JOURNAL
OF
THE PHYSICAL SOCIETY
OF JAPAN

Being a continuation of
"Proceedings of the Physico-Mathematical Society of Japan"

Volume 4 -5

1949-50

Office of the Society:
Faculty of Science, University of Tokyo.

Theory on the Crystallization and Melting of Unvulcanized Rubber. Part I. Crystallization.

By Ryoichi KIKUCHI.

Physics Department, Faculty of Science, University of Tokyo.

(Received December 29, 1947; Revised August 15, 1948).

I. Introduction.

§ 1. Introduction.

Recently, L. A. Wood and N. Bekkedahl(1) have reported new experimental results on the crystallization and melting of unvulcanized rubber in the unstretched state at different temperatures. Their results are summarized as follows:

(1) When we keep a specimen of unvulcanized amorphous rubber at any constant temperature between about +15°C and −50°C, it begins to crystallize and its volume gradually decreases (Fig. 1).(2) We should like to denote the ordinate, "Decrease in volume (in percent)," of Fig. 1 by $w(t)$ which is a function of time t for a constant temperature.

(2) The arrows in Fig. 1 indicate the estimated values for half the total decrease of volume at each temperature. Wood and Bekkedahl considered the reciprocal of this time to be a measure of the average rate of crystallization during the first half of the volume decrease, and it is plotted against temperature in Fig. 2. We should like to call this time briefly the "half-time", and denote it by t_h.

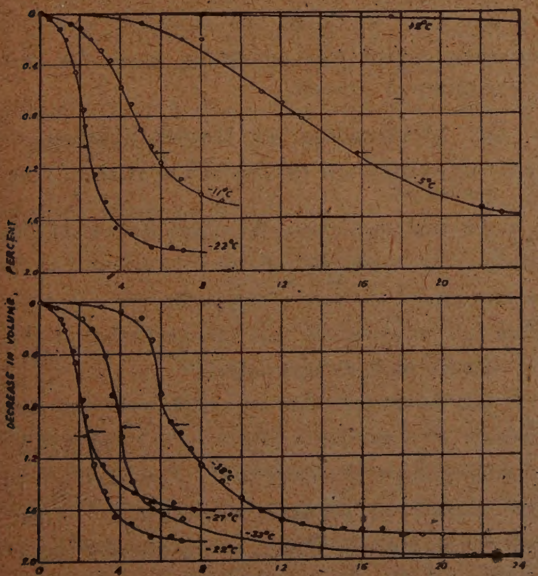

Fig. 1. Crystallization of rubber at different temperatures as indicated by decrease in volume.

(3) As the temperature of crystallized rubber is gradually raised, its volume increases suddenly in some "region" of temperature, and eventually reaches the value corresponding to amorphous state as shown in Fig. 3. This phenomenon seems to be the melting of the crystal, but peculiarly the situa-

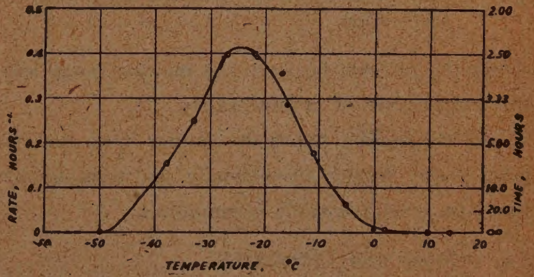

Fig. 2. Rate of crystallization of rubber.

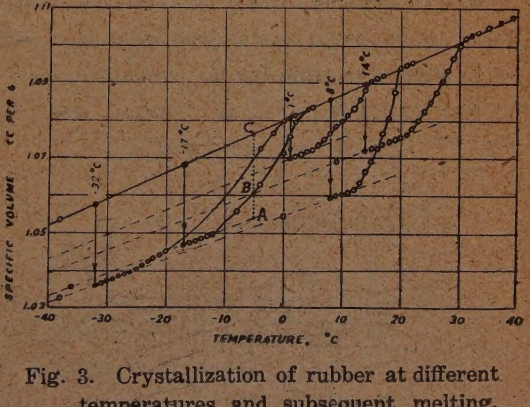

Fig. 3. Crystallization of rubber at different temperatures and subsequent melting. Concering the marks A, B and C, refer to the beinning of § 11, Part II.

H551 63

tion and the width of this melting-region varies according to the previous crystallization temperature.

(4) The range of melting is not dependent on the extent of crystallization and is definitely determined by the temperature at which crystallization occurs. Fig. 4 is derived from Fig. 3 and shows the relation between the melting range and the temperature of crystallization.

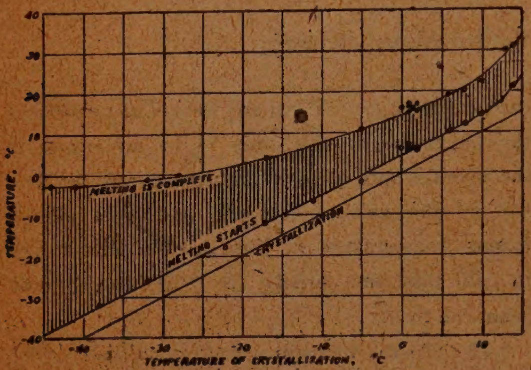

Fig. 4. Melting range of crystalline rubber as a function of the temperature of crystallization.

In the present paper the author tries to explain these results theoretically and consistently based on some allowable assumptions.

§ 2. Models and Definitions.

Adopting the conception of the "micell" (das ausgefranste Micell⁽³⁾) as a fundamental model of rubber crystal, we define as follows.

A part of a chain molecule of rubber which works as a unit in the case of Brownian motion or crystallization is called an "element".

When l elements in each of g chain molecules arrange themselves in parallel lines with the atomic configurations corresponding to crystalline state, this aggregation is called an "l-grain" and l is called the "size" of the grain (Fig. 5).

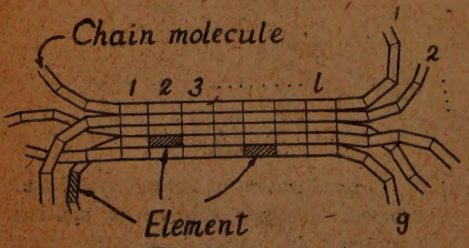

Fig. 5. l-grain.

At an adjacent place to a stable grain, another new one springs up. A group of grains grown with mutual connections as is shown in Fig. 6 is called

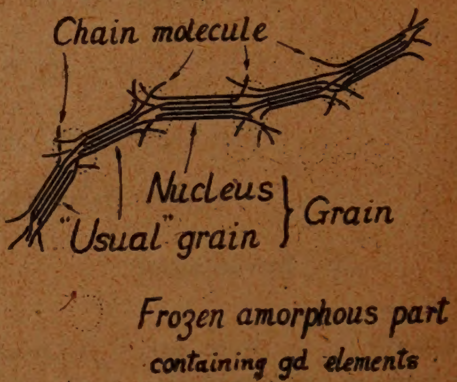

Fig. 6. Linear Cluster.

a "cluster." The grain which formed earliest in a cluster is called a "nucleus", and those grains which are not muclei are called "usual" grains.

As crystallization goes on, narrow amorphous parts are left between two adjacent grains. Their motions being restricted by the surroundings, elements in these amorphous parts do not crystallize afterwards,⁽⁴⁾ and might be called "frozen amorphous elements." Those amorphous elements which are not "frozen" are called "free." Elements which are in grains are called "crystallized elements." We put the ratio between the "frozen" amorphous and the "crystallized" elements as $(r-1)$: 1, r indicating the numberof elements dropping out of free amorphous phase per one "crystallized" element.

II. Mechanism for Crystallization.

§ 3. Crystallization Process at the Higher Temperatures.

As mentioned above Wood and Bekkedahl considered the reciprocal of the "half-time" to be a measure of the rate of crystallization. But before talking about the rate, the mechanism of crystallization must be scrutinized.⁽⁵⁾

Let us consider that an amorphous phase containing L elements is held at T_c°K, and crystallization goes on gradually in it. Letting $P(t)$ be the number of elements remaining in "free" amorphous phase at time t, and considering the definition of r at the end of the preceding section, the number of elements $Q(t)$ then having crystallized is expressed as

$$Q(t) = \frac{1}{\gamma}\{L-P(t)\}. \tag{3.1}$$

Concerning the crystallization process, we make following assumptions: (1) The number of nuclei growing between t and $t+dt$ is $uP(t)dt$, with coefficient u depending only on the crystallizing temperature T_c but not on t; (2) From a nucleus a cluster grows linearly to right and left as in Fig. 6, and the number of newly shaped grains in time dt for a cluster is $2cdt$, c depending only on T_c but not on t. A cluster shown in Fig. 6 will be called a "linear cluster" (cf. Fig. 8); (3) The "size" of each grain is equal in avarage and is l_a depending on T_c; (4) The densities in "free" and "frozen" amorphous states are equal and are different from that in the grain.

From these assumptions we get the following equation for the number of crystallized elements,(6)

$$\frac{1}{\gamma}\{L-P(t)\} = gl_a\int_0^t 2cd\xi\int_0^\xi uP(\tau)d\tau, \tag{3.2}$$

the solution of which is readily transformed into

$$Q(t) = \frac{L}{\gamma}\left\{1-\cos(\sqrt{2cugl_a\gamma}t)\right\}, \tag{3.3}$$

which again, for small values of t, can be expanded as

$$Q(t \doteqdot cugl_aLt^2. \tag{3.4}$$

If, instead of the above assumption (2), we assume that a cluster grows two-dimensionally or three-dimentionally, $Q(t)$ becomes proportional to t^3 or to t^4, respectively, so far as t is small. Which of these cases is realized can be determined by Fig. 1.

The relation between $w(t)$ in Fig. 1 and $Q(t)$ is easily shown to be

$$w(t) = 100\frac{v_a-v_c}{v_a}\cdot\frac{Q(t)}{L}, \tag{3.5}$$

where v_a and v_c denote the specific volume of amorphous and crystalline states, respectively.

Fig. 7 represents log w vs. log t curves corresponding to Fig. 1. From these curves we can conclude that for the higher temperatures than about -30°C, $w(t)$ is proportional to t^2 and (3.4) is realized. (3.4) might be called the "t^2-law for crystallization."

When t is equal to the half-time t_h, we obtain from (3.4) and (3.5)

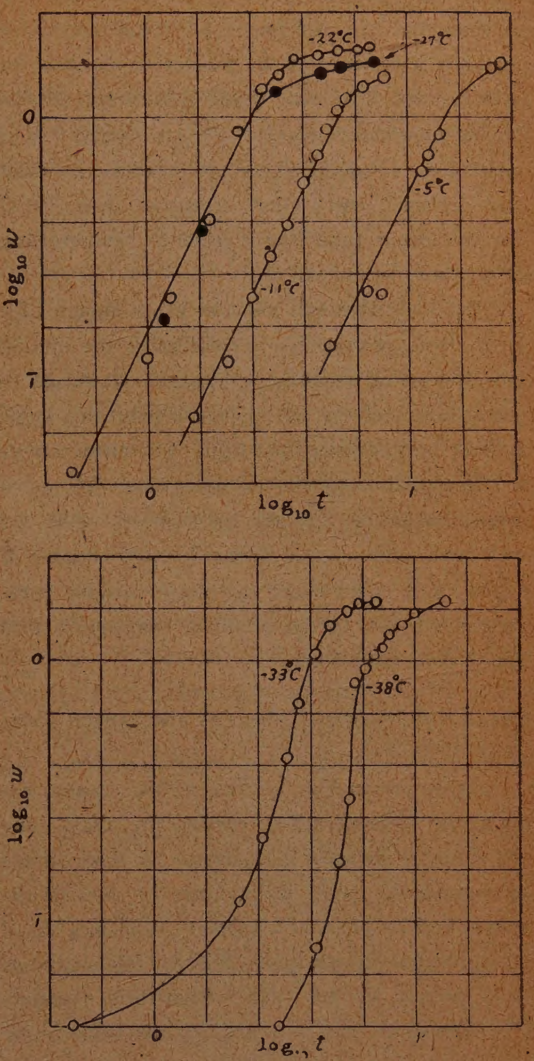

Fig. 7. log w vs. log t curves derived from Fig. 1.

$$w(t_h) = 100\frac{v_a-v_c}{v_a}cugl_a\gamma t_h^2. \tag{3.6}$$

Combining this formula with the equation which is nothing but the definition of $w(t_h)$ in Fig. 1

$$w(t_h) = 100\frac{1}{2}\cdot\frac{v_a-v_c}{\gamma v_a}, \tag{3.7}$$

we have

$$\frac{1}{t_h} = \sqrt{2cugl_a\gamma}, \tag{3.8}$$

which is what Fig. 2 represents. Substituting (3.8) into (3.4), we have

$$Q(t) = \frac{L}{2\gamma}\left(\frac{1}{t_h}\right)^2 t^2. \tag{3.9}$$

Therefore, we can conclude that, so far as γ is assumed to be independent of temperature, $1/t_h$ really is a measure of the rate of crystallization, as Wood and Bekkedahl rightly considered, for the higher temperature region. By the "higher" temperatures we shall mean the temperatures at which the "t^2-law" holds, that is higher than -30°C. At the same time the "lower" temperatures mean those below -30°C.

But (3.3) does not hold for large values of t as it does not take into consideration the mutual interference of neighboring clusters. It should be added here that, by taking into account this interference in an appropriate form, we can construct a differential equation to determine $P(t)$ as a generalization of (3.2), the solution of which fits well with experimental points for large values of t, too. But to introduce too many variable parameters is futile, so the details of comparison with Fig. 1 are omitted here.

§ 4. Crystallization Process at the Lower Temperatures.

As we see in Fig. 7, the "t^2-law" cannot explain the crystallization curves for -33°C and -38°C, and some other mechanisms for them should be considered. Now we assume, in place of the assumption (2) § 3, that a cluster grows in a shape of a tree as illustrated in Fig. 8. We shall call the cluster of this form the "dendriform" cluster. If c represents, just as c in (3.2), the velocity for a grain to grow at a place adjacent to an already formed one, the total number of grains included in a cluster grown from a nucleus generated at $t=0$, is

$$2gl_a(\mu+2\mu+2^2\mu+\ldots\ldots+2^{\frac{ct}{\mu}-1}\mu)=2gl_a\mu(2^{\frac{ct}{\mu}}-1), \quad (4.1)$$

where μ has the meaning illustrated in Fig. 8.

Modifying the method of § 3 a little, we get the next equation for the number of elements $P(t)$ remaining in "free" amorphous phase[6]

$$\frac{1}{\gamma}\{L-P(t)\}=\int_0^t uP(\tau)2gl_a\mu(2^{\frac{c(t-\tau)}{\mu}}-1)d\tau, \quad (4.2)$$

which can easily be transformed into the differential equation

$$\frac{\mu}{c\ln 2}\frac{d^2P}{dt^2}-\frac{dP}{dt}+2gl_a\mu u\gamma\cdot P=0, \quad (4.3)$$

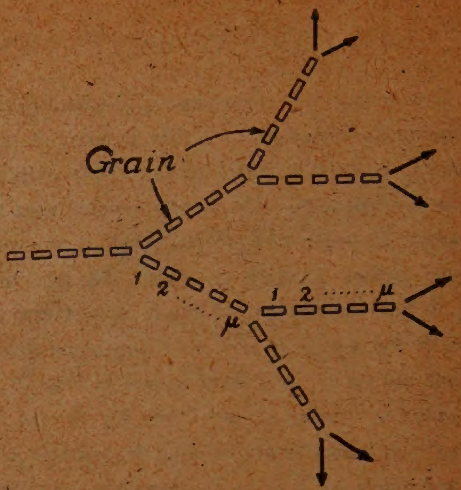

Fig. 8. Dendriform Cluster.

with the initial conditions $P=L$, $\frac{dP}{dt}=0$ at $t=0$. When μ approaches to infinity, (4.3) becomes effectively identical with the differential equation derived from (3.2) with slight modification in a numerical coefficient, confirming that the linear cluster can be considered as a special case of the dendriform one. On the contrary when μ is small, the peculiarity of the latter becomes evident, and if we put

$$\alpha^2\equiv 1-\frac{4\mu ugl_a\gamma}{b}, \text{ and } b\equiv\frac{c\ln 2}{2\mu}, \quad (4.4)$$

the solution of (4.3) becomes

$$P(t)=Le^{bt}\left\{\cosh(\alpha bt)+\frac{1}{\alpha}\sinh(\alpha bt)\right\} \quad (4.5)$$

And again, putting $\frac{1}{\alpha}\equiv 1+\varepsilon$, and combining (4.5) with (3.5), when ε is small and t is not so small, we get

$$w(t)\doteqdot 100\frac{v_a-v_c}{\gamma v_a}\frac{\varepsilon}{2}e^{2bt}. \quad (4.6)$$

To check this equation, Fig 9 was drawn after the data of Fig. 1 with log w and t as axes, and it shows that the "expoential law" (4.6) is realized for the curves of the "lower" temperatures. In this region Fig. 2 cannot be said, in a strict sense, to represent the rate, for combining (4.6) with (3.6) we get

$$\frac{1}{t_h}=\frac{c\ln 2}{-\mu\ln\varepsilon} \quad (4.7)$$

which cannot be connected directly with b which is the parameter representing the rate in (4.6).

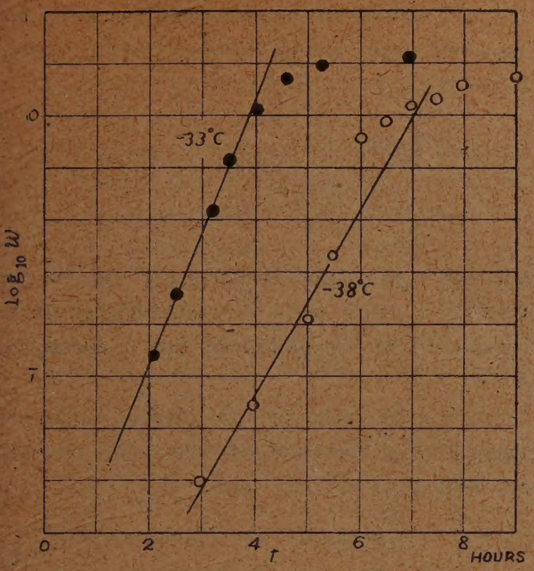

Fig. 9. log w vs. t curves derived from Fig. 1.

III. Rate of Crystallization.

§ 5. Models and Definitions in More Detail.

Before we proceed further, we assume in more detail the process of crystallization and the properties of grains as follows:

(1) In the amorphous phase, chain molecules can assume various different forms for the same energy content, and have entropy due to the number of possible configurations. We denote this entropy S per element and put the internal energy for this phase as zero.

(2) In the first step of the formation of an "l-grain," an "l-activated complex" is formed having the shape shown in Fig. 10. Elements in the activated complex have value zero for both entropy and internal energy.

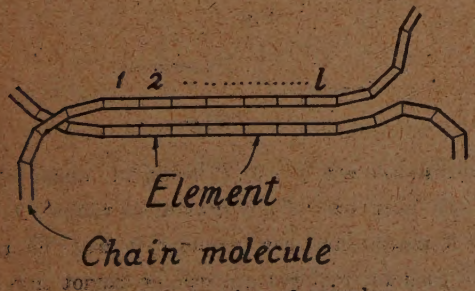

Fig. 10. l-activated complex.

(3) An element in a grain has the value $-E$ of internal energy and zero of entropy.

(4) A grain does not exist alone but appears and disappears together with a "frozen amorphous part" composed of $g\delta$ elements, each of which has the values zero of both entropy and internal energy. The value of δ is, as shown in Fig. 6, $2d$ for a nucleus and d for other "usual" grains.

When we want to emphasize the presence of the frozen amorphous part we write such as "l-δ-grain." The existence of this part is important because it exerts influence upon the crystallization energy of a grain, the latter having meaning only for a system containing both the grain and the frozen amorphous part belonging to it, as they two appear and disappear at the same time. Therefore the crystallization energy per element of an "l-δ-grain" is $-El/(l+\delta)$.

(5) In both amorphous and crystalline states thermal motion (chiefly vibration) is assumed nearly equal and the difference of volumes in the two states multiplied by the atmospheric pressure small compared with ST or E. Hence the free energy per element (chemical potential) for each state is as follows:

$$\left.\begin{aligned}\phi_{am}&=-ST &&\text{for amorphous state}\\ \phi_{ac}&=0 &&\text{for activated complex}\\ \phi_{l\delta}&=-El/(l+\delta) &&\text{for } l\text{-}\delta\text{-grain}\end{aligned}\right\}. \qquad (5.1)$$

(6) The temperature defined by equating ϕ_{am} and $\phi_{l\delta}$

$$T_m=\frac{E}{S}\frac{l}{l+\delta} \qquad (5.2)$$

will be called the "characteristic melting point" for an l-δgrain, as the latter melts at temperatures higher than T_m. Introducing T_0, defined by $E=ST_0$, the formula for the "size" $l(T,\ \delta)$ of a grain of melting point T°K is

$$l(T,\ \delta)=\delta\frac{T}{T_0-T}. \qquad (5.3)$$

T_0 gives the melting point of a grain for which $l/\delta\rightarrow\infty$.

§ 6. Rate of Formation of a Grain.

For the process of formation of a grain from amorphous state through activated complex, so far as the rate of transfer from the latter to the final crystal is fast enough, the rate-determining factors are the following two: (1) The rate of diffusion of elements in the course of formations of an activated complex from amorphous phase, and (2) The number of activated complex in equilibrium with the amorphous phase, when the diffusion velocity is sufficiently large.

In the lower region of temperature (1) has the chief effect and both u and c are proportional to $\exp(-U/kT)$, where U is the activation energy for diffusion of an element. Though the details are not described here, this assumption can explain qualitatively the variation of the rate of crystallization in the lower temperature region.

On the contrary in the higher temperature region, (2) is rate determining, and the number of l-activated complex in equilibrium with amorphous phase is, after Eyring(7), proportional to

$$\exp\{-2l(\phi_{ac}-\phi_{am})/kT\} = \exp(-2lS/k), \qquad (6.1)$$

where 2 in the power represents two molecules participating in the activated complex and k is the Boltzmann's constant. Number of l-grains, $r(l, T)$, crystallizing in unit time is proportional to (6.1) and it

$$r(l, T) = A\exp(-2lS/k). \qquad (6.2)$$

At a temperature T, grains smaller than $l(T, \delta)$ of (5.5) being unable to crystallize, the total number of grains formed in unit time $r_\delta(T)$ is

$$r_\delta(T) = \int_{l(T,\delta)}^{\infty} r(l, T)dl = A\frac{k}{2S}\exp\{-2l(T, \delta)S/k\}. \qquad (6.3)$$

The rate of formation of a grain, u and c, are proportional to (6.3).

The total number of elements $P_d(T)$ crystallizing in "usual" grains in unit time is

$$P_d(T) = \int_{l(T,d)}^{\infty} glr(l, T)dl, \qquad (6.4)$$

and therefore, the average number of elements gl_α for a "usual" grain is

$$gl_\alpha = <gl>_{Av} = \frac{P_d(T)}{r_d(T)} = g\frac{k}{2S}\left\{1+2l(T, d)\frac{S}{k}\right\}. \qquad (6.5)$$

§ Comparison with Experiments.

For the higher temperature region, the theoretical results of the former section can be compared with Fig. 2 which represents (3.9). Supposing the number of nuclei is much smaller than that of "usual" grains, we get, from (6.3), (6.5), (5.3) etc.,

$$\frac{1}{t_h} = \sqrt{2cugl_\alpha\gamma}$$
$$= B\left(1+2q\frac{T}{T_0-T}\right)^{\frac{1}{2}}\exp\left(-3q\frac{T}{T_0-T}\right) \qquad (7.1)$$

where B is a function containing γ etc., but is considered simply as a constant for preliminary comparison with experiments, and q stands for Sd/k.

In Fig. 11, points and the broken curve are those of Fig. 2 and the solid line is the theoretical result (7.1) with the values

$$T_0 = 310°\text{K}, \qquad B = 500,$$
$$q = 0.5\text{-}0.005\,(T\text{-}273), \qquad (7.2)$$

which were selected so as to get the best fit with experimental results, and the probable error of T_0 is about ±20°.

Though the formula (7.1) and the values of (7.2) have merely an approximate meaning, the satisfactory agreement shown in Fig. 11 indicates that such a theory is plausible. Especially as mentioned at the end of § 5, T_0 being the upper limit of the existence of any crystal of rubber, $T_0 = 310°$K means that, however long it may be held at a constant temperature, rubber cannot crystallize above 37°C. Though in reality, some evidences of rubber crystals near 50°C were reported(11), the value of (7.3) with its probable error does not

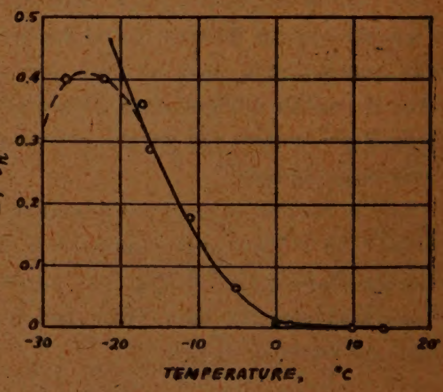

Fig. 11

○ } Experiment

——— Theory

seem irrational, considering the possibility of variation of this threshold value with the change in previous thermal treatments or in compositions of the rubber sample.

This theory will be concluded in the following paper, Part II with the same title(8).

References and Notes.

(1) L. A. Wood and N. Bekkedahl, J. Appl. Phys. **17** (1946) 362.

(2) Figs. 1, 2, 3 and 4 are duplications of the corresponding figures in the reference (1), except for marks A, B and C in Fig. 3 for which explanation will be given in § 11 of Part II.

(3) W. Abitz, O. Gerngross and K. Hermanns, Naturwiss. **34** (1930) 754, etc.

(4) G. S. Parks, J. Chem. Phys. **4** (1936) 459, L. R. G. Treloar, Trans. Faraday Soc. **37** (1941) 81.

(5) Cf. F. von Gölera nd G. Sachs, Zeits. f. Phys. **77** (1932) 281; M. Avrami, J. Chem. Phys. **7** (1939) 1103; **8** (1940) 212; **9** (1941) 177.

(6) Strictly speaking, number of elements crystallized as nuclei $ugl_{tt}\int_0^t P(\tau)d\tau$ should be added in the right hand side of (3.2) and (4.2), but physically it is assumed negligible compared with the rest of the terms so far as t is small.

(7) S. Glasstone, K. J. Laidler and H. Eyring, "The Theory of Rate Processes" (McGraw-Hill Book Co., New York, 1941) p. 185ff.

(8) R. Kikuchi, J. Phys. Soc. Japan, **4** (1949) 7.

Theory on the Crystallization and Melting of Unvulcanized Rubber. Part II. Melting.

By Ryoichi KIKUCHI.

Physics Department, Faculty of Science, University of Tokyo.

(Received December 29, 1947; Revised August 15, 1948).

This is the continuation of the paper, Part I with the same title,(1) and the explanation of the melting properties of rubber crystals discovered by L. A. Wood and N. Bekkedahl(2) will be given here. We shall utilize the same notations and definitions as Part I without explanation hereafter, and sections and figures will be numbered through both parts.

IV. Melting.

§ 8. Melting of a Linear Crystal.

Clusters grown at T_c°K contain various sizes of grains but their distrubution $n_0(l, T_c)$ is definitely proportional to the rate of crystallization as a function of l, that is $r(l, T_c)$, Eq. (6.2), at least at the moment of crystallization. Now we assume that a grain crystallized with the size l enlarges to $l+\lambda$ in time,(3) the distribution for l assymptotically becoming

$$\left.\begin{array}{ll} n(l, T_c) = D\exp\{-2(l-\lambda)S/k\} & l \geqq l(T_c)+\lambda \\ n(l, T_c) = 0 & l < l(T_c)+\lambda \end{array}\right\} \quad (8.1)$$

(cf. Fig. 12).

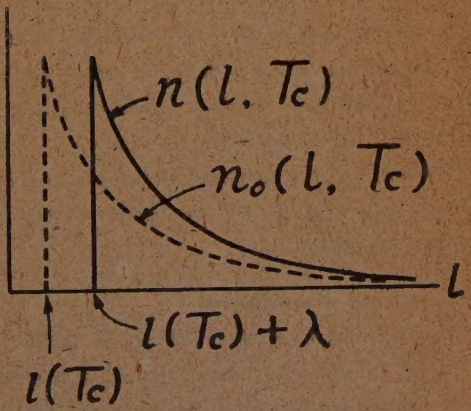

Fig. 12

In the next place, we assume that the melting of a linear crystal occurs after the following mechanisms: (1) Melting proceeds step by step from both ends of a cluster; (2) A grain with the characteristic melting point T°K does not melt until the temperature becomes higher than T°K.

For example, when we raise the temperature of a cluster crystallized at T_c°K to T°K, melting proceeds from both ends step by step until a grain with its characteristic melting point T'°K ($T' > T$) places at the edge of the cluster, and then the melting stops there. Until the temperature becomes higher than T'°K the melting does not resume.

§ 9. Evaluation of the Probability.

For preparation we solve the next question on probability: "One of cards marked 'R' the number of which is R and those marked 'W' the number of which is W, is placed upside-down at random at each of the M sites in a line, M being equal to $R+W$. Turning the cards one by one from both ends and continuing so far as the mark 'R' appears, what is the average number of cards that is to be turned?"

The probability $\Psi(s)$ of finding an 'R' at the s-th site from an end, after all of the $(s-1)$th have been 'R', being

$$\Psi(s) = \frac{R}{M}\cdot\frac{R-1}{M-1}\cdots\cdots\frac{R-s+1}{M-s+1}, \qquad (9.1)$$

the average number of cards $m(M, R)$ asked is

$$m(M, R) = 2\langle s\rangle_{Av} = 2\sum_{s=1}^{R}\Psi(s) = \frac{2R}{M-R+1} \qquad \text{for } R \leqq M-1 \quad (9.2a)$$

$$m(M, R) = R \qquad \text{for } R \geqq M-1 \quad (9.2b)$$

It is important because at $R = M-1$, $m(M, R)$ is an angled curve as a function of R, and this results in a distinct point at which the melting ends as will be shown below (cf. § 11).

Though, strictly speaking, (9.2a) holds for only integral values of R, we assume its validity for non-integral values, too.

§ 10. Melting of a Cluster.

Suppose that a cluster formed at T_c°K and of "size" M (when grains contained in a cluster are M in number, we shall call its "size" M), is brought to T°K ($T > T_c$). Then from (8.1) the number of grains R having the characteristic melting point below T°K is given by

$$R = \int_{l(T_c)}^{l(T)} n(l, T_c)dl = D\frac{k}{2S}\left\{e^{-2l(T_c)\frac{S}{k}} - e^{-2(l(T)-\lambda)\frac{S}{k}}\right\}, \qquad (10.1)$$

and M is equal to $R(T = T_0)$:

$$M = \int_{l(T_c)}^{\infty} n(l, T_c)dl = D\frac{k}{2S}e^{-2l(T_c)\frac{S}{k}}. \qquad (10.2)$$

In a cluster crystallized at T_c°K, avearge size of a grain which has melted at T°K, $gl_a(T_c, T)$ is

$$gl_a(T_c, T) = \frac{\displaystyle\int_{l(T_c)+\lambda}^{l(T)} gle^{-2(l-\lambda)\frac{S}{k}}dl}{\displaystyle\int_{l(T_c)+\lambda}^{l(T)} e^{-2(l-\lambda)S/k}dl}. \qquad (10\text{-}3)$$

Considering R and M thus calculated as to be the corresponding quantity in (9.2), $m(M, R)$ represents the number of grains which have melted at T°K. Then, in order to compare with experiments, combining $m(M, R)$ with (10.3) and $gl_a(T_c)$ in (6.5) which is nothing but $gl_a(T_c, T_0)$, the proportion $y(T, M)$ of *elements* which have melted below T°K in a cluster of size M becomes

$$y(T, M) = \frac{gl_a(T_c, T)}{gl_a(T_c)}\cdot\frac{m(M, R)}{M}. \qquad (10.4)$$

In the next place considering the facts that the width of the frozen amorphous part left between two neighboring grains, being d directly after the crystallization, becomes gradually $d-\lambda$, $l(T_c)$ and $l(T)$ has the form

$$l(T_c) = d\frac{T_c}{T_0-T_c}, \quad l(T) = (d-\lambda)\frac{T}{T_0-T}. \qquad (10.5)$$

Then if we define T_b by

$$(d-\lambda)\frac{T_b}{T_0-T_b} = d\frac{T_c}{T_0-T_c} + \lambda, \qquad (10.6)$$

it gives the temperature at which melting begins, because at $T = T_b$, we get easily $R = 0$ from (10.5) and (10.1).

Using T_b, (10.4) becomes

$$y(T, M)\begin{cases} = \dfrac{2}{M\cdot x(T)+1}\cdot Y(T) \equiv y_1(T, M) & T \leqq T_m' \qquad (10.7a) \\ = Y(T) \equiv y_2(T, M) & T \geqq T_m' \qquad (10.7b) \end{cases}$$

where

$$Y(T) = 1 - \frac{1+2q\left(1-\dfrac{\lambda}{d}\right)\dfrac{T}{T_0-T}}{1+2q\left(1-\dfrac{\lambda}{d}\right)\dfrac{T_b}{T_0-T_b}}\cdot x(T), \qquad (10.8)$$

$$x(T) = \exp\left\{-2q\left(1-\frac{\lambda}{d}\right)\left(\frac{T}{T_0-T}-\frac{T_b}{T_0-T_b}\right)\right\}, \quad (10.9)$$

and T_m' is determined by the equation

$$M \cdot x(T_m') = 1. \quad (10.10)$$

It would be mentioned here that at $T = T_m'$, $R = M-1$ and T_m' gives the point at which melting apparently ends for the cluster (cf. § 11).

§ 11. The Melting Curve Averaged over Clusters with Various Different Sizes.

From our standpoint we can interpret the ratio $\overline{AB}/\overline{AC}$ in Fig. 3 of Part I to be the proportion of the number of elements which have melted at -5°C to the total number of crystallized elements at -17°C. In order to compare this quantity with our theory we have to average $y(T, M)$ over M, because $y(T, M)$ are concerned only with clusters of the size M and the rubber crystallized at any temperature contains clusters of various different sizes.

To proceed along this line, the distribution of number of clusters with the size M must be determined, in advance. Though this distribution should be derived theoretically from assumptions concerning the procedure of crystallization, so far as the preliminary theory is concerned we can do with the next assumption: "The number of clusters with the size between M and $M+dM$ is constant, i.e. is independent of M."(4)

Then averaging $y(T, M)$ of (10.7) over M, we get

$$\begin{aligned} z(T) &\equiv < y(T, M) >_{AV} \\ &= \frac{1}{M_m}\left\{\int_{1/x(T)}^{M_m} y_1(T, M)dM + \int_0^{1/x(T)} y_2(T, M)dM\right\} \\ &= \frac{Y(T)}{M_m \cdot x(T)}\left[2 \ln\left\{\frac{M_m x(T)+1}{2}\right\}+1\right] \quad \text{for } T \leqq T_m \end{aligned} \quad (11.1a)$$

$$z(T) = \frac{1}{M_m}\int_0^{M_m} y_2(M)dM = Y(T) \quad \text{for } T \geqq T_m \quad (11.1b)$$

where T_m is determined by the equation

$$M_m \cdot x(T_m) = 1 \quad (11.2)$$

and M_m gives the maximum size of clusters crystallized at T_c°K, being of the order (5)

$$M_m \approx \left(\frac{c}{ugl_a\gamma}\right)^{\frac{1}{2}} \quad (11.3)$$

It should be noted here concerning (11.1), that $z(T)$ changes its functional form and suffers a remarkable change of tangent at T_m just as $y(T, M)$ at T_m', and is, for T greater than T_m,

$$1 > z(T) \gtrsim 1 - \frac{1}{M_m}, \quad \text{for } T > T_m. \quad (11.4)$$

Therefore, T_m can be considered to be the point at which melting apparently ends.

The formula (11.1) can be compared with the experiment with appropriate values of parameters. Figs. 13 and 14 give this comparison, with the values of T_0 and q given in (7.2) and with

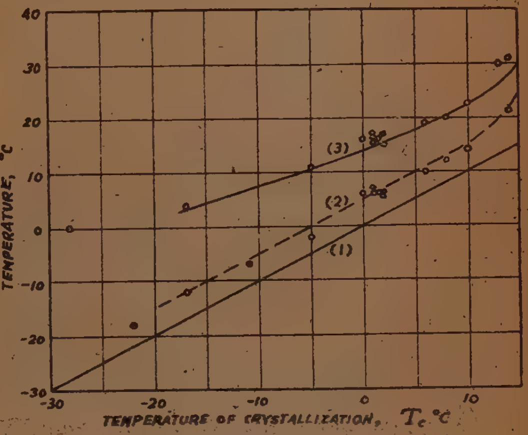

Fig. 13.

(1): Temperature of crystallization T_c.

(2): Assigned values of T_b.

(3): Theoretical values of T_m by (11.2).

○ : Experimental points.

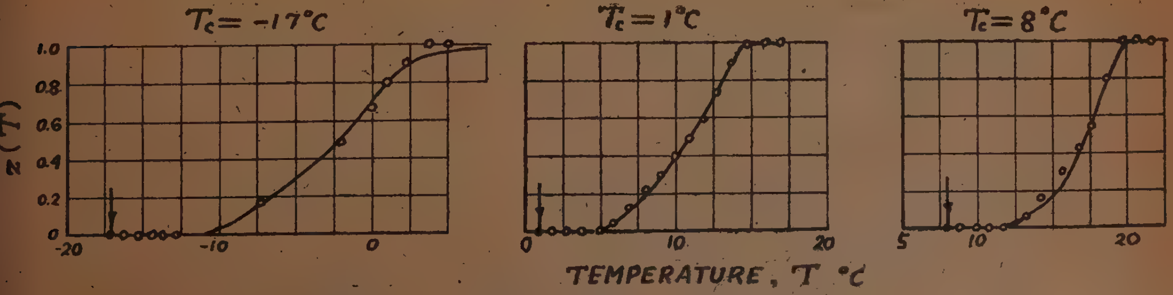

Fig. 14. ○ Experiment —— Theory.

$$\left.\begin{array}{l} T_b - T_c = 5^\circ \text{ (below } 10^\circ\text{C)} \\ M_m = 40 \text{ at } T_c = 1^\circ\text{C} \end{array}\right\} \quad (11.5)$$

M_m having the functional form (11.4).

These figures indicate that (11.1) agrees enough well with the experiment so far as the "linear crystal" is concerned, except the region over about 10°C. This discrepancy above 10°C is not explained yet.

V. Conclusion.

§ 12. Discussions and Conclusion.

Melting of the "dendriform" clusters :—For this crystalline form, two theoretical curves for melting could be constructed by assuming laws for the process of melting, but the conclusion is not yet drawn owing to the complexity of formulae. Qualitatively, the reason for the broadening of the temperature range of melting for the lower temperatures seems to be due to the larger values of the size of a cluster M_m as the temperature becomes lower.

Recrystallization :—When a rubber is held at a constant temperature half-way of melting or above the temperature at which the melting has been apparently finished, the rubber begins to decrease its volume gradually. Wood and Bekkedahl called this phenomenon the "recrystallization," the peculiarity of which is that the rate of decrease in volume is larger than the case of primary crystallization. This phenomenon is explained without difficulty by our theory. Namely, not to speak of the case in which the melting is apparently not completed yet, in the case, too, in which the rubber is brought to the temperature higher than that at which the melting has ended appearently, the crystal does not melt completely and at least some quantity of the order of (11.5) is left, which plays a role of nuclei for recrystallization, causing a larger rate of decrease in volume. Though this seems very interesting and important for more thorough investigaton, more experimental data are desirable.

Furthermore, other exprimental results, too, reported by Wood and Bekkedahl, e.g. various facts concerning the stark rubber, can be explained at least qualitatively by our models.

In conclusion we should like to point out that the present theory includes some new bold models concerning the "micell" of high polymers. Though in the present stage these models are nothing but hypotheses, we hope in the near future its validity will be examined experimentally by attacks from various sides.

The author wishes to express his cordial thanks to Prof. T. Sakai, the late Mr. Y. Ochi, Messrs. A. Ishihara and H Ichimura for their encouraging discussions.

References and Notes.

(1) R. Kikuchi, J. Phys. Soc. Japan. **4**, (1949) 1.

(2) L. A. Wood and N. Bekkedahl, J. Appl. Phys. **17**, (1946) 362.

(3) The author thinks this assumption less serious than the following two. The former was introduced so as to distinguish the point at which melting begins (cf. Figs. 3 4, 13, and 14). Even without this assumption, so far as the latters are recognized, the theoretical melting curves in Fig. 14 do not change essentially, only starting smoothly from the temperature at which crystallization has occurred.

(4) This distribution of clusters is derived when the interference in the growth of neighboring clusters is taken into account in such a form that the rate of growth of a cluster is proportional to $P(t)$ defined in § 3 (cf. the end of § 3, Part I).

(5) If, in accordance with § 3 Part I, clusters are assumed to grow independently of one another, we can derive the result

$$M_m = \sqrt{\frac{\pi}{2}}\left(\frac{c}{ugl_a\gamma}\right)^{\frac{1}{2}},$$

and if the assumption marked (4) in § 11 is allowed, we get

$$M_m = 2\left(\frac{c}{ugl_a\gamma}\right)^{\frac{1}{2}},$$

On the Ammonia Molecule, I.

By Masataka MIZUSHIMA.

Physics Department, Faculty of Science, University of Tokyo.

(Received, May 6, 1948)

§ 1. Introduction.

The structure of ammonia molecule NH_3 has been investigated since the earliest day of molecular physics, and the conclusion was that this molecule has a pyramidal structure with the N-atom on its apex, belonging to the symmetry group C_{3v}. Many experimental results were explained very well by this model. But it is also known that this molecule has an inversion motion i. e., N-atom can vibrate through the center of the triangle formed by the three H-atoms. Since potential energy does not change when one reflect all particles at the origin, there must be two equilibrium configurations. By this double minimum character of potential, the vibrational ground state of this molecule is composed of two nearly degenerate states, wave functions of which are respectively positive and negative for the reflection of all particles at the origin. The transition between these two states corresponds to the inversion motion.

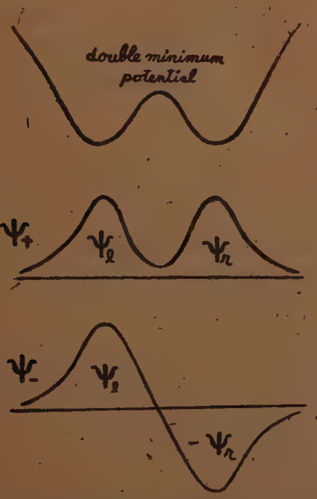

Fig. 1. The double minimum potential and its associating wave functions.

The energy splitting in this so-called inversion doubling(1) is about 0.8 cm.$^{-1}$, which is about one tenth of the energy difference between each rotational states. Thus we are permitted in approximating the wave function of this molecule by the product of rotational, vibrational and the rest parts.

$$\Psi = \psi\Theta\Phi \qquad (1)$$

where Ψ is the total, ψ, the vibrational, Θ, the symmetric rotational wave functions respectively. For ψ we take ψ_+ and ψ_- corresponding to the above mentioned positive and negative states respectively. It can be seen that both $|\psi_+|^2$ and $|\psi_-|^2$ have the center of symmetry.

§ 2. Dielectric Constant of Ammonia.*

In quantum mechanics we may define permanent dipole moment of a molecule by the next formula

$$\mu = \int \psi^{*} \mu \psi d\tau , \qquad (2)$$

where ψ is the vibrational wave function of the molecule, and μ is the dipole moment vector. In the case of ammonia this definition gives us

$$\mu_+ = \int |\psi_+|^2 \mu d\tau \quad \text{or} \quad \mu_- = \int |\psi_-|^2 \mu d\tau$$

for the dipole moment of each state. But since $|\psi_+|^2$ and $|\psi_-|^2$ have the center of symmetry both μ_+ and μ_- vanish identically. Thus it may seem curious that dielectric constant of ammonia gas obeys the famous Debye's formula of polar gas:

$$\frac{\epsilon-1}{4\pi} = \frac{Np^2}{3kT} + \alpha$$

with $p = 1, 48 \cdot 10^{-18}$ e.s.u. c.g.s. This may be explained as follows.

---

* Dr. M. Yasumi obtained the same result in his unpublished study.

Van Vleck[2] showed that in quantum mechanics, the quantity p appearing in the Debye's formula can be expressed as

$$p^2 = \frac{\sum\limits_{r}\sum\limits_{j'} (j|\mu|j')^2 c^{-E_j/kr}}{\sum\limits_{r} e^{-E_r/kr}}, \tag{3}$$

where j is the quantum number and $(j|\mu|j')$ is the matrix element of the electric dipole vector. In the case of ammonia at room temperature vibrationally exited states do not contribute to (3). Therefore, if we designate rotational states by r and the positive and negative states by $+$ and $-$ respectively, (3) becomes

$$\begin{aligned} p^2 = \{\sum_{r}\sum_{r'}[(+,\, r|\mu|+,\, r')^2 + (-,\, r|\mu|-,\, r')^2 e^{-\frac{\epsilon_r}{kr}} \\ +(+,\, r|\mu|,-,\, r')^2 \\ +(-,\, r|\mu|+,\, r')^2 e^{-\frac{\epsilon_r}{kr}}] e^{-\frac{E_{+,r}}{kr}}\} / \sum e^{-\frac{E_{+,r}}{kr}} (1+e^{-\frac{\epsilon_r}{kr}}), \end{aligned} \tag{4}$$

where ϵ_r is the energy difference between $\Psi_{+,r}$ and $\Psi_{-,r}$ states, the positive states being lower.

In (4) $(+, r|\mu|+, r)$ and $(-, r|\mu|-, r)$ vanish identically by the above discussion, and ϵ_r/kT is very small and nearly independent of r, hence defining d by

$$d = \int \psi_+^* \mu \psi_- d\tau \tag{5}$$

we obtain

$$p^2 = \sum_{r}\sum_{r'} (r|d|r')^2 e^{-\frac{E_r}{kr}} / \sum e^{-\frac{E_r}{kr}},$$

which is the same expression as when we take d the permanent dipole moment of the molecule. Thus, though there is no permanent dipole moment in the sense of (2), we can as well conclude that Debye's formula is valid. Since d is nearly independent of r we conclude that $p^2 = d^2$, so that from the experimental data[3] we can obtain the numerical value of the matrix element d

$$d = \left|\int \psi_+^* \mu \psi_- d\tau\right| = 1.48 \cdot 10^{-18} \text{ e.s.u. c.g s.} \tag{6}$$

The physical meaning of this matrix element is clear, for, if we take Wall and Glockler's[4] approximation, ψ_+ and ψ_- become

$$\psi_+ = \frac{1}{\sqrt{2}}(\psi_r + \psi_l) \qquad \psi_- = \frac{1}{\sqrt{2}}(\psi_r - \psi_l),$$

where ψ_r and ψ_l are the so called right and left configuration's wave functions. With them we can easily prove that

$$d^2 = \left(\int \psi_r \mu \psi_r d\tau\right)^2 = \left(\int \psi_l \mu \psi_l d\tau\right)^2,$$

that is, d corrospends to the dipole moment of classical pyramidal structure of the ammonia molecule.

§ 3. Molecular Beam of Ammonia.

When an inhomogeneous electric field is applied on a molecular beam of polar molecule, the path of this beam is somehow deflected, degree of which being determined by the electric dipole moment of this molecule. Schoeffers[5] attempted to measure the dipole moment of the ammonia molecule by the molecular beam method, but, paying no attension to the inversion doubling, failed to obtain the correct interpretation of the experimental results. In his experiment energy perturbation was smaller than ϵ, therefore, the inversion doubling play an essential role in this case; we shall make re-calculation from this point of view.

When an electric field of strength F is applied on a molecule, the energy of the latter will be expressed as

$$E = E^{(0)} + E^{(1)}F + E^{(2)}F^2 + \cdots.$$

Then the force acting on the molecule in the a direction is

$$K_a = -\frac{\partial E}{\partial a} = -\frac{\partial F}{\partial a}(E^{(1)} + 2E^{(2)}F) + \cdots \tag{7}$$

If the field is inhomogeneous in a direction perpendicular to the beam, it is shown[5] that the deflection of a molecule at the end of the path is given as follows

$$s = \frac{K}{4E_t} l_1^2 \left(1 + \frac{2l_2}{l_1}\right)$$

where l_1 and l_2 are the length of path in and out of the field respectively, and E_t is the translational energy of this molecule.

We can calculate E by means of the perturbation theory, with the wave function (1); perturbation function being $-F\mu\cos\theta$.

It may be seen that d, the matrix element of μ defined in (5), is parallel to the molecular axis, so that θ is the angle between the field direction and the molecular axis. Then

$$(J, K, M\,|\cos\theta|\,J, K, M)^2 = \left[\frac{KM}{J(J+1)}\right]^2, \quad (8)$$

$$(J, K, M\,|\cos\theta|\,J-1, K, M)^2 = \frac{(J^2-K^2)(J^2-M^2)}{(2J-1)(2J)^2(2J+1)}. \quad (8)'$$

In general (8)′ is much smaller than (8), so that neglecting this non-diagonal term, we can obtain following expression for E

$$E_{\pm, J, K, M} = E^{(0)}_{\pm, J, K, M} \mp \frac{d^2}{\epsilon_{J, K}}\left[\frac{KM}{J(J+1)}\right]^2 F^2$$

and, from (7), for K

$$K_{\pm, J, K, M} = \pm\frac{2d^2}{\epsilon_{J, K}}\left[\frac{KM}{J(J+1)}\right]^2 F\frac{\partial F}{\partial s} \quad (9)$$

On the other hand, if the translational energy E_+ is distributed between molecules according to the Maxwell-Boltzmann law, it can be proved that $J(0)$, the intensity of the beam at the point $s = 0$, is

$$J(0) = J_a\left(\frac{s_\alpha}{a} + 1\right)\exp\left(-\frac{s_\alpha}{a}\right), \quad (10)$$

where J_0 is the intensity of the beam when field is not applied, and a is its width shown in Fig. 2; s_α is given by the following formula

$$s_\alpha = \frac{K}{4kr}l_1^2\left(1 + \frac{2l_2}{l_1}\right)$$

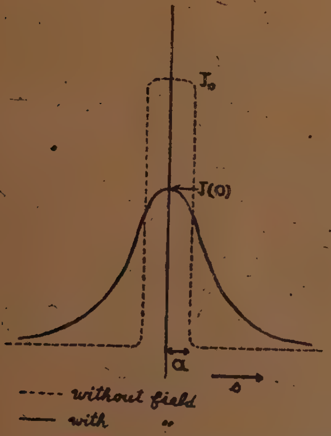

Fig, 2. Intensity curve in the molecular beam experiment of ammonia.

ϵ_r is about 1.57 10^{-16} erg., being nearly independent of J and K, and the numerical value of d is given in (5). Thus on inserting experimental constants, we can ebtain $J(0)/J_0$ for each rotational states. Again assuming Maxwell-Boltzmann distribution between rotational states, we can calculate final value for $J(0)/J_0$. In Table I we compare thus calculated values with the experimental results of Schoeffers; the agreement is satisfactory.

Table I

Experiment number	$J(0)/J_0$ obs.	$J(0)/J_0$ calc.
1	0.87	0.88
4	0.63	0.55 (0.09)
7	0.41	0.38

The value shown in bracket is calculated by Schoeffers paying no attention to the inversion doubling, which shows clearly the important role played by this doubling.

Appendix: The Relative Concentration for Each Rotational State.

In these and the following calculations it is needed to know the relative concentration of each rotational states.

Table II.

The relative concentrations of rotational states of ammonia at $T = 297°K$. (Indicated by G)

J	$\|K\|$	G
0	0	2.000
1	1	5.554
	0	5.453
2	2	8.077
	1	7,645
	0	7.509
3	3	18.600
	2	8.491
	1	8.035
	0	7.889
4	4	9.274
	3	16.315
	2	7.443
	1	7.047
	0	6.919
5	5	8.281
	4	7.000
	3	12.364
	2	5.641
	1	6.339
	0	5.245
6	6	13.489
	5	5.515
	4	4.680
	3	8.232
	2	3.777
	1	3.597
	0	3.492
7	7	5.055
	6	7.968
	5	3 258
	4	2.766
	3	4.866
	2	2.220
	1	2.130
	0	2.064
8	8	3 505
	7	2.666
	6	4.202
	5	1.717
	4	1.459
	3	2.564
	2	1.170
	1	1.103
	0	1.083
9	9	4.522
	8	1.661
	7	1,262
	6	1.984
	5	0.813
	4	0.688
	3	1.216
	2	0.555
	1	0.524
	0	0.517
10	10	1.004
	9	1.924

The energy of each state can be obtained by the next formula.

$$E_{J,K} = \{19.453J(J+1)-7.451K^2\}\cdot 10^{-16}\ \text{ergs}.$$

On the statistical weight of each state following considerations must be made; a) space degeneracy of each J-state is $2J+1$, b) K-state and $-K$-state are in the same energy level, c) the existence of nuclear spin $\frac{1}{2}$ in the hydrogen atom makes the statistical weights of $K = 0, 3, 6, 9, \cdots$ states twice of these of the other states. Thus we can calculate the relative concentration for each state by means of Maxwell-Boltzmann law.

In the above table results are shown for $T = 297°K$

References.

(1) G. Herzberg: *Infrared and Roman Spectra of Polyatomic Molecules* (D. Van Nostrand Co., New York, 1945), p. 26.

(2) J. H. Van Vleck: *The Theory of Electric and Magnetic Susceptibilities* (Oxford, 1932), p. 186.

(3) P. Debye: *Polare Molekeln* (Leipzig, 1929), p. 192.

(4) E. T. Wall and G. Glockler: J. Chem. Phys. **5** (1937), 314.

(5) H. Schoeffers: Phys. Zeits. **41** (1940), 89, 98.

(6) O. Stern: Zeits. f. Phys. **41** (1900), 563.

(7) W. Good: Phys. Rev. **70** (1946), 213.

Crystallite Theory of Liquid.

III. The Viscous Flow.

By Akiya OOKAWA.

Kobayashi Institute of Physical Research, Kokubunji, Tokyo.

(Received May 6, 1948.)

§ 1. Introduction and Summary.

It was proposed previously¹⁾,²⁾ a molecular model of liquid and solid having a structure of a mosaic of fine fragments, each of which has a perfect crystalline pattern throughout its own domain and meets at well-defined interfaces with each other.

Throughout these procedures the non-vibrational thermal mode of the system has simply been represented by the independent translational mode of each crystallites without special care for its appropriateness, which may however be accused of the doubtful predominance or the uncertain existence probability of such a gas-like thermal mode in the condensed system under consideration. In fact it was once proposed by Brillouin³⁾ that the non-vibrational thermal mode in liquid shall correspond to some transverse thermal mode in solid and that it shall be represented by the "vortex" mode in liquid, which is in natural accord with a requirement of absence of the dilatation in the condensed system.

On the other hand, it was already remarked in the previous papers¹⁾,²⁾ that the thermal motion of an intercrystalline boundary between crystallites with different orientations is accompanied by the relative shear movement of the two crystallites and that this motion of the boundary, which takes place equally in alternative directions in natural state, becomes predominant in one direction in a shear stressed state, resulting a macroscopic flow of the system.

The decision between the different viewpoints concerning the non-vibrational thermal mode in natural state as well as the choice of the most predominant process of flow under external stress can only be given by a deliberation on the energy spectrum representing the ground state and the excited states of the system under consideration respectively.

Now, the ground state and the excited states are characterized substantially by two factors as follows:

a) The activation energy for the movement of a specified crystallite.

The misfit potential energy at boundaries between a specified crystallite and its surrounding ones is proportional to its momentary surface area and it depends on the translational coordinate of the specified crystallite, such a situation having been neglected throughout the previous conventional treatments by smoothing out the potential energy with respect to that coordinate. It is evident, however, that there exists a ground state corresponding to a configuration of symmetrical distribution of the intercrystalline boundaries such as to minimize the total intercrystalline surface area, and that there accompanies an increase of the internal surface area in the process of shear motion of a specified crystallite, which is a main cause of the activation energy for such an excited state.

b) The correlation of the movements of many crystallites.

When a specified crystallite displaces itself independently of its neighbouring ones, it has as its necessary results some localized strain energy in excess to the increase of the misfit potential energy above considered. In the extreme case of incompressible system, some well-defined cooperative movement of the total crystallites of the system, such like the degenerated one of the transverse mode in solid, shall be the only possible irreversible process allowed to liquid. In this case the correlation between the displacements of infinitely separated crystallites are perfect. For such an excited state to be realized, however, the total crystallites of the system must be activated simultaneously. In regard of some compressibility of the real system, however, the displacements of the constituent crystallites of the system do not necessarily maintain such a perfect correlation to each other, but the degree of correlation between two specified crystallites decreases with the distance separating them, since the activation of an excited state for increasing distance of correlation is progressively unprobable.

It will be demonstrated in this paper that the non-vibrational thermal mode of normal liquid in natural state can substantially be represented rather by the independent displacement of the constituent crystallites, as previously assumed, than by the vortex mode of the total system, with conceivable exception of a specific liquid of enormously minute misfit energy such as possibly the liquid helium. It will followingly be explained, that the normal liquid in shear stressed state behaves Newtonian in main but tends to non-Newtonian system as the quasistatic character of the system is much destroyed with increase of the applied force. The plastic behaviour of the solid in general can also be explained on the supposition of some non-equilibrium character in the solidification process from the melt. For the moment, however, we must be satisfied rather with a qualitative results in regard of a poor state of the present theory.

§ 2. Non-Vibrational Thermal Mode of Liquid in Natural State.

According to the proposed molecular model the system has a foam-like structure, each foam corresponding to a discrete crystallite of an uniform size αa. The ground state of the minimum potential energy corresponds to a configuration of such a symmetrical distribution of the intercrystalline boundaries as to minimize the total internal surface area.

When a specified crystallite displaces itself, its surrounding boundaries must be set in motion, deviating from the above symmetrical distribution. The specified crystallite may, in extreme case, even be once annihilated and a new differently oriented crystallite may be generated there at the expense of the neighbouring crystallites. In any process the total internal surface area varies itself cyclically, both the period and the amplitude of the variation being obviously sympathetic with the coarseness of the foam structure. We suppose that the amplitude of the varying surface area is given by $\gamma(\alpha a)^2$. Then the configurational excess energy of a crystallite due to its independent displacement is given by $\gamma\alpha^2\varepsilon_{ol}$, where ε_{ol} is the misfit potential energy per unit lattice area, and the suffix t means its dependence on the degree of orientational order of the system.

The configurational excess energy above considered is yet to be modified a little. since the misfit potential energy per unit area shall also vary cyclically with the location of the boundary. The period of this variation is of the order of the lattice constant and the amplitude of the varying energy depends on the relative orientation of the two crystallites meeting there, which is in much analogy with the dependence of the activation energy for translation of the "dislocation" on its width. An elementary activation energy of order of $\alpha^2\varepsilon'_{ot}$ for a crystallite of size αa, therefore, is to be added to the above value, to obtain the total configurational activation energy

$$\varepsilon_c^* = \gamma\alpha^2\varepsilon_{ot} + \alpha^2\varepsilon'_{ot} = \alpha^2(\gamma+\gamma')\varepsilon_{ot} \tag{1}$$

for an independent displacement of a single crystallite, since the unit energy ε'_{ot} can be expected to be a small fraction γ' of the unit misfit energy ε_{ot}.

As was already remarked in the introduction, however, an independent displacement of a specified crystallite is necessarily accompanied by some localized strain energy. This situation may be represented as in Fig. 1, where an independent displacement AA′ or BB′ of order of $\beta^{1/3}x$ of a crystallite is resulted from the thermal displacement x of its boundary MN, β being the available volume coefficient previously[1,2] defined. The strain energy may accordingly be estimated to be of the order of

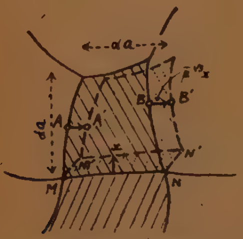

Fig. 1. An independent displacement AA′ or BB′ of a crystallite, resulting from the thermal displacement of its boundary MN.

$$\varepsilon_e^* = \frac{1}{2c}\left(\frac{1}{2}\beta^{1/3}\alpha a/\alpha a\right)^2(\alpha a)^3 = \frac{1}{8c}\alpha^3\beta^{2/3}a^3, \tag{2}$$

where the mean value of local strain and the size of strain field are approximated respectively by $\beta^{1/3}\alpha a/2\alpha a$ and $(\alpha a)^3$, c being the compressibility.

Summing up the configurational excess energy (1) and the elastic strain energy (2),

$$\varepsilon_c^* + \varepsilon_e^* = \alpha^2(\gamma+\gamma')\varepsilon_{ot} + \alpha^3\beta^{2/3}a^3/8c \tag{3}$$

gives the excess energy over the ground state of an excited state for a specified crystallite to be displaced independently of the others.

But the independent displacement of a specified crystallite is not the unique one in the non-vibrational thermal modes of liquid, a well-defined correlated displacement of many crystallites being also conceivable. Now the situation that the excess energy of the system is composed of two components, the configurational energy and the strain energy, may be represented schematically as in Fig. 2.* Fig. 2 (a) represents the ground state, where each constituent crystallite is situated in one of the potential troughs without resulting remarkable strain relative to each other. The excited state for a single crystallite, displaced independently of the others, is depicted in (b). The excited state for three adjacent crystallites, displaced in such a correlation as to uniform the strain energy, is depicted in (c). The excess energy of the last state is of the order of

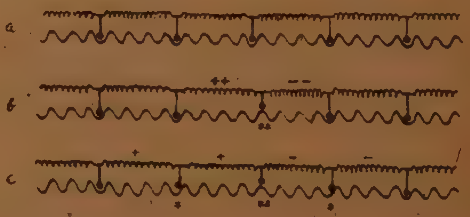

Fig. 2. Schematic representation of the ground state (a), the singly excited state (b), and the triply excited state (c). The elements noted * are excited, and the regions noted ± are strained.

$$2\varepsilon_c^* + \varepsilon_e^*/2, \tag{4}$$

since the mean value of strain is half times and the size of strain field is twice times as great as that of singly excited state. Prosecuting the analogous consideration, we obtain the excess energy of the excited state for the correlated displacement of n adjacent crystallites of the order of

---

* A scheme originating from LENNARD-JONES[4]), who intended to depict somewhat different situation from the present one.

$$n\varepsilon_c^* + \varepsilon_e^*/n\,. \tag{5}$$

The first excited state next to the ground state is that corresponding to a positive integer n most approximate to n^* given by

$$n^* = (\varepsilon_e^*/\varepsilon_c^*)^{1/2}, \tag{6}$$

which minimizes expression (5).

For the estimation of n^*, according to Eqs. (1), (2), and (6), we suppose

$$r + r' \sim 1/2$$

in accord with the viscosity data (see section 3). Putting

$$c \sim 10^{-12}, \quad a^3 \sim 10^{-23}(\text{c.g.s.});$$
$$\varepsilon_{00} = 350k, \quad \bar{\beta}_0 = 10^{-3}, \quad \alpha_0^3 \sim 10$$

for the perfect disordered (liquid) state, we obtain n^* of the order of unity. Thus, the tacit supposition of representing the non-vibrational thermal mode in liquid by the independent displacement of a single crystallite is ascertained, so long as the thermal energy is small compared with the excess energy (1). Such a liquid shall be denoted the "normal liquid" here.

It is to be noted that a system characterized with a much smaller compressibility or an enormously minute misfit energy shows abnormal behaviour, the correlated displacement of many adjacent crystallites being much more probable than the independent displacement of a single crystallite. Such a liquid shall be denoted as the "super liquid" specifically.

§ 3. Viscous Flow of Normal Liquid in Stressed State.

We now proceed on the consideration of the rate of shear strain of normal liquid under external applied force. The quantities α and β take the values corresponding to the perfect disordered state. The excited group of n adjacent crystallites, displacing themselves correlatively with each other, shall be denoted as the "exciton" of order n, or the exciton 'n,' for abbreviation.

At first the existence probability of the respective excited state in natural state is to be estimated. The partial partition function of an exciton 'n' for its translational mode is given by

$$(2\pi m_n^* kT)^{1/2}(\delta/h) \exp\left[-(n\varepsilon_c^* + \varepsilon_e^*/n)/kT\right]$$

where the effective mass m_n^* and the period δ of the cyclical displacement are the appropriate quantities corresponding to this exciton and the energy level of the ground state is taken for the standard of energy. The period of displacement δ of the order of

$$\bar{\beta}_0^{1/3}\alpha_0 a \tag{7}$$

can be estimated, referring to Fig. 1. As the partition function of the ground state is of the order of

$$kT/h\nu\,,$$

the frequency ν being the appropriate quantity corresponding to that state, the relative probability of an exciton 'n' is given by

$$\frac{h\nu}{kT}\,\frac{(2\pi m_n^* kT)^{1/2}\delta}{h}\,e^{-(n\varepsilon_c^* + \varepsilon_e^*/n)/kT}. \tag{8}$$

When there is an applied force F in one direction, the energy gain due to this force per unit displacement process is $n(\alpha_0 a)^2 F\delta$. Here two kinds of the exciton, the positive exciton and the negative exciton, are to be distinguished from each other (see Fig. 3). Since by the presence of the external force the excitation of the positive one is favoured and that of the negative one is unfavoured respectively by a factor

$$\exp\left[\pm n\delta(\alpha_0 a)^2 F/2kT\right]$$

in the case of a symmetrical barrier, the respective existence probability of the exciton is given by

$$\frac{h\nu}{kT}\,\frac{(2\pi m_n^* kT)^{1/2}\delta}{h} \exp\left[-\left\{n\varepsilon_c^* + \frac{\varepsilon_e^*}{n} \mp \frac{n}{2}\delta(\alpha_0 a)^2 F\right\}\Big/ kT\right]. \tag{9}$$

Denoting the average velocity of the exciton 'n' with $\bar{c}_n$, the relative velocity between two layers of mean separation of the order of the crystallite size, $\alpha_0 a$, is

$$u_n = \bar{c}_n \frac{h\nu}{kT}\,\frac{(2\pi m_n^* kT)^{1/2}\delta}{h} \cdot e^{-(n\varepsilon_c^* + \varepsilon_e^*/n)/kT}\, 2\sinh\frac{n\delta(\alpha_0 a)^2 F}{2kT}, \tag{10}$$

and the rate of shear strain, consequently, is

$$D_n = u_n/(\alpha_o a)\,. \tag{11}$$

An estimation in general of the average velocity $\bar{c}_n$ of the exciton is much complicated to be made here. If we suppose, however, that the exciton gives up its energy gain fed by the external force to the neighbouring crystallites in the form of the thermal elastic wave as soon as it proceeds one period of displacement, we can approximate $\bar{c}_n$ with its quasistatic mean value

$$\int_0^\infty \exp\left(-\frac{m_n^*\dot{x}^2}{2kT}\right)\dot{x}d\dot{x} \Big/ \int_0^\infty \exp\left(-\frac{m_n^*\dot{x}^2}{2kT}\right)d\dot{x} = \left(\frac{kT}{2\pi m_n^*}\right)^{1/2}. \tag{12}$$

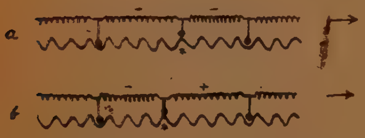

Fig. 3. Schematic representation of the positive exciton (a) and the negative exciton (b), both of order 1.

Substituting Eq. (10), with δ and $\bar{c}_n$ given by Eqs. (7) and (12), into Eq, (11), we obtain

$$D_n = 2\beta_o^{1/3}\nu \exp\left[-\frac{n\varepsilon_c^* + \varepsilon_e^*/n}{kT}\right] \sinh\frac{n\beta_o^{1/3}(\alpha_o a)^3 F}{2kT} \tag{13}$$

for the partial rate of shear strain due to the exciton 'n.'

The total rate of shear strain D, then, is given by summing up the quantities D_n over the conceivable order of the exciton, n, that is

$$D = \sum_n D_n = 2\beta_o^{1/3}\nu \sum_n \exp\left[-\frac{n\varepsilon_c^* + \varepsilon_e^*/n}{kT}\right] \sinh\frac{n\beta_o^{1/3}(\alpha_o a)^3 F}{2kT} \tag{14}$$

This general formula (14) can be written substantially as

$$D = \beta_o^{2/3}(\alpha_o a)^3 \frac{\nu}{kT} \exp\left[-\frac{\varepsilon_c^* + \varepsilon_e^*}{kT}\right] F\,, \tag{15}$$

so long as the condition

$$\varepsilon_c^* - \beta_o^{1/3}(\alpha_o a)^3 F \gg kT \gg \beta_o^{1/3}(\alpha_o a)^3 F \tag{16}$$

is provided, as will be evidenced by the observation of flow for normal liquid under sufficiently weak applied force.

Equation (15) represents a proportional relation between the rate of shear strain and the applied force, that is the Newtonian behaviour of the normal liquid under sufficiently weak external force. The coefficient of viscosity η is

$$\eta = \frac{kT}{\beta_o^{2/3}(\alpha_o a)^3\nu} \exp\left[\frac{\varepsilon_c^* + \varepsilon_e^*}{kT}\right], \tag{17}$$

an expression similar to that usually given for the viscosity of liquid.

The expression (17) on the present theory, however, has a peculiarity different from the usual ones, since the crystallite size α_o in equilibrium state is, as was already shown previously,[1] a function of the temperature. Yet the percentage variation of α_o is neglegibly small compared with that of $1/T$ at ordinary temperature range with the exception of the range near the critical point, where a larger increase of η than usual can be expected owing to a marked increase of α_o thereby. The estimated value of the activation energy $(\varepsilon_c^* + \varepsilon_e^*)$ is a few kcal. per mole, in the same order as the experimental value, but that of the frequency factor $kT/\{\beta_o^{2/3}(\alpha_o a)^3\nu\}$ is of the order of 10^{-2}, too larger than the observed value.

The establishment of the linear relation (15) between the rate of shear strain and the applied force is founded on the supposition of conservation of the quasistatic equilibrium of the system under external applied force. But it is restrained, as is evident in its derivation process, by at least two factors; the approximation of $\bar{c}_n$ by its equilibrium value (12), and the satisfaction of the condition (16). In respect to the latter, it may be noted that the relative probability of the positive exciton of increasing order is progressively enhanced with an increase of the applied force. Whereas the correlated displacement of many adjacent crystallites has been utterly left out of our consideration of normal liquid in natural state, it is indispensable to take into account such a correlated displacement of many crystallites, in order to characterize in strict the dynamical properties of liquid under sufficiently large external force. In any case, it can be expected that the liquid under sufficiently large external force shall behave rather non-Newtonian, an unneglegible magnitude of the correlated displacements of many adjacent crystallites being superposed upon the independent displacement of the single crystallite.

In concluding this section it is noted at the moment that such a super-liquid as defined in the preceding section imposes us an expectation of a superfluidity under external applied force, because the applied force is effective with a magnification factor n for activation of the exciton of large order n, which is the predominant non-vibrational thermal mode in the case of the super-liquid.

§ 4. Non-Vibrational Thermal Mode and Plastic Flow of Solid.

In the case of solid the quantities α, β and ε_{0l} take the values appropriate to the ordered state. The orientational order of the solid is, according to the previous consideration,[2] of the order of

$$t \simeq 1-\exp[-\alpha_1{}^2K_1/8kT], \tag{18}$$

nearly equal to unity owing to the large value of the crystallite size α_1. Therefore, we may characterize the solid state by $t=1$, as was the case there, and we obtain the relations

$$\varepsilon_{01} = K_1(s_1+s_2+s_3) \tag{19}$$

and

$$\beta_1 = s_1 s_2 s_3\,, \tag{20}$$

referring to Eqs. (14) and (15) there.

These are yet to be averaged, for the purpose of a use in the present representations, over the possible orientations of the crystallite with the appropriate weight factor $\exp[-\alpha_1{}^2\varepsilon_{01}/kT]$, that is

$$\bar{\beta}_1 = \int e^{-\alpha_1{}^2\varepsilon_{01}/kT} s_1 s_2 s_3\, d\omega \Big/ \int e^{-\alpha_1{}^2\varepsilon_{01}/kT} d\omega\,, \tag{21}$$

$$\bar{s}_1 = \bar{s}_2 = \bar{s}_3 \simeq (s_1 s_2 s_3)^{1/3} = \bar{\beta}_1{}^{1/3}. \tag{22}$$

The integrals in Eq. (21), when executed by the same conventional method as before, gives

$$\bar{\beta}_1 = [\{I_o(x)-I_1(x)\}/\{8I_o(x)\}]^3\,, \quad x = \alpha_1{}^2K_1/8kT\,. \tag{23}$$

Expanding the modified Bessel functions asymptotically, Eq. (23) is transformed approximately to

$$\bar{\beta}_1 \simeq (kT/2\alpha_1{}^2K_1)^3 \tag{24}$$

and it follows, according to Eq. (22),

$$\bar{s}_1 = \bar{s}_2 = \bar{s}_3 \simeq kT/2\alpha_1{}^2K_1\,. \tag{25}$$

In regard of the Eqs. (1), (2), (19), (24), and (25), we obtain

$$\varepsilon_c{}^* \simeq (3/2)(\gamma+\gamma')kT\,, \tag{26}$$

$$\varepsilon_e{}^* \simeq (a^3/8c\alpha_1)(kT/K_1)^2\,. \tag{27}$$

Eq. (6) then becomes

$$n^* = \left[\left(\frac{kT}{K_1}\frac{a^3}{cK_1}\right) \Big/ \left\{12(\gamma+\gamma')\alpha_1\right\}\right]^{1/2} \sim \alpha_1{}^{-1/2}; \tag{28}$$

where the last term is the estimated value assuming appropriate values as in section 2. Since the equilibrium size α_1 of the crystallite is very great in the ordered state, the first excited state corresponds to the exiton $n=1$, the positive integer most approximate to n^*. This is the affirmation of the previous tacit supposition of representing the non-vibrational thermal mode in solid by an independeut displacement of a single crystallite.

Next, the general relation between the rate of shear strain and the applied force is formally the same with Eq. (14) for liquid and so is given by

$$D = 2\bar{\beta}_1{}^{1/3}\nu\sum_n \exp\left[-\frac{n\varepsilon_c{}^*+\varepsilon_e{}^*/n}{kT}\right] \cdot\sinh\frac{n\bar{\beta}_1{}^{1/3}(\alpha_1 a)^3F}{2kT}\,, \tag{29}$$

where the energies $\varepsilon_a{}^*$ and $\varepsilon_e{}^*$ are given by Eqs. (26) and (27). Then it is transformed to

$$D = \frac{\nu kT}{\alpha_1{}^2K_1}\sum_n \exp\left[-\frac{3}{2}n(\gamma+\gamma')\left\{1+\left(\frac{n^*}{n}\right)^2\right\}\right] \cdot\sinh\frac{n\alpha_1 a^3F}{4K_1}\,, \tag{30}$$

which is essentially equivalent to

$$D \simeq \frac{\nu kT}{\alpha_1{}^2K_1}\sum_n \left[\exp\left\{-\frac{3}{2}(\gamma+\gamma')+\frac{\alpha_1 a^3F}{4K_1}\right\}\right]^n \tag{31}$$

in regard of the large value of $\alpha_1 a^3F/4K_1$ in the case of the stressed solid.

When the argument of the exponential function in (31) is positive, the correlated displacement of increasing number of adjacent crystallites is to be realized predominantly. Whereas the Eqs. (26) and (27) are derived on the supposition of an independent displacement of the constituent crystallites, the result is concluded inconsistent with its presumption. This fact means an inadequacy of the present procedure for the treatment of a flow of solid.

In the deliberation as above, however, it is supposed that the system is always in the thermodynamical equilibrium state. It is to be recognized here that the real solid can not be expected to be in equilibrium unconditionally. The deviation of the real solid from the ideal state of perfect crystal is known as being especially sensitive to the mechanical as well as the thermal experience of the system, as is evidenced in the phenomena such as the strain hardening and the resoftening of the material. The fact that the lattice defects in the solid in general are predetermined by its history shows the difficulty of attainment of the thermodynamical equilibrium state for solid.

Founded on these brief deliberations, it may well be reasonable, or rather true, for the real solid to suppose

$$t = 1-\varepsilon \tag{32}$$

instead of Eq. (18). ε is an *a priori* constant characterizing the degree of deviation of a specified solid from the true equilibrium state. It may be essentially predetermined, we suppose, by the situations at solidification. Eq. (19) is modified accordingly to

$$\varepsilon_{0,1-\varepsilon} = (3/8)\varepsilon K_1 + K_1(s_1+s_2+s_3)\,, \tag{33}$$

but the weighted averages $\bar{\beta}_1$, $\bar{s}_1$, *etc.*; are yet unaltered.

Then the general relation (31) between the rate of shear strain and the applied force has the form

$$D = A\sum_n \exp(-nB)\sinh(nCF)$$
$$\simeq \frac{A}{2}\left\{\frac{1}{1-\exp(-B+CF)} - \frac{1}{1-\exp(-B-CF)}\right\}, \tag{34}$$

where

$$A = \frac{\nu kT}{\alpha_1{}^2 K_1}\,,\quad B = \frac{3}{8}\alpha_1{}^2(\gamma+\gamma')\varepsilon\frac{K_1}{kT}\,,\quad C = \frac{\alpha_1 a^3}{4K_1}\,, \tag{35}$$

and the smaller term independent of α_1 is omitted.

Since the argument B is positive and larger than CF in the most range of the applied force (see below), D can substantially be represented by the first term without marked loss in rigour as follows;

$$D = A\exp(-B)\sinh(CF)$$
$$= (A/2)\{\exp(-B+CF) - \exp(-B-CF)\}\,. \tag{36}$$

The factors other than 'sinh' in Eq. (36) is extraordinarily small and so we require an application of much larger external force to effect an observable rate of shear strain. The final relation (36), therefore, can not be simplified anymore. The solid in stressed state shows thus a non-Newtonian, but plastic characters throughout the most range of the applied force.

The steady-state creep rate in several metals generally appears to obey the law

$$\text{Rate} = A\exp(-\varepsilon_0/kT)\,,$$

where the activation energy ε_0 is of order of an electron volt[7]. Supposing $\varepsilon_0 = 0.75$ ev, we obtain

$$B = 28 \tag{37}$$

at room temperature. The plastic behaviour according to Eq. (36) is strongly dependent on the crystallite size α_1. Some results, calculated on the supposition of several values of order 10^{-4} cm for $\alpha_1 a$, are given in Table I and II, which are shown graphically in Fig. 4 by weak applied force.

Table I. Th evalues of the crystallite size $\alpha_1 a$ and the constants A, C and ε in Eq. (36), calculated according to Eqs. (35) and (37).

	I	II	III
$\alpha_1 a$ (cm)	5.52×10^{-5}	1.66×10^{-4}	3.32×10^{-4}
ε	1.64×10^{-5}	1.82×10^{-6}	$4.55\times10^{-}$
A	9.83×10^{3}	1.09×10^{3}	2.72×10^{2}
C	1×10^{-7}	3×10^{-7}	6×10^{-7}

Table II. Relation between the rate of shear strain and the applied force, calculated according to Eq. (36).

$F\times10^{-7}$ (dyn/cm^2)	D ($cm/cm\cdot sec$)		
	I	II	III
0.4	2.78×10^{-9}	1.14×10^{-9}	1.03×10^{-9}
0.8	6.12×10^{-9}	4.13×10^{-9}	1.14×10^{-8}
1.2	1.02×10^{-8}	1.38×10^{-8}	1.26×10^{-7}
1.6	1.61×10^{-8}	4.58×10^{-8}	1.39×10^{-6}
2.0	2.47×10^{-8}	1.52×10^{-7}	1.54×10^{-5}
2.4	3.71×10^{-8}	5.05×10^{-7}	1.69×10^{-4}
2.8	5.57×10^{-8}	1.68×10^{-6}	1.86×10^{-3}
3.2	8.32×10^{-8}	5.56×10^{-6}	2.05×10^{-2}

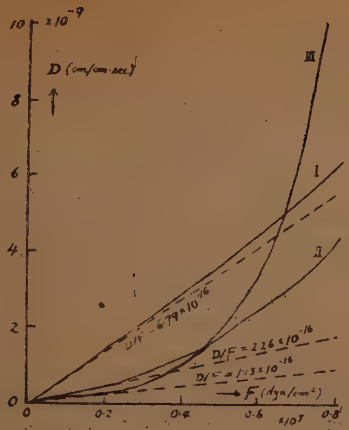

Fig. 4. Relation between the rate of shear strain D of solid and the applied force F, calculated according to Eq. (36). The notations I, II, and III are the same as in Tab. I.

The approximate expression (36) is known to be sufficient to represent the rigorous expression (34), in the range of the applied force as taken above. With further increase of the applied force, however, it can not be justified anymore. The rate of shear strain is expected, according to Eq. (34), to increase much more drastically thereby, because the correlated displacement of the adjacent crystallites can be neglected no more.

It is to be noted for the last that the excitons have been supposed to be independent of each other by the derivation of Eq. (34). The interaction between the excitons, however, should not be neglegible with the increasing population of the excitons, the overlapping of the strain fields as well as the co-possession of the intercrystalline boundaries for neighbouring excitons being the conceivable mechanism of such an interaction. In regard of the experimental facts concerning the slip band, the strain hardening, and the resoftening, *e.g.*, these interactions should be taken into account specifically.

More extended deliberations on these hyper-interactions and the non-equilibrium character represented by ε shall be postponed to the succeeding report.

In conclusion the author wishes to express his sincere thanks to Dr. S. Oka and Dr. S. Miyake for their hearty encouragement and useful discussions. He is also obliged to the National Research Council, for the expenditure of which this study is executed.

References.

(1) A. Ookawa, J. Phys. Soc. Japan **2** (1947), 108.
(2) A. Ookawa, J. Phys. Soc. Japan **3** (1948), 295.
(3) L. Brillouin, J. phys. rad. **7** (1936), 153.
(4) J. E. Lennard-Jones, Proc. Phys. Soc. **52** (1940), 44.
(5) W. Boas, E. Schmid, Zeits. Phys. **100** (1936), 463.

La Théorie du Champ Unitaire et la Théorie Quantique.

Par Giiti Iwata.

Institut de Physique, Université Tokyo.

(Reçu 11 Mai, 1948).

De la théorie du champ unitaire, telle que je comprends, combinée avec la théorie quantique, je déduirai les deux conclusions suivantes,

1) La masse d'une particule se diminue quand elle est chargée de l'électricité.

2) La charge électrique a l'unité.

La première est convenable à exprimer la différence entre la masse du neutron et celle du proton.

La seconde exprimerait l'existence du quantum électrique.

Pour déduire ces deux conclusions, on part de

l'explication courte de la théorie du champ unitaire.(1)

On ajoute la nouvelle variable x^0 aux anciennes variables x^1, x^2, x^3, x^4 pour qu'on obtienne la transformation de jauge

$$x^{0\prime} = x^0 + f(x^1, x^2, x^3, x^4)$$

outre que les transformations de coordonnées

$$x^{r\prime} = f^r(x^1, x^2, x^3, x^4), \quad r = 1, 2, 3, 4.$$

Ces transformations à cinq dimensions sont la base de la théorie du champ unitaire.

Nous supposons que tous les tenseurs ne contiennent la variable x^0 que sous la forme de $\exp(\lambda x^0)$, où la constante λ est nommée l'indice projectif du tenseur. Un tenseur dont l'indice est λ, se multiplie par un facteur $\exp(-\lambda f)$ pour la transformation précédente de jauge, qu'on peut écrire sous les formes différentielles

$$\begin{aligned} dx^{0\prime} &= \frac{\partial x^{0\prime}}{\partial x^\rho} dx^\rho = dx^0 + \frac{\partial f}{\partial x^r} dx^r \\ dx^{r\prime} &= dx^r \\ \rho &= 0, 1, 2, 3, 4; \quad r = 1, 2, 3, 4. \end{aligned}$$

Ainsi un vecteur contrevariant A^ρ de l'indice 0 se transforme suivant les lois

$$A^{0\prime} = A^0 + \frac{\partial f}{\partial x^r} A^r, \quad A^{r\prime} = A^r$$

et un vecteur covariant φ_ρ de l'indice 0 se transforme suivant

$$\varphi_0' = \varphi_0, \quad \varphi_r' = \varphi_r - \varphi_0 \frac{\partial f}{\partial x^r}.$$

Pour les transformations de coordonnées, ils se transforment suivant

$$A^{0\prime} = A^0, \quad A^{r\prime} = \frac{\partial x^{r\prime}}{\partial x^s} A^s$$

$$\varphi_0' = \varphi_0, \quad \varphi_r' = \frac{\partial x^s}{\partial x^{r\prime}} \varphi_s.$$

c'est que A^0 et φ_0 sont invariants, A^r et φ_r passent pour des vecteurs de l'espace à quatre dimensions.

Si l'on regarde la transformation d'un tenseur covariant symétrique $\gamma_{\rho\sigma}$ de second ordre, dont l'indice est nul, les $\gamma_{\rho 0}$ ne sont que les composantes d'un vecteur covariant. On peut donc poser que

$$\gamma_{00} = 1, \quad \gamma_{\rho 0} = \varphi_\rho,$$

De ce tenseur $\gamma_{\rho\sigma}$ on constitue un tenseur covariant symétrique

$$\gamma_{\rho\sigma} - \varphi_\rho \varphi_\sigma = g_{\rho\sigma}$$

dont les composantes contenantes l'indice 0 n'existent pas. Les g_{rs} sont invariantes pour la transformation de jauge, et se transforment pour les transformations de coordonées suivant les mêmes lois que les composantes d'un tenseur de l'espace à quatre dimensions.

L'on peut donc considérer les φ_r comme les composantes des potentiels électromagnétiques, g_{rs} comme celles des potentiels de la gravitation. En définissant la métrique de l'espace à cinq dimensions par l'équation

$$d\sigma^2 = \gamma_{\rho\sigma} dx^\rho dx^\sigma$$

on peut établir la théorie du champ unitaire. Les composantes covariantes

$$\gamma_{\rho\sigma} = \begin{bmatrix} 1 & \varphi_s \\ \varphi_r & \varphi_r \varphi_s + g_{rs} \end{bmatrix}$$

donnent les composantes contrevariantes

$$\gamma^{\rho\sigma} = \begin{bmatrix} 1 + g^{ij}\varphi_i\varphi_j & -g^{si}\varphi_i \\ -g^{rj}\varphi_j & g^{rs} \end{bmatrix}.$$

Si l'on définit les moments d'une particule de la masse m par l'équation

$$p_\rho = m \gamma_{\rho\sigma} \frac{dx^\sigma}{d\sigma},$$

on a

$$\gamma^{\rho\sigma} p_\rho p_\sigma = m^2.$$

De la même manière que dans la théorie de la relativité générale, on définit que la passe d'une particule soit la géodésique caractérisée par le principe de variation

$$\delta \int m \, d\sigma = 0$$

Après un calcul fort court, on en déduit que

$$\frac{dp_0}{d\sigma} = 0.$$

C'est que la première composante p_0 des moments d'une particule est constante le long de la passe. Le principe de variation donne les équations de mouvement d'un particule chargée électriquement

$$\frac{d^2 x^r}{d\sigma^2} + \Gamma^r_{uv} \frac{dx^u}{d\sigma} \frac{dx^v}{d\sigma} + \frac{p_0}{m} \varphi^r{}_s \frac{dx^s}{d\sigma} = 0$$

où

$$\Gamma^r_{uv} = \frac{1}{2}g^{rs}\left(\frac{\partial g_{us}}{\partial x^v}+\frac{\partial g_{vs}}{\partial x^u}-\frac{\partial g_{uv}}{\partial x^s}\right)$$

$$\varphi^r{}_s = g^{ru}\varphi_{us}, \quad \varphi_{us} = \frac{\partial \varphi_u}{\partial x^s}-\frac{\partial \varphi_s}{\partial x^u}.$$

Il me semble que ces équations nous permettent d'identifier p_0 pour la charge électrique de cette particule. Mais la distance infinitésimale $d\sigma$ n'est égale à la distance infinitésimale ds de l'espace à quatre dimensions, définie par

$$ds' = g_{rs}dx^r dx^s$$

et on doit écrire les équations de mouvement d'une particule chargée en usant ds. Donc on récrit les équations de la passe sous la forme suivante

$$\frac{d^2x^r}{ds^2}+\Gamma^r_{uv}\frac{dx^u}{ds}\frac{dx^v}{ds}+\frac{p_0}{m}\frac{d\sigma}{ds}\varphi^r{}_s\frac{dx^s}{ds} = 0$$

D'autre part, dans la théorie de la relativité générale on a les équations de la passe (m_e étant la masse d'une particule chargée)

$$\frac{d^2x^r}{ds^2}+\Gamma^r_{uv}\frac{dx^u}{ds}\frac{dx^v}{ds}+\frac{e}{m_e}\varphi^r{}_s\frac{dx^s}{ds} = 0.$$

En comparant des deux équations on peut conclure aux deux manières

$$1)\quad p_0\frac{d\sigma}{ds} = e, \quad m = m_e$$

$$2)\quad p_0 = e \quad m_e = m\frac{ds}{d\sigma}$$

On se souvient ici que

$$d\sigma^2 = \gamma_{\rho\sigma}dx^\rho dx^\sigma = (\varphi_\rho dx^\rho)^2+g_{rs}dx^r dx^s$$

$$= \left(\frac{p_0}{m}d\sigma\right)^2+ds^2$$

d'où

$$\frac{ds}{d\sigma} = \sqrt{1-\left(\frac{p_0}{m}\right)^2}.$$

En outre, l'équation

$$m^2 = \gamma^{\rho\sigma}p_\rho p_\sigma$$

s'écrit à la forme suivante

$$= p_0{}^2+g^{rs}(p_r-p_0\varphi_r)(p_s-p_0\varphi_s).$$

Le second membre de cette expression est très semblable à l'expression du carré de la masse m_e d'une particule chargée. Cette expression s'écrit

$$m_e{}^2 = g^{rs}(p_r-e\varphi_r)(p_s-e\varphi_s).$$

Si l'on prend la deuxième hypothèse que la première composante des moments soit la charge électrique, on peut alors écrire

$$m^2 = m_e{}^2+p_0{}^2,$$

$$\frac{m_e}{m} = \sqrt{1-\left(\frac{p_0}{m}\right)^2} = \frac{ds}{d\sigma}.$$

On en déduit que la masse d'une particule chargée diminue selon la relation écrite au dessus.

La charge électrique se mesure en unité de la masse. En supposant que le proton soit le neutron chargé, on peut calculer la quantité de la charge électrique du proton par les valeurs des masses de ces particules. La valeur ainsi calculée de e serait environ un vingtième de la masse du proton.

Si cette relation s'applique aux cas familiers, l'électron déchargé de l'électricité, en cas qu'il existe, aurait environ une vingtième masse du proton, et la masse du méson chargé serait plus petite que celle du méson neutral.

Pour qu'on arrive à la deuxième conclusion, on doit combiner la théorie quantique à la théorie du champ unitaire.

Nous supposons que l'indice projectif λ de la fonction d'onde Ψ ne soit pas nul. De la même manière que dans la théorie quantique, on remplace les moments p_ρ par les opérateurs

$$p_\rho = \frac{h}{i}\nabla_\rho \quad 2\pi h = \text{constante de Planck}$$

où les ∇_ρ désignent les dérivations covariantes de l'espace à cinq dimensions. Puisque la valeur propre de p_0 est e, on a

$$p_0\Psi = e\Psi,$$

d'autre part,

$$p_0\Psi = \frac{h}{i}\nabla_0\Psi = \frac{\lambda h}{i}\Psi,$$

on a donc

$$e = \frac{\lambda h}{i}, \quad \lambda = \frac{ie}{h}.$$

Et puis, pour la transformation de jauge la fonction d'onde se multiplie par un facteur $\exp(-ief/h)$, dont le module est 1. Cette transformation de jauge s'appelle la transformation de la première espèce. L'introduction de la variable x^0 éclaircit la liaison de cette transformation avec celles des potentiels électromagnétiques.

On emprunte ici une hypothèse à MM. Einstein-Bergmann.(2) Selon cette hypothèse l'univers est périodique par rapport à la variable x^0. En désignant la longueur de la période par l, on arrive à la relation suivante

$$\exp(iel/h) = 1.$$

pour qu'on ait la fonction d'onde univalente. On en déduit que

$$el/h = 2\pi n, \quad n : \text{entier},$$

d'où

$$e = 2\pi nh/l.$$

En résumé, la valeur de la charge électrique n'est qu'un des multiples de $2\pi h/l$.

Si l'on emploie la valeur e du proton calculée au dessus, la valeur de la longueur de la période l serait environ 10^{-12} cm. Mais la variable x^0 n'est pas observée jusqu'à présent. L'existence en est très doutée par les physiciens. Parce que cette variable est conjuguée à la charge électrique, qu'on observe celle-ci tous les cas, et que la valeur de l est très petite, cette variable n'apparaîtra à jamais avec raison aux yeux de l'homme. Cependant je crois qu'elle existe.

Références.

(1) O. Veblen: Projektive Relativitaetstheorie (1933)

(2) A. Einstein and P. Bergman: Annals of Math., **36** (1938) 683.

On Thermal Hysteresis in Irreversible Iron-Nickel Alloys.

By Yosiaki TINO.

The Institute of Physical and Chemical Research, Tokyo.

(Read April 11, 1948; Received June 3, 1948)

§ 1. Introduction.

When pure iron is heated through A_3-point and then cooled with an ordinary velocity, it is observed that the temperature of the $\alpha \rightarrow \gamma$ transformation is not the same with that of the $\gamma \rightarrow \alpha$ transformation, the latter being considerably lower than the former. This thermal hysteresis in pure iron becomes smaller and smaller till the $\alpha \rightleftarrows \gamma$ transformations occur at almost the same temperatures, as the velocity of heating and cooling decreases. It is also true that alloys containing small quantities of nickel behave similarly to pure iron, but with further increasing content of nickel, the hysteresis becomes larger and larger, which cannot be prevented even with an extremely slow velocity. In this respect the hysteresis(1) in Fe-Ni alloys is different from that in pure iron, and is a characteristic feature of the alloys, which has long made it very difficult to establish the phase diagram of the system.

The cause of such hysteresis, in which this paper will be concerned, is explained as follows:

1. According to many experimental results, the location of the phase boundaries in the diagram is considered to be as shown in Fig. 1. It is here assumed that the boundaries of region $(\alpha+\gamma)$ in the figure are displaced upwards on heating and

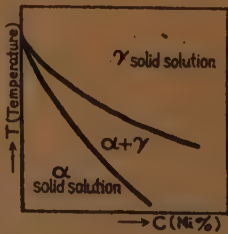

Fig. 1.

downwards on cooling; accordingly the equilibrium position of the region $(\alpha+\gamma)$ is extremely difficult to obtain. For example, the phase diagram proposed by E. Scheil(2) is drawn only for alloys with small nickel content, and that by P.D. Merica(3) is only of use for practical purposes.

2. There is another idea held by Dr. Takeuti(4), by which the hysteresis is ascribed to the fact that the lattice alone is transformed without any change of concentration on cooling or heating, and that such lattice transformation occurs only at the time when they are superheated or supercooled beyond the region $(\alpha+\gamma)$. Consequently the alloys, which are heated or cooled into the region $(\alpha+\gamma)$, remain in the supersaturated state α or γ, as the change of concentration by diffusion is difficult to proceed effectively during heating or cooling; so beyond the region $(\alpha+\gamma)$ the lattice transformation $\alpha\rightarrow\gamma$ or $\gamma\rightarrow\alpha$ takes place.

Now comparing the above two ideas, the latter seems very plausible and especially according to it, the phase diagram can be easily established by the measurement of temperatures of lattice transformations; hence the present writer will adopt the latter standpoint so far as the phase diagram is concerned, and then the following question arises: If the alloys are held at various temperatures for long periods of time instead of being heated or cooled with a velocity, the transformation with the change of concentration $\alpha\rightarrow\alpha+\gamma$ or $\gamma\rightarrow\alpha+\gamma$ will progress within the region $(\alpha+\gamma)$, which should result in disappearance of the hysteresis; but this is true only for alloys with small nickel content as first described. Thus the cause of the remarkable hysteresis is not yet explained satisfactorily.

§ 2. Experimental Results (a)

In the present investigation, the nature of A_3-transformation in Fe-Ni alloys was examined chiefly by means of magnetic measurement for six kinds of alloys containing from 5 to 30% Ni in the following manner.

The specimen in the form of a bar was placed in a silica tube, round which a platinum wire was wound anti-inductively. The temperature was measured by a thermo-couple consisting of platinum and platinum-rhodium wires which were placed in the silica tube furnace. In order to protect the specimen from oxidation at high temperature, the silica tube furnace was connected to a vacuum pump, and the furnace was inserted in a magnetizing coil provided with a water-jacket, inside which a constant magnetic field H_{ex} = 190 Oersteds was given.

By the use of such arrangements, magnetization at various constant temperatures was measured as a function of time. The results obtained are described below, and for convenience alloys with lower nickel content are first explained in this section.

The cases of 5, 10 and 15% Ni alloys are shown in Figs. 2-4; the thick line of the figures represents the hysteresis loop. As to reaction rates for isothermic transformations, some examples are given in the figures.

By cooling after each isothermic transformation in heating process, a group of curves as shown in these figures is obtained. The forms of these curves tell us that two-phase-transformation with the change of concentration $\alpha\rightarrow\alpha+\gamma$ proceeded at each constant temperature, and that the

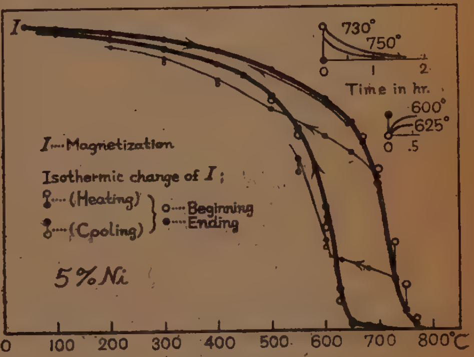

Fig. 2.

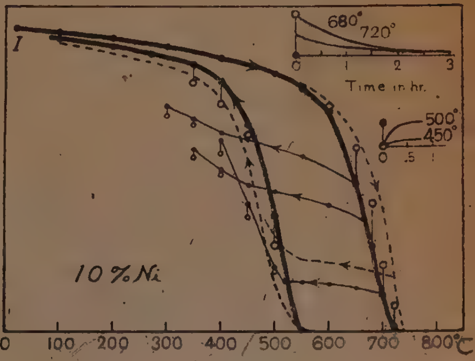

Fig. 3.

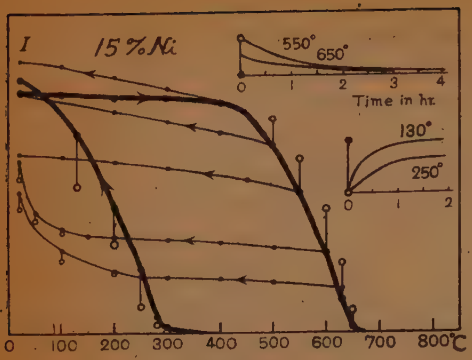

Fig. 4.

precipitated γ phase could be supercooled up to the lattice transformation point characteristic of the new concentration. Thus the region $(\alpha+\gamma)$ of the phase diagram is known to exist between the beginning and the end point of such transformation in heating process.

On cooling the γ solid solution, no matter how long it may be maintained at any temperature in the region $(\alpha+\gamma)$, the transformation $\gamma\rightarrow\alpha+\gamma$ is extremely difficult to proceed, except alloys of low nickel content. (5% Ni alloy is usually considered to belong to the exceptional group.) When, however, the γ solid solution is cooled beyond the region $(\alpha+\gamma)$, the lattice transformation $\gamma\rightarrow\alpha$ begins to occur and continues to do so with falling temperature. This seems apparently two-phase-transformation with the change of concentration $\gamma\rightarrow\alpha+\gamma$ occurring as in the heating stage, but this is not the case. The qualitative difference between the transformation on heating and that on cooling may be also seen in different rates of reactions for both kinds of transformations shown in Figs. 2-4.

The hysteresis obtained in the above manner is compared with that obtained by heating and cooling with an ordinary velocity (10°/1∼2 min.) in Fig. 3 (10% Ni alloy), where the latter hysteresis is drawn in broken lines. It is noted that the transformation $\gamma\rightarrow\alpha$ on cooling begins at identical temperatures in both cases.

In 15% Ni alloy, on abnormal increase of magnetization is seen in Fig. 4 when the specimen is cooled from 400°; but this abnormality cannot be seen when the experiment is done by a dilatometric measurement, so that it seems to be a magnetic event having no connection to phase changes. The same abnormality is seen in alloys of higher nickel content.

The most important result in this section is that, the transformation $\gamma\rightarrow\alpha+\gamma$ on cooling is extremely difficult to proceed in the region $(\alpha+\gamma)$, while the transformation $\alpha\rightarrow\alpha+\gamma$ on heating proceeds easily in the same region.

§ 3. Consideration of the Cause of Hysteresis.

According to the principles of thermodynamics, the free energy of coexistent state of α and γ phases is represented by a common tangent as shown in Fig. 5, and the points of tangency give concentrations of the equilibrium mixture $(\alpha+\gamma)$, that is, C_1 and C_2 in the figure, which being plotted against various temperatures, the region $(\alpha+\gamma)$ of the phase diagram is obtained. And so it is sufficient to consider such common tangents in order to construct the diagram; it is not necessary to refer to the complete forms of the α and γ curves. For example, which of γ, γ' and γ'' curves in Fig. 5 is the form of the γ curve, is out of the question so far as a common tangent is fixed. As a matter of fact, however, the α and γ curves must have certain forms.

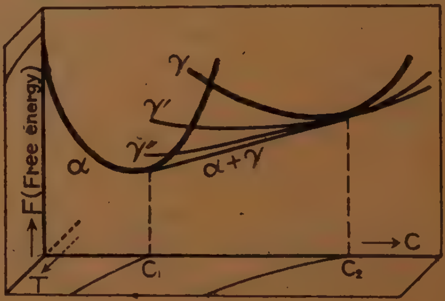

Fig. 5.

The present writer assumes that the slope of the γ curve against the common tangent is in general much smaller than that of the α curve in the region $(\alpha+\gamma)$, such as γ'' curve shown in Fig. 5; so the common tangent is situated much nearer to the γ curve than to the α curve. Consequently in the space composed of F(free energy), T(temperature) and C(concentration), the γ surface should come so near to the surface representing the coexistent state $(\alpha+\gamma)$. Then in a section of the FTC-space by a plane C = constant, the $(\alpha+\gamma)$ curve is still situated so near to the γ curve, as shown in Fig. 6.

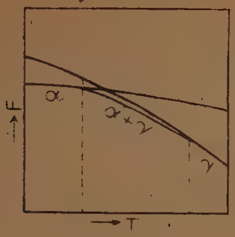

Fig. 6.

This figure tells us that the transformation $\gamma \rightarrow \alpha+\gamma$ on cooling is extremely difficult to proceed, because the decrease in free energy (volume energy) accompanying the transformation, that is, the distance ΔF between the γ and $(\alpha+\gamma)$ curve is so small that it is overcome by the increase of surface energy during nuclear formation (cf. R. Becker's theory(5).) Thus the writer's assumption is inclusive of the experimental fact in the previous section, or conversely the experimental fact is abstracted into the assumption.

Now the hysteresis, as first described, becomes more marked with further increasing content of nickel, which can be realized from the writer's standpoint as follows:

The change of free energy ΔF accompanying the transformation $\gamma \rightarrow \alpha+\gamma$ becomes gradually smaller as the content of nickel in iron increases, in other words, the distance ΔF between the γ and $(\alpha+\gamma)$ curve shown in Fig. 6 is not yet so small in the concentration range below 5% Ni, but it becomes very small in the neighbourhood of 10% Ni and more, which is to result in the remarkable hysteresis.

As the concentration of nickel increases furthermore, the distance ΔF becomes still smaller. However there must be a certain limit of the smallness, beyond which the quantity ΔF can no more decrease. At this very stage of ΔF, the distinction between the γ and $(\alpha+\gamma)$ surface comes to lose its physical meaning, that is, the $(\alpha+\gamma)$ surface melts into the γ surface. Then there should be a critical concentration C_k, above which the stable γ phase only can exist.

Thus it has been found that a limiting line must be drawn at the concentration C_k in the phase diagram (Fig. 7). Consequently any alloy, the temperature and concentration of which is

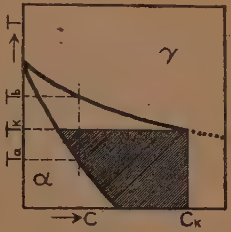

Fig. 7.

situated within the shaded region in the figure, cannot be in the state of two-phase-equilibrium, because the concentration of γ phase of equilibrium mixture $(\alpha+\gamma)$ becomes indefinite in this case.

Now we come to consider the hysteresis in these special alloys, a section of the FTC-space by a plane $C' =$ constant (higher nickel content) being shown in Fig. 8, where × signs on the curve $(\alpha+\gamma)$ represent

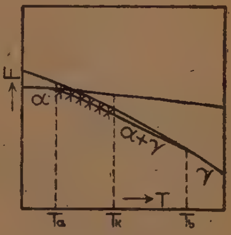

Fig. 8.

the section of the shaded region. It is seen here that the α solid solution, which is heated beyond the temperature T_a, cannot transform to the most stable state $(\alpha+\gamma)$ till it is heated beyond the temperature T_k in the figure. (Considering from the figure, therefore, the lattice transformation $\alpha \rightarrow \gamma$ seems to proceed between these two temperatures; but this is not the case, because such transformation cannot occur within the region $(\alpha+\gamma)$ according to Dr. Takeuti's conclusion(4), on which the present phase diagram is considered.) Hence the transformation $\alpha \rightarrow \alpha+\gamma$ on heating takes place only at the time when it is heated beyond the constant temperature T_k, which should be characteristic of the hysteresis in alloys with higher nickel content.

The above theoretical deduction will be compared with the experimental results in the following section.

§ 4. Experimental Results (b).

The results of observation for 20, 25 and 30% Ni alloys are shown in Fig. 9-11. In the first place, each specimen being heated from room temperature, any isothermic transformation is not observed till about 400° is reached, and from the temperature the transformation $\alpha \rightarrow \alpha+\gamma$ abruptly proceeds. It is a remarkable fact that each transformation point is nearly constant, though the concentration is considerably different from each other. Reaction rates for the transformation at different constant temperatures are also shown in these figures.

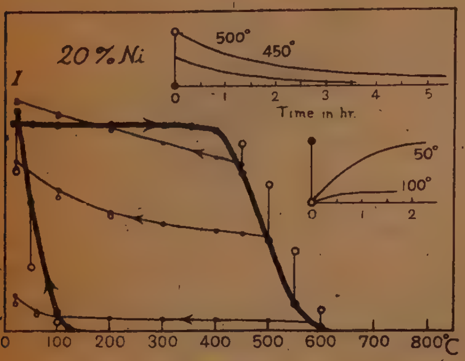

Fig. 9.

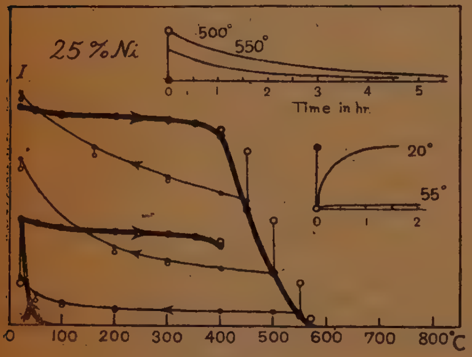

Fig. 10.

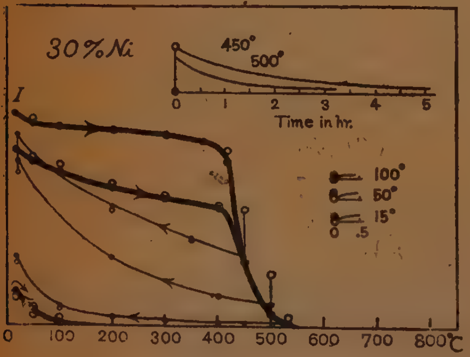

Fig. 11.

When, next, the γ solid solution is cooled, the γ phase remains unchanged till its lattice transformation point is attained, where the transformation $\gamma \rightarrow \alpha$ begins. For example, the lattice transformation $\gamma \rightarrow \alpha$ is observed in 20 and 25% Ni alloys, as shown in Figs. 9–10, but it cannot be observed in 30% Ni alloy (Fig. 11.), where a curve of the ferromagnetic γ phase only appears. This phase is reversible with regard to the temperature, as seen from the figure. The lattice transformation $\gamma \rightarrow \alpha$ of this alloy occurs when it is immersed in liquid air.

The above facts tell us that there exists actually such shaded region in the phase diagram as deduced in the previous section (Fig. 7), as well as the bordering line of the region T_k = about 400°.

The phase diagram constructed from the experimental results (a) and (b) is shown in Fig. 12.

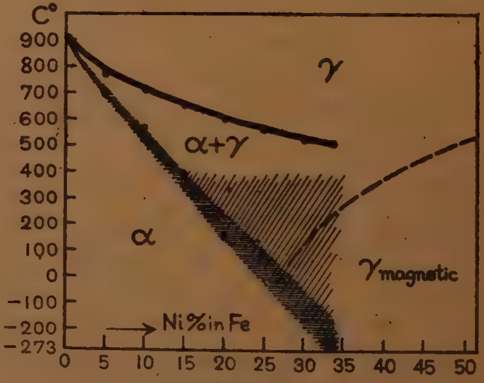

Fig. 12.

The upper boundary of the region $(\alpha+\gamma)$ in the diagram is obtained by connecting the temperatures, in which the magnetization of α phase disappears, and the lower boundary is composed of the points, where the magnetization of α phase reappears. It is seen that the lower boundary does not form a continuous smooth curve; so it is represented as a band in the diagram. This may be due to the difficult formation of pure α solid solution; for the so-called α solid solution is considered to contain more or less γ solution, especially in the alloys with higher nickel content.

As seen from the above, the common tangents, by which the coexistent states of two phases $(\alpha+\gamma)$ are represented, are only uniquely definite above 400°. In order to represent this relation, the part of region ($\alpha+\gamma$) which is situated below the limiting temperature is shaded, as shown in Fig. 12. The shaded region is to spread into contact with the upper boundary of the diagram, as seen in Fig. 7; but this is not so, because alloys containing more than about 35% Ni, just at which the lower boundary in Fig. 12 passes through absolute zero, cannot be cooled beyond the temperature T_a in Fig. 8, below which the α phase would appear. Consequently about 35% Ni is the limititing concentration, above which the γ phase only ex sts, that is, the remarkable hysteresis is no longer observed. (cf. Fig 8. The transformation $\gamma \rightarrow \alpha+\gamma$ is extremely difficult to proceed.) Thus it has been realized how irreversible alloys pass into reversible ones.

The magnetic-transformation curve of the γ solution of the alloys is drawn in a broken line in the phase diagram (Fig. 12). The fact that the irreversible alloys in the neighbourhood of 30% Ni may have the ferromagnetic γ phase, seems to have influence upon behaviours of the alloys, such as for example, on the form of curve obtained by cooling after isothermic transformation $\alpha \rightarrow \alpha+\gamma$, and on an abnormal bend observed in the heating curve, as seen in Figs. 9–11.

§ 5. Conclusion.

In discussing the hysteresis in irreversible Fe-Ni alloys, the cooling process cannot be similarly treated as the heating process —at least aside from alloys of very low nickel content. That is, the transformation $\alpha \rightarrow \alpha+\gamma$ proceeds easily, but the transformation $\gamma \rightarrow \alpha+\gamma$ is extremely difficult to proceed. Moreover with further increasing content of Ni, there appears a temperature range, in which even the transformation $\alpha \rightarrow \alpha+\gamma$ cannot proceed, not to speak of the transformation $\gamma \rightarrow \alpha+\gamma$. And when the concentration increases beyond 35% Ni, the remarkable hysteresis disappears; irreversible alloys pass into reversible ones.

In order to explain these phenomena, the present writer assumed that the free energy of γ phase in the region ($\alpha+\gamma$) is very near in value to that of the coexistent state of the two phases. From this viewpoint, he arrives at the conclusion that the remarkable irreversibility is caused by such relation betweeen free energies as above described.

It is seen from several diagrams of Fe-Ni alloys hitherto proposed that one end of the region ($\alpha+\gamma$) remains open to the γ field, indicating the very fact that the ($\alpha+\gamma$) surface is situated so near to the γ surface in the FTC-space, that is, the above assumption. As a matter of fact, similar types of the region ($\alpha+\gamma$) are seen in the iron sides of the diagrams of Fe-Mn alloys, Fe-Pt alloys, etc.; and the remarkable hysteresis is reported to be induced in these alloys as well$^{(6)}$.

The present investigation was done throughout by the kind guidance of Prof. K. Honda, to whom the writer expresses his sincere thanks. And to Prof. T. Hirone, whose kind encouragement was given during the work, he also expresses his hearty thanks.

References.

(1) J.S. Marsh: The Alloys of Iron and Nickel, **1** (1938), 32
(2) E. Scheil: Archiv f. d. Eisenhüttenwesen, **9** (1935–1936), 163
(3) P.D. Merica: Metals Handbook (1936), 271
(4) S. Takeuti: Nippon Kinzoku Gakkai-si, **6** (1942), 361, 497
(5) R. Becker: Ann. d. Phys., **32** (1938), 128
(6) T. Ishiwara: Sci. Repts. Tohoku Univ. **19** (1930), 509
M. Hansen: Der Aufbau der Zweistofflegierungen, (1936), 721

On the Physical Cleaning of Surfaces. I. Spectra of Gliding Sparks on Contaminated Glass Surfaces.

By Koreo KINOSITA, Mituo SUMI, and Takasi OWAKI.

Department of Applied Physics, Faculty of Engineering, University of Nagoya.

(Read, March 29, 1948; Received, June 9, 1948).

Emission spectra of the gliding sparks on glass surfaces with various grades of contamination were examined.

When the glass plate is shifted for each shot so as to make every spark run on a virgin track in the contamination film (*shifted sparks*), the spectrogram on which the light of thousands of such sparks is accumulated is characterized by the presence of the λ3883 sequence of the CN violet bands and the *0—0* member (λ3852) of the C_2 Deslendres-D'Azambuja bands. On the contrary, when sparks run every time on the same track (*fixed sparks*), the CN and C_2 bands do not appear. "Shifted" sparks on glass surfaces thoroughly cleaned beforehand by means of chemical procedures are similar to the latter. These experiments certify the well-known surface cleaning action of gliding sparks, and indicate furthermore that the hydrocarbon molecules (*e. g.* those of fatty acids), which are supposed to be the main constituents of the contamination film, are not only detatched from the surface but decomposed thereby.

The technique of shifting sparks developed here may find applications in the field of spectral analysis by virtue of its superior sensitivity.

§ 1. Introduction.

One of the most remarkable features of thoroughly cleaned surfaces of glass and other materials is their excellent wettability. This is clearly shown by the "breath figures."(1). If one breathes on a surface of glass, the moisture condenses in minute droplets on any slightly contaminated regions to form a temporary mist; on perfectly clean regions it condenses as a uniform water film which may be invisible, or may show interferance colors momentarily. The former type of condensation is called the "white" and the latter the "black" condensation respectively.

One can obtain such clean surfaces by washing with appropriate chemicals. A number of procedures are known besides, however, which might be named generically the "physical" cleaning methods; they are: (1) sweeping the surface with a hot flame momentarily(2) or (2) with surface gliding sparks(1), (3) inserting the specimen in a low pressure glow discharge(3), (4) bombarding the surface with low speed electrons(4), *et al*(5). Historically these were found in the course of studies on breath figures. The third method above mentioned is now in general use as a preliminary treatment for glass surfaces to be coated by vacuum evaporation technique; nevertheless, the mechanism of these physical cleaning procedures is not yet clear. Strong(5) suggests that electronic or ionic bombardment plays the rôle, whereas Tanner and Lockhart(6) who describe the glow discharge cleaning technique in German optical coating practice use the term "electrostatic cleaning", both without any convincing explanations. A more detailed study seems to be necessary.

The authors took up the cleaning action of surface gliding sparks for the time and tried to find the key by examining their emission spectra.

§ 2. Experimentals.

Intermittent condensed spark discharge was obtained by means of a simple device shown in Fig. 1(a). It is a matter of prime importance to have the sparks run closely on the surface, for which purpose we adopted the electrode configuration in Fig. 1(b).

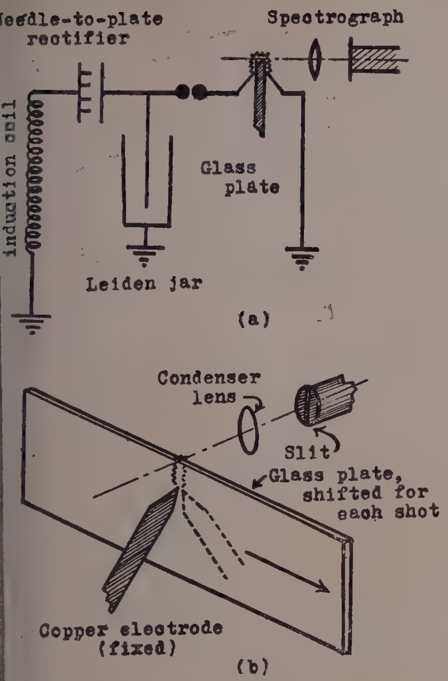

Fig. 1.

he essential difficulty in getting a spectro- of gliding sparks on a contamination film that one spark shot is too feeble for photo- ing and yet the contamination is removed s very shot; the subsequent sparks run only e cleaned-up track. This we overcame by g the glass plate slightly for each shot, as ated in Fig. 1. The light of thousands of on a contamination film could thus be ac- ated on a single spectrogram. For brevity, ll the spectrogram taken in this way, which ected to show some peculiar features char- tic to the contamination film, the S-spectro- and the one photographed without shifting ss plate (sparks on the breath figure produc- the first shot) the F-spectrogram.

and F-spectrograms were taken, mainly with ll glass prism spectrograph,* of the sparks following specimens: *i. e.*, ordinary glass thoroughly washed and then coated with hin films of grease, paraffine, soap, or human ; the same kind of plates washed with soapy ; and the ones washed carefully with chromic austic soda, and distilled water.

§ 3. Results.

S-spectrograms of the sparks on contaminated glass surfaces are characterized by the presence of the *0–0*, *1–1*, *2–2* and *3–3* members of the CN violet bands (λλ3883, 3871, 3862 and 3855) and the *0-0* member (λ3852) of the C_2 Deslendres-D'Azambuja bands. *Cf.* Photo. 1. The response is so sensitive as can be recognized in the case of samples washed carefully with hot soapy water which are all but clean and show nearly "black" condensation. (The extraordinary sensitivity of the breath figure response for the cleanliness of suafaces is well known.)

F-spectrograms of the same samples completely lack the CN and C_2 bands and in the main are similar to the ordinary spark in the air. So are the S- and F-spectrograms for specimens thoroughly cleaned by chemical procedures.

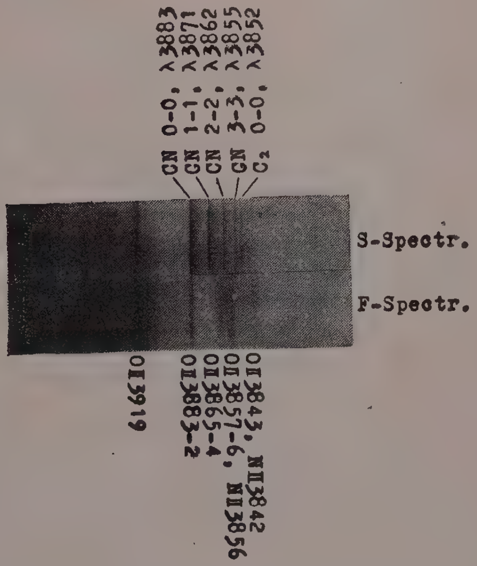

Photo.1. Spectra of Gliding Sparks on Paraffine-coated Glass Plate.

Photo. 1.

Other lines to be noticed are Na λ5893 and Ca λλ4227, 3969, 3934. Details of the observations are summarized in Table I.

The appearance of Na D-lines in the case of grease coated glass, Na and Ca lines in the case of soap- and sweat-coated specimens is quite natural so far as S-spectrograms are concerned. But rather marked intensity of D-lines in the F-spectrograms for these specimens calls our attention. Whether

---

Shimadzu Wavelength Spectrometer.

Table I.

S and F denote "shifted spark" spectogram and "fixed spark" spectoram resp.

		CN λλ3883, 3871, 3862 and 3855 bands. C_2 λ3852 band.	Na D-lines λ5893	Ca	
				λ4227	λλ3969, 39
Ordinary copper spark in the air		absent	(trace)	absent	absent
Gliding spark on grease-coated glass	S	distinct	rather intehse	faint	faint
	F	absent	distinct	indistinguishable*	trace
Gliding spark on parffine-coated glass	S	distinct	present	trace	trace
	F	absent	present	indistinguishable*	faint
Gliding spark on soap-coated glass	S	distinct	very intense	distinct	distinct
	F	absent	intense	absent**	trace
Gliding spark on sweat-coated glass	S	distinct	intense	rather distinct	distinct
	F	absent	intense	absent**	trace
Gliding spark on glass washed with soapy water	S	present	present	trace	faint
	F	absent	distinct	trace	faint
Gliding sparks on chemically cleaned glass	S	absent	present	trace	faint
	F	absent	distinct	trace	faint

* Because of the broadening of the neighboring air lines.
** Presumably because of under-exposure.

this is due to the fact that these lines are very readily excited, or it is because Na atoms have the tendency to adhere to the glass surface and cannot be removed even when hydro-carbons are completely cleaned up, is not yet clear. The existence of Na and Ca lines in the sparks on clean glasses is believed to be due to the destruction, especially at the edge, of glass itself.

Too much stress must not be layed however, upon the intensity descriptions in Tab. I. Quantitative results can hardly be expected owing to the fluctuations of the intensity of the sparks. Quite dense distribution of numerous air lines is another hindrance. Some inconsistencies in Table I may originate in these points.

It is to be mentioned, in addition, that Ca atoms look like to jump up from the glass surface and emit the light, as judged from the spectrograms. This can be seen in Photo. 2.

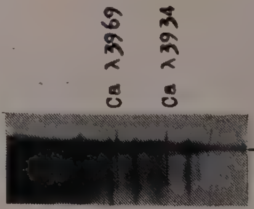

Upper edge of the glass plat

Photo.2. Ca Atoms Look Like to
Jump Up and Emit the Light.

Photo. 2.

§ 4. Discussion.

There is conclusive evidence that perfe clean surfaces of glass and other materials sh the "black" condensation. As to whether *converse* holds, however, some workers seem t rather suspicious: they point out that the elec charge remaining on the surface after the cle ing process may play a part in the increase wettability, and do not agree to regard the bl condensation as a sufficient proof for perfect cleanliness. In fact, the rôle of the remaining charge may not be trivial, although it is a matter of question whether it could be the cause of the black condensation. One of the authors (K.K.) noticed in his previous experiments(7) that the breath figures and the so-called electric figures are closely related.

Anyhow, our observations described in the preceding section seem to offer a positive evidence that gliding sparks actually clean up the surface, and furthermore, suggest some details of their cleaning action.

We consider the main constituents of the ordinary contamination on glass surfaces to be hydrocarbons, probably some fatty acid molecules standing perpendicularly on the surface. This view has some backing of electron diffraction data(8). The appearance of the CN and C_2 bands in the S-spectrogram of the sparks on artificially and naturally contaminated glass surfaces indicates that these hydrocarbon molecules are decomposed to pieces; free carbon atoms produced in this way combine with activated nitrogen of atmospheric origin to form CN molecules. This is not striking if one considers together numerous spectroscopic(9) and mass-spectroscopic(10) data on the decomposition of hydrocarbon molecules in gaseous state by means of electric discharge or electron impact, but a quantitative examination of the data suggests that more detailed studies are necessary as to the mechanism of the production of CN and C_2 molecules in our case.*

The absence of the CN and C_2 bands in the F-spectrogram might be regarded as a proof of the removal of the hydro-carbon contamination from the track of sparks.

Thus we are inclined to Strong's ideas (*cf.* § 1). More detailed investigations are needed, however; for instance, evaporation by local heating due to ionic bombardment would have to be taken into account. The influence of surface charge complicates the situations further.

The sensitivity of the *shifting spark method* developed here may be worthy of note. Applications in spectral microanalysis are suggested. Further studies along this line are desirable.

The authors wish to express their cordial thanks to Prof. T. Suga for his interests and valuable advices throughout the work, and to Prof. K. Noguchi for reading the manuscript. The work was carried out under the financial support of the Scientific Research Expenditure of the Department of Education.

References.

(1) See, among others, T. J. Baker: Phil. Mag. **44** (1922), 752.

(2) J. Aitken: Proc. Roy. Soc. Edin. (1893), 94. *Cf.* also Baker, *loc. cit.*

(3) J. Strong: Publ. A. S. P. **46** (1934), 18.

(4) P. H. Carr: R. S. I. **1** (1930), 711.

(5) Strong reports that faint breath figures could be obtained by ultraviolet irradiations. J. Strong: R. S. I. **6** (1935), 97.

(6) H. A. Tanner and L. B. Lockhart, Jr.: J. O. S. A. **36** (1946), 701.

(7) Reported in the Annual Meeting of the Soc. Appl. Phys. Jap., 1948.

(8) See, *e. g.*, H. Kamogawa: Nippon Sugaku-Buturigakukaisi **17** (1943), 396.

(9) See, *e. g.*, G. H. Diecke und W. Lochte-Holtgreven: Zeits. f. Phys. **62** (1930), 767.

(10) See, *e. g.*, T. Kambara: J. Phys. Soc. Jap. **2** (1947), 25.

---

* The electron impact data show that electron energy of considerable magntitude, say > 100 V, is necessary to obtain a detectable quantity of C^+ or C_2^+ ions as a dissociation product of hydro-carbon molecules, whereas the energy of the greater part of the electrons in the spark is evaluated much lower (several volts); some chemical reactions may take place in the present case which, *e. g.* through dehydrogenation, facilitate the decomposition. Further studies are now in preparation.

On States not in Thermal Equilibrium (Induction of the Equation of Motion of Gas)

By Toyoki KOGA,

Faculty of Engineering, University of Nagoya.

(Read May 10, 1947. Received May 11, 1948)

As the object of study we take a gas which is assumed for simplicity to be constructed of molecules of a single kind. In thermal equilibrium, being an object of thermodynamics or statistical mechanics, this gas has properties which satisfy the equation of state of the perfect gas with sufficient approximation. But not in thermal equilibrium, the process towards equilibrium is not quasi-static nor reversible and the state is more complicated. Therefore, the conceptions available to construct the laws of thermodynamics are not used directly. We adopt here other conceptions. In this discussion, we may touch the problems of polyatomic molecules only formally but not concretely, as the mode of the partition of energy is complicated here. Therefore, excluding the case of monatomic molecules, the results of this discussion are not directly applicable to some kinds of practical problems, for instance, to the phenomenon of the absorption of energy in supersonic waves. But still we hope our aim will be understood; we intend to know the essential nature of irreversible phenomena or to approach the principle of irreversible problems.

§ 1. The Six Kinds of Variables of a Gas not in Equilibrium.

We take a point in the space (large enough) filled up with a gas. Here we consider dynamical quantities of the gas. For convenience we now introduce following notations:—

(m); the mass per unit volume,

$(M)_i$; the momentum per unit volume,

(E); the energy per unit volume,

$[m]_i$; the mass passing through an element of surface vertical to the axis i per unit area per unit time,

$[M]_{ij}$; the momentum component passing through an element of surface per unit area per unit time,

$[E]_i$; the energy passing through an element of surface per unit area per unit time,

where i and j are the three orthogonal directions x, y, z and $(M)_i$ is identical with $[m]_i$.

If we take $\tilde{\rho}$, $\tilde{p}$, $\tilde{T}$, u, v, w as the six parameters, these six are expressed as follows:—

$$(m) = \tilde{\rho},$$

$$(M)_x = \tilde{\rho}u,\ (M)_y = \tilde{\rho}v,\ (M)_z = \tilde{\rho}w,$$

$$(E) = (E')+(E''),$$

$$(E') = \frac{1}{2}\tilde{\rho}(u^2+v^2+w^2)+\tilde{\rho}c_{v'}\tilde{T},\ (E'') = \tilde{\rho}c_{v''}\tilde{T},$$

$$[m]_x = (M)_x,\ \ldots\ \text{etc.},$$

$$[M]_{xx} = \tilde{\rho}u^2+\tilde{p}-\frac{2}{3}\varepsilon_2\tilde{\rho}\frac{\partial u}{\partial x}+\frac{2}{9}\varepsilon_2\tilde{\rho}\left(\frac{\partial u}{\partial x}+\frac{\partial v}{\partial y}+\frac{\partial w}{\partial z}\right),$$

$$[M]_{xy} = \tilde{\rho}uv-\frac{1}{3}\varepsilon_2\tilde{\rho}\left(\frac{\partial v}{\partial x}+\frac{\partial u}{\partial y}\right),\ \ldots\ \text{etc.},$$

$$[E]_x = u(E)+u\left\{[M]_{xx}-\tilde{\rho}u^2\right\}+v\left\{[M]_{xy}-\tilde{\rho}uv\right\}$$
$$+w\left\{[M]_{xz}-\tilde{\rho}uw\right\}+\sigma_p\frac{\partial\tilde{p}}{\partial x}+\sigma_T\frac{\partial\tilde{T}}{\partial x},\ \ldots\ \text{etc},$$

where the coefficients ε_2, σ_p, σ_T are determined from the properties of the molecule of the gas and $\tilde{\rho}$, $\tilde{p}$, $\tilde{T}$, Especially $c_{v'}$ is equal to 3/2. R/M, where R is the gas constant and M is the molecular weight. The equation corresponding to that of state in equilibrium is

$$\tilde{p}\tilde{\rho}^{-1} = \frac{2}{3}c_{v'}\tilde{T} \tag{1.2}$$

We may call $\tilde{\rho}$ the density and u, v, w the velocity, but $\tilde{p}$ is, as stated later, not the pressure which is measureed in equilibrium, nor $\tilde{T}$ is considered as the temperature which has a certain meaning only in equilibrium. From their forms we see that (m) and (E) are scalars, (M), $[m]$, $[E]$ are vectors and $[M]$ is a tensor.

§ 2. Verification.

It is not essentially reasonable to apply conceptions of thermodynamics to the case of non-equilibrium state. But as the first approximation, let us cut out a small domain of the field and consider it as to be in equilibrium state. In this approximation, we can use conceptions of density, pressure, temperature, etc. in each domain as in equilibrium. Thus the field is divided into a great number of small cells, and in each cell the state is considered to be in equilibrium. Further each cell must be so small that we can differentiate quantities all over the field, as if they are continuous. Now, in this artificially constructed field, we caluculate the quantities corresponding to (m), (M), ... etc. mentioned in § 1. The method is similar to Meyer's1) but more generalised2). Now let us introduce notations; $\bar\rho$ for density, $\bar p$ for pressure, $\bar T$ for temperature, $\bar u$, $\bar v$, $\bar w$ for mass-velocity. c'_v for heat capacity of unit mass at constant volume concerning transversal random motions of molecules, $\bar c_{v''}$ for heat capacity concerning rotational and vibratory motions, $\delta/2$ for the radius of an assumed elastic sphere for a molecule*, k for Bolzmann's constant, m for the mass of one molecule, $\bar n$ for the number of molecules in unit volume, $\bar c$ for transversal speed of random motion, where the symbol '—' is used to express quantities of the artificial state. Then the result is as follows: —

$$\left\{\varepsilon_i/t\right\} \equiv -\varepsilon_i\frac{1}{\rho}\frac{d\rho}{dt} - \varepsilon_i\left(\frac{\partial u}{\partial x}+\frac{\partial v}{\partial y}+\frac{\partial w}{\partial z}\right)$$
$$+\frac{3}{2}\varepsilon_i\frac{1}{\bar T}\frac{d\bar T}{dt}-\varepsilon_{i+2}\frac{m}{2k\bar T^2}\frac{d\bar T}{dt}$$

$$\left\{\varepsilon_i\bar u/t\right\} \equiv -\varepsilon_i\frac{d\bar u}{dt}-\frac{1}{3}\varepsilon_{i+2}\left(\frac{1}{\rho}\frac{\partial\rho}{\partial x}-\frac{3}{2}\frac{1}{\bar T}\frac{\partial\bar T}{\partial x}\right)$$
$$-\frac{1}{3}\varepsilon_{i+4}\frac{m}{2k\bar T^2}\frac{\partial\bar T}{\partial x}, \;\ldots\ldots \text{etc.},$$

$$(\bar m) = \bar\rho(1+\{\varepsilon_0/t\}),$$

$$(\bar M)_x = \rho(\bar u+\bar u\{\varepsilon_0/t\}+\{\varepsilon_0\bar u/t\}), \;\ldots\ldots \text{etc.},$$

$$(\bar E) = (\bar E')+(\bar E''),$$

$$(\bar E') = \frac{1}{2}\bar\rho(u^2+v^2+w^2)(1+\{\varepsilon_0/t\})$$
$$+\bar\rho\bar u\{\varepsilon_0\bar u/t\}+\bar\rho\bar v\{\varepsilon_0\bar v/t\}+\rho\bar w\{\varepsilon_0\bar w/t\}$$
$$+\bar\rho c_{v'}\bar T+\frac{1}{2}\bar\rho\{\varepsilon_2/t\}$$
$$-\frac{1}{3}\bar\rho\varepsilon_2\left(\frac{\partial\bar u}{\partial x}+\frac{\partial\bar v}{\partial y}+\frac{\partial\bar w}{\partial z}\right),$$

$$(\bar E'') = \bar\rho c_{v''}\bar T(1+\{\varepsilon_0/t\})-\varepsilon_0\bar\rho\bar c_{v''}\frac{d\bar T}{dt},$$

$$[\bar m]_i = (\bar M)_i,$$

$$[\bar M]_{xx} = \bar p+\bar\rho\bar u^2(1+\{\varepsilon_0/t\})$$
$$-\frac{2}{3}\bar\rho\varepsilon_2\frac{\partial u}{\partial x}+2\rho\bar u\{\varepsilon_0\bar u/t\}+\frac{1}{3}\rho\{\varepsilon_2/t\},$$

$$[\bar M]_{xy} = \bar\rho\bar u\bar v(1+\{\varepsilon_0/t\})-\frac{1}{3}\bar\rho\varepsilon_2\left(\frac{\partial\bar v}{\partial x}+\frac{\partial\bar u}{\partial y}\right)$$
$$+\bar\rho\bar u\{\varepsilon_0\bar v/t\}+\bar\rho\bar v\{\varepsilon_0\bar u/t\}, \;\ldots\ldots \text{etc.},$$

$$[\bar E]_x = [\bar E']_x+[\bar E'']_x,$$

$$[\bar E']_x = \frac{1}{2}\bar\rho(\bar u^2+\bar v^2+\bar w^2)[\bar u(1+\{\varepsilon_0/t\})+\{\varepsilon_0\bar u/t\}]$$
$$+\bar\rho\bar u\left[\bar u\{\varepsilon_0\bar u/t\}-\frac{2}{3}\varepsilon_0\frac{\partial\bar u}{\partial x}+\frac{\bar p}{\rho}+\frac{1}{3}\{\varepsilon_2/t\}\right]$$
$$+\rho\bar v\left[\bar u\{\varepsilon_0\bar v/t\}-\frac{1}{3}\varepsilon_2\left(\frac{\partial\bar u}{\partial y}+\frac{\partial\bar v}{\partial x}\right)\right]$$
$$+\bar\rho\bar w\left[\bar u\{\varepsilon_0\bar w/t\}-\frac{1}{3}\varepsilon_2\left(\frac{\partial\bar u}{\partial z}+\frac{\partial\bar w}{\partial x}\right)\right]$$
$$+\frac{1}{2}\bar\rho\{\varepsilon_2\bar u/t\}+\frac{1}{2}\bar\rho\bar u\{\varepsilon_2/t\}-\frac{1}{3}\bar\rho\varepsilon_2\frac{d\bar u}{dt}$$
$$-\frac{1}{3}\bar\rho\varepsilon_2\bar u\left(\frac{\partial u}{\partial x}+\frac{\partial v}{\partial y}+\frac{\partial w}{\partial z}\right)+\bar\rho\bar u c_{v'}\bar T,$$

$$[\bar E'']_x = \bar\rho\bar u\bar c_{v''}\bar T+\rho\bar u\bar c_{v''}\left(-\varepsilon_0\frac{d\bar T}{dt}+\bar T\{\varepsilon_0/t\}\right)$$
$$-\frac{1}{3}\bar\rho\bar c_{v''}\varepsilon_2\frac{\partial\bar T}{\partial x}+\bar\rho c_{v''}\bar T\{\varepsilon_0\bar u/t\}, \;\ldots\ldots \text{etc.},$$

$$\varepsilon_{2\nu} = \frac{4}{\pi\bar n\sigma^2}(2k\bar Tm)^{\frac{1}{2}-\nu}I_{2\nu+3}, \quad \nu = 1,2,3, \ldots\ldots$$

$$I_{2\nu+3} = \int_0^\infty\frac{\xi^{2\nu+3}}{\psi(\xi)}exp(-\xi^2)d\xi,$$

$$\psi(\xi) = \xi\,exp(-\xi^2)+(2\xi^2+1)\int_0^\xi exp(-\eta^2)d\eta,$$

$$\xi = c\sqrt{2k\bar Tm}, \tag{2,1}$$

Now $\bar\rho$, $\bar p$, $\bar T$, $\bar u$, $\bar v$, $\bar w$ and $\bar c_{v''}$ are artificial, and their values are left to our selection. We take from the first the molecular distribution fully near that of the natural state of which the deviation from equilibrium is assumed to be not large. Now let us attempt to make $(\bar m)$, $(\bar M)$, ... etc. equal to (m), (M), ... etc. making use of arbitrariness permitted. In this attempt, the terms constructed of differential coefficients being of small values, the alterations caused in them by arbitrariness of values of $\bar{\rho}$, $\bar{p}$, $\bar{T}$, ... etc. are negligibly small.

---

* After Sutherland δ is a function of T3).

1) $(\bar{m}) = (m)$, suitablly selecting $\bar{\rho}$ in $(\bar{m})$, as every term other than ρ is of small magnitude of higher order.

2) $(\bar{M})_x = (M)_x = [\bar{m}]_x = [m]_x$, suitablly selecting $\bar{u}$, where ρ has already been determined in 1). Similarly,

$(\bar{M})_y = (M)_y = [\bar{m}]_y = [m]_y$, suitablly selecting $\bar{v}$,

$(\bar{M})_z = (M)_z = [\bar{m}]_z = [m]_z$, suitablly selecting $\bar{w}$.

3) $(\bar{E}'') = (E'')$, suitablly selecting $\bar{c}_{v''}$. That is to say, the energy of vibration and rotation of molecules is distributed in a different manner from that in equilibrium state.

4) $(\bar{E}') = E'$, suitablly selecting $\bar{T}$.

5) $[\bar{M}]_{ii} = [M]_{ii}$, suitablly selecting $\bar{p}$.

Thus the six quantities $\bar{\rho}$, $\bar{p}$, $\bar{T}$ .... etc. and $\bar{c}_{v''}$ are all decided, and there is no arbitrariness left. We must here examine whether the selections above mentioned are not contradictory to the other cases.

6) $\bar{p}\bar{\rho}^{-1} = \frac{2}{3} c'_v \bar{T}$. The examination is as follows: — from (2.1) we get

$$\bar{p}-\frac{2}{3}\bar{\rho}c_{v'}\bar{T} = \frac{1}{3}([\bar{M}]_{xx}+[\bar{M}]_{xy}+[\bar{M}]_{xz})-\frac{2}{3}(\bar{E}'),$$

from 3) and 4) and 5) above

$$= \frac{1}{3}([M]_{xx}+[M]_{xy}+[M]_{xz})-\frac{2}{3}(E').$$

On the other hand, from the definition of energy,

$$(E') = \frac{1}{2}([M]_{xx}+[M]_{xy}+[M]_{xz}).$$

Therefore,

$$p\rho^{-1} = \frac{2}{3}c_{v'}\bar{T}.$$

To express the quantities of (2.1) more briefly before progressing further, let us write down as follows: —

$$\left.\begin{aligned}
\tilde{\rho} &= \rho(1+\{\varepsilon_0/t\}),\\
u &= \bar{u}+\{\varepsilon_0/t\bar{u}\},\\
v &= \bar{v}+\{\varepsilon_0\bar{v}/t\},\\
w &= \bar{w}+\{\varepsilon_0\bar{w}/t\},\\
\tilde{p} &= \bar{p}+\frac{1}{3}\rho\{\varepsilon_2/t\}\\
&\quad -\frac{2}{9}\rho\varepsilon_2\left(\frac{\partial\bar{u}}{\partial x}+\frac{\partial\bar{v}}{\partial y}+\frac{\partial\bar{w}}{\partial x}\right),\\
c_{v'}\tilde{T} &= c_{v'}\bar{T}(1-\{\varepsilon_0/t\})+\frac{1}{2}\{\varepsilon_2/t\}\\
&\quad -\frac{1}{3}\varepsilon_2\left(\frac{\partial\bar{u}}{\partial x}+\frac{\partial\bar{v}}{\partial y}+\frac{\partial\bar{w}}{\partial z}\right).
\end{aligned}\right\}\qquad(2.2)$$

Then (2.1) becomes consistent with (1.1), where

$$\sigma_p = -\frac{5}{2}\varepsilon_0\frac{\tilde{p}}{\tilde{\rho}}+\frac{5}{3}\varepsilon_2-\frac{1}{6}\varepsilon_4\frac{\tilde{\rho}}{\tilde{p}}$$

$$\sigma_T = \frac{25}{18}c_{v'}\varepsilon_0\tilde{\rho}+\frac{5}{9}c_{v'}\varepsilon_4\frac{\tilde{\rho}^2}{\tilde{p}}$$

$$-\frac{1}{18}\varepsilon_6 c_{v'}\frac{\tilde{\rho}^3}{\tilde{p}^2}-\frac{1}{3}\rho c_{v''}\varepsilon_2$$

7) $[\bar{M}]_{xy}-\tilde{\rho}uv = [M]_{xy}-\tilde{\rho}uv$, ... etc.; these are all constructed of terms of small value, so it is not necessary to change any parameters. In other words, the selections above mentioned are not contradictory in this case too.

8) $[\bar{E}]_x = [E]_x$, ... etc.; are these satisfied? There is no parameter left at our disposal. Consequently we must verify that these relations are satisfied automatically from foregoing selections. From (2.1) and the foregoing verifications, $[\bar{E}]_x$ becomes as follows: —

$$[\bar{E}]_x = u(E)+u\{[M]_{xx}-\tilde{\rho}u^2\}+v\{[M]_{xz}-\tilde{\rho}uv\}$$
$$+w\{[M]_{xz}-\tilde{\rho}uw\}+\sigma_p\frac{\partial\tilde{p}}{\partial x}+\sigma_T\frac{\partial\tilde{T}}{\partial x}.$$

Of the terms in the bracket in the right side, the first is the energy convected by the flow, the second, third and fourth terms are the works done by stress. The last terms $\sigma_p\frac{\partial\tilde{p}}{\partial x}+\sigma_T\frac{\partial\tilde{T}}{\partial x}$ is of small value of the first order, and the error in it is of small one of higher order. Thus

$$[\bar{E}]_x = [E]_x.$$

Similarly

$$[\bar{E}]_y = [E]_y,\ [\bar{E}]_z = [E]_z.$$

Further, between $\tilde{\rho}$, $\tilde{p}$, and $\tilde{T}$, there is a relation analogous to the equation of state in equilibrium. Namely

$$\tilde{p}\tilde{\rho}^{-1} = \frac{2}{3}c_{v'}\tilde{T}. \qquad (2,3)$$

From (2.2)

$$\tilde{p}\tilde{\rho}^{-1} = \bar{p}\tilde{\rho}^{-1}(I-\{\varepsilon_0/t\})+\frac{1}{3}\{\varepsilon_2/t\}$$
$$-\frac{2}{9}\varepsilon_2\left(\frac{\partial\bar{u}}{\partial x}+\frac{\partial\bar{v}}{\partial y}+\frac{\partial\bar{w}}{\partial z}\right).$$

On the other hand

$$\frac{2}{3}c_{v'}\tilde{T} = \frac{2}{3}c_{v'}\bar{T}(1-\{\varepsilon_0/t\})+\frac{1}{3}\{\varepsilon_2/t\}-\frac{2}{9}$$
$$\varepsilon_2\left(\frac{\partial u}{\partial x}+\frac{\partial\bar{v}}{\partial y}+\frac{\partial\bar{w}}{\partial z}\right).$$

Thus (2.3) is verified

§ 3. The Laws of Conservation (The Equations of Motion).

Mass, momentum and energy must be conserved respectively. Let us express these laws in the form of equations as follows: —
with respect to mass,

$$\frac{\partial(m)}{\partial t}=-\frac{\partial[m]_x}{\partial x}-\frac{\partial[m]_y}{\partial y}-\frac{\partial[m]z}{\partial z}, \tag{3,1}$$

with respect to momentum,

$$\frac{\partial(M)_i}{\partial t}=-\frac{\partial[M]_{ix}}{\partial x}-\frac{\partial[M]_{iy}}{\partial y}-\frac{\partial[M]_{iz}}{\partial z}, \tag{3,2}$$

where $i=x,\ y,\ z$, and with respect to energy,

$$\frac{\partial(E)}{\partial t}=-\frac{\partial[E]_x}{\partial x}-\frac{\partial[E]_y}{\partial y}-\frac{\partial[E]_z}{\partial z}. \tag{3,3}$$

Here we substitute for (m), $[m]_x$, ... etc. the values of (1.1), then (3.1) becomes

$$\frac{\partial\tilde{\rho}}{\partial t}=-\frac{\partial(\tilde{\rho}u)}{\partial x}-\frac{\partial(\tilde{\rho}v)}{\partial y}-\frac{\partial(\tilde{\rho}w)}{\partial z},$$

This is what is called the equation of continuity, but here we must interpret the meaning of the variables as stated in § 5. Next with respect to momentum,

$$\begin{aligned}\frac{\partial(\tilde{\rho}u)}{\partial t}=&-\frac{\partial}{\partial x}\Big[\tilde{\rho}u^2+\tilde{p}-\frac{2}{3}\tilde{\rho}\varepsilon_2\frac{\partial u}{\partial x}+\frac{2}{9}\tilde{\rho}\varepsilon_2\\&\left(\frac{\partial u}{\partial x}+\frac{\partial v}{\partial y}+\frac{\partial w}{\partial z}\right)\Big]\\&-\frac{\partial}{\partial y}\left[\tilde{\rho}uv-\frac{1}{3}\rho\varepsilon_2\left(\frac{\partial v}{\partial x}+\frac{\partial u}{\partial y}\right)\right]\\&-\frac{\partial}{\partial z}\left[\tilde{\rho}uw-\frac{1}{3}\rho\varepsilon_2\left(\frac{\partial w}{\partial x}+\frac{\partial u}{\partial z}\right)\right],\text{ etc.,}\end{aligned}$$

Finally,

$$\begin{aligned}\frac{\partial(E)}{\partial t}=&-\frac{\partial}{\partial x}\Big[u(E)+u([M]_{xx}-\tilde{\rho}u^2)+v([M]_{xy}\\&-\tilde{\rho}uv)+w([M]_{xz}-\tilde{\rho}uw)+\sigma_p\frac{\partial\tilde{p}}{\partial x}+\sigma_r\frac{\partial\tilde{T}}{\partial x}\Big]\\&-\frac{\partial}{\partial y}[\,''\,]-\frac{\partial}{\partial z}[\,''\,],\end{aligned}$$

the equation of energy. In this equation we see that the term $\sigma_p\frac{\partial\hat{p}}{\partial x}$ has no analogue in usual text books[4]. If we here omit $\tilde{c}_{v''}$ (the case of monatomic gas), by solving these five equations and (2.3), we can get the six variables $\tilde{\rho}$, $\tilde{p}$, $\tilde{T}$, u, v, w as functions of x, y, z, t. That is to say, the six variables are determined by the sex equations. As a matter of course, the values of the six must be given on the boundary. In other words, they must be measured experimentally. Concerning $\tilde{c}_{v''}$ we can not say concretely.

§ 4. The Boundary Conditions.

All the results mentioned above are caluculated on the assumption that the field of gas extends infinitely and continuously. But in fact, we must consider the existence of walls. On a wall the molecules are thought to reflect at random following Maxwell's law corresponding to the temperature of the wall[5]. In order to take the existence of the wall into account, we may imagine the inner region of the wall as replaced by the uniform field of gas. Then on the boundary surface the field is not continuous and the differential coefficients of the variables of state vanish all over the replaced field. The values thus calculated will contain a parameter l which is the length of the distance from the point P in question to the wall. When the lengh l becomes large enough, the values agree with those of a point in the field extended infinitely and continuously; that is to say, l disappears as we have seen in (2.1). Let us take here l equal to the mean free path λ, and consider a certain quantity X. If we take x the distance in the outer direction from the wall,

$$X_{x=\lambda}-X_{x=0}=\lambda\left(\frac{\partial X}{\partial x}\right)_{\text{mean}}$$

where $\left(\frac{\partial X}{\partial x}\right)_{\text{mean}}$ is decided after the equation valid near the wall. As it is improbable that $\left(\frac{\partial X}{\partial x}\right)$ should take a discontinuous or singular value, taking λ minute we may put

$$X_{x=\lambda}-X_{x=0}=0, \tag{4,1}$$

From this discussion, as the values *on* a wall we can take the values *near* a wall (near but so far as the influence of l on the equation may be neglected). In other words, we can take the equations introduced in the foregoing paragraph valid all over the field, and as the boundary conditions we adopt the values experienced on the surface of the wall. Thus as the boundary conditions on a wall, we may take as follows: —

$$\left.\begin{array}{l}
\text{1) } u,\ v,\ w \text{ are zero,} \\
\text{2) } \tilde{T} \text{ is the temperature of the wall,} \\
\text{3) } p_{xx} = \tilde{p} - \frac{2}{3}\varepsilon_2\tilde{\rho}\frac{\partial u}{\partial x} + \frac{2}{9}\varepsilon_2\tilde{\rho}\left(\frac{\partial u}{\partial x} + \frac{\partial v}{\partial y}\right. \\
\qquad \left. + \frac{\partial w}{\partial z}\right),\ p_{xy} = -\frac{1}{3}\varepsilon_2\tilde{\rho}\left(\frac{\partial v}{\partial x} + \frac{\partial u}{\partial y}\right), \text{ etc.} \\
\qquad \text{is the stress (tensor),} \\
\text{4) } \sigma_p\frac{\partial \tilde{p}}{\partial x} + \sigma_T\frac{\partial \tilde{T}}{\partial x}, \text{ etc.} \\
\qquad \text{is the flow of energy.}
\end{array}\right\} \quad (4,1)$$

Thus we have seen that all the variables in the equations of § 3 are measured only on walls by experimental methods. In the field of a gas we must abandon our aim to measure those parameters experimentally; we know only the equations.

§ 5. On the Measurement of States.

In equilibrium we may consider without breaking generality the system stays still in all, so (M) in (1.2) becomes zero. In consequence u, v, w are zero and there remain only three parameters, namely $\tilde{\rho}$, $\tilde{p}$, and $\tilde{T}$. Moreover, the differential coefficients concerning x, y, z and t vanish. In this case we see that

$$(m) = \tilde{\rho}, \qquad (5,1)$$

$$(E) = \tilde{\rho}(c_{v'} + \bar{c}_{v''})\tilde{T}, \qquad (5,2)$$

$$[M]_{ii} = \tilde{p}. \qquad (5,3)$$

Thus the three quantities (m), (E) and $[M]_{ii}$ correspond respectively to the three parameters $\tilde{\rho}$, $\tilde{p}$ and $\tilde{T}$.

A group of molecules reflecting from a surface of a solid body obey Maxwell's law of distribution corresponding to the temperature of the body. In equilibrium, therefore, choosing the temperature of the solid body suitably, we can measure (E) and $[M]_{ii}$ on the surface of the body.

In non-equilibrium states, on the other hand, distribution of the molecules of a gas does not follow Maxwell's law. Nevertheless the reflecting molecules obey the law corresponding to the temperature of the surface. Thus the measurement becomes difficult. We know only the six equations in § 3 and conditions on walls as stated in § 4.

References.

(1) J. H. Jeans: The Dynamical Theory of Gases, 4th edition (1925), p. 291.

(2) Recently Mr. Naruo Takeda succeeded to express Boltzmann's equation in the form of an integral equation. Making use of it, this result (2.1) is deduced easily. This author's method, however, is more complicated. In a short time, these will be published in the Journal of this society (vol. 4, Nos. 4~6).

(3) loc. cit. ante. 1) p. 284.

(4) S. Chapmann and T. G. Cowling: The Mathematical Theory of Non-uniform Gases, Cambridge (1939), chap. 7.

L. Prandtl und O. Tietjens: Hydro-und Aeromechanik, Berlin (1931), iv.

A. Busemann: Gasdynamik, Handbuch der Experimentalphysik iv, teil 1, Leipzig (1931), 358.

(5) loc. cit. ante. 1) p. 117.

Discharge Mechanism of Geiger-Müller Counters(*) (I). The Motion and Quantity of Positive Ions.

By Hiroo KUMAGAI, Koichi SHIMODA, Iwao OGAWA,
Yasuo TORIKAI and Teisuke KODAMA.

Institute of Science and Technology, University of Tokyo.

(Received, June 28, 1948).

§ 1. Introduction.

Although many excellent experiments have been performed by several workers, there remain many uncertain and obscure points on the mechanism of discharge in Geiger-Mllüer Counters. The authors carried out a series of experiments upon the thema in 1943, the results of which are summarized briefly in the followings. Especially, the motion and quantity of the positive ions, spread-speed of the discharge along the central wire and the time-distribution of the so-called *Nachentladungen* were observed by making use of a cathode-ray oscillograph.* The counters were usually filled with argon-alcohol gas mixture to the pressure of about 10-cm Hg.

§ 2. Oscilloscopic Observation of the Motion of the Positive Ion Sheath.

Double-grid counters as illustrated in Fig. 1 were constructed and the electric pulses from a grid, the wall or the wire were led to a C. R. O. through a suitable amplifier. To fascillitate the oscilloscopic observation of the pulse form, a suitable triggering sweep circuit (Fig. 2,) was devised and was found very useful throughout the work. An amplified voltage pulse at the input terminal causes the discharge of a thyratron tube, immediately followed by the charge-up process of the parallel capacitor C_1 through R_1 with the time constant C_1R_1, which was ordinarily about 2×10^{-3} sec. The potential at the cathode is applied to the C. R. O. sweep-plate. At the beginning of the charge-up process, the cathode potential of the thyratron are sufficiently higher than the grid, so that the time sweep once initiated is not disturbed by the closely succeeding pulses. The cathode potential decreases purely exponentially except for the first 10^{-4} sec.

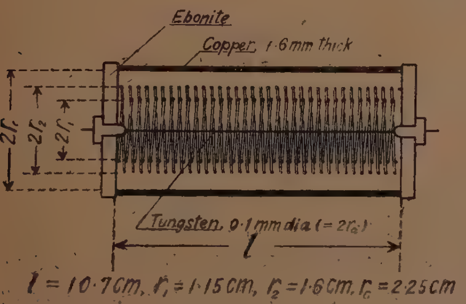
Ebonite
Copper, 1·6 mm thick
$2r_1$
$2r_2$
$2r_c$
Tungsten, 0·1 mm dia (= $2r_a$)
l
$l = 10{\cdot}7$ cm, $r_1 = 1{\cdot}15$ cm, $r_2 = 1{\cdot}6$ cm, $r_c = 2{\cdot}25$ cm

Fig. 1.

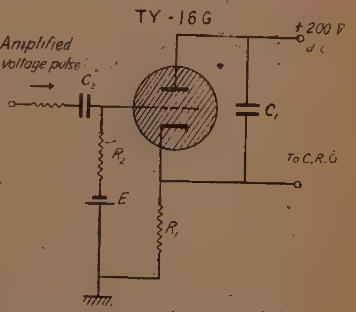

Fig. 2.
Trigger sweep circuit.
C_1: 0.01 μF
C_2: 0.02 μF
R_1: 20 $K\Omega$, 40 $K\Omega$, 100 $K\Omega$, 200 $K\Omega$, 400 $K\Omega$.
R_2: 100 $K\Omega$.
E: Grid-bias Supply.

Now it has been generally accepted that the large quantity of positive ions produced near the central wire of a counter during the growth of the discharge form a concentic cylinder around

---

[*] Studies performed in 1943 at the Physics Department, Faculty of Science, University of Tokyo, and published in Ref. (1), (2), (3), (4).

the wire ('positive ion sheath') and expand towards the cathode wall. According to this view, the potential variation of the outer grid or the wall must become suddenly pronounced when the sheath passes the nearest grid. In fact we have observed a series of characteristic figures on the oscillographic screen (as shown in Fig. 3) when we have taken signals from the anode wire A, inner grid G_1, outer grid G_2 and the cathode wall C. The time t_1, t_2 and T indicated in Fig. 4, should correspond to the transit time of the sheath through G_1, G_2 and C (arrival) respectively.

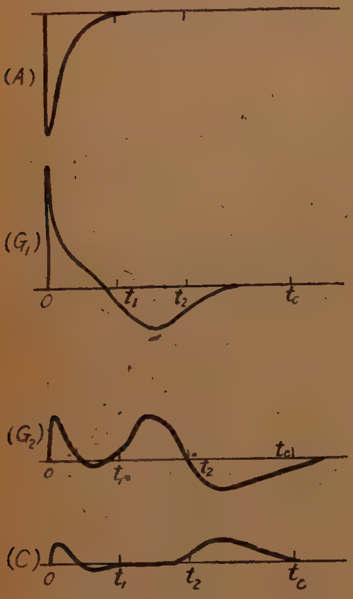

Fig. 3.

§ 3. Some Calculation on the Pulse Form of the Wall (or Grid) Potential.

Let us denote the charge per unit length on the central wire before the discharge by Q_0, the charge on the wire after the discharge by Q, the ion quantity per unit length by q and the radius of the thin ion sheath by r_s. Then, so long as the ion sheath moves inside G_1, the voltage U_1 on G_1 is given by

$$U_1 = \int_{r_a}^{r_1} \frac{2Q_0}{r} dr = \int_{r_a}^{r_s} \frac{2Q}{r} dr + \int_{r_s}^{r_1} \frac{2(Q+q)}{r} dr \qquad (1)$$

Small differences of the wire and the grid potential due to the resistances R and R_1 (see Fig. 5) are here neglected to the first approximation. After integration,

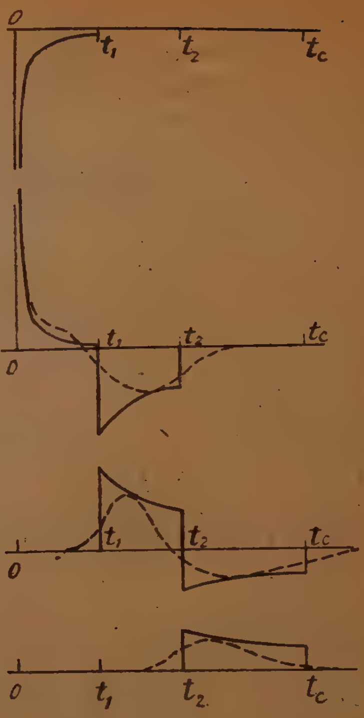

Fig. 4.

$$U_1 = \frac{Q_0}{c_1} = \frac{Q}{c_1} + 2q \log (r_1/r_s), \qquad (2)$$

or

$$Q = c_1 U_1 - 2c_1 q \log (r_1/r_s), \qquad (3)$$

where

$$1/c_1 = 2 \log (r_1/r_a).$$

Therefore, Q and q_1 (charge on G_1) vary with time as the ions move towards the grid, and the induced potential difference on the wire and the grid are given by

$$\Delta\varphi_a = -Ri_a = -Rl\frac{dQ}{dt} = -Rc_1 ql/t,$$

and

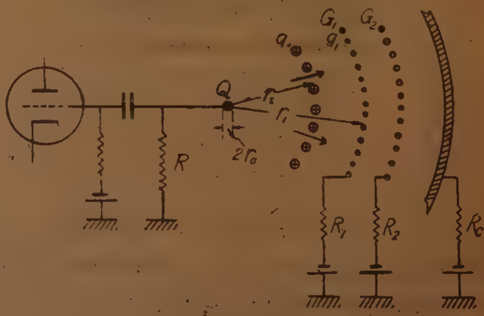

Fig. 5.

$$\Delta\varphi_1 = -R_1 i_1 = -R_1 l \frac{dq_1}{dt} = +Q_1 c_1 q l/t$$

$$(t < t_1,\ l: \text{counter length})$$

respectively, using the ralation:

$$Q + q + q_1 = 0$$

and

$$r_s^2 \backsim t$$

as derived in § 4.

When the ion sheath passes through G_1, $\Delta\varphi_a$ becomes zero by the shielding action of G_1, and then φ_2 varies according to the similar formula. Successive processes can be similarly calculated. Full lines in Fig. 4 indicate the results of calculation and the dotted lines are drawn with some corrections on the broadening of the ion sheath. The latters agree fairly well with the observed patterns.

§ 4. Estimation of the Mobilities of the Positive Ions.

Using the observed transit time t_1 or t_2, we can estimate the mobility k of the positive ions produced by the discharge process. By definition,

$$v = \frac{dr_s}{dt} = k \cdot \frac{p_0}{p} \cdot F, \tag{4}$$

where

$v = \frac{dr_s}{dt}$: velocity of the ions

p_0: standard (1 atmospheric) pressure

p: pressure in the counter

and F is the electric field strength due to other charges than q, and is given by

$$F(r) = \frac{Q}{r} = \left\{ \frac{U_1}{\log(r_1/r_a)} - q \cdot \frac{\log(r_1/r_s)}{\log(r_1/r_a)} \right\} \Big/ r$$

by (3)

When we calculate the motion of the ion sheath, we can put

$$F(r) = \frac{U_1}{\log(r_1/r_a)} \cdot \frac{1}{r} \tag{5}$$

approximately, as the largest part of the time is spent in the region $r_s \fallingdotseq r_1$ and $\log(r_1/r_s) \fallingdotseq 0$. Then we have

$$k \fallingdotseq \frac{p}{2p_0} \cdot \frac{\log(r_1/r_a)}{U_1} \cdot \frac{r_1^2}{t_1},$$

neglecting r_a^2 against r_1^2. Similar formula can be obtained for t_2 also.

Table I.

Ar	C_2H_5OH	k
65mm Hg	0mmHg	1.30
80	10	1.02
30	10	0.78
12	10	0.52
0	21	0.33

We can thus determine k for various mixture of argon and alcohol vapor. The results are shown in Table I. The observed values for impure argon and for alcohol alone are both in fair agreement with the widely accepted data. The decreasing tendency of k for increasing alcohol is quite reasonable. It is remarkable that the k values for argon alone and that for 80-mm Hg argon and 10-mm Hg alcohol do not show any remarkable difference in spite of the fact that the counters with argon alone show quite unstable counting characteristics while those with the latter mixture show perfect self-quenching properties. Therefore, it is quite doubtful that the useful self-quenching character of the alcohol-filled counter might be explained by the small value of k.

§ 5. Deadtime of a Counter.

When we observe the counting pulses by intense radiation by a C. R. O. provided with the triggered-sweep circuit already mentioned, we can see such patterns as shown in Fig. 6.* They show that there happens no successive discharge during a certain time interval τ ($\sim 10^{-4}$ sec.) after a primary one, and that the pulses just after τ are relatively small and fluctuating in size, and the size become ordinary after about 10^{-3} sec. This means that there exists certain "deatime" τ characteristic of each counter.

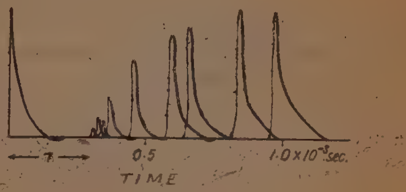

Fig. 6.

---

* Such patterns have been clearly photographed afterwards by O. Minakawa(5) and by C. O. Muelhause and H. Friedman.(6)

The same circuit can also be employed in the study of the time distribution of the "Nachentladungen."(7) Fig. 7 shows an example of N. E. distribution in the case of a gridless counter. It is due to the existence of τ that the N. E. excitation probability is zero just after the primary discharge.

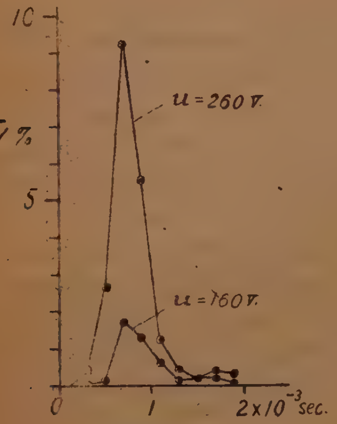

Fig. 7.

We have measured the deadtime for gridless counters with various wall diameters, the results of which are shown in Table II. All counters used were filled with 80-mm Hg argon and 10-mm Hg alcohol.

Table II shows that the deadtime τ is roughly proportional to the square of the counter radius r_c when the 'overvoltage' u (= applied wall voltage U *minus* threshold voltage U_t of the counter) is the same, and decreases when u increases. A typical example is presented in Fig. 8 of the next section. This result can be explained as follows: When the radius of the ion sheath is r_s, the charge Q on the wire is given by

$$Q = cU - 2cq \log(r_c/r_s), \tag{6}$$

Table II.

Counter radius. r_c	(Working voltage) − (Thereshold voltage.) u	Deadtime. τ	$\tau/r_c^2 \times 10^8$
mm	volt	$\times 10^{-4}$sec.	
8	180	0.52	81
11.5	160	1.7	128
12.7	260	1.1	68
20	160	5.2	130
20	260	2.8	70

where

$$1/c = 2 \log(r_c/r_a)$$

analogous to (3). Now it is quite natural to assume that at the end of the deadtime ($t = \tau$, $r_s = r_q$) the charge on the wire should recover the value Q_t at the threshold voltage, namely

$$Q = Q_t \doteq cU_t.$$

Substituing this value in (6), we get

$$u \doteq 2q \log(r_c/r_q), \tag{7}$$

Further, from (4) and (5) in § 4,

$$r_q^2 = \frac{p_0}{p} \cdot k \cdot U \cdot \frac{2}{\log(r_c/r_a)} \cdot \tau \tag{8}$$

and

$$q \backsim u \quad \text{(experimentally)}. \tag{9}$$

Therefore, combining (7), (8) and (9), r_c^2/τ keeps roughly constant so far as the values of U and $\log(r_c/r_a)$ in (8) are nearly the same.

§ 6. Determination of the Ion Quantity from the Observed Deadtime.

From the observed deadtime τ and the ion mobility k above mentioned, we can determine the ion quantity q per unit lengh of the counter for each discharge. Namely, from (7) and (8) (§ 5.),

$$q = u \Big/ \left\{ \log r_c^2 - \log\left(\frac{p_0}{p} \cdot k \cdot U \cdot 2\tau / \log(r_c/r_a) \right) \right\}.$$

An example of the result is shown in Fig. 8. The counter used was filled with 80-mm Hg argon and 10-mm Hg alcohol vapor and $r_a = 0.05$ mm, $r_c = 2$ cm. The observed ion quantity q amounts to about 10^{-10} coulomb/cm, which is considerably greater than so far has been thought(7) (up to 1943). This was checked afterwards by a sensitive galvanometer*.

§ 7. Quenching Mechanism of an Alcohol-Containing Counter

As is mentioned in the last paragraph, the ion quantity q is considerably large and is even larger than the initial charge $Q_0 = cU$ on the wire, if u is sufficiently great. The observed q *vs.* u curve shows a slight bend at the point where q becomes

---

* The results were also in accordance with the experiments formerly performed by T. Tamura, Kyûshû Univ.(8).

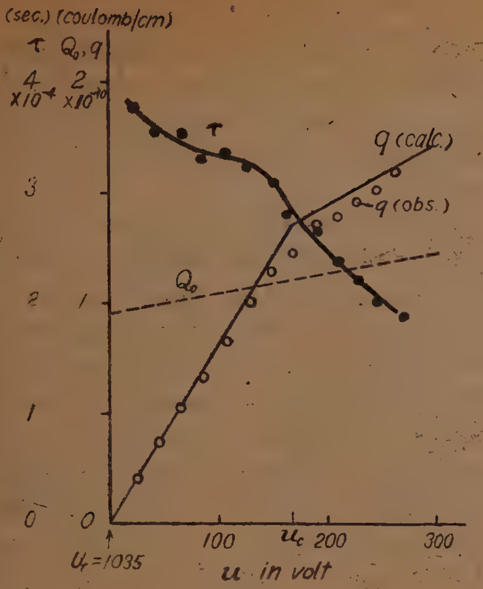

Fig. 8.

a little greater than Q_0. This is also the case when we plot the observed pulse heights on the oscillograph screen against u. To explain this feature, we proceed as follows concerning the quenching mechanism of a discharge. If all the positive ions produced are concentrated very closely to the surface of the central wire when the discharge is quenched (*i. e.* when the growth of the discharge stopped), the electric field near the wire would be inverse in the case of $Q_0 < q$; in this case electrons cannot reach the wire, as they must collide with the gas molecules many times in the inverse field region due to the considerably high pressure. Thus, if $Q_0 < q$, it is natural to assume that the positive ions must be distributed some distance apart from the surface of the wire at the end of each discharge, Q and the field near the wire then being approximately zero. When the positive ions move towards the wall, this field recovers gradually. And when the field takes the same value as that at the threshould voltage, the deadtime is over and the counter becomes ready to the next discharge. On the other hand, when u is not so large and is smaller than certain critical value u_c so that $Q_0 > q$, it is likely that the ions are the more densely distributed the nearer to the wire, which form a different distribution from the case of $q > Q_0$. (See Fig. 9 (a)).

Now the *threshold* condition of a discharge, proposed by Trost ⁽⁷⁾, says that the field strength at

$$r' = r_a + \frac{kn}{p} \qquad (10)$$

takes certain critical value E_{min}, where kn is a constant characteristic to the nature of the gas. We may suppose that the *quenching* condition is also given by this statement.

Adopting such a hypothesis, the large amount of positive ions can be understood as follows. Namely, if the ions are produced inside and outside of r', only those which lie outside of r' weaken the field at $r = r'$, so that the ion quantity are permitted to take a remarkably greater value than is expected when total charge q are thought to take part in reducing the field just at the surface of the wire.

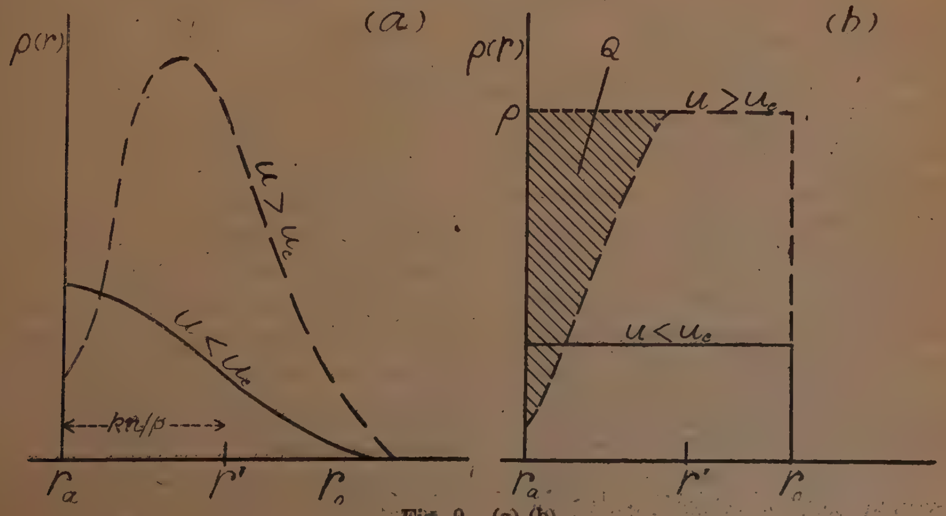

Fig. 9. (a) (b).

Replacing the ion distribution above mentioned (Fig. 9 (a)) by a square-type one for simplicity (Fig. 9 (b)) and assuming our quenching condition, we have tried an approximate calculation of q-u characteristics. Thus we put (for $u < u_c$)

$$\begin{aligned} \rho(r) &= \rho = \text{const.} & r_a < r < r_0 \\ &= 0 & r_0 < r < r_c \end{aligned}$$

where r_0, the outer limit of the ion cloud is treated as an undetermined parameter independent of u, while ρ is to increase with u. Such a simplification makes the electrostatic problem rigorously soluble, and putting the field at $r = r'$ equal to $E_{\min} = 2Q_t/r'$, we get

$$u = \left(\frac{1}{c}+1\right)q - \frac{2r_0^2}{r_0^2-r_a^2}\cdot q\cdot\log\frac{r_0}{r_a} - \frac{1}{c}\cdot\frac{r'^2-r_a^2}{r_0^2-r_a^2}\cdot q. \quad (11)$$

Thus q is proportional to u so long as $u < u_c$. Further when $u > u_c$, q given by (11) results in negative value of Q and the real quantity of the ion is tentatively taken to be equal to q reduced by $|Q|$ approximately, in order to fulfil the condition $Q = 0$.

In the case of Fig. 8, $r_a = 0.05$ mm, $U_t = 1035$ volts, and $kn/p = 0.15$ mm interpolated from Trost's data, so that r' is 0.2 mm. The calculated q *vs.* u curve, assuming $r_0 = 0.237$ mm, is shown in Fig. 8 in a full line, which is in good agreement with the experimental curve. Moreover, r_0 value here assumed is quite consistent with the other facts, *e. g.*, that the growth of discharge is localized in the extreme neighborhood of the wire as shown by many workers(9).

Discharge Mechanism of Geiger-Müller Counters, (II). Experiments with a Separated Cathode Counter.

By Hiroo KUMAGAI, Koichi SHIMODA, Iwao OGAWA,
Yasuo TORIKAI, and Teisuke KODAMA.

Institute of Science and Technology, University of Tokyo.

(Received, June 28, 1948).

§ 8. Apparatus and Circuits.

The counter and circuits used are shown in Fig. 10. The counter wall is made of brass and divided into five parts insulated each other by ebonite rings. The inner diameter of the counter wall is 3.8 cm and the total length is 55 cm. All parts of the divided wall except III (Fig. 10), have mica windows for admittance of β-rays. The central wire of the counter is made of tungsten and its diameter is 0.1 mm. The central wire is maintained at a positive high voltage, 1000 to 2000 volts, and each separated wall is grounded or maintained at a positive or negative low voltage. The pulses from the wall are amplified properly and applied to a C. R. O. or to a "scale of two" counting apparatus.

§ 9. Probability of the Propagation of Discharge.

The counter is filled with 80-mm Hg of argon and 10-mm of alcohol. The middle three, II, III, and IV, or the middle one, III, of the divided parts of wall are maintained at a proper positive voltage by a dry cell and so the electric field at the middle portion of the counter is suppressed. By counting individual pulses from the either end of wall by a scale of two counting apparatus at the various potentials of the central wire, the probability of

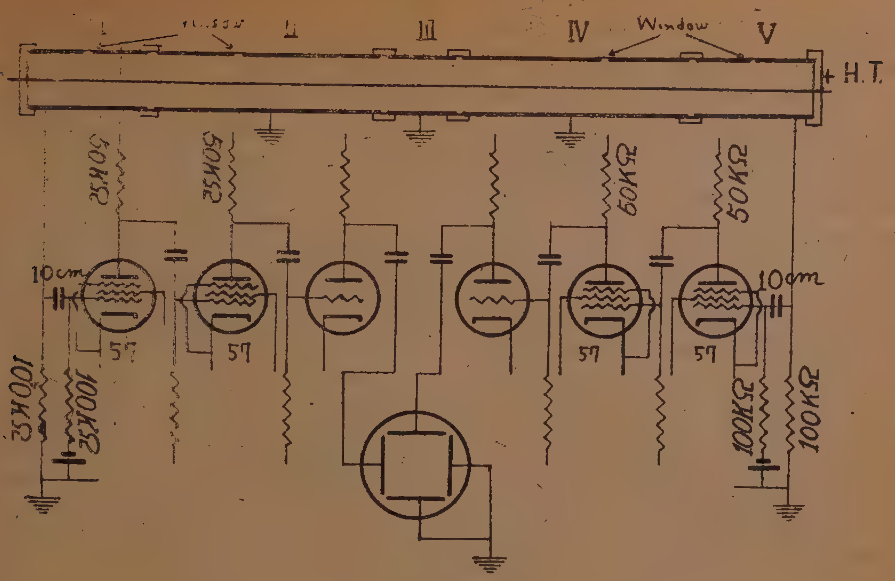

Fig, 10.

the propagation of discharge which depends upon the potential of the central wire is determined in the following way. It is assumed that when β-rays are admitted into I, the counting rate at wall I or V is respectively n_1 or n_2 per minute and when the source of β-rays is removed away, the counting rate is respectively n_3 or n_4 per minute. Thus the probability, α, that the discharge at the region I propagates to the region V, can be computed from

$$n_1 = N + n_3,$$

$$n_2 = \alpha N + n_4,$$

where N is the increment of discharges by β-rays at I per minute

The values of α for various potentials of the central wire are plotted in Fig. 11, the middle three walls being maintained at 135 volts. The curve shows that the probability of propagation is nearly zero at first and becomes perfectly unit above about 135 volts over the threshold voltage. This confirms that photo-electrons liberated from the wall do not greatly contribute to the propagation of the discharge and the discharge grows mainly along the central wire.

§ 10. Probability of Induction of Discharge by Photo-Electrons Liberated from the Wall.

The pulses from walls I and V are applied to

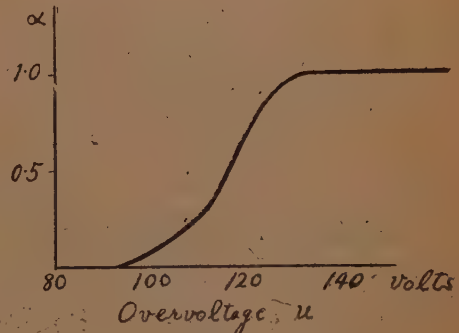

Fig. 11.

abscissa and ordinate axis of the C. R. O. and the β-rays are admitted into I. When the field at the middle portion of the counter is suppressed by the same method as in the previous section, the majority of pulses sweep in the direction of abscissa or ordinate axis independently each other, but a small number of pulses sweeping in the direction of just 45° are observed. And the latter pulses always sweep in the direction of 45° and any delay of the induced pulse was not observed. This shows that a small fraction of discharges in I proceed into V, and the pulses in I and V arise at the same time within 10^{-6} sec. This induction would be caused by the liberation of electrons from the wall or gas by more penetrating photons than those considered in the usual propagation of discharge. The probability of this induction can be estimated by counting sweeps in the direction of 45° on the C. R. O. screen and is plotted against the potential of the central wire in Fig. 12. This probability depends upon the range of portion of the counter at which the field is suppressed but does not depend upon the suppressing voltage. As shown in Fig. 12, this probability is very small and it clarifies that the propagation of discharge takes place immediately along the central wire.

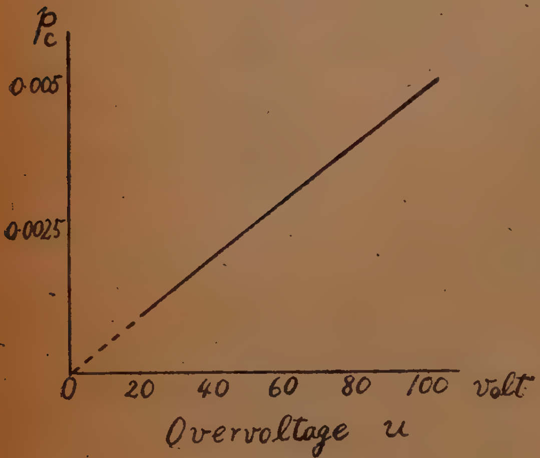

Fig. 12.

§ 11. Velocity of the Propagation of Discharges.

As was described above, it is clear that the discharge in Geiger-Müller counters mainly grows forward along the central wire. In this section we describe on the measurement of velocity of this propagation. It is expected that the measurement of this velocity would play an important rôle in discussing the mechanism of the propagation of discharge. The circuits used are the same as in the previous section. In this case, however, the middle portions of counter wall are always grounded. When two pulses from I and V arise at the same instant, the figure on the C. R. O. screen is such as shown in Fig. 13. (a). When β-rays are admitted into one end of walls, the figures shown in Fig. 13. (b), (c) or (d) are observed. In these figures the pulse in the other end of walls is delayed by the time which correspends to the voltage rise v in the ordinate axis and the time can be calculated from the pulse shape. From this time and the length of counter, the velocity of the propagation of discharges can be measured. In Table III, this velocity in the case that the counter is filled with 80-mm Hg of argon and 10-mm of alcohol is shown as a function of the voltage of central wire. In Fig. 14, the velocity is plotted for various filling gases. The velocity of the propagation of discharge depends upon the field at the middle portion of counter, *e. g.*, when the middle three walls are maintained at some positive potential, the velocity decreases by the reduction of the field at that portion.

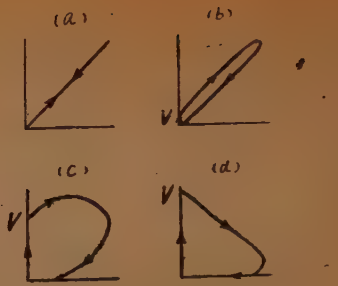

Fig. 13.

Table III.

Voltage of central wire (volts)	Time for propagation (sec.)	Velocity of propagation (cm./sec.)
1120	1.6×10^{-5}	3.9×10^{6}
1140	1.4×10^{-5}	3.7×10^{6}
1160	9.4×10^{-6}	5.2×10^{6}
1180	7.7×10^{-6}	6.0×10^{6}
1200	6.4×10^{-6}	7.2×10^{6}
1220	4.8×10^{-6}	9.6×10^{6}
1240	3.8×10^{-6}	1.2×10^{7}

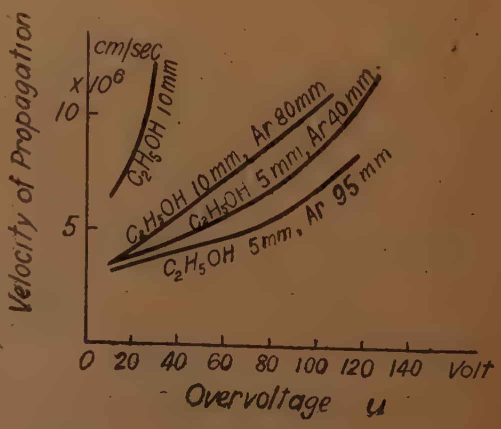

Fig. 14.

The mechanism of propagation would be illustrated by the model shown in Fig. 15. The dis-

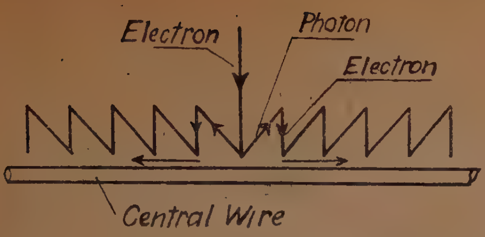

Fig. 15.

charge propagates along the central wire by secondary electron avalanches excited by the preceding one. Most of the electron causing the secondary avalanche are produced within about 1 mm from the wire (9) (10) (11). These secondary electrons are produced probably by very absorbable photons produced by the preceding avalanche. Thus the discharge grows forward by a number of small steps. The length of the path of electrons in each step is about 0.4 mm.(10) Although the mobility of electrons in high field is not known, the time for one step is estimated to be about 10^{-9} sec. When the velocity of propagation is 10^7 cm/sec., one centimeter of the wire is covered by about 100 steps.

Similar measurements of the propagation of discharges have been made recently by Wantuch,(12) Hill and Dunworth,(13) and their results are in perfect accordance with ours.

§ 12. Irregularity of the Size of Pulses.

The size of pulses in Geiger-Müller counter is not constant at the constant supply voltage and the irregularity is observed. Particularly at a little above the threshold voltage, the phenomena appear extremely. As for the main causes of the irregularity, we assume the following three. The first cause is the ripple in the high tension source. This is directly shown by the following experiment. When the ripples in the high tension source are applied to absciassa axis of the C R. O. through a proper condenser and the pulses from the counter are applied to the ordinate axis, then the pulses stand in order of height as shown in Fig. 16 schematically. During low potentials, the variation of heights by the ripple of high tension source is great. Observing figures on the C. R. O. screen in detail, however, there are smaller pulses among the normal ones. These smaller ones would be the second pulses appeared before positive ions formed by the preceding discharge go away sufficiently from the central wire. This is the second cause of irregularity of pulses. In order to observe this effect in more details, the experiments on the propagation velocity were modified and performed where the starting point of pulses is shifted simultaneously by the ripple of high tension source. The circuit used is shown in Fig. 17. The result is schematically shown in Fig. 18. Fig. 18 shows that the smaller pulses among the usual larger ones have smaller velocities of the propagation of discharge and they causes smaller pulses at the opposite end of walls. These facts verify the second cause above mentioned. The third cause for the irregularity of pulse-heights is considered as follows: near the threshold voltage the probability that secondary electron avalanches are excited by the preceding one, is not perfectly unity but a little less than unity. And so the discharge does not propagate completely within the counter but disappears on the way. This suggestion is proved by the following experiments. First, although the ripple of high tension source is minimized as much as possible, the irregularity is yet remarkable near

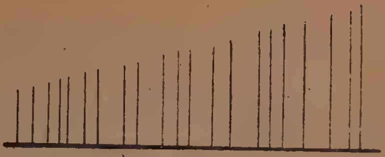

Fig. 16.

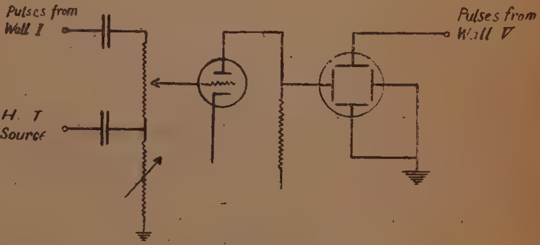

Fig. 17.

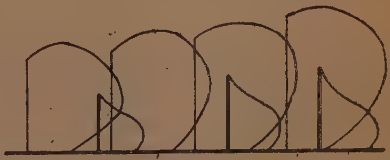

Fig. 18.

the threshold voltage, but when the length of the counter is shortened, the degree of the irregularity diminishes by far and the degree increases with the length of the counter.

Next, we observed the propagation of discharge near the threshold voltage using the same circuit as shown in Fig. 17. The figures observed is schematically shown in Fig. 19. In the region of low voltage, the discharges do not propagate. The limiting voltage below which the discharge does not propagate would be the voltage at which the probability that secondary electron avalanches are excited by the preceding one is unity. Further, Fig. 19. shows that above the limiting voltage there exist yet smaller pulses that do not propagate from end to end of the counter among the normal ones. This would be understood as due to the above mentioned second cause.

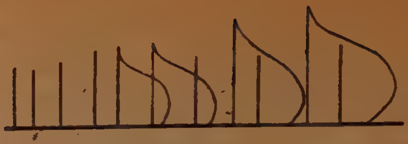

Fig. 19.

Discharge Mechanism of Geiger-Mlüler Counters, (III). Origin of the "*Nachentladung*".

By Hiroo KUMAGAI, Koichi SHIMODA, Iwao OGAWA,
Yasuo TORIKAI, and Teisuke KODAMA.

Institute of Science and Technology, University of Tokyo,

(Received, June 28, 1948).

§ 13. The Time Distribution of N. E.

If N. E. were to take place when the positive ions reach the counter wall, this must be clearly demonstrated in the observed time distribution of N. E. Our result with a gridless counter (*e. g.* Fig. 7, part I), however, shows that almost all the N. E. occur before the positive ions reach the wall.

Moreover, we have observed the time distribution of N. E. in the case of double-grid counters at various grid voltages. The results are shown in Fig. 20, where $\overline{w}$ denotes the observed probability of N. E. in each time interval of 0.9×10^{-4} sec. after a primary discharge, and the applied inner grid voltage is shown as U_t (threshold voltage) $+u$(over voltage). Further, the notation (5 acc, 10 ret) means the application of 5 % voltage between the inner and outer grids, 10 % voltage between the outer grid and the cathode wall, taking the voltage between the wire and the wall as 100 %. The notation "ret" designates the retarding field for the photoelectrons from the wall, and "acc." represents the accelerating field.

We see in Fig. 20 that the distribution in the case of (5-5 ret.) is quite similar to that of a gridless counter (Fig. 7). In the case of photo-electron accelerating field between the grids and the wall, characteristic types are obtained in each cases. Generally speaking, certain peaks in the curve becomes prominent when the overvoltage becomes greater. These peaks correspond to the time just after the ions pass through the inner or outer grid. Besides, on observing the pulse form from the outer grid, it was found that certain characteristic pulses (as shown in Fig. 21) appeared very frequently just in the time interval where $\overline{w}$ shows prominent maximum. This must be considered as a

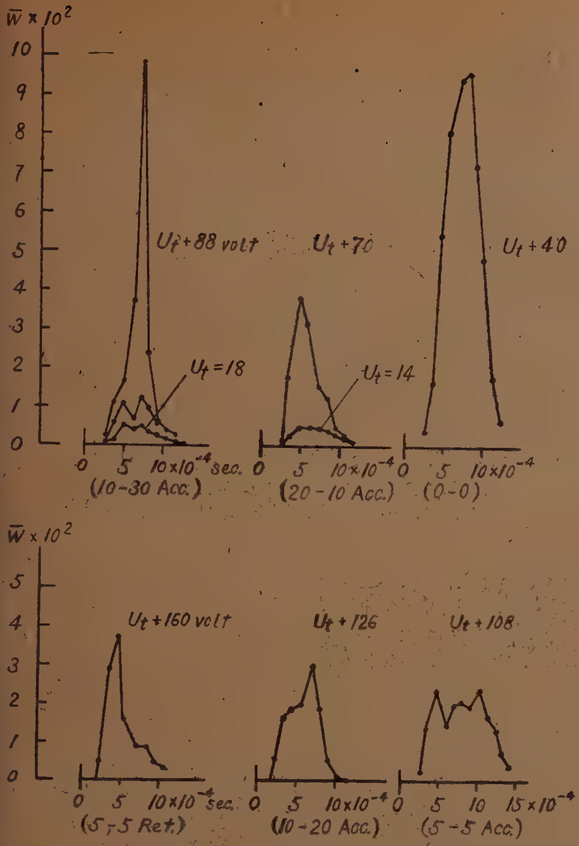

Fig. 20.

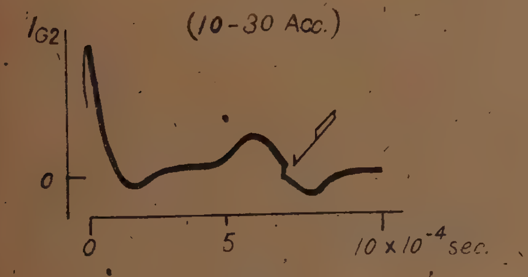

Fig. 21.

result of small discharge in the vicinity of the corresponding grid caused by the electron liberated from the gas by certain action of positive ions when they pass through the somewhat stronger field between the grids and the wall. If the liberated electron is not directed to the grid but accelerated toward the wire, it would give rise to a N.E. Taking account for the existence of such a phenomena, it may be concluded that the great multitude of the positive ions produce some electrons in the gas by certain unknown mechanism when they come to the field of about 500 Volt/cm.

When the overvoltage u is smaller, positive ions come already to the weak field during the deadtime, causing relatively small number of N.E. by this mechanism. When u becomes greater, however, deadtime becomes smaller, and the positive ions are as yet located in the appreciably strong field at the end of deadtime. This may result in an abundance of N.E. due to the mechanism discussed above.

One of the probable mechanism of this liberation of electrons by positive ions will be the electron emission by the impact of metastable ions with other molecules.

§ 14. Special Type Double-Grid Counter with Divided Wire.

In order to investigate the induction of discharge in the other part of the counter by the photoelectrons from the wall, a counter of the special type as illustrated in Fig. 22, was constructed. The central wire is divided and insulated each other by a thin glass rod, and the both grids are located relatively in such a way that the photons emitted near the wire do not hit the outer grid. Grids and the wall are all made of brass.

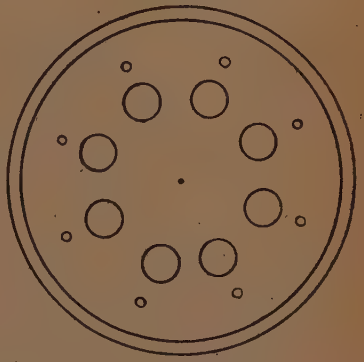

Fig. 22.

The obtained probability p_c for the induction of discharge by the discharge in the other part of the counter are plotted in Fig. 23, against the inner grid voltage U_{g1} for various field distribution between grids and the wall. We find that p_c varies remarkably as the field distribution changes. The result seems to confirm the fact that the induced discharges are caused by photoelectrons liberated from the wall or the grids. Namely, q_c vs. U_{g1} curves for various cases coincide splendidly so far

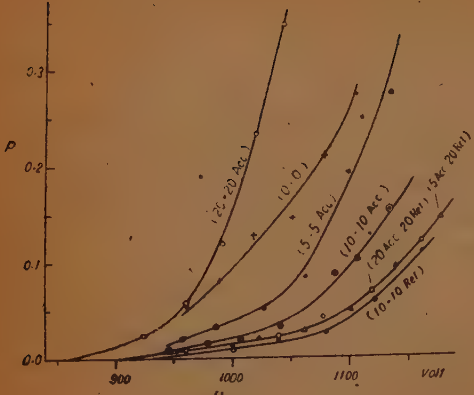

Fig. 23.

as the field between the outer grid and the wall is directed to retard the photoelectrons from the wall, taking account of the difference in the threshold voltage. In these cases, the sense of the field between the inner and outer grids plays no rôle because no photo-electron is liberated from the outer grid. The observed p_c must be all due to photoelectrons from the inside surface of the inner grid. Besides, p_c-value in the case of (5-5 acc.) is about three times as much as that of (10–10 ret.), which is explained clearly as the ratio of solid angle effective for the photo-electron liberation. Moreover, the curves for (5–5 acc.) and (10-10 acc.) show complete similarity. This is understood because the phenomena of the photoelectron liberation is independent of the field strength near the surface. Application of too strong field near the grid (20-20 acc.) causes small increase in p_c. This is perhaps due to small discharge near the grid and emission of penetrating photons in this region.

§ 15. Photoelectron as a Cause of N.E.

Fig. 24 shows the probability p of N. E. in the special counter described in § 14. There are found some relations between this figure and Fig. 23.

(i) Firstly, p-curves seem to be decomposed into two parts, namely first part of small inclination and second part of large inclination. And the part of small inclination keeps the same form so long as the field between the outer grid and the wall is in the sense of electron retarding, and the p-values are smaller than any other cases. This seems to be an evidence that photoelectrons are one of the origin of N. E. The part of large inclination of p-curve is likely, on the other hand, to correspond to the unknown action of positive ions.

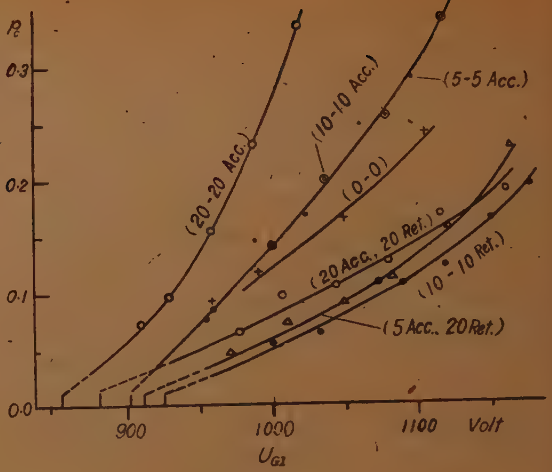

Fig. 24.

(ii) Secondly, it is seen that p decreases appreciably when the field between the two grids increase in the sense of electron accelerating, so far as the field does not exceed too great a value.

As for the question how the photoelectrons, liberated instantaneously after the primary discharge, give rise to a delayed N. E. with such a long time interval as $10^{-4} \sim 10^{-3}$ seconds, there is as yet no decisive confirmation. From some basis, however, it may be plausible that the photoelectrons are captured by some of the gas molecules and form so-called negative ions. According to their small mobility, they are able to cause N. E. in the time interval just observed.

Moreover, if we assume that the electrons are more likely captured by gas molecules in a weak field than in a strong field, our result on the time distribution of N. E. by (5-5 acc.) and the large value of p in the absence of field between grids and the wall (Fig. 24) are explained easily.

Although we have made some assumptions on the origin of N. E. on the basis of our experiments, many further experiments should be carried out in order to decide the real origin of N. E. completely.

§ 16. Summary of Discussions.

Summarizing the fact hitherto established, it is possible to outline the discharge process in G—M counters as follows ;—

(i) A discharge grows in such a way that an electron avalanche taking place in the neighborhood of the wire due to the primary electrons, in turn gives rise to another avalanche and so on. Thus more and more avalanches take place along the central wire, until the production is stopped by the shielding action of the accumulated ion cloud.

(ii) The outer limit of the ion cloud at this instant is roughly given by r_0 (§ 7), which also stands for the starting point of the avalanches.

(iii) The probability that an avalanche induces another one becomes unity when the field at $r' = r_a + kn/p$ takes a certain value E_{min} ($\doteqdot 2Q_t/r'$). The discharge growth is possible whenever the field $E(r')$ exceeds E_{min}. The same condition is valid for both cases of starting and quenching of the discharge.

(iv) Several experiments, especially measurements on the discharge spread along the wire in § 11, suggest that the successive induction of avalanches might be caused by the very absorbable photons (mean range r_0) through the photo-ionization processes. These photons are produced by the preceding avalanche.

(v) After the discharge growth comes to an end, the produced ions move towards the wall, so that the shielding action of the ions decreases gradually, and when the field near the wire is recovered to the threshold value, the deadtime is over and the counter is again ready to the succeeding discharge.

(vi) As to the origin of the N. E., we have obtained the conclusion that there seems to be two kinds of N. E., *i. e.* those which are caused by photoelectrons liberated from the wall, and those caused by positive ions through certain unknown mechanism. Decisive conclusion, however, cannot be drawn until more critical experiments are performed. Along this line, Dr. Minakawa(14)(15)(16)(17) has reported many excellent and interesting researches, especially about the so-called "*Spontan-entladung.*"

References.

(1) K. Shimoda and I. Ogawa ; J. Phys.-Math. Soc. Japan **17** (1943), 235, 241, 489, 491. (in Japanese).

(2) K. Shimoda and I. Ogawa ; Proc. Phys.-Math. Soc., Japan **25** (1943), 445.

(3) Y. Torikai and T. Kodama ; Proc. Imp. Acad., Tokyo **19** (1943), 481

(4) Y. Torikai and T. Kodama ; Proc. Phys. Soc., Japan **2** (1947), 6. (in Japanese).

(5) O. Minakawa ; Proc. Imp. Acad., Tokyo **19** (1943), 642.

(6) C. O. Muelhause and H. Friedman ; Rev. Sci. Inst. **17** (1946), 506.

(7) A. Trost ; Zeits. f. Phys. **105** (1937), 399.

(8) T. Tamura ; Report of Researches, Faculty of Science, Kyûshû Univ. (Phys. Part) **1** (1945), 27.

(9) H. G. Stever ; Phys. Rev. **59** (1941), 765.

(10) O. Minakawa . Proc. Imp. Acad., Tokyo **18** (1942), 468.

(11) H. Aoki and others ; J. Phys. Math. Soc. Japan **16** (1942), 65, 388. (in Japanese)

(12) E. Wantuch ; Phys. Rev. **71** (1947), 646.

(13) J. M. Hill and J. V. Dunworth ; Nature **158** (1946), 833.

(14) O. Minakawa ; Proc. Imp. Acad., Tokyo **18** (1942), 468, 644 ;

(15) O. Minakawa ; *ibid.* **19** (1943), 19, 246, 377.

(16) O. Minakawa ; *ibid.* **20** (1944), 288.

(17) O. Minakawa ; *Kagaku* **14** (1944), 18, 125, 212.

Specific Heat and Thermal Expansion of $BaTiO_3$.

By Shozo SAWADA and Gen SHIRANE.

The Second Faculty of Engineering, University of Tokyo.

(Received June 30. 1948.)

Abstract.

The specific heat and thermal expansion of barium titanate ceramics were measured between room temperature and 250° C., and their anomalies were confirmed. The specific heat, that was measured by Sykes' method showed a λ-type anomaly at the Curie temperature, but the magnitude of the anomaly at the peak was considerably small, amounting to only 0.005～0.015 cal/gr. °C. We measured the thermal expansion with an optical dilatometer, and observed a contraction in the transition region. The thermal expansion coefficient showed a negative peak at the Curie temperature. The specific heat and thermal expansion vs. temperature curves and the positions of their peaks varied slightly for different samples by the condition of their preparation.

§ 1. Introduction.

A few years ago, remarkable dielectric properties of barium titanate $BaTiO_3$ were discovered. The dielectric constant of this material is very high and moreover shows a peak at about 105～125° C. From these facts it is expected that there will probably be a phase transition at this peak point and this transition will be accompanied with anomalies of specific heat and thermal expansion.

In order to ascertain this point, we measured these quantities. At first, measurements were performed in air, then in vacuum. Results were not different essentially in both cases. Measurement in air was already reported briefly in a short note of this Journal(1). In the course of our experiment, we found several papers on the electrical and thermal properties of this peculiar material. The comparison of our result with another authors will be mentioned later.

§ 2. Preparation of Samples.

Samples were ceramic barium titanate sintered in a gas furnace. At first, $BaCO_3$ and TiO_2 were sieved and mixed in a mole ratio 1 : 1. To obtain an intimate mixing these were suspended in distilled water and stirred completely, then dried and the lumps were ground. The powdered preparations were pressed into discs (diameter 5cm, thickness ca. 1cm). Then these were embedded in pure Al_2O_3 powder in a crucible and sintered in a gas furnace using the oxidizing flame. Temperature was raised up to about 1400°C during 5 hours, and maintained at this temperature for about 1 hour, then cooled during about 10 hours to room temperature. The matures were a little porous. (Sample B.)

To obtain nonporous bodies, pressed material was calcined for 1 hour, before sintering, at such temperature that the calcines still retained property of forming compact masses when pulverized and again subjected to pressure (about 1250°C). The finely ground calcines (sometimes moistened with water) were pressed again and sintered at 1400°C as before. The matures are hard and nonporous. (Sample A.)

To determine the Curie temperature of the sample, the dielectric constant ϵ was measured by a quartz oscillator with frequency 1303 k. c., and will be illustrated later, comparing with specific heat and thermal expansion data.

§ 3. Specific Heat.

a) Apparatus and measurement.

Apparatus for our measurement of specific heat C_p of the sample is shown in Fig. 1 (reduced size 2/3). The method is similar to that of Sykes'(2), but several points are modified so as to fit powdered insulator samples. The sintered material is finely pulverized and contained in a copper vessel b whose content is 5 c.c., and the heating energy is supplied by the heater h_1 which is embedded in the sample directly.

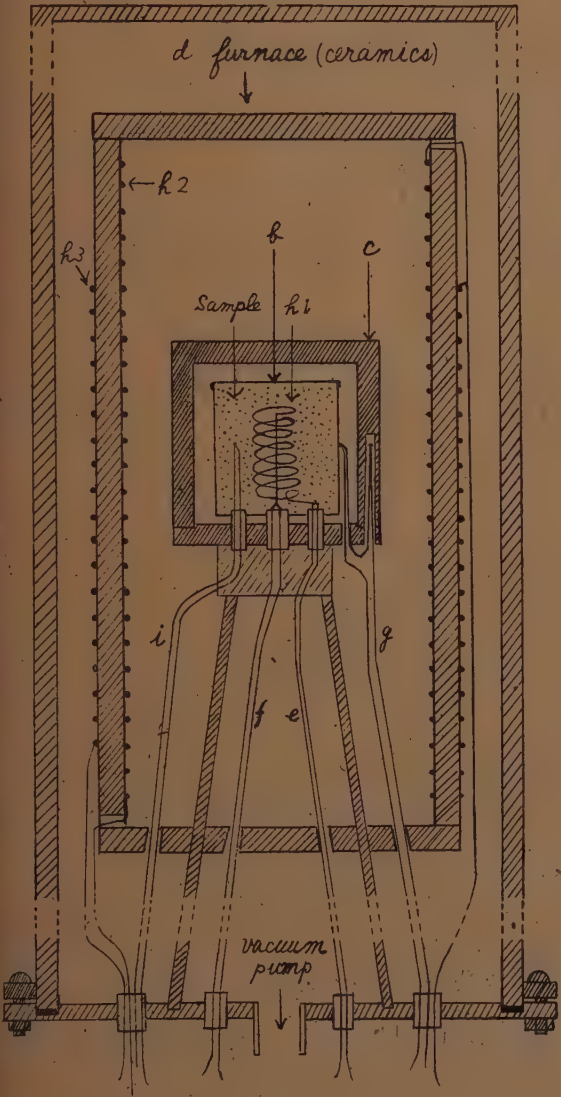

Fig. 1

Fig. 1. Apparatus for measuring the specific heat.

Vessel b is surrounded by a copper case c, and this case is heated by the electric furnace d, which has two heaters h_2 and h_3. The ratio of the currents of these heaters is varied so that the temperature distribution in the furnace is almost uniform.

Heating the sample by heater h_1 (its voltage being held constant), the temperature difference between b and c is measured by alumel-chromel differential thermo-couple g(10^{-7}V./div.) and is made zero by adjusting carefully the currents of heaters h_2 and h_3. There would be in principle no transfer of energy between b and c, and all the energy from heater h_1 would be used to raise the temperature of the sample. Measuring the temperature of the sample by alumel-chromel thermo-couple i and a potentiometer of the precise class, the specific heat of the sample is obtained by a simple calculation. But in practice, there may be some energy transfer between b and c caused by a slight non-uniformity of the temperature distribution inevitably presents in the azimuthal and vertical directions; this energy transfer and C_p of vessel b and heater h_1 etc., (called C_x), are included in directly observed specific heat and this value was estimated by measuring the specific heat of SiO_2, which was determined precisely by Moser(3); this energy is about 1/4 of that supplied by heater h_1. Thus the C_p of the sample can be calculated by the formula

$$mC_p = \frac{vi\Delta t}{J\cdot\Delta T} - C_x,$$

where J is the mechanical equivalent of heat; Δt time required to raise the temperature of the sample by ΔT; v, i voltage and current of heater h_1 respectively, measured through lead wires e and f; and m the mass of the sample (ca. 15gr.). At first, measurements were carried out in air, and then in vacuum. For the removal of the moisture, samples were thoroughly preheated in both cases.

Electric furnace d, which has two heaters inside and outside of the ceramic holder, is suitable to keep the temperature difference between b and c zero, since the inside heater can vary the temperature of c with little time lag. This fact is very important in practice especially near the Curie point. The temperature difference between b and c is smaller than 1/100°C. in our experiments. The outside heater changes the temperature distribution and diminishes the transfer of energy between b and c. This apparatus was set in a vacuum vessel.

In practical measurements the value of ΔT was in general chosen so as to correspond to 0.1 mV, of alumel-chromel thermo-couple (ca. 2.4°C.), and 0.05 mV. near the Curie point. The heating rate was about one degree per minute.

b) Results and discussions.

We measured the specific heat of several samples, and observed the λ-type anomalies at the Curie temperature. A typical C_p vs. temperature curve is illustrated in Fig. 2. This sample A, that was sintered at 1400°C. after calcination at 1250°C., is hard and nonporous.

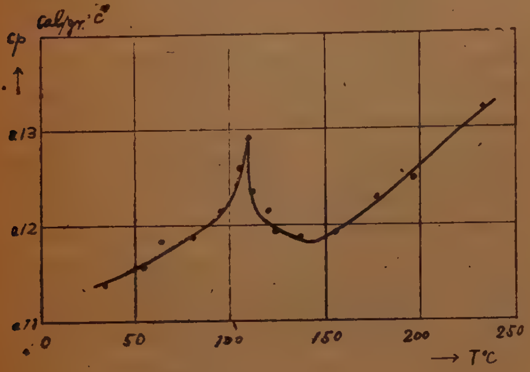

Fig. 2

Fig. 2. C_p of sample A

As is shown the anomaly is considerably small and the magnitude of the anomaly at the peak is about 0.010 cal./gr.°C for this sample. Latent heat was not observed. Some of the measuring points are illustrated in figure with solid circles. The peak of C_p is at 112°C. (±2°C.) for this sample. For reference, the dielectric constant ε of this sample is shown in Fig. 3. The peak of C_p and ε are observed at nearly the same temperature. The degree of sintering and other conditions shift the position of the peak between 105~115°C. and change the form of the curve slightly. For example, C_p of sample B that was sintered at 1380°C. without calcination is shown in Fig. 4.

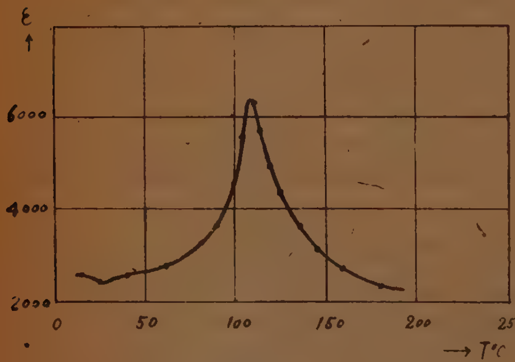

Fig. 3

Fig. 3. ε of sample A

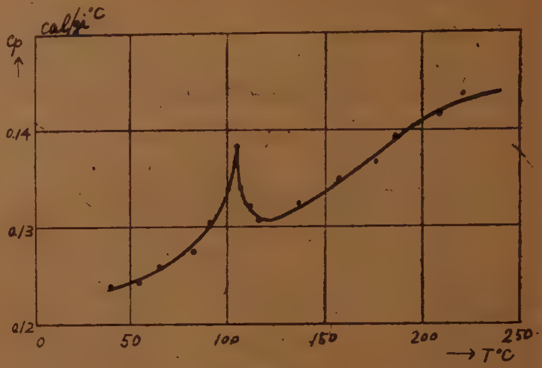

Fig. 4

Fig. 4. C_p of sample B

As can be seen from Fig. 1, the radial temperature distribution in the sample is not uniform, so the thermo-couple shows the temperature of the sample only in the average, and Δt is the time necessary to heat the sample in some temperature range. As the thermal conductivity of $BaTiO_3$ is much lower than that of metals this effect is not negligible, especially near the Curie temperature. For this reason, the form of the peak is apt to be deformed. Moreover, the great change of the specific heat in this range makes it difficult to keep the temperature difference between b and c zero, and in consequence observed values fluctuate. A secondary small hump was observed in many cases at about 10°C. above the Curie point, but its amount is almost comparable with fluctuations of observed values and the existence of this hump has not yet been confirmed.

So far as we can know at present, Vul and Goldman(4) observed an abrupt change of the specific heat at 125°C (details of it can not been known); Miyake and Ueda(5) expected an anomalous change of the specific heat in a wider temperature range; and Harwood, Popper and Rushman(6) observed a change in the C_p amounting to about 0.0025 cal./gr.°C. From the reasons mentioned above, it is difficult to ascertain which of the abrupt change and the λ-type anomaly actually occurs.

§ 4. Thermal Expansion.

a) Apparatus and measurements.

The thermal expansion was observed by a dilatometer of a new type illustrated in Fig. 5 (reduced to 1/3 of the original size). The two quartz rods (radius r) are held between the two samples of about 4 cm. in length (l and l') and quartz holder. The rotation of rods, caused by the thermal dilatation of the samples is observed by mirrors attatched to their ends, using telescope and scale. Linear thermal expansion coefficient β is calculated by the equation

$$\beta = \frac{2r}{(l+l')(2D+a)} \cdot \frac{\Delta x}{\Delta T} + \beta',$$

where a is the distance between two mirrors, D the scale distance, Δx the change of scale reading in the temperature range ΔT, and β' the thermal expansion coefficient of the quartz holder. When $D = 300$cm. and $r = 0.15$cm., this apparatus allows us to measure the dilatation such as $\Delta l/l = 10^{-6}$. To make the temperature distribution in the furnace uniform, temperature of three points inside the furnace are measured by three thermo-couples, inserted as shown in the figure, and the currents of three heaters h_1, h_2, and h_3 are adjusted appropriately. The electric furnace is set in a vacuum vessel which has two windows in the path of light and four windows in the lateral sides so as to make the mounting of samples easy.

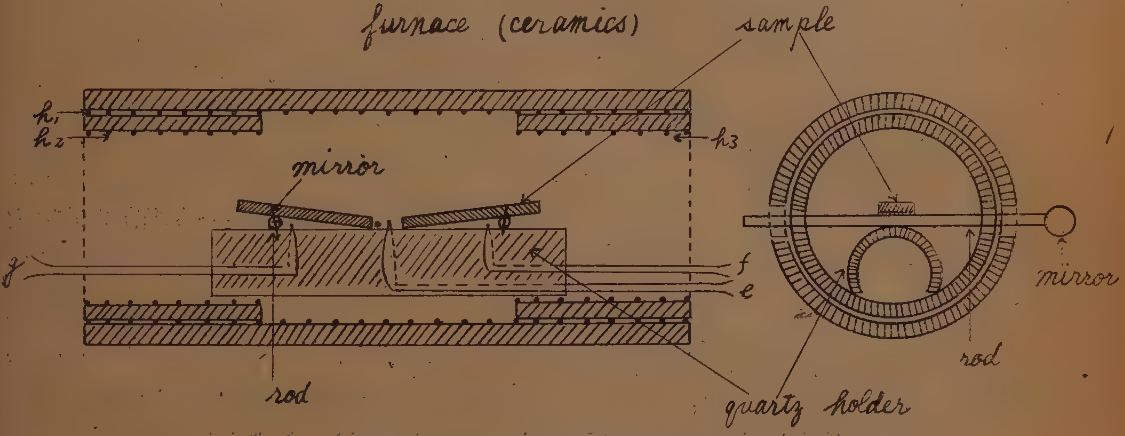

Fig. 5 Apparatus for measuring the thermal expansion.

This apparatus is very simple, so there is no room for various errors to enter. Only possible source of error is a slip between samples and quartz holder or rods; this fear can be removed by the fact that the scale reading coincides exactly at heating and cooling measurements. The value of thermal expansion coefficient of copper measured by this apparatus is in good agreement with those of other authors.

b) Results and discussions.

An example of observed values of the thermal expansion of sample A is shown in Fig. 6 and 7; Fig. 6 shown directly the scale reading, which is proportional to length at each temperature. Using these values the thermal expansion coefficient β is obtained and plotted in Fig. 7. It can be seen from the figure, β decreases gradually from room temperature, and a contraction is observed in the range of 10°C near the transition point. In this sample, a negative peak was observed at 106°C (±2°C.). For both heating and cooling the same curve was obtained within the accuracy of our measurement.

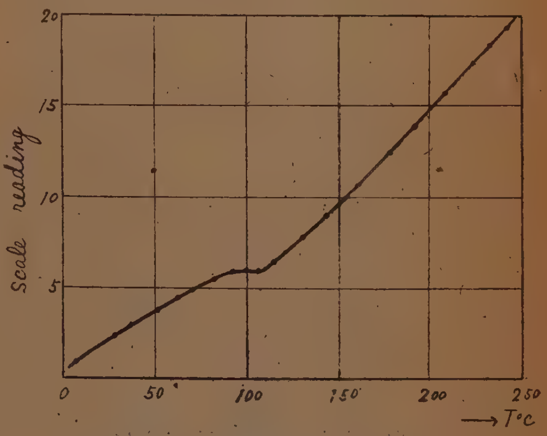

Fig. 6

Fig. 6 Scale reading of sample A.

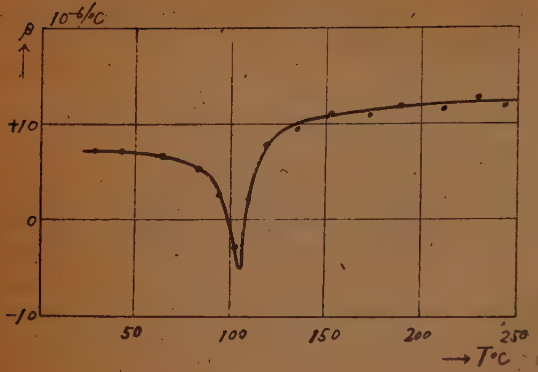

Fig. 7
Fig. 7 β of sample *A*.

As in the case of the specific heat, the position of the peak and the form of the curve vary slightly for different samples; but the result is reproducible with the same sample. When a sample contains impurities or the sintering is not complete, the minimum of β is observed, but contraction does not occur. For example in Fig. 8, β of sample *B* 's plotted. Also for a sample in which no contraction occurs, this can be observed after the more complete sintering. This fact will be explained assuming that the more complete sintering changes the sample into the more complete barium titanate crystals.

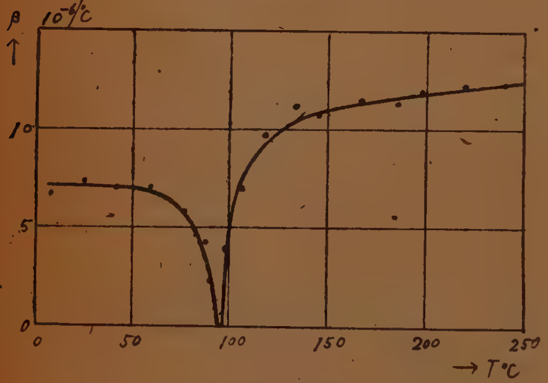

Fig. 8
Fig. 8 β of sample *B*.

Our observed value of the thermal expansion coefficient agrees well with that determined by X-ray investigation. Ueda(7) observed an anomaly of the cubic expansion coefficient near the transition point, using liquid paraffin. And von Hippel and co-workers(8) measured β between −80°C and 1200°C, using a simple dilatometer, and in their experiment the sample showed practically no increase in length in the neighbourhood of the transition point. We consider that, however, it would be difficult to ascertain the small contraction as we have observed with the precision of their apparatus.

§ 5. Conclusion.

The facts reported above confirm the anomalies of the specific heat and thermal expansion. Of course, it is desirable to perform measurements, especially of the thermal expansion coefficients in the three crystallographic axes, with single crystals.

But it will not be probable that the specific heat is essentially different in ceramics and single crystals, although there can be much internal stress in ceramics than in single crystals. In order to determine precisely the integrated value of the anomaly, the entropy change in the transition and the form of curves, accuracy of our measurement is not sufficiently high. Although their determination is very important in order to decide the true nature of the transition, difficulties are very great from the inevitable restriction on measuring the specific heat of such powdered insulators.

In conclusion, we wish to express our sincere thanks to Prof. Y. Takagi and Mr. S. Nagasaki for their kind encouragement in the course of our experiment.

References.

(1) S. Sawada, G. Shirane and H. Sugawara: J. Phys. Soc. Jap., **2** (1947), 90.
(2) C. Sykes: Proc. Roy. Soc., A **143** (1935), 422.
(3) Moser: Phys. Zeits., **37** (1936), 737.
(4) B. M. Vul and I. M. Goldman: C. R. U. S. S. R., **49** (1945), 177.
(5) S. Miyake and R. Ueda: J. Phys. Soc. Jap., **1** (1946), 32.
(6) M. G. Harwood, P. Popper and D. F. Rushman: Nature, **160** (1947), 58.
(7) R. Ueda: Lecture at the Annual Meeting in 1947 of the Physical Society of Japan.
(8) A. von Hippel, R. G. Breckenridge, F. G. Chesley and L. Tisza: Ind. and End. Chem., **38** (1946), 1097.

Short Notes

A New Absorption Band in Colored Rock-Salt Crystal.

By Yoichi Uchida, Masayasu Ueta and Yoshio Nakai; *Department of Physics, Faculty of Science, University of Kyoto.* (Received: November. 5, 1948)

In absorption in addition to well-known F, F' and U bands of colored alkali halide crystals, M, R and V bands have been also discovered in the absorption spectrum of KCl crystal, and a number of notable properties of all these bands were summarized in Seitz's recent paper(1).

Besides these we have found a new band called K. The purpose of this note is to describe conditions for appearance and some properties of this band.

K band may be induced in the clear rock-salt crystal by pushing electrons in from a pointed cathode, just as the case of F center(2) except the crystal is at the temperatures below about 420°c. Another procedure is as follows: F centers are produced by pushing electrons in from a pointed cathode at about 570°c as usual and the crystal is quenched to below 450°c, then an electric field of about 300volt is applied with flat electrodes. By this process, F decoloration fades away, and the sample shows the new absorption.

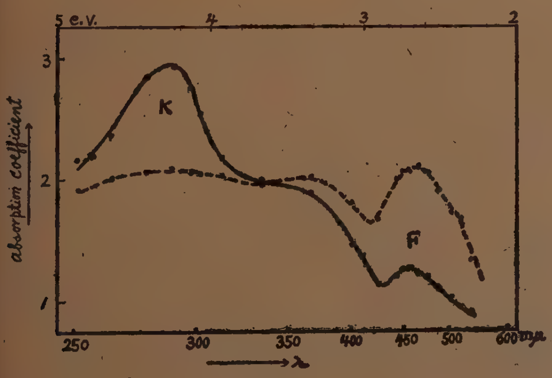

Fig. 1

Absorption curve of NaCl containing K-center (full line), and the same, after losing the power of luminescence (dotted line).

Crystals prepared by the above two methods give almost identical absorptions (Fig. 1). It has a principal maximum at 290m μ (K-band) and a subsidiary maximum of F center. The continuum ranging between K and F may be ascribed to a colloid, for it appears also in a crystal previously colored by F center and then it is diffused away by heating.

When irradiated by the light lying in the new absorption, it is found that the sample shows luminescence with its maxima coinciding with F and F' emission bands due to the transitions from the bottom of the conduction band to the ground states of F and F' centers respectively. By continued irradiation, however, the power of luminescence fades. The absorption curve of a crystal which has lost luminescence-power was examined. It will be seen that absorption coefficient decreases at K and increases at F bands (Fig. 1).

Now Seitz(3) and others suggested that at lower temperatures densities of pair or quartet of vacancies increase in NaCl crystal. If a quartet captures an electron, the binding force of positive ion vacancies will decrease and they repel each other and there will remain a F_2^+ center i.e. a center consisted of two negative ion vacancies plus an electron. F_2 center may have a higher ionization potential than F center, for, from Franck-Condon curves imagined for formations of F_2^{2+} from $F^+ + F^+$ and F_2^+ from $F + F^+$ respectively (Fig. 2), the distance between AB corresponding to ionization energy of F center must be smaller than that of CD corresponding to K absorption. Then, if we suppose the carrier of K band is identical with F_2^+ center, the K band would situate at shorter wavelength than F band as observed, and the dissociation energy of K center may be below 1.7 e.v.

Another support for our picture mentioned above will be as follows: when crystal containing F center is heated at about 450°C without electric field, decoloration disappears very rapidly. This phenomenon has been interpreted as separate

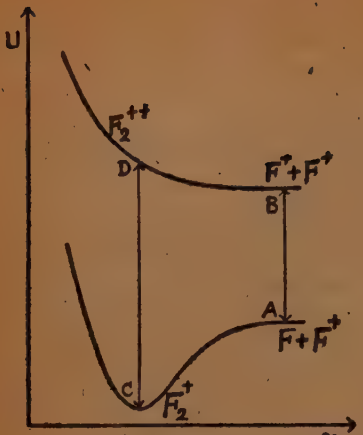

Fig. 2
Franck-Condon curves for K and F absorption.

diffusion of electrons and negative ion vacancies dissociated from F centers. Similar experiment was carried out on the crystal containing K centers. K decoloration is found to disappear appreciably only at temperatures higher than 550°c, showing the higher ionization potential of K than F center.

An incident light-quantum may excite an electron into the conduction band from K center, which will immediately dissociate into two negative ion vacancies. Stepwise recombinations of the conduction electron with a negative ion vacancy and then with the F center produced will radiate F and F' bands respectively. Hence this process transforms K centers into F centers.

Detailed results will be reported later on.

References.

(1) F. Seitz, Rev. Mod. Phys. **18**, (1946) 384
(2) R. W. Pohl, Zeits. f. Metallkunde **26**, (1934) 217; A. L. Hughes, Rev. Mod. Phys. **8**, (1936) 299
(3) F. Seitz, loc. cit.

Variation of the Capacity of Crystal Rectifiers with Bias.

Akio Kobayashi and Kenzi Arita; *Research Laboratory, Tokyo Shibaura Electric Co. Kawasaki, Kanagawa-ken.* (Read October 6, 1947, Received August 11. 1948)

It was cleared by Schottky and Deutschmann(1) that the capacity of cuprous oxide rectifiers varied with bias. According to the modern theory(2), this effect is attributed to the ionized layer of impurity centers near the surface of the semi-conductor. Fig. 1 shows the energy levels at the contact between metal and semi-conductor. The capacity per unit area is given as follows:

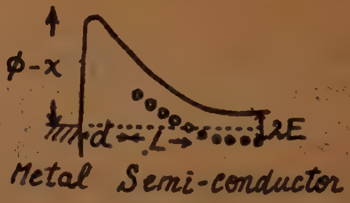

Fig. 1
Energy levels at the contact between metal and semi-conductor.

$$C=\frac{\varepsilon}{4\pi}\left(d^2+\frac{\varepsilon(V_0'-V)}{2\pi eN}+\frac{2\varepsilon hT}{\pi e^2N^2}sinh^2\frac{E}{2kT}\right)^{-\frac{1}{2}}, \qquad (1)$$

where d is the thickness of the stoichiometric layer, ε the dielectric permittivity, E the activation energy of impurity levels, N the concentration of impurity levels, V applied voltage, $V_0'=\phi-\chi-2E$, ϕ the work function of Cu, χ the electron affinity of Cu_2O.

Then

$$\frac{1}{C^2}=\frac{4\pi}{\varepsilon}\left\{d^2+\frac{\varepsilon(V_0'-V)}{2\pi eN}+f(T)\right\} \qquad (2)$$

Thus, plotting $1/C^2$ for biases, we must have a line whose slope is determined by concentration of impurity centers N. The value of d is determined by the point where the line crosses with the abscissa, neglecting the temperature dependent part and putting in eq. (2) V_0' which is given by another experiment.

The authors measured the impedance of a Cu_20 rectifier in the range from 2 volts in the easy flow direction to 3 volts in the hard flow direction. The results are shown in Fig. 2. We obtained by static current *vs.* voltage characteristics 0.7 eV for the value of ϕ-χ, and by its temperature dependence 0.2 eV for E. Therefore $V_0'=0.3$ volts.

By inclination of the curve in Fig. 2 we obtain the value N

$$N=5\times10^{15} \text{ per cm}^3.$$

This value agrees with the value Ng iven by the

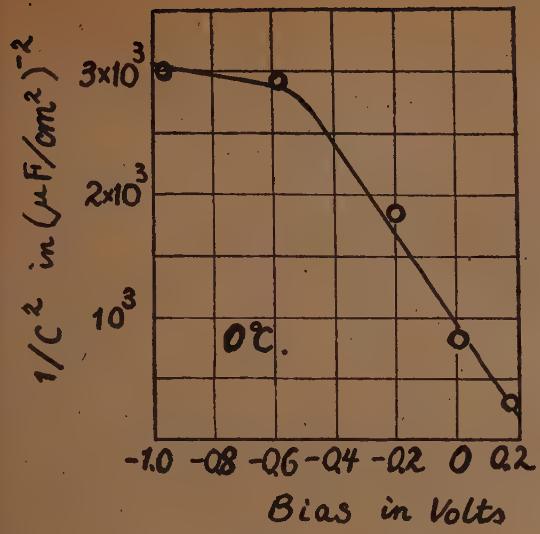

Fig. 2

Fig, 2 $1/C^2$ versus V curve.

capacity at zero bias. The observed V_0' is 0.25 volt. Therefore d may be neglected for our sample. The centers of circles of impedance diagram were deviated at large biases in the direction of easy flow and they were not circles by closer experiments.

References

(1) W. Schottky and W. Deutschmann, Phys. Zeits. **30**, (1929) 839.

(2) R. Kubo, Proc. Phys. Soc. Japan (in Japanese), **2**, (1947) 108.

H. A. Bethe, see Torrey and Whitmer, Crystal Rectifiers, p. 73, (1948).

On the Laminar Sub-Layer in the Turbulent Boundary Layer, I.

By Yutaka SHIGEMITSU.

Railway Technical Research Institute, Tokyo.

(Read March 28, 1948 ; Received June 2, 1948).

Summary of Parts I–III.

The purpose of the study dealt with in this paper is to investigate the state of flow near the surface of a body in a turbulent boundary layer and to contribute to the theories of surface friction or heat transfer in turbulent motion. In part I, the mechanism of the flow in a laminar sub-layer is explained with a conception of the stability of laminar boundary layer ; and the equations of motion and the boundary conditions are derived. In Part II, a method of an approximate solution is shown for the flow along a flat plate, and the solution is compared with experimental data. Then it is proved that the power or the logarithmic law of velocity distributions of the turbulent boundary layer is improved in the vicinity of the plate surface. In Part III, a similar approximate method of solution is shown for particular flow patterns in which a parameter used in the equation is constant and a group of these solutions are derived. And with these solutions in use, a method to calculate the velocity profiles in any sub-layer is derived, assuming that the turbulent boundary layer is developing from the forward stagnation point, and the results are compared with those of the experiments. It appears that the work described in this paper is useful as one of the theoretical grounds on which the general state of flow near the surface of body in turbulent boundary layer it determined.

PART I. On the Mechanism of a Laminar Sub-Layer.

§ 1. Introduction.

In the investigation of a turbulent boundary layer, the most fundamental difficulty is that the effects of the viscosity caused by turbulent motion are not exactly expressed in any physical quantities concerning the mean motion in the whole region of the turbulent boundary layer. Since L. Prandtl proposed his mixture length theory, many investigations have been made on it, but on account of this difficulty even the equations of motion are not completely established, and though some empirical formulae in regard to the velocity distribution have been derived, they are not likely to be adaptable for the case of flow with a pressure gradient.

On the other hand, it is only in the vicinity of the boundary that the turbulent boundary layer has direct effects upon the body in the flow. And it has been known that in this part of flow, the turbulent agitating motion is prevented by the existence of the surface of the body: and there is a laminar sub-layer in which the effect of viscosity caused by molecular motion is much stronger than that of turbulent motion. Also it is well known that it is very thin and the velocity gradient at the boundary is so large that the surface friction is much larger than in the laminar boundary layer, and that it also plays an important role in the heat transfer from the body into the turbulent flow. And since the complicated effects of turbulence are approximately neglected in this layer, the above-mentioned difficulty in the turbulent boundary layer is avoided: and there is a possibility that the state of flow can be investigated theoretically as in the laminar boundary layer.

It was T. E. Stanton(1) who first proved the existence of a laminar sub-layer by experiments, but since then there have been few detailed investigations on it; moreover they are limited in the case of flow without a pressure gradient. By these investigations it has been explained that on account of the very small thickness of the laminar sub-layer the velocity distribution in it is linear; and between the turbulent part and the sub-layer, it is assumed that there is a transition region in order that the velocity distribution in the whole region of turbulent boundary layer may be smoothly connected. Thus, it has been defined that the part of flow near the boundary in which the velocity distribution is supposed to be linear is the laminar sub-layer; but further there has been no detailed definition about it. However, it is noteworthy that when u_1, δ_1, and ν are respectively taken as the mean velocity outside the laminar sub-layer, its thickness, and the kinematic viscosity, such a hypothesis has been generally believed that at the boundary of a laminar sub-layer,

$$\frac{u_1\delta_1}{\nu} = \text{const.}$$

Nevertheless, it is doubtful whether the preceding hypothesis may be directly extended in the case of flow with a pressure gradient. Particularly for the important case in which turbulent separation occurs there has been no definite theory on the laminar sub-layer.

From the above point of view, the author desires to consider the fundamentals of the mechanism of the laminar sub-layer and to investigate its state of flow with any pressure gradient.

§ 2. A Hypothesis on the Lower Critical Reynolds Number of Transition.

After the famous Reynolds' experiments on the transition from laminar to turbulent flow in a tube, it has been found that the Reynolds Number of transition is changeable according to the state of flow, and it decreases with increasing turbulence in the flow. But there is a limit to the Reynolds Number, below which the flow retains to be laminar however large disturbances may be superposed. This limit of the value is generally called lower critical Reynolds Number of transition from laminar to turbulent flow.

For the flow along a flat plate, it is also generally believed that when the δ-Reynolds Number (which is composed of the thickness of the boundary layer and the velocity of the main flow,) is considered, it has the same character as for the flow in a tube. This character seems to be retained also for the flow with a pressure gradient. In the case of a negative value of dp/dx, it is well-known that the transition occurs not so easily as for the flow along a flat plate, and the lower critical Reynolds Number of transition is supposed to be higher than that. And in the case of a positive value of dp/dx, the transition occurs very easily and yet it also seems to have a lower critical Reynolds Number, although this value may be very small. In general, for the flow of the laminar boundary layer around a body, the δ-Reynolds Number has already become considerably large, at the point where the value of dp/dx becomes positive. But when this value is assumed to be not so large, for instance, for the flow around a circular cylinder of an ordinary size, it is recognized, from the curve of the pressure distribution, that irrespective of the state of the main flow, there is a small part of the laminar boundary layer even in the region where dp/dx is positive. From the above experimental facts, the lower critical Reynolds Number of transition is assumed to decrease more and more with an increase in the value of dp/dx from negative to positive.

As for the existence of the lower critical Reynolds Number for the flow along a flat plate, there has been an explanation as follows: The δ-Reynolds Number, $U\delta/\nu$, represents itself as the ratio of the inertia force to the viscous force in the boundary layer, and when this number is below its critical value, the viscous force is so much stronger than the inertia force in it, that the flow remains to be laminar owing to its viscous force, however large disturbances by inertia force may be added.

The above explanation is generally believed to be correct for the flow without a pressure gradient, but it is desired to extend this explanation to the flow with a pressure gradient. The above-mentioned idea in regard to the relationship between the ratio of the two forces and the existence of the lower critical Reynolds Number of transition seems to be adaptable for the flow with a pressure gradient. But in this case of flow, the effect of the pressure gradient also must be considered. And in consideration of the above described experimental facts as for the relationship between the Reynolds Number of transition and the pressure gradient, the author desires to introduce such a hypothesis that for the laminar boundary layer flow, when the state of flow differs far from that of the ideal fluid and the viscous force is very large in comparison with the inertia force and the pressure force, the flow continues to be laminar, however large turbulence may exist in the main flow. In other words, it is assumed that there is such a limit of the ratio between the two forces which appear in the ideal flow and the viscous force that below this limit of the value the flow keeps its stability independent of the state of the main flow.

For the flow with a pressure gradient, the forces as the ideal fluid are due to the charge of momentum and the charge of pressure, and in the laminar boundary layer, the former force is approximately proportional to ρU^2 and the latter is to $-(dp/dx)\delta$, and the viscous force is represented approximately by $\mu U/\delta$. Therefore, the ratio between these forces and the viscous force are described respectively as

$$\frac{U\delta}{\nu}, \tag{2,1}$$

and

$$-\frac{dp}{dx}\frac{\delta^2}{\mu U}. \tag{2,2}$$

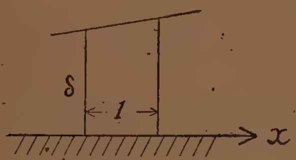

Fig. 1.

In these expressions, (2,1) is the δ-Reynolds Number, R, and (2,2) is the same as the parameter "λ" of the laminar boundary layer flow, derived by the Kármán-Pohlhausen's theory. But R and λ are not assumed to have the same coefficient of ratio, and so when κ is taken as the ratio of these coefficients, the ratio of the forces as the ideal fluid to the viscous force in the boundary layer is represented by

$$R+\kappa\lambda. \tag{2,3}$$

Therefore, on the above-mentioned hypothesis, when the value of (2,3) becomes smaller than a certain limit (which is shown by c,) the flow remains to be laminar independent of the main flow. Namely the following hypothesis is derived that when the condition of

$$R+\kappa\lambda \leqq c \tag{2,4}$$

holds for the boundary layer flow with any pressure gradient, its state of flow keeps the stability however large disturbances may be superposed.

§ 3. The Characteristics of Laminar Sub-layer and its Equations of Motion.

In a turbulent boundary layer, the flow contains large turbulent motion, but at the surface of a body, the velocity of a fluid can be supposed to vanish and, so the vorticity also diffuses into the flow from the surface, as in the case of the laminar boundary layer. In the region of the diffusion of vorticity, the effect of viscosity caused by molecular motion is undoubtedly conspicuous as in the laminar boundary layer, but for the flow in the case of the turbulent boundary layer, there is a characteristic feature, that is: the vorticity diffuses in the turbulent agitating motion; outside the region where molecular viscosity is large, there are large fluctuating motion and finite shearing stress owing to the turbulent motion.

In turbulent boundary layer, the laminar sub-layer can be generally defined as the region where the effect of molecular viscosity is large, and on account of its very small thickness, its equations of motion may be easily derived as that of the laminar boundary layer. And yet at the next stage we meet a fundamentally difficult problem; that is how to consider the physical meaning of the above-mentioned different conditions outside laminar sub-layer and how to describe it mathematically in the equations of motion.

For this problem, it will be desirable to consider it on the basis of the stability of laminar boundary layer which was described in the last chapter. In the turbulent boundary layer, when x- and y-axis are taken as in figure 2 and u as the mean velocity at a point (x, y), the ratio of the sum of inertia force and pressure force to viscous force of the fluid between this point and the boundary of a body is written by (2, 3) as below

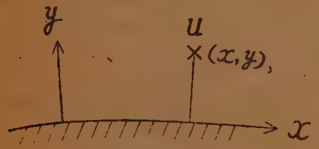

Fig. 2.

$$R+\kappa\lambda = \left(uy+\kappa\frac{dU}{dx}\frac{U}{u}y^2\right)\nu^{-1}. \qquad (3.1)$$

This value vanishes as y tends to zero and so there is a value of y where

$$R+\kappa\lambda = c.$$

When this value is shown as y_1, at least in the region of

$$0 \leqq y \leqq y_1,$$

the flow must remain laminar independently of the turbulent motion outside this region.

In general, in the turbulent boundary layer the turbulence is not isotropic and it has complicated characters, but at present we have little knowledge about it. However, as a matter of fact, its intensity is very large along the surface of the body, and so when the turbulent motion in turbulent boundary layer is regarded as disturbances superposed upon the above-mentioned laminar part near the surface of body, its intensity can be supposed to have such a magnitude as is used in the definition of the lower critical Reynolds Number of transition in the last chapter. Therefore, in the turbulent boundary layer, it is considered that in the region of

$$0 \leqq y \leqq y_1,$$

the flow is laminar and outside of it the flow is turbulent. This region of the laminar flow can be defined as laminar sub-layer, and a finite value of y_1 can be taken as the thickness of the laminar sub-layer (that is shown by δ_1).

When u_1 is taken as the mean velocity at a point of $y=\delta_1$, one of the above-described distinctions between laminar sub-layer and laminar boundary layer is shown by a condition such as

$$\frac{u_1\delta_1}{\nu}+\kappa\left(-\frac{\delta_1{}^2}{\rho}\frac{dp}{dx}\right)\Big/(\nu u_1) = c. \qquad (3,2)$$

Another important feature of this turbulent motion is that there is a finite value of Reynolds shearing stress, and so at the boundary of laminar sub-layer, such a condition that

$$\left(\frac{\partial u}{y\partial}\right) = \frac{u_1}{\delta_1}m, \qquad (33)$$

is necessary. In (3,3), m is a non-dimensional number of a finite value and ought to be determined according to the mechanism of turbulent motion outside the laminar sub-layer.

The conditions at the boundary of the laminar sub-layer are determined by (3,2) and (3,3) and as for the motion of a fluid in this layer, it is determined by the equations of motion of viscous fluid. Moreover, on account of the very small thickness, the equations of motion can be simplified to the "Prandtl's equations" of laminar boundary layer. Then the equations which determine the motion of fluid in the laminar sub-layer are written as

$$\left.\begin{aligned} u\frac{\partial u}{\partial x}+v\frac{\partial u}{\partial y} &= -\frac{1}{\rho}\frac{dp}{dx}+\nu\frac{\partial^2 u}{\partial y^2} \\ \frac{\partial u}{\partial x}+\frac{\partial v}{\partial y} &= 0, \end{aligned}\right\} \qquad (3,4)$$

and the boundary conditions are

$$\left.\begin{aligned} u &= 0 \quad \text{at} \quad y=0 \\ u &= u_1 \quad \text{at} \quad y=\delta_1, \end{aligned}\right\} \qquad (3,5)$$

where u_1 and δ_1 are determined indirectly by (3,2) and (3,3), and so the conditions (3,5) can be written as

$$\left.\begin{aligned} u &= 0 \quad \text{at} \quad y=0 \\ R+\kappa\lambda = c, \quad \left(\frac{\partial u}{\partial y}\right) &= \frac{u_1}{\delta_1}m \quad \text{at} \quad y=\delta_1. \end{aligned}\right\} \qquad (3,5')$$

In the case of the laminar boundary layer, the boundary condition outside the layer is

$$u=U \quad \text{at} \quad y\to\infty,$$

and U is given directly as the velocity of the potential flow, while the thickness is increasing at the rate of $x/\sqrt{R_x}$, until a transition from laminar to turbulent flow or laminar separation occurs. In the turbulent boundary layer near the surface of a body, a laminar boundary layer is also developing, but in the region of $y > \delta_1$, the laminar flow is breaking into a turbulent flow with the fluid in the region of $y < \delta_1$ keeping its stability as a laminar sub-layer along the boundary of a body. But δ_1 and u_1 are not given directly by the condition of turbulent flow outside a sub-layer, and these values are decided by (3,5′) which represent the above-mentioned character that the state of flow outside laminar sub-layer is different from that of laminar boundary layer.

In the foregoing part, as the equations of motion and the boundary conditions of laminar sub-layer, (3,4) and (3,5′) have been derived; while in the following parts some discussions will be made on these approximate solutions.

Before going further the author wishes to record here a debt of gratitude for the kind guidance throughout the present work, to Messrs. Kondo, Tadokoro, Maekawa, Yamanouchi, and other research members in the hydrodynamical-laboratory of the Railway Technical Research Institute.

Reference.

(1) Stanton, T. E.: Porc. Roy. Soc. A 97, 413 (1920).

Theoretical Determination of Proper Frequencies of the Resonant Circuit of the Cavity Magnetrons.*

By Masao KOTANI and Hidetoshi TAKAHASHI.

Department of Physics, University of Tokyo.

(Received, June 11, 1948)

§ 1. Introduction

Since the most important factor to determine the frequency of microwaves generated by a magnetron is the proper frequencies of electric oscillation of the resonant circuit constructed in the anode block of metal, it is important for the design of a magnetron to know quantitatively the relation between the proper frequencies and the dimensions of the resonant circuit. In this paper we describe an analytical treatment of the electromagnetic oscillations of these resonant circuits, which gives results agreeing closely with experiment. Our discussion will be concerned with magnetrons with typical resonant circuits as shown in Fig. 1, (a) and (b). These are known in Japan under the names "Tachibana (mandarine) type" and "Umebachi (plum-flower) type" respectively. Cylindrical cavities are all alike in size in case of Umebachi-type, while they are alternately large and small in case of Tachibana-type.

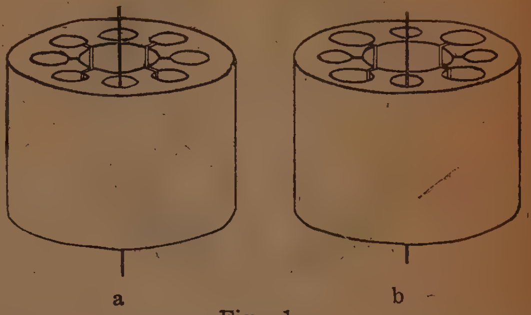

Fig. 1.

In the following we denote by A the central cylindrical cavity, where electron motion takes place, and by B the resonant cavities arranged circumferentially which are connected to the space A through narrow slots. In case of Tachibana-

---

[*] The essential part of this work was completed during the world war II.

type, large and small cavities are distinguished as B and B′.

As a simplifying assumption we neglect the effect of the finite thickness of the metallic block and assume the electromagnetic field corresponding to the proper mode of oscillation to be independent of the coordinate z measured along the cathode. Though in actual magnetron the thickness of the anode block is not very large compared with the anode radius, this thickness seems to play only secondary roles in our present problem, and so we simplify our analysis by treating the problem as a two-dimensional one.

Our next assumption is that the dimensions (breadth and depth) of the slots are small in comparison with B and B′. This assumption has as its consequence the situation that the dimensions of the slots are far smaller than the wave-length, and the electromagnetic field near the slots may be treated as quasi-static.

Though the present method is applicable, at least in principle, to cases when the shape of resonant cavities B, B′ is general, we confine ourselves to the case of cavities of circular form, which is not only simple in theoretical treatment but also important in practice. Thus we consider the anode block such as shown in Fig. 2 as the typical Tachibana-type circuit. Radii of larger and smaller cavities are denoted by R and R' respectively, while the radius of the central cavity is written as R_0. The anode surface is divided into 2 ν segments by 2 ν slots located equidistantly on the circle A. In short, our problem is to find two-dimensional proper oscillation of connected cavity as shown in the figure.

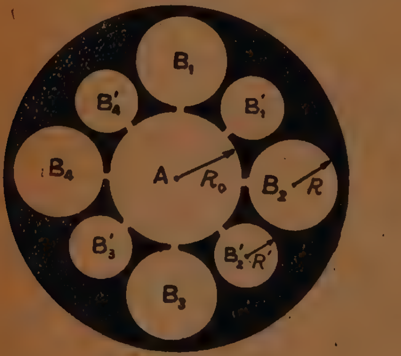

Fig. 2.

§ 2. General Assumptions on the Radio-Frequency Field.

In order to determine the proper oscillation of such a complicated hollow cavity, we obtain first the oscillating electromagnetic field in each of the cavities A, B₁, B₁′, B₂, ... for arbitrarily chosen value of the frequency ω, and adjust this frequency so that the fields may join smoothly at the slots. Then the conditions of continuity give equations for the determination of ω and $\lambda = \frac{2\pi c}{\omega}$.

Now, in case of two-dimensional oscillations of relatively long wave-length, radiofrequency currents flow on the wall of B, B′ (and eventually of A also) in a plane perpendicular to z, and positive and negative surface charges appear on both sides C, D of the slots, just as on pair of electrodes of an electrostatic condenser. Then the magnetic field $\boldsymbol{H}$ has z-component only, whereas the electric field $\boldsymbol{E}$ has no component parallel to z. Hence we may denote the z-component of $\boldsymbol{H}$ as $He^{j\omega t}$ and the x-,y-component of $\boldsymbol{E}$ as $E_x e^{j\omega t}$, $E_y e^{j\omega t}$, where ω is the circular frequency to be determined by the following analysis. E_x, E_y and H are functions of x and y only; they are connected by the following relations:

$$\frac{\partial^2 H}{\partial x^2}+\frac{\partial^2 H}{\partial y^2}+k^2 H=0, \tag{1}$$

$$k=\frac{\omega}{c}=\frac{2\pi}{\lambda},$$

$$E_x=-\frac{j}{k}\frac{\partial H}{\partial y}, \quad E_y=\frac{j}{k}\frac{\partial H}{\partial x}, \tag{2}$$

which are derived from Maxwell's equations.

In the mode in which we are interested, charges of opposite signs accumulate periodically on both sides of the slots, and a strong field appears locally in their neighbourhood. Since, however, the wave-length is assumed to be far larger than the dimension of the slot, this local field may be approximated by electrostatic one, apart from the factor $e^{j\omega t}$. [x and y components of $\boldsymbol{E}$ must of course satisfy, $\Delta E+k^2E=0$. But when the wave-length $\frac{2\pi}{k}$ is large compared with the length over which the field varies appreciably, the last term k^2E may be neglected.] This circumstance has its consequence that the concept of (electrostatic) potential is applicable as far as the consideration is limited within the neighbourhood of a single slot. Let (the amplitude of) the potential difference across the slot connecting the larger cavity $B_\nu \equiv B_0$ with A be V. Then, according to the theory of polyphase oscillation, the potential difference across the slot connecting $B_n (n = 1, 2, \ldots\ldots, \nu)$ and A is

$$V \exp\left(2\pi i \zeta \frac{n}{\nu}\right),$$

where ζ is an integer. Similarly, the potential difference across the slot connecting B_n' and A can be written as

$$V' \exp\left(2\pi i \zeta \frac{n+\frac{1}{2}}{\nu}\right), \quad n = 1, 2, \ldots\ldots \nu.$$

Oscillation of push-pull type, which is most common in practice, is characterized by $\zeta = 0$ and opposite signs of V and V'.

§ 3. Electromagnetic Field in a Single Cavity.

Fig. 3 shows one of the larger cavities B, projected on the x-y plane. Circle with O as its centre and of radius R coincides with the wall of the cavity, except at the small part of length 2δ near the slot. Now, take polar coordinates r, ϕ as shown in the figure. If the copper is assumed to be a perfect conductor, tangential component E_ϕ (ϕ-component) of the electric field along the circle $r = R$, $(E_\phi)_{r=R}$ takes non-vanishing values only within the interval $-\frac{\delta}{R} < \phi < \frac{\delta}{R}$. In this interval $(E_\phi)_{r=R}$ can be given approximately by solving electrostatic field in the neighbourhood of the slot when the potential difference of C and D is V. Now, from this knowledge of $(E_\phi)_{r=R}$, we can determine, not only the electric field within the cavity, but also the magnetic field, with the help of (1) and (2). For this purpose we first expand $(E_\phi)_{r=R}$ in Fourier series of ϕ

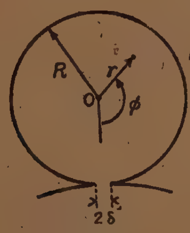

Fig. 3.

$$(E_\phi)_{r=R} = \sum_{m=0}^{\infty} C_m \cos m\phi, \tag{3}$$

in which C_m is given as follows

$$C_0 = \frac{1}{2\pi} \int_{-\frac{\delta}{R}}^{-\frac{\delta}{R}} (E_\phi)_{r=R}\, d\phi, \quad C_m = \frac{1}{\pi} \int_{-\frac{\delta}{R}}^{-\frac{\delta}{R}} (E_\phi)_{r=R} \cos m\phi\, d\phi. \tag{4}$$

Since $\int_{-\frac{\delta}{R}}^{\frac{\delta}{R}} (E_\phi)_{r=R}\, R\, d\phi$ is equal to V, we have, in the limit $\delta \to 0$,

$$C_0 = \frac{V}{2\pi R}, \quad C_m = \frac{V}{\pi R}. \quad (m \geqq 1) \tag{5}$$

Now, as a function satisfying (1), H can be expanded in the form

$$H = \sum_{m=0}^{\infty} A_m J_m(kr) \cos m\phi. \tag{6}$$

Substitution of (6) into (2) gives

$$E_\phi = \frac{j}{k} \frac{\partial H}{\partial r} = j \sum_{m=0}^{\infty} A_m J_m'(kr) \cos m\phi.$$

This function must coincides with (3) when $r = R$. Hence we must have

$$j A_m J_m'(kR) = C_m.$$

A_m can be obtained from these relations, and (6) takes the form

$$H \equiv H(r, \phi) = -j \sum C_m \frac{J_m(kr)}{J_m'(kR)} \cos m\phi. \tag{7}$$

Thus we have succeeded in determining H from $(E_\phi)_{r=R}$.

If we assume that the breadth of the slot is sufficiently small in comparison with R, electromagnetic field in the region not too close to the slot is almost identical with the field for the limiting case $\delta = 0$. Accordingly, for points whose distance from the slot is fairly large as compared with δ, we can substitute the values (5) for C_m without serious error. Hence we have

$$H = -\frac{jV}{\pi R} \left\{ \frac{J_0(kr)}{2 J_0'(kR)} + \sum_{m=1}^{\infty} \frac{J_m(kr)}{J_m'(kR)} \cos m\phi \right\}. \tag{8}$$

This formula, which neglects δ, is not valid in the immediate neighbourhood of the slot. In fact, if we put $r=R$, $\phi=0$ in (8), the series diverges and gives $H=\infty$, an absurd result. We can, however, take a region—which we shall call "intermediate region"—whose points are at distances from the slot large compared with δ, but small compared with R. For points in such intermediate region, (8) is valid, but the same formula can be simplified, taking into account the relations

$$(\text{distance from the slot}) \ll R.$$

But as the series so obtained converges very slowly, it is convenient to write it in the following form

$$H=-\frac{jkV}{\pi}\Big[\frac{J_0(kr)}{2kRJ_0'(kR)}+\sum_{m=1}^{\infty}\Big\{\frac{J_m(kr)}{kRJ'_0(kR)}-\frac{1}{m}\Big(\frac{r}{R}\Big)^m\Big\}\cos m\phi+\sum_{m=1}^{\infty}\frac{1}{m}\Big(\frac{r}{R}\Big)^m\cos m\phi\Big] \quad (9)$$

In this form the last series expresses the part which diverges at $r=R$, $\phi=0$; this series can be easily summed as follows

$$\sum_{m=1}^{\infty}\frac{1}{m}\Big(\frac{r}{R}\Big)^m\cos m\phi=\log\frac{R}{\rho},$$

$$\rho=\sqrt{R^2+r^2-2Rr\cos\phi}.$$

ρ is nothing but the distance from the slot. In the former series in (9) we may put $r=R$, $\phi=0$, and the result can be written in the form

$$H=-\frac{jkV}{\pi}\Big\{f(kR)+\log\frac{R}{\rho}\Big\}, \quad (10)$$

in which the function f is defined by

$$f(x)=\frac{J_0(x)}{2xJ'_0(x)}+\sum_{m=1}^{\infty}\Big\{\frac{J_m(x)}{xJ'_m(x)}-\frac{1}{m}\Big\}. \quad (11)$$

4. Electromagnetic Field in the Neighbourhood of a Slot.

Next we shall derive expressions for H valid in the neighbourhood of a slot. The field in this region depends on the detailed form of the slot, but as the dimension of the slot is far smaller than the wave-length, we can use electrostatic approximation. Let the electrostatic potential at the point (x, y) be $\Phi(x, y)$, when the potentials of both sides C and D of the slot are $+\frac{V}{2}$ and $-\frac{V}{2}$ respectively, and denote the complex potential by

$$\chi=\Phi+j\Psi,$$

where the function Ψ is conjugate to Φ. Then according to the so-called Cauchy-Riemann's equation we have

$$\frac{\partial\Phi}{\partial x}=\frac{\partial\Psi}{\partial y}, \quad -\frac{\partial\Phi}{\partial y}=\frac{\partial\Psi}{\partial x} \quad (12)$$

for E_x and E_y. Comparing (12) to (2) we find

$$H=-jk(\Psi+C). \quad (13)$$

The constant C can be determined by the condition that (13) and (10) should be identical in the intermediate region.

As a concrete example, let us consider an infinitely thin slot as shown in Fig. 4. For this case the complex potential is given by

$$\chi=\frac{V}{\pi}\sin^{-1}\frac{z}{\delta}, \quad z=x+jy.$$

For points somewhat distant from the slot $|z|\gg\delta$, so that we may write

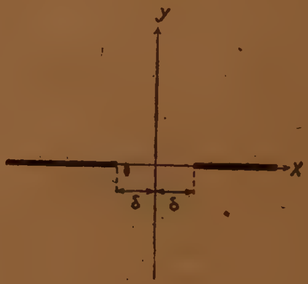

Fig. 4

$$\chi=\begin{cases}\frac{V}{2}+j\frac{V}{\pi}\log\frac{2z}{\delta} & (y>0)\\ \frac{V}{2}-j\frac{V}{\pi}\log\frac{2z}{\delta} & (y<0)\end{cases}$$

Hence in the intermediate region we have

$$\Psi\doteqdot\begin{cases}\frac{V}{\pi}\log\frac{2\rho}{\delta} & (y>0)\\ -\frac{V}{\pi}\log\frac{2\rho}{\delta} & (y<0)\end{cases}$$

where ρ is equal to $|z|$ and is the same quantity as ρ in (10). Substitution of this equation into (13) gives

$$H\doteqdot\begin{cases}-\frac{jkV}{\pi}\log\frac{2\rho}{\delta}-jkC, & (y>0) \quad (14)\\ +\frac{jkV}{\pi}\log\frac{2\rho}{\delta}-jkC. & (y<0) \quad (14')\end{cases}$$

Now, in the intermediate region mentioned above, both (14') and (10) must be true. If we equate these two expressions ρ drops automatically and C is determined as follows:

$$C = \frac{V}{\pi}\left\{f(kR)+\log\frac{2R}{\delta}\right\}. \tag{15}$$

From (14) and (15), we find the following expression for H valid in the intermediate region on the side of A$(y<0)$:

$$H = -\frac{jkV}{\pi}\left\{f(kR)+\log\frac{2R\rho}{\delta}\right\}. \tag{16}$$

In case the form of the slot is arbitrarily given, we can still write

$$H = \mp\frac{jkV}{\pi}\log\frac{2\rho}{\delta^*} - jkC,$$

where "the equivalent breadth of the slot" δ^* is a length characteristic of any slot, and can be determined by solving electrostatic problem. Using this δ^* we obtain generally

$$H = -\frac{jkV}{\pi}\left\{f(kR)+\log\frac{4R\rho}{(\delta^*)^2}\right\} \tag{17}$$

which is applicable to the intermediate region in A around the slot connecting A and B_0.

Similarly, we find for the intermediate region M_n in A, around the slot between A and B_n (See Fig. 5)

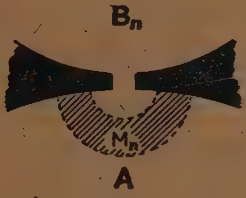

Fig. 5

$$H = -\frac{jkV}{\pi}e^{2\pi i\zeta\frac{n}{\nu}}\left\{f(kR)+\log\frac{4R\rho}{(\delta^*)^2}\right\}, \tag{18}$$

and for the intermediate region M_n' near the slot between A and B_n'

$$H = -\frac{jkV'}{\pi}e^{2\pi i\zeta\frac{n+\frac{1}{2}}{\nu}}\left\{f(kR')+\log\frac{4R'\rho}{(\delta'^*)^2}\right\} \tag{19}$$

Finally, we shall find the expression for H valid in A, except in the immediate neighbourhood of the slots. The procedure is quite similar to that used to find the field in the cavity B_0. The only difference is that the intervals in which E_ϕ does not vanish are 2ν in number and lie equidistantly along the wall of A (anode surface). Short calculations give for the region M_n

$$H = \frac{jk}{\pi}e^{2\pi i\zeta\frac{n}{\nu}}\left[V\left\{f_{\zeta/\nu}(kR_0)+\log\frac{R_0}{\nu\rho}\right\}+V'g_{\zeta/\nu}(kR_0)\right] \tag{20}$$

and for M_n'

$$H = \frac{jk}{\pi}e^{2\pi i\zeta\frac{n+1/2}{\nu}}\left[Vg_{\zeta/\nu}(kR_0)\right.$$
$$\left.+V'\left\{f_{\zeta/\nu}(kR_0)+\log\frac{R_0}{\nu\rho}\right\}\right] \tag{21}$$

In these formulas functions $f_{\zeta/\nu}$, $g_{\zeta/\nu}$ are used, which are defined as follows:

$$f_{\zeta/\nu}(x) = \frac{1}{2}\sum_{m=0}^{\infty}\left\{\frac{\nu J_{\zeta+m\nu}(x)}{xJ'_{\zeta+m\nu}(x)}-\frac{1}{m+1}\right\}$$
$$+\frac{1}{2}\sum_{m=0}^{\infty}\left\{\frac{\nu J_{\nu-\zeta+m\nu}(x)}{xJ'_{\nu-\zeta+m\nu}(x)}-\frac{1}{m+1}\right\}, \tag{22}$$

$$f_{0/\nu}(x) = \frac{\nu J_0(x)}{2xJ_0'(x)}+\sum_{m=1}^{\infty}\left\{\frac{\nu J_{m\nu}(x)}{xJ'_{m\nu}(x)}-\frac{1}{m}\right\},$$

$$g_{\zeta/\nu}(x) = \frac{\nu}{2}\sum_{m=-\infty}^{+\infty}(-1)^m\frac{J_{|\zeta+m\nu|}(x)}{xJ'_{|\zeta+m\nu|}(x)}. \tag{23}$$

Numerical tables of $f(x)$, $f_{\zeta/\nu}(x)$ and $g_{\nu/\nu}(x)$ are given in the next paper for several important values of ζ and ν.

§ 5. Equations to Determine the Proper Frequencies.

Now, since both (18) and (20) are valid in the same region M_n, they must reduce to the same expression. The condition of agreement is

$$V\left\{f(kR)+f_{\zeta/\nu}(kR_0)+\log\frac{4RR_0}{\nu(\delta^*)^2}\right\}+V'g_{\zeta/\nu}(kR_0) = 0 \tag{24}$$

Similarly, equating (19) and (21) we find

$$Vg_{\zeta/\nu}(kR_0)+V'\left\{f(kR')+f_{\zeta/\nu}(kR_0)+\log\frac{4R'R_0}{\nu(\delta'^*)^2}\right\} = 0. \tag{25}$$

Elimination of V/V' from these two equations gives

$$\left\{f(kR)+f_{\zeta/\nu}(kR_0)+\log\frac{4RR_0}{\nu(\delta^*)^2}\right\}\left\{f(kR')+f_{\zeta/\nu}(kR_0)\right.$$
$$\left.+\log\frac{4R'R_0}{\nu(\delta'^*)^2}\right\}-(g_{\zeta/\nu}(kR_0))^2 = 0. \tag{26}$$

This is the required (transcendental) equation which enables us to calculate the proper wave-number $k=\frac{2\pi}{\lambda}$ or proper wave-length λ. The results derived from (26) will be discussed in the following paragraphs.

For the following discussions we make use of several properties of functions $f(x)$, $f_{\zeta/\nu}(x)$ and $g_{\zeta/\nu}(x)$. They are given here for convenience

$$f_{\nu-\zeta/\nu}(x)=f_{\zeta/\nu}(x), \tag{27}$$

$$\begin{aligned} &g_{\nu-\zeta/\nu}(x)=g_{\zeta/\nu}(x), \\ &g_{\frac{\nu}{2}/\nu}(x)\equiv 0,\ (\nu,\ \text{even}) \end{aligned} \tag{28}$$

$$\left.\begin{aligned} f_{\zeta/\nu}(x)+g_{\zeta/\nu}(x)&=f_{\zeta/2\nu}(x)-\log 2, \\ f_{\zeta/\nu}(x)-g_{\nu/\nu}(x)&=f_{\nu-\zeta/2\nu}(x)-\log 2, \end{aligned}\right\} \tag{29}$$

$$\frac{1}{2}\left\{f_{\zeta/2\lambda}(x)+f_{\nu-\zeta/2\nu}\right\}=f_{\zeta/\nu}(x)+\log 2. \tag{30}$$

For small values of x these functions behave as follows:

$$f(x)=-\frac{1}{x^2}+\frac{1}{8}+O(x^3), \tag{31}$$

$$\left.\begin{aligned} f_{0/\nu}(x)&=-\frac{\nu}{x^2}+\frac{\nu}{8}+O(x^2), \\ f_{\zeta/\nu}(x)&=-\frac{1}{2}\left\{\Psi\left(\frac{\zeta}{\nu}\right)+\Psi\left(1-\frac{\zeta}{\nu}\right)\right\}-\gamma+O(x^2), \\ &\gamma\ (\text{Euler's constant})=0.5772\ldots\ldots \end{aligned}\right\} \tag{32}$$

$$\left.\begin{aligned} g_{0/\nu}(x)&=-\frac{\nu}{x^2}+\frac{\nu}{8}-\log 2+O(x^2), \\ g_{\zeta/\nu}(x)&=\frac{1}{2}\left\{\Psi\left(\frac{\zeta}{\nu}\right)+\Psi\left(1-\frac{\zeta}{\nu}\right)-\Psi\left(\frac{\zeta}{2\nu}\right)\right. \\ &\quad\left.-\psi\left(1-\frac{\zeta}{2\nu}\right)\right\}+O(x^2). \end{aligned}\right\} \tag{33}$$

§ 6. Proper Oscillations of Umebachi Type Circuits.

Firstly, let us apply the results obtained above to the case when the radius R' of the smaller cavities B_1', B_2', ... is made to vanish. The circuit is then one of Umebachi type with ν slots. Since

$$\lim_{R'\to 0} f(kR')$$

is infinite, (26) reduces to

$$f(kR)+f_{\zeta/\nu}(kR_0)+\log\frac{4RR_0}{\nu(\delta^*)^2}=0, \tag{34}$$

which is the equation for the proper wave-length of the Umebachi type circuit with ν slots.

For given values of R, R_0, δ, ν, this equation has infinite number of roots, and they all have real physical meaning as long as the corresponding wave-length λ is sufficiently large in comparison with the dimension of the slots. However, if the breadth of the slot δ^* is very small, oscillations are possible, whose wave-lengths are fairly large as compared with the dimension of the circuit, and tend logarithmically to infinity with $\delta^*\to 0$. To show this, we assume $kR\ll 1$, $kR_0\ll 1$, and apply the approximate formulas (31), (32). Then (34) is reduced to

$$\left.\begin{aligned} &\left(\frac{1}{R^2}+\frac{\nu}{R_0{}^2}\right)\frac{1}{k^2}\doteqdot\frac{\nu+1}{8}+\log\frac{4RR_0}{\nu(\delta^*)^2},\ (\zeta=0) \\ &\frac{1}{R^2}\frac{1}{k^2}\doteqdot\frac{1}{2}\left\{\Psi\left(\frac{\zeta}{\nu}\right)+\Psi\left(1-\frac{\zeta}{\nu}\right)\right\}+\gamma+\log\frac{4RR_0}{\nu(\delta^*)^2} \end{aligned}\right\} \tag{35}$$

(35) gives one value of k or λ for each value of ζ. Though these wave-lengths grow indefinitely as δ^* tends to zero, the dependence is only logarithmic, so that in most practical cases approximation (35) is too crude, and we have to use (34) for numerical work.

On account of periodic nature of dependence on ζ, it is sufficient to take only ν consecutive values of ζ; for example, $\zeta=0, 1, 2, \ldots, \nu-1$. Moreover, equation (34) is invariant with respect to the substitution $\zeta\to\nu-\zeta$. Hence we obtain $\frac{\nu}{2}+1$ different frequencies

$$\left.\begin{aligned} &\zeta=0 \\ &\zeta=1 \text{ and } \zeta=\nu-1 \\ &\zeta=2 \text{ and } \zeta=\nu-2 \\ &\ldots\ldots\ldots \\ &\zeta=\frac{\nu}{2} \end{aligned}\right\} \tag{36}$$

(If ν is odd the last line is to be replaced by

$$\zeta=\frac{\nu-1}{2} \text{ and } \zeta=\frac{\nu+1}{2},$$

and the number of different frequencies is $\frac{\nu+1}{2}$)

If δ^* is sufficiently small, the wave-length for $\zeta=0$ is fairly short, and those for the other modes $1\leqq\zeta\leqq\frac{\nu}{2}+1$ are large, and are nearly equal. Among these long wave-length modes, the wave-length is minimum for $\zeta=\frac{\nu}{2}\left(\text{or }\frac{\nu\pm 1}{2}\right)$. Thus the push-pull oscillation has the shortest wave-length among the low frequency group. A few numerical examples illustrating the dependence of λ on ζ are given in Table I.

TABLE I

Typical Examples of Calculated Resonant Frequencies

(a) 8 cavities, Umebachi type

$R = 3$ mm, $\delta^* = 0.165$ mm (Breadth and length of slots being 1.25 mm and 1 mm respectively)

ζ		0	1	2	3	4
$\lambda_{(mm)}$	$R_0 = 6_{mm}$	29	61	54	52	51
	$R_0 = 4.5_{mm}$	23.4	59.5	52.8	50.7	50.1

(b) 8 cavities, Tachibana type

$R_0 = 6\ mm,\ R_0 = 3\ mm,\ R' = 2\ mm,\ \delta^* = 0.165\ mm$

ζ	0	1	2
$\lambda_{(mm)}$	25.4	37.9	53.8
	42.3 (push-pull)	52.2	

(c) 10 cavities, Tachibana type

$R_0 = 6\ mm,\ R = 3.5\ mm,\ R' = 2.5\ mm,\ \delta^* = 0.098\ mm$, (Breadth and length of slots being 1 mm)

ζ	0	1	2
λ_{mm}		48.6	47.2
	54.0	(66)	67.1

Next we examine the magnetic induction flux through cavities. If we assume $kR \ll 1$, $kR_0 \ll 1$ in (7) and similar equation representing H in A, we obtain:

$$\text{in } \mathrm{B}_n: \quad H \doteqdot j\frac{V}{k\pi R^2}e^{2\pi l\zeta\frac{n}{\nu}} \tag{37}$$

$$\text{in A}: \quad H \doteqdot \begin{cases} -j\dfrac{\nu V}{k\pi R_0^{\ 2}}, & (\zeta = 0) \\ 0. & (0 < \zeta < \nu) \end{cases} \tag{38}$$

These formulas show that the magnetic field is nearly uniform in any of the cavities. Consequently, uniform current flows on the wall of each cavity, and charges appear only on both sides of slots. According to (38), no flux passes through the central cavity A, except for the mode $\zeta = 0$. Especially in push-pull mode, flux of the same magnitude pass through all B-cavities, alternately in one and the other direction. Short wave-length mode $\zeta = 0$ is unique in that equal flux passes through all B-cavities in the same direction, the return flux passing through A in the opposite idrection.

§ 7. Proper Oscillation of Tachibana Type Circuit.

We now go on to discuss general Tachibana type circuit. In this case, for each value of ζ two proper oscillations of LC type exist according to (26). Although the split number is 2ν, it is sufficient to choose ζ in the interval $0 \leqq \zeta \leqq \frac{\nu}{2}$, and we obtain twice as many proper oscillations as in (36). In the long wave-length approximation similar to (35), (26) can be transformed into a quadratic equation in $\frac{1}{k^2}$, and the inspection of this equation shows that in general the longer wave-length are a little longer than proper wave-lengths of Umebachi circuit having ν larger (B) cavities only, while the shorter wave-lengths are a little shorter than those of circuit with ν smaller (B′) cavities only. Especially when ν is even and $\zeta = \frac{\nu}{2}$, mutual interactions between B and B′ cavities vanish on account of (28), and (26) splits into two equations as follows:

$$f(kR) + f_{\frac{\nu}{2}/\nu}(kR_0) + \log\frac{4RR_0}{\nu(\delta^*)^2} = 0,$$

$$f(kR') + f_{\frac{\nu}{2}/\nu}(kR) + \log\frac{4R'R_0}{\nu(\delta^*)^2} = 0.$$

These are nothing but the equations to determine proper wave-lengths for the cases in which smaller cavities or larger cavities are absent. In case $\zeta = \frac{\nu}{2}$, we have push-pull type oscillation in larger (smaller) cavities, and no flux passes through smaller (larger) cavities. These latter cavities are "dead". The situation may be easily understood by means of Fig. 6.

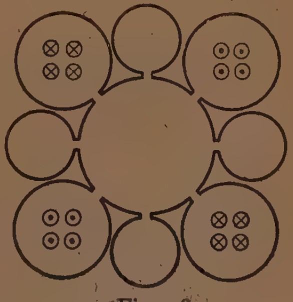

Fig. 6

Push-pull type oscillation in case of 2ν slots Tachibana circuit, which is the most common and important mode in practice, is the proper oscillation of the longest wave-length in the class $\zeta = 0$. Its wave-length can be obtained by solving (26).

Now, the functions $f_{0/\nu}(x)$, $g_{0/\nu}(x)$ take very large values for small values of $x = kR_0$. Hence its wave-length is fairly shorter than the longest wave-lengths of the classes $0 < \zeta \leq \frac{\nu}{2}$. In case of push-pull mode, magnetic flux through larger cavities does not exactly cancel the flux through smaller cavities, and a certain amount of flux passes through the central cavity A. Relative amount of this flux through A is large if the difference between B and B′ is considerable, and in the limit when one kind of cavities,—B′ say—dissappears, the oscillation tends to the mode $\nu = 0$ of ν-slots Umebachi type magnetron treated in the preceding paragraph, and the flux through A is just equal to ν times the flux through any one of the B cavities. On the contrary, if the difference between B and B′ disappears, the mode goes over to push-pull mode of 2ν-slots Umebachi circuit, and we have no flux through A.

In short, LC-like modes of 2ν-slots Tachibana type circuits are classified into 4 groups. In the order of decreasing wave-length, they are as follows:

(1) the longer wave-length mode for $0 < \zeta \leq \frac{\nu}{2}$,
(larger cavities are mainly effective)
(2) the longer wave-length mode for $\zeta = 0$,
(push-pull mode of 2ν-slots circuit)
(3) the shorter wave-length modes for $0 < \zeta \leq \frac{\nu}{2}$.
(smaller cavities are mainly effective)
(4) the shorter wave-length mode for $\zeta = 0$.

§ 8. Transition from 2ν-slots Tachibana Type Circuit to 2ν-slots Umebachi Type Circuit.

Finally we discuss the transition from 2ν-slots Tachibana circuit to 2ν-slots Umebachi circuit, letting $R' \rightarrow R$, $\delta'^* \rightarrow \delta^*$. In this limit equation (24), (25) are evidently satisfied by taking

$$V' = V, \quad f(kR)+f_{\zeta/\nu}(kR_0)+g_{\zeta/\nu}(kR_0)+\log\frac{4RR}{\nu(\delta^*)^2}=0, \tag{38}$$

$$V' = -V, \quad f(kR)+f_{\zeta/\nu}(kR_0)-g_{\zeta/\nu}(kR_0)+\log\frac{4RR_0}{\nu(\delta^*)^2}=0. \tag{39}$$

With the use of (29), these equations can be written as

$$V' = V, \quad f(kR)+f_{\zeta/2\nu}(kR_0)+\log\frac{4RR_0}{2\nu(\delta^*)^2}=0 \tag{38'}$$

or

$$V' = -V, \quad f(kR)+f_{\zeta+\nu/2\nu}(kR_0)+\log\frac{4RR_0}{2\nu(\delta^*)^2}=0. \tag{39'}$$

(38′) and (39′) are nothing but the equations for 2ν-slots Umebachi circuit (See (34)). Moreover, since we have put $e^{2\pi i\zeta\frac{n}{\nu}}V$ for the potential difference across the slot between B_n and A, and $e^{2\pi i\zeta\frac{n+1/2}{\nu}}V'$ for the potential difference across the slot between B_n' and A, we can write them in a single formula

$$e^{2\pi i\bar{\zeta}\frac{n}{2\nu}}V \qquad n = 1,\ 2,\ \ldots\ldots,\ 2\nu$$

with $\bar{\zeta} = \zeta$ in case $V' = V$, and $\bar{\zeta} = \zeta + \nu$ in case $V' = -V$. Then, (38′) and (39′) can be unified into

$$f(kR)+f_{\bar{\zeta}/2\nu}(kR_0)+\log\frac{4RR_0}{2\nu(\delta^*)^2}=0,$$

$$\bar{\zeta} = 0,\ 1,\ 2,\ \ldots\ldots,\ 2\nu-1.$$

Thus the transition is completed. Hence, of the two ζ- modes in Tachibana type circuit, one tends to ζ- and the other to $\zeta+\nu$- mode. This latter may be classified as $\nu-\zeta$ type as well. Especially the push-pull mode in Tachibana circuit, which is the longer wave-length mode with $\zeta = 0$, tends to $\zeta = \nu$ mode of 2ν-slots Umebachi type circuit. The behaviour of the resonant wave-lengths of various modes as R' changes from 0 to R, is shown qualitatively in Fig. 7.

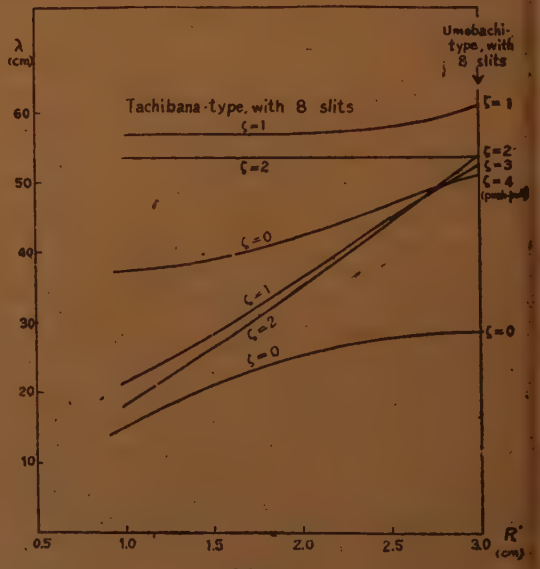

Fig. 7

Correspondence between Tachibana and Umebachi type circuits.
($2\nu = 8$, $R_0 = 6$ mm, $R = 3$ mm, $R' = 1 \sim 3$ mm.)

Numerical Tables of Functions useful for the Calculation of Resonant Frequencies of a Cavity Magnetron.

By Masao KOTANI and Hidetoshi TAKAHASHI.

Department of Physics, University of Tokyo.

(Received June 11, 1948).

In the preceding paper* we have described a method to calculate characteristic frequencies of resonant circuit of a cavity magnetron. Special attention was paid to the so-called Tachibana and Umebachi type circuits, which are shown in Fig. 1 of I. Final formulae obtained are (26) and (34) of I. In order to solve these transcendental equations we have to know the functions $f(x)$, $f_{\zeta/\nu}(x)$ and $g_{\zeta/\nu}(x)$ numerically. These functions are tabulated in the present paper, for several values of ν which may be practically important.

In case of Umebachi type circuit, whose cylindrical cavities are all of the same size, the transcendental equation (34) can be solved quite easily by a graphical method. Putting $kR_0 = x$, and writing

$$\frac{R}{R_0} \equiv c, \quad \log\frac{4RR_0}{\nu(\delta^*)^2} \equiv A,$$

the equation to be solved can be written as

$$f_{\zeta/\nu}(x) = -A - f(cx). \tag{1}$$

Now draw the graph of $f_{\zeta/\nu}(x)$ on a sheet of paper, taking the abscissa in logarithmic scale, and draw $-f(y)$ on another sheet of transparant paper, in the same way. Place the latter sheet on the former and let the coordinate axes coincide at first. Then translate the upper sheet parallel to itself, downwards by an amount A and horizontally to the right by an amount $\log c$ (See Fig. 1). Then the abscissa of the crossing points of two curves, read on the scale of the lower sheet, give values of $x = kR'$, which satisfy (1).

Since the convergence of series of defining the functions $f(x)$, $f_{\zeta/\nu}(x)$ and $g_{\zeta/\nu}(x)$ is rather slow, some artifice was necessary to compute their sums. We found it convenient to sum first several terms of these series directly, and to expand the remainder in powers of x. As an example, we give here the formula for $f_{0/\nu}(x)$, which was used in numerical calculation

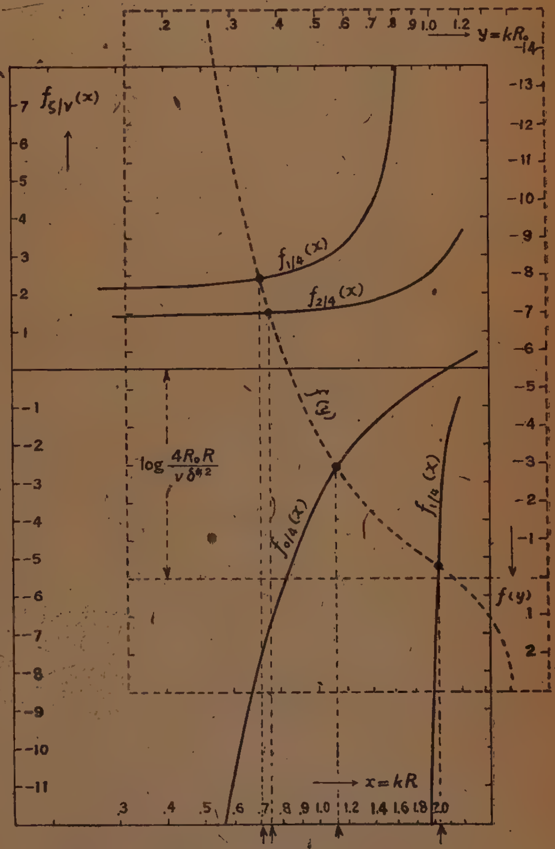

Fig. 1.

$$f_{0/\nu}(x) = \frac{\nu J_0(x)}{2xJ_0'(x)} + \sum_{m=1}^{n}\left(\frac{\nu J_{m\nu}(x)}{xJ'_{m\nu}(x)} - \frac{1}{m}\right) + R_n,$$

$$R_n = a_n\left(\frac{x}{2}\right)^2 + b_n\left(\frac{x}{2}\right)^4 + \cdots,$$

where

---

* Henceforth referred to as I.

$$a_n = \sum_{m=n+1}^{\infty} \frac{2}{m^2\nu(m\nu+1)}$$

$$= \frac{2}{\nu}\Psi'(n+1)+2\Psi(n+1)-2\Psi\left(n+1+\frac{1}{\nu}\right),$$

$$b_n = \sum_{m=n+1}^{\infty} \frac{2(3m\nu+4)}{m^3\nu^2(m\nu+1)^2(m\nu+2)}$$

$$= -\frac{2}{\nu^2}\Psi''(n+1)-\frac{7}{\nu}\Psi'(n+1)-\frac{2}{\nu}\Psi'\left(n+1+\frac{1}{\nu}\right)$$

$$-\frac{19}{2}\Psi(n+1)+10\Psi\left(n+1+\frac{1}{\nu}\right)-\frac{1}{2}\Psi\left(n+1+\frac{2}{\nu}\right),$$

in which $\Psi(u)=\dfrac{d}{du}\log\Gamma(u)$, and $\psi'(u)$, $\psi''(a)$,... are their derivatives.

Table I.

$f(x)$

x	$f(x)$	x	$f(x)$	x	$f(x)$	x	$f(x)$	x	$f(x)$
0.200	−24 867	0.600	−2.5235	1.000	−0.438	1.400	0.948	1.800	18.248
0.210	−22,5361	0.610	−2.428	1.010	−0.406	1.410	0.998	1.810	24.255
0.220	−20.5201	0.620	−2.337	1.020	−0.375	1.420	1.050	1.820	35.925
0.230	−18.7610	0.630	−2.250	1.030	−0.343	1.430	1.104	1.830	68.450
0.240	−17.2176	0.640	−2.167	1.040	−0.312	1.440	1.160	1.840	650.273
0.250	−15.8542	0.650	−2.087	1.050	−0.281	1.450	1.218	1.850	−87.800
0.260	−14.6454	0.660	−2.011	1.060	−0.251	1.460	1.279	1.860	−41.351
0.270	−13.5681	0.670	−1.938	1.070	−0.220	1.470	1.343	1.870	−27.135
0.280	−12.6039	0.680	−1.867	1.080	−0.190	1.480	1.409	1.880	−20.239
0.290	−11.7375	0.690	−1.799	1.090	−0.160	1.490	1.479	1.890	−16.165
0.300	−10.9560	0.700	−1.733	1.100	−0.130	1.500	1.552	1.900	−13.473
0.310	−10.2485	0.710	−1.670	1.110	−0.100	1.510	1.629	1.910	−11.561
0.320	− 9.6026	0.720	−1.609	1.120	−0.069	1.520	1.710	1.920	−10.132
0.330	− 9.0211	0.730	−1.551	1.130	−0.039	1.530	1.795	1.930	− 9.023
0.340	− 8.4866	0.740	−1.494	1.140	−0.008	1.540	1.886	1.940	− 8.136
0.350	− 7.9969	0.750	−1.439	1.150	+0.023	1.550	1.982	1.950	− 7.411
0.360	− 7.5472	5.760	−1.386	1.160	0.054	1.560	2.085	1.960	− 6.806
0.370	− 7.1333	0.770	−1.334	1.170	0.085	1.570	2.195	1.970	− 6.294
0.380	− 6.7512	0.780	−1.284	1.180	0.116	1.580	2.312	1.980	− 5.854
0.390	− 6.3979	0.790	−1.235	1,190	0.147	1.590	2.438	1.990	− 5.472
0.400	− 6.0705	0.800	−1.188	1.200	0.179	1.600	2.573	2.000	− 5.137
0.410	− 5.7665	0.810	−1.142	1.210	0.211	1.610	2.719	2.010	− 4.841
0.420	− 5.4836	0.820	−1.098	1.220	0.243	1.620	2.878	2.020	− 4.576
0.430	− 5.2199	0.830	−1.055	1.230	0.276	1.630	3.051	2.030	− 4.338
0.440	− 4.9737	0.840	−1.012	1.240	0.310	1.640	3.241	2.040	− 4.123
0.450	− 4.7435	0.850	−0.971	1.250	0.344	1.650	3.449	2.050	− 3.928
0.460	− 4.5278	0.860	−0.930	1.260	0.378	1.660	3.680	2.060	− 3.750
0.470	− 4.3254	0.870	−0.890	1.270	0.413	1.670	3.937	2.070	− 3.586
0.480	− 4.1353	0 880	−0.852	1.280	0.449	1.680	4.224	2.080	− 3.435
0.490	− 3.9564	0.890	−0.814	1.290	0.485	1.690	4.548	2.090	− 3.295
0.500	− 3.7878	0.900	−0.777	1.300	0.522	1.700	4.917	2.000	− 3.165
0.510	− 3.6287	0.910	−0.741	1.310	0.560	1.710	5.341		
0.520	− 3.4784	0.920	−0.705	1.320	0.598	1.720	5.834		
0.530	− 3.3362	0.930	−0.670	1.330	0.637	1.730	6.414		
0.540	− 3.2015	0.940	−0.635	1.340	0.678	1.740	7.107		
0.550	− 3.0738	0.950	−0.601	1.350	0.720	1.750	7.950		
0.560	− 2.9525	0.960	−0.568	1.360	0.763	1.760	8.999		
0.570	− 2.8372	0.970	−0.535	1.370	0.807	1.770	10.340		
0.580	− 2.7276	0.980	−0.502	1.380	0.852	1.780	12.117		
0.590	− 2.6231	0.990	−0.470	1.390	0.899	1.790	14.585		

Table II.

$f_{\zeta/8}(x)$

x \ ζ	0	1	2	3	4
0.2	−199.0	4.060	2.087	1.529	1.388
0.3	−87.88	4.112	2.096	1.533	1.391
0.4	−48.99	4.188	2.108	1.538	1.395
0.5	−30.99	4.291	2.125	1.544	1.400
0.6	−21.20	4.425	2.146	1.553	1.406
0.7	−15.30	4.595	2.171	1.562	1.413
0.8	−11.47	4.812	2.201	1.574	1.421
0.9	−8.834	5.088	2.236	1.587	1.430
1.0	−6.947	5.442	2.277	1.602	1.441
1.1	−5.548	5.904	2.324	1.618	1.453
1.2	−4.477	6.523	2.379	1.637	1.466
1.3	−3.640	7.385	2.441	1.658	1.481
1.4	−2.972	8.652	2.513	1.681	1.497
1.5	−2.427	10.68	2.596	1.707	1.515
1.6	−1.976	14.40	2.693	1.738	1.534
1.7	−1.596	25.86	2.805	1.767	1.555
1.8	−1.271	76.42	2.936	1.801	1.578
1.9	−0.9895	−50.81	3.092	1.838	1.603
2.0	−0.7415	−17.83	3.279	1.881	1.630
2.1	−0.5198	−10.35	3.506	1.928	1.659
2.2	−0.3184	−7.036	3.788	1.980	1.690
2.3	−0.1323	−5.170	4.144	2.037	1.724

$f_{\zeta/10}(x)$

x \ ζ	0	1	2	3	4	5
0.2	−248.7	5.063	2.558	1.787	1.476	1.388
0.3	−109.9	5.128	2.569	1.791	1.478	1.389
0.4	−61.24	5.223	2.585	1.797	1.481	1.392
0.5	−38.74	5.351	2.605	1.803	1.485	1.395
0.6	−26.51	5.517	2.630	1.813	1.489	1.399
0.7	−19.13	5.730	2.661	1.823	1.495	1.404
0.8	−14.34	6.000	2.707	1.836	1.502	1.409
0.9	−11.05	6.344	2.740	1.850	1.510	1.415
1.0	−8.689	6.785	2.789	1.866	1.518	1.422
1.1	−6.940	7.361	2.847	1.884	1.528	1.430
1.2	−5.604	8.134	2.913	1.905	1.539	1.439
1.3	−4.559	9.210	2.989	1.928	1.550	1.448
1.4	−3.725	10.79	3.077	1.953	1.563	1.458
1.5	−3.045	13.32	3.178	1.982	1.577	1.470
1.6	−2.483	17.98	3.296	2.013	1.593	1.482
1.7	−2.010	32.30	3.435	2.048	1.610	1.495
1.8	−1.606	95.49	3.595	2.086	1.628	1.509
1.9	−1.256	−63.55	3.787	2.128	1.647	1.525
2.0	−0.9480	−22.33	4.017	2.175	1.669	1.541
2.1	−0.6731	−12.97	4.297	2.227	1.692	1.558
2.2	−0.4237	−8.836	4.645	2.284	1.716	1.577
2.3	−0.1936	−6.506	5.087	2.349	1.743	1.597

$f_{\zeta/12}(x)$

x \ ζ	0	1	2	3	4	5	6
0.2	−298.5	6.069	3.044	2.083	1.650	1.447	1.387
0.3	−131.8	6.147	3.057	2.087	1.652	1.449	1.389
0.4	−73.49	6.261	3.076	2.094	1.655	1.451	1.390
0.5	−46.48	6.414	3.100	2.102	1.659	1.454	1.393
0.6	−31.81	6.613	3.129	2.112	1.664	1.457	1.395
0.7	−22.96	6.868	3.166	2.124	1.670	1.461	1.399
0.8	−17.21	7.192	3.209	2.138	1.677	1.465	1.403
0.9	−13.26	7.604	3.259	2.154	1.685	1.470	1.407
1.0	−10.43	8.133	3.318	2.173	1.693	1.476	1.412
1.1	−8.331	8.824	3.386	2.194	1.703	1.482	1.417
1.2	−6.729	9.751	3.464	2.217	1.714	1.489	1.423
1.3	−5.476	11.04	3.555	2.244	1.726	1.497	1.430
1.4	−4.475	12.94	3.660	2.273	1.740	1.505	1.437
1.5	−3.661	15.97	3.780	2.305	1.754	1.515	1.445
1.6	−2.987	21.56	3.915	2.341	1.770	1.524	1.453
1.7	−2.420	38.74	4.084	2.381	1.788	1.535	1.463
1.8	−1.936	114.6	4.277	2.425	1.806	1.547	1.472
1.9	−1.517	−76.29	4.506	2.473	1.827	1.558	1.483
2.0	−1.149	−26.81	4.780	2.527	1.849	1.572	1.493
2.1	−0.8202	−15.60	5.115	2.587	1.872	1.586	1.506
2.2	−0.5222	−10.64	5.530	2.654	1.898	1.601	1.518
2.3	−0.2474	−7.847	6.059	2.729	1.926	1.617	1.532

$f_{\zeta/4}(x)$

ζ / x	0	1	2
0.2	−99.50	2 101	1.394
0.3	−43.94	2.129	1.394
0.4	−24.49	2.170	1.401
0.5	−15.49	2.225	1.432
0.6	−10.59	2.295	1.453
0,7	− 7.637	2.386	1.478
0.8	− 5.716	2.500	1.508
0.9	− 4.395	2.644	1.543
1.0	− 3.456	2.829	1.584
1.1	− 2.740	3.068	1.631
1.2	− 2.199	3.387	1.685
1.3	− 1.773	3.828	1.748
1.4	− 1.431	4.473	1.820
1.5	− 1.149	5.499	1.903
1.6	− 0.9139	7.377	2.000
1.7	− 0.7135	13.12	2.112
1.8	− 0.5397	38.42	2.243
1.9	− 0.3866	−23.79	2.399
2.0	− 0.2491	− 8.670	2.586
2.1	− 0.1237	− 3.516	2.813
2.2	− 0.00729	− 1.835	3.094
2.3	+ 0.1028	− 0.8735	3.451

$f_{\zeta/5}(x)$

ζ / x	0	1	2
0.2	−124.4	2 576	1.480
0.3	− 54.93	2.610	1.487
0.4	− 30.62	2.659	1.498
0.5	− 19.36	2.725	1.511
0.6	− 13.25	2.810	1.528
0.7	− 9.556	2.919	1.549
0.8	− 7.157	3.058	1.573
0.9	− 5.509	3.233	1.602
1.0	− 4.326	3.458	1.634
1.1	− 3.448	3.751	1.672
1.2	− 2.776	4.143	1.716
1.3	− 2.249	4.687	1.765
1.4	− 1.826	5.484	1.822
1.5	− 1.481	6.757	1.887
1.6	− 1.194	9.092	1.961
1.7	− 0.9505	16.26	2.048
1.8	− 0.7415	47.87	2.147
1.9	− 0.5588	−31.64	2.264
2.0	− 0.3967	−11.02	2.403
2.1	− 0.2505	− 6.333	2.589
2.2	− 0.1164	− 4.253	2.772
2.3	+ 0.00868	− 3.075	3.025

$f_{\zeta/6}(x)$

ζ / x	0	1	2	3
0.2	−149.2	3.065	1.654	1.390
0.3	− 65.91	3.105	1.661	1.390
0.4	− 36.74	3.163	1.672	1.393
0.5	− 23.24	3.241	1.686	1.409
0.6	− 15.90	3.342	1.704	1.419
0.7	− 11.47	3.471	1.725	1.431
0.8	− 8.595	3.635	1.749	1,445
0.9	− 6.619	3.844	1.779	1.461
0.0	− 5.202	4.111	1.812	1.480
1.1	− 4.150	4.460	1.851	1.501
1.2	− 3.346	5.927	1.896	1.524
1.3	− 2.716	5.576	1.948	1.550
1.4	− 2.212	6.528	2.007	1.580
1.5	− 1.801	8.051	2.074	1.612
1.6	− 1.460	10.85	2.149	1.648
1.7	− 1.172	19.44	2,243	1.688
1.8	− 0.9252	57.37	2.349	1.732
1.9	− 0.7104	−38.06	2.473	1.780
2.0	− 0.5209	−13.31	2.621	1.834
2.1	− 0.3504	− 7.699	2.800	1.894
2.2	− 0.1952	− 5.212	3.021	1.961
2.3	− 0.05105	− 3.808	3.299	2.036

Table III.

$g_{\zeta/4}(x)$

ζ / x	0	1
0.2	−100.2	1.265
0.3	− 44.64	1.290
0.4	− 25.19	1.325
0.5	− 16.24	1.383
0.6	− 11.30	1.436
0.7	− 8.357	1.517
0.8	− 6.444	1.619
0.9	− 5.132	1.751
1.0	− 4.194	1.920
1.1	− 3.500	2.143
1.2	− 2.971	2.443
1.3	− 2.561	2.863
1.4	− 2.234	3.485
1.5	− 1.971	4.485
1.6	− 1.755	6.333
1.7	− 1.575	12.05
1.8	− 1.425	37.31
1.9	− 1.296	−26.33
2.0	− 1.186	− 9.858
2.1	− 1.089	− 6.137
2.2	− 1.004	− 4.508
2.3	− 0.9282	− 3.604

$g_{\zeta/5}(x)$

x \ ζ	0	1	2
0.2	−125.1	1.794	0.3856
0.3	−55.62	1.825	0.3891
0.4	−31.32	1.871	0.3941
0.5	−20.07	1.933	0.4009
0.6	−13.95	2.014	0.4088
0.7	−10.27	2.117	0.4187
0.8	−7.873	2.249	0.4307
0.9	−6.231	2.417	0.4449
1.0	−5.056	2.633	0.4616
1.1	−4.185	2.917	0.4811
1.2	−3.521	3.298	0.5039
1.3	−3.004	3.830	0.5305
1.4	−2.592	4.614	0.5617
1.5	−2.258	5.872	0.5984
1.6	−1.982	8.192	0.6417
1.7	−1.752	15.34	0.6938
1.8	−1.558	46.93	0.7548
1.9	−1.390	−32.60	0.8294
2.0	−1.244	−12.00	0.9212
2.1	−1.116	−7.331	1.035
2.2	−1.000	−5.276	1.180
2.3	−0.8954	−4.125	1.369

$g_{\zeta/6}(x)$

x \ ζ	0	1	2
0.2	−149.9	2.311	0.6974
0.3	−66.61	2.349	0.7028
0.4	−37.44	2.405	0.7104
0.5	−23.94	2.480	0.7202
0.6	−16.60	2.578	0.7327
0.7	−12.18	2.704	0.7478
0.8	−9.304	2.863	0.7659
0.9	−7.333	3.067	0.7872
1.0	−5.921	3.328	0.8122
1.1	−4.874	3.671	0.8413
1.2	−4.076	4.131	0.8751
1.3	−3.453	4.772	0.9143
1.4	−2.956	5.716	0.9599
1.5	−2.553	7.229	1.013
1.6	−2.220	10.02	1.072
1.7	−1.941	18.60	1.148
1.8	−1.704	56.51	1.235
1.9	−1.500	−38.92	1.339
2.0	−1.321	−14.19	1.466
2.1	−1.163	−8.593	1.621
2.2	−1.020	−6.120	1.816
2.3	−0.8895	−4.732	2.066

Determination of Cross Section for the Photo-Disintegration of Deuteron.

Ken-ichi SHINOHARA, Toshihiro OKADA, and Susumu MORITA.

Department of Physics, Faculty of Science, Kyushu University.

(Received June 19, 1948).

§ 1. Introduction.

The cross section for the photo-disintegration of deuteron has been measured by several authors. In their pioneer work, Chadwick, and Goldhaber(1) used an ionization chamber which is filled with deuterium and connected to a linear amplifier. They detected the photo-protons produced by the 2.6 Mev gamma-rays emitted from ThC″ and roughly estimated the value of the cross section as 5×10^{-28} cm², with an accuracy of the factor of 2. Richardson and Emo(2) used a cloud chamber and obtained 11×10^{-28} cm² as the value of the cross section for the 3.0 Mev gamma-rays emitted from Na^{24}, with an accuracy of the factor of 2. Because of the uncertainty in the intensity of the gamma-rays used, it was not possible to get an accurate value of the cross section in the latter experiment. Finally, Halban(3) used the method of counting the photo-neutrons, which are produced by the gamma-rays of ThC″, at the centre of a large water tank and slowed down by the surrounding water. He obtained the value of $(10\pm0.8)\times10^{-28}$ cm². His measurement is probably the most accurate of the three mentioned above, but, nevertheless, there is some possibility of a rather large error entering in his measurement, as the method he used in counting the neutrons is indirect.

Theoretical calculation, on the other hand, carried out by Rarita and Schwinger(4) gave a much larger value as the cross section of this process. It is about 3/2 of the value obtained by Halban, and does not seem to show an agreement with the experiment. In view of the importance of the process concerned, we have attempted to carry out a most careful expriment with the gamma-rays from ThC″, and compared the result with the theory.

An ionization chamber filled with deuterium and connected to a linear amplifier has been used, as in the case of the experiment of Chadwick and Goldhaber. The experiment, therefore, consisted of two parts: the counting of the photo-protons liberated in the ionization chamber and the determination of the intensity of the gamma-rays emitted by ThC″ used.

§ 2. Exprimental Arrangement for Counting the Photo-protons.

The ionization chamber used is shown diagramatically in Fig. 1. Its collecting electrode *A* is made of iron rod, 0.5 cm in diameter and 7.5 cm long. It is connected to the grid of the first valve of the linear amplifier. The outer electrode *B* is made of brass cylinder, 10 cm in diameter and 10 cm long. The front side of the chamber is provided with a small window *W*. It is covered with a thin mica sheet of 2.0 cm stopping power and served to test the operating condition of the ionization chamber and the linear amplifier, by introducing the alpha-particles of Po, at frequent intervals.

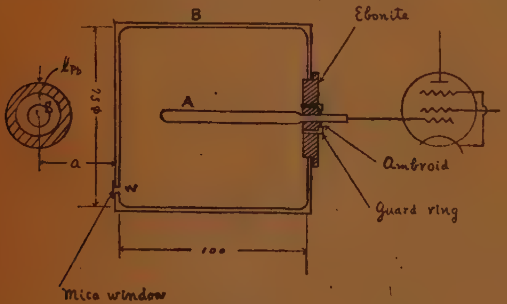

Fig. 1.

Two such ionization chambers were prepared. One of them was filled with deuterium and the other with ordinary hydrogen, both at one atmospheric pressure. The voltage on the outer electrode was always kept at 1500 volts. The output of the linear amplifier was fed into the vertical axis of a Braun tube oscillograph, while its horizontal axis was driven by an alternating voltage of 200 cycles per second. The resulting movement of the spot on the screen was photographed with a Leica camera. The film was kept at rest during each exposure, which lasted for 1/3–1/2 min.

The linearity and the sensitivity of the linear amplifier were tested by applying an alternating voltage of 1,000 cycles per sec. from a standard oscillator through a condenser to the outer electrode of the ionization chamber, at the same time supplying the steady voltage of 1,500 volts to this electrode. It was found that the output of the amplifier including the oscillograph changed perfectly linearly to the applied alternating voltage in the range of the output pulses of several times the noise level. Since the pulses due to the photo-protons amounted to only 2 to 3 times the noise level, the linearity of the present amplifier was supposed to be sufficient for our purpose. The sensitivity of the amplifier, measured on the photographic film was found to be 0.17 mv/mm.

The gamma-ray source was RdTh and was enclosed in a glass tube of 2.5 cm in diameter*. The lengh of the source was about 2 cm. It was placed at *S* in Fig. 1. The distance *a* (Fig. 1) between its centre and the front face of the ionization chamber was taken either as 4.0 cm or 6.0 cm. The source was surrounded by a lead sheet of 0.5 cm or 1.0 cm, in order to cut down the soft gamma-rays and lower the noise level.

§ 3. Results of Counting the Photo-Protons.

In order to elimnate the backgound counts and obtain the true photo-proton counts, the following four series of measurements were carried out.

1. The ionization chamber filled with D_2 was used and the gamma-ray source was placed at S.

---

* The gamma-ray source was kindly loaned by Dr. Sagane of the Tokyo University.

2. The ionization chamber filled with D_2 was used, but no gamma-ray source at S.

3. The ionization chamber filled with H_2 was used and the gamma-ray source was placed at S.

4. The ionization chamber filled with H_2 was used and no gamma-ray source at S.

The pulses recorded in the first arrangement can be divided into two classes. The pulses belonging to the first class had a breadth of about 2×10^{-4} sec and showed the characteristic features of the heavy ionizing particles. The size of the pulses was consistent with the energy of the photo-protons as estimated from the binding energy of the deuteron, the quantum energy of the gamma-rays, and the sensitivity of the amplifier. Most of them are obviously due to the photo-protons, but it is also possible that a few are caused by the contaminated alpha-particles and the accidental accumulation of the secondary electrons liberated by the gamma-rays. Pulses belonging to the second class had a much irregular appearance and their breadth was of the magnitude usually more than ten times of those belonging to the first class. They are probably caused by occasional small discharge due mainly to the insufficient insulation, in the high tension supplies and in the ionization chamber. We have also included large pulses caused by the contaminated alpha-particles in this second class.

The pulses obtained in the second arrangement consisted almost entirely of those belonging to the second class and their number was nearly the same as those in the first arrangement. The pulses belonging to the first class were very few in number.

Almost all the pulses photographed in the third and the fourth arrangement belonged to the second class. Their numbers were nearly the same, in both cases, as those in the first and the second ar-

Table I.

Date	gas	$a^{1)}$ in cm	$l_{pb}^{2)}$ in cm	with the source		without the source		n_p per min.
				No. of pulses of the 1st kind per min.	No. of pulses of the 2nd kind per min.	No. of pulses of the 1st kind per min.	No. of pulses of the 2nd kind per min.	
March, 12. 1943	D_2	4.0	1.0	7.6 ± 1.1	5.9 ± 1.1	0.6 ± 0.3	5.0 ± 1.0	6.6 ± 1.2³⁾
,,	D_2	4.0	1.0	5.2 ± 1.1	6.6 ± 1.2	0.5 ± 0.3	5.2 ± 1.2	4.5 ± 1.2³⁾
,,	D_2	4.0	1.0	51. ± 1.0	6.1 ± 1.1	0	9 ± 3	4.9 ± 1.0³⁾
,,	H_2	4.0	1.0	0.6 ± 0.3	4.8 ± 1.0	0	3.4 ± 1.0	—
,,	H_2	4.0	1.0	0	3.4 ± 0.9	0.3 ± 0.3	4.3 ± 1.2	—
May, 1. 1943	D_2	4.0	0.5	10.8 ± 1.6	5.2 ± 1.1	2.4 ± 1.0	5.7 ± 1.8	8.4 ± 1.9
,,	D_2	4.0	0.5	8.0 ± 1.3	5.9 ± 1.1	0	4.8 ± 1.8	8.0 ± 1.3
,,	D_2	4.0	0.5	8.3 ± 1.1	4.6 ± 0.8	0	0.8 ± 0.6	8.1 ± 1.1
,,	D_2	4.0	0.5	9.2 ± 1.4	4.0 ± 0.9	0	6.0 ± 1.7	9.2 ± 1.4
,,	H_2	4.0	0.5	1.3 ± 0.6	2.9 ± 0.8	0	0	—
,,	H_2	4.0	0.5	2.0 ± 0.8	1.7 ± 0.7	0.6 ± 0.4	4.0 ± 1.1	—
May, 3. 1943	D_2	4.0	0.5	6.9 ± 1.2	8.7 ± 1.4	0	6.0 ± 1.6	6.9 ± 1.2
,,	H_2	4.0	0.5	0.8 ± 0.5	2.9 ± 0.9	0.8 ± 0.6	4.8 ± 1.4	—
May, 6. 1943	D_2	4.0	1.0	6.8 ± 1.3	4.9 ± 1.1	0	4.0 ± 1.6	6.8 ± 1.3
,,	D_2	6.0	1.0	4.1 ± 0.7	7.0 ± 1.0	0	6.2 ± 1.4	4.1 ± 0.7
,,	H_2	4.0	1.0	0	4.2 ± 1.2	0.5 ± 0.5	4.0 ± 1.4	—
May, 8. 1943	D_2	6.0	1.0	3.3 ± 0.7	4.8 ± 0.9	0	4.7 ± 1.2	3.3 ± 0.7
,,	D_2	6.0	1.0	3.9 ± 0.8	5.7 ± 1.0	0	4.2 ± 1.0	3.9 ± 0.8
,,	D_2	6.0	1.0	4.0 ± 0.9	5.4 ± 1.0	0.4 ± 0.3	5.7 ± 1.1	4.0 ± 0.9
,,	H_2	6.0	1.0	0	3.0 ± 1.0	0	4.0 ± 1.3	—

(1): Distance between the source and the front face of the ionization chamber
(3): Thickness of the lead sheet surrounding the source.
(3): The values reduced to those on May, 1943, from the decay of RdTh.

rangements.

From these results, the difference of the number of the pulses belonging to the first class, in the first and the second arrangement, was taken as the number of photo-protons. The experimental results are given in Tab. I and the weighted mean of the number of photo-protons recorded per min. is given in the last column of the table.

§ 4. Measurement of the Intensity of the Gamma Ray Source.

Since the RdTh source contained a considerable quantity of Ra, it was necessary, first, to determine the ratio of the amount of RdTh and Ra contained in it. Alpha-rays emitted by the source was used for this purpose*.

The method of the measurement is shown in Fig. 2. As the RdTh source was in the form of a solution and some glass wools were enclosed with it in the glass tube, its small amount was taken out and put in a small cavity of 8 mm in diameter and 0.5 mm deep, made on a glass plate and covered with a thin mica sheet of 7-8 mm stopping power. This served as the alpha-ray source and was placed at S. The space A is connected through an air reservoir to a vacuum pump and its pressure could be adjusted to any value below atmospheric pressure. The space B and the ionization chamber was always kept at 1 atm, and the effective depth of the ionization chamber was about 3 mm. Both of the space A and B were filled with air. The ionization chamber was connected to the linear amplifier and its output drove, through a scale-of-eight counter, a thyratron recording circuit. The number of alpha-particles counted was 300-500 per min.

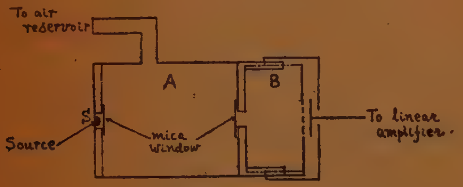

Fig. 2.

There are only three radioactive elements in the Ra and RdTh series which emits alpha particles of range longer than 5 cm. They are RaC′, ThA and ThC′. In the equilibrium state of RdTh series, ThA emits one alpha-particles of 5.68 cm range, and ThC′ emits 0.65 alpha-particles of 8.62 cm range, per disintegration of RdTh. In the Ra series, RaC′ emits one alpha-particle of 6.95 cm range per disintegration of Ra. An example of the relation obtained between the number of the alpha particles counted and the pressure of the air in the space A is shown in Fig. 3.

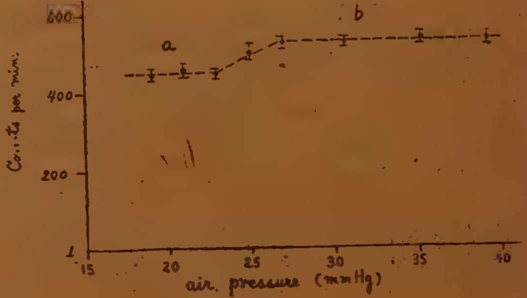

Fig. 3.

There is a sudden jump in the curve at the point where the range of the ThA alpha-particles ends. The ratio R of the number of alpha particles on both sides of the jump can be expressed by

$$R=\frac{C_{Ra}+0.65\times1.09\,C_{RdTh}}{C_{Ra}+1.65\times1.09\,C_{RdTh}}=\frac{C_{Ra}+0.71\,C_{RdTh}}{C_{Ra}+1.80\,C_{RdTh}} \tag{1}$$

where C_{Ra} is the amount of Ra expressed in mg, and C_{RdTh}, the amount of RdTh expressed in gamma-ray equivalent of Ra. C_{RdTh} should be multiplied by a factor 1.09, since RdTh disintegrates at the rate of 1.09 times more than Ra, when they are both in equilibrium with their daughter substances and the gamma-ray intensities are also equal. It is therefore,

$$\frac{C_{Ra}}{C_{RdTh}}=\frac{1.80\,R-0.71}{1-R} \tag{2}$$

Table II shows the results of the measurement. The second column gives the dates on which the measurements were done, and the third and the fourth column give the number of alpha particles counted per minutes before (part b) and after (part a) the ThA jump, respectively. The last column gives the ratio R.

---

* The method has been suggested by Dr. Sagane.

Table II.

Source	Date	No. of pulses per min. at part a.	No. of pulses per min. at part b.	R
No. 1	Oct. 6, 1943	376 ± 8.6	434 ± 10.5	$0.86_6 \pm 0.02_9$
,,	Oct. 10, 1943	438 ± 7.4	503.5 ± 4.6	$0.85_9 \pm 0.01_6$
,,	Oct. 15, 1943	303 ± 4.4	351 ± 4.2	$0.86_5 \pm 0.01_6$
,,	Oct. 17, 1943	287 ± 3.5	337.5 ± 5.8	$0.85_0 \pm 0.01_8$
,,	Oct. 18, 1943	263 ± 6.6	400 ± 7	$0.87_7 \pm 0.03_0$
No. 2	Oct. 22, 1943	426 ± 5.5	489.6 ± 4.5	$0.87_0 \pm 0.01_6$
			mean	$0.86_3 \pm 0.00_8$

The source No. 1 was enclosed in the cavity on the 4th of Oct. 1943, and No. 2, on the 20th of Oct. 1943. The fact that the ratio R does not change with the time shows that the RdTh source was at a sufficiently equilibrium state. From Tab. II we get

$$\frac{C_{Ra}}{C_{RdTh}} = 6.13 \pm 0.25 \quad \text{(Oct. 1943)}$$

$$= 5.25 \pm 0.21 \quad \text{(May, 1943)}$$

On the other hand, the total amount of the radioactive substances S, expressed in its gamma ray equivalent with Ra, has been determined by comparing the intensity of the gamma rays emitted by it with that of a 1.01 mg of Ra. Comparison was made with a gold-leaf electroscope, and the gamma rays were filtered with 3 mm of lead before entering it. The result is

$$C_{Ra} + C_{RdTh} = 0.94_0 \ mC.$$

Therefore, we get, finally,

$$C_{RdTh} = 0.150 \pm 0.01 \ mC \quad \text{(May, 1943)}$$

§ 5. The Cross Section of the Photo-Disintegration.

With the geometrical arrangement shown in Fig. 1, the number of the photo-protons emitted in the ionization chamber per min., can be expressed by

$$n_p = \frac{N_\gamma \sigma n}{2} I e^{-(\mu_{Pb} l_{Pb} + \mu_{Br} l_{Br})} \cdot \{2b + \sqrt{a^2+b^2} - \sqrt{(a+2b)^2+b^2}\} \qquad (3)$$

if a point source of the gamma-rays is assumed.

In (3), a is the distance between the source and the front side of the ionization chamber facing the source, and was taken, either, as 4.0 or 6.0 cm. b is the length of the ionization chamber and is also equal to its diameter, being equal to 10 cm. N_γ is the number of the gamma-ray quantum of 2.62 Mev emitted per min. from RdTh of 1 mg Ra gamma-ray equivalent. Since the 2.62 Mev. quantum is known to be emitted at a rate of one at each disintegration of ThC″ and since, in equilibrium with its daughter substances, the atoms in the RdTh series disintegrate at a rate of 1.09 times of those of Ra series, when their intensities measured with the gamma-rays are equal, the value of N_γ is equal to

$$N_\gamma = 3.70 \times 10^7 \times 0.35 \times 60 \times 1.09 = 0.849 \times 10^9,$$

where 3.70×10^7 is the number of Ra atoms disintegrating per sec. and mg. and 0.35 is the part of the RdTh disintegrating into ThC″, n is the number of deuterium atoms per cc in the ionization chamber, and is equal to 5.4×10^{19}. I is the intensity of RdTh source and is equal to 0.150 ± 0.01 mg Ra equivalent in gamma-ray intensity. μ_{Pb} and μ_{Br} are the absorption coefficient of lead and brass for the gamma-rays of 2.62 mev. and are taken as 0.461_6 cm^{-1} and 0.315 cm^{-1}, respectively. l_{Pb} is the thickness of the lead plate surrounding the source to cut down soft gamma-rays, and l_{Br} is the thickness of the brass plate forming the front side of the ionization chamber, and finally, σ is the cross section of the photo-disintegration process.

Actually, the RdTh source was not a point source but was distributed in a volume in the glass tube. We, therefore, tried to calculate the correction due to this finite size of the source by assuming, either, the source to be distributed uniformely in a sphere of 2.5 cm in diameter or in a cylinder of 2.5 cm in diameter and of equal height. The calculation was done numerically and it was found that, in either case, the correction amounted to only 2% and they were nearly equal for both cases. Table III gives the values of σ thus obtained, with three different arrangements.

Table III.

a in cm	l_{pb} in cm	n_p/min	$\sigma\times10^{-23}$ cm^2
4.0	0.5	8.0 ± 0.6	18.6 ± 2.1
4.0	1.0	5.6 ± 0.6	16.5 ± 2.3
6.0	1.0	3.8 ± 0.4	16.4 ± 2.3
		mean	17.2 ± 1.5

The errors in the values of σ were estimated from the geometrical conditions, the errors in the measurement of n_p and I. The final value of σ obtained as the weighted mean of the three measurements is $(17.2\pm1.5)\times10^{-23}$ cm^2.

This value of the cross section is higher than any of the previous measurements. According to the theoretical calculation carried out by Rarita and Schwinger, the cross section should be 12×10^{-23} cm^2 for the electric dipole transition, and 3.3×10^{-23} cm^2 for the magnetic dipole one. The total cross section, therefore, becomes 15.3×10^{-23} cm^2. Thus our results, unlike the previous results, agrees within the limit of the experimetal error, with the theoretical calculation.

References.

(1) J. Chadwick and M. Goldhaber, Proc. Roy. Soc., **151** (1935), 479.
(2) J. Richardson and L. Emo, Phys. Rev., **53**, (1938), 234.
(3) H. von Halban, Jr., Comptes rendus, **206**, (1938), 1170.
(4) W. Rarita and J. Schwinger, Phys. Rev., **59**, (1941), 436.
(5) A. Ricoux, J. de phys., **8**, (1937), 388.

Thomas-Fermi-Dirac Equation for not Completely Degenerate Electron Gases.

By Isaaki YOKOTA

Niigata Higher School

(Received June 28, 1948)

The Thomas-Fermi method, or statistical method in many-electron problems of quantum mechanics is sometimes very useful in itself or as the first approximation to the more elaborate procedures. But the ordinary Thomas-Fermi equation concerns only with the ground state of many-electron systems, i. e. with the completely degenerate electron gases, so it corresponds only to the states at absolute zero temperature. The equation generalized so as to include the cases at any temperature has been derived by Marshak, Bethe(1) and by Prof. Sakai(2) independently, and has been applied to some astrophysical problems by the formers.

On the other hand, as has been shown by Jensen,(3) the exchange energy of electrons, which was not taken into consideration in the original equation of Thomas and Fermi, becomes appreciable when the electron density is not so large (when $n\leq1/a_0^3$, where n is the number of electrons per cm^3 and a_0 the Bohr's radius of hydrogen atoms), as the density of kinetic energy increases as $n^{5/3}$, whereas that of exchange energy increases as $n^{4/3}$ with electron density n. The improved equation which takes into consideration the effect of exchange has been first derived by Dirac(4) for completely degenerate system and is known under the name of the Thomas-Fermi-Dirac equation.

The aim of the present work is to take into consideration both effects of temperature and exchange upon the electron distribution through the evaluation of the effects of temperature on the density of exchange energy.

We treat a system composed of electrons and atomic nuclei in thermal equilibrium, the latters being at rest. The method we adopt is the variational one in which we first calculate the density of free energy at any point of the system with given electron density, temperature and electrostatic potential under the assumption of Fermi distribution. Integrating the expression thus obtained over the whole space, we have the total free energy of the system, which is minimized under the additional condition that the total number of electrons is given. The result and variational equation together with the Poisson equation gives the required one.

The above procedures are essentially the same as those adopted by Jensen(3) in his derivation of Thomas-Fermi-Dirac equation valid at absolute zero temperature, in which he minimized the energy instead of the free energy in our case.

We, however, shall treat the effects of temperature only in the first approximation, so that our equation may be applied only to the cases when the temperature is far below the degeneration temperature at any part of the system considered.

So our equation can not be applied to the thermally excited atoms or molecules in isolation but only to the systems of collective electrons as has been treated by Marshak and Bethe,(1) and will find some application in theory of metals and in astrophysics.

Now we shall calculate the exchange energy per unit volume for the assembly of free electrons as a function of electron density and temperature. Considering a system of free electrons enclosed within a cube of unit volume, we assume that the kinetic energies of electrons are distributed according to Fermi distribution. This assumption is not consistent with our procedures, because, as Bardeen(5) has pointed out, the exchange energies should modify the distribution function, especially in somewhat remarkable degree near the top of the filled region. Regarding this subject, however, we have no experimental evidences up to the present, and it is possible that the correlation energies which we leave out of consideration in this paper might have an effect compensating that of exchange.(6)

Now the exchange energy between two free electrons with momenta $\hbar\vec{k}_1$ and $\hbar\vec{k}_2$ and with parallel spins is, as well known, given by

$$\varepsilon_{ex}(\vec{k}_1, \vec{k}_2) = -\frac{4\pi e^2}{|\vec{k}_1-\vec{k}_2|^2}. \tag{1}$$

So the exchange energy per unit volume can be expressed in the double integral in $\vec{k}$ space:

$$u_{ex} = -2\iint \frac{4\pi e^2}{|\vec{k}_1-\vec{k}_2|^2} f(\varepsilon_1) f(\varepsilon_2) \frac{d\vec{k}_1\, d\vec{k}_2}{(2\pi)^6}. \tag{2}$$

where $f(\varepsilon)$ is the Fermi function with $\varepsilon = \hbar^2k^2/2m$. To carry out the integration, we first average the integrand over all angles between $\vec{k}_1$ and $\vec{k}_2$, and we have

$$u_{ex} = -\frac{2\pi e^2\hbar^2}{m} C^2 \iint \log\left|\frac{\sqrt{\varepsilon_1}+\sqrt{\varepsilon_2}}{\sqrt{\varepsilon_1}-\sqrt{\varepsilon_2}}\right| \times f(\varepsilon_1) f(\varepsilon_2)\, d\varepsilon_1\, d\varepsilon_2, \tag{3}$$

where

$$C = 2\pi \frac{(2m)^{3/2}}{h^3}. \tag{4}$$

In this expression we have transformed the integral variables from k's to ε's. The approximate value of the integral can be evaluated when the temperature is not so high.* After some calculation we find

---

* The first step of integration can be carried out as usual according to the Sommerfeld's method. But in the second step the integrand has the singularities at $\varepsilon = \varepsilon_0$, ε_0 being the *"Grenzenergie"* in Fermi distribution, and some devices are necessary in calculation.

$$u_{ex} = -\frac{2\pi e^2 \hbar^2}{m} C^2 \left\{2\varepsilon_0^2 + \frac{\pi^2}{6}(kT)^2 \times\left(-2\log\frac{\varepsilon_0}{kT} + \gamma\right)\right\}, \tag{5}$$

where γ is a numerical constant which contains some definite integrals.** But its numerical value is trivial for our present purposes.

As well known, ε_0 is given by

$$\varepsilon_0 = \varepsilon_{00} - \frac{\pi^2}{12}\frac{(kT)^2}{\varepsilon_{00}},$$

where ε_{00} is the "*Grenzenergie*" at absolute zero temperature and can be expressed as a function of the electron density n only:

$$\varepsilon_{00} = \frac{h^2}{2m}\left(\frac{3}{8\pi}\right)^{2/3} n^{2/3}.$$

Substituting these in (5), we have at once

$$u_{ex} = -\frac{3}{2}e^2\left(\frac{3}{8\pi}\right)^{1/3} n^{4/3} + \frac{32\pi^3 m^2 e^2}{9h^4}(kT)^2 \times\left[\log\frac{h^3}{(2mkT)^{3/2}}\frac{3}{8\pi}n - \frac{3}{4}(\gamma-2)\right], \tag{6}$$

which is the desired expression for the density of the exchange energy.

It is easy to see that the density of the kinetic free energy f_{kin} can be written in terms of the electron density and the temperature as follows:

$$f_{kin} = \frac{3h^2}{10m}\left(\frac{3}{8\pi}\right)^{2/3} n^{5/3} - \frac{\pi^2 m}{2h^2}\left(\frac{8\pi}{3}\right)^{2/3}(kT)^2 n^{1/3}. \tag{7}$$

Now the density of free energy f consists of three parts, the kinetic (7), the exchange (8) and the potential terms:

$$f = f_{kin} + u_{ex} + u_{pot}, \tag{8}$$

the last being given by

$$u_{pot} = -en\left(\Phi + \frac{1}{2}\varphi\right), \tag{9}$$

where Φ and φ are the potentials due to nuclei and electrons respectively, and the latter is connected with n through the Poisson equation

$$\Delta\varphi = 4\pi e n. \tag{10}$$

Integrating (8) over all space, we have the total free energy of the system:

$$F = \int (f_{kin} + u_{ex} + u_{pot})\,d\tau, \tag{11}$$

Now thermodynamic principles require that the free energy of the system in the thermal equilibrium must have the minimum value consistent with the given temperature and external parameters. This requirement, together with the subsidiary condition that the total number of electrons

$$N = \int n\,d\tau$$

must be constant, gives the variational equation

$$\frac{\delta F}{\delta n} - \mu = 0, \tag{12}$$

where $\delta F/\delta n$ is the functional derivative of F with respect to n, and μ is the Lagrangian multiplication factor with minus sign and corresponds to the chemical potential per electron.

From (6), (7), (9) and (11) we find the explicit expression of (12):

$$\frac{h^2}{2m}\left(\frac{3}{8\pi}\right)^{2/3} n^{2/3} - 2e^2\left(\frac{3}{8\pi}\right)^{1/3} n^{1/3} - (kT)^2\left[\frac{\pi^2 m^2}{6h^2}\left(\frac{3}{8\pi}\right)^{2/3} n^{-2/3} - \frac{32\pi^3 m^2 e^2}{9h^4} n^{-1}\right] - e\left(\Phi + \varphi + \frac{\mu}{e}\right) = 0. \tag{13}$$

Now we put

$$\overline{\Psi} = \Phi + \varphi + \frac{\mu}{e} = V + \frac{\mu}{e} \tag{14}$$

where V is the potential at the point considered. Then we see from (10) and (13) that $\overline{\Psi}$ satisfies

$$(\Delta\overline{\Psi})^{2/3} - \frac{2^{16/3}\pi^{4/3} m e^{8/3}}{3^{2/3} h^2}(\Delta\overline{\Psi})^{1/3} - (kT)^2\left[\frac{2^{8/3}\pi^{10/3} m^2 e^{4/3}}{3h^4}(\Delta\overline{\Psi})^{-2/3} - \frac{2^8\pi^4 m^3 e^4}{3^2 h^6}(\Delta\overline{\Psi})^{-1}\right] = \frac{2^{13/3} m e^{5/3}}{3^{2/3} h^2}\overline{\Psi}, \tag{15}$$

which is the required equation.

We see that the equation (15) agrees with the ordinary Thomas-Fermi-Dirac equation when the temperature is absolute zero, as it must be. Also we see that, if we omit the terms which originate

---

** $\gamma = 2 - 4\log 2 + \frac{12}{\pi^2}\gamma_1 - \gamma_2 + 2\gamma_3$

where

$$\gamma_1 = \int_0^\infty x\log x\frac{dx}{e^x+1}, \quad \gamma_2 = \int_0^1 \frac{e^x-1}{x}\frac{dx}{e^x+1}, \quad \gamma_3 = \int_1^\infty \frac{1}{x}\frac{dx}{e^x+1}.$$

from exchange effect, we have the same equation as obtained by Marshak, Bethe and Prof. Sakai.

In conclusion, the author wishes to express his cordial thanks to Prof. Ochiai for his kind interest in this work.

References.

(1) R. E. Marshak & H. A. Bethe: Astrophys. J. **91** (1940), 239.
(2) T. Sakai: Proc. Phys.-Math. Soc. Jap. **24** (1942), 254.
(3) H. Jensen: Zeits. f. Phys. **89** (1934), 713.
(4) P. A. M. Dirac: Proc. Camb. Phil. Soc. **26** (1930), 376.
(5) J. Bardeen: Phys. Rev. **50** (1936), 1098.
(6) F. Seitz: *The Modern Theory of Solids* (New York, 1939), 422.

Viscosity of High Polymer Solutions, I. Rigid Skein Model.

By Nobuhiko SAITÔ.

Kobayasi Institute of Physical Research, Kokubunzi, Tokyo.

(Read September 9, 1947; Received July 6, 1948)

§1. Introduction.

Since Kuhn's treatment(1) the skein model for high polymers has been used by several authors(2),(3),(4) in the theory of viscosity of dilute solutions. We also adopt this model although there are some facts which are contradictory to this over-simplified model. The assumptions are the followings; 1, a high polymer molecule is composed of spherical particles connected by rigid rods and is not deformed by the flow; 2, the mass of the molecule can be neglected; 3, the flow of the liquid is not disturbed by rigid rods and there is no interaction among the parts of the flow arround different particles; 4, the forces by the flow, acting on the spherical particles, are those of Stokes; 5, the solution is so dilute that the molecules behave independently.

Huggins(2) treated the case of the most general internal configuration of a molecule; however, only in the two dimensional case. Debye's theory(4), though it is the simplest, grasps the essential points, discussing the case of the spherical symmetry of the internal configuration. We intend to treat the Huggins' model for the three dimensional case.

§2. Kinematical Behavior of a Macromolecule in a Laminar Flow.

Let x, y, z be a coordinate system referred to a fixed space, and ξ, η, ζ referred to a molecule. The origins can be chosen to be the same. The transformation between them is determined by a matrix $A=(a_{ik})$. The coordinates of the ith particle are $r_i(x_i, y_i, z_i)$ in $x\,y\,z$-system or $s_i(\xi_i, \eta_i, \zeta_i)$ in $\xi\,\eta\,\zeta$-system, and between them there exists the following relation

$$r_i = A s_i \tag{1}$$

The velocity of the liquid is assumed to be

$$u = Gr, \qquad G = \begin{pmatrix} 0 & 0 & 0 \\ g & 0 & 0 \\ 0 & 0 & 0 \end{pmatrix} \tag{2}$$

in $x\,y\,z$-system or

$$v = Bs, \qquad B = (b_{ik}) = A^{-1}GA \tag{3}$$

in $\xi\,\eta\,\zeta$-system. Therefore the velocity of the ith particle relative to the flow will be $[\omega, s_i] - v$ in $\xi\,\eta\,\zeta$-system, $\omega(\omega_\xi, \omega_\eta, \omega_\zeta)$ being the angular velocity of the rotation of the molecule. Hence the force upon the ith particle is

$$K_i = -f\eta_0\, a_i([\omega\, s_i] - \mathrm{B}\, s_i), \tag{4}$$

where a_i, η_0, f are respectively the radius of the ith particle, the coefficient of viscosty of the solvent, and a constant. The moment of force about the origin due to the ith particle is

$$\boldsymbol{M}_i = [\boldsymbol{s}_i, \boldsymbol{K}_i] = -f\eta_0\, a_i[\boldsymbol{s}_i, [\boldsymbol{\omega}, \boldsymbol{s}_i] - \mathrm{B}\,\boldsymbol{s}_i], \tag{5}$$

By the assumption 2, $\sum \boldsymbol{K}_i$ and $\sum \boldsymbol{M}_i$ must vanish. We can choose the origin of the coordinate system to be the center of mass and $\xi\,\eta\,\zeta$-axes to be the principal axes of the moment of inertia of the molecule when a_i is regarded as if it were the mass of the particle. Then the relation $\sum \boldsymbol{K}_i = 0$ is always satisfied and the relation $\sum \boldsymbol{M}_i = 0$ leads to the following three relations.

$$\left.\begin{aligned} \omega_\xi(Q+R) &= b_{32}Q - b_{23}R, \\ \omega_\eta(R+P) &= b_{13}R - b_{31}P, \\ \omega_\zeta(P+Q) &= b_{21}P - b_{12}Q, \end{aligned}\right\} \tag{6}$$

where

$$P = \sum a_i \xi_i^2, \quad Q = \sum a_i \eta_i^2, \quad R = \sum a_i \zeta_i^2, \tag{7}$$

and the relations

$$\sum a_i \xi_i \eta_i = 0, \ \sum a_i \eta_i \zeta_i = 0, \ \sum a_i \zeta_i \xi_i = 0 \tag{8}$$

are used. From the definition of B, we have

$$\left.\begin{aligned} \omega_\xi &= g(a_{12}\, a_{23} Q - a_{13}\, a_{22} R)/(Q+R), \\ \omega_\eta &= g(a_{13}\, a_{21} R - a_{11}\, a_{12} P)/(R+P), \\ \omega_\zeta &= g(a_{11}\, a_{22} P - a_{12}\, a_{21}\, Q)/(P+Q), \end{aligned}\right\} \tag{9}$$

where a_{ik} may be expressed by the Eulerian angles θ, φ, ψ. On the other hand we have generally

$$\left.\begin{aligned} \omega_\xi &= \dot\vartheta \sin\psi - \dot\varphi \sin\theta, \\ \omega_\eta &= \dot\theta \cos\psi + \dot\varphi \sin\psi \sin\theta, \\ \omega_\zeta &= \dot\psi + \dot\varphi \cos\theta. \end{aligned}\right\} \tag{10}$$

From these relations we can determine the motion of a macromolecule in a laminar flow. In particular when $P = Q$,

$$\left.\begin{aligned} \dot\theta &= -\frac{g}{4}\,\frac{P-R}{P+R}\sin^2\theta \sin 2\varphi, \\ \dot\varphi &= \frac{g}{2}(1 - \frac{P-R}{P+R}\cos 2\varphi), \\ \dot\psi &= \frac{g}{2}\cos\theta\,(1 - \sin\theta \\ &\quad + \frac{P-R}{P+R}\sin\theta \cos 2\varphi \end{aligned}\right\} \tag{11}$$

which shows the same motion as that of the ellipsoid of revolution derived by Jeffery(8), if we appropriate P, $Q(=P)$ and R to a^2, $b^2(=a^2)$ and c^2, squares of the halves of the axial lengths of the ellipsoid.

§ 3. Influence of the Brownian Motion.

The distribution function $\rho(\theta, \varphi, \psi)$ of the orientation of molecules is influenced by two effects. The one is the effect of the systematic movement of a molecule calculated above, and the other that of the rotational Brownian motion. If the rotational frictional constants w_ξ, w_η, w_ζ about three principal axes are all equal to unity, we have the following equation for the rate of change of the distribution function,

$$\partial\rho/\partial t = -\mathrm{div}\ \omega\rho + kT\ \mathrm{div\ grad}\ \rho. \tag{12}$$

However, when w_ξ, w_η, w_ζ are not equal to each other as is the case under consideration, we can proceed as follows.(5) The energy dissipation by an infinitesimal rotation of a molecule in a fluid at rest is described by

$$\begin{aligned} dW = {} & w_\xi(\sin\psi d\theta - \sin\theta \cos\psi d\varphi)^2 \\ & + w_\eta(\cos\psi d\theta + \sin\theta \sin\psi\, d\varphi)^2 \\ & + w_\zeta(\cos\theta d\varphi + d\psi)^2. \end{aligned} \tag{13}$$

Putting

$$\left.\begin{aligned} dy^1 &= \sqrt{w_\xi}(\sin\psi d\theta - \sin\theta \cos\psi d\varphi), \\ dy^2 &= \sqrt{w_\eta}\,(\cos\psi d\theta + \sin\theta \sin\psi d\varphi), \\ dy^3 &= \sqrt{w_\zeta}\,(\cos\theta\, d\theta + d\psi), \end{aligned}\right\} \tag{14}$$

then

$$dW = (dy^1)^2 + (dy^2)^2 + (dy^3)^2. \tag{15}$$

On the other hand dW is a quadratic form of $d\theta$, $d\varphi$ and $d\psi$, that is,

$$dW = \sum g_{ik}\, dx^i\, dx^k. \tag{16}$$

where

$$\left.\begin{aligned} &(dx^1, dx^2, dx^3) = (d\theta, d\varphi, d\psi) \\ &g_{11} = w_\xi \sin^2\psi + w_\eta \cos^2\psi + w_\zeta \cos^2\theta \\ &g_{12} = g_{21} = -(w_\xi - w_\eta)\sin\theta \sin\psi \cos\psi \\ &g_{13} = g_{31} = 0 \\ &g_{22} = w_\xi \sin^2\theta \cos^2\psi + w_\eta \sin^2\theta \sin^2\psi + w_\zeta \cos^2\theta \\ &g_{23} = g_{32} = w_\zeta \cos\theta \\ &g_{33} = w_\zeta. \end{aligned}\right\} \tag{17}$$

Using the variables dy^1, dy^2, dy^3, Eq. (12) holds in the usual sense of div and grad. As for the variables dx^1, dx^2. dx^3, therefore, Eq. (12) must hold with the operators div and grad in the meaning of the Riemanian geometry with fundamental tensors g_{ik} defined by Eqs. (17). In our problem of viscosity, it is sufficient to deal with the stationary state $\partial\rho/\partial t = 0$. And further if we assume $P = Q$ for the sake of simplicity, then $w_\xi = w_\eta = w$ (see § 4) and Eq. (12) becomes

$$\dot{\theta}\frac{\partial\rho}{\partial\theta}+\dot{\varphi}\frac{\partial\rho}{\partial\varphi}+\dot{\psi}\frac{\partial\rho}{\partial\psi}+\rho\dot{\theta}\frac{\cos\theta}{\sin\theta}+\rho\left(\frac{\partial\dot{\theta}}{\partial\theta}+\frac{\partial\dot{\varphi}}{\partial\varphi}+\frac{\partial\dot{\psi}}{\partial\psi}\right)$$
$$=\frac{kT}{w}\left[\frac{1}{\sin\theta}\frac{\partial}{\partial\theta}\left(\sin\theta\frac{\partial\rho}{\partial\theta}\right)+\frac{1}{\sin^2\theta}\frac{\partial^2\rho}{\partial\varphi^2}\right] \qquad (18)$$

Substituting $\dot{\theta}, \dot{\varphi}, \dot{\psi}$ from Eqs. (11), and putting $\frac{R-P}{R+P}=p$, $\frac{kT}{w}=D$, we have

$$g\left(p\frac{\sin2\theta\sin2\varphi}{4}\frac{\partial\rho}{\partial\theta}+\frac{1+p\cos2\varphi}{2}\frac{\partial\rho}{\partial\varphi}\right.$$
$$\left.-\frac{3p}{2}\sin^2\theta\sin2\varphi\rho\right)$$
$$=D\left(\frac{1}{\sin\theta}\frac{\partial}{\partial\theta}\left(\sin\theta\frac{\partial\rho}{\partial\theta}+\frac{1}{\sin^2\theta}\frac{\partial^2\rho}{\partial\varphi^2}\right)\right. \qquad (19)$$

This is the same form as the equation for the ellipsoid of revolution in a laminar flow derived by J. M. Burgers(6) and A. Peterlin,(7) and its solution was given by them.

§ 4. Frictional Constants.

It is a simple matter to calculate the frictional constants. We need not take account of the gradient of flow. In our case it is necessary only those for rotation, i.e., w_ξ, w_η, w_ζ. For the resultant moment of force about the origin we have

$$\boldsymbol{M}=\sum[\dot{\boldsymbol{s}}_i, \boldsymbol{K}_i]=-f\eta_0\sum a_i[\boldsymbol{s}_i,[\boldsymbol{\omega}, \boldsymbol{s}_i]]$$
$$=-f\eta_0(P+Q+R)\boldsymbol{\omega}$$
$$+f\eta_0\sum a_i(\xi_i\omega_\xi+\eta_i\omega_\eta+\zeta_i\omega_\zeta)\boldsymbol{s}_i,$$

that is

$$M_\xi=-f\eta_0\,\omega_\xi(Q+R), \qquad \text{etc.} \qquad (20)$$

On the other hand the frictional constants w_ξ, w_η, w_ζ are defined by

$$M_\xi=-w_\xi\,\omega_\xi, \qquad \text{etc.} \qquad (21)$$

Therefore,

$$w_\xi=f\eta_0(Q+R), \qquad \text{etc.} \qquad (22)$$

We have assumed $P = Q$, then

$$w_\xi=w_\eta=w=f\eta_0(P+R). \qquad (23)$$

§ 5. Intrinsic Viscosity.

The increase of the energy dissipation per unit volume per unit time to that for the pure solvent, W_0, caused by the presence of high polymers is

$$W-W_0=N\{-\sum(\boldsymbol{K}_i,[\boldsymbol{\omega},\boldsymbol{s}_i]-\boldsymbol{v}_i)\}$$
$$=Nf\eta_0g^2\left\{\frac{P}{2}\cos^2\theta+\frac{(P-R)^2}{P+R}\sin^4\theta\cos^2\varphi\right.$$
$$\left.\times\sin^2\varphi+\frac{PR}{P+R}\sin^2\theta\right\}\equiv Nf\eta_0g^2F, \qquad (24)$$

where N is the number of molecules in 1 c.c. of the solution and W_0 equals to $\eta_0 g^2$. The effective viscosity η is defined by

$$W=\eta g^2. \qquad (25)$$

Then

$$(\eta-\eta_0)/\eta_0=\eta_{sp}=NfF. \qquad (26)$$

Having assumed that the solution is very dilute, η_{sp}/NM here obtained is nothing but the intrinsic viscosity, M being the mass of the molecule.

Eq. (24) is very similar to that for the ellipsoid of revolution derived by Jeffery,(8) which contains complicated integrals in place of our constant coefficients.

F must be averaged by ρ. When g is small

$$F=\frac{7P^2+21PR+2R^2}{30(P+R)}$$
$$-\left(\frac{g}{D}\right)^2\frac{16R-11P}{25200}p^3+\cdots\cdots. \qquad (27)$$

In particular when $P = Q = R$,

$$F=\frac{P}{2}=\frac{1}{6}(P+Q+R). \qquad (23)$$

This is the result already obtained by Debye.(4)

§ 6. Discussion.

Although we have assumed the molecules to be rigid, it seems absurd at first sight because of its vivid micro-Brownian motion in a solution. However, this micro-Brownian motion has no effect on the viscosity. This is easily recognized when we consider a molecule in a solution at rest, where also molecules change their internal configurations by micro-Brownian motions, but the energy dissipation does not take place. We have only to consider rigidly fixed configurations one by one, and then average for such configurations. It is supposed in the preceding sections that P, Q and R are invariant during such micro-Brownian motion. If there is a velocity gradient, however, the micro-Brownian motion will be different from the case at rest. Nevertheless, when it is too strong to be effected by the velocity gradient, it would be reasonable to regard the molecules to be rigid.

In conclusion we wish to express our hearty thanks to Dr. S. Oka for his valuable suggestions given to this work.

References.

(1) W. Kuhn: Zeits. phys. Chem. A. **161** (1932), 1; 427.
(2) M. L. Huggins: J. Phys. Chem. **42** (1938), 911; **43** (1939), 439.
(3) H. A. Kramers: J. Chem. Phys. **14** (1946), 415.
(4) P. Debye: J. Chem. Phys. **14** (1946), 636.
(5) R. Gans: Ann. d. Phys. **86** (1928), 628.
F. Perrin: J. de phys. Rad. **5** (1934), 497.
(6) J. M. Burgers: *Second Report on Viscosity and Plasticity* (1938) Chap. III, 113.
(7) A. Peterlin: Zeits. f. Phys. **111** (1938), 232.
(8) G. B. Jeffery: Proc. Roy. Soc. **A 102** (1923), 161.

Viscosity of High Polymer Solutions, II. Influence of Rubber Elasticity.

By Nobuhiko SAITÔ.

Kobayasi Institute of Physical Research, Kokubunzi, Tokyo,

(Read May 22, 1948; Received July 22, 1948).

§ 1. Introduction.

In the preceding paper, Part I,(1) we have treated the viscosity of dilute high polymer solutions with a rigid skein model, which is justified in the case of such a small velocity gradient that the statistical molecular sizes, that is, P, Q and R defined by Eqs. (7) in Part I, do not change with time. Strictly speaking, however, this is not true. The micro-Brownian motion will be effected more or less by a velocity gradient, which causes the change in P, Q and R. It is the purpose of this article to give a remark concerning the effect of this change in P, Q and R in the two dimensional case.

§ 2. Effect of the Change of the Internal Configuration.

In Part I it has been shown that if P, Q and R for one molecule are equal to those for another, the contribution to the viscosity is the same. Therefore, it may be permitted to take in place of a complicated internal configuration such a model for a high polymer as is shown in Fig. 1, that is, four spherical particles are symmetrically connected by two rods, one of which is perpendicular to the other. Moreover, if a molecule changes its internal configuration by the flow, it will exhibit a rubber-like elasticity and then the rods connecting particles will have to be replaced by springs. Further it is assumed that the angle between the two springs is not deformed and equals $\pi/2$, and the mass of a molecule can be neglected.

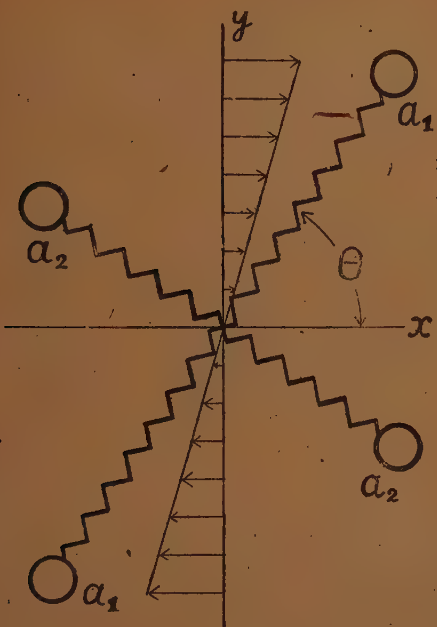

Fig. 1.

The treatments are almost analogous to those in Part I. It may be unnecessary to describe the detail. Let the lengths of the springs be $2s_1$ and $2s_2$, which are the functions of the angle θ between the major axis and x-axis, and the coefficients of elasticity of the springs k_1, k_2 respectively. In the absence of the velocity gradient, s_1 and s_2 are constants s_{10} and s_{20} respectively. The velocity gradient is supposed to be g, as is shown in Fig. 1. The resultant moment of force acting on a molecule must vanish, which determines the angular velocity of the rotation of the molecule, that is,

$$\dot{\theta} = \omega(\theta) = -g\frac{a_1 s_1^2 \sin^2\theta + a_2 s_2^2 \cos^2\theta}{a_1 s_1^2 + a_2 s_2^2}. \qquad (1)$$

From the conditions for equilibrium of forces in a spring we have,

$$\left.\begin{aligned} f\eta_0 a_1(gs_1 \sin\theta\cos\theta - ds_1/dt) &= k_1(s_1 - s_{10}), \\ f\eta_0 a_2(-gs_2 \sin\theta\cos\theta - ds_2/dt) &= k_2(s_2 - s_{20}), \end{aligned}\right\} \qquad (2)$$

where the constants, f, η_0, a_1, a_2 have the same meanings as defined in Part I. Putting $k_1/f\eta_0 a_1 = \tau_1$, $k_2/f\eta_0 a_2 = \tau_2$ the above equations become

$$\left.\begin{aligned} (g\sin\theta\cos\theta - \tau_1)s_1 + \tau_1 s_{10} - ds_1/dt &= 0, \\ (-g\sin\theta\cos\theta - \tau_2)s_2 + \tau_2 s_{20} - ds_2/dt &= 0. \end{aligned}\right\} \qquad (3)$$

The distribution function $\rho(\theta)$ of the orientation of molecules is determined by

$$\left.\begin{aligned} -\rho\dot{\theta} + D\partial\rho/\partial\theta &= \text{const}, \\ D = \frac{kT}{w} &= \frac{kT}{2f\eta_0}\frac{1}{a_1 s_1^2 + a_2 s_2^2}. \end{aligned}\right\} \qquad (4)$$

These equations (3) and (4) can be solved by power series of g, which are assumed to take the following forms

$$\left.\begin{aligned} s_1 &= F_0 + gF_1 + g^2F_2 + \cdots, \\ s_2 &= G_0 + gG_1 + g^2G_2 + \cdots, \\ \dot{\theta} &= gH_1 + g^2H_2 + \cdots, \\ \rho &= \rho_0 + g\rho_1 + g^2\rho_2 + \cdots, \end{aligned}\right\} \qquad (5)$$

where F_0, F_1, $\cdots$, G_0, G_1, $\cdots$, H_1, H_2, $\cdots$, ρ_0, ρ_1, $\cdots$ are functions of θ only. Substituting these series into the preceding equations, it is possible to determine these coefficients of powers of g successively. Thus we obtain

$$\left.\begin{aligned} s_1 &= s_{10}\Big[1 + \frac{g}{\tau_1}\sin\theta\cos\theta + g^2\Big\{\frac{\sin^2\theta\cos^2\theta}{\tau_1^2} \\ &\qquad + \frac{\cos 2\theta}{2\tau_1^2}(1 - p\cos 2\theta)\Big\} + \cdots\Big] \\ s_2 &= s_{20}\Big[1 - \frac{g}{\tau_2}\sin\theta\cos\theta + g^2\Big\{\frac{\sin^2\theta\cos^2\theta}{\tau_2^2} \\ &\qquad - \frac{\cos 2\theta}{2\tau_2^2}(1 - p\cos 2\theta)\Big\} + \cdots\Big] \\ \dot{\theta} &= -\frac{g}{2}(1 - p\cos 2\theta) \\ &\qquad + g^2\frac{PR}{(P+R)^2}\sin 2\theta\cos 2\theta\left(\frac{1}{\tau_1} + \frac{1}{\tau_2}\right) + \cdots \end{aligned}\right\} \qquad (6)$$

$$\begin{aligned} \rho = \frac{1}{2\pi}\Big[1 &+ \frac{gp}{4D_0}\sin 2\theta + g^2\Big\{\frac{p^2}{16D_0^2}\cos 2\theta \\ &- \frac{p^2\cos 4\theta}{64D_0^2} - \frac{\cos 4\theta}{16D_0(P+R)}\left(\frac{R}{\tau_1} + \frac{P}{\tau_2}\right)\Big\} + \cdots\Big], \end{aligned} \qquad (7)$$

where

$$R = 2a_1 s_{10}^2, \quad P = 2a_2 s_{20}^2, \quad p = \frac{R-P}{R+P}, \quad D_0 = \frac{kT}{f\eta_0(Q+R)}. \qquad (8)$$

§ 3. Viscosity.

The increase of the energy dissipation per unit time caused by one molecule in the direction of θ is easily obtained as in Part I, with the result that

$$\Delta W = 2f\eta_0[g^2(a_1s_1^2\sin^2\theta+a_2s_2^2\cos^2\theta)+\theta(a_1s_1^2+a_2s_2^2)$$
$$+(a_1\dot{s}_1^2+a_2\dot{s}_2^2)-2g\{-\dot{\theta}(a_1s_1^2\sin^2\theta+a_2s_2^2\cos^2\theta)$$
$$+(a_1s_1\dot{s}_1-a_2s_2\dot{s}_2)\sin\theta\cos\theta\}]. \qquad (9)$$

Substituting Eqs. (6) into Eq. (9), and averaging with the distribution function ρ (Eq. (7)), we finally obtain

$$\frac{\overline{\Delta W}}{f\eta_0 g^2} = \frac{P+R}{4}\left(1-\frac{p^2}{2}\right)+\frac{P+R}{16}p^2\left\{\frac{p^2}{64D_0^2}\right.$$
$$\left.+\frac{1}{8D_0(P+R)}\left(\frac{R}{\tau_1}+\frac{P}{\tau_2}\right)\right\}+g[\cdots]+\cdots \qquad (10)$$

If we assume $P=R$, $\tau_1 \doteq \tau_2 \doteq \tau$, then $p=0$, and Eq. (10) reduces to

$$\overline{\Delta W} = f\eta_0 g^2\left[\frac{P}{2}-\frac{1}{4}\frac{P}{\tau^2}g^2\cdots\right] \qquad (11)$$

This result shows a sort of structural viscosity. The second term explains the deviation from Staudinger's rule for intrinsic viscosity, which is derived from the first term only as is shown by Debye.⁽²⁾

§ 4. Streaming Double Refraction.

Following the simplest theory of the streaming double refraction due to Boeder,⁽³⁾ it is possible to calculate the double refraction. Polarizability tensor of a molecule will vary with the deformation. Therefore, its principal values may be described by introducing two constants α and β, as follows,

$$\left.\begin{aligned} &c_1 = c_{10}+\alpha(s_1-s_{10}) \\ &c_1 = c_{20}+\beta(s_2-s_{20}) \quad c_3 = c_{30} \end{aligned}\right\} \qquad (12)$$

If the molecule makes an angle θ with x-axis, the polarizability tensor c_{ik} becomes

$$\left.\begin{aligned} &c_{11} = c_1\cos^2\theta+c_2\sin^2\theta \\ &c_{12} = c_{21} = (c_1-c_2)\cos\theta\sin\theta \\ &c_{22} = c_1\sin^2\theta+c_2\cos^2\theta. \\ &c_{31} = c_{13} = c_{23} = c_{32} = 0, \quad c_{33} = c_{30} \end{aligned}\right\}. \qquad (13)$$

By averaging with ρ (Eq. (7)), we obtain the polarizability tensor of the flowing solution in a Couette apparatus. In this way we have

$$\bar{c}_{11}-\bar{c}_{22} = \frac{c_{10}-c_{20}}{64}\frac{g^2p}{D_0^2}+\frac{5g^2}{32\pi}\left(\frac{\alpha s_{10}}{\tau_1^2}+\frac{\beta s_{20}}{\tau_2^2}\right)$$
$$+\frac{1}{32\pi}\frac{g^2p}{D_0}\left(\frac{\alpha s_{10}}{\tau_1}-\frac{\beta s_{20}}{\tau_2}\right). \qquad (14)$$

$$2\bar{c}_{12} = \frac{c_{10}-c_{20}}{16\pi}\frac{gp}{8D_0}+\frac{g}{8\pi}\left(\frac{\alpha s_{10}}{\tau_1}+\frac{\beta s_{20}}{\tau_2}\right). \qquad (15)$$

The extinction angle χ is determined by

$$\tan 2\chi = \frac{2\bar{c}_{12}}{\bar{c}_{11}-\bar{c}_{22}}. \qquad (16)$$

The strength of the double refraction Δn is approximately proportional to $\{(\bar{c}_{11}-\bar{c}_{22})^2+4c_{12}^2\}^{1/2}$,

$$\Delta n \backsim \sqrt{(\bar{c}_{11}-\bar{c}_{22})^2+4\bar{c}_{12}^2}. \qquad (17)$$

Assuming $P=R$, $\tau_1=\tau_2=\tau$, $c_{10}=c_{20}=c_{30}=c_0$

$$\tan 2\chi = 4\tau/5g \qquad (18)$$

$$\Delta n \backsim \frac{\alpha s_{10}g}{4\pi\tau}+\text{highen order of } g^2 \qquad (19)$$

The first terms of Eqs. (14) and (15) come from "Eigenanisotropie" or "Formanisotropie" and the second from "Dehnungsanisotropie". Assuming that α and β are positive, as is easily seen from Eqs. (17), (14) and (15), and that Δn is larger than the case when $1/\tau_1$ and $1/\tau_2$ are zero, which explains to some extent the deviation from Boeder's theory of various experiments of Signer and Gross,⁽⁴⁾ although complete explanation of all the phenomena can not be given.

In conclusion we wish to express our sincere thanks to Dr. S. Oka for his useful discussions given to this work.

References.

(1) N. Saitô: J. Phys. Soc. Japan. **4** (1949), 85.
(2) P. Debye: J. Chem. Phys. **14** (1946), 636.
(3) P. Boeder: Zeits. f. Phys. **75** (1930), 258.
(4) R. Signer: Zeits. phys. Chem. **A 150** (1930), 257.
R. Signer: H. Gross, Zeits. phys. Chem. **A 165** (1933), 161.
R. Signer: Trans. Faraday Soc. **32** (1936), 296.

The Dispersion of the Piezoelectric Modulus in Rochelle Salt Crystal at Low Frequencies.

By Heiji KAWAI and Masakazu MARUTAKE.

Kobayashi Institute of Physical Research, Kokubunji, Tokyo.

(Read May 23, 1948; Received July 21, 1948)

§ 1. Introduction.

Previously⁽¹⁾ the authors reported the dispersion of the dielectric constant in rochelle salt at 1～100 cycles per second. It is well known that the dielectric constant ε_a and the piezoelectric modulus d_{14} of the rochelle salt have similar characteristics and their ratio, *i.e.* the non-load voltage sensitivity, is almost independent of the temperature and the humidity.⁽²⁾⁽³⁾ Therefore, it is anticipated that the piezoelectric modulus has also dispersion at the low frequency as the dielectric constant does. In this experiment, the piezoelectric modulus of rochelle salt (d_{14}) and the ratio of the piezoelectric modulus to the dielectric constant (d_{14}/ε_a) were measured at 1/3～25 cycles, and it was found that the piezoelectric modulus has the same dispersion as the dielectric constant and that their ratio is independent of frequency in the same frequency range. This result is very different from Schulwas-Sorokin's data,⁽⁴⁾ partly because of the different results about the dielectric constant.⁽⁵⁾

§ 2. Experiment.

The measuring apparatus is shown schematically in Fig. 1. A is a cylinder which has an eccentric center of rotation O, and rotating with various frequencies (1/3～20 cycles), pushes the spring S. (Two springs of phosphor-bronze and piano wire were used which have natural frequencies of 50 and 30 cycles, respectively.) Then the voltage difference produced on the crystal is measured and the piezoelectric modulus d_{14} is obtained. The thin a-cut crystal plate, two sides of which are inclined 45° both to b-and c-axis, was used. The circuit diagrams are shown in Fig. 2. A is an a. c. milliammeter of a rectifier type to which was added an oil damper in order to make possible the measurements in the low frequency range.

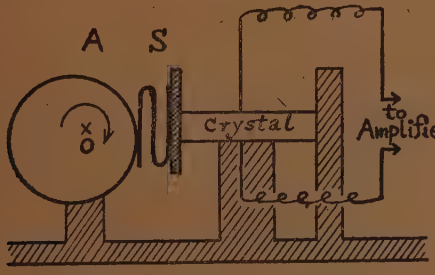

Fig. 1. Measuring apparatus.

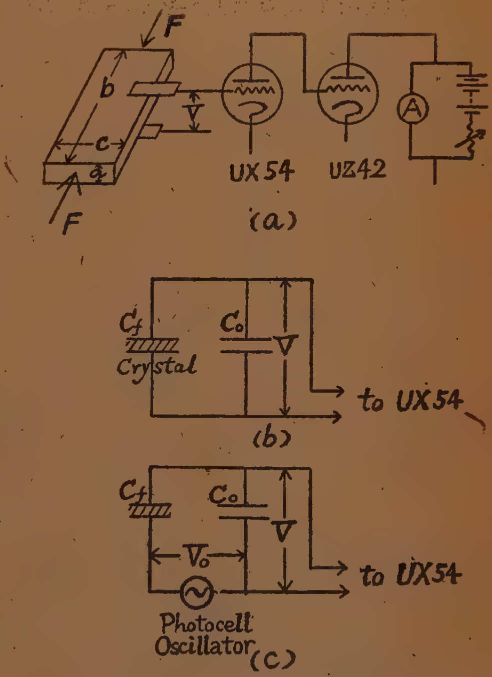

Fig. 2. The circuit diagrams.

Now, denote the thickness and the length of the two sides of the plate by a, b and c, respectively. ($a = 9$ mm, $b = 2.4$ cm, $c = 1.8$ cm.) When the normal force F is applied on the side plane of the length c, and the load impedance is Z (v. Fig. 2.), the voltage between two electrodes is

$$V = -\frac{\frac{1}{2}\frac{b}{a}d_{14}F}{C_f+\frac{1}{i\omega Z}}, \qquad (1)$$

where $C_f = bc\varepsilon_a/4\pi a$ is the capacity of the freely deformable crystal plate, ω is the circular frequency and $i^2=-1$.(6)(3)

(a) The measurement of d_{14}/ε_a.

The circuit (*a*) of Fig. 2 was used. In this case $Z=\infty$, and (1) becomes

$$V = -\frac{2\pi}{c}\frac{d_{14}}{\varepsilon_a}F. \qquad (2)$$

$F = 16$ grams weight (effective value) was applied.

(b) The measurement of d_{14}.

The circuit of Fig. 2 (*b*) was used. In this case $Z = 1/i\omega C_o$, and (1) becomes

$$V = -\frac{b}{2a}\frac{d_{14}}{C_f+C_o}F. \qquad (3)$$

$F = 160$ grams weight and C_o of about ten times C_f ($10^{-4}\sim10^{-3}\,\mu F$) were used, where C_o is the capacity of an air or a mica condenser.

(c) The measurement of ε_a.

The measurement of ε_a was also done, using the circuit (*c*) of Fig. 2. The low frequency oscillator was constructed with the photo-cell and the eccentrically rotating circular plate light interruptor. In this case, when input voltage is V_o, output voltage is obviously

$$V = V_o\frac{C_f}{C_o}. \qquad (4)$$

The results are shown in Fig. 3, where the values of d_{14}/ε_a, d_{14} and ε_a were calculated by (2), (3) and (4), respectively.

All the experiments were done at room temperature and room humidity. Therefore the values of d_{14} and ε_a may be those of somewhat indefinite condition, because they vary very slowly with temperature and humidity. Also, the measurements were difficult at the temperature higher than 15°C because of the large surface leakage in the room humidity. In fact the value of d_{14}/ε_a at 17°C in Fig. 3 shows the tendency to decrease with frequency, which seems to be due to the surface leakage. Accordingly the measurements above the Curie temperature (23°C) were done while heating and descicating the crystal, and it was found that

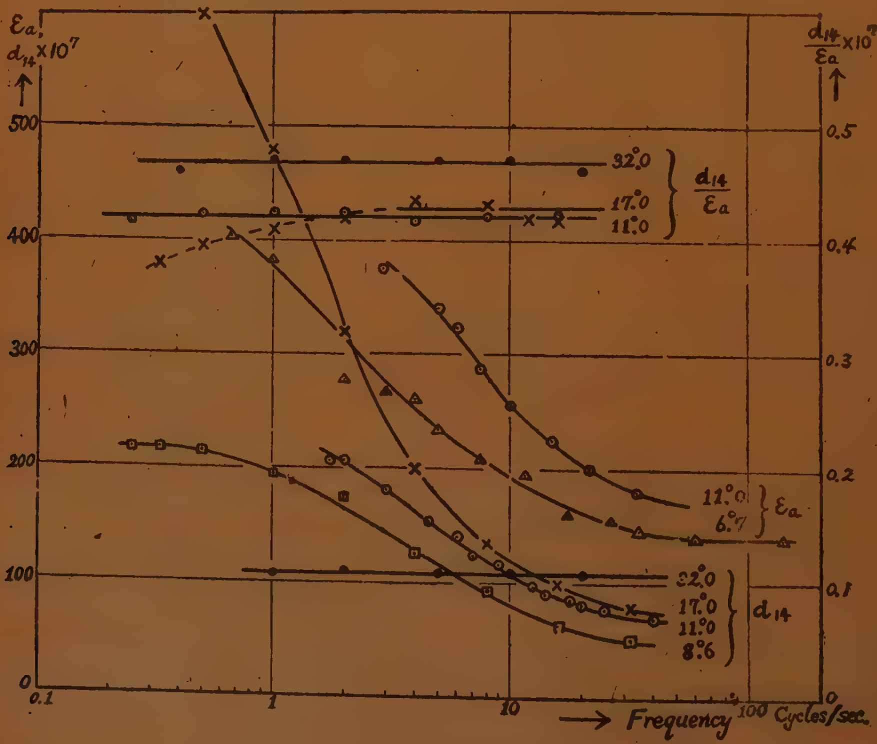

Fig. 3. Measured values of d_{14}/ε_a, d_{14} and ε_a.

d_{14} as well as d_{14}/ε_a has no dispersion, as Fig. 3 shows.

§ 3. Results.

In this experiment, it was found that d_{14}/ε_a is independent of the frequency (from 1/3 to 25 cycles) at the various conditions, though ε_a has a dispersion which depends on the temperature and the humidity. Consequently d_{14} was found to have the same dispersion as ε_a below the Curie temperature, which disappears above it. When Mueller's theory(2) is applied to these results, the origin of the dispersion of ε_a and d_{14} will be found in the properties of the dielectric constant of the clamped crystal, or the clamped dielectric constant of rochelle salt will have dispersion at low frequencies. Then the static phenomena (*e.g.* the spontaneous polarization) and the dynamic ones (*e.g.* the dielectric constant at high frequency) can not be treated with the same value of the clamped dielectric constant, and Mueller's opinion must be modified in the ferroelectric range.

References.

(1) H. Kawai and M. Marutake: J. Phys Soc. Jap. **3** (1948), 8.
(2) H. Mueller: Phys. Rev. **57** (1940), 829; **58** (1940), 565.
(3) H. Kawai: J. Phys. Soc. Jap. **3** (1948), 105; **2** (1947), 113.
(4) R. D. Schulwas-Sorokin: Phys. Zeits. Sowj. **12** (1937), 685.
(5) R. D. Schulwas-Sorokin and M. V. Posnov: Phys. Rev. **47** (1935), 166.
(6) Y. Kakiuchi: J. Phys. Soc. Jap. **1** (1946), 31.

On the Mean International Electrical Units.

By Syûzô MIYAKE.

Electrotechnical Laboratory, Tokyo.

(Read May 23, 1948; Received August 3, 1948.)

§ 1. Introduction.

The international electrical units, which were put into practice in conformity with the decision of the International Conference on Electrical Units and Standards in 1908, were abolished on January 1st, 1948 in accordance with the resolution of the International Committee of Weights and Measures in 1946 and turned its position over to the absolute electrical units. The change of the electrical units in Japan is expected to be delayed a little by some special circumstances.

The measurements, which were carried out to find distinctly the difference existed among the international units which have been established and maintained in various countries respectively, were the former International Comparisons. The summarized report of our participation in the International Comparisons can be found in "The Half a Century History of the Electrotechnical Laboratory" written in Japanese. The comparisons under the auspices of the International Bureau of Weights and Measures were carried out four times concerning resistance and three times concerning electromotive force, and the results are shown in Tables I and II(1)(2).

Suffix M of Ω shows the mean. A, E, F, G, J, U shows respectively the initial of French for the name of country.

Table I.

The Comparison of the Units of Resistance of Various Countires.

		Nov., 1933	March, 1935	Dec., 1936	Feb., 1939
		Ω_M	Ω_M	Ω_M	Ω_M
Germany	Ω_A	$+10.6\mu\Omega$	$+9.8\mu\Omega$	$+6.6\mu\Omega$	$+9.1\mu\Omega$
America	Ω_E	-6.4	-5.5	-3.7	-3.2
France	Ω_F	$+73.0$	$+69.5$	—	—
(modified)	Ω_F	—	0.0	$+0.9$	$+3.7$
England	Ω_G	-5.2	-3.6	-3.9	-6.5
Japan	Ω_J	-8.3	-11.2	-10.0	-14.4
USSR	Ω_U	$+9.5$	$+10.6$	—	—
(modified)	Ω_U	—	0.0	-0.4	$+0.8$

Table II.

The Comparison of the Units of E.M.F. of Various Countries.

		Dec., 1934	Jan., 1937	Feb., 1939
		V_M	V_M	V_M
Germany	V_A	$-4\mu V$	$-7.3\mu V$	$-5.5\mu V$
America	V_E	-12	-9.5	-11.2
France	V_F	-76	—	—
(modified)	V_F	0	$+0.7$	$+18.5$
England	V_G	$+5$	$+7.6$	$+6.5$
Japan	V_J	-2	$+0.7$	$+1.3$
USSR	V_U	$+13$	—	—
(modified)	V_U	0	-5.5	-23.1

Suffixes are the same as in Table I.

As the results of the comparisons of resistance in 1935 and of electromotive force in 1934, the mean international units were established upon the mean values of the units of five countries, Germany, America, England, Japan, and USSR. While, France deviating from the above five countries, made her units in accordance with the mean international units after having modified her own units. Hereafter, from an independent standpoint, USSR amended and made her own units in accordance with the mean international units. Therefore glaring attentions are necessary to pay for the fact that the sum of the difference since the year of 1936, Tables I and II, do not prove zero.

Now, since the establishment of the mean international units the mean value of units maintained by the above six countries has been pledging themselves to be unchangeable as yet. The relation between the mean international units and the absolute units has been recognized by the International Committee in 1948. It runs as follows:

1 mean international ohm = 1.00049 absolute ohms,

1 mean international volt = 1.00034 absolute volts.

The International Comparison, which was in abeyance since 1939 as a result of the World War II, was revived in 1947. Being invited to take part in the comparisons, the electrical standards of our laboratory were forwarded to the International Bureau of Weights and Measures. The measurements of the comparison are now going on. Great hopes are entertained for the publishment of the results with keen interest.

The point that the author wants to discuss in this papers is to investigate closely the pledge "the mean international units maintained by six countries are unchangeable", which was decided at the time when the mean units were established.

§ 2. The Theory of the Mean Units.

$i = 1, 2, 3, 4, 5, 6.$

$x_i(0)$: the true value of various countries' units in its initial time.

$x_i(t)$: the true value of various countries' units in the time instant "t".

$x_m(t)$: the mean unit at the time instant "t".

k_i : the coefficient of the secular change of various countries' units.

k_m : the coefficient of the secular change of the mean units.

Suppose these, and the relation will be followed thus:

$$x_i(t) = x_i(0) + k_i t. \qquad (1)$$

$$x_m(t) = 1/6 \sum x_i(t). \qquad (2)$$

$$x_m(t) = x_m(0) + k_m t. \qquad (3)$$

$$k_m = 1/6 \sum k_i. \qquad (4)$$

Till now this k_m has been pledged to be equal to zero, but in the manganin standard resistors, which have been maintaining the unit of resistance practically, it is well known that they increase their values gradually, even though they are of superior quality, with the lapse of time. Therefore, k_i is understood to be zero or a positive quantity. Consequently k_m, mean value, is not asserted to be zero. Similarly in the cadmium standard cells, which have been maintaining the unit of electromotive force in effect, it is known as a matter of common knowledge that their values decrease gradually, even though they are of superior quality, as the years go by. Hence k_i is taken to be zero or a negative quantity. Therefore, it will not proper to pledge k_m, mean value, is to be zero. If it be so, we shall consider what value k_m has.

Put

$$\delta_i(t) = x_i(t) - x_m(t). \tag{5}$$

This is the difference between various countries' units and the mean units, and nothing but the numerical value measured at the International Comparisons.

Rewriting (5), it follows that,

$$\begin{aligned}\delta_i(t) &= x_i(0) + k_i t - x_m(0) - k_m t\\ &= \delta_i(0) + (k_i - k_m)t.\end{aligned}$$

After transferring $\delta_i(0)$ to the left-side, square and sum up with respect to "i". Then we have,

$$\begin{aligned}\sum\{\delta_i(t) - \delta_i(0)\}^2 &= (\sum k_i^2 - 2k_m \sum k_i + 6k_m^2)t^2\\ &= (\sum k_i^2 - 12\,k_m^2 + 6\,k_m^2)t^2\\ &= (\sum k_i^2 - 6\,k_m^2)t^2. \end{aligned} \tag{6}$$

Assume a relation between $\sum k_i^2$ and k_m, that k_i takes a positive quantity only including zero (in case of resistance) or takes a negative quantity only including zero (in case of electromotive force), and also the distribution is considered to conform to the Gaussian error function.

If so, it turns out as follows by the theory of errors,

$$\sqrt{\frac{\sum k_i^2}{6}} = 1.2533\,k_m,$$

or

$$\sum k_i^2 = 9.425\,k_m^2. \tag{7}$$

Putting (7) into (6), we have

$$k_m^2 = \frac{\sum\{\delta_i(t) - \delta_i(0)\}^2}{3.425\,t^2}. \tag{8}$$

Thus k_m can be obtained by using δ_i and t.

§ 3. Numerical Examples.

Among the values of Tables I and II, if we adopt the subsequent values of δ_i since the establishment of the mean international units taking the French and USSR's modified units into consideration, Tables III and IV can be obtained. "t" shall be counted by month taking the time of the establishment of the mean international units as the initial.

Table III.

The Value of $\delta_i(t)$ as to Resistance.

		$t=0$	$t=21$	$t=47$
		$\delta_i(0)$	$\delta_i(21)$	$\delta_i(47)$
Germany	δ_A	$+11.5\,\mu\Omega$	$+8.3\,\mu\Omega$	$+10.8\,\mu\Omega$
America	δ_E	-3.7	-2.0	-1.5
France	δ_F	$+1.8$	$+2.6$	$+5.4$
England	δ_G	-1.9	-2.1	-4.7
Japan	δ_J	-9.5	-8.2	-12.6
USSR	δ_U	$+1.8$	$+1.4$	$+2.6$

Table IV.

The Value of $\delta_i(t)$ as to Electromotive Force.

		$t=0$	$t=25$	$t=50$
		$\delta_i(0)$	$\delta_i(25)$	$\delta_i(50)$
Germany	δ_A	$-1.9\,\mu V$	$-5.1\,\mu V$	$-3.3\,\mu V$
America	δ_E	-9.8	-7.3	-8.9
France	δ_F	$+2.2$	$+2.9$	$+20.7$
England	δ_G	$+7.1$	$+9.8$	$+8.7$
Japan	δ_J	$+0.2$	-2.9	$+3.6$
USSR	δ_U	$+2.2$	-3.3	-20.8

The coefficient of secular change of the mean units calculated from Table III concerning the resistance by the formula (8) is as follows.

In the term from March, 1935 to Dec., 1936,

$$k_m = +0.10\ \mu\Omega/\text{month}.$$

In the term from March, 1935 to Feb., 1939,

$$k_m = +0.069\ \mu\Omega/\text{month}.$$

In the same way the results calculated from Table IV concerning the electromotive force is as follows.

In the term from Dec., 1934 to Jan., 1937,

$$k_m = -0.17\ \mu V/\text{month}.$$

In the term from Dec., 1934 to Feb., 1939,

$$k_m = -0.32\ \mu V/\text{month}.$$

The values of k_m above obtained, concerning the resistance, are close to the value anticipated once, but concerning the electromotive force it appears to be larger than expectation.

The followings can be regarded as the cause without such a satisfactory coincidence.

(a) The International Comparisons have been performed only three times since the establishment of the mean international units. Consequently we ran short of data for investigation.

(b) The way of judgement in which the units of various countries increase or decrease linearly with time admits of further investigation.

(c) There is enough ground for investigation in seeking for k_m on the assumption in accordance with the Gaussian error function (one side of positive or negative region) for the distribution of k_i.

(d) Further on there is room to be left for investigation for the present pledge on which the mean units are decided in comparison with the same weight for those countries where the units are maintained with various constancy.

4. Conclusion.

Passing discussion upon the pledge adopted in the case of introducing the mean international units to data—the mean value of the units which have been maintained by six countries is unchangeable with lapse of time—the secular change of the mean units is tried to be calculated on the assumption that the units of various countries sustain linear change with time and the distribution of the coefficients of secular change is done in accordance with the Gaussian error function. The results of calculation appear to be a little larger as compared with what it is. With the increase of the materials for the International Comparisons in the future, the author believes that the above theory will be proved helpful to the exact maintenance of the electrical units by having these assumptions amended so as to be in accordance with practice.

References.

(1) C. R. Acad. Sci. (Paris), t. **209** (1939), p. 23.
(2) Procès-Verbaux du Comité International des Poids et Mesures, t. **19** (1939), pp. E 62 et E 63.

The Patch Effect of Crystal Rectifiers.

By Akio KOBAYASHI and Kenzi ARITA.

Reseach Laboratory, Tokyo-Shibaura Electric Co., Kawasaki, Kanagawa-ken.

(Read May 23, 1948; Received August 11, 1948)

Abstract.

The complex plane impedance diagram of crystal rectifiers were usually analysed as a circle. The observed results on cuprous oxide rectifiers deviated considerably from a circle. To analyse the results, the writers used the series resistance, R_s, of the bulk part of Cu_2O derived from static current-voltage characteristics. Then, $Z-R_s = Z_l$ gave the impedance of blocking layer, and $Y_l = 1/Z_l$, its admittance. Denoting the zero frequency conductance by Y_{l_0}, and putting $Y_l-Y_{l_0} = G+i\omega C$, dispersion of G and C was defined experimentally, at various biases and temperatures. A patch theory of the blocking layer proposed to explain the dispersion agrees with the observed results quantitatively.

§ 1. Introduction

To find the series resistance, R_s, the rectifying resistance, R_p, and the shunting capacity, C, of which the equivalent circuit of crystal rectifiers consist, we use the so-called impedance-diagram, which is the complex-plane locus of the impedances measured at various frequencies. As the form of this diagram, Schottky and Deutchman,(1) and the writers in the previous paper(2) assumed it as a circle with the center on the real axis, while Wood(3) Fink and Adler(4), and Tomura(5) as a circle with the center below the real axis. They defined R_s and R_p from the points of intersection of the circle with the real axis. Wood, Fink and Adler, and Tomura obtained the law of $C \propto \omega^{-\alpha}$ for the dispersion of C. Considering that $\lim_{\omega\to 0} \omega^{-\alpha} = \infty$, this law cannot hold when the frequency becomes very small.

We define the term "relaxation of rectification" to imply the failure of the simple expression $Y_l = i\omega C + 1/R_p$ (both R_p and C independent of frequency), that is, the increase of conductance and decrease of capacitance along with the rise in frequency. The effect of relaxation on frequency is small in general when its period is large compared with the relaxation time. So we may expect at small frequency the capacitance to be nearly constant and the frequency dependent part of conductance to be nearly zero, in other words the impedance and admittance curves cut the real axis at right angle, when frequency becomes zero.

The irregular change of R_s with bias by Schottky and Deutchmann's work may be attributed to a rough measurement of impedance or the inadequacy of the analysis by circle. As for the papers of Wood, Fink and Adler, and Tomura only a part of the circular arc is covered by observed points.

§ 2. Experiments and Analysis.

From the log J versus $1/T$ curves for various biases, the activation energy for backward current was estimated to be about 0.32 eV, which was considerably lower than that of slowly cooled samples whose activation energies were 0.5 to 0.7 eV. This means that for some parts of the blocking layer, the thickness is very small and the image force lowers the value of effective contact potential difference.

Fig. 1 shows the differential resistance $R' = \partial V/\partial J$ derived from the static current-voltage characteristics. R' becomes nearly constant for the higher forward bias. Considering the fact that at this voltage region the rectifying resistance of the blocking layer itself becomes very small, it may be allowed to identify the value of R' at $+3$ volts to the series resistance R_s. The linearity of the log R_s vs. $1/T$ plot may show that the value thus determined may not be incorrect.

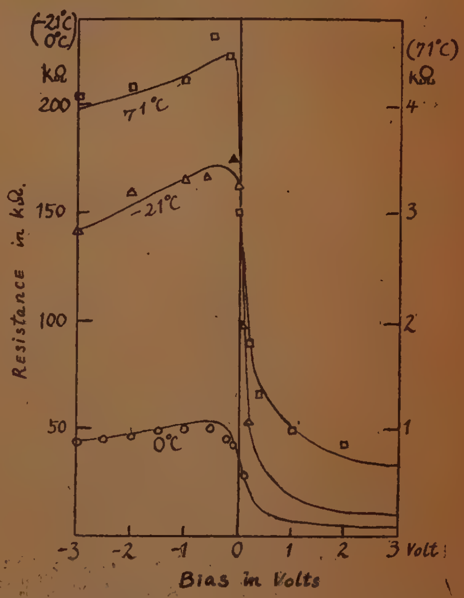

Fig. 1. Differential resistance derived from static current—voltage characteristics and zero-frequency impedances from a. c. measurement.

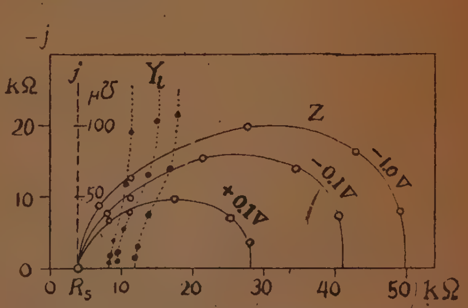

Fig. 2. Impedance and admittance diagram for 0°C.

The observed impedance diagrams at 0 °C for three different biases are shown in Fig. 2 for example. To analyse this result, the above-mentioned value of R_s, common to over-all biases, is plotted at first, then $Y_l = 1/Z_l = 1/(Z - R_s)$ is plotted on the same figure in suitable scale, the origin being R_s. To compare the a.c. impedance with the d.c. characteristics, we obtain the zero frequency admittance (or conductance), Y_{l0}, by the extrapolation Y_l onto the real axis, then $Z_0 = R_s + 1/Y_{l0}$. Z_0's are plotted in Fig. 1.

The fact that the admittance becomes ever smaller and contracts near the R_s, supports the correctness of this analysis.

Putting $Y_l - Y_{l0} = G + i\omega C$, G/ω and C are plotted against frequency in Fig. 3 for three temperatures and five biases. At higher temperatures, C is near almost flat at lower frequencies as is shown very clearly in this figure.

Conspicuous features of the dispersion of C and G/ω are as follows.

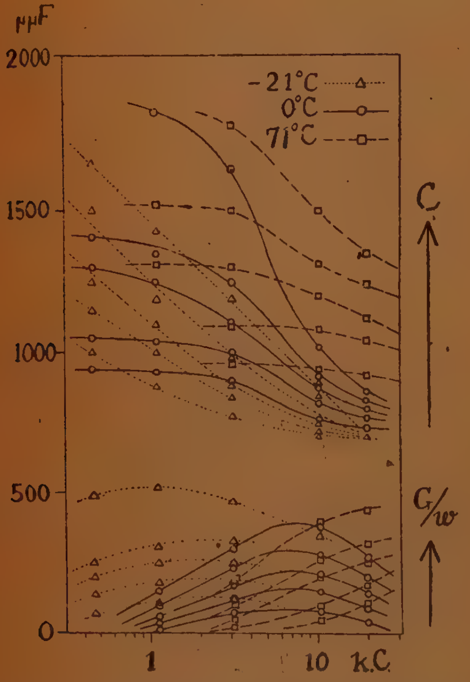

Fig. 3. Dispersion of C and G/ω for several biases and temperatures. Each group of curves for three temperatures and for both C and G/ω corresponds to the values of backward bias 0, −0.6, −1, −2 and −3 volts from up to below.

1) Curves upon the whole shift to larger frequency with the increasing temperature.

2) The values of C and G/ω decrease with the increasing backward bias.

3) The steepest change of C corresponds with the maximum of G/ω.

4) The activation energy of ω_m, where G/ω has the maximum value, is 0.32 eV.

§ 3. Theory.

To exlain the observed dispersion of C and G/ω, the equivalent circuit shown in Fig 4 is proposed by the writers. This is the simplest case of Wagner's theory of dielectric after-effect. The origin of these heterogeneity, say patches, are due to the local variation of contact potential difference and that of the thickness of the barrier layer. For the sake of simplicity, two parts of different thickness are considered. The r_s corresponds with the spreading resistance for the thinner part of the blocking layer, whose equivalent circuit is prescribed as r_p and c_1.

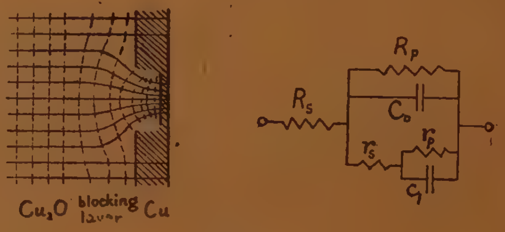

Fig. 4.

Fig. 4. Equipotential surfaces of patches having the extra spreading resistance and its equivalent circuit.

Then

$$Y_l = \frac{1}{R_p} + i\omega C_0 + \frac{1 + i\omega\tau}{r_p + r_s + i\omega\tau r_s}, \quad (\tau = c_1 r_p).$$

$$Y_{l0} = \frac{1}{R_p} + \frac{1}{r_p + r_s} \tag{1}$$

$$Y_{l\infty} = \lim_{\omega \to \infty} Y_l = \frac{1}{R_p} + \frac{1}{r_s} \tag{2}$$

Putting $Y_l - Y_{l0} = G + i\omega C$,

$$\frac{G}{\omega} = \frac{\{\omega\tau r_s/(r_s + r_p)\}^2}{(r_s + r_p)^2 + (\omega\tau r_s)^2} C_1,$$

$$C = C_0 + \frac{r_1^2}{(r_s + r_p)^2 + (\omega\tau r_s)^2} C_1.$$

If we define the ω for maximum G/ω with ω_m,

$$\omega_m = \frac{r_s + r_p}{r_s r_p c_1}, \tag{3}$$

$$\frac{G}{\omega} = \left(\frac{r_p}{r_s + r_p}\right)^2 C_1 \frac{\omega/\omega_m}{1 + (\omega/\omega_m)^2}, \tag{4}$$

$$C = C_0 + \left(\frac{r_p}{r_s + r_p}\right)^2 C_1 \frac{1}{1 + (\omega/\omega_m)^2}. \tag{5}$$

§ 4. Discussion.

From eqs. (4) and (5) the maximum value of G/ω is a half of the total change of C by frequency. This agrees very well with the curves in Fig. 3. The second qualitative agreement is as follows; the temperature dependence of ω_m may be defined by $(r_s+r_p)/r_sr_p$, C being nearly independent of temperatures. Then its activation energy is a weighted mean of that of r_s and r_p. This may explain the value of the observed activation energy 0.32 eV. The curves C and G/ω are shifted toward higher frequency by increasing bias, because r_p increase with bias. These facts again explain the observation. But, in order to determine values of R_p, r_s, r_p, c_1 and C_0 and dependence of capacity on bias, closer experiments will be needed.

References.

(1) W. Schottky and W. Deutschmann. Phys. Zeits. **30** (1929) 839.

(2) A. Kobayasi and K. Arita, J. of Phys. Soc. Japan, **4** (1949) 58.

(3) L. A. Wood, Rev. Sci. Inst. **4** (1933) 434.

(4) C. G. Fink and E. Adler, Trans. Am. Electrochem. Soc. **79** (1941) 577.

(5) M. Tomura, Tsushin Kogyo, (in Japanese), **2** (1946) 20.

Statistical Theory of Binary Alloys. (IV)
β-Brass Type of Superstructure.

By Yutaka TAKAGI.

Tokyo Institute of Technology.

(Received August 22, 1948.)

If we wish to apply the statistical theory of binary alloys to the problems concerning other co-operative phenomena such as solution, adsorption, melting and so on, we must have a thorough knowledge of the theoretical results covering the entire range of arbitrary alloy compositions. However, many papers appeared heretofore have been chiefly concerned with stoichiometric AB case and AB_3 case, and their main efforts have been always directed to the fundamental refinement of the method itself of statistical approach. So we have undertaken the present investigation with the aim of giving the bird's-eye view over the superlattice phenomena, the degree of order and the configurational specific heat for alloys of various concentrations having been calculated as functions of temperatures.

To start with, for simplicity, we shall concentrate our attention on the β-brass type of superstructure in which the lattice may be decomposed into only two sublattices α and β symmetrically related to each other.

Nothing essentially new nor anything theoretically fundamental is contained in the present paper, but it may rather be regarded as an embodiment of our paper I(1), where abstract formulae were developed without numerical results.

§ 1. Notations and Definitions.

In order to symmetrize the formulae, and at the same time to make the useful applications to wider region of phenomena easier and more intuitive, we shall hereafter use new notations and parameters which are to be defined as follows.

Let us suppose that in a given specimen of an alloy there are N lattice points (sites) occupied by N atoms, of which [A] are A atoms and [B] are B atoms. We shall introduce a new parameter θ, so that

$$[\mathrm{A}] = \frac{N}{2}(1+\theta), \quad [\mathrm{B}] = \frac{N}{2}(1-\theta). \tag{1.1}$$

Let an A be classified as A_α or A_β according to whether it is on a site α or on a site β. Similarly let a B be classified, as B_α or B_β. For the degree of long range order, we shall introduce a new parameter s, slightly modified from that used in the paper I, so that

$$\begin{aligned}[\text{right atoms}] &= [\mathrm{A}_\alpha]+[\mathrm{B}_\beta] = \frac{N}{2}(1+s),\\ [\text{wrong atoms}] &= [\mathrm{A}_\beta]+[\mathrm{B}_\alpha] = \frac{N}{2}(1-s).\end{aligned} \tag{1.2}$$

Then we can write down

$$\begin{aligned}[\mathrm{A}_\alpha] &= \frac{N}{4}(1+\theta+s), \quad [\mathrm{B}_\alpha] = \frac{N}{4}(1-\theta-s),\\ [\mathrm{A}_\beta] &= \frac{N}{4}(1+\theta-s), \quad [\mathrm{B}_\beta] = \frac{N}{4}(1-\theta+s).\end{aligned} \tag{1.3}$$

In order to describe the degree of local order, we have to count the numbers of atom-pairs. Here we shall introduce a parameter r, slightly modified from that used in the paper III(2), so that

$$\begin{aligned}[\text{right pairs}] &= [\mathrm{A}_\alpha\mathrm{B}_\beta]+[\mathrm{B}_\alpha\mathrm{A}_\beta] = \frac{zN}{4}(1+r),\\ [\text{wrong pairs}] &= [\mathrm{A}_\alpha\mathrm{A}_\beta]+[\mathrm{B}_\alpha\mathrm{B}_\beta] = \frac{zN}{4}(1-r),\end{aligned} \tag{1.4}$$

z being the number of nearest neighbours of any lattice point. Then taking account of the identities such as $[\mathrm{A}_\alpha\mathrm{A}_\beta]+[\mathrm{A}_\alpha\mathrm{B}_\beta] = z[\mathrm{A}_\alpha]$ etc., the numbers of four kinds of pairs may be solved as

$$\begin{aligned}[\mathrm{A}_\alpha\mathrm{A}_\beta] &= \frac{zN}{8}(1+2\theta-r),\\ [\mathrm{A}_\alpha\mathrm{B}_\beta] &= \frac{zN}{8}(1+2s+r),\\ [\mathrm{B}_\alpha\mathrm{A}_\beta] &= \frac{zN}{8}(1-2s+r),\\ [\mathrm{B}_\alpha\mathrm{B}_\beta] &= \frac{zN}{8}(1-2\theta-r).\end{aligned} \tag{1.5}$$

§ 2. First Approximation.

It was proved in the paper I that the author's theory which is based on the combinatory formula

$$\frac{[\alpha\beta]!}{[\mathrm{A}_\alpha\mathrm{A}_\beta]!\,[\mathrm{A}_\alpha\mathrm{B}_\beta]!\,[\mathrm{B}_\alpha\mathrm{A}_\beta]!\,[\mathrm{B}_\alpha\mathrm{B}_\beta]!}\left(\frac{[\mathrm{A}_\alpha]!\,[\mathrm{B}_\alpha]!}{[\alpha]!}\right)^{z-1} \times\left(\frac{[\mathrm{A}_\beta]!\,[\mathrm{B}_\beta]!}{[\beta]!}\right)^{z-1}, \tag{2.1}$$

is completely equivalent to the formula of the quasi-chemical method. So, after Fowler and Guggenheim(3), we shall call the results of the above formula the first approximation for the cooperative phenomena.

s-T relation calculated from the formulae

$$\begin{aligned}\frac{r+1}{2} &= \frac{s}{\tanh\frac{z-1}{2z}\Omega}, \quad \Omega = \log\frac{(1+\theta+s)(1-\theta+s)}{(1+\theta-s)(1-\theta-s)},\\ \frac{2v}{kT} &= \log\frac{(1+2s+r)(1-2s+r)}{(1+2\theta-r)(1-2\theta-r)},\end{aligned} \tag{2.2}$$

is shown in the upper half of Fig. 1 for various values of θ, $2v = v_{AA}+v_{BB}-2v_{AB}$. The lower half of the figure shows θ-T_c relation for $s=0$, calculated from the formula which, as stated in the paper I, is identical with Easthope's formula(4), that is

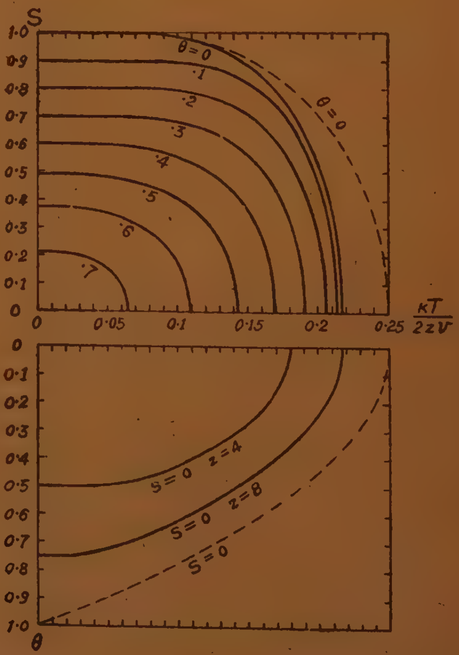

Fig. 1.
Upper part: s-T relation. Full lines are the first approximation for $z=8$. Broken line is zeroth approximation. Lower part: θ-T_c relation. Full lines are the first approximation for $z=4$ and $z=8$. Broken line is zeroth approximation.

$$\exp\left(\frac{2v}{kT_c}\right)=\frac{\left[\frac{z}{z-1}\frac{(1+\theta)(1-\theta)}{2}\right]^2}{\left[1-\frac{z}{z-1}\frac{(1+\theta)(1-\theta)}{2}\right]^2-\theta^2} \tag{2.3}$$

For convenience of comparison, the results of zeroth approximation (see the next section) are shown in broken lines in both parts of the figure.

Fig. 2 shows s_0-θ relation, where s_0 denotes the values of s when $T=0$. The formula which is based upon is as follows:

$$\theta=\frac{\tanh\frac{1}{z-1}\tanh^{-1}s^*-s^*}{\tanh\frac{1}{z-1}\tanh^{-1}s^*+s^*},\quad s_0=s^*(1+\theta). \tag{2.4}$$

r-T relation and σ-T relation are shown for various values of θ in Figs. 3 and 4, where σ denotes the configurational specific heat.

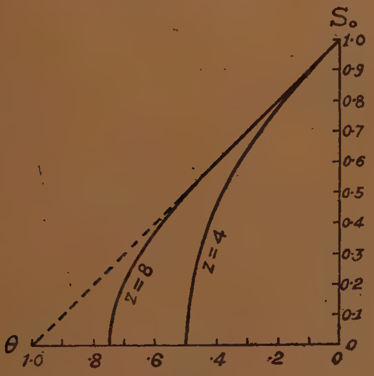

Fig. 2.

s_0-θ relation. Full lines are first approximation for $z=4$ and $z=8$. Broken straight line is zeroth approximation.

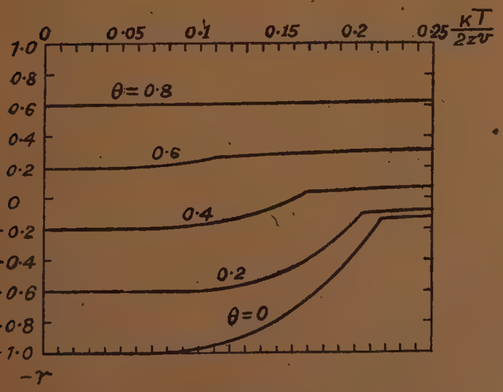

Fig. 3.

r-T relation for $z=8$.

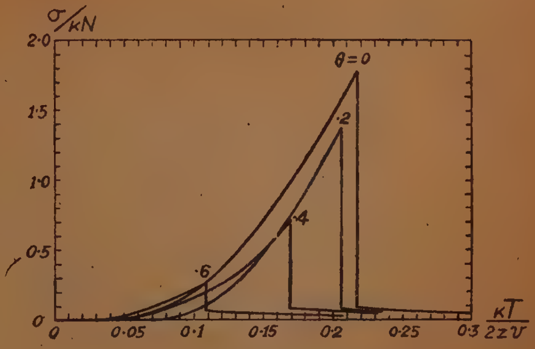

Fig. 4.

Configurational specific heat for $z=8$.

§ 3. Zeroth Approximation.

If we assume, neglecting the repelling or coalescing tendency between like or unlike neighbours,

$$[A_\alpha A_\beta]\propto[A_\alpha]\times[A_\beta],\ \text{etc.}, \tag{3.1}$$

our theory reduces to the theory of Bragg and Williams, that is zeroth approximation after a classification due to Fowler and Guggenheim of the available statistical theories of cooperative phenomena. In this section we shall examine the results of this approximation.

The upper half of Fig. 5 shows the s-T relation for various values of θ, while the lower half

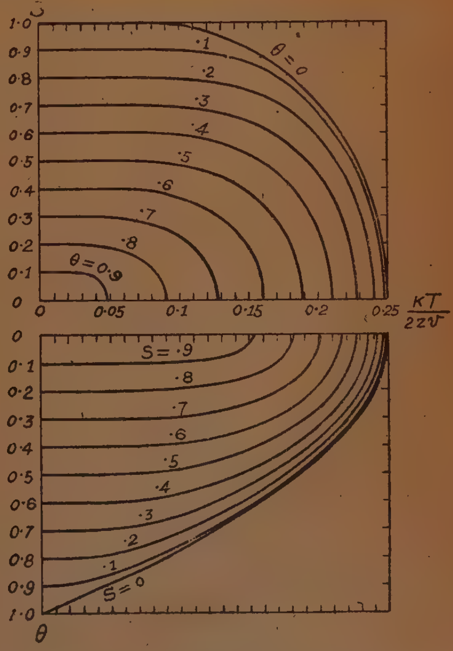

Fig. 5.

s-θ-T surface. Zeroth approximation.

of it shows the θ-T relation for various values of s, the formula employed for them being

$$\frac{kT}{2zv} = \frac{s}{\Omega}, \quad \Omega = \log\frac{(1+\theta+s)(1-\theta+s)}{(1+\theta-s)(1-\theta-s)}. \qquad (3.2)$$

These may be regarded as a plan and a elevation of contour lines of the three dimensional s-θ-T surface. Using the temperature scale as adopted here, the shape and position of this surface is fixed in space irrespective of the number of nearest neighbours.

The configurational specific heat curves for various values of θ are shown in Fig. 6.

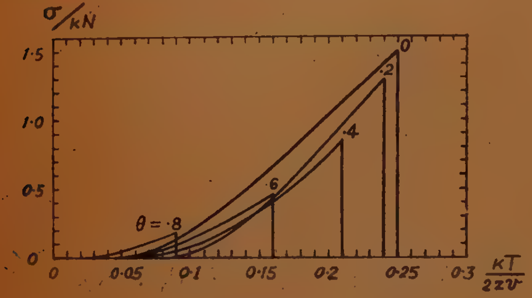

Fig. 6.
Configurational specific heat. Zeroth approximation.

§ 4. Comparison of Two Approximations.

Fig. 7 shows critical values of specific heat as functions of θ. The curve marked with σ_c corresponds to zeroth approximation, while that marked with σ_{c-} corresponds to the first approximation.

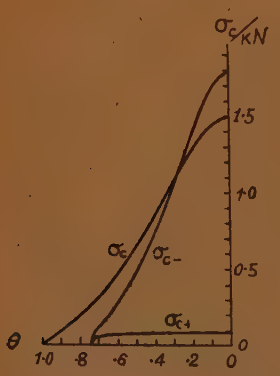

Fig. 7.
Critical values of configurational specific heat at Curie temperatures. σ_c curve: zeroth approximation. σ_{c-} and σ_{c+} curves: first approximation for $z = 8$

The last curve marked with σ_{c+} represents the values immediately above the Curie points which are due to the decay of the residual local order.

The upper part of Fig. 8 shows the configurational energy E for several remarkable temperatures, while the lower part of it the configurational entropy Φ. In both parts of the figure, the left hand sides represent the results of zeroth approximation, while the right hand sides represent the results of the first approximation.

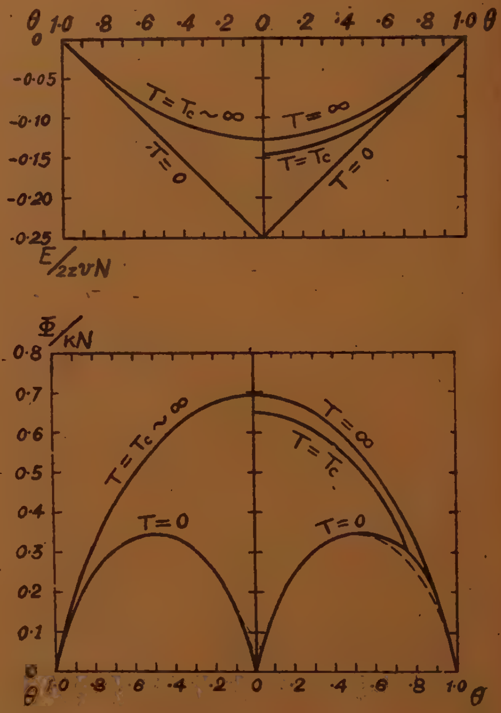

Fig. 8.
Upper figure: E-θ relation. Left hand side corresponds to zeroth approximation. Right hand side is the first approximation, for $z = 8$. Lower figure: Φ-θ relation. Left hand side corresponds to zeroth approximation. Right hand side is the first approximation for $z = 8$. For convenience of comparison, $T = 0$ curve of zeroth approximation is shown by a broken line.

Inner relations between these two stages of approximations may most clearly be apprehended from these curves. For convenience of experimental physicists, energy difference ΔE and entropy difference $\Delta\Phi$ between $T = 0$ and $T = T_c$ are plotted in Fig. 9.

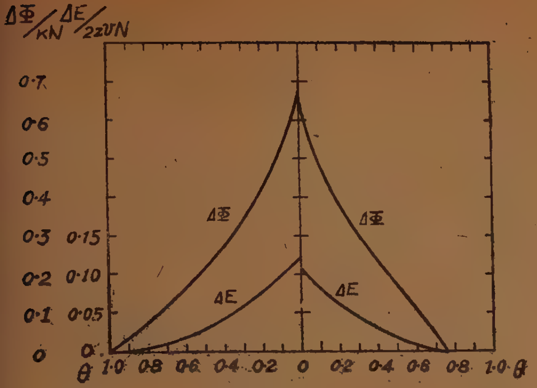

Fig. 9.
ΔE-θ, $\Delta \Phi$-θ relations, where $\Delta E = (E)_{T=T_c} - (E)_{T=0}$, $\Delta \Phi = (\Phi)_{T=T_c} - (\Phi)_{T=0}$. Left hand side corresponds to the zeroth approximation. Right hand side is the first approximation for $z = 8$.

In conclusion the author wishes to express his hearty thanks to Miss. K. Endō and Miss. A. Ōsawa for their helpful assistance in computational works.

References.

(1) Y. Takagi: Proc. Phys.-Math. Soc. Japan, **23** (1941), 44.
(2) Y. Takagi: Proc. Phys.-Math. Soc. Japan, **24** (1942), 333.
(3) R. H. Fowler and E. A. Guggenheim: *Statistical Thermodynamics*, Chapt. XIII, (Cambridge University Press, 1939).
(4) C. E. Easthope: Proc. Camb. Phil. Soc., **33** (1937), 502.

The Second Report on the Hole Theory of Liquid.

By Tsugihiko SATO and Syû ONO.

Institute of Applied Science, Faculty of Engineering, Kyushu University.

(Received August 25, 1948)

§ 1. Introduction.

Recently one of the present authors established the hole theory of liquid¹⁾ which was successful in application to the critical and surface phenomena. While in that paper too many empirical quantities are used to perform the comparison between theory and experiment, we shall in the present paper attempt to eliminate these empirical quantities from the theory and to calculate them theoretically from the interatomic forces, thus an important advance concerning the treatment of the free volume being made. In the previous work¹⁾, only the increase of the free volume due to the increase in the number of the empty cells or "holes" is taken into account, but now its own temperature variation will be considered, although the expansion of the lattice constant or the volume of the elementary cell, which plays an important rôle in the usual cage model of liquid²⁾, cannot be taken into consideration in the hole theory.

§ 2. Partition Function

As in the previous paper, the classical partition function $f(T)$ of an assembly of N identical molecules is

$$f(T) = \{\phi(T)\}^N \Omega(T), \tag{1}$$

$$\phi(T) = \frac{(2\pi mkT)^{3/2}}{h^3} j(T), \tag{2}$$

$$\Omega(T) = \frac{1}{N!}\int\int\cdots\int \exp\left(-\frac{W}{kT}\right) dv_1 dv_2 \ldots dv_N. \tag{3}$$

where $j(T)$ is the partition function for the internal degrees of freedom of a molecule, and W is the potential energy of the whole assembly, being a function of the positional coordinates of all molecules in it. m is the mass of a molecule, k Boltzmann's constant, h Planck's constant, T the absolute temperature, and dv_i the volume element of the ith molecule, the integration being carried to a point outside the container. Here we will restrict the discussion to the case of spherical or approximately spherical molecules.

Then, we divide a whole space inside the container into L cells, L being larger than N. And the integral within the container can be replaced by the integrals within these cells. It is impossible to have more than one molecule in any one of these L cells because of the repulsive energy, provided the volume of these cells is sufficiently small. And $N!$ terms which differ only in interchange of molecules amount to the same value. Thus the multiple integral (3) can be expressed in the form

$$\Omega(T) \doteq \sum \int_{\tau i_1} \int_{\tau i_2} \cdots \int_{\tau i_N} \exp\left(-\frac{W}{kT}\right) dv_1 dv_2 \ldots dv_N, \tag{4}$$

where summation is carried over the $L!/N!\,(L-N)!$ different configurations. This is the number of ways of arranging N molecules in L cells in such a manner that we never have more than one molecule in a cell.

Suppose the intermolecular potential is additive. And we assume that if the size of cell is large enough we can neglect the interaction between the molecules which are not in the nearest neighbor cells. But the size must be small enough not to admit of simultaneous existence of two molecules in a cell. According to these two restrictions, we chose the shape of cells such that their centers constitute the lattice points in a face-centered cubic array. In the presence of the long range intermolecular forces, our theory does not hold, since there cannot be any cells which satisfy the above two requirements. If the intermolecular force decreases with distance as rapidly as van der Waals' attraction, the favorable size of a cell can be determined.

Let ε denote the potential energy of a pair of molecules on the centers of two nearest neighbor cells. And let us denote by XZ the number of pairs of neighboring cells, of which the one is occupied and the other is unoccupied; then the number of pairs of neighboring cells both occupied is $(N-X)Z/2$. Z is the total number of the nearest neighbors, and in the present case the calculation will be carried out for $Z=12$, corresponding to a face-centered cubic lattice. When all molecules rest at the centers of their own cells, the total potential energy of the assembly is $(N-X)Z\varepsilon/2$.

Suppose the cell which is occupied by the ith molecule has w_iZ vacant neighbors and $(1-w_i)Z$ occupied ones in a particular configuration. Let us denote by u_i the potential energy of the ith molecule. If it occupies the cell having w_iZ vacant neighboring cells, u_i is a function of the positional coordinates of the ith molecule and the neighboring $(1-w_i)Z$ molecules. Here we will use the values of the poteitial energy of the molecule surrounded by the neighboring molecules at the centers of their own cells as the approximated value of u_i. This approximate u_i is a function of the coordinates of ith molecule x_i, y_i, z_i under the definite arrangement of the molecules on the Z neighboring lattice points. Furthermore, we assume that u_i can be expressed in the form $u(x_i, y_i, z_i; w_i)$ approximately. Then we have

$$W = \frac{(N-X)Z\varepsilon}{2} + \sum_{i=1}^{N} \left\{ u(x_i, y_i, z_i; w_i) - (1-w_i)Z\varepsilon \right\}.$$

And we can write (4) in the form

$$\Omega(T) = \sum \exp\left\{-\frac{(N-X)Z\varepsilon}{2kT}\right\} q(w_1)q(w_2)\ldots q(w_N), \tag{5}$$

$$q(w_i) = \int_{\tau} \exp\left\{-\frac{u(x_i, y_i, z_i; w_i) - (1-w_i)Z\varepsilon}{kT}\right\} du_i. \tag{6}$$

If we regard the occupied cell as a "molecule" and the unoccupied one as a "hole", our theory will be equivalent to the hole theory of liquid. And our hole theory is also applicable to the vapor phase, as the partition function (3) and the above method of approximation hold for any assembly ruled by classical mechanics.

§ 3. Calculation of Free Volume.

In the preceding section, we have established the hole theory of liquid and vapor. Then we have to calculate the Helmholtz free energy as a function of the temperature and the volume to discuss the thermodynamical behavior of them. It is necessary for this purpose to find the functional form of the cell integral $q(w)$ defined by (6).

When the Z neighboring cells are all empty, i.e. $w_i = 1$, the integrand in (6) is unity and the cell integral becomes $q(1) = \tau$, τ being the volume of a cell. And we denote $q(0)$ by ω; $q(0) = \omega$.

In the usual quasi-crystalline model of liquid, ω is the generalized free volume[2]. In order to calculate this free volume from the intermolecular potential, we assume that the potential within the cell whose nearest neighbors are all occupied is spherically symmetrical about the center of the cell. This potential is called the cage potential. For the purpose of calculating the cage potential, we adopt the procedure of Lennard-Jones and Devonshire[3] and use Lennard-Jones' type of intermolecular potential of the form[3]

$$\phi(r) = \phi_0\left\{\left(\frac{r_0}{r}\right)^{12} - 2\left(\frac{r_0}{r}\right)^6\right\}, \tag{7}$$

where ϕ_0 denotes the minimum value of intermolecular potential and r_0 is the value of the distance r at which this minimum occurs. Then the potential within the cell can be written in the form

$$u(x, y, z; 0) = Z\varepsilon + Z\phi_0\left\{\left(\frac{r_0}{a}\right)^{12} l\left(\frac{r^2}{a^2}\right) - 2\left(\frac{r_0}{a}\right)^6 m\left(\frac{r^2}{a^2}\right)\right\}, \tag{8}$$

$$l(\eta) = (1 + 12\eta + 25.2\eta^2 + 12\eta^3 + \eta^4)(1-\eta)^{-16} - 1, \tag{9}$$

$$m(\eta) = (1+\eta)(1-\eta)^{-4} - 1, \tag{10}$$

where a is the distance between nearest neighbors. Hence ω becomes

$$\omega(T) = 2\pi a^3 \int_0^{1/4} \eta^{1/2} \exp\left[\frac{Z\phi_0}{kT}\left\{-\left(\frac{r_0}{a}\right)^{12} l(\eta) + 2\left(\frac{r_0}{a}\right)^2 m(\eta)\right\}\right] d\eta, \tag{11}$$

ω is evidently a function of the temperature, whereas it is assumed to be independent of temperature in the previous paper. And ε is given by

$$\varepsilon = \phi_0\left\{\left(\frac{r_0}{a}\right)^{12} - 2\left(\frac{r_0}{a}\right)^6\right\}. \tag{12}$$

For an intermediate value of w, $q(w)$ is approximately evaluated in the way adopted in the previous paper. We use the geometrical mean as the approximate value of $q(w)$ for the intermediate w for the convenience of calculation:

$$q(w) = \omega^{1-w}\tau^w.$$

Then the partition function (1) is expressible in the form

$$f(T) = \left\{\phi\omega \exp\left(-\frac{Z\varepsilon}{kT}\right)\right\}^N \sum_X g(N, X) \exp\left(-\frac{X\zeta}{kT}\right), \tag{13}$$

where $g(N, X)$ denotes the number of the distinguishable arrangement of N molecules in L cells with specified value of X, and ζ is defined by

$$2\zeta = -Z\varepsilon - 2kT \ln\frac{\tau}{\omega(T)}. \tag{14}$$

After the long calculation shown in the previous paper, we obtain the Helmholtz free energy

$$F = \frac{Z\varepsilon}{2} - kT\ln(\phi\omega) + L\,kT\left\{x\ln x + (1-x)\ln(1-x)\right\} + \frac{1}{2}LZkT\left\{x \ln\frac{\beta-1+2x}{x(\beta+1)} + (1-x)\ln\frac{\beta+1-2x}{(1-x)(\beta+1)}\right\}, \tag{15}$$

where x and β are defined by

$$x = \frac{N}{L}, \tag{16}$$

and

$$\beta = \left[1 + 4x(1-x)\left\{\exp\left(\frac{2\zeta}{ZkT}\right) - 1\right\}\right]^{1/2} \tag{17}$$

respectively. By differentiating with respect to volume, we obtain the equation of state in the form

$$p = -\frac{NkT}{b}\left\{\ln\left(1-\frac{b}{V}\right) + \frac{Z}{2}\ln\frac{\beta+1-2\frac{b}{V}}{\left(1-\frac{b}{V}\right)(\beta+1)}\right\}, \tag{18}$$

where p is the pressure, V the volume and b is defined by

$$b = Vx = N\tau. \tag{19}$$

§ 4. Comparison with Experimental Data for the Critical Temperature.

It follows from the equation of state (18) that the critical temperature T_c can be determined as a root of the transcendental equation

$$2kT_c = \frac{-Z\varepsilon}{Z\ln\frac{Z}{Z-2} + \ln\frac{\tau}{\omega(T_c)}}, \tag{20}$$

where $\omega(T)$ and ε (negative) are given by (11) and

(12) respectively.

We shall compare the calculated and observed values of the critical temperature of argon.

The values of the constants r_0 and ϕ_0 for argon are

$$r_0 = 3.83 \text{ Å} \text{ and } \phi_0 = 16.5 \times 10^{-15} \text{ ergs},$$

which have been determined by Lennard-Jones from the temperature dependence of the second virial coefficient; and $a = 4.04$ Å is determined from the molar volume of liquid argon at 88°K. The calculated and observed values of the critical temperatures are shown in Table 1. The values of a for neon and nitrogen are determined under the assumption that a/r_0's of these substances are equal to that of argon, because the numerical integration for the different values of a/r_0 is considerably laborious. If these substances fit to Pitzer's definition of perfect liquid[1] which shows correspondence in behavior, the above assumption is acceptable. The calculated critical temperatures shown in parentheses are the ones calculated from the observed values of the heat of evaporation and $\tau/\omega = 20.1$ in the previous paper. The calculated critical temperatures in the present paper seems to be lower than the ones in the previous paper, in which τ/ω was considered to be independent of temperature. τ/ω calculated from the intermolecular forces is 16.7 at the critical temperature and 20.5 at the melting point, whereas the one empirically determined in the previous paper is 20.1.

Table I.

Comparison with experimental data for the critical temperature.

	$\phi_0 \times 10^{15}$ ergs	a Å	T_c (observed) °K	T_c (calculated) °K
A	16.5	3.83	151	135 (155)
Ne	4.98	3.08	44	39 (43)
N_2	13.25	4.17	126	109 (149)

§ 5. Variation of the Densities with Temperature of the Liquid and gas in Equilibrium.

Let us denote the values of x's for the vapor and the liquid in equilibrium by x_G and x_L respectively. And according to the previous paper, these are determided as roots of the equations

$$x_G + x_L = 1, \tag{21}$$

$$\ln \frac{1-x_G}{x_G} = \frac{Z}{Z-2} \ln \frac{\beta(x_G)+1-2x_G}{\beta(x_G)-1+2x_G} \,. \tag{22}$$

Using the above two equations and (20), we can calculate x_L or x_G as a function of the reduced temperature, which is plotted in Fig. 1.

As the mass density can be expressed by $\rho = x/N_0\tau$ from (19), where N_0 is the number of molecules in unit mass, the experimental value of x_L can be obtained by means of the formula $x_L = \rho_L/(\rho_L+\rho_G)$ [cf. Eq. (21)]. This curve is uniformly lower than the one in the previous paper, and in better agreement with the experimental one for the perfect liquid. Thus our refined hole model of liquid gives the sufficient vapor pressure curve without adjustable parameters, removing the defects of the usual quasi-crystalline model. Kamerlingh-Onnes' constant RT_c/p_cV_c calculated from the present theory is 2.92, whereas the experimental values are about 3.4. This calculated value does not depend on ω.

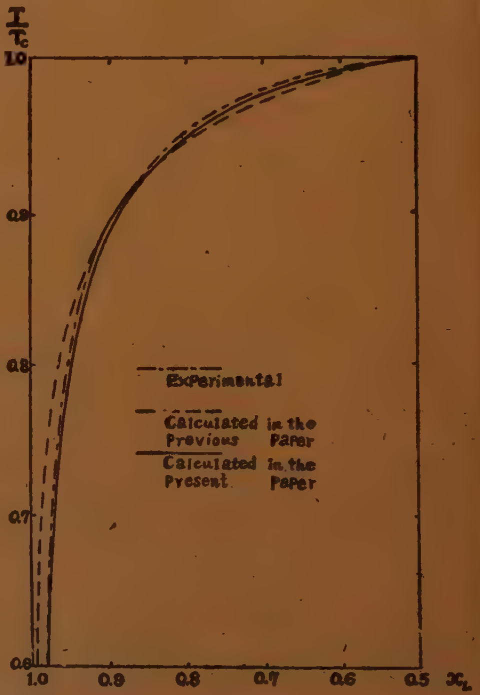

Fig. 1. Variation of density of perfect liquid with reduced temperature.

References.

1) S. Ono, Memoirs of the Faculty of Engineering, Kyushu Univ. 10 (1947), 195; BUSSEIRON

KENKYU (In Japanese) No. 9 (1947), 16.
2) J. E. Lennard-Jones and A. F. Devonshire, Proc. Roy. Soc. A, **163** (1937), 53; **165** (1938), 1.
3) J. E. Lennard-Jones, Proc. Roy. Soc. **106**, (1924), 463.
4) K. S. Pitzer, J. Chem. Phys. **7** (1939), 583.

On the Internal Conversion in M-shell and the Isomer Analysis.

By Makoto TANIHUJI.

Department of Physics, Faculty of Science, Kyūshū University.

(Recieved August 25, 1948.)

§ 1. Introduction.

Since the nuclear isomer was interpreted as an excited state of the same nucleus by v. Weizäcker,⁽¹⁾ the studies of spin change l between excited and ground state have been undertaken by many investigators. Concerning the determination of the l-value, there are two methods:

1) Comparison of the experimental value of the lifetime τ of isomer with Bethe's⁽²⁾ formula.

$$1/\tau = e^2/\hbar c \cdot 2\pi c/\lambda \cdot (2\pi r_0/\lambda)^{2l} (1/l\,!)^2$$

Where $e^2/\hbar c$ is fine-structure constant, c, λ, r_0 are light velocity, wave length, and nuclear radius respectively.

2) When the nucleus falls into the ground state from the isomer level the γ-ray emitted may be converted by the bound electron. The conversion coefficient α depends on l, so the comparison of the experimental value of α with the theoretical value determines l. According to Lowson and Cork⁽³⁾, the measurement of the background γ-ray is troublesome, so the ratio α_K/α_L or α_K/α_M are more easily compared with the theory than the individual values of α_K, α_L, α_M (α_K, α_L, α_M are the conversion coefficients in K, L, M shells respectively.)

Furthermore, experimental physicists have adviced us that α_K/α_M would be more sensitive to l, than α_K/α_L in the case of low energy γ-ray.

§ 2. γ-Radiation and Matrix Elements of Conversion.

The matrix elements of the process in which the bound electrons are ejected by the multipole radiation emitted by the nucleus when the nucleus falls into the ground state from an excited one are given in non-relativistic approximation as follows:

$$H' = \int \Psi_f^* \left\{ -\frac{e\hbar}{mic} \vec{A}\,\mathrm{grad} - \frac{e\hbar}{2\,mic} \mathrm{div}\,\vec{A} + e\varphi \right\} \Psi_0 dv \tag{1}$$

where $\vec{A}$, φ is the electromagnetic potential of γ-radiation, m, e are the electron mass and the charge, and c is the light velocity. The expressions of $\vec{A}$, and φ were given in detail by W. Heitler⁽⁴⁾ in the so-called "primed guage" in which φ' vanishes.

$$\vec{A}' = \vec{A} - \mathrm{grad}\,\lambda, \quad \varphi' = \varphi + \frac{1}{c}\frac{\delta\lambda}{\delta t}, \quad \mathrm{div}\,\vec{A}' = \varphi' = 0. \tag{2}$$

Therefore, we can use these expressions for our calculations.

Now, in the case of α_K, using the expressions of $\vec{A}$, φ given by Heitler, Dancoff and Morrison⁽⁵⁾

calculated the above mentioned matrix element rigorously. But, since their method of calculation is not very practicable for the internal conversion in L and M shells, we prefer the Hebb-Nelson's(6) approximation. Hebb and Nelson, in the calculation of α_L, remarked that $\vec{A}'$ has more strong singularity than $\vec{A}$ in the region of small value of r where conversion takes place chiefly, then, from (2), neglecting $\vec{A}$ compared with $\vec{A}'$, we get

$$\vec{A}' + \operatorname{grad} \lambda = 0 \tag{3}$$

$$\varphi = -\frac{1}{c}\frac{\partial \lambda}{\partial t} \tag{4}$$

Using the Heitler's expression for $\vec{A}'$, φ of the electric α^l pole radiation is found to be as follows:

$$\varphi = -\frac{1}{c}\frac{\partial \lambda}{\partial t} \doteqdot \frac{i\omega}{c}\cdot\frac{a_l^m}{c}\cdot\left(\frac{l}{l+1}\right)^{1/2}\cdot Y_l^m f_l(kr)e^{-i\omega t}$$

where k is the wave number, $\omega = ck$, Y_l^m is the spherical harmonics and α_l^m is the constant which is related to the matrix element of the nuclear multipole moment. Radial function $f_l(kr)$ becomes:

$$f_l(kr) = H_{l+1/2}(kr)/(kr)^{1/2}$$

where $H_{l+1/2}(kr)$ is the Hankel function of the first kind. The matrix element (1) becomes now simply

$$H' = e\int \Psi_f^* \varphi \Psi_0 dv \tag{6}$$

in which we now take Ψ_0 to be the eigen-function of M-shell:

$$\Psi_0 = Y_{l_0}^{m_0}(a_1 + a_2 r + a_3 r^2)e^{-ar} \tag{7}$$

Ψ_f is the eigen-function of the continous level,

$$\Psi_f^* = Y_{l'}^{-m'}\left(\frac{m\pi p}{\hbar}\right)^{\frac{1}{2}}\left[\Gamma(l'+1+in)\Gamma(l'+1-in)\right]^{\frac{1}{2}}$$
$$\cdot\left[\Gamma(l'+1)\Gamma(l'+3/2)\right]^{-1}$$
$$\cdot e^{\frac{n\pi}{2}}\left(\frac{pr}{2}\right)^{l'} e^{-ipr} F(l'+1+in,\ 2l'+2,\ 2ipr) \tag{8}$$

where p is $1/\hbar$ times the momentum of the ejected electron,

$$n = \frac{a}{p} = \frac{z\alpha}{\sqrt{2\nu-(z\alpha)^2}},\quad a = \frac{z'}{a_0},\quad z' = \frac{z}{3} \tag{9}$$

a_0 is the radius of Bohr orbit, z is the nuclear charge, ν is the γ-ray energy devided by mc^2, and α is the fine-structure constant. l_0, m_0; l', m' are the angular momentum quantum numbers specifying the initial and final states. Constants, a_1, a_2, a_3, also specify the initial states.

§ 3. The calculation of α_M

We obtain the transition probability N_e using H' in the last paragraph,

$$N_e = \frac{1}{\hbar^2}|H'|^2 \tag{10}$$

From (5) to (8) we get

$$N_e = K\int r^\delta e^{-\rho r}F(l'+1+in,\ \alpha l'+\alpha,\ 2ipr)dr$$
$$\cdot\int Y_{l_0}^{m_0} Y_l^m Y_{l'}^{m'} d\Omega,\qquad \rho = a+ip \tag{11}$$

In the determination of (11), we have used the expression of $f_l(kr)$

$$f_l(kr) \sim \frac{i\left(\frac{kr}{2}\right)^{-l-\frac{1}{2}}(-1)^{l+1}}{(kr)^{1/2}\Gamma(-l+1/2)},\quad kr \ll 1 \tag{12}$$

K is a constant factor depending on the substate of M-shell. From angular integral of (11) we get the selection rule, and as the result, conversion coefficient $\alpha_M = N_e\Big/\frac{(\sigma_l^m)^2}{\pi^2\hbar k}$ * becomes to be the sum of following terms, multiplied with common factor

$$\frac{1}{z'}\left(\frac{2}{\nu(1+n^2)}\right)^{\frac{2l+1}{2}}\left(\frac{l}{l+1}\right)\cdot\frac{e^{2\pi n}}{1-e^{-2\pi n}}$$

$$\left.\begin{aligned}
l' = l;\ & \frac{1}{9}\cdot\frac{\prod_{j=1}^{l}(j^2+n^2)}{[l'.(2l+1)]^2}\{|3F_{(1)}(l)-6F_{(2)}(l)\\
& +2F_{(3)}(l)|^2 + \frac{2l(l+1)}{(2l-1)(2l+3)}|F_{(3)}(l)|^2\} \equiv A\\
l' = l+1;\ & \frac{2}{3}\cdot\frac{\prod_{j=1}^{l+1}(j^2+n^2)}{[(l+1)!\,(2l+1)(2l+3)]^2}\\
& \cdot\frac{1}{n^2}\cdot\frac{l+1}{2l+1}|2F_{(3)}(l+1)-F_{(4)}(l+1)|^2 \equiv B\\
l' = l-1;\ & \frac{2}{3}\cdot\frac{\prod_{j=1}^{l-1}(j^2+n^2)}{[(l-1)!]^2}\\
& \cdot n^2\cdot\frac{l}{2l+1}|2F_{(1)}(l-1)-F_{(2)}(l-1)|^2 \equiv C
\end{aligned}\right\} \tag{13}$$

---

* c,f. (5) $\frac{(\sigma_l^m)^2}{\hbar\pi k}$ is the number of quanta radiated per unit time.

$$l' = l+2\,;\ \frac{1}{3}\cdot\frac{\prod_{j=1}^{l+2}(j^2+n^2)}{[(2l+1)(2l+3)(2l+5)(l+2)\,!]^2}\cdot\frac{1}{n^4}\cdot\frac{(l+1)(l+2)}{(2l+1)(2l+3)}\,|F_{(5)}(l+2)\,|^2 \equiv D$$

$$l' = l-2\,;\ \frac{1}{3}\cdot\frac{\prod_{j=1}^{l-2}(j^2+n^2)(2l-1)^2}{[(l-2)\,!]^2}\cdot n^4\cdot\frac{l(l-1)}{(2l+1)(2l-1)}\,|F_{(1)}(l-2)\,|^2 \equiv E$$

for each selection rule, where

$$F_{(\delta)}(l') = \left(\frac{n}{n+i}\right)^{\delta+1}\delta\,!\,F(\delta+1,\,l'+1+in,\,2l'+2;\,2ip/\rho). \tag{14}$$

The common factor can be further reduced, and finally we obtain

$$\gamma^{2l+2}\alpha_M = 8\alpha\cdot 3^{2l+2}\cdot\frac{l}{l+1}\cdot\left(\frac{2n}{1+n^2}\right)^{2l+1}\cdot\frac{2\pi n}{1-e^{-2\pi n}}\{A+B+C+D+E\},$$

where $\gamma = z/137$.

As is seen from (14), A, B, C, D, E, in (13) are the hypergeometric functions, which we must estimate numerically for various values of n and l in order to get the result to be compared with experimental data.

§ 4. Numerical Results, Qualitative and Quantitative Considerations.

Before we get into the discussions of the numerical results, we shall consider the results qualitatively. For larger ν, α_M varies with ν as follows.

$$\alpha_M \backsim \left(\frac{2}{\nu}\right)^{l+9/2}.$$

Now, Hebb, Nelson and Dancoff, Morrison have found respectively

$$\alpha_L \backsim \left(\frac{2}{\nu}\right)^{l+7/2},$$

$$\alpha_K \backsim \left(\frac{2}{\nu}\right)^{l+5/2}.$$

Thus

$$\alpha_K/\alpha_M \backsim \left(\frac{2}{\nu}\right)^{-2}, \qquad \alpha_K/\alpha_L \backsim \left(\frac{2}{\nu}\right)^{-1}.$$

So α_K/α_M is more sensitive than α_K/α_L to the tion of ν. The l-dependence is not so simply expressed analytically but may be read in the following Table 1 and the Fig. 1.

The technical remarks about the numerical calculations are added in the Appendix.

Table 1.

$\gamma^{2l+2}\alpha_M$

l / ν/γ^2	1	2	3	4	5
10.0	5.03×10^{-7}	1.40×10^{-7}	3.61×10^{-8}	9.05×10^{-9}	2.27×10^{-9}
7.5	1.39×10^{-6}	5.00×10^{-7}	1.82×10^{-7}	6.30×10^{-8}	2.17×10^{-8}
5.0	6.20×10^{-6}	3.80×10^{-6}	2.15×10^{-6}	1.20×10^{-6}	6.64×10^{-7}
2.5	8.41×10^{-5}	1.22×10^{-4}	1.62×10^{-4}	2.07×10^{-4}	1.46×10^{-4}
1.0	3.44×10^{-3}	1.53×10^{-2}	6.33×10^{-2}	1.66×10^{-1}	8.76×10^{-1}

This table shows that α_M increases with l for small ν, and decreases with l for large ν.

Further the numerical calculations revealed the following points:

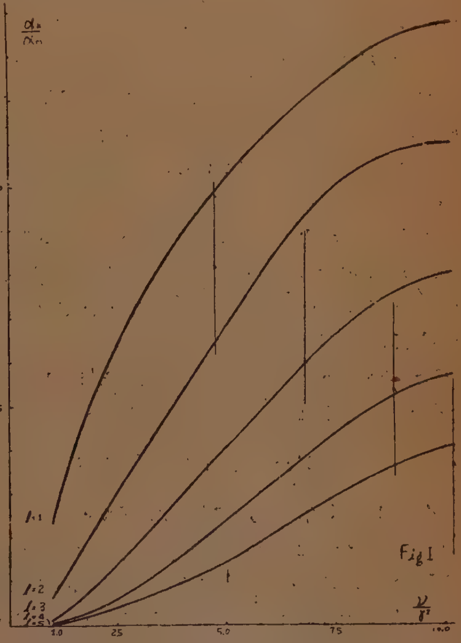

Fig. 1.

1) For large ν; $\alpha_K > \alpha_L > \alpha_M$,

$$\alpha_s > \alpha_p > \alpha_d$$

and

$$\alpha_K/\alpha_M \ll \alpha_s/\alpha_d,$$

where α_s, α_p, α_d are the α caused in s, p, d, state in M-shell. That is, concerning internal conversion coefficient, the angular momentum is more important factor than the energy.

2) For small ν, $\alpha_K \sim \alpha_L \sim \alpha_M$ and $\alpha_s \sim \alpha_p \sim \alpha_d$.

This point is interpreted from the direct interaction between nucleus and its bound electron as Taylor and Mott(7) have pointed out in the case of the quadripole radiation.

§ 5. Comparison with Experimental Data (Isomer Analysis) and Discussions.

Table II shows the experimental data given by Lawson, and Cork

Table II.

Nucleus	γ-ray Energy	α_K/α_L	α_K/α_M	ν/γ^2	l-value obtaned from life time
In	392.7 Kev.	5.4±0.8	15.84	10.33	4
In	337.7 Kev.	4.8±0.6	23±10	8.88	4
In	191.7 Kev.	1.0±0.1	4.6±0.8	5.04	5
Cd	246.7 Kev.	5.9±0.5	30±10	6.85	No data
Cd	172.8 Kev.	6.6±0.6	35±10	4.80	No data

Comparing with Fig. 1 we see that the theoretical α_K/α_M are about four times smaller than the experimental values of Lawson and Cork. This is very dissatisfactory and, in the following, we wish to study the reason of this discrepancy in some detail.

On the way of our calculation, we made following two approximations, one is the neglect of $\vec{A}$ compared with $\vec{A}'$ and the other is the expansion of Hankel function.

For the former we remark that the most singular part of $\vec{A}$, $\vec{A}'$, is respectively

$$|A'| \sim (1/kr)^{l+2}, \quad |A| \sim (1/kr)^{l},$$

so $|A|/|A'| < 1$ gives $kr \ll 1$, $\therefore$ $\lambda \gg r$

but $\bar{r} = n^2 a_0/z$ (n is the principal quantum number).

When $Z = 30 \sim 50$ $\bar{r} \sim 10^{-9}$ which demands $\lambda \gg 10^{-9}$ this condition is only fulfilled by the γ-rays with energy less than 0.13 Mev. The latter approximation is justified also in the same condition.

In the case of α_K, α_L, this critical value of γ-ray energy becomes to be about 1 Mev. and 0.5 Mev. respectively and in the case of α_K, most known isomers satisfy this condition. But in the case of α_L, some known γ-ray energies lie beyond the critical value and for our α_M almost all known γ-ray energies do not fulfill the above mentioned condition. Such circumstances oblige us to change the calculation formalism. Firstly, one must give up Hebb-Nelson's approximation and use for example Dancoff-Morrison's method. Secondly, it may be of some hope to use the asymptotic form of the Hankel function for $kr \to \infty$ for γ-ray energies larger than the above mentioned critical value. And such methos of calculation, if carried out will reveal better agreement with experiments. But such computation will for the M-shell be quite troublesome, and may be left over for future chance. On the other hand accuracy of experimental work in the present stage (see table II) is too low to encourage us to the further laborious numerical works. Gathering these matters, we can conclude that in the present stage of the problem, the accuracy of theoretical and experimental works are still insufficient to decide l uniquely using the data of the internal conversion. As an additional remark, we point out that the results calculated here if enlarged 4,3∼4,5 times, coincide well with the experimental values of the table 1, and this coincidence is better than when

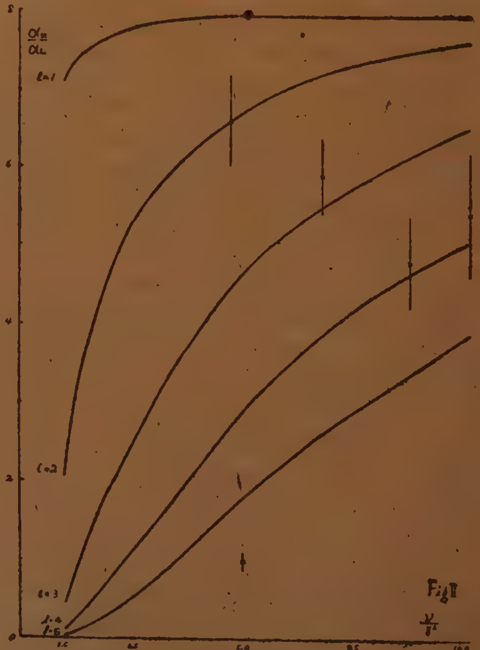

Fig. 2.

using α_K/α_L curve* (see Fig. 2.) Especially for In (191.7 Kev-γ-ray) l is equal to 5, but α_K/α_L curve gives $l > 5$ (perhaps $l = 7$). Decision of l from life time gives $l = 5$, so in low energy α_K/α_M will be more sensitive to l than α_K/α_L.

There are many other problems to be discussed on the internal conversion and isomers, for example, relativistic case of electric and magnetic multipole radiation and etc., in these problems we hope to return in future occasions.

Appendix

The calculations of hypergeometric function which is the main part of our numerical computations has been performed by using the recurrence formula and equation of analytic continuation for hypergeometric functions. In the papers of Dancoff-Morrison and Hebb-Nelson, there are published the results only, and so we wish to remark a few points about the reduction of the formula. In the case of eigen-functions belonging to the continuous levels in the coulomb field, the parameters of the hypergeometric function have a special relation from which it follows as above:

$F(\alpha, \beta, \gamma ; z) = e^{i\alpha} F^{*}(\alpha, \beta, \gamma ; z)$ (* expresses the conjugate complex.)

$e^{-i\alpha} F(\alpha, \beta, \gamma ; z) = \bar{F}(\alpha, \beta, \gamma ; z) =$ real function.

So that all relations between the various hypergeometric functions can be transformed into the $\bar{F}$ relations.

For the $F(\alpha, \beta, \gamma ; z)$, there is following relation

$$\delta(1-z)F(\alpha t, \beta, \gamma ; z) = \{2\delta-\gamma+(\beta-\gamma)z\} F(\delta, \beta, \gamma ; z) + (\gamma-\delta)F(\delta-1, \beta, \gamma ; z)$$

by the aid of which, if δ is an integer, all functions can be expressed by $F(1, \beta, \gamma ; z)$, the latter function on the other hand, can be transformed into the two terminating series by the analytic continuation relation

$$F(a, b, c ; z) = \frac{\Gamma(c)}{\Gamma(a)\Gamma(b)} \left\{ \frac{\Gamma(a)\Gamma(b-a)}{\Gamma(c-a)}(-z)^{-a}F(a, 1-c+a, 1-b+a ; z) + \frac{\Gamma(b)\Gamma(a-b)}{\Gamma(c-b)}(-z)^{-b}F(b, 1-c+b, 1-a+b ; z) \right\}$$

Further, recurrence formula which relates two functions with different l's can be obtained by Gauss' formula

$$\bar{F}_{l+1}(1, \beta, \gamma ; z) = \frac{(2l+3)(1+n^2)}{4\{(l+1)^2+n^2\}} \cdot \left\{ (2l+2)\left[\bar{F}_l(1, \beta, \gamma ; z) - \frac{2ln}{\sqrt{1+n^2}} \right] \right\}$$

where $F_{l+1}(1, \beta, \gamma ; z)$ means that in β and γ, l' is replaced by $(l+1)$.

References

(1) C.F.v. Weizäcker; Naturwiss. **24**, (1936) 813.
(2) Bethe: Rev. Mod. Phys.: **9**, (1937) 69 (§ 87)
(3) J.L. Lawson and J.M. Cork: Phys. Rev. **57**, (1940) 982.
(4) W. Heitler: Proc. Camb. Phil. Soc. **32**, (1936) 112.
(5) S.M. Dancoff and P. Morrison: Phys. Rev. **55**, (1939) 122.
(6) M.H. Hebb and E. Nelson: Phys. Rev. **58**, (1940) 486.
(7) H.M. Taylor and N.F. Mott: Proc. Roy. Soc. **A 142** (1933) 215.

---

* In Fig. I. experimental values of α_K/α_L (4-th column of Table II) are plotted after divided by 4.3.

Tentative Explanation of the Hysteresis Loops of Rochelle Salt.*

Takehiko OGUCHI, Yutaka TAKAGI, and Gen SHIRANE.

Tokyo Institute of Technology.

(Read May 23, 1948, Received November 30, 1948).

§ 1. Introduction.

It is well known that Rochelle salt is ferroelectric substance with hysteresis loops observed under an alternating electric field⁽¹⁾, and that the breadth of this loop becomes narrower and the values of polarization smaller as the temperature approaches to its Curie point.

These phenomena have been considered by many workers to be understood in analogy to ferromagnetism, by assuming ferroelectric domain structure. The existence of domains in Rochelle salt has recently been established from several experiments.⁽²⁾ But since the behavior of domains under an external field has not yet been studied so precisely that the characteristic form of hysteresis loop cannot be derived quantitatively from this point of view.

On the other hand Mueller⁽³⁾ explained these phenomena without referring to its domain structure. In his theory, the hysteresis loop was deduced from equilibrium curve between field E and polarization P, and abrupt changes in polarization were predicted at $D \rightarrow B'$ and at $D' \rightarrow B$ (see Fig. 1).

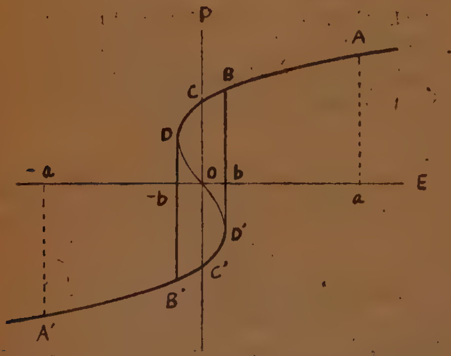

Fig. 1. S-type curve represents the equilibrium relation between P and E. The parts AC and A′C′ correspond to the stable states; CD and C′D′ metastable states; DOD′ unstable state. Thick line represents Mueller's hysteresis loop.

In the present paper, we shall tentatively follow Mueller's view inasmuch as he thought that an essential feature of hysteresis loops should be observed even in one domain crystal, while, instead of his interpretation based upon equilibrium curve, we shall adopt Eyring's rate process theory⁽⁴⁾ for the purpose of explaining the changes of loop-forms depending on frequencies of external field. We shall interpret the hysteresis phenomena as being caused by relaxation effect which should be accompanied by the reorientation of electric dipoles in spontaneously polarized homogeneous substance. Of course, the change of polarization due to the movement of domain boundaries are to be expected, but the change of intrinsic polarization itself must also be brought about as the present theory requires. Because the field energy is of the same order as thermal energy kT in electric case, being a striking contrast to the fact that it is quite negligible as compared with kT in magnetic case.

Thus we have developed a quantitative method for drawing hysteresis loops at any temperature as a function of various conditions of external field, such as frequencies, maximum field strength, and wave forms.

§ 2. Outline of Theoretical Treatment.

The structure of Rochelle salt is well known⁽⁵⁾

---

* This work was read at Kyoto in the Meeting of Physical Society of Japan in the spring of 1948, and translated from Japanese which was once received in the Proceedings of the Physical Society of Japan on May 7, 1948, and has never been published.

and it is accepted that its ferroelectricity is due to the hydrogen bonds. Mason said in his paper(6), that the proton which is responsible for this ferroelectricity is solely the one that lies between an oxygen atom belonging to carboxyl group of tartaric acid and an oxygen atom of neighbouring water molecule. The proton can exist either at A or B of potential wells as shown in Fig. 2, contributing to the crystal dipole moment $+\mu$ or $-\mu$ respectively.

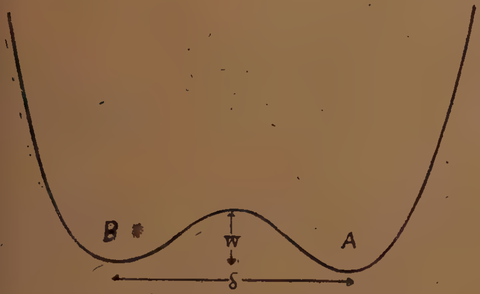

Fig. 2. Potential wells for a proton in a H-bond.

In order to derive two Curie points, Mason made use of the fact that the distance δ between A and B and hence the amount of moment μ may change its value with temperature. We shall adopt the former part of Mason's view. However, we shall for a moment, regard μ as being constant throughout the whole range of temperature, since our main interest consists in exposing the inherent nature of hysteresis loops.

The effective field F which acts on the protons may be written as,

$$F = E + \beta(P + \gamma F)$$

or

$$F = \frac{E + \beta P}{1 - \beta\gamma} \tag{1}$$

where β denotes Lorentz factor and γ is polarizability of remaining parts of the crystal. In this field the energy of proton is $-\mu F$ or $+\mu F$ respectively according to whether it exists in A or B (see Fig. 3).

Let the total number of H-bonds in the crystal be denoted by N and the number of H-bonds which have dipole moment $+\mu$ or $-\mu$ be denoted by a or b respectively. Then

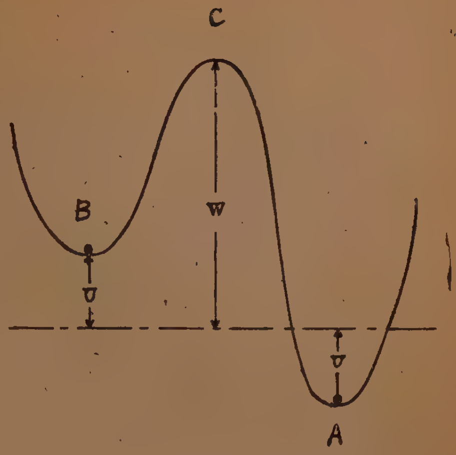

Fig. 3. Potntial wells in the presence of effective field.

$$a = \frac{N}{2}(1+\theta), \quad b = \frac{N}{2}(1-\theta), \tag{2}$$

$$P = \mu(a-b) = N\mu\theta, \tag{3}$$

where

$$\theta = \frac{P}{P_s}, \tag{4}$$

in which P_s represents the saturation polarization of the crystal. The partition function Z of this system may easily be calculated in the Bragg-Williams' approximation

$$Z = \frac{N!}{a!\,b!} e^{\frac{\mu(a-b)F}{kT}}$$

$$= \left(\frac{N}{a} e^{\frac{\mu F}{kT}}\right)^a \left(\frac{N}{b} e^{-\frac{\mu F}{kT}}\right)^b = (Z_A)^a (Z_B)^b \tag{5}$$

Z is of the form as if an a-type H-bond or a b-type H-bond has each the partition function Z_A or Z_B respectively. Making use of this fact we shall assume the change of partition function required for the movement of a proton from B to A is $Z_B \rightarrow Z_A$.

By Eyring's rate process theory, the probability per unit time of such a reaction is given by

$$\vec{k} = \frac{kT}{h}\frac{Z^*}{Z_B} e^{-\frac{W}{kT}} \tag{6}$$

where Z^*kT/h is the partition function for a proton existing at the saddle point C of the potential barrier. Z_B is the partition function of initial state, k and h are Boltzmann's constant and Planck's constant respectively.

Similarly the probability for the reverse process in which a proton moves from A to B is given by

$$\overleftarrow{k} = \frac{kT}{h}\frac{Z^*}{Z_A}e^{-\frac{W}{kT}} \tag{7}$$

In actual case, both processes (6) and (7) take place at the same time. Let the net change be denoted by k_{net}, then

$$k_{net} = \frac{kT}{h}Z^*\left\{\frac{1}{Z_B}e^{-\frac{W}{kT}} - \frac{1}{Z_A}e^{-\frac{W}{kT}}\right\}$$

$$= \frac{kT}{h}Z^*e^{-\frac{W}{kT}}\frac{1}{2}\left\{(1-\theta)e^{\frac{\mu F}{kT}} - (1+\theta)e^{-\frac{\mu F}{kT}}\right\} \tag{8}$$

Whenever one proton moves from B to A, P increases by 2μ. Accordingly,

$$\frac{dP}{dt} = 2\mu k_{net} \tag{9}$$

The rate of the change of P under an external field $E = E_0 \exp(2\pi i\nu t)$ may therefore be written in the form

$$\frac{dP}{dE} = \frac{dP}{dt}\frac{dE}{dt} = \frac{dP}{dt}\frac{1}{2\pi i\nu E} \tag{10}$$

Using (8) and (9), (10) becomes

$$\frac{dP}{dE} = \frac{2\mu kTZ^*}{h2\pi i\nu E}e^{-\frac{W}{kT}}\frac{1}{2}\left\{(1-\theta)e^{\frac{\mu F}{kT}} - (1+\theta)e^{-\frac{\mu F}{kT}}\right\} \tag{11}$$

or using (3),

$$\frac{d\theta}{dE} = \frac{kTZ^*}{Nh2\pi i\nu E_0 e^{2\pi i\nu t}}e^{-\frac{W}{kT}}\left\{(1-\theta)e^{\frac{\mu(E_0 e^{2\pi i\nu t} + \beta N\mu\theta)}{(1-\beta\gamma)kT}} - (1+\theta)e^{-\frac{\mu(E_0 e^{2\pi i\nu t} + \beta N\mu\theta)}{(1-\beta\gamma)kT}}\right\} \tag{12}$$

Solving (12), θ can be decided as a function of T, E_0, ν and t.

The equilibrium state expected from (12) is reducible to the following form:

$$P = P_s \tanh\frac{\mu(E+\beta P)}{(1-\beta\gamma)kT}. \tag{13}$$

(13) just correspondsent to Weiss' formula, and the results of it is shown in Fig. 1. Recently Mason has also given the formula (9) by somewhat different way. But he did not make the further development of the formular (9) for calculating the hysteresis loops.

§ 3. Several Numerical Examples of Hysteresis Loops.

The differential equation (12) cannot be solved analytically but we can obtain the shape of the curve by numerical integration. Several results are shown in Figs. 4~11, where T_c denotes the upper Curie point, E_0 and ν denote maximum amplitude and frequency of the external field respectively. For the values of material constants appearing in the formula we shall adopt what Mason has used, namely

$$\left.\begin{aligned} W &= 1100 \text{ cal/mol} \\ N\mu &= 3700 \text{ esu.} \\ \beta &= 4.07 \\ \gamma &= 0.15 \end{aligned}\right\} \tag{14}$$

Z^* is arbitrarily assumed so as to be convenient for computations, for at present we connot estimate any reasonable value of Z^*. In Fig. 4, the curve for $\nu = 1$ closely resembles the "static" hysteresis loop mentioned in § 1, but the curve for $\nu = 10$ and 100 become resmbling what are observed actually in cathode-ray oscillograms. Fig. 5 shows

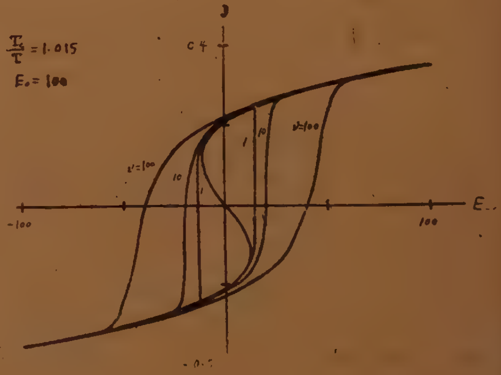

Fig. 4.

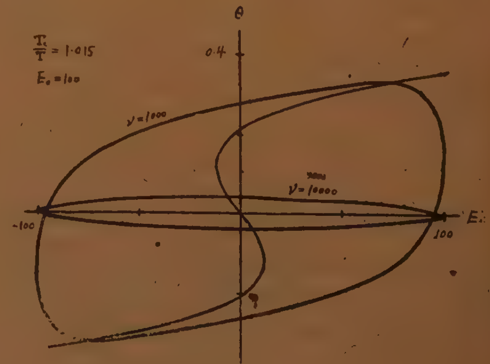

Fig. 5.

the case in which again $T_c/T = 1.015$, $E_0 = 100$ esu. but $\nu = 1000$ and 10000. It is seen that H-bond can no more follow the external electric field, provided that ν is greater than 1000. Fig. 6 shows the case in which as before $T_c/T = 1.015$ and $\nu = 100$ but the amplitude of external field is decreased to $E_0 = 20$ esu. and 15 esu. respectively. Comparing these with the previous curves for $E_0 = 100$ esu., it may be seen that the hysteresis loops become steeper. Fig. 7 shows the case in which as before $T_c/T = 1.015$, $\nu = 100$ but the amplitude is further decreased to $E_0 = 14$ esu. and 12.5 esu., (Coercive force of this crystal being estimated to be just 12 esu.). In such cases, the hysteresis loops become separated into two parts. Whenever $E_0 < 12$ esu., the hysteresis loops are separated into two parts and lie in the neighbourhood of the equilibrium curve. Fig. 8 shows the case in which $E_0 = 100$ esu. and $\nu = 1$, 10 and 100 but the temperature is raised to $T_c/T = 1.0008$. Sinec the temperature is now chosen very close to Curie point, the hysteresis loops become fairly different from previous ones, that is, their breadth becomes narrower and the values of remanence become smaller. Fig. 9 shows the case in which also $T_c/T = 1.0008$, $E_0 = 100$ but $\nu = 1000$ and 10000.

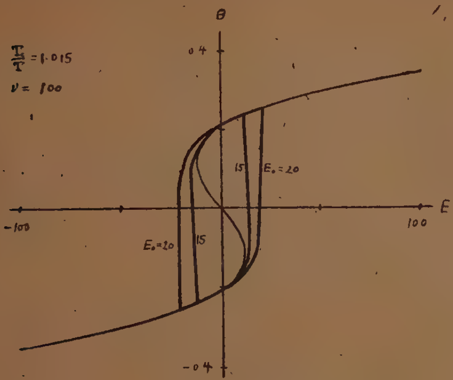

Fig. 6.

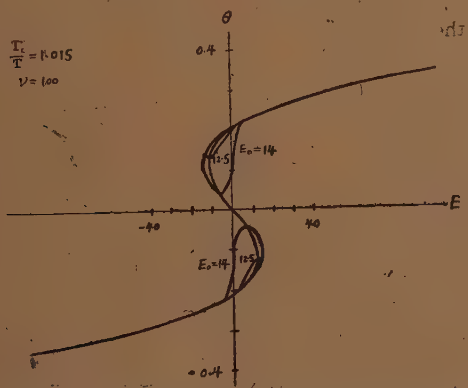

Fig. 7. Hysteresis loops separated into two parts, E_0 being chosen for 14 esu. and 12.5 esu.

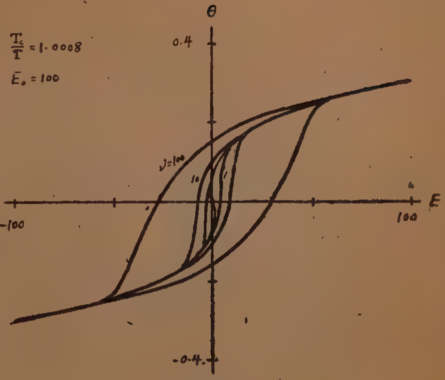

Fig. 8.

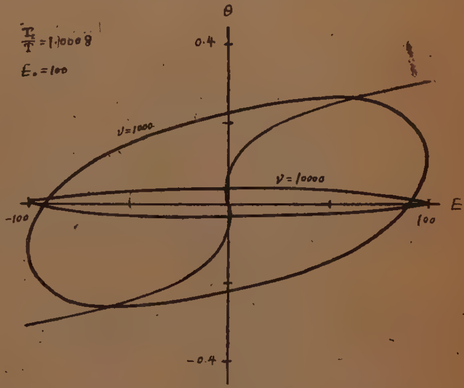

Fig. 9.

Let the temperature is again decreased to previous one, namely, $T_c/T = 1.015$, and let E_0 be fixed at 100 esu. and ν be fixed at 100, and let us investigate the effect of the wave form of external field upon the shape of hysteresis loops. Fig. 10 shows the hysteresis loops to be obtained for a rectified full wave of amplitude of 100 esu. The authors do not know whether there are observations to be compared with these results. Fig. 11 shows the asymmetric hysteresis loops obtained by biasing D. C. field of -60 esu. and $+80$ esu. Mueller has experimentally obtained the similar curves by applying mechanical sheer stresses on Rochelle salt crystals. Considering that Rochelle salt has a large piezoelectric coefficient d_{14} and that sheer stress may be regarded as effectively

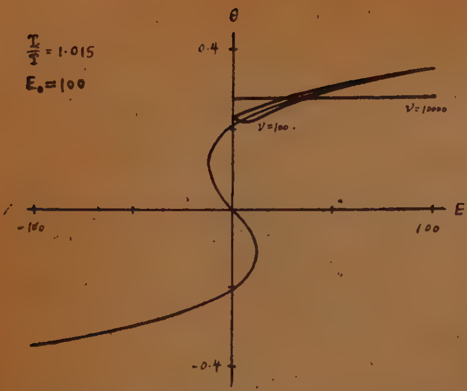

Fig. 10. Hysteresis loops to be obtained for a rectified full wave of amplitude of 100 esu.

equivalent to electric field, it may be allowable to say that the curves of Fig. 11 correspond to what Mueller has obtained.

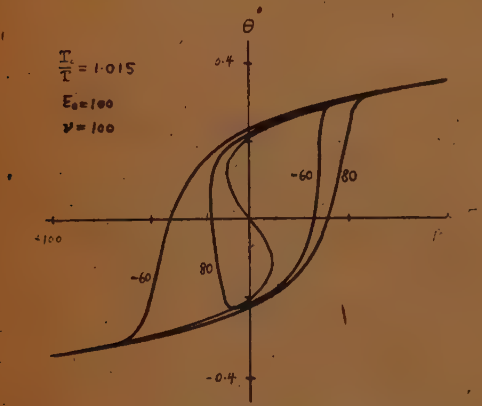

Fig. 11. Hysteresis loops obtained under biasing D. C. field. Numerals beside the curve denote the values of D. C. bias. Amplitude of alternating field is 100 esu. in both cases. The curve specified by −60 lies in the region between −160 esu. and +40 esu.; the curve specified by +80 between −20 and +180 esu.

§ 4. Stability of Hysteresis Loops.

Though some of the hysteresis loops of very curious shapes (see Figs. 5, 7, 9) have not yet been observed, even the authors do not dare to hope the discovery of such curves, because these loops are unstable and will greatly change their shapes under minute external fluctuation.

Now we shall examine the stability of the loops. Put

$$k_{ret} = \lambda. \tag{15}$$

Let us describe the isoclinic lines which are to be calculated from (15) for various values of λ. (Fig. 12). The equilibrium curve is the one for which $\lambda = 0$. In the region to the right side of this curve $\lambda > 0$ while in the region to the left $\lambda < 0$. The more distant are the isoclinic lines from the equilibrium curve, the greater the values of the parameter λ. Now, look at the part enclosed by the circle in Fig. 12. (This part is shown enlarged in Fig. 13). For instance, let the loop deviate from the point P on AB toward Q. Since λ is smaller at Q than the values which is to be expected on the stationary curve AB, that is to say, since $d\theta/dE$ must be smaller there, the integrated curve should be inclined to return toward AB, in such cases, the hysteresis loops are stable. At the part enclosed by the square in Fig. 12, it may easily be seen that they are unstable by similar reasons (Fig. 14).

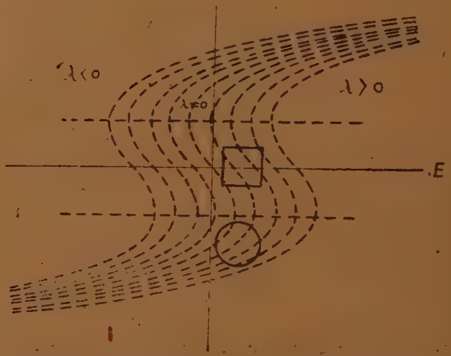

Fig. 12. Isoclinic lines for the differential equation (12).

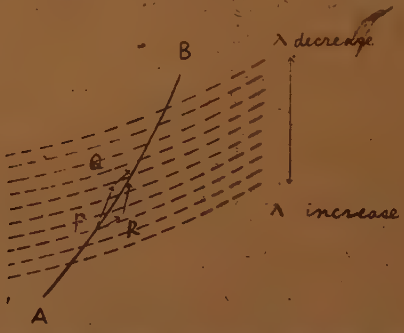

Fig. 13. Broken curves represent the isoclinic lines. Full line AB is the integration curve, being a part of hysteresis loop.

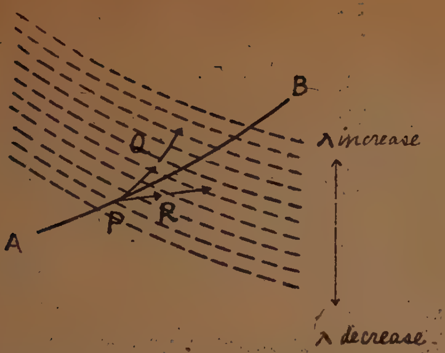

Fig. 14. The part enclosed by the square in Fig. 12, is enlarged.

Hence the stable regions are on the outside of two dotted lines in Fig. 12. In Figs. 5, 7 and 9, the hysteresis loops of which main parts exist in the region between dotted lines are unstable and perhaps not to be observed experimentally.

Finally it should be pointed out that if another value of Z^* be chosen the dependence of the loop-forms upon the frequency may be changed. The frequency ν used in this paper is, therefore, not to be confused with the one practically employed in laboratories.

References.

(1) S. B. Sawyer and C. H. Tower, Phys. Rev. **35** (1930), 269.
(2) S. Miyake, Proc. Phys.-Math. Soc. Japan, **23** (1941), 377, 810.
J. Phys. Soc. Japan, **2** (1947), 98.
W. J. Price, Phys. Rev. **73** (1948), 1132.
(3) H. Mueller, Phys. Rev. **47** (1935), 175, **57** (1940), 829, **58** (1940), 565, 805.
(4) Glasstone, Laidler and Eyring, *The Theory of Rate Processes*, p. 153, McGraw-Hill Co., Ltd.
(5) C. A. Beevers and W. Hughes, Proc. Roy. Soc. A **177** (1941), 251.
(6) W. P. Mason, Phys. Rev. **72** (1947), 854.

Short Notes.

Dielectric Residual Polarization of Barium Titanate Ceramic.

By Etsuro SAWAGUCHI and Tetsuo AKIOKA.
Tokyo Institute of Technology. Faculty of Science, Osaka University.
(Received July 4, 1948).

Among the ferroelectric prorerties of barium titanate it may be especially noted that the polarization *vs.* electric field relation shows a typical hysteresis characteristics,(1)(2) and that a piece of $BaTiO_3$ polycrystalline ceramic may be rendered piezoelectric(3) after the application of high D.C. field. After the removal of polarizing field from the $BaTiO_3$ ceramic, we find by a direct examination that there remains some residual polarization, the amount of which depends on the time of exposure to the field and on field intensity.

For fear of confusion due to leakage conductivity and electric breakdown, very fine polycrystalline ceramic must be used. This claim is fulfilled by refining method. The sample(*) thus obtained appears yellowish, and under a microscopic examination it proves to be an aggregation of numerous minute single crystals. A piece of the sample, silver-plated on both faces, is arranged in a flask so as to be protected from humidity. The two silver electrodes are connected once to the polarizing D.C. source, and secondly to a galvanometer circuit to measure the discharge current from the sample. When the sample is removed from the field, plenty of discharging current flows through a galvanometer, while it decreases rapidly and disappears almost completely after an hour. Thus it seems that the stable polarization is attained. This equilibrium state

---

(*) The dielectric constant measured with 1103 kc/sec is $\varepsilon = 1.2\times10^3$ at room temperature and $\varepsilon = 8\times10^3$ at the Curie point 93°C. (The discrepancies of Curie temperature from other authors' may probably be due to impurities.)

should be attributed to some definite configuration of spontaneously polarized domains.(4) If the temperature of the sample is raised at a constant rate (2.5°C/min.) by an electric furnace set arround the flask, then reappears the discharge current; at first it remains nearly constant then increases steeply to high values near the Curie point. After this rise, it decreases sharply and becomes not perceptible above that point. Since the discharging current is the time derivative of polarization, we can evaluate the residual polarization by integration of the current. Some of the observed values are shown in Fig. 1; here the polarizing field is applied at 25±3°C. It is notable that the curves resemble that of the spontaneous magnetization *vs.* temperature relation in ferromagnetic materials, and our values of the polarization are found on some occasion larger than 5.3 microcoulomb/cm² which is reported by Hulm.(2)

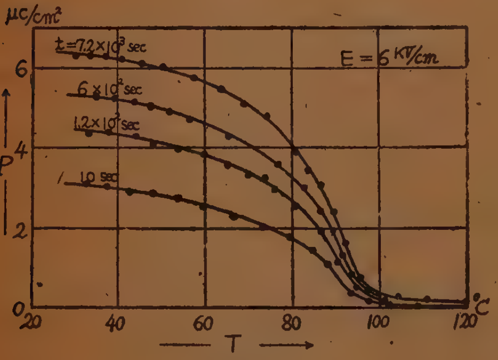

Fig. 1.

The effect of the field intensity *E*, and of the time of exposure *t*, upon the residual polarization *P*, is shown in Fig. 2, the ordinates representing the *P*'s at 30°C. In the time interval as shown in Fig. 2, *P* is nearly a linear function of log *t* when the field is of moderate intensity, but it is different when the field is very weak or very high, namely there seems to be some saturation effect above $E \fallingdotseq 6$ KV/cm.

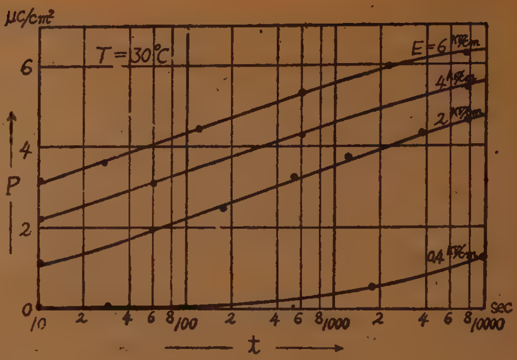

Fig. 2.

When the discharge current disappears above the Curie point, we can no more detect any electric current during either cooling or reheating process. On the contrary, when there remains some residual polarization below the Curie point we can observe that the electric charge is absorbed into the sample during cooling process, this may be accounted for by the increase of spontaneous polarization of Weiss domains as the temperature is lowered. Now it is easy to see that at least in ferroelectric state of the sample the inversion of the domains is responsible for polarizing process. Hence the polarization is affected by the time of exposure as well as the field intensity. A fuller account of the work will be published later.

In conclusion authors express their grateful appreciation to Prof. Y. Takagi and Mr. S. Sawada and Mr. G. Shirane for their kind advice and encouragement.

References

(1) Y. Takagi, E. Sawaguchi, and T. Akioka: J. Phys. Soc. Jap., **3** (1948), 270.
(2) J. K. Hulm: Nature, **160** (1947), 127.
(3) W. L. Cherry, Jr. and Robert Adler: Phys. Rev., **72** (1947), 981.
(4) H. F. Kay and R. G. Rhodes: Nature, **160** (1947), 126.

On the Mechanism of Colouring of Oxidized Copper.

By Yasuhiro Doi. *The Mechanical Labortory, Tokyo, Japan.* (Received Sept. 24, 1948)

When metallic copper is heated in the air, bright colours appear with the growth of the oxide film on the surface of metallic copper. There are two independent theories on the mechanism of the colouration, one is the diffraction theory given by Raman, Wood, Hinshelwood and

Mallock, and the other is the interference theory by Constable etc.

The author will present a new interference condition, considering the phase change of light on the reflection at the metallic copper and oxide boundary. When the light comes normally to the coloured copper surface, a portion of it is thrown back from the surface, of which amplitude ratio to the incident light is

$$R=\frac{r_a+r_b e^{-2A}}{1+r_a r_b e^{-2A}}, \qquad A=2\pi i\frac{ln}{\lambda},$$

where r_a and r_b are Fresnel's coefficients respectively at the air-oxide and the oxide-metal boundaries, l the thickness of the oxide and n the refractive index thereof. We must here notice that r_b should be a complex number on account of the complex refractive index of copper and can be written $|r|e^{i\delta}$, where the azimuth $\delta\sim 3/2\pi$ can be computed by Fresnel's equations with the known values of the refractive indices of copper and oxide and the intensity of the reflected light is then given by

$$RR^*=\frac{r_a^2+|r_b|^2+2r_a|r_b|\cos(2A-\delta)}{1+r_a^2|r_b|^2+2r_a|r_b|\cos(2A-\delta)}.$$

The minimum reflection occours when l and λ satisfy the interference condition

$$2nl/\lambda=\delta/2\pi+(2m-3)/2, \quad m=1,2,\cdots$$

The author has prepared a brightly polished copper plate 100 ~ 50 mm in size and 1 mm thick, and oxidized the surface by heating it in the air about 15 minutes within the temperature range 150 ~ 250 deg. C. The thickness of the oxide film was computed applying the above-mentioned interference condition to the minimum of the spectral reflectivity, which was measured by Martens-Koenig's spectral photometer. As shown in the Table, it has been found to be nearly coincident with the value determined from the amount of the weight decrease after the oxidized copper plate was dipped into thinly diluted sulphuric acid and the oxide film was dissolved off.

Table.

order	colour	wave lenght (Å)		n (Cu_2O)	δ deg	thickness (Å)	
		max	min			optical	weighed
1	brown		4800	2,9	262	190	130
1	red		5200	2,9	265	210	190
1	blue		6200	2,6	283	330	275
1	pale blue		6600				300
1	yellow	5500					490
2	orange		4400	3,1	257	860	580
2	orange red		4800	2,9	262	1030	690
2	orange red		5000	2,9	264	1060	645

Therefore, it is clear that the interference phenomena is mainly responsible for the observed colouring at least in the region of the first order's interference, even if the scattering of the light in the oxide film to the side way might be able to contribute to the brilliancy of the colour.

In the interference condition offered by Constable(1) the phase factor δ was neglected and his computed values of the thickness were two times as large as the values with the author's in the first order region.

The author heartily thanks Dr. H. Hasunuma and Mr. Y. Ukita for their kind discussion on the whole course of his investigation.

Reference.

(1) F. H. Constable: Proc. Roy. Soc. A **115** (1925) p 570.

On The Hysteresis Loops of $BaTiO_3$ Ceramics.

By Shoichiro NOMURA and Shozo SAWADA.
Second Faculty of Engineering, University of Tokyo

(Received Nov. 2, 1948).

The hysteresis loops of $BaTiO_3$ are not novel today. It is considered that the hysteresis phenomena depend upon the electric domain structure, but their essence and behaviour are not yet obvious.

We investigated the relation between maximum polarization and maximum field at each temperature from 20°C. to 150°C., as Hulm,(1) and recognized that the maximum polarization versus temperature curves of hysteresis loops have a maximum when the applied a.c. voltage is smaller than a certain value which changes with temperature. If the applied a.c. voltage is larger, the maximum polarization decreases with temperature as observed by Hulm.

Let us suppose that the ceramics are made of many electric domains and in its single domain the relation between polarization and field is the same as Mason(2) adopted in the paper of rochelle salt. It is natural such phenomena are observed when, we imagine, the spontaneously polarized domains behave as stated above.

In order to make sure the behaviour of domains furthermore, we observed the hysteresis loops of $BaTiO_3$ with biasing d.c. voltage at each temperature. A circuit essentially similar to that of Sawyer and Tower(3) was used to display the polarization on electric field curve at 50 cycles per second on a cathode ray tube, but d.c. batteries were inserted between earth and power transformer in order to give d.c. biasing voltage.

Following figures show one example, in which a.c. voltage is 25kV/cm, and d.c. voltage varies from 0 to 45kV/cm. As the d.c. biasing field becomes stronger, asymmetry of loops appears and the hysteresis loss becomes smaller. When the field is too strong to prevent from "umklappens" of domains, the loss of loops vanishes quitely and the loop becomes an asymmetric single curve as shown by (e). We do not observe any abrupt change of loops when d.c. field strength increases continuously beyond the coersive force, but the bend type of the edge of loops in the side of opposite direction to d.c. field changes passing through some d.c. value as shown by (b) and (c).

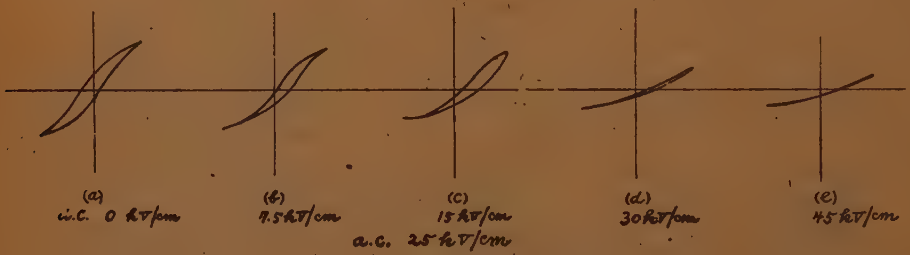

Fig. 1.

One of the other evidences of this fact is shown by changing temperature at a certain adequate d.c. voltage. In this case, the coersive force changing with temperature foments the transformation of bending. It is interesting to see how the total length of hysteresis loops proportional to polarization changes with d.c. biasing field. When the applied d.c. field is too small to contain coersive force, it decreases monotonously with d.c. field, and then becomes flat, while for large field it doesn't decrease initialy, then as It may be due to the coersive field, and coincides with the one that was approximately estimated from the normal hysteresis loops.

before. The d.c. value at which the total length begins to decrease changes with a.c. voltage and temperature. As temperature rises, the region of d.c. voltage in which the polarization decreases gradually becomes smaller and smaller. We can also estimate the coersive force from these facts, and the results are in accordance with the above values in the order.

In addition, it should be mentioned that the treatment of a single crystal in the same manner as we did for ceramics will be interesting.

References

(1) J. K. Hulm: Nature, **160**, (1947) 127.
(2) Mason: Phys. Rev., **72**, (1947) 854.
(3) C. B. Sawyer and C. H. Tower: Phys. Rev., **35**, (1930) 269.

On the Laminar Sub-Layer in the Turbulent Boundary Layer, II.

Part II. On an Approximate Solution for the Flow along a Flat Plate.

By Yutaka SHIGEMITSU.

Railway Technical Research Institute, Tokyo.

(Read March 28, 1948; Received August 3, 1948).

§ 4. A Method of an Approximate Solution of the Equations of Motion When $\lambda = 0$.

In the investigation of turbulent boundary layer, the most important flow pattern is that along a flat plate; and in this case of flow, there has been many detailed experimental and semi-theoretical investigations in comparison with other cases. And so, when we treat the equations of motion of laminar sub-layer, it is desirable to start at first with this case.

The equations of motion and the boundary conditions of laminar sub-layer in this case are

$$u\frac{\partial u}{\partial x}+v\frac{\partial u}{\partial y}=\nu\frac{\partial^2 u}{\partial y^2},\qquad u=\frac{\partial\psi}{\partial y},\quad v=-\frac{\partial\psi}{\partial x},\tag{4,1}$$

and

$$u=0 \text{ at } y=0,\qquad u=u_1 \text{ at } y=\delta_1,\tag{4,2}$$

or

$$u=0 \text{ at } y=0,\qquad \left(\frac{\partial u}{\partial y}\right)_{\delta_1}=\frac{u_1}{\delta_1}m,\quad \frac{u_1\delta_1}{\nu}=c.\tag{4,2'}$$

At first, as the non-dimensional coordinates and the stream function, we write as follows,

$$\xi=x/L,\quad \eta=y/\delta_1,\quad F(\xi,\eta)=\Psi(x,y)/(u_1\,\delta_1);\tag{4,3}$$

where L is a standard length along the x-axis. Then making use of the last condition of (4,2'), we have

$$u=u_1\frac{\partial F}{\partial\eta},\quad v=u_1\left(\frac{\partial F}{\partial\eta}\eta\frac{d\delta_1}{dx}-\frac{\partial F}{\partial\xi}\frac{\delta_1}{L}\right)$$

$$\frac{\partial u}{\partial x}=-\frac{d\delta_1}{dx}\frac{c\nu}{\delta_1{}^2}\frac{\partial F}{\partial\eta}-\frac{u_1}{\delta_1}\frac{\partial^2 F}{\partial\eta^2}\eta\frac{d\delta_1}{dx}+\frac{u_1}{L}\frac{\partial^2 F}{\partial\xi\partial\eta}\tag{4,4}$$

$$\frac{\partial u}{\partial y}=\frac{u_1}{\delta_1}\frac{\partial^2 F}{\partial\eta^2},\quad \frac{\partial^2 u}{\partial y^2}=\frac{u_1}{\delta_1{}^2}\frac{\partial^3 F}{\partial\eta^3},$$

and (4,1) reduces to

$$c\frac{d\delta_1}{dx}\left(\frac{\partial F}{\partial\eta}\right)^2+\frac{\partial^3 F}{\partial\eta^3}=c\frac{\delta_1}{L}\left(\frac{\partial F}{\partial\eta}\frac{\partial^2 F}{\partial\xi\partial\eta}-\frac{\partial^2 F}{\partial\eta^2}\frac{\partial F}{\partial\xi}\right)\tag{4,5}$$

The F and δ_1/L may be expanded in the following power series

$$F=f_0(\eta)+f_1(\eta)\xi+f_2(\eta)\xi^2+\dots,\qquad \delta_1/L=a_0+a_1\xi+a_2\xi^2+\dots,\tag{4,6}$$

and when these are substituted into (4,5), the sum of the coefficients of the same power of ξ must vanish. Then the coefficients of ξ^0 give

$$(ca_1)f_0'^2+f_0'''=(ca_0)(f_0'f_1'-f_0''f_1).\tag{4,7}$$

Now, as the first approximation we take

$$F(\xi,\eta)=f_0(\eta),$$

and then (4,7) reduces to

$$(ca_1)f_0'^2+f_0'''=0,$$

and when, for brevity, σ and f are taken respectively as ca_1 and f_0', the above expression gives

$$\sigma f^2+f''=0.\tag{4,8}$$

This equation is a transformation of (4,1) by using u_1, δ_1, and F, in which u_1 is eliminated by the one condition of (4,2') and simplified to the first approximation. There is the unknown factor σ which is dependent on δ_1 and it must be determined by the other condition of (4,2'). Hence the boundary conditions of (4,8) are $u=0$ at $y=0$ and $u=u_1$, $\frac{\partial u}{\partial y}=\frac{u_1}{\delta_1}m$ at $y=\delta_1$, and these are expressed in the foollowing non-dimensional form;

$$f=0 \quad\text{at}\quad \eta=0,\qquad f=1,\ f'=m \quad\text{at}\quad \eta=1.\tag{4,9}$$

Hence we can determine the form of f and σ by (4,8) and (4,9).

Multiplied by f', (4,8) is easily integrated into

$$\frac{1}{3}(\sigma f^3)+\frac{1}{2}f'^2 = c_1\,,$$

and the integration constant c_1 is determined by (4,9), i.e.

$$c_1 = \frac{1}{2}f'^2(0) = \frac{1}{3}\sigma+\frac{1}{2}m^2.$$

Taking α as $f'(0)$, these reduce to

$$f' = \sqrt{(\alpha^2-\frac{2}{3}\sigma f^3)},$$

$$\frac{1}{3}\sigma+\frac{1}{2}m^2 = \frac{1}{2}\alpha^2.$$

From the above equation, it is known that f can be expressed by an elliptic function of η. These results are

$$\begin{aligned} &f = B[\wp(A\eta)-\{\wp'(A\eta)+2\}^2/\{4\wp^2(A\eta)\}], \\ &A = 0.43679(\alpha\sigma)^{\frac{1}{3}}, \quad B = 1.1447\alpha/(\alpha\sigma)^{\frac{1}{3}}. \end{aligned} \tag{4,10}$$

In these, the moduli of $\wp$-function are given as

$$g_2 = 0, \quad g_3 = -4, \tag{4,11}$$

and as the boundary conditions we get

$$\begin{aligned} &\frac{1}{2}\alpha^2-\frac{1}{2}m^2-\frac{1}{3}\alpha = 0, \\ &B[\wp(A)-\{\wp'(A)+2\}^2/\{4\wp^2(A)\}] = 1. \end{aligned} \tag{4,12}$$

Hence, for a given value of m, α and σ are determined by (4,12) and so f is also determined by (4,10). Namely as the first approximation of (4,6), we get

$$F = f_0(\eta) \quad \text{and} \quad \delta_1/L = a_0+a_1\xi. \tag{4,13}$$

§ 5. The Velocity Distribution in the Laminar Sub-Layer

As for a theoretical ground by which the value of m is determined, we take the condition that at the boundary of laminar sub-layer, the tangent of the velocity profile is equally connected to that of the turbulent part. As the velocity profile of turbulent boundary layer, we will take the "Power-Law" or the "Logarithmic-Law"; these are respectively written as

$$u = U(y/\delta)^{\frac{1}{7}} \tag{5,1}$$

and

$$\frac{u}{U_\tau} = A+\frac{1}{K}\log\frac{U_\tau y}{\nu}, \tag{5,2}$$

where U, δ, and U_τ are respectively the velocity of the fluid outside the turbulent boundary layer, its thickness, and the frictional velocity; and A, K are numerical constants. With (5,1) we obtain

$$\left(\frac{\partial u}{\partial y}\right)_{\delta_1} = \frac{u_1}{\delta_1}\frac{1}{7},$$

and in the "Logarithmic-Law", using the condition of $u_1\delta_1/\nu = c$,

$$U_\tau = \sqrt{(\tau_0/\rho)} = \sqrt{(\alpha c)}\nu/\delta_1 = \sqrt{(\alpha/c)}u_1\,, \tag{5,3}$$

and we get

$$\left(\frac{\partial u}{\partial y}\right)_{\delta_1} = \frac{U_\tau}{K\delta_1} = \frac{u_1}{\delta_1}\left(\sqrt{\frac{\alpha}{c}}\frac{1}{K}\right).$$

Then we get

$$m = \frac{1}{7} \tag{5,4}$$

or

$$m = \sqrt{\frac{\alpha}{c}}\frac{1}{K}. \quad (K = 0.39) \tag{5,5}$$

Taking (5,4), we get $\varkappa = 1.336$, $\sigma = 2.646$ by (4,12) and the velocity distribution in laminar sub-layer is determined by (4,10).

In the theory of turbulent boundary layer, it is well-known that when we take

$$u^* = u/U_\tau\,, \ y^* = U_\tau y/\nu,$$

there is a functional relation between u^* and y^*, which is independent of the Reynolds Number of the main flow. In the above solution of laminar sub-layer, the velocity distribution is given by

$$u/u_1 = f(y/\delta_1),$$

and making use of (5,3), we have the form

$$u^* = \sqrt{(c/\alpha)}f(y^*/\sqrt{(c\alpha)})\,; \tag{5,6}$$

namely in the first approximate solution, the above-mentioned relation between u^* and y^* also holds.

As shown in the Part I of this paper, the physical meaning of c may be called as the lower critical Reynolds Number of transitian for the flow along a flat plate, and as for its numerical value, there are some theoretical investigations by W. Tollmien and others. But their results are believed to be not yet completely correct, and so at present we have no reliable ground to determine the value of c. Hence we will take

$$c = 230, \qquad (5,7)$$

so that (5,6) may agree with the experimental results.

Hence, in the case of the "Power-Law", taking (5,7), we obtain

$$u^* = 13.1 f(y^*/17,5), \qquad (5,8)$$

and in the "Logarithmic-Law", from (5,5) and (4,12) we have $m \doteq 0.193$, $\alpha = 1.31$, $\sigma = 2.53$ and get the form

$$u^* = 13.2 f(y^*/17,4). \qquad (5,9)$$

These results of the velocity distribution in the two cases are shown in Figs. 3, 4, and Table I. In Fig. 4, as to the discrepancy between the "Power-" and the "Logarithmic-Law" and the experimental data near the surface of a body, there has been such an explanation that the velocity distribution in laminar sub-layer is assumed to be linear; and between the turbulent part and the sub-layer, a transition region is supposed to exist so that the velocity distribution may be smoothly connected in the whole region of turbulent boundary layer. But when we take the above solution of the laminar sub-layer, although approximately, we can explain these experimental facts more theoretically.

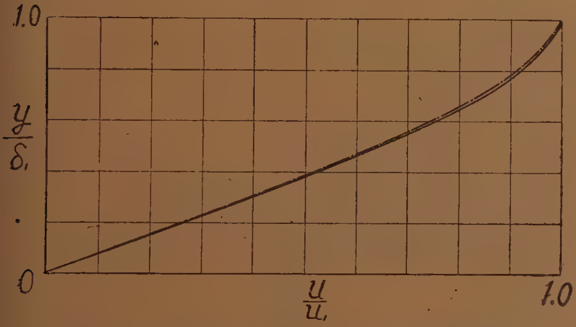

Fig. 3. Velocity distribution in laminar sub-layer. Full line—"Power-Law". Chain line—"Logarithmic-Law".

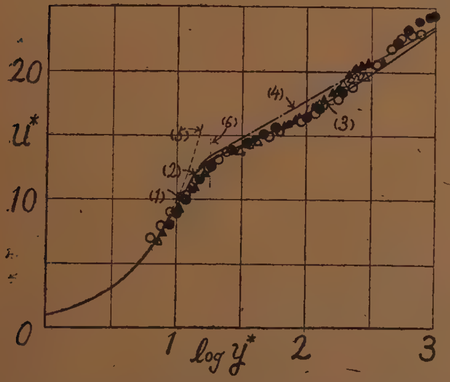

Fig. 4. Universal velocity distribution in turbulent boundary layer. (1)—(5,8), (2)—(5,9), (3)—"Power-Law", (4)—"Logarithmic-Law", (5)—linear velocity distribution, (6)—the boundary of the laminar sub-layer in "Power-Law". ●, ○, ▲, △ are measured points made by Tani and Hama.(1)

Table I.

"Power-Law"		"Logarithmic-Law"	
y/δ_1	u/u_1	y/δ_1	u/u_1
0,0000	0,00000	0,0000	0,00000
,0527	,07038	,0538	,07061
,1054	,14071	,1075	,14119
,1581	,21090	,1613	,21162
,2107	,28074	,2151	,28169
,2634	.35000	,2689	,35119
,3161	,41836	,3226	,41978
,3688	,48543	,3764	,48708
,4215	.55077	,4302	,55263
,4742	,61387	,4839	,61595
,5269	.67420	,5377	,67649
,5795	,73119	,5915	,73367
,6322	,78426	,6453	,78692
,6849	,83281	,6990	,83563
,7376	,87626	,7528	,87923
,7903	,91409	,8066	,91718
,8430	,94578	,8604	,94898
,8957	,97090	,9141	,97419
,9483	,98911	,9679	,99247
1,0000	1,00000	1,0000	1,00000
$m = 0.1424$ $\alpha = 1.3358$		$m = 0.1926$ $\alpha = 1.3133$	

§ 6. The Distribution of the Thickness of the Laminar Sub-Layer and the Turbulent Boundary Layer.

In the last chapter, we obtained the values of σ for the "Power-" and the "Logarithmic-Law", and with these values in use, we can show the distribution of the thickness for the first approximate solution; these are respectively

$$\delta_1/L = \alpha_0 + 0.0115\xi,$$

$$\delta_1/L = \alpha_0 + 0.0110\xi,$$

in which α_0 must be determined by the condition at the point where the turbulent boundary layer start to develop. When we proceed to get higher approximate solutions, the next coefficients of the power series of δ_1/L can be determined step by step. However, in the first approximate solution, the accuracy of the expression for δ_1/L is inadequate, and so concerning the thickness of the sub-layer, we desire to investigate by another well-known method.

For the turbulent flow along a flat plate, the surface friction is written as

$$\tau_0 = \mu\left(\frac{\partial u}{\partial y}\right)_0, \tag{6,1}$$

or

$$\tau_0 = \rho U^2 \frac{d}{dx}\int_0^\delta \frac{u}{U}\left(1-\frac{u}{U}\right)dy. \tag{6,2}$$

When its velocity distribution is assumed to be

$$u = U(y/\delta)^{\frac{1}{7}},$$

and with the condition of $(u_1\delta_1)/\nu = c$, we get

$$\delta_1^{\frac{8}{7}} = \delta^{\frac{1}{7}} c\nu/U, \tag{6,3}$$

hence (6,1) can be expressed by the form

$$\tau_0 = \mu\alpha u_1/\delta_1 = \mu\alpha(c\nu)^{-\frac{3}{4}} U^{\frac{7}{4}} \delta^{-\frac{1}{4}},$$

and when we neglect the effect of laminar sub-layer and calculate the momentum integral of (6,2) using the form of (5,1), it reduces to

$$\tau_0 = \frac{7}{72}\rho U^2 \frac{d\delta}{dx}.$$

Thus we have the condition

$$\frac{7}{72}\rho U^2 \frac{d\delta}{dx} = \mu\alpha(c\nu)^{-\frac{3}{4}} U^{\frac{7}{4}} \delta^{-\frac{1}{4}}, \tag{6,4}$$

and then with (6,3) and (6,4), $\delta(x)$ and $\delta_1(x)$ can be easily integrated. For brevity, when we take the ideal case of flow in which the turbulent boundary layer is developing from the forward stagnation point, these results are

$$\left.\begin{aligned}\delta/x &= 0.3723 R_x^{-\frac{1}{5}},\\ \delta_1/x &= 103.0 R_x^{-\frac{9}{10}},\end{aligned}\right\} \tag{6,5}$$

where $R_x = Ux/\nu$.

The distribution of the thickness can also be derived in the case of the "Logarithmic-Law". By (5,2) we have

$$u_1/U_\tau = A + 1/K \log(U_\tau\delta_1/\nu) \tag{6,6}$$

and

$$U/U_\tau = A + 1/K \log(U_\tau\delta/\nu) \tag{6,7}$$

and with (5,3) we have a condition

$$A = \sqrt{(c/\alpha)} - 1/K \log \sqrt{(\alpha c)}. \tag{6,8}$$

Taking

$$KU/U_\tau = z, \tag{6,9}$$

and eliminating A from (6,7), we obtain

$$\log \delta/x = \log\{\sqrt{(\alpha c)}/K\} - K\sqrt{(c/\alpha)} + z + \log z - \log R_x, \tag{6,10}$$

and when we write U_τ with δ_1 by (5,3), eliminate A by (6,8) and $\log(\delta/x)$ by (6,10), then (6,7) reduces to

$$\frac{K}{\sqrt{(\alpha c)}} R_x \frac{\delta_1}{x} + \log\frac{\delta_1}{x} = \log\frac{\sqrt{(\alpha c)}}{K} + z + \log z - \log R_x. \tag{6,11}$$

From (5,2) and (6,7), we have

$$u/U = 1 - 1/z \log(\delta/y),$$

and then with the momentum equation in use in the whole region of turbulent boundary layer and eliminate δ by (6,10), we obtain

$$e^z(z^2-2z+2)\frac{dz}{dx} = \frac{K^3}{\sqrt{(\alpha c)}} \exp\{K\sqrt{(c/\alpha)}\}\frac{U}{\nu} \tag{6,12}$$

With the previously-described numerical values of α, c and K, (6,12) can be easily integrated, and when the integration constant is determined assuming $\delta = 0$ at $x = 0$, this result becomes

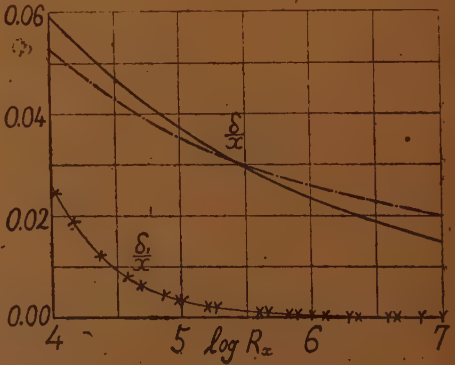

Fig. 5. Distribution of the thickness of turbulent boundary layer and the laminar sub-layer. Full line—"Power-Law". Chain line—"Logaritic-Law". Y—calculated points in "Power-Law", X—calculated points in "Logarthmic-Law".

$$R_x = 1.601e^z(z^2-4z+6)-6. \qquad (6,13)$$

Taking this relationship between z and R_x and using (6,10) and (6,11), we can express δ/x and δ_1/x as a function of R_x.

These results are shown in Fig. 5 in the two cases and we can find that the distribution of the thickness of laminar sub-layer in both cases are almost the same, although those of the turbulent boundary layer are different. As well as the velocity distribution described in the last chapter, the above result seems to show that the state of flow in laminar sub-layer is not so dependent on the state of the flow in turbulent part.

§ 7. Discussions on the Results.

We found the distribution of δ/x and δ_1/x as functions of R_x, and then u_1/U can be shown in the same way by the condition $u_1\delta_1/\nu = c$, and so with the function of (4,10), the state of flow in the laminar sub-layer can be completely estimated.

(i) In the laminar sub-layer, the surface friction is $\tau_0 = \mu\alpha u_1/\delta_1$ and when c_f is taken as the skin friction coefficient, that is $c_f = \tau_0/(1/2\ \rho U^2)$ it is also given as a function of R_x: in the case of the "Power-Law", it reduces to

$$c_f = 0.05792 R_x^{-\frac{1}{5}} \qquad (7,1)$$

and

$$\tau_0 = 0.02262\rho U^2 R_\delta^{-\frac{1}{4}} \qquad (7,2)$$

where $R_\delta = U\delta/\nu$. By means of a dimensional analysis, Blasius derived the "1/7-Power-Law" of the velocity distribution on the basis of his empirical formula of surface friction, such as

$$\tau_0 = 0.0228\rho U^2 R_\delta^{-\frac{1}{4}}. \qquad (7,3)$$

In the above calculation, on the basis of the "Power-Law", (7,2) is conversely derived, and the numerical coefficient is almost the same as (7.3).

In the "Logarithmic-Law", with the numerical value of K in (5,5), c_f is shown as follows by (6,9)

$$c_f = 0{,}30/z^2,$$

and with the relation of (6,13), it is given as a funcion of R_x. These are shown in figure 6 with experimental data.⁽¹⁾

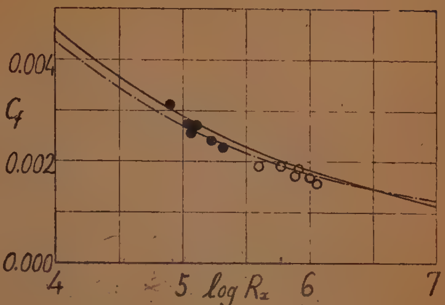

Fig. 6. Distribution of the skin friction coefficient. Full line—"Power-Law". Chain line—"Logarithmic-Law".

(ii) Concerning the distribution of the thickness of laminar sub-layer and turbulent boundary layer, it has been shown that they increase along the surface of a body in different rate. Thus we find that the velocity distribution in the whole turbulent boundary layer flow along a flat plate changes according to the Reynolds Number. For example, in two cases of $R_x = 1.114\times10^5$ and $R_x = 1.098\times10^6$, the velocity distributions in the turbulent boundary layer including laminar sub-layer, are calculated for the "Power-" and the "Logarithmic-Law", and compared with experimental results⁽¹⁾ in Fig. 7.

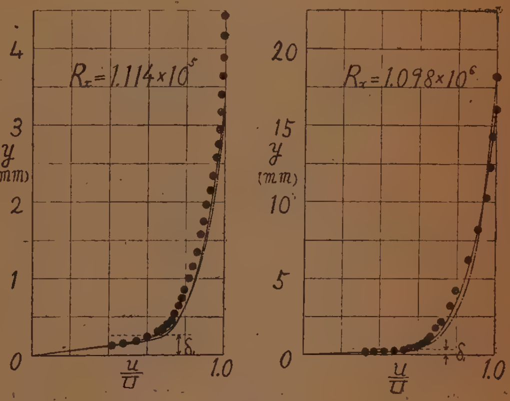

Fig. 7. Velocity distributions in the whole region of turbulent boundary layer at various values of R_x. Full line—"Power-Law" Chain line—"Logarithmic-Law". δ_1 shows the thickness of the laminar sub-layer in "Power-Law".

(iii) In many experiments on turbulent boundary layer, the existence of the laminar sub-layer has been neglected, and it has been believed that for the flow along a flat plate, the velocity distribution is independent of R_x. But when the existence of laminar sub-layer is considered, its effect ought to appear itself; for instance when we take $H = \delta^*/\vartheta$ (δ^* and ϑ are respectively displacement and momentum thicknesses) as one of the parameters to show the state of turbulent boundary layer, it also changes with the value of R_x even for the flow along a flat plate. These facts are recognized by the recent experiments.(1)

By the present investigation, when the effect of laminar sub-layer is neglected, in the "Power-Law", we have from (5,1)

$$\delta^* = 0.1250\delta \quad \vartheta = 0.09722\delta,$$

and

$$H_0 = 1.286. \tag{7,4}$$

(The suffix 0 indicates the case when the laminar sub-layer is neglected, and 1 when it is considered.) But in laminar sub-layer, from the table, we have

$$\int_0^{\delta_1}(1-u/u_1)\,dy = 0.4033\delta_1$$

$$\int_0^{\delta_1}u/u_1(1-u/u_1)\,dy = 0.1392\delta_1.$$

When this effect is considered and the displacement and momentum thicknesses are calculated, we obtain easily the form of H_1 as follows;

$$H_1 = \frac{R_x^{-\frac{1}{10}} + 0.0^3729R_x^{\frac{9}{10}}}{25.8 - R_x^{\frac{1}{10}} - 0.0^3568R_x^{\frac{9}{10}}} \tag{7,5}$$

In the "Logarithmic-Law", in the same manner, the form of H_0 and H_1 are calculated as functions of R_x. These are shown in figure 8 with the experimental data.(1)

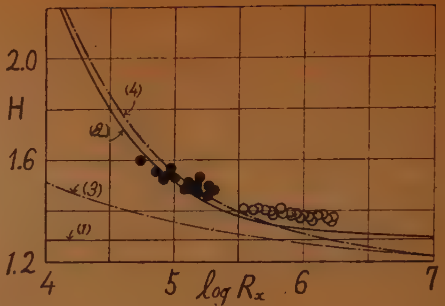

Fig. 8. Distribution of the parameter of "H". (1)—H_0, (2)—H_1: "Power-Law". (3)—H_0, (4)—H_1: "Logarithmic-Law".

In many experiments on turbulent boundary layer, owing to the very small thickness, the existence of laminar sub-layer has been neglected. But when the velocity distribution is measured until the immediate vicinity of the surface of a body, it is clear from the experimental results that, due to the effect of the laminar sub-layer, the state of flow is completely different from that in turbulent part. Hence, apart from the study in turbulent layer, the investigations of laminar sub-layer come to be necessary. In this part of the paper, we investigated whether the fundamental conception of laminar sub-layer described in the last part, might be appropriate or not for the flow without pressure gradient, by comparing the results of the approximate solution with experimental data.

Reference.

(1) Tani and Hama; Senken Hokoku, 1-4. March, 1945.

On the Laminar Sub-Layer in the Turbulent Boundary Layer, III.

By Yutaka SHIGEMITSU

Railway Technical Research Institute, Tokyo.

(Read March 28, 1948; Received September 3, 1948)

Part III. On the Laminar Sub-Layer for the Flow with a Pressure Gradient.

(I) The Case of Constant λ.

§8. A Method of Derivation of an Approximate Solution.

In the equations of motion of laminar sub-layer, the first approximate solution for $\lambda = \textit{constant}$ can be easily obtained as in the case of $\lambda = 0$. The flow of this case corresponds to that of Falkner-Skan in the laminar boundary layer theory and it is important when we treat a flow with any pressure gradient. The derivation of the first approximate solution is the same as described in §4.

The equations of motion and the boundary conditions are

$$u\frac{\partial u}{\partial x}+v\frac{\partial u}{\partial y}=-\frac{1}{\rho}\frac{dp}{dx}+\nu\frac{\partial^2 u}{\partial y^2} \tag{8,1}$$

$$u=\frac{\partial\psi}{\partial y},\qquad v=-\frac{\partial\psi}{\partial x},$$

and

$$\begin{aligned} u&=0 \quad \text{at} \quad y=0\\ u&=u_1 \quad \text{at} \quad y=\delta_1, \end{aligned} \tag{8,2}$$

or

$$u=0 \quad \text{at} \quad y=0$$

$$\left(\frac{\partial u}{\partial y}\right)_{\delta_1}=\frac{u_1}{\delta_1}m,\quad R+\kappa\lambda=c. \tag{8,2'}$$

$$\left(R=\frac{u_1\delta_1}{\nu},\quad \lambda=-\frac{1}{\rho}\frac{dp}{dx}\frac{\delta_1^2}{\nu u_1}.\right)$$

In this case of flow, there is another condition

$$\frac{d\lambda}{dx}=0 \quad \text{or} \quad \frac{dR}{dx}=0. \tag{8,3}$$

When we take ξ, η and $F(\xi,\eta)$ respectively as the non-dimensional coordinates and the stream function as (4, 3), we have

$$u=u_1\frac{\partial F}{\partial\eta},\quad v=u_1\left(\frac{\partial F}{\partial\eta}\eta\frac{d\delta_1}{dx}-\frac{\partial F}{\partial\xi}\frac{\delta_1}{L}\right),$$

$$\frac{\partial u}{\partial x}=-\frac{d\delta_1}{dx}\frac{R\nu}{\delta_1^2}\frac{\partial F}{\partial\eta}-\frac{u_1}{\delta_1}\frac{\partial^2 F}{\partial\eta^2}\eta\frac{d\delta_1}{dx}+\frac{u_1}{L}\frac{\partial^2 F}{\partial\xi\partial\eta}, \tag{8,4}$$

$$\frac{\partial u}{\partial y}=\frac{u_1}{\delta_1}\frac{\partial^2 F}{\partial\eta^2},\quad \frac{\partial^2 u}{\partial y^2}=\frac{u_1}{\delta_1^2}\frac{\partial^3 F}{\partial\eta^3},$$

and (8,1) reduces to

$$R\frac{d\delta_1}{dx}\left(\frac{\delta F}{\delta\eta}\right)^2+\frac{\partial^3 F}{\partial\eta^3}+\lambda=R\frac{\delta_1}{L}\left(\frac{\partial F}{\partial\eta}\frac{\partial^2 F}{\partial\xi\partial\eta}-\frac{\partial^2 F}{\partial\eta^2}\frac{\partial F}{\partial\xi}\right). \tag{8,5}$$

When we expand $F(\xi,\eta)$ and δ_1/L respectively in the power series as (4,6) and substitute in (8,5), we get the following condition as the coefficients of ξ^0;

$$(Ra_1)f_0'^2+f_0'''+\lambda=Ra_0(f_0'f_1'-f_0''f_1).$$

In the same manner in which (4,8) is derived, the equation of motion of the first approximate solution is written as

$$\sigma f^2+f''+\lambda=0, \tag{8,6}$$

where $f=f_0'$ and $\sigma=Ra_1$, and the boundary conditions are also written in the non-dimensional form:

$$\begin{aligned} f&=0 &&\text{at}\quad \eta=0,\\ f&=1,\ f'=m &&\text{at}\quad \eta=1. \end{aligned} \tag{8,7}$$

When (8,6) is integrated and the integration constant is determined, we obtain

$$f'=\sqrt{\left(\alpha^2-\frac{2}{3}\sigma f^3-2\lambda f\right)} \tag{8,8}$$

$$\frac{1}{3}\sigma+\frac{1}{2}m^2+\lambda=\frac{1}{2}\alpha^2,$$

where $\alpha=f'(0)$, and from the above equation, the form of f is derived as

$$f = B[\wp(A\eta)-\{\wp'(A\eta)+2\}^2/\{4\wp^2(A\eta)\}], \qquad (8,9)$$

$$A = 0.43679(\alpha\sigma)^{-\frac{1}{3}}, \quad B = 1.1447\,\alpha/(\varkappa\sigma)^{\frac{1}{3}},$$

where in the $\wp$-function,

$$g_2 = -9.1577\,\lambda/\alpha(\varkappa\sigma)^{\frac{1}{3}}, \quad g_3 = -4.$$

The boundary conditions are

$$\frac{1}{2}\alpha^2-\frac{1}{2}m^2-\frac{1}{3}\sigma = \lambda, \qquad (8,10)$$

$$B[\wp(A)-\{\wp'(A)+2\}^2/\{4\wp^2(A)\}] = 1.$$

Thus the first approximate solution is determined for the flow of some value of λ, when the value of m is determined.

§ 9. The Determination of the Velocity Distribution.

For the turbulent boundary layer with a pressure gradient, there are few investigations in contrast to the flow along a flat plate, and at present we have little knowledge about the velocity distribution. So we have no theoretical or experimental ground to determine the necessary values of the boundary conditions of (8,2'), and we cannot estimate the state of flow in the laminar sub-layer definitely as for the flow without a pressure gradient. However, for the purpose of investigating whether the idea of the laminar sub-layer described in Part I, may be appropriate for the turbulent boundary layer flow with a pressure gradient, we desire to proceed on this investigation.

If we put $m = 0$ and eliminate λ in the solutions of (8,9) and (8,10), the boundary conditions reduce to the simple form

$$g_2 = 4(1-B^3)/B^2 \qquad (9,1)$$

$$B[\wp(A)-\{\wp'(A)+2\}^2/\{4\wp^2(A)\}] = 1,$$

and the values of $\varkappa$ and σ are determined depending on g_2. Hence α and σ can be easily expressed as a function of λ, and they are shown in Table II.

However, in the real state of flow in turbulent boundary layer, m must have a finite value, and as one of the trials to decide it, we take the following condition; that is, at the boundary of laminar sub-layer, the shearing stress is smoothly connected to that of the turbulent part.

Table II.

λ	α	σ	g_2
6,287	3,007	−5,296	7,610
4,978	2,728	−3,764	7,684
3,565	2,402	−2,043	8,000
2,000	2,000	0,000	∞
0,822	1,661	1,678	−3,215
0,000	1,402	2,949	0,000
−0,660	1,177	4,057	3,050
−1,314	0,936	5,255	7,560
−1,968	0,675	6,586	16,25
−2,652	0,376	8,169	44,48
−3,119	0,157	9,393	160,0
−3,438	0,000	10,31	∞

Namely

$$\tau_{\delta_1} = \rho l^2\left(\frac{\partial u}{\partial y}\right)^2 = \mu\left(\frac{\partial u}{\partial y}\right) \qquad (9,2)$$

whereas if the effect of the laminar sub-layer is neglected in the expression of $\tau_{\delta_1} = \rho l^2(\partial u/\partial y)^2$ it follows that

$$l = ky.$$

By experiments, the value of k is known to change depending on the degree of the pressure gradient, but here for brevity we take $k = 0.4$, that is corresponding to the case without a pressure gradient. Hence (9,2) reduces to

$$m = 1/\{0.16(\varkappa-k\lambda)\}. \qquad (9,3)$$

As to the determination of the value of $\varkappa$, we take the condition of turbulent separation point. When it is supposed that the skin friction vanishes at the turbulent separation point, it corresponds, in the above solutions, to the case in which

$$\varkappa = 0. \qquad (9,4)$$

On the other hand, by experiments on turbulent separation, in this case of flow we can take roughly*

---

* These experiments were made with the following equipments; which consisting oftwo flat plates of 100 cm × 50 cm and 20 cm × 50 cm, connected at their ends as in figure 9, and with two end plates. With a method of kerosene-and-lampblack, we determined the location of the turbulent separation, and measured the velocity distribution near the surface of the plate, with a small pitot tube. These are shown in Fig. 10.

$$R = 60. \tag{9,5}$$

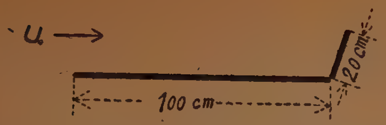

Fig. 9. Illustration of the equipment.

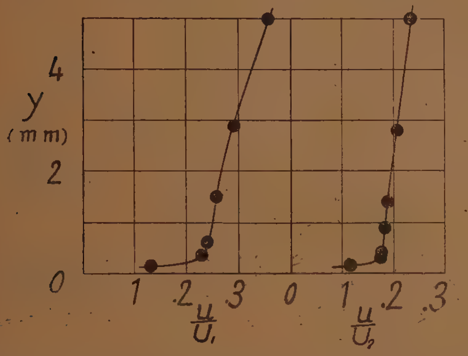

Fig. 10. Velocity distribution near the surface at turbulent separation point. $U_1 = 26$ m/s, $U_2 = 31$ m/s.

Then from (9,4), (9,5), and (8,10), m, λ, and σ can be determined approximately and we get

$$\kappa = -50.9. \tag{9,6}$$

Using these conditions, we obtain the following conditions

$$\left.\begin{aligned} g_2 &\doteqdot 4(1-B^3)/B^2 + 0{,}090/\{B^2(4{,}5+\lambda)^2\sigma\}, \\ B[\wp(A) &- \{\wp'(A)+2\}^2/\{4\wp^2(A)\}] = 1. \end{aligned}\right\} \tag{9,7}$$

For brevity of calculation, at a given value of g_2, the second term of its expression is calculated with the values of B, λ and σ which correspond to the case of $m = 0$, and with this correction term, we determine B as the case of $m \neq 0$. Then the necessary numerical values of the boundary conditions are determined and we can know the velocity distribution in each case of a value of g_2. These results are shown in Tables III, IV and Figs. 11, 12.

Table III.

λ	α	σ	m	g_2
6,147	2,974	—5,178	0,0115	7,610
4,803	2,680	—3,633	0,0132	7,684
3,495	2,378	—2,002	0,0153	8,000
1,963	1,982	0,000	0,0189	∞
0,806	1,646	1,647	0,0231	—3,215
0,000	1,389	2,895	0,0272	0,000
0,648	1,166	3,981	0,0317	3,050
—1,286	0,926	5,141	0,0380	7,560
—1,925	0,667	6,441	0,0473	16,25
—2,584	0,371	7,952	0,0634	44,48
—3,020	0,154	9,081	0,0819	160,0
—3,341	0,000	10,01	0,1042	∞

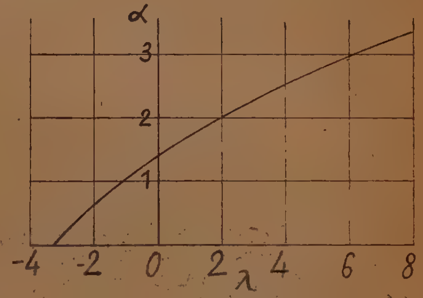

Fig. 11. Distribution of $\alpha(\lambda)$.

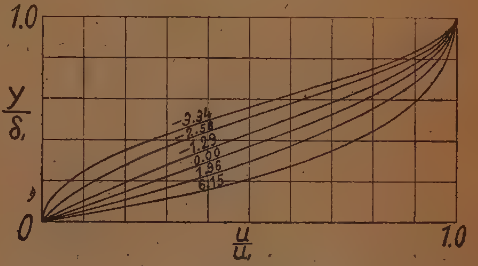

Fig. 12. Velocity distributions in laminar sub-layer. Numbers on contours are values of λ.

At present, we have few experimental works concerning the velocity distribution in laminar sub-layer with a pressure gradient, and it is difficult to discuss the above results by comparing with experimental data. Particularly, as for the mechanism of the turbulent separation, we have no definite knowledge about it, owing to the difficulty of experiments. However, in this investigation, we can propose one way to define it with the phenomena of the separation of the laminar sub-layer. In Fig. 12 the case of $\lambda = -3.34$ ($\alpha = 0$) corresponds to the flow near the surface at the turbulent separation point. By Fig. 12, it is recognized that the state of the velocity distribution in laminar sub-layer changes depending on the pressure gradient, and the relationship between the curvature of the velocity profile and the degree of the pressure gradient, is similar to the laminar boundary layer; and it is not proper to take generally its velocity

Table IV.

λ	6,147	4,803	3,495	1,963	0,806	0,000
η	$f(\eta)$	$f(\eta)$	$f(\eta)$	$f(\eta)$	$f(\eta)$	$f(\eta)$
0,00	0,0000	0,0000	0,0000	0,0000	0,0000	0,0000
,05	,1410	,1281	,1146	,0966	,0813	,0695
,10	,2662	,2443	,2199	,1883	,1606	,1389
,15	,3785	,3490	,3179	,2752	,2377	,2082
,20	,4765	,4428	,4070	,3570	,3126	,2771
,25	,5621	,5265	,4883	,4340	,3851	,3458
,30	,6364	,6006	,5620	,5061	,4549	,4131
,35	,7006	,6660	,6286	,5733	,5219	,4794
,40	,7558	,7234	,6884	,6356	,5857	,5440
,45	,8025	,7736	,7418	,6929	,6461	,6065
,50	,8431	,8172	,7892	,7454	,7027	,6663
,55	,8771	,8548	,8311	,7929	,7554	,7229
,60	,9077	,8870	,8676	,8356	,8036	,7757
,65	,9295	,9144	,8992	,8733	,8472	,8241
,70	,9491	,9374	,9266	,9061	,8858	8,677
,75	,9650	,9564	,9485	,9340	,9192	,9059
,80	,9776	,9716	,9667	,9571	,9471	,9380
,85	,9872	,9834	,9808	,9752	,9692	,9640
,90	,9940	,9920	,9910	,9883	,9855	,9829
,95	,9982	,9975	,9974	,9966	,9958	,9951
1,00	1,0000	1,0000	1,0000	1,0000	1,0000	1,0000

λ	−0,648	−1,286	−1,925	−2,584	−3,020	−3,341
η	$f(\eta)$	$f(\eta)$	$f(\eta)$	$f(\eta)$	$f(\eta)$	$f(\eta)$
0,00	0,0000	0,0000	0,0000	0,0000	0,0000	0,0000
,05	,0591	,0479	,0357	,0218	,0115	,0042
,10	,1198	,0990	,0762	,0500	,0305	,0167
,15	,1819	,1531	,1215	,0882	,0571	,0376
,20	,2454	,2102	,1714	,1256	,0911	,0668
,25	,3098	,2699	,2255	,1727	,1325	,1042
,30	,3749	,3319	,2837	,2256	,1811	,1497
,35	,4402	,3956	,3453	,2840	,2364	,2029
,40	,5052	,4606	,4099	,3472	,2980	,2635
,45	,5699	,5260	,4765	,4145	,3651	,3307
,50	,6318	,5911	,5443	,4843	,4367	,4034
,55	,6919	,6549	,6121	,5569	,5115	,4804
,60	,7488	,7164	,6787	,6292	,5879	,5600
,50	,8018	,7745	,7426	,7001	,6639	,6400
,70	,8500	,8281	,8025	,7677	,7357	,7181
,75	,8927	,8761	,8569	,8301	,8063	,7917
,80	,9291	,9175	,9042	,8852	,8679	,8579
,85	,9584	,9513	,9432	,9313	,9200	,9141
,90	,9808	,9767	,9728	,9666	,9604	,9578
,95	,9943	,9930	,9919	,9898	,9875	,9869
1,00	1,0000	1,0000	1,0000	1,0000	1,0000	1,0000

distribution linear as in the case of flow along a flat plate. Further, by these results, we can suppose that for the turbulent flow around a body, the velocity distribution in the laminar sub-layer changes and the surface friction decreases, as the separation point is approached.

(II) The Case of Variable, λ.

§10. A Method of an Approximate Calculation of the Velocity Distribution of Laminar Sub-Layer with some Pressure Gradient.

The state of flow in laminar sub-layer such that λ is constant along the surface of a body, can not be supposed to exist really, except the flow along a flat plate. In general, the mechanism of the flow in turbulent boundary layer is complicated, moreover it is accompanied by the difficult problem of the transition from laminar to turbulent flow, and even the condition of turbulent separation is not yet established. However, by many experiments, it seems to be recognized that the surface friction at a point is decreasing as it goes from the transition region to separation point, and the qualitative relation between the change of the surface friction and the state of the pressure distribution is similar to that of laminar boundary layer, except the following well-known difference i.e., in the former case the surface friction is very large and the flow does not separate even under the considerably large pressure gradient. These experimental facts seem to be suggested in the theoretical results derived in the last chapter. Hence we can find a possibility that the state of flow near the surface of a body in turbulent boundary layer with any pressure gradient, is estimated by use of the solutions shown in Fig. 12. Of course, on account of the difficulty to determine the necessary values of the boundary condition, the exact discussion can not be expected, but as one of the trials we will proceed to the evaluation.

For the turbulent boundary layer flow, the parameter "λ" of the laminar sub-layer is generally variable along the x-axis, and its velocity distribution can be expressed in the form

$$u = u_1 f(\eta\,;\ \lambda,\ \lambda',\ \lambda'',\ \ldots.),$$

where $\lambda' = d\lambda/d\xi$, etc. But, for brevity, we neglect the effect of the λ', etc., and take

$$u = u_1 f(\eta\lambda),$$

where the form of f is the same as in the last chapter. And then, when dp/dx is given as a function of ξ, we can estimate the state of flow, with the condition of $R+\kappa\lambda = c$ and a group of the above solutions, if we know the distribution of $\lambda(\xi)$.

To determine $\lambda(\xi)$, we use the momentum condition in laminar sub-layer. It is written as

$$\frac{d}{dx}\int_0^{\delta_1} u^2 dy - \bar{u}_1 \frac{d}{dx}\int_0^{\delta_1} u dy$$

$$= -\frac{\delta_1}{\rho}\frac{dp}{dx} - \nu\left\{\left(\frac{\delta u}{\partial y}\right)_0 - \left(\frac{\partial u}{\partial y}\right)_{\varepsilon_1}\right\}, \qquad (10,1)$$

and it reduces to

$$\frac{\delta_1}{\nu u_1 L}\frac{d}{d\xi}\{u_1{}^2\delta_1 F_2(\lambda)\} - \frac{\delta_1}{\nu L}\frac{d}{\delta\xi}\{u_1\delta_1 F_1(\lambda)\}$$

$$\doteqdot \lambda - \alpha(\lambda) + m(\lambda), \qquad (10,2)$$

where

$$F_1(\lambda) = \int_0^1 f(\eta\lambda)d\eta, \quad F_2(\lambda) = \int_0^1 f^2(\eta\lambda)d\eta.$$

But in the velocity distribution in the case of $\lambda =$ *const.*, the condition to determine $m(\lambda)$ is not sufficiently correct, and by the curves in figure 12, it is recognized that m is taken so small. By Part II of this paper, it is known that the curve of the velocity distribution is not so dependent on the value of m, but in the momentum condition, it is necessary to decide the value of $m(\lambda)$ correctly, and now as the correction term of m, we take the following condition

Table V.

λ	$p_1(\lambda)$	$p_2(\lambda)$
6,43	∞	∞
6,147	−0,4134	164,3
4,803	— ,0622	24,36
3,495	— ,0243	9,852
1,963	— ,$0^2$669	3,354
0,806	— ,$0^3$174	1,002
0,000	,0000	0,000
−0,648	,$0^2$292	−0,553
−1,286	,$0^2$778	−0,914
−1,925	,0154	−1,098
−2,584	,0273	−1,090
−3,020	,0396	−1,000
−3,341	,0507	−0,864

$$\frac{\delta_1}{\nu u_1 L}\frac{d}{d\xi}\{u_1{}^2\delta_1F_2(\lambda)\}-\frac{\delta_1}{\nu L}\frac{d}{d\xi}\{u_1\delta_1F_1(\lambda)\}$$

$$=\lambda-\alpha(\lambda)+m(\lambda)+m'(\lambda). \qquad (10,3)$$

We take roughly

$$m'(\lambda)=1,$$

and it becomes

$$d\lambda/d\xi=P_1(\lambda)Q_1(\xi)+P_2(\lambda)Q_2(\xi), \qquad (10,4)$$

where $P_1(\lambda)$ and $P_2(\lambda)$ are calculated with the solutions of $\lambda = \mathit{constant}$ and shown in table 5, and $Q_1(\xi)$ and $Q_2(\xi)$ are determined by the pressure gradient such as

$$Q_1(\xi)=(Ls^{\frac{1}{3}})/\nu^{\frac{2}{3}},\ Q_2(\xi)=(d/d\xi)/s,$$

$$s=-(dp/dx)/\rho. \qquad (10,5)$$

(10,4) is a differential equation to determine the distribution of $\lambda(\xi)$, and its boundary condition ought to be determined by the value of λ at the position where the turbulent boundary layer begins to develop. However, for brevity, we take the ideal case that the turbulent boundary layer is developing from the forward stagnation point. Then we can take by Table V.

$$\lambda=6{,}43, \qquad (10,6)$$

for the value of the stagnation point, as in the Kármán-Pohlhausen's theory in laminar boundary layer. Hence in the above ideal case, we can evaluate the distribution of $\lambda(\xi)$ with any pressure gradient, using the condition of (10,4) and (10,6).

§ 11. An Example of the Calculation.

As an example of the above calculation, we take one of the Schubauer's experiments of an elliptic cylinder⁽¹⁾; that was made at high stream turbulence to make the transition occur near the forward stagnation point as closely as possible.

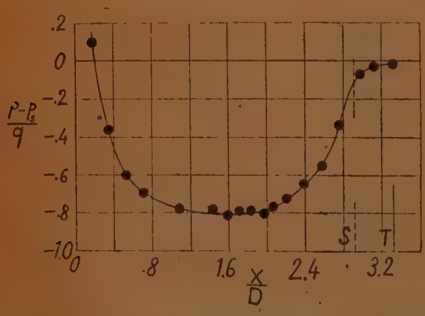

Fig. 13. Pressure distribution around the body.
$x/D=\xi$.
S–Observed separation point.
T–Trailing edge.

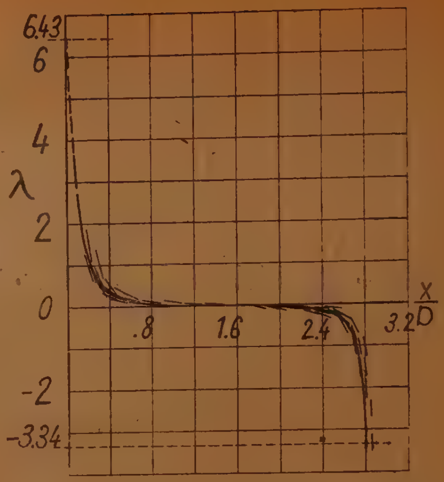

Fig. 14. Graphical calculation of $\lambda(\xi)$.
$x/D=\xi$.

The pressure distribution around the body is shown in Fig. 13, and with this curve, (10,5) are calculated. Then we can get graphically the distribution of $\lambda(\xi)$ by (10,4) and (10,6), and the result is shown in Fig. 14. With this result, we can get the velocity distribution or the surface friction, and these are shown in Figs. 15 and 16 with the experimental results.

This experiment is not necessarily adequate to be compared with the calculation on the hypothesis that the turbulent boundary layer is beginning

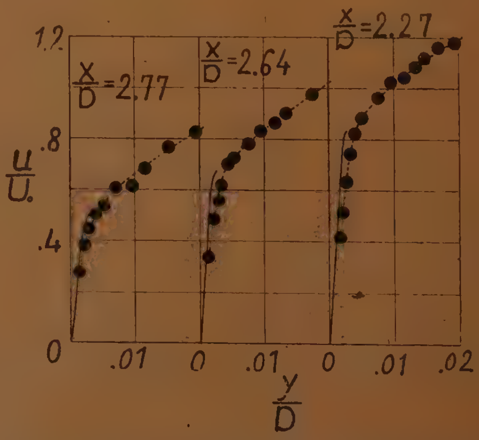

Fig. 15. Velocity distribution of the flow near the body. Dotted line — experimental. Full line—Theoretical.

from the stagnation point; moreover the accuracy of the above graphical calculation is not sufficient. Hence, we can not expect the strict discussion on the comparison between the theoretical and experimental results. However, by these comparisons, it is likely that the state of flow near the surface of the body can qualitatively be explained with the conception of the laminar sub-layer.

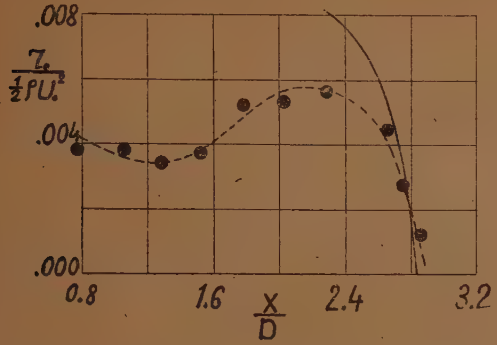

Fig. 16. Distribution of the surface friction near the separation point. Dotted line — Experimental. Full line—Theoretical.

§ 12. Conclusion.

In the foregoing parts of this paper, at first, the mechanism of the state of flow in the laminar sub-layer is explained on a hypothesis concerning the stability of the laminar boundary layer and its equations of motion and the boundary conditions are derived, and then for the purpose of investigating whether this interpretation on the laminar sub-layer may be appropriate, we make comparisons between the approximate solutions of the above equations of motion and the experimental results, for the two cases of the flow with and without a pressure gradient.

For the flow along a flat plate, the well-known hypothesis, that is, at the boundary of the laminar sub-layer, $(u_1\delta_1)/\nu = constant$, can be shown as one of the special case of our hypothesis, and as the approximate calculation, the experimental data concerning the state of flow near the surface, can fairly well be explained with this conception.

For the flow with a pressure gradient, we have now few experimental data, and there is no reliable foundation to determine the necessary numerical values of the boundary condition. Hence, the strict discussion on the propriety of the conception of the laminar sub-layer in this case, needs more detailed experimental works, but at present, it is concluded that we can explain the state of flow near the surface of a body, at least, qualitatively, using the above fundamental conception of the laminar sub-layer. Particularly, the important character, derived in this theory, that the velocity distribution in the laminar sub-layer changes with the pressure gradient in the same manner as the laminar boundary layer, can be supported by the generally believed experimental fact that the surface friction decreases as the separation point is approached.

As for turbulent separation, at present, its mechanism of the flow has scarcely been investigated and there are some attempts to search for the necessary parameter, but none of the undoubted conclusions has been derived. In this study of the laminar sub-layer, we can show the phenomena of the separation of the laminer sub-layer. As for the problem whether it may be the same as the turbulent separation, we have still no clear answer. However, by this investigation, we can propose one interpretation concerning the mechanism of the turbulent separation.

One of the important characteristics in this investigation, lies in the determination of the condition at the boundary of the laminar sub-layer. But in real state of flow, the boundary of the laminar sub-layer and the turbulent part, can not be definitely determined, as in the phenomena of the transition from laminar to turbulent flow along the surface of a body, where there is a large range of transition region between the laminar boundary layer and the fully developed turbulent boundary layer. Hence, it is difficult to determine theoretically the correct value of $m(\xi)$, and at present, we can not expect the complete theoretical treatment as in the theory of the laminar boundary layer. But when the mechanism of the turbulent flow in the turbulent boundary layer comes to be completely investigated, this investigation gives a theoretical ground to the problem, that is, how the correction by the effect of the molecular viscosity near the surface of a body may be estimated.

Reference.

(1) G. B. Schubauer; N. A. C. A. Tech. Rep. No. 652, 1939.

Relaxation Phenomena of Polymers. I. Stress Relaxation of Vulcanized Rubber (Part I.)

By Haruhiko TOHARA

6th Division, Railway Institute of Technical Research, Tokyo

(Received Sept. 16, 1948)

§ 1. Introduction

As soon as a piece of rubber-like material is deformed, each link of its chain molecules is strained in the following manner and its bond angles and atomic distances deviate from their equillibrium values. This stress is transmitted from atom to atom, not through segments* and is similar to that of a material composed of short molecules. The work done by an external force is converted to the potential energy of links and the modulus of elasticity of this sort is of the same order of magnitude as that of short molecular materials, that is of 10^{11}dynes/cm². This large stress decays with time through the following stages.

a. Viscous Segment Motion.

As constrained rotations about single bonds are allowed—although their potential barriers would be much higher than the levels of the thermal agitation,—each link is released from its strain through the thermal motion. The segment is wandering among many configurations which have the same energy with the junctions unmoved on the average. The segment motion is supposed to reach the equilibrium state at ordinary temperature within about 10^{-6} second.

b. Motion of Junctions.

The rubber-like elasticity is due to the thermal motion which tends to increase the configuration entropy of the network. The equillibrium state which corresponds to the maximum entropy is reached through the shift of junctions and this is a rate process. When some of the junctions slip, the equillibrium state which has a larger entropy is attained and it is also a rate process. The slip might have a longer time of relaxation than the shift and the primary cross-links scarcely slip at the temperature range of rubber-like elasticity.

c. Liberation of Junctions.

If two chains liberate themselves at their cross-bond (primary or secondary), their energy increases by the bond energy and the configuration entropy also increases. Consequently at lower temperatures the bonded state is stable, but at higher temperatures the liberated state is stable. It is noticeable that, for not too large deformation, the entropy of liberation increases on the average with the deformation and the transition temperature is lowered. In most cases, secondary cross-bonds do not liberate at ordinary temperature and primary ones break down only at very high temperatures.(1)

The modulus of rubber-like elasticity, including that of the relaxing stress, is about $10^7 \sim 10^8$ dynes/cm².

§ 2. Equations of Relaxation.

W. Kuhn, utilizing Maxwell's equation, introduced the following equations of relaxation and succeeded in the phenomenological representation of relaxation phenomena.(2)

---

* A segment, in our paper, means a part of chain molecule between two adjacent junctions and a link the unit of its motion.

$$d\varepsilon/dt = (1/E_i)(d\sigma_i/dt) + \sigma_i/E_i\tau_i \qquad (2.1)$$

and

$$\sigma = \sum_i \sigma_i \qquad (2.2)$$

where i distinguishes the type of relaxing mechanisms, ε denotes the strain, σ_i, E_i and τ_i respectively the partial stress, the instantaneous modulus of elasticity and the time of relaxation of the type i, and σ is the total stress measured in experiment. For the stress relaxation

$$\varepsilon = 0 \text{ for } t < 0, \qquad \varepsilon = \varepsilon_0 \text{ for } t > 0 \qquad (2.3)$$

the relaxing stress is

$$\sigma = \varepsilon_0 \cdot \sum_i E_i \exp(-t/\tau_i) \qquad (2.4)$$

On the right side of Eq. (2.1) the first term represents the rate of the i-th elastic deformation which obeys the Hooke's law, and the second term, the rate of the i-th plastic flow which is assumed to follow the Newton's law.

Thereafter A. Tobolsky and H. Eyring, modifying Eq. (2.1), gave a new equations of relaxation which were based on the Eyring's kinetic theory of rate processes.(3)(4) Their modification lies in the term of the plastic flow. According to their theory the rate of flow is

$$2n\lambda k^* \sinh(\lambda\sigma/2NkT)$$

where λ denotes the average distance, projected in the direction of the stress, between two neighbouring equillibrium positions in the relaxation process, and k^* the specific rate of that process. N represents the average number of the relaxing points in parallel per unit area perpendicular to the stress and n that of the points in series per unit length parallel to it.

While, on the other hand,

$$k^* = (kT/h)\, K^{\ddagger}$$

and

$$K^{\ddagger} = \exp(-\Delta F^{\ddagger}/kT)$$

where $K^{\ddagger}$ represents the equillibrium constant between the initial and the activated states and $\Delta F^{\ddagger}$ the "free energy of activation" of that process. Then the rate of strain is given as follows:

$$d\varepsilon/dt = (1/E_i)(d\sigma_i/dt) + A_i \sinh(B_i\sigma_i), \qquad (2.5)$$

where

$$\left.\begin{aligned} A_i &= 2n_i\lambda_i(kT/h)\exp(-\Delta F^{\ddagger}/kT) \\ B_i &= \lambda_i/2N_ikT, \end{aligned}\right\} \qquad (2.6)$$

and the total stress, as before,

$$\sigma = \sum_i \sigma_i$$

When the partial stress is small, that is

$$B_i\sigma_i \ll 1$$

Eq. (2.5) reduces to Eq. (2.1), if one writes

$$1/\tau_i = A_iB_iE_i = (n_i/N_i)(E_i\lambda_i^2/h)\exp(-\Delta F_i^{\ddagger}/kT). \qquad (2.8)$$

Relaxation processes of the following type might be observed through the wide ranges of temperature and period of observation.

a. Viscous Segment Motion.

This process includes the energetic stabillization of links which are strained at the instant of deformation as well as the establishment of the thermal equillibrium of segments whose terminals are fixed in space.

b. Shift of Junctions.

These junctions may be cross-links of the primary or secondary nature. The distinction between the shift of junctions and the equillibrium establishment of segments would be somewhat a conceptional one.

c. Slip of Secondary Cross-Links.

The slip includes the reformation of a junction where either of the joined chains is different from the one which was joined before slippage.

d. Liberation of Secondary Cross Links.

Liberated cross-links are not reformed above some critical temperature which is lowered with deformation.

e. Slip and Liberation of Primary Cross-Links.

The slip of primary cross-links would scarcely take place and the liberation of them proceeds at high temperature where rubber-like elasticity no longer holds.

There might be different types of secondary cross-links, of which some is stronger and some weaker. They would manifest different relaxation processes.

If the relaxation time of one process is far apart from the others, one may regard the processes of which the relaxation times are much longer than it as non-relaxing and may disregard the processes of which the relaxation times are much shorter. Therefore one may consider them to consist of one relaxing process and a non-relaxing one.

If a body undergoes a constant strain instantaneously, as before, one gets by integrating Eq. (2.5)

$$\tanh (B_i\sigma_i/2) = \tanh (B_i\sigma_i^0/2)\cdot\exp(-A_iB_iE_it) \tag{2.9}$$

where σ_i^0 denotes the initial value for σ_i. Let, in brief,

$$D_i = \tanh (B_i\sigma_i^0/2) \tag{2.10}$$

then one obtains from Eqs. (2.8), (2.9) and (2.10)

$$B_i\sigma_i/2 = \operatorname{arctanh}[D_i \exp(-t/\tau_i)] \tag{2.11}$$

Expanding the function "arctanh" in the following power series, one obtains

$$B_i\sigma_i/2 = D_i \exp(-t/\tau_i) + (1/3)\, D_i^3 \exp(-3t/\tau_i) + \cdots \tag{2.12}$$

When a long time has elapsed, that is,

$$t \gg \tau_i$$

then

$$\sigma_i \simeq (2D_i/B_i) \exp(-t/\tau_i) \tag{2.13}$$

and one obtains the relaxation time τ_i from the latter part of the stress decay curve. It is convenient, however, to calculate the following function of t/τ with the parameter D

$$\rho(t/\tau,\ D) = \operatorname{arctanh}[D \exp(-t/\tau)]/[D \exp(-t/\tau)] \tag{2.14}$$

Let one define the asymptotic stress decay curve, represented by Eq. (2.13), with σ_i^*

$$\sigma_i^* = (2D_i/B_i) \exp(-t/\tau_i) \tag{2.15}$$

and knowing the value of the parameter D_i, one obtains the stress decay curve as follows:

$$\sigma_i = \rho(t/\tau_i,\ D_i)\, \sigma_i^* \tag{2.16}$$

When the initial stress is large, however, one needs not know the precise value of $B_i\sigma_i^0$, because

$$D_i \simeq 1 \ \textit{if} \ B_i\sigma_i^0 \gg 1.$$

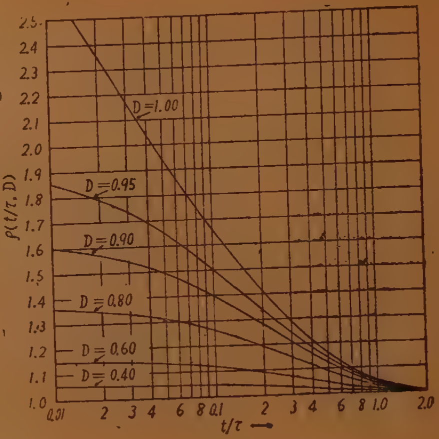

Fig. 1.

$\rho(t/\tau,\ D)$ as a function of t/τ with a parameter D

Now, from Eq. (2.8)

$$\tau_i = (N_i/n_i)(h/E_i\lambda_i^2) \exp(-\Delta S_i^{\ddagger}/k) \exp(\Delta E_i^{\ddagger}/kT) \tag{2.17}$$

where $\Delta E_i^{\ddagger}$ and $\Delta S_i^{\ddagger}$ denote respectively "the energy of activation" and "the entropy of activation" of that relaxation process.

On the right side of Eq. (2.17) each factor except the last depends little on the temperature, and therefore from the relation between τ_i and T, one obtains the value of $\Delta E_i^{\ddagger}$.

I wish to express my sincere thanks to Mr. G. Hirokawa for his continual encouragement, to Prof. T. Sakai, his co-workers especially to Mr. R. Kikuchi, and Mr. A. Ookawa for their good advices and to Mr. T. Matsuda for his assistance.

References

(1) A. V. Tobolsky, I. B. Prettynan, J. H. Dillon, J. Appl. Phys., **15** (1944), 380.
(2) W. Kuhn Zeits. phys. Chem., B **42** (1939), 1. Naturwiss., **40** (1938), 661
K. Beneewitz, H. Rötger, Phys. Zeits., **40** (1939), 416.
(3) A. Tobolsky, H. Eyring, J. Chem. Phys. **11** (1943), 125
(4) Grasstone, Laidler and Eyring, Theory of rate processes (1941), 480 (McGraw-Hill Book Co.)

Relaxation Phenomena of Polymers II. Stress Relaxation of Vulcanized Rubber (Part II.)*

By Haruhiko TOHARA

6th Division, Railway Institute of Technical Research, Tokyo

(Received Sept. 16, 1948)

§ 3. Experimental Apparatus.

The apparatus which we used in measuring the stress relaxation of a sample, when it underwent a constant compression instantaneously, is shown in Fig. 2. The compression is given by a duralmin lever which is supported on the one side by ball bearings and attracted on the other side by an electromagnet, The stress is measured by means of piezo-electric pieces of quartz of which both bases are coated with copper.

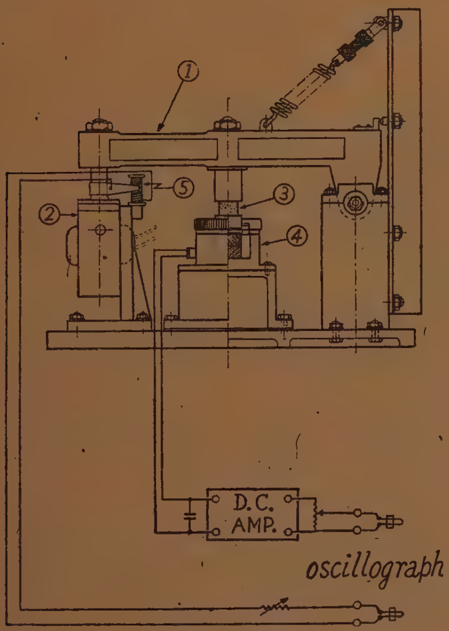

Fig. 2.

Fig. 2 Experimental apparatus recording the stress relaxation. 1: duralmin lever, 2: electromagnet, 3: sample, 4: piezo-electric pieces, 5: constantan wire and slider.

The charge induced on both bases is led to the imput terminal of a direct current amplifier with a waterproofed lead wire which is insulated with amber terminals and polystyrene tubes.

The output current of the amplifier is recorded by a electromagnetic oscillograph, of which the vibrater has its natural period of vibration of about 1/1,000 second. As the lever moves, an attached reed of phosphor-bronze slides on the constantan wire, 0.06 mm in diameter, wound on a fixed bakelite bobbin, and the motion of the lever is recorded on the same oscillogram as the variation of the current.

The apparatus was laid in the low temperature thermostat which was cooled with dry ice and the temperature of the thermostat could be held at a desired temperature within ± 0.5°C by the regulator.

When this apparatus is used, the adequate measuring period is limited to the range of about 0.1 to 10 seconds on account of the natural period of the vibrator as well as the leakage of the piezoelectric charge. We have measured the stress decay of vulcanized natural rubber at various temperatures between −30°C and −50°C and the temperature was measured by a copper-constantan thermo-couple fixed near the sample. This temperature range was chosen from the point of view of the adequate relaxation time for measurement. The piezo-electric pieces and the lead wire were covered for waterproof, but when the apparatus was held below 0°C for several minutes, the water vapour contained in it condensed, and the sensitivity dropped considerably. We, therefore, put the piezo-electric equipment in the thermostat through a small window, closed always but immediately before the measurement, and each measurement was completed within 15 seconds. The bakelite plate, 3 mm in thickness cooled in the thermostat, was inserted between the sample and the piezo-electric equipment to prevent from the heat conduction. The temperature rise of the sample due to the insertion of the equipment was within 0.5 C.

---

* Continued to the preceding paper

The rubber samples — especially low sulphur vulcanizates — cooled in the thermostat, crystallized locally to some extent and the relaxation time of them became longer than before crystallization. The effect of crystallization, however, was below the experimental error within 2 hours. The samples were heated at 50°C for an hour every 2 hours of cooling in order to avoid the crystallization. The samples were cylindrical, 15 mm in diameter 10 mm in height, and both bases of them were prevented by sandpaper from gliding during compression.

The compositions of the samples are listed in Table I.

Table I.

sample	B	D	G
smoked sheet	100	100	100
zinc oxide	5	5	5
stearic acid	1	1	1
tetramethylthiuram-disulphide	1	—	—
dibenzthiazyl-disulphide	—	1	0.8
sulphur	1	3	7.5
vulcanized	138 °C ×30 min	138°C ×30 min	143°C ×30 min
density at 20°C in g/cm³	0.962	0.973	0.992
shore durometer at 20°C	26°	24°	34°

§ 4. Results.

A few examples of the oscillograms of stress relaxation are shown in Photos, 1 ~ 3. The upper line represents the strain, the lower line the stress.

a. Procedure of Analysis.

Finite time is needed during compression and we take the origin of time at the instant when a constant strain is attained.

Finite period of compression brings no error in obtaining the relaxation time, although it makes a correction necessary for obtaining the instantaneous modulus of elasticity.

We divide the total stress $\sigma(t)$ into two partial stresses, of which the first σ_1 may be considered as non-relaxaing and the second $\sigma_r(t)$ relaxes during observation. In determining the partial stresses and the relaxation time, we shall make use of "the method of successive approximation". (Figs. 3 and 4)

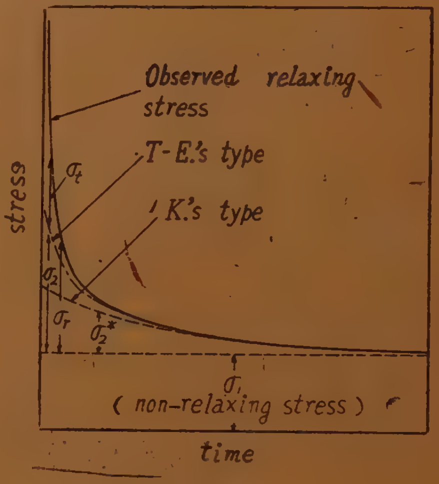

Fig. 3.

Stress decay curve.

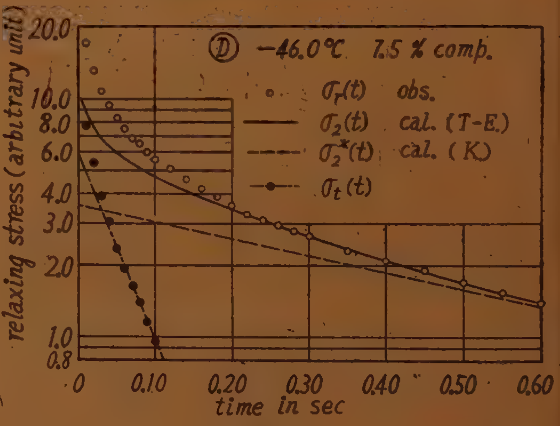

Fig. 4.

Relaxing stress in semi-logarithmic scale.

We consider $\sigma(t_1)-t_1$ must be taken as long as possible — as the zeroth approximation $\sigma_1^{(0)}$ for σ_1 and the latter part of the zeroth approximate relaxing stress

$$\sigma_r^{(0)}=\sigma(t)-\sigma_1^{(0)}$$

gives the roughly approximate relaxation time $\tau_2'^{(0)}$. Then the approximate asymptotic stress

$$\sigma_r^{(0)}(t)/\rho(t/\tau_2'^{(0)};\ 1)\ .$$

gives more approximate time $\tau_2''^{(0)}$, and at last

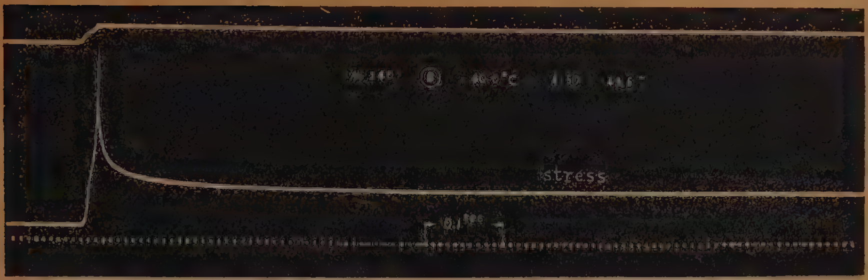

Photo. 1

B. -40.0°C, $\varepsilon = 8.8\,\%$, $E_I = 11.8$ kg/cm², $\tau_2 = 0.182$ sec, $\tau_t = 0.022$ sec,

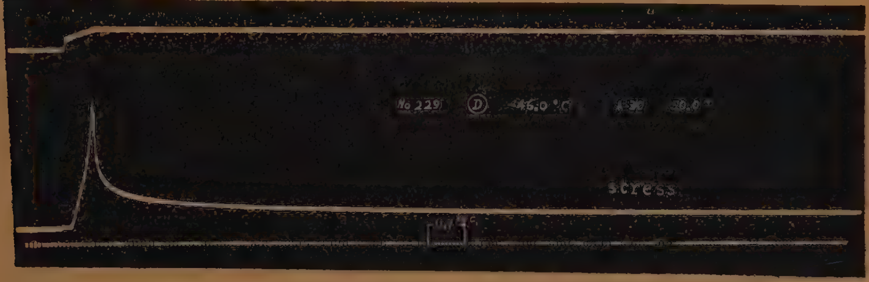

Photo. 2

D. -46.0°C, $\varepsilon = 7.5\,\%$, $E_I \fallingdotseq 11.9$ kg/cm², $\tau_2 = 0.56$ sec, $\tau_t = 0.054$ sec.

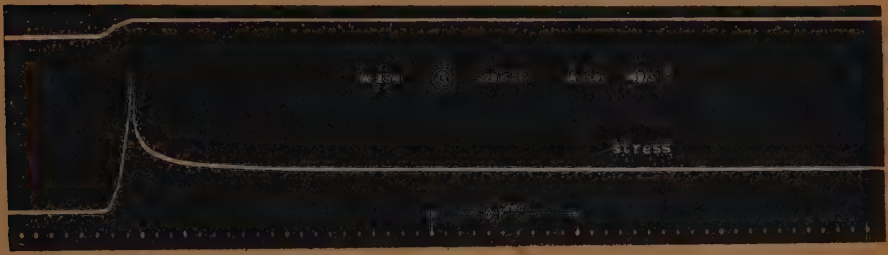

Photo. 3

G. -29.5°C, $\varepsilon = 7.9\,\%$, $E_I = 13.1$ kg/cm², $\tau_2 \fallingdotseq 0.090$ sec, $\tau_t = 0.0083$ sec.

$$\sigma_2^{*(0)}(t) = \sigma_r^{(0)}(t)/\rho(t/\tau_2''^{(0)},\ 1)$$

zeroth approximation $\tau_2^{(0)}$ for τ_2 from its latter part.

To get the relaxation time we draw the relaxing stress on semi-logarithmic section paper with the logarithmic stress, then the slope of the stress-time curve gives it. The same process may be repeated with the first approximate non-relaxing stress

$$\sigma_1^{(1)} = \sigma_1^{(0)} - \sigma_2^{*(0)}(t_1)$$

until $\sigma_1^{(s-1)} - \sigma_1^{(s)}$ becomes within the experimental error.

In most cases the zeroth approximations were already sufficient and in other cases the first approximations were necessary. The accuracy of stress was 0.05 mm on the oscillogram or from 0.007 kg/cm² to 0.011 kg/cm² as the shunt resistance varies, and that of the strain was 0.004, where the strain itself was about 0.08.

In the above procedures the relaxation time τ_2 and the asymptotic stress σ_2^* are determined from the latter portion of a stress decay curve, and

$$\sigma_2 = \rho(t/\tau_2,\ 1)\cdot\sigma_2^*$$

coincides with the observed relaxing stress

$$\sigma_r = \sigma(t) - \sigma_1$$

except at the initial part of it. The latter σ_r, however, is larger than the former σ_2 at that part (transient stage) and the difference

$$\sigma_t = \sigma_r - \sigma_2 \qquad (4.1)$$

introduces a new decaying stress which relaxes apparently exponentially with time and has its relaxation time τ_t. Transient stress σ_t decays more rapidly than σ_2 does and τ_t is about one-tenth of τ_2

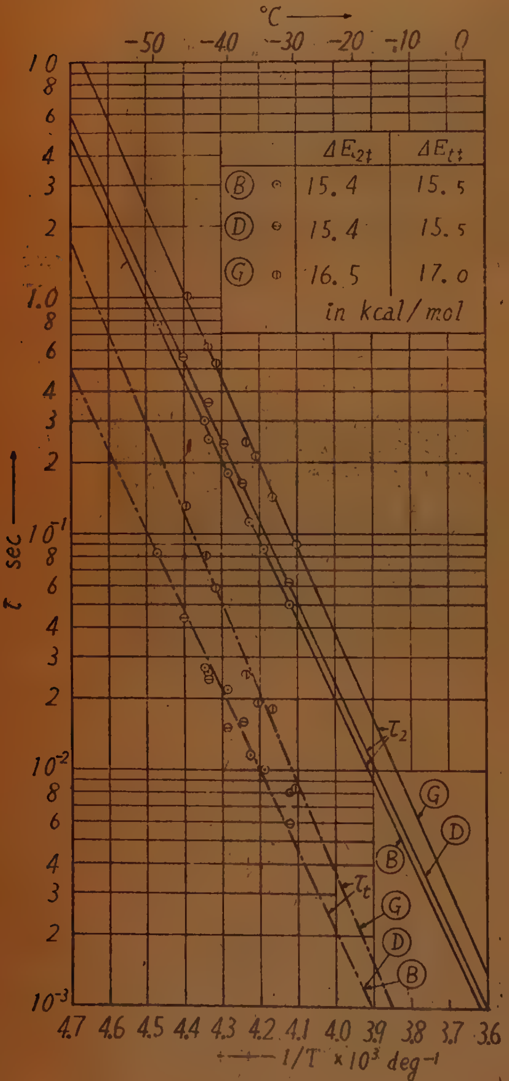

Fig. 5.

Relation between relaxation time and temperature. abscissa is 1/T, ordinate logarithm of relaxation time.

b. Time of Relaxation and Temperature.

As is shown in Fig. 5, both log τ_2 and log τ_t depend linearly on 1/T, and from Eq. (2.17) their slopes give the energies of activation $\Delta E_2^{\ddagger}$ and $\Delta E_t^{\ddagger}$ which are listed in Table II.

Table II

sample	$\Delta E_2^{\ddagger}$	$\Delta E_t^{\ddagger}$
B	15.4 kcal/mol	15.5 kcal/mol
D	15.4	15.5
G	16.5	17.0

The accuracy of $\Delta E_2^{\ddagger}$ was about ± 0.1 kcal/mol and that of $\Delta E_t^{\ddagger}$ about ± 0.5 kcal/mol. It is noticeable that $\Delta E_2^{\ddagger}$ and $\Delta E_t^{\ddagger}$ are nearly equal for each sample and they have the tendency to increase to some extent with the degree of vulcanization.

c. Non-Relaxing Stress and Temperature.

We have measured the stress relaxation of the same samples at some temperatures up to room temperature and any other relaxation phenomenon was hardly observed.

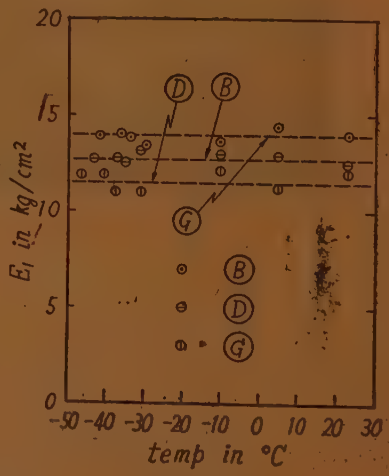

Fig. 6

Modulus of non-relaxing elasticity and temperature.

In Fig. 6 the modulus of non-relaxing elasticity is plotted against temperature and it is likely to be independent of temperature.

If there were no other relaxation process in this temperature range, the modulus of non-relaxing elasticity should be proportional to the absolute temperature.

In our experiment, however, the value of the strain and of the "absolute" stress contain errors of at most several percents, consequently the moduli of elasticity also contain errors of at most about 10 percents, but the relative stress, necessary for determining the relaxation time, is much more reliable.

In obtaining the modulus of elasticity, we divide the apparent modulus by a factor (so-called shape factor) which is the same for samples of the same dimensions, in particular 1.45 for our case, and is approximately calculated according to the strain-energy method.

§ 5. Discussion.

According to our experiment, Eq. (2.9) or (2.11) (Tobolsky-Eyring's relaxation) is more adequate to represent the stress relaxation than Eq. (2.4) (Maxwell's relaxation), and moreover, in our case, Eq. (2.11) is in the best accord with the observed stress decay curve when one assume $D_2 \simeq 1$ among various values of D_2.

What is the mechanism of our relaxing stress σ_3?

As previously mentioned any other relaxation process was hardly observed in the temperature range from -50°C to room temperature during several seconds. On the other hand, E_2 seems to be much smaller than the value 10^{11} dynes/cm^2 which is expected for viscous segment motion (for $D_2 \simeq 1$, it is difficult to determine the initial stress σ_2^0). We should conclude that this stress relaxation is due to the shift of junctions or to the slip of some type of secondary cross-links, we can not, however, decide which of them takes place in our case.

The spectrum of relaxation time in wide range would be useful in determining the mechanism of this stress relaxation. Extrapolating the curve in Fig. 5, we obtain the relaxation time of about $2\sim3\times10^{-4}$ second at 20°C.

The second question is the discrepancy between the observed relaxing stress σ_r and the theoretical one σ_2.

Is the transient stress σ_t due to other type of relaxation process than σ_2? The equality of $\Delta E_2{}^{+}_{+}$ and $\Delta E_t{}^{+}_{+}$ is likely to be a negative evidence for this question. We shall interpret it in the next paper as due to the time-dependence of the number of "effective" junctions which alone carry the relaxing stress.

§ 6. Conclusion

We are convinced that the dispersion of dynamic modulus of elasticity and the absorption of vibration of rubber, at least in the audible frequencies, arise mainly from the relaxation process which we have observed. This relaxation process would be due to the shift of junctions or to the slip of a type of secondary cross-links. Tobolsky-Eyring's equation is more adequate to describe the stress relaxation than Kuhn's one but Tobolsky-Eyring's equation is not perfect in describing the whole stage of it.

This report is a part of the "study of rubber as an antivibration meterial" which was given by the Railway Technical Conference and is in progress.

Multiple Scattering of Fast Electrons.
Part. I. Theoretical Considerations.

By Ken-ichi SHINOHARA.

Department of Physics, Faculty of Science, Kyushu University, Fukuoka.

(Read September 18, 1848; Received October 6, 1948)

Abstract.

The multiple scattering of fast electrons by thin foils has been calculated on the assumption that the electrons are diffracted by minute crystals forming the foil. The method used was that of Williams and the resulting distribution of the projected angles is given. The result shows a better agreement with most of the experiments than the previous theories.

§ 1. Introduction.

Multiple scattering of electrons has been treated, theoretically, by Williams(1) and also by Goudsmit and Saunderson(2). In either case, the elastic scattering of electrons by an atom has been assumed to take place, and the result of a certain number of such collisions has been computed. The comparison of their results with the experiments shows that the experimental results give generally, a much smaller scattering when lead is used as a scatterer and an approximate agreement when light materials such as carbon or aluminium are used.

Since the materials such as lead or aluminium are always composed of minute crystals, it is certain that the interference of electron waves scattered by neighbouring atoms in each minute crystal occurs, instead of independent scattering by atoms taking place. Wheeler(3) has pointed out that, any first order effect of interference of the scattered electron waves coming from different atoms may not reduce the scattering but the higher order interference effect as in the Darwin-Ewald X-ray theory will appreciably reduce the scattering and bring it to a value in accord with the observations. Williams believes, however, that such a higher order interference does not occur.

In spite of these remarks by various authors, it is tried, in this paper, to calculate the scattering by taking into account the first order interference (kinematical treatment) since the method of Goudsmit and Saunderson and of Williams are certainly incomplete in that they neglect the interference effect. The result of the calculation shows that the higher order interference effect will probably not change the present result appreciably.

The scattered electrons, in the present calculation, consist of two parts. One is the beam reflected from various net-planes in the crystal and the other is the diffusely scattered beam due to the heat motion of the atoms in the crystal.

The general procedure followed was that of Williams.

§ 2. Intensity of Reflection from a Minute Crystal.

a. Reflection from a net plane.

If $f_{1i}(\chi)$ is the intensity of the electron beam flected from the i-th net-plane of a crystal of volume δV into a solid angle $d\Omega = \sin\chi\, d\chi\, d\psi$ we have(4)

$$\int f_{1i}(\chi)d\chi = \frac{je^4}{64\,\pi m^2 v^4}[F^K - F^{El}]^2 e^{-2M}\frac{\lambda^3}{\sin^6\frac{\chi_i}{2}}\frac{\delta V}{{v_a}^2} \tag{1}$$

where e, m, v, and λ are, respectively, the charge, mass, velocity and the wave-length of the electron, F^K and F^{El} the crystal structure factors for the nucleus and the electrons, v_a the volume of the unit cell, j the number of planes of like spacing in the crystal and χ_i the Bragg angle. e^{-M} is the term which give the correction for the crystal structure factor to make allowance for the heat motion of the atoms in the crystal. It is the function of the temperature and the scattering angle. For a face-centered cubic lattice such as lead or aluminium, (1) becomes

$$\int f_{1i}(\chi)\,d\chi = \frac{je^4}{64\,\pi m^2 v^4}[4^2(Z-f)^2e^{-2M}]\frac{\lambda^3}{\sin^6\frac{\chi_i}{2}}\frac{\delta V}{v_a{}^2} \tag{2}$$

when all three Miller indices *hkl* are even or odd and is zero otherwise. *Z* is the atomic number and *f* the atomic structure factor for the atoms at rest and *j* is equal to the number of possible permutations of the Miller indices of the plane, taking into account the possibility of negative indices.

Formulas (1) and (2) have been obtained by assuming a wholly random orientation of a minute crystal in the foil and computing the average of the scattered intensity over the orientation.

b. Temperature diffuse scattering.

According to Zachariasen⁽⁵⁾, the temperature diffuse scattering varies rapidly with the scattering direction and exhibits a series of diffraction maxima. His results are not expressed in a simple form and are not easy to take into our calculation. But it was also pointed out by him, that if a rough average of the intensity of the diffuse scattering over the scattering angle is estimated, the resulting intensity distribution is nearly the same as that given by Debye⁽⁶⁾. The Debye formula has, therefore, been used in our calculation. The expression for intensity $f_2(\chi)$ of diffuse scattering is, then,

$$f_2(\chi) = N\frac{e^4}{4\,m^2 v^4 \sin^4\frac{\chi}{2}}(Z-f)^2(1-e^{-2M}) \tag{3}$$

where *N* is the number of atoms in the minute crystal and is given by $N = n\dfrac{\delta V}{v_a}$, if *n* is the number of atoms in the unit cell. For a face centered cubic lattice *n* is equal to 4.

The total intensity of the scattered beam from a minute crystal is, therefore,

$$\sum_i f_{1i}(\chi)+f_2(\chi)$$

§ 3. Calculation of the Distribution of the Projected Angle.

a. General procedure.

In a similar way as in the method of Williams, the projection of the deflection of the particles on the plane at right angles to the line of sight, which is the plane containing the initial direction, is considerd. The distribution of this projected angle ϕ, after the scattering by a minute crystal, is given by

$$P(\phi)\,d\phi = 2\int_0^{\frac{\pi}{2}}\{\sum_i f_{1i}(\chi)+f_2(\chi)\}\cos u\,du\,d\phi \tag{4}$$

where *u* is the angle shown in Fig. 1. AO in Fig. 1 is the direction of the incident beam, and AP, the scattered beam. Then an angle ϕ_1 is defined, such that in traversing the foil of scattering substance, the electron experiences, on the average, one collision which deflects it through more than ϕ_1, i.e.

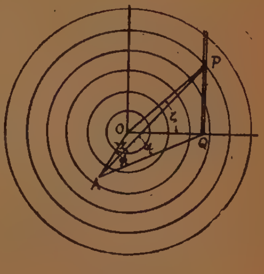

Fig. 1.

$$\frac{t}{\delta V}\int_{\phi_1}^{\frac{\pi}{2}} P(\phi)d\phi = 1, \tag{5}$$

where $\dfrac{t}{\delta V}$ is the number of small crystals per unit area of the foil. $P(\phi)$ decreases rapidly with ϕ so that the upper limit does not enter in (5) as long as ϕ_1 is small.

The collisions giving deflections appreciably less than ϕ_1 will take place in large numbers. These deflections may be in the same or opposite direction and therefore, Williams concluded, that from the theory of errors, the resultant deflection α will conform very nearly to a gaussian distribution.

The gaussian distribution can be written as

$$F(\alpha) = \frac{2}{\pi\alpha_M}\exp\left(-\frac{\alpha^2}{\pi\alpha_M{}^2}\right) \tag{6}$$

where α_M is connected to $\overline{\alpha^2}$ by

$$\alpha_M{}^2 = \frac{2}{\pi}\overline{\alpha^2}. \tag{7}$$

$\overline{\alpha^2}$ can be obtained from the similar quantity $\overline{\phi^2}$ for the scattering by a single minute crystal, instead of a single atom in the case of Williams, by

$$\overline{\alpha^2} = \nu\,\overline{\phi^2}, \tag{8}$$

where ν is the avereage number of collision of the electron in traversing the foil and is given by

$$\nu = N_1\sigma t,$$

N_1 being the number of minute crystals per unit volume and t the thickness of the foil, and σ the cross section of the minute crystal. The volume of the minute crystals in the foil are assumed to be all equal.

b. Calculation of ϕ_1.

In Fig. 2, Let AO be the direction of the incident beam and let the part of the scattered beam which gives a projected angle larger than ϕ_1 falls to the right of the line BC or the left of B′C′. In these regions ϕ is usually large, and the contribution from the beams reflected from net-planes are, usually, negligibly small. The diffusely scattered beam only is important.

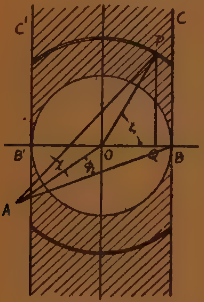

Fig. 2.

From (5), we have, therefore,

$$\frac{4t}{\delta V}\int_{\phi_1}^{\frac{\pi}{2}} f_2(\chi)\zeta \sin\chi\, d\chi = 1 \tag{9}$$

where

$\cos\zeta = \dfrac{\tan\phi_1}{\tan\chi} \approx \dfrac{\phi_1}{\chi}$.* Since e^{-2M} and f are almost equal to zero, at these angles, we can further write, for a face-centered cubic lattice,

$$\int_{\phi_1}^{\frac{\pi}{2}} f_2(\chi)\zeta \operatorname{sid}\chi\, d\chi = \int_{\phi_1}^{\frac{\pi}{2}} \frac{D\delta V}{\chi^3}\zeta d\chi, \tag{10}$$

where

$$D = \frac{16e^4Z^2}{m^2v^4v_a}\delta V \tag{11}$$

Integrating (10) and comparing with (9), we get finally,

$$\phi_1 \fallingdotseq \sqrt{\frac{\pi Dt}{2}}. \tag{12}$$

c. Calculation of σ and α_M.

The number of electrons falling in a narrow region lying between two parallel lines BC and B′C′ contributes to the gaussian distribution. The cross section can be written as

$$\sigma = \sigma_1 + \sigma_2$$

where σ_1 corresponds to the contribution from the beam scattered within the cone of the semi-apex angle ϕ_1, and σ_2 the contribution from the shaded area. σ_1 can be written as

$$\sigma_1 \fallingdotseq \int_0^{\phi_1}\{\sum_i f_{1i}(\chi) + f_2(\chi)\}2\pi\sin\chi\, d\chi$$

Since the beam reflected by a single net-plane is concentrated in the neighbourhood of the Bragg angle, the first term in the parenthesis can be written as:

$$\int_0^{\phi_1}\sum_i f_{1i}(\chi)2\pi\sin\chi\, dx = 2\pi\sum_i \sin\chi_i\int_0^{\phi_1} f_{1i}(\chi)d\chi$$
$$= 2\pi\sum_i \chi_i\int_0^{\phi_1} f_{1i}(\chi)d\chi. \tag{13}$$

$\int_0^{\phi_1} f_{1i}(\chi)dx$, in this expression, can be obtained from (2).

We have therefore,

$$\sigma_1 \fallingdotseq 2\pi\sum_i \chi_i\int_0^{\phi_1} f_{1i}(\chi)d\chi + 2\pi\int_0^{\phi_1}\chi f_2(\chi)d\chi \tag{14}$$

where $f_2(\chi)$ can be obtained from (3)

In estimating the contribution to σ from the shaded area, we will neglect the beam reflected from net-planes, as its intensity decreases much more rapidly than the diffusely scattered beam. We will further use a simplified form for $f_2(\chi)$:

$$f_2(\chi) = \frac{D\delta V}{\chi^4}.$$

Then we get

$$\sigma_2 = \frac{4D\delta V}{3\phi_1^2}. \tag{15}$$

In a similar way $\overline{\phi^2}$ can be obtained:

---

* When the angles ϕ or χ are small, $\tan\phi$, $\sin\chi$, etc., are replaced by ϕ, χ etc.

$$\overline{\phi^2} = \frac{1}{\sigma}\left(\pi\sum_i|\chi_i^3\int_0^{\phi_1} f_{1i}(\chi)d\chi + \pi\int_0^{\phi_1}\chi^3 f_2(\chi)d\chi + \frac{D}{3}\delta V\right). \tag{16}$$

§ 4. Numerical Calculation for Lead and Aluminium.

Calculations have been carried out for lead and aluminium. Atomic structure factors used were those given by James and Brindley(7) for the Thomas model of atoms for lead and for the Hartree distribution for aluminium. Room temperature (290° absolute) was assumed for the temperature of the minute crystal, and the total energy of the electron was assumed to be 4.56 Mev. (wave-length $\lambda = 2.49\times10^{-11}$ cm). The result of the calculation is, for lead

$$\sigma = \left(3.36\times10^5 - \frac{1.66}{\phi_1^2}\right)\delta V, \text{ (in cm}^2\text{)} \tag{17}$$

$$\overline{\phi^2} = \frac{15.60+2.89\log\phi_1}{\sigma}\delta V, \text{ (in radian}^2\text{)} \tag{18}$$

and for aluminium

$$\sigma = \left(3.34\times10^4 - \frac{0.076}{\phi_1^2}\right)\delta V, \text{ (in cm}^2\text{)} \tag{19}$$

$$\overline{\phi^2} = \frac{0.765+0.132\log\phi_1}{\sigma}\delta V. \text{ (in radian}^2\text{)} \tag{20}$$

In most of the experiments, the electrons have a rather broad distribution in energy in the neighbourhood of several Mev. In such a case it was convenient in Williams's treatment, to write the gaussian distribution in the form(8)

$$F(W\alpha) = \frac{2}{\pi W\alpha_M}\exp\left(-\frac{W^2\alpha^2}{\pi W^2\alpha_M^2}\right) \tag{21}$$

In this form, the distribution in $W\alpha$ was theoretically independent of the total energy W, since to a good approximation α_M was inversely proportional to W. Fortunately, this is also the case with the present calculation.

It is easily seen from (12) that when $v \simeq c$, $\frac{\phi_1}{\lambda}$ is independent of the wave-length or the energy of the electrons and from (16), (8), (7) and the expression for σ, $\frac{\alpha_M}{\lambda}$ is also independent of the energy. Since $\lambda = \frac{h}{mv} \simeq \frac{hc}{mc^2} = \frac{hc}{W}$ when the velocity of the electrons is nearly equal to the light velocity, $W\alpha_M$ is independent of the total energy W. The average value of $W\alpha$ computed from the experimental results can, therefore, be directly compared with the present calculation.

§ 5. Comparison with the Theories of Williams and of Goudsmit and Saunderson.

The comparison of the present calculation with those of Williams and of Goudsmit and Saunderson is made in Table I and Fig. 3, for the electron of total energy 4.56 Mev and the scatterer of 0.115 mm lead. In Table I, the second column gives the distribution obtained by Goudsmit and Saunderson as a function of the scattering angle and the third column, the distribution of the projected angle calculated from the same theory. Those two distributions are nearly equal, as has already been pointed out by Goudsmit and Saunderson and also by Williams. The fourth column gives the distribution corresponding to the actual experimental condition using cloud chambers, also calculated from the same theory. The illuminated depth in the cloud chamber was taken as 20 mm and the length of the shortest electron tracks measured was assumed to be 6 cm. This shows also a similar distribution. The fifth column gives the distribution obtained by Williams. The sixth column gives the distribution calculated with the present theory. Fig. 3 gives the distribution of the projected angles in the three theories.

Table I. Comparison of the present theory with the theories of Goudsmit and Saunderson and of Williams for a lead scatterer. $W = 4.56$ Mev. $t = 0.0115$ cm.

α or χ	Goudsmit and Saunderson			Williams	Present
	$f(\chi)$	$F(\alpha)$	$F'(\alpha)$	$F(\alpha)$	$F(\alpha)$
0°	15.3	15.3	15.3	15.3	15.3
5°	14.8	14.8	14.8	14.9	14.8
10°	13.6	13.7	13.7	13.8	13.4
15°	11.8	12.1	12.1	12.2	11.3
20°	9.7	10.1	10.1	10.2	8.9
25°	7.1	7.7	7.7	8.3	6.6
30°	5.0	5.3	5.1	6.3	4.5
35°	3.5	3.7	3.6	4.5	2.9
40°	2.3	2.6	2.5	3.1	1.8
45°	1.5	1.7	1.5	2.1	1.0

The distribution given by Goudsmit and Saunderson shows a slightly smaller scattering than

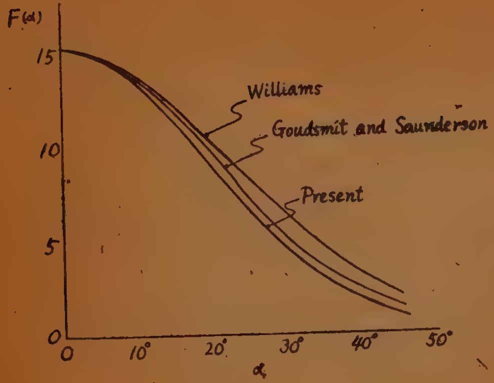

Fig. 3.

Comparison of the present distribution with those of Goudsmit and Saunderson and of Williams for a lead scatterer. $W = 4.56$ Mev. $t = 0.0115$ cm.

that of Williams, and the present calculation shows a still smaller scattering. The last distribution is, certainly, in better agreement with most of the experiments. Since the treatment of Williams and of Goudsmit and Saunderson are both based on the same assumption of independent scattering by neighbouring atoms, the resulting smaller scattering in the case of Goudsmit and Saunderson has been caused almost entirely by the difference in the method of treatment. As the method of Goudsmit and Saunderson is probably more accurate, our calculation, which follows the method of Williams, can also be improved in its exactness, if it is possible to adopt their method. The result will probably be a still smaller scattering, but its exact value is difficult to estimate.

A comparison of the theories with our experiment as well as with others will be given in the next paper.

The present calculation is based on the kinematical theory of diffraction. It may seem necessary that the dynamical treatment such as those of Bethe⁽⁹⁾ should be used. But the actual calculation shows that, it is the diffuse scattering that is giving the main contribution, to the distribution, since, the reflections by net-planes are limited in a rather small angular range. Such a treatment, will, therefore, not change the distribution essentially. It seems, possible, on the other hand, that since the formula of Debye is admittedly not very accurate, a more accurate treatment of the diffuse scattering may improve the distribution to some extent.

The effect of the inelastic scattering is not included in the present theory. It is difficult to estimate its effect. But, since the inelastically scattered electrons are concentrated in an extremely narrow range of angles in the neighbourhood of the direction of incidence, its influence on the result is expected not to be very large.

References.

(1) E. J. Williams: Proc. Roy. Soc., A, 169 (1939), 531; Phys. Rev., 58 (1940), 292.
(2) S. Goudsmit and J. L. Saunderson: Phys. Rev. 57 (1940), 24; Phys. Rev., 58 (1940), 36.
(3) J. A. Wheeler: Phys. Rev., 57 (1940), 352 (A).
(4) A. H. Compton and S. K. Allison: X-rays in Theory and Experiment. 2nd ed. (1936), 417. A slight modification has been made in the formula given in the book in order to apply it to the electron scattering.
(5) W. H. Zachariasen: Phys. Rev., 57 (1940), 597.
(6) P. Debye: Ann. d. Phys., 43 (1914), 49.
(7) J. W. James and G. W. Brindley: Zeits. f. Krist., 78 (1931), 470.
(8) C. W. Sheppard and W. A. Fowler: Phys. Rev., 57 (1940), 273.
(9) H. Bethe: Ann. d. Phys., 87 (1928), 55.

On the Solution of the Laminar Boundary Layer Equations.

By Itiro Tani.

Department of Physical Technology, Second Faculty of Engineering,
University of Tokyo.

(Read April 30, 1946; Received October 13, 1948)

§1. Introduction.

The theory of the laminar boundary layer offers a means of determining the skin friction under the assumption of a given velocity distribution outside the boundary layer. Owing to the mathematical difficulties, however, exact solutions are possible only when the velocity distribution is expressed as a simple function of the distance along the surface. More complicated velocity distributions necessitate recourse to the method of expansion in series or that of step-by-step calculations, but the labor involved is too great for the methods to be of practical use. Approximate method due to Pohlhausen (1921), which had long been recommended for general use, gives a reasonably accurate solution in a region of accelerated flow, but recently its adequacy in a region of retarded flow has been questioned. Separation of flow may actually occur where the solution of Pohlhausen fails to give it. More recently Howarth (1938) put forward another approximate means of solution, which gives fairly reasonable results in a region of retarded flow.

Howarth's solution essentially consists in solving the boundary layer equations for the particular case in which the velocity U outside the boundary layer decreases linearly with the distance x measured along the surface, and utilizing the solution by replacing the actual distribution of U by a circumscribing polygon of infinitesimal sides. Therefore, it is assumed that the velocity distribution at any section depends on the velocity gradient dU/dx at that section only, being affected by the conditions upstream only in so far as this affects the momentum thickness θ. In other words, the velocity distribution across the boundary layer is determined by a parameter such as

$$\sigma = \frac{\theta^2}{\nu}\frac{dU}{dx}.$$

It is to be noticed that Pohlhausen's solution is based on the same assumption.

Now, if the assumption were adequate, we should expect the separation of flow to occur at a certain definite value of σ, whatever be the distribution of velocity outside the boundary layer. That this is not the case, however, is readily seen, since the value of σ giving separation is -0.084 according to Howarth's solution, and -0.068 according to Falkner and Skan's solution (1930, also Hartree 1937) for the case $U = x^{\alpha}$. This has led the writer to believe that σ does not exactly fix the velocity distribution, and that other parameters such as

$$\omega = \sigma^2 U \frac{d^2U}{dx^2} \Big/ \left(\frac{dU}{dx}\right)^2$$

also affect the distribution, the influence becoming more marked as the separation is approached. Since ω is always zero for Howarth's solution and positive for Falkner and Skan's solution near the point of separation, it is probable that the value of σ giving separation increases (i.e. becomes less negative) as ω increases. Recently, the writer (1940) has measured the velocity distribution around an airfoil of the laminar flow type, and also observed the position of transition from laminar to turbulent flow in the boundary layer. On applying Howarth's method of solution to his observed velocity distribution, the writer found the separation well ahead of the transition. This seemed unreasonable, but at that time the problem was pursued no farther, since the velocity distribution had not been measured sufficiently precisely. Probably, however, the unreasonable circumstance will partly be explained by the effect of ω, giving separation too late since ω is negative in the region between velocity maximum and transition for such an airfoil.

An attempt was therefore made to investigate the effect of ω on the velocity distribution across the boundary layer. In view of the practical interest of cases in which ω becomes negative in the neighborhood of the separation, it was decided to solve the boundary layer equations as accurately as possible for the velocity distribution $U = U_0 + cx^n$ with $n = 2$, 4 and 8 (Howarth's solution corresponds to the case $n = 1$). This particular solution is then used as a basis for rough approximation to the solution in the general case.

§ 2. Solution for the Special Case of Velocity Distribution.

We consider, first of all, the solution in series for a velocity distribution outside the boundary layer of the form

$$U = U_0 + cx^n,$$

where x is the distance measured along the surface and c, n and U_0 are constants. The method of solution is the same as given by Howarth for the particular case where $n = 1$.

We assume an expression of the form

$$\psi = \sqrt{\nu x U_0} \sum_{r=0}^{\infty} \xi^r f_r(\eta)$$

for the stream function ψ, where $\xi = 8\,cx^n/U_0$, $\eta = (y/2)\sqrt{U_0/\nu x}$, and y is the distance measured normal to the surface. Substituting this form in the boundary layer equation

$$u\frac{\partial u}{\partial x} + v\frac{\partial u}{\partial y} = U\frac{dU}{dx} + \nu\frac{\partial^2 u}{\partial y^2}$$

(where u and v denote the velocity components in the directions x and y), and equating coefficients of the various powers of ξ on the two sides of the equation, we obtain a series of differential equations

$$f_0''' + f_0 f_0'' = 0,$$

$$f_1''' + f_0 f_1'' - 2nf_0' f_1' + (2n+1) f_0'' f_1 = -n,$$

$$f_2''' + f_0 f_2'' - 4nf_0' f_2' + (4n+1) f_0'' f_2$$

$$= -\frac{1}{8}n + 2nf_1'^2 - (2n+1) f_1 f_1'',$$

$$f_3''' + f_0 f_3'' - 6nf_0' f_3' + (6n+1) f_0'' f_3$$

$$= 6nf_1' f_2' - (2n+1) f_1 f_2'' - (4n+1) f_1'' f_2,$$

$$\dots\dots\dots\dots\dots\dots\dots\dots\dots\dots,$$

where dashes denote differentiations with respect to η. The boundary conditions are (since $u = v = 0$ at $y = 0$) $f_r(0) = f_r'(0) = 0$ for all values of r, and (since $u = U$ at $y = \infty$) $f_0'(\infty) = 2$, $f_1'(\infty) = 1/4$, $f_r'(\infty) = 0$ for $r \geqq 2$.

The solution of the first equation was given by Blasius (1908) and Toepfer (1912). A table of f_0 has been given by Howarth to five decimal places. In view of the importance of f_0, on which all the succeeding functions depend, the integration was carried out afresh by the present writer to give f_0 to seven decimal places.

The solution for $n = 1$ has already been evaluated by Howarth, the functions being obtained up to and including f_6. Calculations for cases where $n = 2$, 4 and 8 were carried out by the writer. Since the determination of f_r requires the knowledge of $f_0, f_1, \dots, f_{r-1}$, the significant figures of the values of f_r decrease as r increases, the effect becoming more serious as n increases. Thus the functions were obtained up to and including f_6 for $n = 2$, f_5 for $n = 4$, and f_4 for $n = 8$.

§ 3. Calculation of the Correction Term.

Unfortunately, however, the series converges so slowly, that the functions so far evaluated are not sufficient to give a sufficiently accurate representation unless the absolute value of ξ is small. Many more functions of the higher order would have been required, but the labor involved would be prohibitive. The difficulty may be avoided by applying an approximate method of procedure, which is originally due to Howarth, and based on the assumption that the functions f_r' of the higher order are expressible with reasonable accuracy in the form $K_r \eta \exp(-\alpha\eta^s)$ where s, α and K_r are constants, s and α retaining the same value, whereas K_r differing for different functions f_r'. The adequacy of the assumption may be justified from the fact that, apart from f_0, f_1 and f_2 which are exceptional, the differential equations defining f_r are of the same form. It was found by trial that $s = 2.94$, 2.57 and 2.22; $\alpha = 0.135$, 0.235 and 0.385 for $n =$ 2, 4 and 8 respectively (Howarth adopted $s = 3$,

$= 0.1$ for $n = 1$).

Now, if we assume that all the functions f_r' for $r > m$ are of the form $K_r\eta\exp(-a\eta^s)$, the velocity distribution is given by

$$u = \frac{U_0}{2}\left\{\sum_{r=0}^{m}\xi^r f_r'(\eta) + F(\xi)G(\eta)\right\},$$

where $G(\eta) = \eta\exp(-a\eta^s)$, $F(\xi)$ is a function of ξ to be determined, and $m = 6, 5$ and 4 for $n = 2, 4$ and 8 respectively. Substituting the expression in the momentum integral of the boundary layer

$$\int_0^\infty \frac{\partial}{\partial x}(u^2 - U^2)dy - U\int_0^\infty \frac{\partial}{\partial x}(u - U)dy = -\nu\left(\frac{\partial u}{\partial y}\right)_{y=0},$$

we have the differential equation for F:

$$(A + BF)\frac{dF}{d\xi} = P + QF + RF^2,$$

where

$$A = 2n\xi\left\{\sum_{r=0}^{m}\xi^r\int_0^\infty f_r'G\,d\eta - \left(1 + \frac{\xi}{8}\right)\int_0^\infty G\,d\eta\right\},$$

$$B = 2n\xi\int_0^\infty G^2 d\eta,$$

$$P = \frac{1}{8}(2nm + 1)f_m(\infty)\xi^{m+1}$$

$$-\frac{1}{2}\sum_{r=1}^{m}\{2n(m+r)+1\}\xi^{m+r}\sum_{i=r}^{m}\int_0^\infty f_i' f'_{m+r-i}\,d\eta,$$

$$Q = -\frac{1}{2}\sum_{r=0}^{m}(2nr+1)\xi^r\int_0^\infty f_r'G\,d\eta + \left(1 + \frac{\xi}{8}\right)\int_0^\infty G\,d\eta,$$

$$R = -\frac{1}{2}\int_0^\infty G^2 d\eta.$$

Starting from the value of ξ for which u is given by $(U_0/2)\sum_{r=0}^{m}\xi^r f_r'$ with sufficient accuracy ($\xi = \pm 0.26$, ± 0.14 and ± 0.06 for $n = 2, 4$ and 8 resp.) and therefore $F = 0$, the equation may be integrated graphically for F. The accelerated flow may be obtained by extending the solution for positive values of ξ, but the calculations need not be carried out much farther, because the limiting case for $\xi \to +\infty$ correponds to the velocity distribution $U = x^n$, for which an exact solution has been given by Falkner and Skan.

On the other hand, the extension for negative values of ξ gives the solution for the retarded flow, where the separation of flow may occur when $(\partial u/\partial y)_{y=0} = 0$, i. e. $F = -\sum_{r=0}^{m}\xi^r f_r''(0)$. Actually, however, slightly before reaching the separation, $A + BF$ becomes zero resulting an infinite value of $dF/d\xi$. This failure must be due to the inexactitude in the form assumed for the correction term, although the integral does not reach the separation by a quantity ($\Delta\xi$) of the order of 10^{-4}. It seems fairly reasonable to assume that it is only in the neighborhood of the point where $A + BF = 0$ that the solution is invalidated. If we assume that the solution given is valid as far as the point $\Delta\xi = 0.01$ before the point for which $A + BF = 0$, we may complete the solution using the relation

$$\left[\frac{\partial u}{\partial y}\frac{\partial}{\partial x}\left(\frac{\partial u}{\partial y}\right)\right]_{y=0} = \nu\left[\frac{\partial^4 u}{\partial y^4}\right]_{y=0},$$

which is obtained by differentiating the boundary layer equation twice with respect to y and putting $y = 0$. The corresponding equation for F is

$$MF + \sum_{r=0}^{m}\xi^r f_r^{V}(0) = \left\{F + \sum_{r=0}^{m}\xi^r f_r''(0)\right\}$$

$$\left\{2n\xi\frac{dF}{d\xi} - F + \sum_{r=0}^{m}(2nr - 1)\xi^r f_r''(0)\right\},$$

where M is the value of $d^4G/d\eta^4$ for $\eta = 0$. An infinite value of M might be deduced from the assumed form for G, but in view of the rough nature of approximation, it seems unadvisable to rely on as far as the higher derivatives. Probably a more reasonable method would be to determine the value of M so as to make F and $dF/d\xi$ continuous at the joining point. By doing so we find separation when $\xi = -0.586$, -0.363 and -0.226 for $n = 2, 4$ and 8 respectively. It is to be noticed that by a small displacement of the joining point the final result remains unaltered within the limits of accuracy here achieved. Howarth obtained $\xi = -0.960$ at separation for $n = 1$.

§ 4. Results of Calculation.

The velocity distribution across the boundary layer, expressed non-dimensionally, is given by

$$\frac{u}{U} = \frac{1}{2(1 + \xi/8)}\left\{\sum_{r=0}^{m}\xi^r f_r'(\eta) + F(\xi)G(\eta)\right\}.$$

Tables 1, 2 and 3 contain values of u/U for several values of ξ and η. Values of σ, ω, $H = \delta^*/\theta$, $T =$

Table I.

Values of u/U etc. for $n = 2$.

η \ ξ	0.300	0	−0.100	−0.200	−0.300	−0.400	−0.500	−0.560	−0.586
0.0	0.000	0.000	0.000	0.000	0.000	0.000	0.000	0.000	0.000
0.2	0.166	0.133	0.120	0.106	0.091	0.073	0.051	0.032	0.011
0.4	0.320	0.265	0.243	0.219	0.193	0.161	0.121	0.086	0.046
0.6	0.461	0.394	0.367	0.337	0.303	0.262	0.208	0.159	0.102
0.8	0.588	0.517	0.488	0.455	0.416	0.370	0.307	0.248	0.176
1.0	0.698	0.630	0.601	0.568	0.529	0.481	0.414	0.348	0.266
1.2	0.789	0.729	0.703	0.672	0.635	0.589	0.522	0.454	0.367
1.4	0.861	0.812	0.790	0.763	0.730	0.688	0.626	0.561	0.473
1.6	0.914	0.876	0.859	0.838	0.810	0.774	0.720	0.661	0.578
1.8	0.950	0.923	0.911	0.895	0.874	0.845	0.800	0.750	0.677
2.0	0.973	0.955	0.947	0.936	0.921	0.900	0.865	0.825	0.764
2.2	0.986	0.976	0.970	0.963	0.953	0.939	0.914	0.884	0.837
2.4	0.993	0.988	0.985	0.980	0.974	0.965	0.948	0.927	0.894
2.6	0.997	0.994	0.993	0.990	0.987	0.981	0.971	0.957	0.935
2.8	0.999	0.997	0.997	0.995	0.994	0.990	0.985	0.976	0.963
3.0	1.000	0.999	0.998	0.998	0.997	0.995	0.992	0.988	0.980
3.2	—	1.000	0.999	0.999	0.998	0.998	0.996	0.994	0.990
3.4	—	—	1.000	1.000	0.999	0.999	0.998	0.997	0.995
3.6	—	—	—	—	1.000	1.000	0.999	0.999	0.998
3.8	—	—	—	—	—	—	1.000	1.000	0.999
4.0	—	—	—	—	—	—	—	—	1.000
σ	0.028	0	−0.012	−0.025	−0.039	−0.056	−0.074	−0.086	−0.092
ω	0.011	0	−0 005	−0.012	−0.020	−0.029	−0.041	−0.050	−0.053
H	2.466	2.591	2.649	2.721	2.814	2.941	3.147	3.387	3.760
T	0.265	0.221	0.202	0.180	0.154	0.122	0.079	0.041	0.000
Ψ	0.305	0.441	0.499	0.568	0.645	0.738	0.848	0.927	0.964

Table II.

Values of u/U etc. for $n = 4$.

η \ ξ	0.180	0	−0.060	−0.120	−0.180	−0.240	−0.300	−0.340	−0.363
0.0	0.000	0.000	0.000	0.000	0.000	0.000	0.000	0.000	0.000
0.2	0.168	0.133	0.121	0.107	0.093	0.077	0.057	0.039	0.014
0.4	0.321	0.265	0.245	0.223	0.199	0.171	0.136	0.103	0.057
0.6	0.460	0.394	0.370	0.344	0-313	0.278	0.232	0.188	0.124
0.8	0.584	0.517	0.492	0.464	0.431	0.392	0.341	0.290	0.212
1.0	0.693	0.630	0.606	0.579	0.547	0.507	0.454	0.400	0.315
1.2	0.784	0.729	0.708	0.683	0.654	0.617	0.566	0.513	0.426
1.4	0.856	0.812	0.794	0.773	0.748	0.716	0.670	0.621	0.538
1.6	0.910	0.876	0.862	0.846	0.826	0.799	0.761	0.718	0.644
1.8	0.947	0.923	0.913	0.901	0.886	0.865	0.836	0.801	0.739
2.0	0.971	0.955	0.949	0.940	0.929	0.915	0.893	0.867	0.818
2.2	0.985	0.976	0.972	0.966	0.959	0.950	0.934	0.916	0.880
2.4	0.993	0.988	0.986	0.982	0.978	0.972	0.962	0.950	0.925
2.6	0.997	0.994	0.993	0.991	0.989	0.985	0.980	0.972	0.956
2.8	0.999	0.997	0.997	0.996	0.995	0.993	0-990	0.985	0.976
3.0	1.000	0.999	0.999	0.998	0.998	0.997	0.995	0.993	0.988
3.2	—	1.000	1.000	0.999	0.999	0.998	0.998	0.997	0.994
3.4	—	—	—	1.000	1.000	0.999	0.999	0.998	0.997
3.6	—	—	—	—	—	1.000	1.000	0.999	0.999
3.8	—	—	—	—	—	—	—	1.000	1.000
4.0	—	—	—	—	—	—	—	—	—
σ	0.035	0	−0.014	−0.029	−0.045	−0.062	−0.082	−0.095	−0.103
ω	0.042	0	−0.019	−0.041	−0.066	−0.095	−0.128	−0.153	−0.169
H	2.470	2.591	2.648	2.718	2.804	2.919	3.088	3.284	3.660
T	0.268	0.221	0.200	0.178	0.152	0.121	0.083	0.047	0.000
Ψ	0.258	0.441	0.515	0.598	0.690	0.794	0.915	1.006	1.067

Table III.

Values of u/U etc. for $n = 8$.

η \ ξ	0.120	0	−0.040	−0.080	−0.120	−0.160	−0.200	−0.215	−0.226
0.0	0.000	0.000	0.000	0.000	0.000	0.000	0.000	0.000	0.000
0.2	0.166	0.133	0.120	0.106	0.091	0.074	0.051	0.038	0.018
0.4	0.315	0.265	0.245	0.223	0.199	0.169	0.130	0.108	0.070
0.6	0.450	0.394	0.371	0.346	0.316	0.280	0.231	0.202	0.151
0.8	0.572	0.517	0.494	0.468	0.437	0.399	0.345	0.312	0.253
1.0	0.681	0.630	0.608	0.584	0.554	0.517	0.463	0.430	0.367
1.2	0.773	0.729	0.710	0.689	0.662	0.628	0.577	0.546	0.484
1.4	0.847	0.812	0.796	0.778	0.756	0.726	0.682	0.654	0.598
1.6	0.903	0.876	0.864	0.850	0.832	0.809	0.772	0.749	0.701
1.8	0.942	0.923	0.915	0.905	0.891	0.874	0.845	0.827	0.788
2.0	0.967	0.955	0.950	0.943	0.934	0.921	0.901	0.887	0.858
2.2	0.983	0.976	0.972	0.968	0.962	0.954	0.940	0.930	0.910
2.4	0.992	0.988	0.986	0.983	0.980	0.975	0.966	0.959	0.946
2.6	0.996	0.994	0.993	0.992	0.990	0.987	0.982	0.978	0.969
2.8	0.998	0.997	0.997	0.996	0.995	0.994	0.991	0.989	0.983
3.0	0.999	0.999	0.999	0.998	0.998	0.997	0.996	0.994	0.991
3.2	1.000	1.000	1.000	0.999	0.999	0.999	0.998	0.997	0.996
3.4	—	—	—	1.000	1.000	1.000	0.999	0.999	0.998
3.6	—	—	—	—	—	—	1.000	1.000	0.999
3.8	—	—	—	—	—	—	—	—	1.000
4.0	—	—	—	—	—	—	—	—	—

σ	0.048	0	−0.018	−0.038	−0.058	−0.080	−0.103	−0.113	−0.119
ω	0.139	0	−0.058	−0.122	−0.194	−0.275	−0.365	−0.402	−0.429
H	2.457	2.591	2.650	2.723	2.814	2.930	3.131	3.260	3.532
T	0.278	0.221	0.198	0.172	0.143	0.108	0.063	0.039	0.000
Ψ	0.174	0.441	0.546	0.660	0.786	0.925	1.083	1.149	1.202

Table IV.

Results of Howarth's solution ($n = 1$).

ξ	0.600	0	−0.200	−0.400	−0.600	−0.800	−0.900	−0.960
σ	0.026	0	−0.012	−0.026	−0.044	−0.064	−0.076	−0.084
ω	0	0	0	0	0	0	0	0
H	2.460	2.591	2.660	2.754	2.885	3.125	3.370	3.830
T	0.265	0.221	0.199	0.173	0.139	0.089	0.051	0.000
Ψ	0.322	0.441	0.498	0.569	0.661	0.775	0.844	0.896

Table V.

Results of Hartree's solution ($U = x^{\alpha}$).

$\frac{2\alpha}{1+\alpha}$	1.000	0.300	0	−0.100	−0.160	−0.180	−0.190	−0.199
σ	0.086	0.045	0	−0.026	−0.049	−0.058	−0.063	−0.068
ω	0	−0.009	0	0.015	0.034	0.044	0.050	0.057
H	2.215	2.361	2.591	2.803	3.093	3.297	3.481	4.030
T	0.360	0.299	0.221	0.164	0.105	0.073	0.049	0.000
Ψ	0.086	0.253	0.441	0.557	0.659	0.702	0.728	0.753

$\theta\tau_0/\rho\nu U$ and $\Psi = 2T-(3+2H)\sigma$ (where τ_0 is the intensity of skin friction, θ and δ^* the momentum and displacement thicknesses) are also included in the tables, whilst the corresponding values deduced from Howarth's results ($n=1$) and Hartree's results ($U=x^{\alpha}$) are presented in Tables 4 and 5 respectively.

Now, if H, T and Ψ are plotted as functions of σ, the curves for different forms of velocity distribution, $U=U_0+cx^n$ with $n=1, 2, 4, 8$ and $U=x^{\alpha}$, are not in agreement, indicating that the velocity distribution across the boundary layer cannot exactly be determined by a single parameter, σ. The separation of curves appears to be due to the effect of ω, the increase in ω resulting in the increase in H and decrease in T for the same value of σ. The effect is considerable in the region of negative σ, i.e. of retarded flow, especially as the separation is approached. Thus, the values of σ giving separation are -0.068 for $U=x^{\alpha}$ ($\alpha = -0.0905$), and -0.084, -0.092, -0.103, -0.119 for $n=1, 2, 4, 8$ in $U=U_0+cx^n$. The corresponding values of ω are $+0.057$, 0, -0.053, -0.169, -0.429 respectively. It is concluded, therefore, that the criterion for separation for $\omega=0$ ($\sigma = -0.084$) gives separation too late when applied to the case $\omega>0$, and too early when applied to the case $\omega<0$.

§ 5. Approximate Solution for the General Case.

The momentum integral of the boundary layer may be put in the form

$$\frac{d}{dx}\left(\frac{U\theta^2}{\nu}\right) = \Psi,$$

where $\Psi = 2T-(3+2H)\sigma$, and integrated in the form

$$U^{k+1}\frac{\theta^2}{\nu} = \left(U^{k+1}\frac{\theta^2}{\nu}\right)_{x=a} + C\int_a^x U^k dx,$$

if it is assumed that $\Psi = C-k\sigma$ in the region $a \leqq x \leqq b$. Since this requires to replace the curve of Ψ against σ by a polygon, the calculation may be performed only by the method of successive approximations. In practice, however, sufficiently accurate results are obtained in the following way: Assuming Ψ to be a function of σ and ω, we have approximately

$$\Psi = 0.441-4.7\sigma+8\sigma^2+\frac{0.13\,\omega}{\omega-0.3},$$

where the last two terms are small. Therefore we obtain for the first approximation

$$\frac{\theta^2}{\nu} = 0.441\,U^{-5.7}\int_0^x U^{4.7}\,dx;$$

the forward stagnation point corresponding to $x=0$. Substituting the first approximation into the neglected terms $8\sigma^2+0.13\,\omega/(\omega-0.3)$, we have for the second approximation

$$\frac{\theta^2}{\nu} = U^{-5.7}\int_0^x\left(0.441+8\sigma^2+\frac{0.13}{\omega-0.3}\right)U^{4.7}dx.$$

Once the value of θ^2/ν is determined in terms of x, we can estimate the skin friction and the velocity distribution by using the results of exact solutions. The criterion for separation may be found from the result mentioned above: $\sigma = -0.068$, -0.084, -0.092, -0.103 and -0.119 for $\omega = +0.057$, 0, -0.053, -0.169 and -0.429 respectively.

This method of estimation, when applied to the measured velocity distribution around the airfoil mentioned above, gives separation somewhat later than that previously calculated. A detailed numerical discussion cannot be made, because the measurement was scarcely accurate enough for the value of d^2U/dx^2 to be determined with the accuracy desired, and, moreover, the value of ω near the separation exceeded the range covered by the solution of the present paper. Nevertheless there seems to be little doubt that the newly estimated point of separation comes much closer to the observed point of transition to turbulent flow.

References.

H. Blasius, Zeits. Math. Phys. 56 (1908), 1.

K. Toepfer, Zeits. Math. Phys. 60 (1912), 397.

K. Pohlhausen, Zeits. angew. Math. Mech. 1 (1921), 252.

V. M. Falkner & S. W. Skan, R. & M., Aero. Res. Comm., No. 1314 (1930).

D. R. Hartree, Proc. Camb. Phil. Soc, 33 (1937), 223.

L. Howarth, Proc. Roy. Soc. A, 164 (1938), 547.

I. Tani & S. Mituisi, Rep. Aero. Res. Inst., Tokyo Imp. Univ., No. 198 (1940).

On the Anomalies of the Small Angle Reflection of Cathode Rays from the Surface of a Single Crystal. Part I. The Usual Dynamical Treatment.

By Kazutake KOHRA and Ken-ichi SHINOHARA.

Institute of Physics, Kyusyu University, Fukuoka, Japan.

(Received October 16, 1948).

Abstract.

A detailed theoretical treatment is given in order to study the anomalies of the small angle reflection of cathode rays from a cleavage face of rocksalt. It is shown that the correction formula of the positions of the reflection spectra by previous authors cannot be applied to the lowest order reflection. There are, moreover, serious discrepancies between the theoretically obtained feature of the lowest order reflection and that obtained experimentally.

§ 1. Introduction.

The reflection of the cathode rays from the cleavage surface of a single crystal has been studied, both experimentally and theoretically, by many authors. It is now well known, that the positions of the reflection spectra deviate from the Bragg formula

$$2d\sin\theta = n\lambda \tag{1}$$

This fact is usually explained by taking account of the effect of the refraction. The Bragg formula modified in this way is

$$\mu_n{}^2-1 = -\sin^2\theta+\frac{n^2\lambda^2}{4d^2}, \tag{2}$$

μ_n being the index of refraction and λ the wave length in the vacuum. The refraction of the beams is, on the other hand, explained as due to the existence of the mean inner potential, E_n, differing from zero, and the following relation has been obtained between E_n and the refractive index:

$$E_n = (\mu_n{}^2-1)\frac{h^2}{2me\lambda^2}\left(1+\frac{h^2}{m^2c^2\lambda^2}\right)^{-\frac{1}{2}}, \tag{3}$$

where e, m, c and h have their usual meanings. However, the value of E_n or μ_n thus obtained is not a constant but is found to depend on the order n of reflection.(1) Both of them approach their respective constant values when n is sufficiently large, and drop to small values for small n. (Fig. 4)

The first explanation of this tendency has been given by Laschkarew(2) from the standpoint of the kinematical theory. This was followed by many quantum mechanical treatments of the problem,(3) (4) (5) but none of them succeeded in explaining apparent change in the inner potential E_n with the order of the reflection quantitatively (1st anomaly). Especially, for the lowest order reflection, serious difficulties appeared in that the existing theory expects the increase of the apparent mean inner potential in the opposite sense to that of the experimental facts (2nd anomaly).

In this paper, we will try to find out how far the conventional quantum mechanical method, neglecting the absorption, can explain the observed fact. The actual calculation is carried out on NaCl, because we have a reliable experimental result due to Yamaguti(6) and also an exact knowledge of the structure factor of the crystal.

§ 2. Theoretical Considetations.

There are two principal ways in treating dynamically the diffraction of electrons in a crystal, corresponding respectively to those of Darwin(7) and of Ewald(8) in the case of X-rays. In the former treatment, the crystal is replaced by parallel atomic planes having certain coefficients of reflection, transmission and absorption. This method is adopted, in the case of electrons by Harding.(9) In the latter treatment, the Schrödinger equation in the field of the crystal is solved.

This method was used by Bethe⁽¹⁰⁾ and others.

Since the method of Bethe is more general in character and is suited to extend to the higher approximations, we will follow his general procedure with the modification that we take the representation of the wave vector used by Kikutchi.⁽¹¹⁾ Such a tretment has already been carried out by Moliére,⁽¹²⁾ but his greatly simplified potential could not allow even the decreasing tendency of the apparent mean inner potential to be explained without introducing the absorption.

(a) Wave functions in the crystal.

Following Bethe, we will first consider the equilibrium of the electron waves in the periodic potential field of a crystal. We will then assume that the crystal is bounded by two parallel net planes and introduce the boundary conditions connecting the waves in the crystal with those in the vacuum. We will start with the Schrödinger equation:

$$\Delta\psi+\frac{8\pi^2 me}{h^2}(E+V)\psi=0, \qquad (4)$$

where V represents the potential field in the crystal and is expanded as:

$$\frac{8\pi^2 me}{h^2}V=\sum v_g e^{2\pi i(\vec{g}\,\vec{r})}, \qquad (5)$$

$\vec{g}$ is a radius vector in the reciprocal lattice. In the case of NaCl, $\vec{g}$ is represented by $(g^1/a\,,\,g^2/a\,,\,g_3/a,)$ where a is the length of the edge of the unit cell, and $g_1\,,\,g_2\,,\,g_3$ are all even or odd integers.

The wave function in the crystal is represented as the superposition of plane waves:

$$\psi=\sum\psi_g e^{i(\vec{k}_g\vec{r})}, \qquad (6)$$

where

$$\vec{k}_g=\vec{k}_0+\vec{g}. \qquad (7)$$

Substituting (6) in (4) and assuming that only ψ_0 and ψ_h are large, we get

$$\left.\begin{aligned}(\kappa^2-k_0^2-V_{11})\,\psi_0-V_{12}\psi_h&=0\\ V_{21}\psi_0-(\kappa^2-k_h^2-V_{22})\,\psi_h&=0\end{aligned}\right\}, \qquad (8)$$

where

$$\left.\begin{aligned}V_{11}&=\sum{}''\frac{v_g v_{-g}}{\kappa^2-k^2_g}, & V_{12}&=-v_{-h}+\sum{}''\frac{v_{-g}v_{g-h}}{\kappa^2-k^2_g},\\ V_{21}&=-v_h+\sum{}''\frac{v_g v_{h-g}}{\kappa^2-k^2_g}. & V_{22}&=\sum{}''\frac{v_{g-h}v_{h-g}}{\kappa^2-k^2_g}.\end{aligned}\right\} \qquad (9)$$

$\sum''$ represents the summation in which the terms with the suffixes o and h are omitted, K the magnitude of the momentum vector of the incident wave in the vacuum, and $\kappa^2=K^2+v_0$.

For a crystal having a center of symmetry, $V_{12}=V_{21}$, and we can further prove that when $\vec{h}$ has the indices $(0\,0\,h)$ as in the case of reflection from a cleavage surface, $V_{11}=V_{22}$. This procedure of taking two amplitudes large, corresponds to the experimental condition that we have one incident and one reflected beams in the vacuum. (8) can be solved if

$$\begin{vmatrix}\kappa^2-k_0^2 & V_{11} & -V_{12}\\ & -V_{12} & \kappa^2-k_h^2-V_{11}\end{vmatrix}=0 \qquad (10)$$

This can be transformed by the use of the quantities D and δ shown in Fig. 1, which is constructed in conformity with the boundary condition that the tangential components of the wave vector in the crystal and in the vacuum are equal at the boundary: it is as follows:

$$\begin{vmatrix}N^2+v_0-(D+\delta)^2-V_{11}\,, & -V_{12}\\ -V_{12} & N^2+v_0-(D-\delta)^2-V_{11}\end{vmatrix}=0$$

or

$$\delta^2=N^2+v_0-V_{11}+D^2\pm\sqrt{4(N^2+v_0\quad V_{11})D^2+V_{12}^2}. \qquad (11)$$

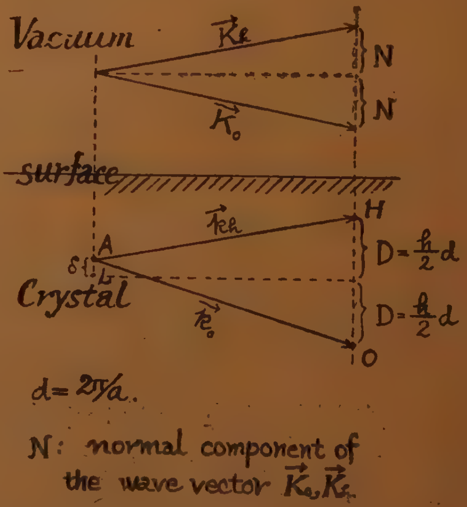

Fig. 1. Diagram of wave vectors.

Since $\delta < D$, we take only the $(-)$ sign in (11) and get*

---

* The two of the four roots are the necessary and sufficient ones to satisfy the boundary conditions considered later. The other two roots which are abandoned, appears in the process of reducing the infinitely many equations for the amplitudes of waves to the two equations (8). This problem has been considered in detail by Lamla.⁽¹³⁾

$$\delta=\pm\{N^2+v_0-V_{11}+D^2-\sqrt{4(N^2+v_0-V_{11})D^2+V_{12}^2}\}^{\frac{1}{2}}=\pm\varDelta. \qquad (12)$$

The relation between the amplitudes of two crystal waves are, then, from (8)

$$\left.\begin{aligned}\psi_h{}'&=\frac{v_0-V_{11}+N^2-(D+\varDelta)^2}{V_{12}}\psi_0{}'=X'\psi_0{}'\\ \psi_h{}''&=\frac{v_0-V_{11}+N^2-(D-\varDelta)^2}{V_{12}}\psi''=X''\psi_0{}''.\end{aligned}\right\}\qquad(13)$$

(b) The reflection coefficient.

Introducing the boundary conditions at the surface of the crystal, we get (See Fig. 2).

$$\begin{aligned}\frac{\varPsi_h}{\varPsi_0}=&\ [\{(N-D-\varDelta)+X'(N+D-\varDelta)\}\\ &\qquad+A\{N-D+\varDelta)+X''(N+D-\varDelta\}]\\ &\times[\{(N+D+\varDelta)+X'(N+D-\varDelta)\}\\ &\qquad+A\{(N+D-\varDelta)+X''(N-D-\varDelta)\}]^{-1},\end{aligned}$$

where

$$A=-\frac{(D+\varDelta-N)e^{i\Delta L}+X'(-D+\varDelta-N)e^{-i\Delta L}}{(D-\varDelta-N)e^{i\Delta L}+X'(-D-\varDelta-N)e^{-i\Delta L}}e^{2i\Delta L}. \qquad (15)$$

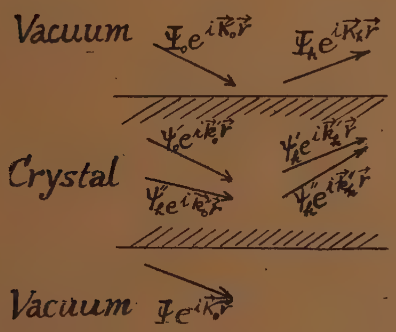
Vacuum
$\varPsi_0 e^{i\vec{K}_0\vec{r}}$
$\varPsi_h e^{i\vec{K}_h\vec{r}}$
Crystal
$\psi_0' e^{i\vec{k}_0'\vec{r}}$
$\psi_h' e^{i\vec{k}_h'\vec{r}}$
$\psi_h'' e^{i\vec{k}_0''\vec{r}}$
$\psi_h'' e^{i\vec{k}_h''\vec{r}}$
Vacuum
$\varPsi e^{i\vec{K}_0\vec{r}}$

Fig. 2.

$\varPsi_0$, $\varPsi_h$ are respectively the amplitudes of the incident and reflected waves in the vacuum, and L the thickness of the crystal.

As the reflection coefficient, we have

$$R=\left|\frac{\varPsi_h}{\varPsi_0}\right|^2. \qquad (16)$$

When $\varDelta$ is real, A and accordingly R are the periodic functions of the thickness of the crystal L. The reflection coefficient depends sensibly on the thickness of the crystal. But, since the real crystal has not a perfectly uniform thickness, we take, as is usually done, the mean of R over L.

When $\varDelta$ is imaginary, A decreases to zero for large L, and R does not depend on L but becomes nearly equal to unity. Selective reflection occurs in this case, and the electrons incident on the crystal is almost totally reflected.

(c) Positions and widths of the reflected spots.

The region of imaginary $\varDelta$ is bounded in terms of N by

$$\left.\begin{aligned}N^2_{\max}&=D^2-v_0+V_{11}\pm|V_{12}|\\ N^2_{\min}&=D^2-v_0+V_{11}-|V_{12}|.\end{aligned}\right\}\qquad(17)$$

Since $D^2-v_0+V_{11}\gg|V_{12}|$ in general,* we can write

$$\left.\begin{aligned}N_{\max}&=\sqrt{D^2-v_0+V_{11}}\left(1+\frac{1}{2}\frac{|V_{12}|}{D^2-v_0+V_{11}}+\dots\right)\\ N_{\min}&=\sqrt{D^2-v_0+V_{11}}\left(1-\frac{1}{2}\frac{|V_{12}|}{D^2-v_0+V_{11}}+\dots\right).\end{aligned}\right\}\qquad(18)$$

The value of N_m which corresponds to the middle point of the selective reflection is given by

$$N_m\fallingdotseq\frac{N_{\max}+N_{\min}}{2}\sqrt{D^2-v_0+V_{11}}, \qquad (19)$$

and the width of the selective reflection, by

$$\varDelta N=N_{\max}-N_{\min}=\frac{|V_{12}|}{\sqrt{D^2-v_0+V_{11}}}\fallingdotseq\frac{|V_{12}|}{N_m}. \qquad (20)$$

The position of the reflection spectra to be expected, when only a constant inner potential v_0 is assumed, is given by

$$N_0=\sqrt{D^2-v_0}, \qquad (21)$$

which is different from N_m, by the quantity V_{11}.

Since the glancing angle is determined by N (Fig. 1), we obtain from (2), (3) and (20);

$$E_n=\frac{8\pi^2me}{h^2}(D^2-N^2{}_m)=\frac{8\pi^2me}{h^2}(v_0-V_{11}); \qquad (22)$$

$$E_0=\frac{8\pi^2me}{h^2}v_0.$$

It is thus clear that the deviation of the reflected beams from the Bragg angle is caused not only by the constant term in the Fourier expansion of the crystal potential, i. e., the mean inner potential v_0, but also all the periodic terms v_g. The value of the apparent mean inner potential should be corrected by

---

* This approximation does not hold for the lowest order reflection.

Table I. Apparent mean inner potential obtained by Yamaguti and the corrected value. (in volts.)

order n	1 (002)	2 (004)	3 (006)	4 (008)	6 (0010)	6 (0012)
Yamaguti's result	1.54±0.15	6.84±0.09	8.00±0.10	8.37±0.09	8.17±0.16	8.36±0.16
ΔE_n	−1.00	+0.93	+0.50	+0.28	+0.17	+0.12
ΔE_n by Uyeda	−0.75	+0.79	+0.48	+0.25	+0.16	+0.11
Corrected value	0.54	7.77	8.50	8.65	8.34	8.48

$$\Delta E_n = E_0 - E_n = \frac{8\pi^2 me}{h^2} V_{11}, \qquad (23)$$

in order to get the true mean inner potential.

§ 3. Comparison with the Experiment.

V_{11} can be divided into two parts, as Uyeda(14) has pointed out;

$$V_{11} = V_{11}' + V_{11}'' = \sum_{g_1 = g_2 = 0}'' \frac{v_g v_{-g}}{\kappa^2 - k_g^2} + \sum_{\text{except } g_1 = g_2 = 0} \frac{v_g v_{-g}}{\kappa^2 - k_g^2}. \qquad (24)$$

The second term depends on the azimuth of the incident plane but the first term does not. The second term can take any value ranging from a negligible small value to a very large one and it can happen even that the denominators of one or more terms become zero. In the last case, however, a simultaneous reflection is occuring, and there are three or more waves of large amplitudes in the crystal. Our theory loses its validity in this case.

We will limit our later calculation to the case where no simultaneous reflection occurs. In the expression (24), $\kappa^2 - k_g^2$ is always large for the terms for which $g_2 \neq 0$, and $v_{-g} v_g / (\kappa^2 - k_g)$ becomes negligibly small. Then, since $(\kappa)_y \fallingdotseq (k_g)_y$, we have, taking (20) into account,

$$\kappa^2 - k_g^2 = N^2 + v_0 - [(k_g)_x^2 + (k_g)_z^2]$$

$$= \left(\frac{h}{2} d\right)^2 + V_{11} - \left[g_1^2 d^2 + \left(g_3 d - \frac{h}{2} d - \delta\right)^2\right],$$

when δ is small,*

$$\kappa^2 - k_g^2 = V_{11} + d^2 [g_3 (h - g_3) - g_1^2].$$

Therefore, we get

$$V_{11} = \sum'' \frac{v_g v_{-g}}{V_{11} + d^2 [g_3 (h - g_3) - g_1^2]}. \qquad (25)$$

Substituting (25) again into V_{11} in the denominator of (25), we have, since V_{11} is small,**

$$V_{11} \doteqdot \sum'' \frac{v_g v_{-g}}{d^2 [g_3 (h - g_3) - g_1^2] + \sum'' \dfrac{v_g v_{-g}}{d^2 [g_3 (h - g_3) - g_1^2]}}. \qquad (25')$$

On the other hand, v_g can be expressed in terms of the crystal structure factor of the nuclear charge Z_g and of the electrons F_g, by

$$v_g = \frac{8\pi^2 n e}{h^2} (Z_g - F_g). \qquad (26)$$

In our calculation, we have used the atomic structure factor obtained by Brill and his coworkers,(15) and in order to take into account of the heat motion of the atoms, Debye's temperature factor modified by Waller and James(16) has been used both on the atomic and on the nuclear structure factors.***

The result of the calculation on the azimuth in which the first term of V_{11}'' in (24) has a finite value and the second term is negligible, is given in Table I and Fig. 3, where it is compared with Yamaguti's experimental result(17) and the value calculated by Yamaguti using Uyeda's formula.(18)

As is seen in Fig. 3, the magnitude of the correction introduced by the periodic terms of the potential is insufficient at the low order reflections (1st anomaly), and even the sign of the correction is, at the lowest order reflection, opposite to the requirement (2nd anomaly).

---

* This approximation is not so good for the lowest order reflection.

** This expression differs slightly from Uyeda's in the denominator.

*** This procedure corresponds to having a time average of the charge density.

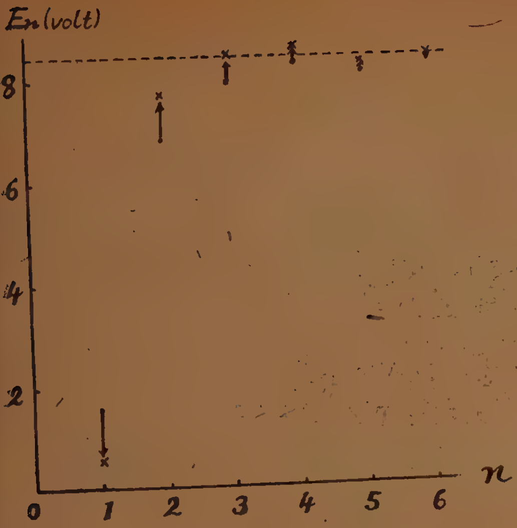

Fig. 3.

(·): The apparent mean inner potential.
(×): The corrected value.
n: Order of reflection.

Since the discrepancy is most remarkable for the lowest order reflection, we will further give a special consideration to that reflection (2nd anomaly). If a value of 8.48 volts* is assumed for the mean inner potential of NaCl, we have immediately from (18);

$$N^2_{\max} = 0.41 = (0.64)^2.$$

$$N^2_{\min} = -2.90 = -(1.70)^2.$$

It is to be noted that, as $N_{\min}$ becomes negative, the expression (20) and consequently the correction formula (23) cannot be used for the lowest order reflection. The negative value of ΔE in (a) and (b) obtained by all prevoius authors from (23) are therefore meaningless.

The actual feature of the intensity curve for the lowest order reflection predicted by the theory is given approximately by the full line in Fig. 4. This is not in accord with the experimental result. The lowest order reflection can be experimentally observed at a small glancing angle and this peak of reflection is not a flat one continuing from zero glancing angle. The observed intensity curve will have an appearance not much different from the one given by the dotted line.

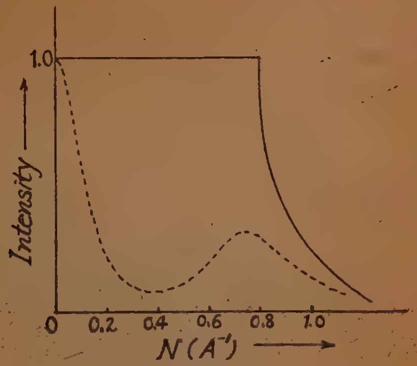

Fig. 4. Intensity curve for the lowest order reflection.

— : The curve expected from the theory.
····· : The approximate feature of the observed curve.
(Schematically drawn.)

It is thus clear that there exists a serious discrepancy between the experiment and the present theory. We will examine the appropriateness of our approximation and also look for other causes which will influence the experiments in the next papar.

References.

(1) T. Yamaguti: Proc. Phys.-Math. Soc. Japan, **16** (1934), 95.
(2) W. E. Laschkarew: Zeits. f. Phys., **86** (1933), 797; **89** (1934), 820.
(3) S. Kikuchi: Sci. Pap. Inst. P. C. R., **26** (1935), 225.
(4) S. Miyake: Sci. Pap. Inst. P. C. R., **27** (1935), 286.
(5) R. Uyeda: Proc. Phys.-Math. Soc. Japan, **20** (1938), 280.
(6) T. Yamaguti: Proc. Phys.-Math. Soc. Japan, **23** (1941), 433.
(7) C. G. Darwin: Phil. Mag., **27** (1914), 675.
J. A. Prins: Zeits. f. Phys., **63** (1930), 477.
(8) P. P. Ewald: Ann. d. Phys., **54** (1917), 519; 557.
M. v. Laue: Erg. d. ex. Naturwis., X (1931), 133.
M. Kohler: Berliner Ber. Phy.-Math., Kl. XIX. (1935), 1.
G. Moliere: Ann. d. Phys, **35** (1939), 272; 297.
(9) J. W. Harding: Phil. Mag., **23** (1937), 271.
(10) H. Bethe: Ann. d. Phys., **87** (1928), 55.
(11) S. Kikuchi: cf. (4).
(12) K. Moliére: Ann. d. Phys., **34** (1939), 461.
(13) E. Lamla: Ann. d. Phys., **34** (1939), 461: Jour. f. d. reine u. angew. Math., **79** (1938), 134.
(14) R. Uyeda: cf. (5).
(15) R. Brill, H. G. Grimm, C. Hermann & C. Peters: And. d. Phys,, **34** (1939), 393.

---

* This value has been obtained by Yamaguti.(19)

(16) J. Waller and R. W. James: Proc. Roy. Soc., **117** (1927), 214.
(17) T. Yamaguti: cf. (7).
(18) R. Uyeda: cf. (5).
(19) T. Yamaguti: cf. (7).

On the Anomalies of the Small Angle Reflection of Cathode Rays from the Surface of a Single Crystal. Part II. The Investigation on the Causes of the Anomalies.

By Kazutake KOHRA and Ken-ichi SHINOHARA.

Institute of Applied Science, Faculty of Engineering, Kyushu University

Department of Physics, Faculty of Science, Kyushu University.

(Recieved October 16, 1948)

Abstract.

The causes of the anomalies in the low order reflection of the cathode rays from the surface of a single crystal have been considered. It is shown that the anomalies cannot be attributed to the effect of the azimuth nor the poorness of the approximation of the calculation, but can be explained, for the greater part, by a simple geometrical consideration.

§ 1. Introduction.

In Part 1,⁽¹⁾ it is shown that, theoretically, the region of the selective reflection is given by the normal components of the wave vectors:

$$\left.\begin{aligned} N_{\max} &= \sqrt{D^2-v_0+V_{11}+|V_{12}|}\,, \\ N_{\min} &= \sqrt{D^2-v_0+V_{11}-|V_{12}|}\,. \end{aligned}\right\} \qquad (1)$$

and the value of the true mean inner potential E_0 can be obtained by applying the correction ΔE_n to the apparent mean inner potential E_n for the higher reflections:

$$E_0 = E_n + \Delta E_n\,, \qquad (2)$$

where

$$\Delta E_n = \frac{8\pi^2 me}{h^2} V_{11}\,. \qquad (3)$$

We have seen that these results are not in accord with the experiment and there exist the so-called 1st and 2nd anomalies. In an effort to find out the causes of these anomalies, we will first consider the appropriateness of the assumptions which have been adopted for V_{11} and V_{12} in calculating (1) and (3). We will then study other physical conditions.

§ 2. The Effect of the Azimuth.

As described in Part 1, both V_{11} and V_{12} are divided into the two parts, the part which does not depend on the azimuth and the part which depends on it:

$$V_{11} = \sum_{g_1=g_2=0}'' \frac{v_g v_{-g}}{\kappa^2-k_g^2} + \sum_{\text{except } g_1=g_2=0} \frac{v_g v_{-g}}{\kappa^2-k_g^2} = V_{11}' + V_{11}'' \qquad (4)$$

$$V_{12} = -v_h + \sum_{g_1=g_2=0}'' \frac{v_g v_{h-g}}{\kappa^2-k_g^2} + \sum_{\text{except } g_1=g_2=0} \frac{v_g v_{h-g}}{\kappa^2-k_g^2} = -v_h + V_{12}' + V_{12}'' \qquad (5)$$

In part 1, we carried out the calculation for the cases when the parts depending on the azimuth V_{11}'' and V_{12}'' are negligibly small. The magnitudes of these second terms, however, change greatly as the azimuth of the incident plane is varied with respect to the crystal axis. For example, in the (1 0 0) azimuth, viz., when the incident plane is parallel to the (1 0 0) plane, if the primary beam is directed at an angle required for the (0 0 4n) reflection, simultaneous reflection occurs and the beam is reflected at the same time, also by the (2n 0 2n) and ($\bar{2n}$ 0 2n) planes. (Fig. 1). In this case, then, the present theory loses its applicability. If the beam is directed at an angle required for the (0 0 2(2n+1) reflection, no simultaneous reflection occurs, but several terms in V_{11}'' become rather large. For the latter case, we can calculate ΔE_n and $N_{\max}$, $N_{\min}$ from (1) and (3); for the (0 0 6) reflection,

$$\Delta E_n = (0.50-1.79) = -1.29, \quad \text{(in volts)} \qquad (6)$$

and for the (0 0 2) reflection,

$$\left.\begin{aligned} N^2_{\max} &= 0.26 = (0.51)^2, \\ N^2_{\min} &= -5.85 = -(2.42)^2. \end{aligned}\right\} \qquad (7)$$

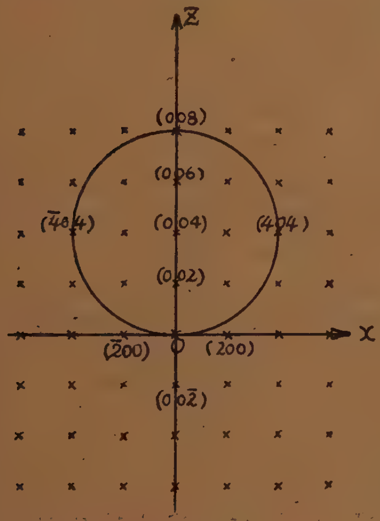

Fig. 1. Reciprocal lattice and Ewald's sphere.

In Part I, the value obtained for ΔE_n was 0.50 (in volts) for the (0 0 6) reflection, and $N^2_{\max} = 0.41 = (0.64)^2$ and $N^2_{\min} = -2.90 = -(1.70)^2$ have been obtained for the (0 0 2) reflection. From (6) we see that the sign of ΔE_n in the (0 0 6) reflection in this azimuth becomes even opposite to that obtained in Part I, and, consequently, the apparent mean inner potential becomes larger than the true one*. As for the (0 0 2) reflection, it is seen from (7) that the essential theoretical feature is not different, even in this special azimuth, from the one shown in Part I, and there still remains the discrepancy between the theory and the experiment.

It is, therefore, concluded that the effect of the azimuth can not explain the 1st and 2nd anomalies, although it has the considerable effect on the higher order reflections.

§ 3. Test of the Higher Approximation.

We have assumed, in our calculation, that V_{11} and V_{12} are both constants. This approximation loses its validity when the glancing angle becomes small. In this case we must take V_{11} and V_{12} as the functions of N and δ. We can write (Fig. 2)

$$\kappa^2-k_g{}^2 = N^2+v_0-\left(g_3 d-\frac{h}{2}d-\delta\right)^2, \qquad (8)$$

then we have

$$\frac{1}{\kappa^2-kg^2} = \frac{1}{d^2 g_3(h-g_3)}\left(1-\frac{\zeta^2}{dg_3(h-g_3)}\right.$$
$$\left.+\frac{\delta(2g_3-h)}{dg_3(h-g_3)}-\frac{\delta^2}{d^2 g_3(h-g_3)}+\cdots\right). \qquad (9)$$

when the summation in V_{11} and V_{12} is limited to the terms not depending on the azimuth, $(g_1 = g_2 = 0,\ g_3 \neq 0)$, where,

$$\zeta^2 = N^2+v_0-\left(\frac{h}{2}d\right)^2. \qquad (10)$$

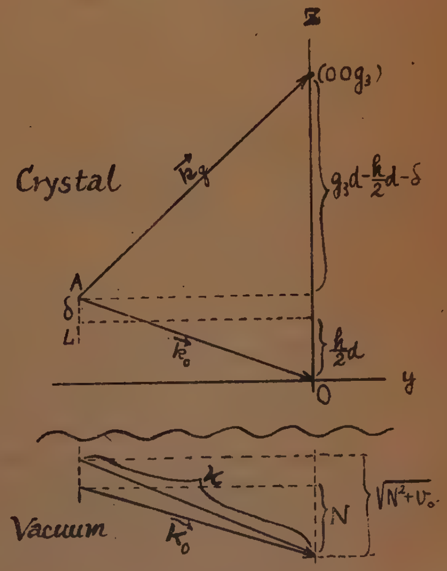

Fig. 2.

---

* This tendency seems to be found not only for the (0 0 6) reflection, but in the other higher order reflections. This fact seems not to have been noticed by any previous authors, although, in the usual experiments, such a special azimuth has not been used.

Usually the last three and the higher terms are neglected and only the first term is used in calculating the dispersion equation. If the higher terms are not neglected we have, instead of (11) in Part I, as the dispersion equation:

$$\delta^4+0.239\,\delta^3-(2\,\zeta^2+5.191)\delta^2-(0.238\,\zeta^2+0.012)\delta$$
$$+\zeta^4+0.494\,\zeta^2-0.520=0 \qquad (11)$$

In (11) proper numerical values are already inserted for the atom factors and other quantities.

Since the terms of δ^3 and δ in this equation are small, they can be negleted to get an approximate solution. The region of negative δ^2 in the resulting quadratic equation for δ^2 will then give the region of the selective reflection appoximately. The actual solution of the biquadratic equation (11) will probably be such that they are given by complex quantitics of which imaginary part are not much different from the ones obtained by solving the quadratic equation in δ^2. The region of selective reflection thus obtained is give by

$$\left.\begin{array}{l} N^2_{\text{max}} \doteq 0.38 \doteq (0.62)^2, \\ N^2_{\text{min}} \doteq -2.84 \doteq -(1.69)^2 \end{array}\right\} \qquad (12)$$

With this higher approximation, the feature of the theoretical diffraction pattern does not show much change, and the experimental fact cannot, still, be explained. It seems possible that the discrepacy of the experimental result with the calculated one does not lie in the poorness of the approximation, but in some other causes, which we have not yet considered.

§ 4. The Effective Cross Section of the Incident Beam Striking the Surface of the Crystal.

Since thd incident beam of electrons has a finite cross section and the crystal, too, is of the finite size, the total number of electrons striking the crystal surface varies with the galncing angle. In Fig. 3, let p be the width of the electron beam in the plane of incidence and, l, the width of the crystal, in the same plane. All incoming electrons can strike the crystal if the glancing angle is larger than α determined by:

$$\sin\alpha=\frac{p}{l} \qquad (13)$$

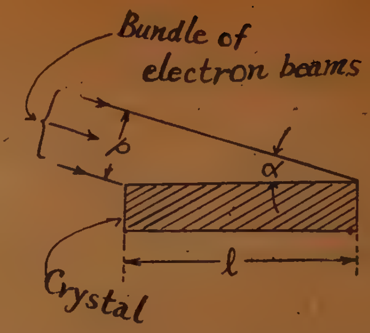

Fig. 3. Geometrical condition of the electron beams and the crystal.

At a small angle, only a part of the electrons can strike the surface and this fraction of the effective beam decreases almost linearly with the glancing angle. If we suppose l and p to be about 3 mm and 0.1 mm. respectively, we have $\alpha=0.03$, which corresponds to $N=4.71A^{-1}$ when $\lambda=0.04\,A^{-1}$ (about 40 kv.).

Fig. 4 shows the feature of the reflection spectra. Curve *a* represents the fraction of the beam actually striking the surface as a function of N, the dotted curve *b*, the reflectivity expected from the dynamical theory, and the full curve *c*, the intensity of reflected beam obtained by modifying the curve *b* with the use of the curve *a*.

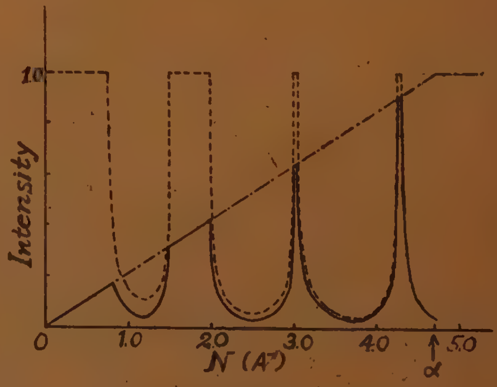

Fig. 4. Intensity curves.

a) -·-·-·- : The intensity curve of the effective incident beam.

b) - - - - - : The curve expected by the dynamical theory.

c) ——— : The curve obtained by modifying curve *b* with curve *a*.

The curve *c* shows a maximum of the reflected beam at a small glancing angle, in conformity with the experimental result. The maxima of the 2nd, 3rd, and 4th order reflections are shifted to the upper limits of the selective reflections.

If we assume that the positions of the low order reflections are measured at each maximum of the full curve c, we get, as the correction for the apparent mean inner potential for the lowest order (0 0 2) and the second order (0 0 4) reflections;

$$\varDelta E_{002} \doteqdot 5.48,$$
$$\varDelta E_{004} = 1.74. \qquad \text{(in volts.)}$$

The corresponding experimental values of Yamaguti⁽²⁾ are

$$\varDelta E_{002} = 6.98$$
$$\varDelta E_{004} = 1.64 \qquad \text{(in volts.)}$$

The agreement between the experimental and the theoretical values are fairly good.

§ 5. Discussions.

We think that the anomalies in the low order reflections (the 1st and the 2nd anomalies) are accounted for, for the greater part, by taking the geometrical consideration in addition to the dynamical effect of all the periodic terms in the Fourier expansion of the crystal potential.

Some other probable causes such as the distortion of the spacings near the surface, the adsorbed layers on it and the effect of absorption of electrons have already been discussed by some authors as responsible for the anomalies. Yamaguti's⁽³⁾ consideration on the effect of the distortion of spacings near the surface shows that, in order to explain the anomalies, the spacings must be taken as very much expanded, which is utterly inadmissible from the theory of the ionic binding. The theory expects, rather, the contraction of the spacing. Harding⁽⁴⁾ studied the effect of the adsorbed layers. He shows that such layers will affect the width and the shape of the reflected spot to some extent, but we do not believe that they can explain the anomalous positions of the low order reflections satisfactorily.

The effect of the absorption of the electrons in the crystal will be treated in the next paper where it will be shown that the inclusion of this effect will modify the curve c and a better agreement will be obtained with the observed feature of reflection.

References.

(1) K. Kohra and K. Shinohara: J. Phys. Soc. Jap. **4** (1949), 155.
(2) T. Yamaguti: Proc. Phys.-Math. Soc. **23** (1941), 433.
(3) T. Yamaguti: cf. (1).
(4) J. W. Harding: Camb. Phil. Mag. **23** (1937), 271.

On the Velocity of Displacement of Magnetic Domain Boundary.⁽¹⁾

By Takasi HUZIMURA and Tatsuya KATAYAMA.

Research Institute for Iron, Steel and other Metals, Tohoku University.

(Read April 10, 1948; Received October 25, 1948)

It is usually supposed that the elementary process of magnetization is reduced to the displacement of boundary between magnetic domains. However, exact theories concerning the mechanism of the displacement of this boundary have not been published. The velocity of displacement, of course, is affected by the electric current in the ferromagnetic substance induced by the discontinuous change of magnetization, yet it is still assumed that the essential factor is not the action of this eddy current.*

---

* We confirm this conclusion from the experimental results about temperature dependence of propagation velocity of a magnetic boundary in a metallic ferromagnetic substance. The results will be published in J. Phys. Soc. Jap.

Recently one of the the writers(2) treated this problem quantum-mechanically on the basis of a simple model of the domain boundary and found that if no eddy current is induced the velocity will be independent of temperature. In connection with his theoretical result, it is desired to confirm the theory by a measurement of the displacement velocity of the domain boundary. In order to eliminate the influence of eddy current which occurs in metallic ferromagnetica accompanied with the reversal of magnetic domain, one may observe the said velocity on the ferromagnetic semi-conductor, instead of ordinary metallic ferromagnetica, and for this reason, the present authors observed the Barkhausen effect of semi-conductor, Fe_3O_4, at temperatures, 10°C and −140°C, and elucidated a conclusion on the dependence of the displacement velocity on the temperature. The results obtained agree with the theoretical result stated above. In the following lines, we will describe the methods and the results of our measurement.

The form of the specimen is a rectangular rod of the dimensions 14×2×2 mm.[3], the axis of which lies along the [100]-direction of a natural magnetite single crystal. As this sample has an allotropic transformation temperature near −150°C[3], the experiments are carried out at two points above the transformation temperature, namely 10°C and −140°C. The magnetic hysteresis curves at both temperatures are shown in Fig. 1. The measuring circuits of the Barkhausen effect are schematically shown in Fig. 2. In the figure, C is a magnetizing solenoid, B is another solenoid placed coaxially with C and gives a smoothly varying magnetic field. A is a search coil, the length and diameter of which are 30 mm. and 3.5 mm. respectively and with a total number of 10000 turns. E is a Braun-tube oscillograph. The search coil is large enough compared with the specimen (S), so that the magnetic reversal occured at any point of the specimen induces electro-motive forces under the same condition in the coil. A, B and S are installed in a Dewer's vessel and cooled in the evaporating gas of liquid air. When the temperature of the specimen reaches −140°C, the observation of the Barkhausen effect is carried out.

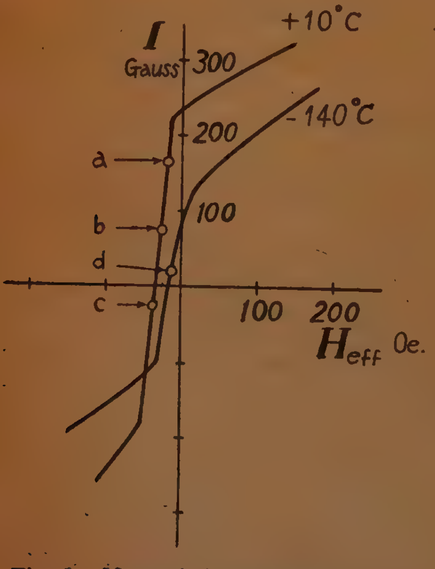

Fig. 1. Magnetic hysteresis curves of Magnetite crystal in [100]-direction.

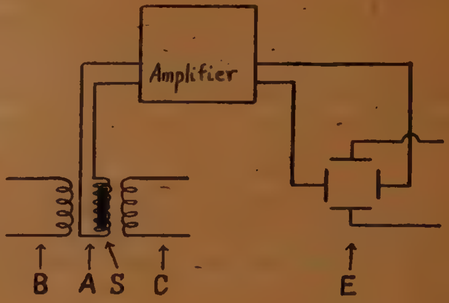

Fig. 2. Measuring circuit.

This specimen is once magnetized near saturation by means of applying the magnetic field of 300 Oersted by the solenoid C, then, brought to the desired stage of magnetization: when another smoothly varying field is superposed by B, a number of Barkhausen impulses appear on the fluorescence screen of the Braun-tube oscillograph. The range of field change is 1.5 Oersted and its rate of change is 0.02 Oersted per sec. When sweeping speed of the spot of Braun-tube is suitable, one can observe that the form of Barkhausen impulses are simple structureless peaks and they appear one by one and do not overlap each other, so that one is able to measure the time of duration of each impulse by means of its oscillograms. Times of duration for a large number of impulses at constant temperature and around a certain magnetization of the specimen are measured, and thus one can determine the occurrence frequency of the time of duration. At first, the observations are made at three points on the descending branch of the hysteresis curve (marked a, b, c in Fig. 1) at

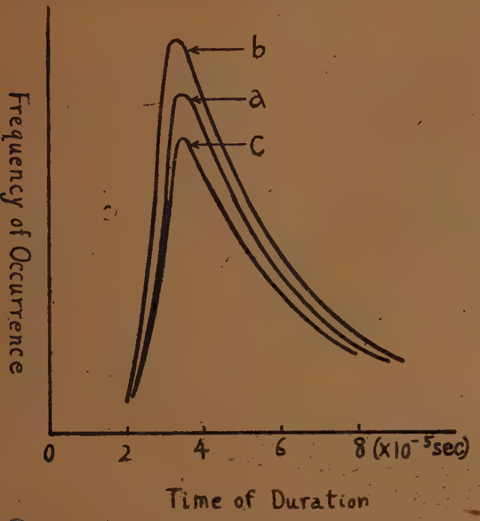

Fig. 3. Three distribution curves of duration time on magnetic hysteresis curve at 10°C. Total numbers of impulses are for a 243, for b 227 and for c 215.

100°C. Three distribution curves of the occurrence of duration time are given in Fig. 3. As it shows, the said distributions are not essentially changed by the intensity of magnetization. Next, the observations of the time of duration at-140°C ($I =$ 30 gauss, pointed in Fig. 1) is made, and the result is duplicated in Fig. 4 together with that at 10°C (b). Observed values of the time of duration of each simple Barkhausen jump lie between 2 and 9×10^{-5} sec. One may find from these results that the values of the time of duration corresponding to maximum frequency c incide with at 10°C and -140°C and are independent of its intensity of magnetization.

Now we shall discuss on the theoretical results above stated, that the displacement velocity of the boundary is independent of temperature. One will find that the present experiment supports this theoretical results. Because it is usually supposed that the distribution of domain boundaries in the ferromagnetic substance depends mainly on its internal stress distribution; now, the stress distribution is not so greatly affected by the fall of temperature, so that it will be concluded that the distribution of domain boundary does not change

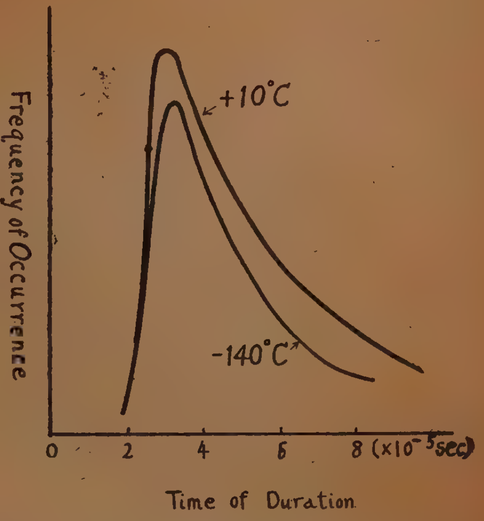

Fig. 4. The distribution curves of duration time at 10°C (point b in Eig. 1) and --140°C (point d in Fig. 1).

Total numbers of impulses are for b 227 and for d 179.

at both temperatures. As an evidence for it, the statistical size of each single Barkhausen jump at 10°C and —140°C is also observed and it is found that this does not change with temperature. Consequently, from observed coincidence of the time of duration of the Barkhausen jump at different temperatures, one may conclude that the velocity of the diplacement of magnetic boundary is not affected by temperature.

Moreover, a discussion on the observed invariance of the distribution of the duration time at various portions of the magnetization curve at the same temperature is given here. One of the present authors also found theoretically that the displacement velocity of the boundary by an isothermal magnetization is proportional to the magnetic field acting at the domain boundary. This theoretical result contradicts apparently with the observed invariance of the velocity. However, the discontinuous displacement of the domain boundary occurs when the field acting at the domain boundary in question takes an appropriate value against the brake action due to the so-called critical field H_0⁽⁴⁾ and the influence of free pole in the ferromagnetic substance and the surface energy of domains. The magnetic field around the domain boundary is the superposition of the external field and the action of free magnetic pole at domain boundary. As the free pole distribution is not known, one can not know the magnetic field due to the free pole, so that one can not find the exact value of the magnetic field at the displacing domain boundary. Consequently, it is very difficult to verify whether or not the said contradiction between theory and experiment really exists.

In conclusion the writers wish to express their hearty thanks to Dr. T. Hirone under whose direction the work was done.

A part of the present study was carried out by fund defrayed from the Ministry of Education (Item number 1306).

References.

(1) Report of the Research Institute for Iron, Steel and other Metals, Tohoku University.
(2) T. Katayama: A report will be published in this Journal earlier than this paper.
(3) T. Okamura: Sci. Rep. **21** (1922), 193.
(4) K. J. Sixtus and L. Tonks: Phy. Rev. **37**, (1931) 930. Phys. Rev. **42**, (1932) 419.

Probabilities of Beta Decay and Orbital Electron Capture for the Forbidden Transitions.*

By Seitaro NAKAMURA, Soei SIMA and Minoru KOBAYASI.

Physics Institute, University of Tokyo *Now at Shanghai, China* *Physics Institute, University of Kyoto*

(Received February 26, 1949).

Abstract.

Total probabilities for the beta decay and the orbital electron capture are calculated according to the Fermi theory in the case of the first and the second forbidden transitions. In this case, the ratio of the probabilities for the positron emission to those for the K-electron capture are also estimated as a function of the nuclear charge and the nuclear radius.

§ 1. Introduction.

The theory of the bata decay first proposed by Fermi was successful in explaining the general features of the experiments, but in finer detail the theory remains much to be refined. As the experimental materials available to test the theory we have: 1) the shapes of the continuous spectra of the beta rays, 2) the selection rules for the beta decay and 3) in the case of positron emitters, the relative values of the probabilities of the positron emission to those of the orbital electron capture. To accomplish the theoretical analysis less ambiguously, Konopinski and Uhlenbeck[1] developed the theory for the forbidden transitions. And thus the electron spectra of some radioactive elements, such as RaE, P^{32}, and Na^{24} which deviate appreciably from the Fermi theory and rather fit in with the so-called K-U type, could excellently be reproduced by the corresponding forbidden formula. This result seems to promise possibilities for trusting the Fermi theory without any modifications. Konopinski and Uhlenbeck's calculations, however, ended in deciding the energy distribution curve. In this circumstance, we proceed in the following to evaluate the formula of total probabilities for the forbidden beta decay and orbital electron capture. This may serve as one of the theoretical tools for testing the theory in the case of 2) and 3) mentioned above. The main features of the results are shown as follows:

A). For the forbidden transitions the dependence of the probability formula on the nuclear constructions, i. e., the nuclear charge Ze and the nuclear radius ρ, becomes more sensitive than for the allowed ones. Therefore, the relationship between the half life of the beta emitters and the maximum energy of the particles has a different form as would at first be expected, such as the pure seventh power law in the first forbidden transitions. This indicates that the Sargent rule should be carefully adopted in the forbidden cases:

---

* The work had already been done in 1943, but the publication was delayed on account of the war circumstances.

B) The ratio of the probabilities of the positron emission to those of the K-electron capture is given for the forbidden transitions with the consideration of the L-electron capture, the contribution of the latter being found to be 20% to the former when Z is small.

C) By using the empirical values of the life times of the radioactive elements and the maximum energy of the beta particles, we have calculated the semi-empirical values for the matrix elements of beta decay in the forbidden transitions in some simple cases. The values thus estimated for the matrix elements are subject to further theoretical study.

§ 2. Total Probabilities for the First and the Second Forbidden Transitions.

The Fermi theory of beta decay which was remarkably extended to the case of the forbidden transitions by Konopinski and Uhlenbeck(1) predicts the number of electrons $P(W)dW$ emitted into the energy range dW at W in the following expression,

$$P(W)\,dW = \frac{G^2}{2\pi^3}\,C(\pm Z, W)\,F(\pm Z, W)\,p(W_0-W)^2\,W\,dW \qquad (1)$$

which is contrasted to the allowed one,

$$P(W)\,dW = \frac{G^2}{2\pi^3}\,C_0F(\pm Z, W)\,p(W_0-W)^2\,W\,dW. \qquad (2)$$

Here $p = (W^2-1)^{1/2}$ is the momentum of the electron, W_0 its maximum energy, G is the dimensionless Fermi constant. The units of time, length, and energy are h/mc^2, h/mc, and mc^2, respectively. $F(\pm Z, W)$ represents the effect of the nuclear charge Ze to the electron, which is given

$$F(\pm Z, W) = \frac{4}{\{\Gamma(1+2s)\}^2}\,(2p\rho)^{2s-2}\,e^{\pm\frac{\alpha ZW}{p}} \cdot \left|\Gamma\left(s+i\frac{\alpha ZW}{p}\right)\right|^2 \qquad (3)$$

where Z and $-Z$ mean the case of the electron and the positron, respectively, ρ is the nuclear radius, $s = \sqrt{1-\alpha^2Z^2}$. $C(\pm Z, W)$ represent correction factors which are certain functions of p, W, Z, ρ, and the nuclear matrix elements, and are fully listed in Konopinski and Unlenbeck's paper. Especially, in the case of allowed transition it reduces the simple matrix element $|\int\sum_k V^*Q_kUd\tau|^2$ but in the forbidden cases they involve the combined influences from the relativistic effects of the nuclear motion and from the higher rotation states of the electron (other than the s electron).

In order to obtain the total probabilities for the beta decay in the forbidden transitions, we performed the elementary but tedious integrations of (1) in the energy interval ($W = 1$, $W = W_0$). Since Z is not so large, i.e. $Z<30$, for the important cases, we have approximated $F(\pm Z, W) = 1$, whose error is estimated to about 1% when $Z<30$. As is well known, the marked dependence of the formula on the nuclear charge Ze appears through the correction factors $C(\pm Z, W)$, not through $F(\pm Z, W)$ in the forbidden transitions. For the five interactions of the Fermi type,

$$\{V^*\beta_k Q_k u)(V^*\beta\varphi_{.k}\},$$

$$\{V^* Q_k u)(\psi^k\varphi)_k-(V^*\vec{\alpha}_k Q_k u)(\psi^*\vec{\alpha}\varphi)_k\},$$

$$\{(V^*\beta_k\vec{\sigma}_k Q_k u)(\psi^*\beta\vec{\sigma}\varphi)_k+(V^*\beta_k\vec{\alpha}_k Q_k u)(\psi^*\beta\vec{\alpha}\varphi)_k\},$$

$$\{(V^*\vec{\sigma}_k Q_k u)(\psi^k\vec{\sigma}\varphi)_k-(V^*\gamma_{5k} Q_k u)(\psi^*\gamma_5\varphi)_5\},$$

$$\{(V^*\beta_k\gamma_{5k} Q_k u)(\psi^*\beta\gamma_5\varphi)_k\}, \qquad (4)$$

the results of the integrations are given below.

$$\frac{1}{\tau_{1S}} = \frac{G^2}{\Pi^2}|\int\vec{r}|^2\left\{I_3(W_0^6)+\frac{\alpha^2Z^2}{4\rho^2}I_0(W_0^4)\right\}$$

$$\frac{1}{\tau_{1V}} = \frac{G^2}{\Pi^2}\Big[|\int\vec{r}|^2\left\{J_4(W_0^6)+\frac{\alpha^2Z^2}{4\rho^2}I_0(W_0^4)\pm\frac{\alpha Z}{\rho}I_1(W_0^5)\right\}$$
$$+|\int\vec{\alpha}|^2 I_0(W_0^4)+i\{(\int\vec{\alpha})(\int\vec{r})^*-(\int\vec{\alpha})^*(\int\vec{r})\}$$
$$\cdot\left\{I_2(W_0^5)\pm\frac{\alpha Z}{2\rho}I_0(W_0^4)\right\}\Big].$$

$$\frac{1}{\tau_{1T}} = \frac{G^2}{\Pi^2}\Big[|\int\vec{\sigma}\cdot\vec{r}|^2\left\{I_5(W_0^6)+\frac{\alpha^2Z^2}{4\rho^2}I_0(W_0^4)\pm\frac{\alpha Z}{\rho}I_1(W_0^5)\right\}$$
$$+|\int\vec{\alpha}|^2 I_0(W_0^4)$$

$$+|\int\vec{\sigma}\times\vec{r}|^2\left\{I_8(W_0^6)+\frac{\alpha^2Z^2}{4\rho^2}I_0(W_0^4)\pm\frac{\alpha Z}{\rho}I_2(W_0^5)\right\}$$

$$-\{(\int\tilde{\sigma}\times\vec{r})(\int\vec{\alpha})^*+(\int\vec{\sigma}\times\vec{r})^*(\int\vec{\alpha})\}$$

$$\cdot\left\{I_2(W_0^5)\pm\frac{\alpha Z}{2\rho}I_0(W_0^4)\right\}+(\Sigma_{ij}|B_{ij}|^2)\,I_9(W_0^6)\Big].\tag{5}$$

$$\frac{1}{\tau_{1A}}=\frac{G^2}{\Pi^2}\Big[|\int\vec{\sigma}\vec{r}|^2\left\{I_6(W_0^6)+\frac{\alpha^2Z^2}{4\rho^2}I_0(W_0^4)\pm\frac{\alpha Z}{\rho}I_1(W_0^5)\right\}$$

$$+|\int\gamma_5|^2I_0(W_0^4)-i\{(\int\vec{\sigma}\cdot\vec{r})(\int\gamma_5)^*-(\vec{\sigma}\vec{r})^*(\int\gamma_5)\}$$

$$\cdot\left\{I_2(W_0^5)\pm\frac{\alpha Z}{\rho}I_0(W_0^4)\right\}$$

$$+|\int\vec{\sigma}\times\vec{r}|^2\left\{I_7(W_0^6)+\frac{\alpha^2Z^2}{4\rho^2}I_0(W_0^4)\right\}$$

$$+\Sigma_{ij}|B_{ij}|^2I_9(W_0^6)\Big].$$

$$\frac{1}{\tau_{2s}}=\frac{G^2}{\pi^2}(\Sigma|R_{ij}|)^2\left\{I_{15}(W_0^8)+\frac{\alpha^2Z^2}{48\rho^2}I_{10}(W_0^6)\right\}.$$

$$\frac{1}{\tau_{2V}}=\frac{G^2}{\pi^2}\Big[\{\Sigma|R_{ij}|^2\}$$

$$\cdot\left\{I_{16}(W_0^8)+\frac{\alpha^2Z^2}{48\rho^2}I_{10}(W_0^6)\pm\frac{\alpha Z}{90\rho}I_{14}(W_0^7)\right\}$$

$$+\{\Sigma|A_{ij}|^2\}I_9(W_0^6)-i\{R_{ij}A_{ij}^*-R_{ij}^*A_{ii}\}$$

$$\cdot\left\{I_{12}(W_0^7)\pm\frac{\alpha Z}{24\rho}I_{11}(W_0^6)\right\}$$

$$+|\int\vec{\alpha}\times\vec{r}|^2\left\{I_7(W_0^7)+\frac{\alpha^2Z^2}{4\rho^2}I_0(W_0^4)\right\}\Big],$$

$$\frac{1}{\tau_{2T}}=\frac{G^2}{\pi^2}\Big[\{\Sigma|S_{ijk}|^2\}\Big]\frac{1}{72}I_{17}(W_0^8)$$

$$+\{\Sigma|T_{ij}|^2\}\frac{1}{12}$$

$$\cdot\left\{I_{19}(W_0^8)+\frac{\alpha^2Z^2}{16\rho^2}I_1{}^0(W_0^6)\pm\frac{\alpha Z}{30\rho}I_{14}(W_0^7)\right\}$$

$$+\{\Sigma|A_{ij}|^2\}I_9(W_0^6)-\{\Sigma T_{ij}A_{ij}^*+\Sigma T_{ij}^*A_{ij}\}$$

$$\cdot\frac{1}{2}\left\{I_{12}(W_0^7)\pm\frac{\alpha Z}{24\rho}I_{11}(W_0^6)\right\}$$

$$+|\int\vec{\alpha}\times\vec{r}|^2\left\{I_5(W_0^6)+\frac{\alpha^2Z^2}{4\rho^2}I_0(W_0^4)\right\}$$

$$\frac{1}{\tau_{2A}}=\frac{G^2}{\pi^2}\Big[\{\Sigma|S_{ijk}|^2\}\frac{1}{72}I_{17}(W_0^8)+\{\Sigma|T_{ij}|^2\}$$

$$\cdot\frac{1}{12}\left\{I_{18}(W_0^8)+\frac{\alpha^2Z^2}{16\rho^2}I_{10}(W_0^6)\right\}\Big].\tag{6}$$

Here the same notations are adopted as those in Konopinski and Uhlenbeck's paper, and the dependence of the formula on W_0 is found to have the following expressions:

$$I_0(W_0^4)=\left(\frac{W_0^4}{2\cdot3\cdot5}-\frac{3W_0^2}{4\cdot5}-\frac{2}{3\cdot5}\right)R+\frac{1}{4}W_0L,$$

$$I_2(W_0^6)=\left(\frac{W_0^5}{2\ 5\cdot9}-\frac{7W_0^3}{2\cdot5\cdot9}-\frac{9W_0}{5\cdot8}\right)R+\left(\frac{W_0^2}{4}+\frac{1}{3\cdot8}\right)L$$

$$I_3(W_0^6)=\left(\frac{W_0^6}{2\cdot3\cdot5\cdot7}-\frac{13W_0^4}{3\cdot4\cdot5\cdot7}-\frac{4W_0^2}{7\ 9}+\frac{2}{5\cdot7\cdot9}\right)R$$

$$+\frac{W_0^3}{12}L,$$

$$I_4(W_0^6)=\left(\frac{W_0^6}{2\cdot7\cdot9}-\frac{79W_0^4}{4\cdot5\cdot7\cdot9}-\frac{109W_0^2}{3\cdot4\cdot5\cdot7}-\frac{2}{3\cdot5\cdot7}\right)R$$

$$+\left(\frac{W_0^3}{4}+\frac{W_0}{12}\right)L,$$

$$I_5(W_0^6)=\left(\frac{W_0^6}{2\cdot5\cdot7\cdot27}+\frac{W_0^4}{4\cdot5\cdot7\cdot27}+\frac{167W_0^2}{4\cdot5\cdot7\cdot27}+\frac{2}{7.27}\right)R$$

$$-\left(\frac{W_0^3}{4\cdot9}+\frac{W_0}{4\cdot9}\right)L,$$

$$I_6(W_0^6)=\left(\frac{W_0^6}{2\ 5\cdot27}-\frac{17W_0^4}{4\cdot5\cdot27}-\frac{41W_0^2}{2\ 5\cdot27}\ \frac{2}{5\cdot27}\right)R$$

$$+\left(\frac{5W_0^3}{4\cdot9}+\frac{W_0}{2\cdot9}\right)L,$$

$$I_7(W_0^6)=\left(\frac{W_0^6}{2\cdot5\cdot7\cdot9}-\frac{19W_0^4}{5\cdot7\cdot8\cdot9}+\frac{29W_0^2}{3\cdot5\cdot7\cdot16}+\frac{1}{3\cdot5\cdot7}\right)R$$

$$-\left(\frac{W_0}{3\cdot16}\right)L,$$

$$I_8(W_0^6)=\left(\frac{W_0^6}{2\cdot3\cdot5\cdot7}-\frac{11W_0^4}{5\cdot7\cdot8}-\frac{901W_0^2}{5\cdot7\cdot9\cdot16}-\frac{1}{7\cdot9}\right)R$$

$$+\left(\frac{W_0^3}{6}+\frac{W_0}{16}\right)L,$$

$$I_9(W_0^6)=\left(\frac{W_0^6}{2\cdot5\cdot7\cdot9}-\frac{59W_0^4}{5\cdot7\cdot9\cdot16}-\frac{407W_0^2}{5\cdot7\cdot9\cdot32}\right.$$

$$\left.-\frac{1}{2\cdot5\cdot7\cdot9}\right)R+\left(\frac{W_0^3}{3\cdot8}+\frac{W_0}{3\cdot32}\right)L,$$

$$I_{10}(W_0^6)=\left(\frac{W_0^6}{3\cdot7}-\frac{179W_0^4}{3\ 4\cdot5\cdot7}-\frac{1889W_0^2}{3\cdot5\cdot7\cdot8}-\frac{26}{3\cdot5\cdot7}\right)R$$

$$+\left(2W_0^3+\frac{7W_0}{8}\right)L,$$

$$I_{11}(W_0^6)=\left(\frac{W_0^6}{5\cdot7}-\frac{33W_0^4}{4\cdot5\cdot7}-\frac{901W_0^2}{3\ 5\cdot7\cdot8}\right.$$

$$\left.-\frac{2}{3\cdot7}\right)R+\left(W_0^3+\frac{3W_0}{8}\right)L,$$

$$I_{12}(W_0^7) = \left(\frac{W_0^7}{4\cdot5\cdot7\cdot9} - \frac{W_0^5}{2\cdot7\cdot9} - \frac{247\,W_0^3}{5\cdot7\cdot9\cdot16} - \frac{2}{5\cdot7\cdot9}\right) R + \left(\frac{W_0^4}{3\cdot8} + \frac{W_0^2}{3\cdot16}\right) L,$$

$$I_{14}(W_0^7) = \left(\frac{W_0^7}{4\cdot7} - \frac{67\,W_0^5}{7\cdot8} - \frac{2161\,W_0^3}{7\cdot32} - \frac{1175\,W_0}{7\cdot64}\right) R + \left(\frac{15\,W_0^4}{2} + \frac{45\,W_0^2}{8} + \frac{15}{64}\right) L,$$

$$I_{15}(W_0^7) = \left(\frac{W_0^8}{4\cdot5\cdot7\cdot27} - \frac{17\,W_0^6}{5\cdot7\cdot8\cdot27} - \frac{4\,W_0^4}{3\cdot7\cdot25} + \frac{W_0^2}{25\cdot27} - \frac{1}{7\cdot25\cdot27}\right) R + \frac{W_0^5}{3\cdot5\cdot8} L,$$

$$I_{16}(W_0^8) = \left(\frac{W_0^8}{4\cdot5\cdot81} - \frac{31\,W_0^6}{7\cdot8\cdot81} - \frac{199\,W_0^4}{4\cdot5\cdot7\cdot27} - \frac{31\,W_0^2}{5\cdot7\cdot81} + \frac{1}{5\cdot7\cdot81}\right) R + \left(\frac{W_0^5}{3\cdot8} + \frac{W_0^3}{4\cdot9}\right) L,$$

$$I_{17}(W_{08}) = \left(\frac{W_0^8}{2\cdot7\cdot81} - \frac{103\,W_0^6}{4\cdot5\cdot7\cdot81} - \frac{1139\,W_0^4}{4\cdot7\cdot25\cdot27} - \frac{134\,W_0^2}{7\cdot25\cdot81}\right) R + \left(\frac{W_0^5}{4\cdot5} + \frac{W_0^3}{4\cdot9}\right) L,$$

$$I_{18}(W_0^8) = \left(\frac{W_0^8}{5\cdot7\cdot81} - \frac{5\,W_0^6}{4\cdot7\cdot81} + \frac{11\,W_0^4}{7\cdot8\cdot27} + \frac{26\,W_0^2}{5\cdot7\cdot81} - \frac{2}{5\cdot7\cdot81}\right) R - \frac{W_0^3}{8\cdot9} L,$$

$$I_{19}(W_0^8) = \left(\frac{4\,W_0^8}{5\cdot7\cdot81} - \frac{11\,W_0^6}{4\cdot5\cdot27} - \frac{4831\,W_0^4}{7\cdot8\cdot25\cdot27} \quad \frac{398\,W_0^2}{7\cdot25\cdot81} + \frac{2}{25\cdot81}\right) R + \left(\frac{W_0^5}{2\cdot5} - \frac{W_0^3}{8\cdot9}\right) L, \tag{7}$$

where

$$R = (W_0^2-1)^{1/2}, \text{ and } L = \log(W_0+(W_0^2-1)^{1/2}). \tag{8}$$

Some noticiable features will be mentioned here concerning the forbidden beta decays,

A) In the forbidden formulas, the influence of the nuclear charge appears through the terms involving factors $\alpha Z/\rho$, $\alpha^2 Z^2/\rho^2$, which show the stronger dependence on Z, in contrast to the allowed formulas, where the slower dependence of $F(\pm Z, W)$ on Z predominates.

B) The dependence of the total probabilities on W_0, which might roughly be estimated as the 7-th power law in the first forbidden transitions, the 9-th power law in the second forbidden transitions is seen to be broken down in (7), especially when W_0 is small. This is due to the fact that, besides the terms containing the highest power of W_0, another terms containing the lower power of W_0, which may be comparable with the former on account of the factors $\alpha Z/\rho$, or $\alpha^2 Z^2/\rho^2$.

C) On evaluating the nuclear matrix elements in the forbidden transitions, some questions are to be mentioned. Since (5), (6) involve more than one nuclear matrix element, one would be necessary to know about the nuclear states, if one expects to discuss the validity of the results on the experiments. But in some special cases, where they reduce to one nuclear matrix element, we could evaluate the dependence of the life time on W_0 and Z unambiguously. For instance, if the following conditions are satisfied in the tensor interactions, i. e.,

1) $\Delta j = \pm 2$, in the first forbidden, which means $B_{ij} \neq 0$, all others $= 0$, or

$\Delta j = \pm 3$, in the second forbidden, which means $S_{ijk} \neq 0$, all others $= 0$, we could easily determine the total probabilities.

2) If we neglect the difference in the Coulomb energy in the initial and final nuclei, we can utilize the convenient relations such as,

$$\int \vec{\alpha} = i W_0 \int \vec{r} \tag{8a}$$

$$A_{ij} = i W_0 R_{ij} \tag{8b}$$

which was cited in Konopinski and Uhlenbeck's paper. In this case, also, we could make all the terms into unity.

Thus we have the corresponding Sargent rules for the forbidden transitions in these cases, as will be shown in Fig 1.

It may, however, be argued, that the diagrams which we have chosen are hardly suitable to the forbidden cases, since here the life-time, τ, of the beta decay shows an additional dependence on Z or ρ, besides the essential dependence on W_0. In this situation, we should prefer to evaluate the semi-empirical matrix elements in each case and expect further study by reviewing them. For instance, one can calculate the semi-empirical values for the matrix elements of beta decay in the first forbidden transitions by the help of the approximate relation (8a) the result of which is shown in the following table.

Here $T_0 = 3\times10^3$ sec is assumed. The value of

Table I.

Elements	Li^8	B^{12}	N^{16}	F^{20}	Na^{24}	Al^{28}	P^{32}	Cl^{36}	Sc^{44}	V^{48}	Mn^{52}
$\lvert\int\vec{r}\rvert^2(10^{-28}\,\mathrm{cm}^2)$	5	200	90	10	10	60	0.1	6	0.6	0.04	0.2
$-\mathrm{Log}_{10}\frac{\lvert M\rvert^2}{T_0}$	5.41	3.86	5.08	5.85	6.18	5.01	7.87	7.8	5.17	7.22	6.05

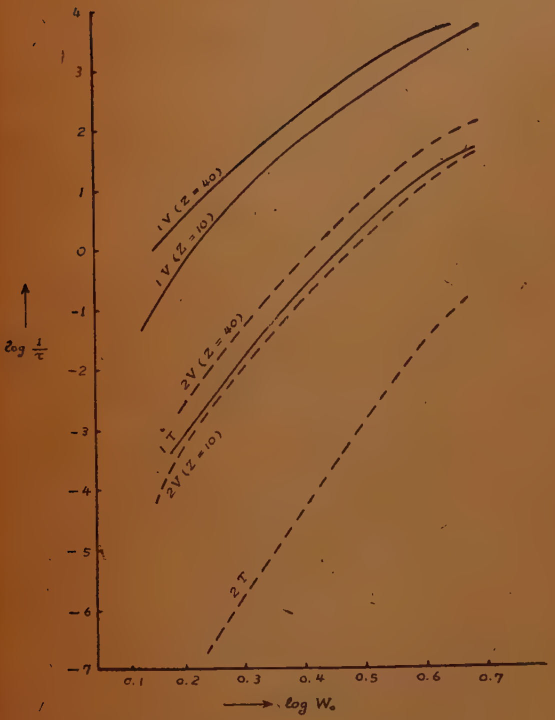

Fig. 1. Sargent Rules for the Forbidden Transitions

$\log_{10}\frac{|M|^2}{T_0}$ are cited for the comparison with the elaborate calculations by J. Itoh[2)], where the allowed functions are adopted to the function of W_0. As far as the matrix elements $\int\vec{r}$ or R_{ij} are concerned, it does seem that there is a correlation between the forbidden beta decay and the dipole or the quadrupole radiation of nuclear gamma. It must, of course, be mentioned that in the latter case we have to do with the charge distribution on the nuclei, while in the former case it is a matter of the neutron-proton distributions.

§ 3. K- or L-Electron Capture for the Forbidden Transitions.

As a natural extension of the preceeding discussions, we have calculated the probabilities of K-electron capture for the first and the second forbidden transitions on the Fermi theory. Calculated probabilities for the K-electron capture are given as the following expressions:

$$P^K=\frac{G^2}{4\pi}q^2(2\alpha Z)^3e^{-2\rho\alpha Z}(2\rho\alpha Z)^{2(S-1)}C_K$$

$$C_K^{1S}=\left|\int\vec{r}\right|^2\left(\frac{q^2}{3}\frac{1+\varepsilon}{4\pi}+\frac{1-\varepsilon}{4\pi\rho^2}+\frac{q}{3}\frac{\sqrt{1-\varepsilon^2}}{2\pi\rho}\right)$$

$$C_K^{1V}=\left|\int\vec{r}\right|^2\left(\frac{q^2}{3}\frac{1+\varepsilon}{4\pi}+\frac{1-\varepsilon}{4\pi\rho^2}-\frac{q}{3}\frac{\sqrt{1-\varepsilon^2}}{2\pi\rho}\right)$$
$$+\left|\int\vec{\alpha}\right|^2\left(\frac{1+\varepsilon}{4\pi}\right)+i\{(\int\vec{\alpha})(\int\vec{r})^*-(\int\vec{\alpha})^*(\int\vec{r})\}$$
$$\left\{\frac{q}{3}\frac{1+\varepsilon}{4\pi}-\frac{\sqrt{1-\varepsilon^2}}{4\pi\rho}\right\}$$

$$C_K^{1T}=\left|\int\vec{\sigma}\vec{r}\right|^2\left\{\frac{q^2}{9}\frac{1+\varepsilon}{4\pi}+\frac{1-\varepsilon}{4\pi\rho^2}+\frac{q}{3}\frac{\sqrt{1-\varepsilon^2}}{2\pi\rho}\right\}$$
$$+\left|\int\alpha\right|^2\frac{1+\varepsilon}{4\pi}$$
$$+\left|\int\vec{\sigma}\times\vec{r}\right|^2\left(\frac{q^2}{6}\frac{1+\varepsilon}{4\pi}+\frac{1-\varepsilon}{4\pi\rho^2}-\frac{q}{3}\frac{\sqrt{1-\varepsilon^2}}{2\pi\rho}\right)$$
$$+\{(\int\vec{\sigma}\times\vec{r})(\int\alpha)^*+(\int\vec{\sigma}\times\vec{r})^*(\int\alpha)\}$$
$$\times\left\{-\frac{q}{3}\frac{1+\varepsilon}{4\pi}+\frac{\sqrt{1-\varepsilon^2}}{4\pi\rho}\right\}+\Sigma|B_{ij}|^2\left(\frac{q^2}{12}\frac{1+\varepsilon}{4\pi}\right).$$

$$C_K^{1A}=\left|\int\vec{\sigma}\cdot\vec{r}\right|^2\left(\frac{q^2}{9}\frac{1+\varepsilon}{4\pi}+\frac{1-\varepsilon}{4\pi\rho^2}-\frac{q}{3}\frac{\sqrt{1-\varepsilon^2}}{2\pi\rho}\right)$$
$$+\left|\int\gamma_5\right|^2\frac{1+\varepsilon}{4\pi}+i\{(\int\vec{\sigma}\cdot\vec{r})(\int\gamma_5)^*-(\int\vec{\sigma}\vec{r})^*(\int\gamma_5)\}$$
$$\left\{-\frac{q}{3}\frac{1+\varepsilon}{4\pi}+\frac{\sqrt{1-\varepsilon^2}}{4\pi\rho}\right\}$$
$$+\left|\int\vec{\sigma}\times\vec{r}\right|^2\left(\frac{q^2}{6}\frac{1+\varepsilon}{4\pi}+\frac{1-\varepsilon}{4\pi\rho^2}+\frac{q}{3}\frac{\sqrt{1-\varepsilon^2}}{2\pi\rho}\right)$$
$$+\Sigma|B_{ij}|^2\frac{q^2}{12}\frac{1+\varepsilon}{4\pi}.$$

$$C_K^{2S}=\Sigma|R_{ij}|^2\left\{\frac{q^4}{30}\frac{1+\varepsilon}{4\pi}+\frac{2}{15}q^3\frac{\sqrt{1-\varepsilon^2}}{4\pi\rho}+\frac{1}{3}q^2\frac{1-\varepsilon}{4\pi\rho^2}\right\}.$$

$$C_K^{2V}=\Sigma|R_{ij}|^2\left\{\frac{q^4}{30}\frac{1+\varepsilon}{4\pi}-\frac{2}{15}q^3\frac{\sqrt{1-\varepsilon^2}}{4\pi\rho}+\frac{1}{3}q^2\frac{1-\varepsilon}{4\pi\rho^2}\right\}$$
$$+|A_{ij}|^2\frac{q^2}{12}\frac{1+\varepsilon}{4\pi}-i(\Sigma R_{ij}A_{ij}^*-\Sigma R_{ij}^*A_{ij})$$

$$\left\{\frac{q^3}{30}\frac{1+\varepsilon}{4\pi}-\frac{q^2}{6}\frac{\sqrt{1-\varepsilon^2}}{4\pi\rho}\right\}$$

$$+|\int\vec{\alpha}\times\vec{r}|^2\left(\frac{q^2}{6}\frac{1+\varepsilon}{4\pi}+\frac{2}{3}q\frac{\sqrt{1-\varepsilon^2}}{4\pi\rho}+\frac{1-\varepsilon}{4\pi\rho^2}\right)$$

$$C_K^{2T}=\sum|S_{ijk}|^2\frac{1}{72}\left(\frac{q^4}{15}\frac{1+\varepsilon}{4\pi}\right)+\sum|T_{ij}|^2\frac{1}{12}$$

$$\left\{\frac{q^4}{15}\frac{1+\varepsilon}{4\pi}-\frac{2}{5}q^3\frac{\sqrt{1-\varepsilon^2}}{4\pi\rho}+q^2\frac{1-\varepsilon}{4\pi\rho^2}\right\}$$

$$+\sum|A_{ij}|^2\frac{1}{12}q^2\frac{1+\varepsilon}{4\pi\rho}-\{\sum T_{ij}A_{ij}^*+\sum T_{ij}^*A_{ij}\}$$

$$\times\frac{1}{4}\left\{\frac{q^3}{15}\frac{1+\varepsilon}{4\pi}-\frac{1}{3}q^2\frac{\sqrt{1-\varepsilon^2}}{4\pi\rho}\right\}$$

$$+|\int\vec{\alpha}\,\vec{r}|^2\left(\frac{q^2}{9}\frac{1+\varepsilon}{4\pi\rho}+\frac{2}{3}\frac{\sqrt{1-\varepsilon^2}}{4\pi\rho}+\frac{1-\varepsilon}{4\pi\rho^2}\right)$$

$$C_K^{2A}=\sum|S_{ijk}|^2\frac{1}{72}\left(\frac{q^4}{15}\frac{1+\varepsilon}{4\pi}\right)+\sum|T_{ij}|^2\frac{1}{12}$$

$$\left\{\frac{q^4}{15}\frac{1+\varepsilon}{4\pi}+\frac{2}{5}q^3\frac{\sqrt{1-\varepsilon^2}}{4\pi\rho}+q^2\frac{1-\varepsilon}{4\pi\rho^2}\right\}.$$

Here the wave fnnctions for the *K*-electron are properly the solution of Dirac's relativistic wave equations. ε represents the total energy of the electron captured, q the energy of the neutrino emitted.

In order to compare the results with experiments, the ratio σ of the probabilities for the positron emission to those for the *K*-electron capture may certainly the most available. We have thus evaluate σ in the same special cases as was performed with regard to the beta decay in the forbidden transitions. The results are listed in the Table II.

Table II.

II) Neglecting the Coulomb energy between the initial and the final nuclei :

$\sigma_{1V}=\dfrac{P_{1V}^*}{P_{1V}^K}$	The First Forbidden Case (Vector Interaction)		
	$Z=10$	$Z=20$	$Z=40$
$W_0=1.5$	23.6	3.2	0.33
2.0	46.1	6.2	0.65
1.5	219.0	26.6	2.60
3.0	581.2	68.3	6.52
4.0	2027	236.3	22.72
5.0	5072	625.1	54.83

$\sigma_{2V}=\dfrac{P_{2V}^*}{P_{2V}^K}$	The Second Forbidden Case (Vector Interaction)		
	$Z=10$	$Z=20$	$Z=30$
$W_0=1.5$	0.2	0.01	0.002
2.0	4.1	0.31	0.051
2.5	19.2	1.54	0.255
3.0	68.1	5.98	0.851
4.0	208.8	18.80	2.954
5.0	510.5	48.72	7.645

II) Favoring Selection Rules;

$\sigma_{1T}=\dfrac{P_{1T}^*}{P_{1T}^K}$	The First Forbidden Case (Tensor Interaction)		
	$Z=10$	$Z=20$	$Z=40$
$W_0=1.5$	0.04	0.004	0.0004
2.0	1.19	0.135	0.014
2.5	4.16	0.483	0.048
3.0	7.34	0.857	0.086
4.0	25.20	2.242	0.288
5.0	46.90	5.586	0.544

$\sigma_{2T}=\dfrac{P_{2T}^*}{P_{2T}^K}$	The Second Forbidden Case (Tensor Interaction)		
	$Z=10$	$Z=20$	$Z=40$
$W_0=1.5$	0.38	0.04	0.004
2.0	1.77	2.07	0.208
2.5	158.8	19.17	1.913
3.0	732.4	84.92	8.443
4.0	9382	1271	105.8
5.0	26614	30913	304.6

Here the dependence of σ on Z, W_0, and ρ is seen much more remarkable in the forbidden transitions than in the allowed one. Since, in the forbidden transitions, the total angular momentum carried away by the electron and the neutrino may not always be zero, the contributions of *L*-electron capture should not be overlooked. Meanwhile the probabilities of *L*-electron capture will be estimated, by using the *L*-Wave in the Dirac equation of the electron in the Coulomb field of initial nuclei. The results are indicated, referring to the actual cases of Be^7, V^{48}, and Zn^{65}, in comparison with the contributions of their *K*-electron capture, where the contributions of the *L*-electron capture are found to be about 10% to those of the *K*-electron capture.

Table. III.

	${}_4\mathrm{Be}^7$				${}_{23}\mathrm{V}^{48}$				${}_{30}\mathrm{Zn}^{65}$			
	P_{1S}^{K}	P_{1S}^{L}	P_{2S}^{K}	P_{2S}^{L}	P_{S}^{K}	P_{1S}^{L}	P_{2S}^{K}	P_{2S}^{L}	P_{1S}^{K}	P_{1S}^{L}	P_{2S}^{K}	P_{2S}^{L}
$W_0=1.0$	0.0008	0.0003	0.00096	0.00069	1.221	0.144	1.460	0.185	7.124	0.487	8.636	0.743
1.5	0.0018	0.0006	0.00261	0.00193	2.030	0.232	3.709	0.469	11.740	0.783	21.836	1.940
2.0	0.0030	0.0010	0.00601	0.00401	3.108	0.345	7.988	1.006	17.817	1.158	46.792	4.256
2.5	0.0048	0.0015	0.01229	0.00927	4.490	0.485	15.329	1.933	25.542	1.619	89.499	8.312
3.0	0.0073	0.0021	0.02307	0.01746	6.227	0.653	27.156	3.424	35.120	2.170	157.522	14.902

In any cases, the screening effect of the K-electron may certainly be taken into account, for instance, if $Z=4$ the effective nuclear charge is estimated as about 2, which reduces the probabilities of the L-electron capture considerably. The ratio of the probabilities between the K-and L-electron captures is found to be almost independent of W_0.

The authors wish to thank Professor H. Yukawa, under whose direction the work was carried out, for his advicés and encouragements in the pursuit of the problem.

References.

(1) Konopinki and Uhlenbeck, Phys. Rev. **60**(1941) 308.

(2) J. Itoh, Proc. Phys.-Math. Soc. Japan, **22** (1940) 530.

(3) M. E. Rose, Phys. Rev. **51** (1937) 484.

On the Transition in KH_2PO_4*.

Gen SHIRANE and Takehiko OGUCHI.

Second Faculty of Engineering, University of Tokyo.

(Received March 8, 1948).

§ 1. Introduction.

The transition in KH_2PO_4 has been treated successfully by Slater(1). His theory is based upon the following three assumptions. First :—each phosphate has always two hydrogens close to it; and second :—there is always one on the connecting line between each pair of phosphate groups; and third :—the dipole moment pointing along the $\pm c$ direction of the crystal is more stable than that at right angles to this direction. It is found that the theory predicts a sudden transition from the polarized state at low temperature to the unpolarized state at high temperature, that is, this phase change is of the first order. Takahashi(2) has proved that this singular aspect of the transition is not caused from an approximation in statistical treatment but it is an exact result of this model. In an actual crystal there are phosphate groups each of which has any number of neighbouring hydrogen other than two, that is, HPO_4 or H_3PO_4, and there are possibilities that there may be two hydrogens or none on a bond. Slater has predicted that the discrepancy between theory and experiments would be caused either by the fact that first and second assumptions are inadequate or by the fact that there is internal stress in an actual crystal. He has felt that the latter is likely to be the case. Takagi(3) has tried the modification of Slater's first assumption, namely, he has considered besides H_2PO_4, both H_3PO_4 and HPO_4 at the expense of a finite energy. As expected, it is found in his paper that the transition is not sudden but takes place through some temperature range. This modification, however, would imply the formation of ions, such as H_3PO_4, HPO_4, a type of which is known to be very rare in the similar case of ice, and would also be probably rare in this crystal from the chemical standpoint. So we shall modify the second assumption.

---

* This paper, which was originally written in Japanese to be published in *Nihon Butsuri-gakkai-shi*, has now been translated into English according to the request of the editorial committee.

We shall assume that either two hydrogens or none can be located on a bond at the expense of a finite energy. Though internal energy is increased by this assumption, the configurational entropy increases more rapidly so that calculated aspects of the transition in KH_2PO_4 are fairly improved.

§ 2. Outline of the Theory of Transition.

Let the hydrogen bond having two hydrogens or none be called b_0 and b_0' respectively. Since the crystal is neutral the number of b_0 is equal to that of b_0'. So hereafter both these numbers will be denoted by the same symbol b_0. Let us denote a bond by b_+ if it has a hydrogen near the upper corner of the phosphate and b_- if it has a hydrogen near the under corner of the phosphate. We shall also use the notations D_+, D_-, D_0 to specify the direction of dipole moment of phosphate groups, and to denote the total numbers of any species contained in the crystal we shall use especially the italic type of the symbols.

If there are N phosphate groups and $2N$ hydrogens, then

$$D_+ + D_- + D_0 = N \tag{2.1}$$

$$b_+ + b_- + 2b_0 = 2N. \tag{2.2}$$

D_+, D_- and D_0 are related to b_+, b_- and b_0 as

$$b_+ + b_0 = 2D_+ + D_0 \tag{2.3}$$

$$b_- + b_0 = 2D_- + D_0. \tag{2.4}$$

From the chemical standpoint, it is easily seen that b_+ and b_- are more stable than b_0, hence

$$b_+ + b_- + 2\varepsilon_T \rightleftarrows 2b_0 \tag{2.5}$$

namely ε_T (>0) is required for this reaction to occur. Thus Slater's treatment corresponds to a limiting case when ε_T tends infinity. Since $\pm c$ directions of the crystal are the directions of easiest polarization so

$$D_\pm + 2\varepsilon_0 \rightleftarrows D_0. \tag{2.6}$$

When we arrange these bonds at random, the number of configuration is

$$\frac{(2N)!}{b_+!\,b_-!\,(b_0!)^2} \tag{2.7}$$

From these configurations (2.7), we must select only the reasonable ones satisfying the assumption that each phosphate has always two hydrogens close to it. If we consider solely b_+ and b_- bonds, there are six different ways to arrange them on the four lines belonging to each phosphate group to build H_2PO_4. Now, since we permit the existence of b_0's and b_0''s the number of possible arrangements increases to $6\times16=96$. For example, the upper side of D_+ is shown in Fig. 1.

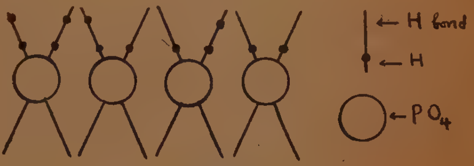

Fig. 1.

The number of configurations W is easily given by a similar way as used by Takagi :(4)

$$W = \frac{(b_+ + b_0)^{2(b_+ + b_0)}(b_- + b_0)^{2(b_- + b_0)}}{(b_+ + b_- + 2b_0)^{b_+ + b_- + 2b_0}\, b_+^{\,b_+}\, b_-^{\,b_-}\, b_0^{\,2b_0}} \times \frac{4D_0^{\,D_0} N^N}{D_+^{\,D_+} D_-^{\,D_-} D_0^{\,D_0}}. \tag{2.8}$$

When the crystal is placed in an electric field E_c along the c-axis, the internal energy is

$$U = -(D_+ - D_-)\mu E_c + D_0\varepsilon_0 + 2b_0\varepsilon_T \tag{2.9}$$

We can calculate with equations (2.8) and (2.9) how the general tendency of the transition changes for various values of ε_T, and compare these computations with former theories and experiments.

§ 3. Detailed Results of Calculations.

For convenience, we shall put

$$D_+ - D_- = N\nu_c\,,\; D_0 = N\nu_0\,,\; b_0 = N\tau. \tag{3.1}$$

From the conditions for stable states

$$\frac{\partial F}{\partial \nu_c}=0;\quad \frac{1-\nu_0+\nu_c}{1-\nu_0-\nu_c}\left(\frac{1-\gamma+\nu_c}{1-\gamma-\nu_c}\right)^2\left(\frac{1-\nu_c}{1+\nu_c}\right)^4=e^{\frac{2\mu E_c}{kT}} \tag{3.2}$$

$$\frac{\partial F}{\partial \nu_0}=0;\quad \frac{4(1-\nu_0+\nu_c)(1-\nu_0-\nu_c)}{{\nu_0}^2}\doteq e^{\frac{2\varepsilon_0}{kT}} \tag{3.3}$$

$$\frac{\partial F}{\partial \gamma}=0;\quad \frac{(1-\gamma+\nu_c)(1-\gamma-\nu_c)}{\gamma^2}\doteq e^{\frac{2\varepsilon_\gamma}{kT}}. \tag{3.4}$$

(3.3) and (3.4) respectively show the existence of quasi-chemical equilibrium of the following reactions:

$$\mathrm{D}_+ + \mathrm{D}_- + 2\varepsilon_0 \leftrightarrows 2\mathrm{D}_0 \tag{3.5}$$

$$\mathrm{b}_+ + \mathrm{b}_- + 2\varepsilon_\gamma \leftrightarrows 2\mathrm{b}_0 \,. \tag{3.6}$$

Now, put $\frac{1}{2}\log\frac{1+\nu_c}{1-\nu_c}=R$, that is, $\tanh R=\nu_c$, then (3.2) becomes

$$\frac{1-\nu_0+\nu_c}{1-\nu_0-\nu_c}\left(\frac{1-\gamma+\nu_c}{1-\gamma-\nu_c}\right)^2=e^{\frac{2\mu E_c}{kT}+8R}. \tag{3.7}$$

From (3.3), (3.4) and (3.7), the following compatibility condition

$$2e^{-\frac{\varepsilon_0}{kT}}\sinh R=(1+2e^{-\frac{\varepsilon_\gamma}{kT}}\sinh^2 R)\sinh\left(\frac{\mu E_c}{kT}+R\right)$$
$$-2e^{-\frac{\varepsilon_\gamma}{kT}}(1+2e^{-\frac{2\varepsilon_\gamma}{kT}}\sinh^2 R)^{\frac{1}{2}}\sinh R\cosh\left(\frac{\mu E_c}{kT}+R\right) \tag{3.8}$$

is obtained. ν_0 and γ are solved respectively as follows:

$$\nu_0=1/\cosh R\left\{\cosh R+\left(\frac{1}{4}e^{\frac{2\varepsilon_0}{kT}}+\sinh^2 R\right)^{\frac{1}{2}}\right\} \tag{3.9}$$

$$\gamma=1/\cosh R\{\cosh R+(e^{\frac{2\varepsilon_\gamma}{kT}}+\sinh^2 R)^{\frac{1}{2}}\}. \tag{3.10}$$

From these equations (3.8), (3.9) and (3.10), various quantities, such as spontaneous polarization, specific heat and susceptibility can be obtained.

The spontaneous polarization P_c in the direction of c-axis is

$$P_c=N\mu\tanh R. \tag{3.11}$$

Put $E_c=0$ in (3.8), then

$$2\sinh R=e^{\frac{\varepsilon_0}{kT}}\sinh R+2e^{\frac{\varepsilon_0-2\varepsilon_\gamma}{kT}}\sinh^2 R$$
$$-2e^{\frac{\varepsilon_0-\varepsilon_\gamma}{kT}}(1+e^{-\frac{2\varepsilon_\gamma}{kT}}\sinh^2 R)^{\frac{1}{2}}\sinh R\cdot\cosh R \tag{3.12}$$

from this

$$R=0$$

or

$$\sinh^2 R\doteq\frac{(1-2e^{-\frac{\varepsilon_0}{kT}})^2-4e^{-\frac{2\varepsilon_\gamma}{kT}}}{(e^{-\frac{2\varepsilon_\gamma}{kT}}+2e^{-\frac{\varepsilon_0}{kT}})4e^{-\frac{2\varepsilon_\gamma}{kT}}} \tag{3.13}$$

are obtained. Fig. 2 shows $P_c/N\mu$ vs. kT/ε_0 curves calculated from (3.13) for various values of $\varepsilon_\gamma/\varepsilon_0$. Thus, if ε_γ is chosen as finite value, the transition becomes of the second order type, and at the same time the critical temperature, let it be denoted by T_γ, is lowered as the value of $\varepsilon_\gamma/\varepsilon_0$ decreases. T_γ is given as limiting case in which $R\to 0$ in (3.12),

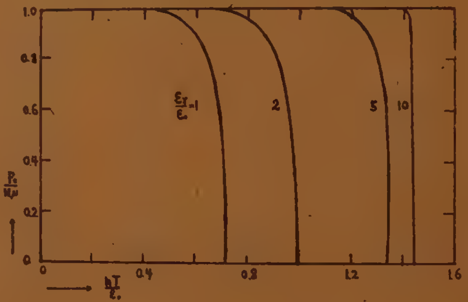

Fig. 2.

$$1-2e^{-\frac{\varepsilon_0}{kT_\gamma}}=2e^{-\frac{\varepsilon_\gamma}{kT_\gamma}}. \tag{3.14}$$

This formula of transition temperature is just the same as that obtained by Takagi from his alternative set of assumptions. The general aspect of the curves calculated from both sets of assumptions are nearly equal, too.

We shall inquire how ν_0 and γ increase with temperature. In the region of $T<T_\gamma$, ν_0 and γ are given from (3.9) and (3.10) but in the region of $T>T_\gamma$, $R\equiv 0$, so

$$\nu_0=\frac{2e^{-\frac{\varepsilon_0}{kT}}}{1+2e^{-\frac{\varepsilon_0}{kT}}} \tag{3.15}$$

$$\gamma=\frac{e^{-\frac{\varepsilon_\gamma}{kT}}}{1+e^{-\frac{\varepsilon_\gamma}{kT}}}. \tag{3.16}$$

These values are shown in Fig. 3. (3.15) agrees with the Slater's result. This shows that D_0 is independent of b_0 in the region $T>T_\gamma$. When $T\to\infty$, it is obtained that $\nu_0\to\frac{4}{6}=0.667$ and

$$\gamma \to \frac{1}{2} = 0.5.$$

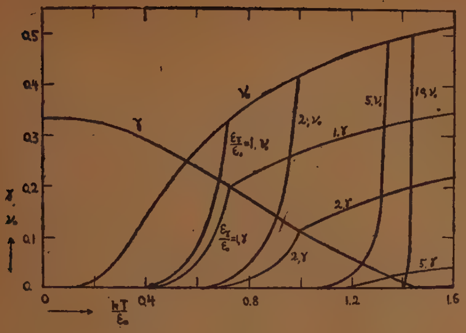

Fig. 3.

If the formula (3.14) of transition point is substituted into (3.16) then

$$\gamma = \frac{1-2e^{-\frac{\varepsilon_0}{kT_\gamma}}}{3-2e^{-\frac{\varepsilon_0}{kT_\gamma}}} \tag{3.17}$$

is deduced, and this shows a locus of γ at $T = T_\gamma$.

Specific heat Cv is obtained as following calculations:

$$\frac{C_v}{N} = \varepsilon_0 \frac{\partial \nu_0}{\partial T} + 2\varepsilon_\gamma \frac{\partial \gamma}{\partial T}. \tag{3.18}$$

According to whether $T \gtrless T_\gamma$, (3.9), (3.10) or (3.15), (3.16) are substituted into ν_0 and γ. The results are shown in Fig. 4.

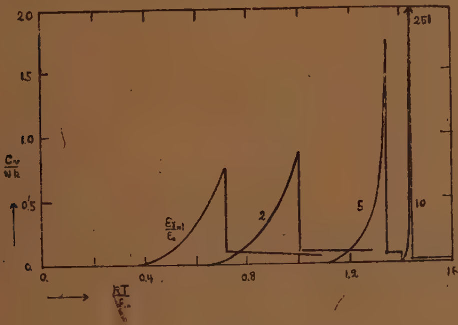

Fig. 4.

If we differentiate (3.8) with Ec and put $Ec \to 0$, $R \to 0$, then we obtained

$$\lim_{E_c \to 0}\left(\frac{dR}{dE_c}\right) = \frac{\mu}{kT} \frac{1}{2e^{-\frac{\varepsilon_0}{kT}} + 2e^{-\frac{\varepsilon_\gamma}{kT}} - 1}. \tag{3.19}$$

Therefore susceptibility χ_c in the direction of c-axis is

$$\frac{\varepsilon_0}{N\mu^2}\chi_c = \frac{\varepsilon_0}{kT} \frac{1}{2e^{-\frac{\varepsilon_0}{kT}} - 1 + 2^{-\frac{\varepsilon_\gamma}{kT}}}. \tag{3.20}$$

The relation between $\frac{1}{\chi_c}\frac{N\mu^2}{\varepsilon_0}$ and temperature is shown in Fig. 5. They generally obey Curie-Weiss' law.

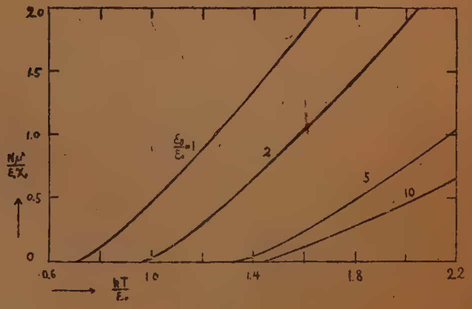

Fig. 5.

§ 4. Comparison with Experiments and Former Theories.

Reviewing the authors' results and comparing them with those derived by Takagi with alternative set of assumptions, one finds that (1) the formulae of transition point are in complete agreement if ε_γ and γ are equated to ε_τ and τ, and that (2) the temperature dependence of spontaneous polarization, specific heat and susceptibility are almost in agreement when the values of $\varepsilon_\gamma/\varepsilon_0$ and $\varepsilon_\tau/\varepsilon_0$ amount from 5 to 10.

Though the transition is of the second order, the temperature change of Pc, Cv are very sharp and look as if it were the first order transition. This tells us that the cooperations through the hydrogen bonds of KH_2PO_4 are so severe that either the existence of b_0, b_0' or the existence of HPO_4^-, H_3PO_4, does not considerably destroy the hydrogen bonds.

The temperature dependences of spontaneous polarization and specific heat when $\varepsilon_\gamma/\varepsilon_0$ is 5 ~ 10, agree well with experiments. Based upon the data of Bantle(5), in which transition point was found to be 123°K, we can estimate the energies as follows:

Table I.

$\varepsilon_\gamma/\varepsilon_0$	5	10	∞
ε_0(cal/mol)	181	170	169
ε_γ(cal/mol)	907	1700	∞

In Table II, ν_0, γ and the corresponding energy at transition temperature are given:

Table II.

$\varepsilon_T/\varepsilon_0$	5	10	∞
ν_0	0.4875	0.4990	0.5
$\nu_0\varepsilon_0$(cal/mol)	88.24	84.83	84.5
γ	0.0238	0.001	0
$2\gamma\varepsilon_T$(cal/mol)	43.2	3.4	0

It is generally accepted that the energy required for breaking one hydrogen bond lies between 1 and 9 kcal/mol from experiments on various substances. The fact that our ε_T is found to be 0.9 ~ 1.7 kcal/mol, though being somewhat small, may be said reasonable.

Moreover, in an actual crystal, as pointed out by Slater, it is also reasonable to say that the transition curve is rounded off on account of internal strain, then the value of $\varepsilon_T/\varepsilon_0$ would be somewhat larger than 5 ~ 10 and agreement with regard to the energy of hydrogen bonds may be still more improved.

In conclusion the authors wish to express their sincere gratitudes to Prof. Y. Takagi for the suggestion of this problem and the kind guidance during the course of this work.

References.

(1) J. C. Slater: J. Chem. Phys. **9** (1941) 16.
(2) H. Takahashi: Proc. Phys-Math. Soc. Japan. **23** (1941) 1069.
(3) Y. Takagi: Nippon Butsurigakukaishi (in Japanese) **3** (1948) 80.
J. Phys. Soc. Japan **3** (1948) 273. short note.
(4) Y. Takagi: Nippon Suubutsugakukaishi (in Japanese) **17** (1943) 280.
J. Phys. Soc. Japan **3** (1948) 271. short note.
(5) W. Bantle: Helv. Phys. Acta. **5** (1942) 373.

Short Notes.

Further Experiments on the Parallel Wire-and-Plate Type Counter.

By Kazuzi HASHIMOTO, Munemaru IMAI & Heiichi HAGIWARA.

Hitachi Central Laboratory.

(Received November. 16, 1948).

In a recent paper one of the authors described the idea and design of the parallel wire-and-plate type counter.(1) On the preliminary test of this counter it was found that there were some induced discharge phenomena on the special central wire affected by neighbouring one. At the beginning of the test made on this counter in any case, it will be inportant and interesting to determine the probability of the coincident discharge, and simultaneously to measure the effective volume of the central wires.

Fig. 1 shows one representative parallel-counter picked out of several test counters which contain various intervals of central wires. Three central wires are put between two parallel plates. The central wires in this case are arranged 2.5 cm. apart from each other, and the parallel copper plates, by which the wires are sandwiched, are both 15 cm. long and 3.5 cm wide. When certain X-ray beam is striking a voluntarily selected point of the counter as shown in Fig. 1 the central wire No. 1 is closed to the passing X-ray beam so that the individual counting rate of No. 1 will be the largest, and No. 2, No. 3 be smaller in due order.

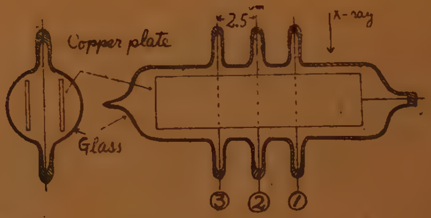

Fig. 1. Lateral and cross section of the parallel-counter.

Let the notation ①, ②, ③, be the counting rate observed from each individual central wire, No. 1, No. 2 and No. 3 and notations ③$_1$, ③$_2$, etc. with suffix, mean the counting rate of No. 3 central wire when No. 1 or No. 2 are in counting condition. Then, the percentage of induced discharge probability, e.g. counting probability of No.

3 that is caused by the discharge of neighbouring wire No. 2 or No. 1 will be computed as follows.

$$\frac{\textcircled{3}_2-\textcircled{3}}{\textcircled{2}}\times 100\,\%,\ \text{or}\ \frac{\textcircled{3}_1-\textcircled{3}}{\textcircled{1}}\times 100\,\%$$

Thus, the percentage of probabilities of the central wire concerning the mutual distance of the wires were obtained as shown in Fig. 2

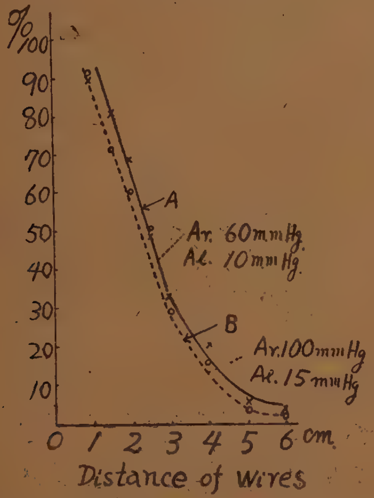

Fig. 2. The percentage of induced discharge probability at one central wire concerning the distance from adjacent one.

In the parallel-counter if the cosmic ray or charged particles passes through the region far apart from the central wire, there will be few or no chance of count.

The counting rate of such rays may be increased gradually as they approach more and more closely to the central wire.

Those effective volumes accessory to the central wire were measured by experimental method shown in Fig. 3.

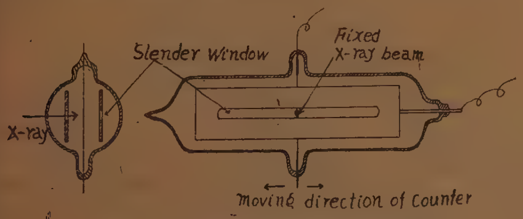

Fig. 3. Experimental method. X-ray beam is coming into the slender window from the back of this paper.

A long and slender window was drilled at the center of each parallel plate in the counter in order to lead a narrow X-ray beam (CuKα = 1.54A) only through the gas without striking the cathode metal.

If the counter slides right and left at right angle to the passing X-ray beam after setting the central wire to the beam the curve of the counting rate concerning the wire position will denote the curve similar to the so-called probability curve which has a maximum counting rate at the center. The experimental fact denoted the remarkable result beyond the expectation as shown in Fig. 4.

It will be clear that the maximum point does not lie at central wire, but lies rather on both sides 1.3 ~ 1.5 cm apart from the central wire. It was found that there are irregular sensibility in the parallel-counter. These phenomena were independent of the counter pressure, copper plate distance or X-ray wave length.

These phenomena are very remarkable but their explanation is not yet incapable.

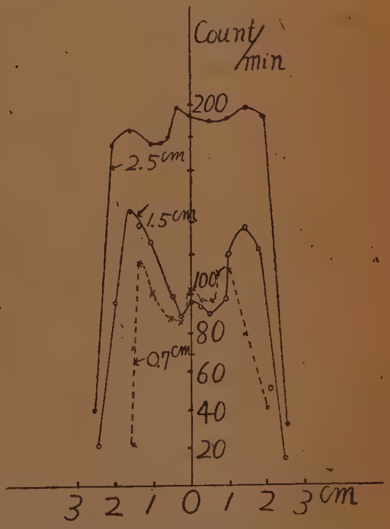

Fig. 4. Sensitive Curves. (Plate distance; 2.5, 1.5, 0.7 cm.)

Reference.

(1) K. Hashimoto: J Phys. Soc. Japan. 3 (1948) 151.

X-ray Studies on Cetyl Alcohols.

By Kenzo SANO* and Yoshinobu KAKIUCHI.

Institute of Science and Technology,

University of Tokyo.

(Received November 26, 1948)

The solid cetyl alcohol $CH_3(CH_2)_{14}CH_2OH$ is known to show anomalous behaviors in thermal and electrical properties, and from these facts it was concluded that there is two modifications in its crystal structure(1). The knowledge about the mechanism of the transformation is, however, still left quite obscure. A. Müller(2) has observed the X-ray diffraction of normal paraffines C_nH_{2n+2} ($n = 21 \sim 29$), at various temperatures, and found that the spacings corresponding to (110) and (200) planes become nearer as the temperature rises until they coincide perfectly with each other at a certain temperature. He concluded that paraffine molecules begin to rotate around their long axis above the transformation point, and as the result the symmetry of the crystal becomes higher in high temperature modification.

The present authors expected the same type of transformation in cetyl alcohol as in the paraffines, and found that it was really the case. The K_α radiation from copper target was thrown upon the sample of cetyl alcohol 0.5 mm in thickness and its Debye rings were observed. The temperature was controlled by flowing the cold and hot water through the mantle covering the space around the sample.

Both (200) and (110) spacings are almost the same with that of paraffines (3.8 and 4.2 A) at lower temperatures, showing the similar arrangement of molecules in cetyl alcohol and the paraffines. Those two spacings coincide in exactly the same manner as in the paraffines at the temperature near 20°C (Fig. 1). Therefore, we may conclude that the transformation in cetyl alcohol is also *rotational* in its character.

The X-ray reflection from (001) plane was also observed in a usual manner, and c spacing is found to be constant throughout the whole temperature region studied (5~45°C)(3).

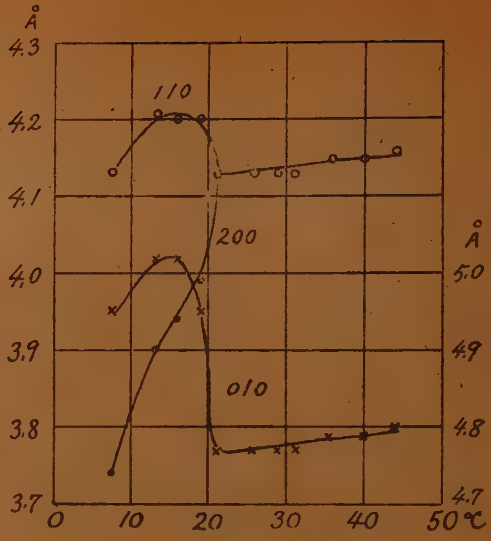

Fig. 1. (200), (110) and (010) spacings.

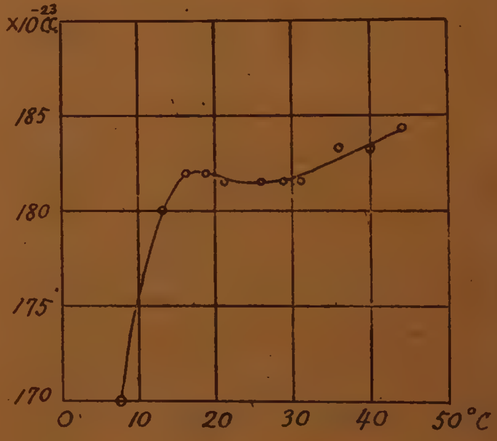

Fig. 2. Volume of a unit cell.

Photo 1. Debye Photographs.

The volume of the unit cell is calculated from the dimensions of the cell, as shown in Fig. 2. The abrupt change is observed at the transformation point. This result agrees with the dilatometric observation by Higasi and Kubo. The transformation temperature obtained in the present experiment is much lower than that observed by these authors. This discrepancy will perhaps due to the fact that the transformation temperature is affected by the presence of water as they mentioned. The specific heat measurement is also in the course of its development.

According to the authors' opinion, the anomalous electric behaviors of cetyl alcohol will, therefore, be closely related to the rotation of molecules around their long axis.

References.

(1) K. Higasi and M. Kubo: Sci. Pap. I. P. C. R. **36** (1936) 286.

(2) A. Müller: Proc. Roy. Soc. **A 138** (1932) 514.

(3) D. A. Wilson and Ott: J. Chem. Phys. **2** (1934) 231.

---

* Now at Yamanashi higher technical school.

A New Type of Fine Structure in the Spectrum of NeII.

By Shigeki Suwa.

Institute of Science and Technology, University of Tokyo.

(Received January 29, 1949.)

The lines of NeII coming from a hollow cathode discharge tube filled with a few mm Hg of neon were investigated here for fine structure. The tube used was just the same as reported by Prof. K. Murakawa(1). Strong lines, belonging mainly to the combination $3s-3p$ and partly to $3p-3d$, were examined by two quartz Lummer-Gehrcke plates (thickness = 5.6 mm and 4.4 mm) placed before the slit of a Hilger quartz E_2 spectrograph.

It was found that, when the neon was pure, every strong NeII line showed a fine structure which was not yet known, and that in this case the isotope effect previously reported(2) was obscured by this structure. An enlargement of interference patterns of some lines is reproduced in Fig. 1, and Fig. 2 gives, as an example, the microphotometer curve of λ 3727; the structure of λ 3727 is sketched qualitatively in Fig. 3. Each line showed a similar structure which consisted of a central main component and wings broadened symmetrically on both sides of the main component; and in every case the intensity fell rapidly at the edge of these wings. The distances of these edges from the centre, $\Delta\nu_1$ and $\Delta\nu_2$, were measured and the results are given in Table I. It can be seen from the table that the lines whose initial and final terms belong to the same family (namely the same multiplicity and the same series limit) have nearly equal breadth, while the breadths of the lines belonging to different family are somewhat different.

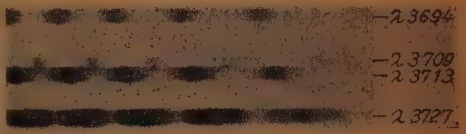

Fig. 1. An enlargement of interference patterns of NeII lines taken with a quartz Lummer plate of thickness 4.4 mm.

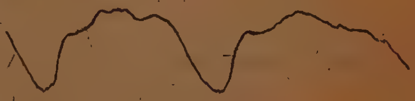

Fig. 2. Microphotometer curve of λ 3727 of NeII.

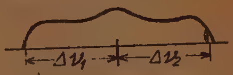

Fig. 3. The structure of λ 3727 of NeII.

Iron or aluminium hollow cathodes of various sizes were used, and various metals such as Mg, Pb and Tl were inserted in the cathode, but in each case it was found that the structure was always the same, except that the intensity of the wings relative to the central main component varied from case to case.

It is a remarkable fact that the lines of NeI and the lines due to the cathode material do not shown the above mentioned structure, even when they are as strong as the NeII lines which appear

Table I. Breadths of the new type of fine structure of NeII lines.

wave length (A.U.)	Allocation(3)	Breadth	
		$\Delta\nu_1$ (cm^{-1})	$\Delta\nu_2$ (cm^{-1})
	$3s\,(^3P)-3p(^3P)$ Doublet System		
3727.1	$3s\ ^2P_{1/2}(^3P)-3p\ ^2D_{3/2}(^3P)$	0.31	0.33
3713.1	$3s\ ^2P_{3/2}(^3P)-3p\ ^2D_{5/2}(^3P)$	0.30	0.29
3643.9	$3s\ ^2P_{3/2}(^3P)-3p\ ^2D_{3/2}(^3P)$	0.31	0.31
3482.0	$3s\ ^2P_{3/2}(^3P)-3p\ ^2S_{1/2}(^3P)$	~0.3	~0.3*
3392.8	$3s\ ^2P_{1/2}(^3P)-3p\ ^2P_{3/2}(^3P)$	0.31	0.30
3378.3	$3s\ ^2P_{1/2}(^3P)-3p\ ^2P_{1/2}(^3P)$	0.22	0.34
3323.8	$3s\ ^2P_{3/2}(^3P)-3p\ ^2P_{3/2}(^3P)$	0.32	0.38
	$3s\,(^3P)-3p\,(^3P)$ Quartet System		
3777.2	$3s\ ^4P_{1/2}(^3P)-3p\ ^4P_{3/2}(^3P)$	~0.25	~0.25*
3766.3	$3s\ ^4P_{3/2}(^3P)-3p\ ^4P_{5/2}(^3P)$	~0.25	~0.25*
3694.1	$3s\ ^4P_{5/2}(^3P)-3p\ ^4P_{5/2}(^3P)$	0.26	0.28
3664.1	$3s\ ^4P_{5/2}(^3P)-3p\ ^4P_{3/2}(^3P)$	0.24	0.25
3355.1	$3s\ ^4P_{3/2}(^3P)-3p\ ^4D_{3/2}(^3P)$	0.29	0.28
3297.7	$3s\ ^4P_{5/2}(^3P)-3p\ ^4D_{5/2}(^3P)$	~0.25	~0.25*
	$3s\,(^1D)-3p\,(^1D)$		
3574.6	$3s\ ^2D_{3/2}(^1D)-3p\ ^2F_{5/2}(^1D)$	0.21	0.23
3568.5	$3s\ ^2D_{5/2}(^1D)-3p\ ^2F_{7/2}(^1D)$	0.12	0.20
3319.8	$3s\ ^2D_{3/2}(^1D)-3p\ ^2P_{1/2}(^1D)$	0.15	0.20
3232.4	$3s\ ^2D_{3/2}(^1D)-3p\ ^2D_{3/2}(^1D)$	0.28	0.26
	$3p\,(^3P)-3d\,(^3P)$		
3244.2	$3p\ ^4D_{5/2}(^3P)-3d\ ^2F_{7/2}(^3P)$	0.20	0.27
3218.2	$3p\ ^4D_{7/2}(^3P)-3d\ ^4F_{9/2}(3P)$	0.29	0.29

* These lines were not measured; the breadth was estimated by eyes.

at the same time and exhibit the above mentioned structure.

The breadth $\Delta\nu_1$ or $\Delta\nu_2$ is far larger than that expected from the Doppler effect due to ordinary thermal motion. This effect is expected to be of the order of 0.1 cm^{-1} and the NeI lines showed really this breadth. Therefore, this phenomenon must be ascribed to a particular effect characteristic of only Ne$^+$ ions. This may be either due to an external electric field or interatomic interactions.

This phenomenon is important when one considers the fact that the hollow cathode discharge tube has been generally accepted as a convenient light source free from any external perturbation.

It is hoped to obtain by a more detailed future investigation a more definite conclusion as to its origin.

The cost of this research has been partly defrayed from the Scientific Research Expenditure of the Department of Education.

The author wishes to express his cordial thanks to Prof. K. Murakawa for his encouragement throughout this work.

References.

(1) K. Murakawa, Sci. Pap. Inst. Phys. Chem. Res., **18** (1932), 191.

(2) K. Murakawa and S. Suwa, Phys. Rev. **74** (1948), 1535.

(3) The classification of NeII was given by T.L. Bruin and C. J. Bakker, Zeits. f. Phys. **69** (1931), 19.

On the Precipitation in Single Crystals of Beryllium-Copper Alloy.

Shin-ya MIYATANI.

Institute of Science and Technology, University of Tokyo, Komaba, Meguroku, Tokyo.

(Received February 8, 1949).

As the first step towards clarifying the mechanism of precipitation in Be-Cu alloy, study of single crystals has been undertaken. Crystals of Be-Cu (Be 2.0±0.3 %) of about 2 mm in linear dimension were quenched from 870°C. in water, aged at 350°C., and then etched with $HCl+FeCl_3 \cdot 6H_2O$. The crystallographic orientation of the matrix was determined by a goniometer[1] and by microscopic photographs. The twins were utilized as standards, since it is known that the copper alloy crystals twin on {111}. Microscopic observation of the aged sample revealed a set of regular streaks[2][3]. Fig. 1 shows an example of microscopic photographs, and Fig. 2 and 3 show two examples of the stereographic projections. Very close to the normals to these streaks we obtained {110} poles of the matrix (α-phase), but poles of other simple Miller-indices (e. g. {100}, {111}, {210}) were farther off. We may, therefore, assume that in Be-Cu crystals the precipitant precipitates on layers which are parallel to the {110} planes of of the matrix.

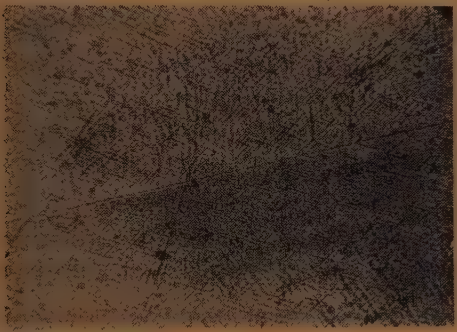

Fig. 1. Beryllium-Copper (Be 2 %). Heated 3 hours at 870°C. and quenched, aged 2 hours at 350°C., etched with $HCl+FeCl_3 \cdot 6H_2O$. Magnification 270×.

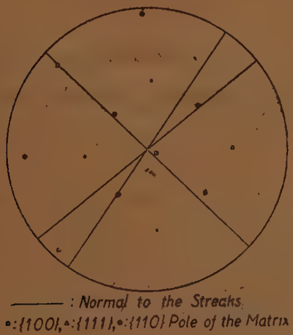
——— : Normal to the Streaks
•:{100}, ▴:{111}, •:{110} Pole of the Matrix

Fig. 2. Stereographic Projection. Cu+2 % Be. Heated 3 hours at 870°C and quenched, aged 1 hour at 350°C. Streaks with three different directions are shown.

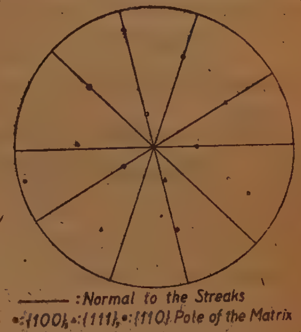
——— : Normal to the Streaks
•:{100}, ▴:{111}, •:{110} Pole of the Matrix

Fig. 3. Stereographic projection of the crystal shown in the upper half of Fig. 1. Streaks with five different directions are shown.

Laue patterns were also examined. The analysis of the asterisms which were obtained when the crystals were annealed after quenching seems not to contradict with the above-mentioned assumption.

A part of the expenditure for carrying out the present experiment was defrayed from Scientfic Research Expenditure of the Department of Education.

References.

(1) S. Barrett and L. H. Levenson: A. I. M. E. **137** (1940), 76.

(2) Siemens-Konzern: Beryllium and Its Alloys, (1929).

(3) D. Harker and M. J. Murphy: A. I. M. E. Metals Div. **161** (1945), 75.

Micro-second Decay of the Thermionic Emission from Oxide Cathode.

By Hazimu KAWAMURA, Akira SHINOHARA, and Yoshio EMOTO.

Mazda Research Laboratories, Tokyo-Shibaura El. Co., Kawasaki, Kanagawa-ken.

(Received February 14, 1949).

We are measuring micro-second decay of the oxide cathode, by the similar method to that of Sproull.(1)

As shown in Fig. 1, the decay curves are composed of two sorts of exponential decays, having period of about 20 micro-seconds and several hundred micro-seconds respectively. The later decay with longer period is common to all cathodes, but the degree of the former decay is very different in variaty of cathodes. We are investigating this decay of the shorter period.

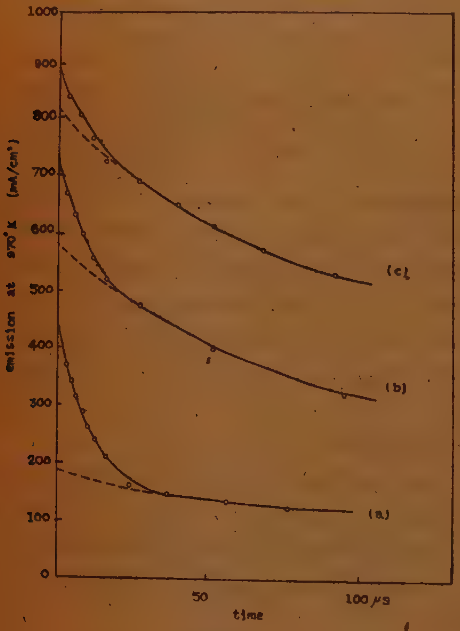

Fig. 1

The results we have obtained are:

1) That the decay is remarkable, when the surface of the core metal of nickel has been oxidized previously;

2) And that the decay disapears in few minutes, when the emission current of several hundreds milli-amperes per cm^2 is drawn out from the cathode at 1000°—1200°K of the cathode temperature, as shown in Fig. 1. Curve a) in Fig. 1 is for the initial state, and b) and c) are the decay curves for the same cathode from which the emission current of 400 ma/ m^2 was drawn for 20 sec. and 50 sec. respectively.

From these results we are now supposing, that the blocking layer at the interface of oxide and core metal, due to the formation of barium nickelate ($BaNiO_3$), give rise to this decay. A part of the emission current through the layer of the oxide is composed of ion current through layer. The Ba ions which are concentrated at the interface by this ion current should reduce the $BaNiO_3$ to BaO and Ni, which results in extinguishing the blocking layer.

Reference.

(1) R. L. Sproull Phys. Rev. **67** 166 (1945).

On the Diffraction of Electromagnetic Waves by Screens and Holes of Perfect Conductors (I)

On a Dual Relation between the Diffractions of Electromagnetic Waves by Screens and that by Holes of Perfect Conductors.

By Tosio Aoki.

Meiji Technological College, Tobata.

(Received September 18, 1948)

Consider a surface S with an arbitrary shape on the xy-plane, let the remainder of the xy-plane be $\bar{S}$ and assume that the medium is homogeneous and isotropic. The object of this paper is to estalish a dual relation between the diffraction by S, which is an infinitely thin and conducting screen, and that by $\bar{S}$ which is also an infinitely thin and conducting screen, but in this case S is a hole.

Definitions and notations. The point conjugate o the point $P = (x, y, z)$ with respect to the xy-lane is $(x, y, -z)$ and denoted by $\bar{P}$. The conjugate vector to the vector $\boldsymbol{A} = (A_x, A_y, A_z)$ with repect to the xy-plane is $\bar{\boldsymbol{A}} = (A_x, A_y, -A_z)$.

$\overset{e}{\boldsymbol{J}}(Q)$ and $\overset{m}{\boldsymbol{J}}(Q)$ represent electric and magnetic current distributions (at a point Q) both being vector functions of a point. These need not be restricted to be point-, or line-, or surface-distributions. $\boldsymbol{J}(Q) = (\overset{m}{\boldsymbol{J}}(Q), \overset{e}{\boldsymbol{J}}(Q))$ represents an electromagnetic current distribution.

$\boldsymbol{E}(P)$ and $\boldsymbol{H}(P)$ represent electric and magnetic fields (at a point P) induced by $\boldsymbol{J}(Q)$, both being vector functions of a point. $\boldsymbol{F}(P) = (\boldsymbol{H}(P), \boldsymbol{E}(P))$ represents an electromagnetic field.

$(\boldsymbol{H}(P), \boldsymbol{E}(P))$ is said to be e-symmetric with respect to the xy-plane if

$$\boldsymbol{H}(\bar{P}) = -\bar{\boldsymbol{H}}(P), \quad \boldsymbol{E}(\bar{P}) = \bar{\boldsymbol{E}}(P) \quad \text{for all } P,$$

hat, is,

$$H_x(x, y, -z) = -H_x(x, y, z),$$
$$E_x(x, y, -z) = E_x(x, y, z),$$
$$H_y(x, y, -z) = -H_y(x, y, z),$$
$$E_y(x, y, -z) = E_y(x, y, z),$$
$$H_z(x, y, -z) = H_z(x, y, z),$$
$$E_z(x, y, -z) = -E_z(x, y, z).$$

Let S be a perfect conductor in the xy-plane and the electromagnetic current which is denoted by $\boldsymbol{J}_U(Q) = (\overset{m}{\boldsymbol{J}}_U(Q), \overset{e}{\boldsymbol{J}}_U(Q))$, be distributed in the half space $z > 0$ only, and let us consider one of such cases fixed and call it U-case. The electromagnetic field in this U-case is denoted by $\boldsymbol{F}_U(P) = (\boldsymbol{H}_U(P), \boldsymbol{E}_U(P))$.

Contrary to the above case, let $\bar{S}$ be a perfect conductor and the electromagnetic current, given by $\boldsymbol{J}_V(Q) = \boldsymbol{J}_U^*(Q)$, be distributed in $z < 0$ only, and let us call it V-case and denote the field by $\boldsymbol{F}_V(P) = (\boldsymbol{H}_V(P), \boldsymbol{E}_V(P))$. The symbol $*$ means $\boldsymbol{J}^*(Q) = (\overset{e}{\boldsymbol{J}}(Q), \overset{m}{\boldsymbol{J}}(Q))$, therefore $\boldsymbol{J}_V(Q) = (\overset{\bar{e}}{\boldsymbol{J}}_U(Q), \overset{\bar{m}}{\boldsymbol{J}}_V(Q))$.

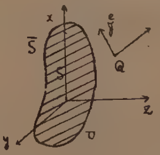

Fig. 1

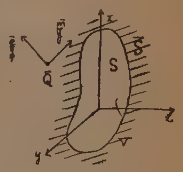

Fig. 2

Now it is easily shown that by a moderate change of the fundamental units, the Maxwell's differential equations can be transformed into the following form

$$(1) \qquad \begin{cases} \nabla \times \boldsymbol{E} + \delta \dfrac{\partial \boldsymbol{H}}{\partial t} = -\overset{m}{\boldsymbol{J}}, \\ \nabla \times \boldsymbol{H} - \delta \dfrac{\partial \boldsymbol{H}}{\partial t} = \overset{e}{\boldsymbol{J}}. \end{cases}$$

In this new fundamental units system we have the following

Theorem. i.

$$\boldsymbol{H}_{U_{\text{II}}} = \boldsymbol{E}_V, \quad \boldsymbol{E}_{U_{\text{II}}} = -\boldsymbol{H}_V \quad (z > 0),$$
$$\boldsymbol{H}_{V_{\text{II}}} = \boldsymbol{E}_U \quad \boldsymbol{E}_{V_{\text{II}}} = -\boldsymbol{H}_U \quad (z < 0),$$

where the fields with suffixes U_{II} *and* V_{II} *indicate the secondary fields of U- and V-cases respectively.*

ii. *Each of the fields* U_{II} *and* V_{II} *is e-symmetric.*

iii. *About the Poynting vectors.*

$$S_{U_{II}} = S_V \quad (z > 0), \quad S_{V_{II}} = S_U \quad (z < 0).$$

Preceding the proof we introduce the notion of the Riemann space. Let Ω_1 and Ω_2 be three-dimensional Euclidean spaces which have the same medium as that of U(and V)-case. Put Ω_1 upon Ω_2 and cut each of them along a corresponding surface S and connect the right side of S in Ω_1 with the left side of S in Ω_2, and the left side of S in Ω_1 with the right side of S in Ω_2. The upper Ω_1 is called a real space and the lower Ω_2 an imaginary space, and these two spaces put together are denoted by Ω and called a Riemann space with two sheets.

Let $J(Q)$ be a given electromagnetic current distribution in Ω and the solution which satisfies Maxwell's equations and given boundary conditions in Ω be called the electromagnetic field in Ω. When we want to indicate the branch surface and the current distribution explicitly we denote the field by $F(P, S, J(Q))$ instead of $F(P) = (H(P), E(P))$.

Now we shall give the outline of the proof of the Theorem.

$J_U(Q_1)$ denotes the current distribution that lies in Ω_1 only and is equal to $J_U(Q)$ of U-case, and $J_U(Q_2)$ denotes the current distribution that lies in Ω_2 only and is equal to $J_U(Q)$, and we have

$$(2) \quad \begin{cases} F_U(P) = F(P, S, J_U(Q_1)) + F(P, S, \tilde{J}_U(\bar{Q}_2)), \\ F_V(P) = F(P, \bar{S}, \overset{*}{J}_U(\bar{Q}_1)) + F(P, \bar{S}, \overset{\tilde{*}}{J}_U(Q_2)), \end{cases}$$

$$(P \in \Omega_1)^{(1)}$$

where $\sim$ is defined by $\tilde{J} = (\overset{\bar{m}}{J}, -\overset{\bar{e}}{J})$.

The primary fields of U- and V-cases can be represented in the Riemann space in the form

$$(3) \quad \begin{cases} F_{U_I}(P) = F(P, S, J_U(Q_1)) + F(P, S, J_U(Q_2)), \\ F_{V_I}(P) = F(P, \bar{S}, \overset{*}{J}_U(Q_1)) + F(P, \bar{S}, \overset{*}{J}_U(Q_2)). \end{cases}$$

From (2), (3) and

$$F_U = F_{U_I} + F_{U_{II}}, \quad F_V = F_{V_I} + F_{V_{II}}$$

we get

$$(4) \quad \begin{cases} F_{U_{II}}(P) = F(P, S, \tilde{J}_U(\bar{Q}_2)) - F(P, S, J_U(Q_2)), \\ F_{V_{II}}(P) = F(P, \bar{S}, \overset{\tilde{*}}{J}_U(Q_2)) - F(P, \bar{S}, \overset{*}{J}_U(\bar{Q}_2)). \end{cases}$$

From this we have the Theorem. ii.

Further we can transform (4) to

$$(5) \quad F_{U_{II}}(P) = F(P, \bar{S}, \tilde{J}_U(\bar{Q}_1)) - F(P, \bar{S}, J_U(Q_2)) \qquad (P \text{ in } z > 0),$$

$$(6) \quad F_{V_{II}}(P) = F(P, S, \overset{\tilde{*}}{J}_U(Q_1)) - F(P, S, \overset{*}{J}_U(\bar{Q}_2)) \qquad (P \text{ in } z < 0).$$

Since $J = (\overset{m}{J}, \overset{e}{J})$, we have $\overset{*}{\tilde{J}} = (-\overset{e}{J}, \overset{m}{J}) = -\overset{\bar{*}}{J}$. The field induced by the current distribution J is $F = (H, E)$, then we define F^* as $F^* = (\bar{E}, \bar{H})$ and $\tilde{F}$ as $\tilde{F} = (\bar{H}, -\bar{E})$. So, if we change J into $\overset{*}{\tilde{J}}$, F changes into $\overset{*}{\tilde{F}}$ that is,

$$(7) \quad F(S, \overset{*}{\tilde{J}}(Q)) = \overset{*}{\tilde{F}}(S, J(Q)) = \overset{*}{\tilde{F}}.$$

From (5) and (7)

$$\overset{*}{\tilde{F}}_{U_{II}} = \overset{*}{\tilde{F}}(\bar{S}, \overset{*}{\tilde{J}}_U(\bar{Q}_1)) - \overset{*}{\tilde{F}}(\bar{S}, J_U(Q_2))$$
$$= F(\bar{S}, \overset{*}{\tilde{\tilde{J}}}_U(Q_1)) - F(\bar{S}, \overset{*}{\tilde{J}}_U(Q_2)).$$

Since $\overset{*}{\tilde{\tilde{J}}} = J^*$ and $\overset{*}{\tilde{J}} = -\tilde{J}^*$ we have

$$\overset{*}{\tilde{F}}_{U_{II}} = F(\bar{S}, \overset{*}{J}_U(\bar{Q}_1)) + F(\bar{S}, \overset{\tilde{*}}{J}_U(Q_2)),$$

this is equal to F_V by (2), therefore

$$\overset{*}{\tilde{F}}_{U_{II}} = (-E_{U_{II}}, H_{U_{II}}) = F_V = (H_V, E_V),$$

that is,

$$H_{U_{II}} = E_V, \quad E_{U_{II}} = -H_V \quad (z > 0).$$

The proof of the half of the Theorem. i. is completed.

In the same way, $\overset{*}{\tilde{F}}_{V_{II}} = F_U$ results from (6), (7) and (2), so we have another half of the Theorem. i.

iii. is a direct consequence of i. Thus the Theorem was proved perfectly.

As a special case of the Theorem we see that the diffraction theory of screens (or holes) with electric sources is equivalent to that of holes (or screens) with magnetic sources. As another special case, the case in which H-waves polarized in one direction project themselves on a screen (or hole) is equivalent to the case in which E-waves polarized in the conjugate direction project themselves on a hole (or screen). Therefore, if we can understand one of these cases completely we can also understand the others.

Generally we have the following

Corollary. If we learn one of the fields U, V, U_{II} and V_{II} for $z>0$ or $z<0$ we can learn all others at the same time, where the primary fields U_{I} and V_{I} are given.

Further it will be easily proved that the Theorem is an extension of the principle of images.

Concerning the diffraction by holes and screens there is the Babinet's principle. This principle asserts that if we define a black body as a body with properties of perfect absorption and perfect non reflexion, then the sum of two fields, the field with S as a black screen and the field with $\bar{S}$ as a black screen, is equal to the primary field (without a diffracting body) in the opposite side of the source with respect to the screen.

In fact, let S be a black screen, $J(Q)$ be in $z>0$ and if we define the diffracted field by S as the solution of the Maxwell's equations in the Riemann space with two sheets with the branch surface S, we have

$$F(P, S, J_U(Q_1))+F(P, \bar{S}, J_U(Q_1)) = \boldsymbol{F}_{U_{\mathrm{I}}}(P),$$
$$(P \text{ in } z<0)$$

This is the so-called Babinet's principle.

However, Sommerfeld⁽³⁾ pointed out that this principle lacks in clearness and that it is most reasonable to consider the field as the solution of the Maxwell's equations in the Riemann space with infinite sheets, so the above relation is as vague as the definition of black bodies.

Then, if we substitute black screens by screens of perfect conductor, what form does the Babinet's principle take? When S is a screen of perfect conductor the field $\boldsymbol{F}_U$ induced by $J_U(Q)$ in $z>0$ is expressed, by (2), as

$$\boldsymbol{F}_U = F(S, J_U(Q_1))+F(S, \tilde{J}_U(\bar{Q}_2)).$$

Similarly the field $\boldsymbol{F}_{U'}$ that has the same current distribution $J_U(Q)$, but now $\bar{S}$ being a screen, is expressed as

$$\boldsymbol{F}_{U'} = F(\bar{S}, J_U(Q_1))+F(\bar{S}, \tilde{J}_U(\bar{Q}_2)).$$

The sum of the above two fields is

$$(8)\quad \boldsymbol{F}_U+\boldsymbol{F}_{U'} = \boldsymbol{F}_{U_{\mathrm{I}}}+2F(S, \tilde{J}_U(Q_2)),\quad (z<0).$$

The last term on the right represents the effect in $z<0$ of the real space by the source in $z<0$ of the imaginary space, and generally is considered smaller than the primary $\boldsymbol{F}_{U_{\mathrm{I}}}$.

References.

(1) Cf. 小谷正雄, 木原太郎, 穴及細隙よりの電波の漏洩の理論.

(2) Riemann-Webers: Differentialgleichungen der Physik II. P. 440.

On the Diffraction of Electromagnetic Waves by Screens and Holes of Perfect Conductors (II)

Approximate Formulas and their Applications

By Tosio AOKI.

Meiji Technological College, Tobata.

(Received September 18, 1948)

On the diffraction of waves by screens and holes, until now only a few cases of screens of half planes, infinitely long slits and rectangular screens were discussed.

Since we have given in (I) the dual relation between the diffracted field by a screen and that by the corresponding hole, it is sufficient to study one of these fields, especially its field in the half space. So we shall here give the approximate formulas of diffracted fields through holes and give their applications to the above cases and further to circular holes and elliptical holes. Thus the diffraction problems by screens and holes, though approximate, are discussed systematically and some new results may be expected.

§ 1. General Approximate Formulas.

Let S be a hole, $\bar{S}$ be an infinitely thin conducting screen, both be on the xy-plane and cover the whole plane together*. We assume that the medium is homogeneous and isotropic dielectric and its inductive capacities are ε and μ, and that the electromagnetic current distribution $J(Q) = (\overset{m}{J}(Q), \overset{e}{J}(Q))$ is in the left half space ($z < 0$) alone. In the following we shall observe the diffracted fields through S at a point $P = (x, y, z)$ in the right half space ($z > 0$).

The field we now observe is one of V-cases mentioned in (I), so applying the notion of Riemann spaces, from (I)-(2), we have

(1) $F_V(P) = F(P_1, \bar{S}, J(Q_1) + F(P_1, \bar{S}, \tilde{J}(\bar{Q}_2))$.**

Put

$$F(P, \bar{S}, J(Q_1)) = (\boldsymbol{H}_1(P), \boldsymbol{E}_1(P)),$$

$$F(P, \bar{S}, \tilde{J}(\bar{Q}_2)) = (\boldsymbol{H}_2(P), \boldsymbol{E}_2(P)),$$

there exist

$$(2) \quad \begin{cases} \boldsymbol{H}_2(P_1) = \bar{\boldsymbol{H}}_1(\bar{P}_2), & \boldsymbol{H}_2(P_2) = \bar{\boldsymbol{H}}_1(\bar{P}_1), \\ \boldsymbol{E}_2(P_1) = -\bar{\boldsymbol{E}}_1(\bar{P}_2), & \boldsymbol{E}_2(P_2) = -\bar{\boldsymbol{E}}_1(\bar{P}_1), \end{cases}$$

so we shall only observe the first term on the right side of (1). Since

$$(3) \quad \begin{cases} F(P_1, \bar{S}, J(Q_1)) = F(P_2, S, J(Q_1)), \\ F(P_2, \bar{S}, J(Q_1)) = F(P_1, S, J(Q_1)) \end{cases}$$

it is sufficient to observe the field $F(P, S, J(Q_1))$ after all.

Now set

$$F(P, S, J(Q_1)) = (\boldsymbol{H}'(P), \boldsymbol{E}'(P))$$

and applying the Green's theorem in the Riemann space, after somewhat complicated calculations, we get the following results.

$$(4) \quad \begin{cases} \boldsymbol{H}'(P) = \dfrac{1}{4\pi}\displaystyle\int_{S^+}\left(\boldsymbol{H}_I\frac{\partial\psi}{\partial n} - \psi\frac{\partial \boldsymbol{H}_I}{\partial n}\right)da \\ \quad -\dfrac{1}{4\pi}\displaystyle\int_{C^+}\psi\boldsymbol{H}_I\times d\boldsymbol{s} + \frac{1}{4\pi i\omega\mu}\int_{C^+}\nabla\psi\boldsymbol{E}_I\cdot d\boldsymbol{s} \\ \quad +\dfrac{1}{2\pi}\nabla\times\displaystyle\int_{S_2^-}\psi\boldsymbol{n}\times\boldsymbol{H}'da \\ \quad -\dfrac{1}{2\pi i\omega\mu}\nabla\times\nabla\times\displaystyle\int_{S_2^-}\psi\boldsymbol{n}\times\boldsymbol{E}'da, \\ \boldsymbol{E}'(P) = \dfrac{1}{4\pi}\displaystyle\int_{S^+}\left(\boldsymbol{E}_I\frac{\partial\psi}{\partial n} - \psi\frac{\partial \boldsymbol{E}_I}{\partial n}\right)da \\ \quad -\dfrac{1}{4\pi}\displaystyle\int_{C^+}\psi\boldsymbol{E}_I\times d\boldsymbol{s} - \frac{1}{4\pi i\omega\varepsilon}\int_{C^+}\nabla\psi\boldsymbol{H}_I\,d\boldsymbol{s} \\ \quad +\dfrac{1}{2\pi}\nabla\times\displaystyle\int_{S_2^-}\psi\boldsymbol{n}\times\boldsymbol{E}'da \\ \quad -\dfrac{1}{2\pi i\omega\varepsilon}\nabla\times\nabla\times\displaystyle\int_{S_2^-}\psi\boldsymbol{n}\times\boldsymbol{H}'da, \end{cases}$$

where

---

* Notations are used correspondingly to (I).

** $P_1(P_2)$ is the point in $\Omega_1(\Omega_2)$ which has the same coordinates as P.

$\psi = e^{ikr}/r,\ k^2 = \omega^2 \varepsilon \mu,$

$$r = ((x-x')^2+(y-y')^2+(z-z')^2)^{1/2};$$

$P = (x, y, z)$ is an observing point,

$P' = (x', y', z')$ is an integral point on S,

the field depends on t by $\exp(-i\omega t)$,

$(\boldsymbol{H}_I, \boldsymbol{E}_I)$ means the primary field of $\boldsymbol{F}_V = (\boldsymbol{H}, \boldsymbol{E})$,

$\int_{S^+} da$ means the surface integral on $z = +0$ of S,

$\int_{S^-} da$ means the surface integral on $z = -0$ of S in Ω_2,

$\boldsymbol{n}$ is a unit vector normal to S and points to the positive z-axis on $z = +0$ and the negative z-axis on $z = -0$,

$\int_{C^+} d\boldsymbol{s}$ means the line integral along C which is the contour of S and $\bar{S}$ at the same time, and its direction, looking from the right side $z > 0$, is counter-clockwise, $d\boldsymbol{s}$ the line element vector on C.

The Kirchhoff-Huygens' solutions are the first each one term on the right side of (4) and the Kottler's solutions⁽¹⁾ which were obtained as a "Sprungwertproblem" are the first each three terms on the right side of (4), that depend on the primary field only.

In virtue of (1), (2) and (3) we can express $\boldsymbol{F}_V$ by $(\boldsymbol{H}', \boldsymbol{E}')$ such as

$$\boldsymbol{H}(P) = \boldsymbol{H}'(P_2)+\bar{\boldsymbol{H}}'(\bar{P}_2),$$
$$\boldsymbol{E}(P) = \boldsymbol{E}'(P_2)-\bar{\boldsymbol{E}}'(\bar{P}_2),$$

Substitute (4) for $\boldsymbol{E}'$ and $\boldsymbol{H}'$ of the above equations and change their forms a little, we have

$$(4)\quad \begin{cases} \boldsymbol{H}(P) = \dfrac{1}{2\pi}\displaystyle\int_{S^+}\left(\boldsymbol{H}_{In}\frac{\partial\psi}{\partial n}-\psi\frac{\partial \boldsymbol{H}_{It}}{\partial n}\right)da \\ \qquad -\dfrac{1}{2\pi}\displaystyle\int_{C^+}\psi \boldsymbol{H}_{In}\times d\boldsymbol{s}-\frac{1}{2\pi i\omega\mu}\int_{C^+}\nabla\psi \boldsymbol{E}_{It}\cdot d\boldsymbol{s} \\ \qquad +\dfrac{1}{\pi i\omega\mu}\nabla\times\nabla\times\displaystyle\int_{S_2^-}\psi \boldsymbol{n}\times \boldsymbol{E}_t' da, \\ \boldsymbol{E}(P) = \dfrac{1}{2\pi}\displaystyle\int_{S^+}\left(\boldsymbol{E}_{It}\frac{\partial\psi}{\partial n}-\psi\frac{\partial \boldsymbol{E}_{In}}{\partial n}\right)da \\ \qquad -\dfrac{1}{2\pi}\displaystyle\int_{C^+}\psi \boldsymbol{E}_{It}\times d\boldsymbol{s}+\frac{1}{\pi}\nabla\times\int_{S_2^-}\psi \boldsymbol{n}\times \boldsymbol{E}_t' da, \end{cases}$$

where the fields with suffix $\boldsymbol{n}$ represent their normal components in the direction of positive z-axis and the fields with suffix t their tangential components on the xy-plane.

Considering physically, as the first approximate formulas of $\boldsymbol{H}$ and $\boldsymbol{E}$ we can generally adopt the sum of the terms which depend only on the primary field on the right side of (5). As the second we adopt $\boldsymbol{H}$ and $\boldsymbol{E}$ of (5) in which $\boldsymbol{E}'$ is substituted by the first approximate formula.

§ 2. Spherical Waves.

In the case of the radiation from a dipole located at $Q = (x_0, y_0, z_0)$ of finite distance we can transform the surface integrals of the first approximate formulas of (5) into line integrals, the result is⁽²⁾

$$(6)\quad \begin{cases} \boldsymbol{H}(P) \simeq \boldsymbol{H}_0(P)+\bar{\boldsymbol{H}}_0(\bar{P}), \\ \boldsymbol{E}(P) \simeq \boldsymbol{E}_0(P)-\bar{\boldsymbol{E}}_0(\bar{P}), \end{cases}$$

where in the case of the magnetic dipole $\boldsymbol{p}\Psi$ (Hertz vector)

$$(5)\quad \begin{cases} \boldsymbol{H}_0 = \boldsymbol{H}_I^* + \dfrac{1}{4\pi}(k^2\boldsymbol{p}+(\boldsymbol{p}\cdot\nabla^0)\nabla^0)\Phi - \dfrac{1}{4\pi}\displaystyle\int_C \boldsymbol{A}\times d\boldsymbol{s} \\ \qquad -\dfrac{1}{4\pi}\nabla\displaystyle\int_C \boldsymbol{B}\cdot d\boldsymbol{s}, \\ \boldsymbol{E}_0 = \boldsymbol{E}_I^* + \dfrac{i\omega\mu}{4\pi}\boldsymbol{p}\times\nabla^0\Phi + \dfrac{i\omega\mu}{4\pi}\displaystyle\int_C \boldsymbol{B}\times d\boldsymbol{s} \\ \qquad -\dfrac{1}{4\pi i\omega\varepsilon}\nabla\displaystyle\int_C \boldsymbol{A}\cdot d\boldsymbol{s}, \end{cases}$$

in the case of the electric dipole $\boldsymbol{p}\Psi$

$$(6)\quad \begin{cases} \boldsymbol{H}_0 = \boldsymbol{H}_I^* - \dfrac{i\omega\varepsilon}{4\pi}\boldsymbol{p}\times\nabla^0\Phi - \dfrac{i\omega\varepsilon}{4\pi}\displaystyle\int_C \boldsymbol{B}\times d\boldsymbol{s} \\ \qquad +\dfrac{1}{4\pi i\omega\mu}\nabla\displaystyle\int_C \boldsymbol{A}\cdot d\boldsymbol{s}, \\ \boldsymbol{E}_0 = \boldsymbol{E}_I^* + \dfrac{1}{4\pi}(k^2\boldsymbol{p}+(\boldsymbol{p}\cdot\nabla^0)\nabla^0)\Phi - \dfrac{1}{4\pi}\displaystyle\int_C \boldsymbol{A}\times d\boldsymbol{s} \\ \qquad -\dfrac{1}{4\pi}\nabla\displaystyle\int_C \boldsymbol{B}\cdot d\boldsymbol{s}, \end{cases}$$

in which

$$(\boldsymbol{H}_I^*(P), \boldsymbol{E}_I^*(P)) = \begin{cases} (\boldsymbol{H}_I(P), \boldsymbol{E}_I(P)) & \text{if} \quad P \in L, \\ 0 & \text{if} \quad P \notin L, \end{cases}$$

L is the right part $(z > 0)$ of the cone which has the vertex at Q and C as its guiding curve,

$$\psi = e^{ikr}/r,\ \Psi = e^{ik\xi}/\xi,\ \Phi = \int_C \psi\Psi\frac{\boldsymbol{r}\cdot\boldsymbol{v}\times d\boldsymbol{s}}{r-\boldsymbol{r}\cdot\boldsymbol{v}},$$

$$r = \overline{P'P},\quad \boldsymbol{r} = \overrightarrow{P'P},\quad \xi = \overline{QP'},$$

$\boldsymbol{v}$ is the unit vector with its direction QP', P' is a point on C,

$$\boldsymbol{A} = \psi\Psi(k^2\boldsymbol{p}-(k^2+2ik\xi^{-1}-2\xi^{-2})(\boldsymbol{p}\cdot\boldsymbol{v})\boldsymbol{v}),$$

$$B=\psi\Psi(ik-\xi^{-1})(\boldsymbol{p}\times\boldsymbol{v}),$$

$$\nabla_0=x\frac{\partial}{\partial x^0}+y\frac{\partial}{\partial y^0}+z\frac{\partial}{\partial z^0},$$

$$\nabla=x\frac{\partial}{\partial x}+y\frac{\partial}{\partial y}+z\frac{\partial}{\partial z}.$$

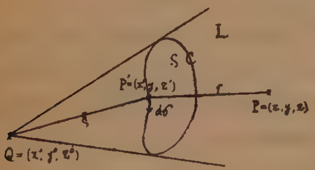

Fig. 1

§ 3. Plane Waves.

The Hertzvectors of *H*- and *E*-waves polarized in a direction $\boldsymbol{p}$ are represented by $\boldsymbol{p}e^{ik\xi}$. Let $\boldsymbol{k}_0$ be the unit vector which represents the direction of their propagation. Similarly to § 2 we have the following result.

$$(7)\quad\begin{cases}\boldsymbol{H}(P)\simeq\boldsymbol{H}_0(P)+\bar{\boldsymbol{H}}_0(\bar{P}),\\ \boldsymbol{E}(P)\simeq\boldsymbol{E}_0(P)-\bar{\boldsymbol{E}}_0(\bar{P}),\end{cases}$$

where in the case of *H*-wave

$$(7.1)\quad\begin{cases}\boldsymbol{H}_0=\boldsymbol{H}_I{}^*+\frac{k^2}{4\pi}(\boldsymbol{p}-(\boldsymbol{p}\cdot\boldsymbol{k}_0)\boldsymbol{k}_0)\Phi-\frac{k^2}{4\pi}\int_C\psi\Psi(\boldsymbol{p}\\ \qquad-(\boldsymbol{p}\cdot\boldsymbol{k}_0)\boldsymbol{k}_0)\times d\boldsymbol{s}-\frac{ik}{4\pi}\nabla\int_C\psi\Psi(\boldsymbol{p}\times\boldsymbol{k}_0)\cdot d\boldsymbol{s},\\ \boldsymbol{E}_0=\boldsymbol{E}_I{}^*+\frac{k\omega\mu}{4\pi}\boldsymbol{p}\times\boldsymbol{k}_0\Phi-\frac{k\omega\mu}{4\pi}\int_C\psi\Psi(\boldsymbol{p}\times\boldsymbol{k}_0)\\ \qquad\times d\boldsymbol{s},\end{cases}$$

in the case of *E*-wave

$$(7.2)\quad\begin{cases}\boldsymbol{H}_0=\boldsymbol{H}_I{}^*-\frac{k\omega\varepsilon}{4\pi}\boldsymbol{p}\times\boldsymbol{k}_0\Phi+\frac{k\omega\varepsilon}{4\pi}\int_C\psi\Psi(\boldsymbol{p}\times\boldsymbol{k}_0)\times d\boldsymbol{s}\\ \qquad-\frac{i\omega\varepsilon}{4\pi}\nabla\int_C\psi\Psi(\boldsymbol{p}-(\boldsymbol{p}\cdot\boldsymbol{k}_0)\boldsymbol{k}_0)\cdot d\boldsymbol{s},\\ \boldsymbol{E}_0=\boldsymbol{E}_I{}^*+\frac{k^2}{4\pi}(\boldsymbol{p}-(\boldsymbol{p}\cdot\boldsymbol{k}_0)\boldsymbol{k}_0)\Phi-\frac{k^2}{4\pi}\int_C\psi\Psi(\boldsymbol{p}\\ \qquad-(\boldsymbol{p}\cdot\boldsymbol{k}_0)\boldsymbol{k}_0)\times d\boldsymbol{s},\end{cases}$$

in which

$$(\boldsymbol{H}_I{}^*(P),\ \boldsymbol{E}_I{}^*(P))=\begin{cases}(\boldsymbol{H}_I(P),\ \boldsymbol{E}_I(P)) & P\in L,\\ 0 & P\notin L,\end{cases}$$

$$\psi=e^{ikr}/r,\quad\Psi=e^{ik\xi},\quad\Phi=\int_C\psi\Psi\frac{\boldsymbol{r}\cdot\boldsymbol{k}_0\times d\boldsymbol{s}}{r-\boldsymbol{r}\cdot\boldsymbol{k}_0},$$

ξ is the distance from some constant phase plane to a point on C parallel to the direction $\boldsymbol{k}_0$.

§ 4. Half Planes and Infinitely Long Slits.

The solution of the problem of the diffraction by a half plane has been obtained by Sommerfeld⁽³⁾ by the use of a contour integral representation. Epstein⁽⁴⁾ and Crudelli⁽⁵⁾ also solved it as a boundary value problem. The diffraction through infinitely long slits were studied by Sieger⁽⁶⁾ and Morse-Rubenstein⁽⁷⁾ exactly. Computing (7), (7.1) and (7.2) we can obtain the same results as these approximately.

§ 5. Holes of Finite Dimensions.

General approximate formulas have been obtained from (5), but in this § we shall study the diffracted fields of plane waves through holes of finite dimensions at large distances especially.

Set the origin in the neighborhood of the hole. We calculate (5) by the use of orthogonal coordinates $(x,\ y,\ z)$, spherical coordinates $(R,\ \theta,\ \varphi)$ and cylindrical coordinates $(\rho,\ \alpha,\ z)$ according to circumstances. Let the propagation vector of the given plane be $\boldsymbol{k}(R=k,\ \theta=\theta_0,\ \varphi=\varphi_0)$ and $\boldsymbol{p}$ be the unit vector which lies in the plane normal to $\boldsymbol{k}$ at the origin and in the xy-plane at the same time and directs at the angle $\varphi_0-\pi/2$ to the positive x-axis. The field whose electric field is polarized in the direction $\boldsymbol{p}$ is called *E*-wave and the field whose magnetic field is polarized in the direction $\boldsymbol{p}$ is called *H*-wave.

In the case of *H*-wave

$$(8)\quad\begin{cases}\boldsymbol{H}\simeq-\boldsymbol{p}\frac{ik^3}{2\pi}\cos\theta_0\frac{e^{ikR}}{R}\int_S Kda-\boldsymbol{R}\frac{k^2}{2\pi}\cos\theta_0\\ \qquad\frac{e^{ikR}}{R}\int_C K\cos(\beta-\varphi_0)ds,\\ \boldsymbol{E}=\frac{ik^2\omega\mu}{2\pi}\cos\theta_0(\boldsymbol{q}\cos\theta-\boldsymbol{n}\sin\theta_0)\frac{e^{ikR}}{R}\int_S Kda\\ \qquad+\boldsymbol{n}\frac{k\omega\mu}{2\pi}\cos\theta_0\frac{e^{ikR}}{R}\int_C K\sin(\beta-\varphi_0)ds.\end{cases}$$

written in components, they are

$$\begin{cases}H_R\simeq\frac{ik^3}{2\pi}\sin\theta\cos\theta_0\sin(\varphi-\varphi_0)\psi_0\int_S Kda\\ \qquad-\frac{k^2}{2\pi}\cos\theta_0\,\psi_0\int_C K\cos(\beta-\varphi_0)ds,\\ H_\theta\simeq\frac{ik^3}{2\pi}\cos\theta\cos\theta_0\sin(\varphi-\varphi_0)\psi_0\int_S Kda,\end{cases}$$

$$\left\{\begin{array}{l}
H_\varphi \simeq \dfrac{ik^3}{2\pi}\cos\theta_0\cos(\varphi-\varphi_0)\psi_0\displaystyle\int_S Kda, \\
E_R \simeq \dfrac{ik^2\omega\mu}{2\pi}\cos\theta\cos\theta_0(\sin\theta\cos(\varphi-\varphi_0)-\sin\theta_0) \\
\quad \psi_0\displaystyle\int_S Kda+\dfrac{k\omega\mu}{2\pi}\cos\theta\cos\theta_0\,\psi_0\displaystyle\int_C K \\
\quad \sin(\beta-\varphi_0)ds, \\
E_\theta \simeq \dfrac{ik^2\omega\mu}{2\pi}\cos\theta_0(\cos^2\theta\cos(\varphi-\varphi_0)+\sin\theta\sin\theta_0) \\
\quad \psi_0\displaystyle\int_S Kda-\dfrac{k\omega\mu}{2\pi}\sin\theta\cos\theta_0\,\psi_0\displaystyle\int_C K\sin(\beta-\varphi_0) \\
\quad ds, \\
E_\varphi \simeq -\dfrac{ik^2\omega\mu}{2\pi}\cos\theta\cos\theta_0\sin(\varphi-\varphi_0)\psi_0\displaystyle\int_S Kda,
\end{array}\right. \tag{9}$$

in the case of E-wave

$$\left\{\begin{array}{l}
\boldsymbol{H} \simeq \dfrac{ik^2\omega\varepsilon}{2\pi}(\boldsymbol{n}\cos\theta_0\sin\theta_0-\boldsymbol{q}\cos^2\theta_0)\psi_0\displaystyle\int_S Kda \\
\quad +\dfrac{k\omega\varepsilon}{2\pi}\sin\theta_0\,\psi_0\displaystyle\int_C K\boldsymbol{n}\times d\boldsymbol{s}-\boldsymbol{R}\dfrac{k\omega\varepsilon}{2\pi}\psi_0\displaystyle\int K \\
\quad \sin(\beta-\varphi_0)ds, \\
\boldsymbol{E} \simeq -\boldsymbol{p}\dfrac{ik^3}{2\pi}\cos\theta\psi_0\displaystyle\int_S Kda-\boldsymbol{n}\dfrac{k^2}{2\pi}\psi_0\displaystyle\int_C K \\
\quad \cos(\beta-\varphi_0)ds,
\end{array}\right. \tag{10}$$

written in components, they are

$$\left\{\begin{array}{l}
H_R \simeq \dfrac{ik^2\omega\varepsilon}{2\pi}(\cos^2\theta\sin\theta_0-\sin\theta\cos^2\theta_0 \\
\quad \cos(\varphi-\varphi_0))\displaystyle\int_S Kda-\dfrac{k\omega\varepsilon}{2\pi}\sin\theta\sin\theta_0\psi_0 \\
\quad \displaystyle\int_C K\sin(\beta-\varphi)ds-\dfrac{k\omega\varepsilon}{2\pi}\psi_0\displaystyle\int_C K\sin(\beta-\varphi_0)ds, \\
H_\theta \simeq -\dfrac{ik^2\omega\varepsilon}{2\pi}\cos\theta(\sin\theta\sin\theta_0+\cos^2\theta_0\cos(\varphi-\varphi_0)) \\
\quad \psi_0\displaystyle\int_S Kda-\dfrac{k\omega\varepsilon}{2\pi}\cos\theta\sin\theta_0\psi_0\displaystyle\int_C K\sin(\beta-\varphi)ds, \\
H_\varphi \simeq \dfrac{ik^2\omega\varepsilon}{2\pi}\cos^2\theta_0\sin(\varphi-\varphi_0)\psi_0\displaystyle\int_S Kda \\
\quad +\dfrac{k\omega\varepsilon}{2\pi}\sin\theta_0\,\psi_0\displaystyle\int_C K\cos(\beta-\varphi)ds, \\
E_R \simeq \dfrac{ik^3}{2\pi}\sin\theta\cos\theta\sin(\varphi-\varphi_0)\,\psi_0\displaystyle\int_S Kda \\
\quad -\dfrac{k^2}{2\pi}\cos\theta\,\psi_0\displaystyle\int_C K\cos(\beta-\varphi_0)ds, \\
E_\theta \simeq \dfrac{ik^3}{2\pi}\cos^2\theta\sin(\varphi-\varphi_0)\psi_0\displaystyle\int_S Kda \\
\quad +\dfrac{k^2}{2\pi}\sin\theta\,\psi_0\displaystyle\int_C K\cos(\beta-\varphi_0)ds, \\
E_\varphi \simeq \dfrac{ik^3}{2\pi}\cos\theta\cos(\varphi-\varphi_0)\psi_0\displaystyle\int_S Kda,
\end{array}\right. \tag{11}$$

in which

$$\psi_0 = e^{ikR}/R,$$

$$K = \exp(ikd(x'\cos\delta+y'\sin\delta))$$

$$= \exp(ik\rho d\cos(\alpha-\delta)),$$

$$d = (\sin^2\theta-2\sin\theta\sin\theta_0\cos(\varphi-\varphi_0)+\sin^2\theta_0)^{1/2},$$

$$\tan\delta = (\sin\theta_0\sin\varphi_0-\sin\varphi\sin\varphi)/(\sin\theta_0\cos\varphi_0-\sin\theta\cos\varphi),$$

$$\boldsymbol{q} = (1, \pi/2, \varphi_0), \quad d\boldsymbol{s} = (ds, \pi/2, \beta).$$

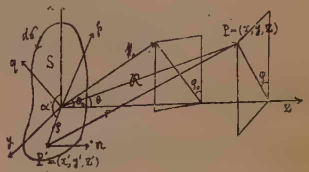

Fig. 2,

§ 6. Circular Holes.

Set the origin at the center of the given circular hole with radius a. In the case of plane waves incident at this hole the diffracted field at a point (R, θ, φ) of large distances is obtained from (8)–(11). In this case, by the symmetry of its shape without losing generality we can assume that the direction of the polarization coincides with the x-axis.

In the case of H-wave

$$\left\{\begin{array}{l}
H_R \simeq 0, \\
H_\theta \simeq -ik^2a\cos\theta\cos\theta_0\cos\varphi\psi_0L, \\
H_\varphi \simeq ik^2a\cos\theta_0\sin\varphi\psi_0L, \\
E_R \simeq 0 \\
E_\theta \simeq ik\omega\mu a\cos\theta_0\sin\varphi\psi_0L, \\
E_\varphi \simeq ik\omega\mu a\cos\theta\cos\theta_0\cos\varphi\psi_0L,
\end{array}\right. \tag{12}$$

in the case of E-wave

$$\left\{\begin{array}{l}
H_R \simeq 0, \\
H_\theta \simeq -ik\omega\varepsilon a\cos\theta\sin\varphi\psi_0L, \\
H_\varphi \simeq -ik\omega\varepsilon a\cos\varphi\psi_0L, \\
E_R = 0, \\
E_\theta \simeq -ik^2a\cos\varphi\psi_0L, \\
E_\varphi \simeq ik^2a\cos\theta\sin\varphi\psi_0L,
\end{array}\right. \tag{13}$$

where

$$L = J_1(kad)/d^*, \qquad \psi_0 = \exp(ikR)/R,$$

$$d = (\sin^2\theta-2\sin\theta\sin\theta_0\sin\varphi+\sin^2\theta_0)^{1/2}.$$

---

* J_1 is the Bessel function of the first order.

Let F be the energy flow, at the observing point (R, θ, φ), G be the energy flow of geometrical optics through the hole and W be the total transmission energy and put

$$I=2\pi R^2F/G, \quad T=W/G$$

we call I the relative intensity and T the transmission coefficient.

In the case of H-wave

$$(14)\ \begin{cases} I\simeq 2\cos\theta_0(1-\sin^2\theta\cos^2\varphi)L^2, \\ T\simeq\dfrac{1}{\pi}\cos\theta_0\displaystyle\int_0^{\pi/2}d\theta\int_0^{2\pi}\sin\theta(1-\sin^2\theta\cos^2\varphi)L^2d\varphi, \end{cases}$$

in the case of E-wave

$$(15)\ \begin{cases} I\simeq 2\sec\theta_0(1-\sin^2\theta\sin^2\varphi)L^2, \\ T\simeq\dfrac{1}{\pi}\sec\theta_0\displaystyle\int_0^{\pi/2}d\theta\int_0^{2\pi}\sin\theta(1-\sin^2\theta\sin^2\varphi)L^2d\varphi. \end{cases}$$

§ 7. Elliptical Holes.

Let the semimajor and semiminor axes of the given elliptical hole be a and b, the origin be located at its center and semimajor axis coincide with the x-axis and the direction of the polarization of plane waves. The diffracted fields by the hole are obtained similarly to the previous §.

In the case of H-wave

$$(16)\ \begin{cases} H_R\simeq 0, \\ H_\theta\simeq ik^2ab\cos\theta\cos\theta_0\sin(\varphi-\varphi_0)\psi_0M, \\ H_\varphi\simeq ik^2ab\cos\theta_0\cos(\varphi-\varphi_0)\psi_0M, \\ E_R\simeq 0, \\ E_\theta\simeq ik\omega\mu\, ab\cos\theta_0\cos(\varphi-\varphi_0)\psi_0M, \\ E_\varphi\simeq -ik\omega\mu\, ab\cos\theta\cos\theta_0\sin(\varphi-\varphi_0)\psi_0M, \\ I\simeq 2ab\cos\theta_0(1-\sin^2\theta\sin^2(\varphi-\varphi_0))M^2, \\ T\simeq\dfrac{1}{\pi}ab\cos\theta_0\displaystyle\int_0^{\pi/2}d\theta\int_0^{2\pi}\sin\theta(1-\sin^2\theta \\ \qquad \sin^2(\varphi-\varphi_0))M^2d\varphi, \end{cases}$$

in the case of E-wave

$$(17)\ \begin{cases} H_R\simeq 0, \\ H_\theta\simeq -ik\omega\varepsilon\, ab\cos\theta\cos(\varphi-\varphi_0)\psi_0M, \\ H_\varphi\simeq ik\omega\varepsilon\, ab\sin(\varphi-\varphi_0)\psi_0M, \\ E_R\simeq 0, \\ E_\theta\simeq ik^2ab\sin(\varphi-\varphi_0)\psi_0M, \\ E_\varphi\simeq ik^2ab\cos\theta\cos(\varphi-\varphi_0)\psi_0M, \\ I\simeq 2ab\sec\theta_0(1-\sin^2\theta\cos^2(\varphi-\varphi_0))M^2, \\ T\simeq\dfrac{1}{\pi}ab\sec\theta_0\displaystyle\int_0^{\pi/2}d\theta\int_0^{2\pi}\sin\theta(1-\sin^2\theta\cos^2 \\ \qquad (\varphi-\varphi_0))M^2d\varphi, \end{cases}$$

in which

$$\psi_0=\exp(ikR)/R,\ \ M=J_1(kf)/f,\ \ f=(a^2(\sin\theta_0\cos\varphi_0 \\ -\sin\theta\cos\varphi)^2+b^2(\sin\theta_0\sin\varphi_0-\sin\theta\sin\varphi)^2)^{1/2}.$$

§ 8. Rectangular Holes.

Let two sides of the given rectangular hole be $2a$ and $2b$, and the origin be located at its center. The diffracted fields of plane waves by the hole are obtained in the same manner as the previous §.

In the case of H-wave

$$(18)\ \begin{cases} H_R\simeq 0, \\ H_\theta\simeq\dfrac{2}{\pi}ik^3\cos\theta\cos\theta_0\sin(\varphi-\varphi_0)\psi_0AB, \\ H_\varphi\simeq\dfrac{2}{\pi}ik^3\cos\theta_0\cos(\varphi-\varphi_0)\psi_0AB, \\ E_R\simeq 0, \\ E_\theta\simeq\dfrac{2}{\pi}ik^2\omega\mu\cos\theta_0\cos(\varphi-\varphi_0)\psi_0AB, \\ E_\varphi\simeq -\dfrac{2}{\pi}ik^2\omega\mu\cos\theta\cos\theta_0\sin(\varphi-\varphi_0)\psi_0AB, \\ I\simeq\dfrac{2k^2}{\pi ab}\cos\theta_0(1-\sin^2\theta\sin^2(\varphi-\varphi_0))A^2B^2, \\ T=\dfrac{k^2}{\pi^2ab}\cos\theta_0\displaystyle\int_0^{\pi/2}d\theta\int_0^{2\pi}\sin\theta(1-\sin^2\theta \\ \qquad \sin^2(\varphi-\varphi_0))A^2B^2d\varphi, \end{cases}$$

and in the case of E-wave

$$(19)\ \begin{cases} H_R\simeq 0, \\ H_\theta\simeq -\dfrac{2}{\pi}ik^2\omega\varepsilon\cos\theta\cos(\varphi-\varphi_0)\psi_0AB, \\ H_\varphi\simeq\dfrac{2}{\pi}ik^2\omega\varepsilon\sin(\varphi-\varphi_0)\psi_0AB, \\ E_R\simeq 0, \\ E_\theta\simeq\dfrac{2}{\pi}ik^3\sin(\varphi-\varphi_0)\psi_0AB, \\ E_\varphi\simeq\dfrac{2}{\pi}ik^3\cos\theta\cos(\varphi-\varphi_0)\psi_0AB, \\ I\simeq\dfrac{2k^2}{\pi ab}\sec\theta_0(1-\sin^2\theta\cos^2(\varphi-\varphi_0))A^2B^2, \\ T\simeq\dfrac{k^2}{\pi^2ab}\sec\theta_0\displaystyle\int_0^{\pi/2}d\theta\int_0^{2\pi}\sin\theta(1-\sin^2\theta \\ \qquad \cos^2(\varphi-\varphi_0))A^2B^2d\varphi, \end{cases}$$

in which

$$\psi_0 = \exp(ikR)/R,$$

$$A = \sin(ka(\sin\theta_0\cos\varphi_0 - \sin\theta\cos\varphi))/k(\sin\theta_0\cos\varphi_0 - \sin\theta\cos\varphi),$$

$$B = \sin(kb(\sin\theta_0\sin\varphi_0 - \sin\theta\sin\varphi))/k(\sin\theta_0\sin\varphi_0 - \sin\theta\sin\varphi).$$

The problem studied by Stratton and Chu(8) is the special case of the above and it is easily proved that their solutions coincide with ours.

References.

(1) F. Kottler; Ann. d. Phys. **71**, (1923) 457.

(2) The proof is omitted. Cf. von A. Rubinowicz; Ann. d. Phys. **53**, (1917) 257.

(3) Sommerfeld; Math. Ann. **47**, (1896) 317.

(4) Epstein; Diss. Munich (1914).

(5) Crudelli; Nuovo Cimento **11**, (1916) 277.

(6) Sieger; Ann. d. Phys. **27**, (1908) 626.

(7) M. Morse and J. Rubenstein; Phys. Rev. **54**, (1938) 895.

(8) Stratton and Chu; Phys. Rev. **56**, (1939) 99.

On the Ammonia Molecule (II).

By Masataka MIZUSHIMA.

(*Physics Department, Faculty of Science, University of Tokyo.*)

(Received; Nov. 12, 1948)

§ 1. Introduction.

In the previous paper(1) we discussed on the wave function of the ammonia molecule, and then calculated the effect of inhomogeneous electric field on the molecular beam of ammonia. In this paper, consideration on the intermolecular potential between ammonia molecules is made, and using the results we proceed to calculate the half-width of the spectral line in the "inversion spectra"(2) of this molecule.

It is pointed out(3) that the wave function of the ammonia molecule can be classified into + and − classes, owing to the fact that the potential energy of this molecule is not changed when all atoms are inverted at the center. The wave function of this molecule can be factorized into vibrational, rotational, and the other parts, with good approximation, so that for the + and − states with rotational quantum numbers J, K, and M

$$\Psi_+ = \psi_+\Theta_{J,K,M}\Phi \quad \text{and} \quad \Psi_- = \psi_-\Theta_{J,K,M}\Phi \tag{1}$$

respectivly; where ψ_+ and ψ_-, the vibrational parts, does not and does change sign respectivily when the above operation is made. Thus for the matrix elements of dipole vector μ we obtain

$$\int\psi_+\mu\psi_+d\tau = \int\psi_-\mu\psi_-d\tau = 0 \tag{2}$$

and from the susceptibility data

$$\mu \equiv \left|\int\psi_+\mu\bar{\psi}_-d\tau\right| = 1.48\cdot10^{-18}\ \text{e.s.u.} \tag{3}$$

§ 2. Intermolecular Perturbation between the Ammonia Molecules.

When two molecules are in the distance R to each other, the perturbation potential may be approximately represented by the well known formula

$$V = -\frac{\mu\mu'}{R^3}(2\cos\theta\cos\theta' - \sin\theta\sin\theta'\cos\varphi) \tag{4}$$

where θ and φ are two angles which describe the inclination of μ. The wave function which describes the unperturbed two molecular system may be assumed to be

$$\begin{aligned}\Psi = \sum_{M,M'}\big(&a_{M,+}^{M',-'}\Theta_{J,K,M}\Theta_{J',K',M'}\psi_+\psi_{-'}\\ &+a_{M,-}^{M',+'}\Theta_{J,K,M}\Theta_{J',K',M'}\psi_-\psi_{+'}\\ &+a_{M,+}^{M',+'}\Theta_{J,K,M}\Theta_{J',K',M'}\psi_+\psi_{+'}\\ &+a_{M,-}^{M',-'}\Theta_{J,K,M}\Theta_{J',K',M'}\psi_-\psi_{-'}\big)\end{aligned} \tag{5}$$

where $a_{M,+}^{M',-'}$ etc. are coefficients which are to be suitably determined. The perturbation energy in this system is obtained as the roots of the following determinantal equations.

$$\left|\begin{array}{c|c} \begin{matrix}\epsilon-E & & \\ & \epsilon-E & 0 \\ 0 & & \ddots\end{matrix} & A \\ \hline A & \begin{matrix}\epsilon-E & & \\ & \epsilon-E & 0 \\ 0 & & \ddots\end{matrix}\end{array}\right| = 0 \qquad (6)$$

$$\left|\begin{array}{c|c} \begin{matrix}-E & & \\ & -E & 0 \\ 0 & & \ddots\end{matrix} & A \\ \hline A & \begin{matrix}2\epsilon-E & & \\ & 2\epsilon-E & 0 \\ & & \ddots\end{matrix}\end{array}\right| = 0 \qquad (6')$$

where we take the energy of unperturbed system in $(J, K, +; J', X', +')$-state as zero, $(J, K, -; J', L', +')$ or $(J, K, +; J', K', -')$-state as ϵ, (ϵ does depend on the rotational quantum numbers, but the dependence may safely be neglected in this section). The non-diagonal elements can be obtained by (2), (3), and the integration with the symmetric rotator wave functions. Thus the matrix elements of submatrix A are as follows,(4)

$$A_{M_i, M_i'}^{M_j, M_j'} = \frac{\mu^2}{R^3}\frac{KK'}{J(J+1)J'(J'+1)}$$

$$\Big\{-2M_iM_i'\delta(M_j, M_i)\,\delta(M_j', M_i')$$

$$\pm\frac{1}{2}[(J-M_i+1)(J+M_i)(J'-M_i')(J'+M_i'+1)]^{1/2}$$

$$\delta(M_j, M_{i-1})\,\delta(M_j', M_i'{}_{+1})$$

$$\pm\frac{1}{2}[(J+M_i+1)(J-M_i)(J'-M_i'+1)(J'+M_i')]^{1/2}$$

$$\delta(M_j, M_{i+1})\,\delta(M_j', M_i'{}_{-1})\Big\} \qquad (7)$$

The solutions of these secular equations may easily be obtained when the eigen-value of A-matrix $e_1, e_2, \cdots e_{(2J+2)\,(2J'+1)}$ are known, as (see the appendix),

$$E_n = \epsilon \pm e_m \quad \text{from (6)} \qquad (8)$$

and

$$E_n' = \epsilon \pm \sqrt{\epsilon^2+e_m^2} \quad \text{from (6')} \qquad (8')$$

where e_m may be put to be

$$e_m = \frac{a_m}{R^3} \qquad (9)$$

and the mean square of e_m's is

$$\langle e_m^2\rangle_{Av} = \frac{2}{3}\cdot\frac{\mu^4}{R^6}\cdot\frac{K^2K'^2}{J(J+1)J'(J'+1)} \qquad (10)$$

§ 3. Intermolecular Potential in Various States.

When we substitute (8) or (8′) into each column of (6) or (6′) respectively we obtain the corresponding wave functions. Thus (8) is the energy of state

$$\sum_M(\psi_+\theta_{J,K,M}\psi_-'\theta_{J',K',M'} \pm \psi_-\theta_{J,K,M}\psi_+'\theta_{J',K',M'}) \qquad (11)$$

and (8′)

$$\sum\{(-\epsilon\mp\sqrt{\epsilon^2+e_m^2})\,\psi_+\theta_{J,K,M}\psi_+'\theta_{J',K',M'}$$

$$\mp e_m\psi_-\theta_{J,K,M}\psi_-'\theta_{J',K',M'}\} \qquad (11')$$

respectively.

On the other hand, if two molecules apart far e_m becomes so small that $\epsilon < e_m$; in this case (8′) may be approximated by $\epsilon\pm\left(\epsilon\pm\frac{a_m^2}{2\epsilon R^6}\right)$ which has the same form as the second order perturbation. In (12′), + and − respectively correspond to $\psi_+\theta_{J,K,M}\psi_+'\theta_{J',K',M'}$ and $\psi_-\theta_{J,K,M}\psi_-'\theta_{J',K',M'}$ states. As the two energy levels of (8′) do not cross each other, assumption of adiabatic change enable us to conclude that the signs in our formula (11′) correspond to the above two states respectively.

In the case of (8) we can also apply the same criterion. Strictly speaking, energy ϵ of $(J, K, -; J', K', +')$ state and $(J, K, +; J', K', -')$ state are not equal to each other, as pointed out in section 2; thus also in this case intermolecular potential may be expressed in the second order perturbation form, when intermolecular distance is large. The sign of the second order perturbation term for the system in $(J, K, +; J', K', -')$ state is the same as that of $\epsilon_{J,K,+}+\epsilon_{J',K',-'}-\epsilon_{J,K,-}-\epsilon_{J',K',+'}$ and that for the system in $(J, K, -; J', K', +')$ state is the reverse.

Thus this quantity determines the sign which is to be taken for each state in (8). The results are summarized in Table I.

Table I.
Intermolecular Potential

J', K' \ J, K	$+$	$-$
$+'$	$\epsilon-\sqrt{\epsilon^2+e_m^2}$	$\epsilon\mp e_m$
$-'$	$\epsilon\pm e_m$	$\epsilon+\sqrt{\epsilon^2+e_m^2}$

when $\epsilon_{J,K,+}+\epsilon_{J',K',-'}-\epsilon_{J,K,-}-\epsilon_{J',K',+'}>0$, upper sign
and when " <0, lower sign
must be taken respectively.

§ 4. Formula for the Calculation of Half-Width.

We have deduced a formula for the calculation of half-width of spectral line in the other paper,(5) which is

$$A=\int F(\alpha)(1-\cos P_\alpha)\,d\alpha, \tag{12}$$

and the frequency shift of intensity maximum is

$$B=\int F(\alpha)\sin P_\alpha d\alpha. \tag{13}$$

In these formulae,

$$P_\alpha=\left\{\int_{-\infty}^{\infty}\frac{p_i(x)-p_f(x)}{\hbar}dx\right\}_\alpha, \tag{14}$$

where $p_i(x)$ and $p_f(x)$ are the intermolecular perturbation in the initial and the final states of optical process as a function of time x; α denotes the character of collision. In the case of absorption line

$$\int F(\alpha)\,d\alpha=\sum_{J,K,M}\int_0^\infty\int_0^\infty\frac{4}{\sqrt{\pi}}\left(\frac{m}{4kT}\right)^{3/2}V^3\rho$$

$$\exp\left(\frac{m}{-4kT}V^2\right)dV\,d\rho\,G(J,K,M)\,n \tag{15}$$

where m, the mass of molecule, V, the relative velocity of collision, ρ, the parameter of collision, Gn, the number of molecules in J, K, M state in unite volume.

§ 5. Calculation of Half-width in the Inversion Spectrum of Ammonia.

The so-called "inversion spectrum" correspond to the transtion $\psi_+\rightarrow\psi_-$, without any change in the other quantum number. Thus from the Table I we obtain for p_i-p_f in this case, the following same expression for both cases when the colliding molecule is in + and − states

$$p_i-p_f=\epsilon-\sqrt{\epsilon+{}^2e_m{}^2}\mp e_m \tag{16}$$

It may be estimated that the collision whose perturbation energy does not exceed about 10^{-13} erg. contributes little to A or B, so that (16) can be approximated by

$$\left(\text{when } R<\sqrt[3]{\left|\frac{a}{\epsilon}\right|}=p_0\right)$$

$$\begin{cases} p_i-p_f=\epsilon-\dfrac{\epsilon^2}{2a}R^3 & (17) \\ \qquad\qquad\qquad\text{or} & \\ p_i-p_f=\epsilon-\dfrac{2a}{\epsilon R^3} & (17') \end{cases}$$

$$(\text{when } R>\rho_0)\qquad p_i-p_f=0$$

for, the perturbation energy at ρ_0($\doteqdot$20 Å) is about 10^{-13} erg.

When R is smaller than about 1 Å, exchange force becomes appreciable, but its contribution to A does not exceed $10^{-11}n$*, while the contribution by the above force is about $10^{-9}n$ as is seen by (20), so that we may neglect the contribution of exchange force in the following calculation.

The mean translational energy of molecules at room temperature being much greater than the intermolecular potential at about 1 Å, we may assume in the following that the path of molecule is not curved by the intermolecular force; thus expressing the perturbation energies by time x, we obtain

$$\begin{cases} p_i-p_f=\epsilon-\dfrac{\epsilon^2}{2a}(\rho^2+V^2x^2)^{3/2} \\ p_i-p_f=\epsilon-\dfrac{2a}{\epsilon(\rho^2+V^2x^2)^{3/2}} \end{cases}$$

$$\text{for}\qquad \rho^0>R=(\rho^2+V^2x^2)^{1/2} \tag{18}$$

$$p_i-p_f=0\qquad\text{for}\qquad \rho^0<(\rho^2+V^2x^2)^{1/2}. \tag{18'}$$

In the case of (18) integration by x yields

$$\hbar P=\frac{2}{V}\left\{\frac{7}{8}\epsilon-\frac{3\rho^2\epsilon^2}{16a}\left(\frac{a}{\epsilon}\right)^{1/3}\right\}\sqrt{\left(\frac{a}{\epsilon}\right)^{2/3}-\rho^2}$$

$$+\frac{3\epsilon^2\rho^4}{8a}\log\left[\frac{\sqrt{\left(\frac{a}{\epsilon}\right)^{2/3}-\rho^2}+\left(\frac{a}{\epsilon}\right)^{1/2}}{-\sqrt{\left(\frac{a}{\epsilon}\right)^{2/3}-\rho^2}+\left(\frac{a}{\epsilon}\right)^{1/2}}\right]$$

---

* This upper limit of contribution can be obtained by the Lorentz model discussed in the paper (5).

$$\doteqdot \frac{\epsilon}{4V}\left[7\left(\frac{a}{\epsilon}\right)^{1/3}-5\left(\frac{\epsilon}{a}\right)^{1/3}\rho^2\right]$$

thus

$$\int_0^{\rho_0}(1-\cos P)\,\rho\,d\rho=\frac{-2\hbar V}{5\epsilon}\left(\frac{a}{\epsilon}\right)^{1/3}$$

$$\left\{\sin\left(\frac{7\epsilon}{4V\hbar}\left(\frac{a}{\epsilon}\right)^{1/3}\right)-\sin\left(\frac{\epsilon}{2V\hbar}\left(\frac{a}{\epsilon}\right)^{1/3}\right)-\frac{5\epsilon}{4V\hbar}\left(\frac{a}{\epsilon}\right)^{1/3}\right\}$$

$$\equiv X(a, V)$$

integration $X(a)\equiv\int_0^\infty V^3X(a, V)\exp\left(-\frac{m}{4kT}V^2\right)dV$ was numberically performed, the results of which are shown in Table II. Thus

In evaluating $<XY>_{AV}$ or $<Y>_{AV}$, a being not obtained as an explicit function of M, we assume that the levels in a J, K-state are distributed according to Gauss' law; in this case we may put

$$a'=\frac{KK'}{\sqrt{J(J+1)J'(J'+1)}}$$

by (10) in evaluating $<X>_{AV}$ or $<Y>_{AV}$ and then multiply the results by suitable factors.* In averaging them we use the table of molecular distribution shown in the appendix of the proceeding paper.

Table II.

$a'=a\Big/\left\{\sqrt{\frac{2}{3}}\mu^2\right\}=0.1$	0.2	0.3	0.4	0.5	0.6	0.7	0.8
$X\cdot10^{-4}=$ 0.60	1.17	1.49	2.27	2.82	3.33	3.85	5.35

$$A_1=\frac{4}{\sqrt{\pi}}\left(\frac{m}{4kT}\right)^{3/2}<X(a)>_{AV}n \tag{19}$$

where $<X(a)>_{AV}$ is the average of $X(a)$ over the rotational states of colliding molecules.

In the case of (18′)

$$\hbar P=2\left\{\epsilon-\frac{2a}{\rho^2}\left(\frac{\epsilon}{a}\right)^{1/3}\right\}\sqrt{\left(\frac{a}{\epsilon}\right)^{2/3}-\rho^2}\Big/V\doteqdot-\frac{4a}{\rho^2V}$$

thus

$$\int_0^{\rho}(1-\cos P)\,\rho\,d\rho=\frac{1}{2}\left(\frac{a}{\epsilon}\right)^{2/3}\left\{1-\cos\left(\frac{4a}{V\hbar}\left(\frac{\epsilon}{a}\right)^{1/3}\right)\right\}$$

$$+\frac{2a}{V\hbar}S_i\left\{\frac{4a}{V\hbar}\left(\frac{\epsilon}{a}\right)^{1/3}\right\}\equiv Y(a, V)$$

where

$$S_i(x)=\int_x^\infty\frac{\sin y}{y}\,dy$$

Integration $Y(a)\equiv\int_0^\infty V^3Y(a, V)\exp\left(-\frac{m}{4kT}V^2\right)dV$ is also calculated numerically, ressult of which are shown in Table III, thus

$$A_2=\frac{4}{\sqrt{\pi}}\left(\frac{m}{4kT}\right)^{3/2}<Y(a)>_{AV}n \tag{19′}$$

Table III.

$a'=$	0.2	0.3	0.4	0.5	0.6	0.7
$Y\cdot10^{-4}=$	14.9	20.6	25.8	30.4	34.9	39.1

§ 6. Numerical Calculation and Comparison with Experiment.

Good(2) reported the line shape of $J=3, K=3$ line. Applying the criterion in section 3 that (19) or (19′) must be used when $\epsilon_{J,K,+}+\epsilon_{J',K',-'}-\epsilon_{J,K,-}-\epsilon_{J',K',+'}<0$ or >0, respectively, we can conclude from the experimental data that when the rotational quantum number of the colliding molecules are $J, K=4, 4; 5, 5; 6, 6; 7, 7; 8, 8; 9, 9; 10, 10\cdots\cdot$etc., (19), and in the other cases (19′) must be used respectively, for the line $J, K=3, 3$.

The results thus obtained are

$$A_1=0.330\cdot10^{-10}n$$

$$A_2=6.72\cdot10^{-10}n$$

the final result is

$$A=7.05\cdot10^{-10}n \tag{20}$$

which is compared with the experimental data in Table IV. Agreement is satisfactory.

---

* Since X is approximately proportional to $a^{4/3}$, the suitable factor for A is $\frac{3}{7}2^{2/3}\dfrac{\Gamma\left(\frac{16}{3}\right)}{\Gamma\left(\frac{3}{2}\right)}$, and by the same reasoning the suitable factor for A_2 is $\frac{4}{7}2^{3/8}\dfrac{\Gamma\left(\frac{15}{8}\right)}{\Gamma\left(\frac{3}{2}\right)}$.

Bleaney and Penrose(6) reported that the half-width of 17 lines vary in proportion to $\left(\frac{K^2}{J(J+1)}\right)^{1/2}$, approximately. In Table III. we see that Y is approximately proportional to $a^{3/4}\propto\left(\frac{K^2}{J(J+1)}\right)^{3/8}$ thus if we neglect the contribution A_2 to A, A is seen to be proportional to $\left(\frac{K^2}{J(J+1)}\right)^{3/8}$. Contribution of A_2 is to make this proportionality more close to the experiment.

Table IV.

pressure mm-Hg		5×10^{-2}	2.5×10^{-2}	1.5×10^{-2}
half-width	obs.	0.57	0.57	0.34
Mc/sec.	calc.	1.15	0.58	0.34

That the line shift B is zero is easily concluded by the fact that the mean of e_m being zero, there are equal number of collisions with different sign and the same absolute value. This fact also agrees with experiment.

§ 7. Summary.

Intermolecular potential between ammonia molecules was calculated, and then its results were used in the calculation of half-width and frequency shift in the inversion spectrum of ammonia. The calculated results agree very well with experiment.

§ 8. Aknowledgment.

I wish to express my gratitude to Prof. Kotani, Assist. Prof. Takahashi, Dr. Yasumi and Mr. Usui for their helpful discussions on this paper.

Appendix.

Solution of (6) and (6′).

If T is a transformation matrix such that

$$TAT^{-1}=\begin{bmatrix} e_1 & & 0 \\ & e_2 & \\ 0 & & \ddots \\ & & & e_r \end{bmatrix} \qquad (21)$$

(6) and (6′) can be transformed as follows

$$\begin{vmatrix} T & 0 \\ 0 & T \end{vmatrix}\begin{vmatrix} \begin{matrix}\epsilon-E & & \\ & \epsilon-E & \\ & & \ddots\end{matrix} & A \\ A & \begin{matrix}\epsilon-E & & \\ & \epsilon-E & \\ & & \ddots\end{matrix} \end{vmatrix}\times\begin{vmatrix} T^{-1} & 0 \\ 0 & T^{-1} \end{vmatrix}=\begin{vmatrix} \begin{matrix}\epsilon-E & & \\ & \epsilon-E & 0 \\ 0 & & \ddots \end{matrix} & \begin{matrix}e_1 & & \\ & e_2 & 0 \\ 0 & & \ddots \\ & & & e_r\end{matrix} \\ \begin{matrix}e_1 & & \\ & e_2 & 0 \\ 0 & & \ddots \\ & & & e_r\end{matrix} & \begin{matrix}\epsilon-E & & \\ & \epsilon-E & 0 \\ 0 & & \ddots \end{matrix} \end{vmatrix}=0 \qquad (22)$$

$$\begin{vmatrix} T & 0 \\ 0 & T \end{vmatrix}\begin{vmatrix} \begin{matrix}-E & & \\ & -E & \\ & & \ddots\end{matrix} & A \\ A & \begin{matrix}2\epsilon-E & & \\ & 2\epsilon-E & \\ & & \ddots\end{matrix} \end{vmatrix}\times\begin{vmatrix} T^{-1} & 0 \\ 0 & T^{-1} \end{vmatrix}=\begin{vmatrix} \begin{matrix}-E & & \\ & -E & 0 \\ & & -E \\ 0 & & & \ddots \end{matrix} & \begin{matrix}e_1 & & \\ & e_2 & 0 \\ 0 & & \ddots \\ & & & e_r\end{matrix} \\ \begin{matrix}e_1 & & \\ & e_2 & 0 \\ 0 & & \ddots \\ & & & e_r\end{matrix} & \begin{matrix}2\epsilon-E & & \\ & 2\epsilon-E & 0 \\ 0 & & \ddots \end{matrix} \end{vmatrix}=0 \qquad (22')$$

From (22), solution (8) is easily obtained,

In (22′), replacing some rows and columns to each other and multiplying some rows by (—), we obtain

$$\begin{vmatrix} \begin{matrix}2\epsilon-E & & \\ & 2\epsilon-E & 0 \\ 0 & & \ddots \end{matrix} & \begin{matrix}e_1 & & \\ & e_2 & 0 \\ 0 & & \ddots \\ & & & e_r\end{matrix} \\ \begin{matrix}-e_1 & & \\ & -e_2 & 0 \\ 0 & & \ddots \\ & & & -e_r\end{matrix} & \begin{matrix}E & & \\ & E & 0 \\ 0 & & \ddots \end{matrix} \end{vmatrix}$$

multiplying it with (22′)

$$\begin{vmatrix} \begin{matrix}-E(2\epsilon-E)-e_1^2 & 0 & \\ & -E(2\epsilon-E)-e_2^2 & \\ 0 & & \ddots \end{matrix} & 0 \\ 0 & \begin{matrix}E(2\epsilon-E)-e_1^2 & 0 & \\ & E(2\epsilon-E)+e_2^3 & \\ 0 & & \ddots \end{matrix} \end{vmatrix}=0 \qquad (23)$$

the solution of which is easily seen to be (8′),

References.

(1) M. Mizushima: J. Phys. Soc. Japan, **4** (1948) 11.

(2) W. Good: Phys: Rev. **70**, (1946) 213

(3) G. Herzberg: *Infa-Red and Raman Spectra of Polyatomic Molecules.* (Van Norsted, New York, 1945)

(4) H. Margenau and D. J. Warren: Phys. Rev. **51**, (1935) 748

(5) M. Mizushima: This Journal (in press),

(6) B. Bleaney and R. P. Penrose: Phys. Rev. **70**, (1946) 775

The Temperature Dependence of Initial Permeability of Iron Single Crystals under External Tension.

By Yuzo TOMONO.

Physical Institute, Faculty of Science, University of Tokyo.

(Received: Nov. 12, 1948.)

§ 1. Introduction.

At room temperature the initial permeability of iron single crystal increases as the external tension, applied to the measuring direction, becomes stronger, but shows a gentle decrease after the tension surpasses some critical value. This phenomenon was found by Dr. Kaya and Taoka.(1) We further performed the same experiment at various higher temperatures.

When we apply a tension on the ferromagnetic substance which has positive magneto-striction, the volume of magnetic domains, magnetized to the tension direction, increases at the expense of domains orthogonally magnetized. Then the magnetisation process is for the most part, 180° wall motion. For this motion, Becker-Kersten's internal stress theory(2) is not applicable. We must consider the local field theory(3) or wall-energy theory.(4)

According to the researches of Dr. Kaya and Taoka, the initial permability of iron crystal reaches maximum at nearly 600 gr./mm² external tension. Supposing that this maximum appears when the internal force has been overcome by the external tension, then we can estimate the mean value of internal force about 600 gr./mm². Our problem is how this mean value changes at higher temperature, so that we may know the character of internal force from this temperature depenence.

§ 2. Specimens, Apparatus and Measuring Method.

Our specimens are three cylindrical pieces which are directed near to the crystallographic main axes, as illustrated in Table I. These were produced through recrystalisation method.

Table I.

name of specimen	length	cross sectional area	direction cosines		
[100]	254.0 mm	3.05 mm²	0.973	0.171	0.145
[110]	267.0	2.97	0.718	0.696	0.039
[111]	230.4	3.24	0.659	0.542	0.522

To measure the magnetisation, we used an astatic magneto-meter suspended by a very fine, long quarz fibre. The intensity of the applied magnetic field was from 0.001 to 0.015 Oe.

The non-inductive Pt furnace heats the specimens. The uniform temperature range of furnace was about 30 cm. Outside the furnace, magnetizing coil was wound. Both ends of the specimen were inserted into holders made of non-magnetic Monel metal and loaded by moving Tombac bellow. The amount of external tension was measured by the elongation of phosphor bronze spring. Its largest error was 20 gr. The degree of vacuum inside the furnace was 10^{-4} mm Hg. Total sketch of our apparatus is shown in Fig. 1.

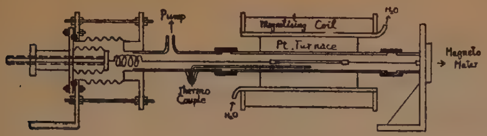

Fig. 1.

As Dr. Simizu's research(5) shows, the cooling velocity about 150°C, where the magnetic aging takes place, affects the initial permeability of iron. To avoid this aging effect, we cooled specimens as rapidly as possible about this temperature. The cooling velocity was 18°C/minute, but it was not sufficient to quench the aging. Before measuring initial permeability, two sorts of demagnetisation were performed. One is the thermal method and the other is demagnetisation in alternating field, whose amplitude was 25 Oe.

§ 3. Experimental Results.

Just below Curie temperature, the initial permeability when not loaded, increases above 10000 abruptly and decreases straightly down as Fig. 2, 3 and 4 show. Near room temperature, thermal demagnetisation (T. D.) gives a little higher initial permeability than alternating field demagnetisation (A. D.). At higher temperature their relation becomes reverse, and just below Curie temperature they coincide. On specimen [100] a little abrupt change is seen below 150°C, showing that our cooling velocity was not enough to quench the magnetic aging. This abrupt change is not seen on [110] and [111].

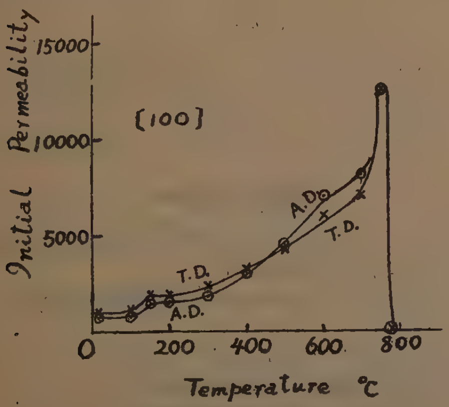

Fig. 2.

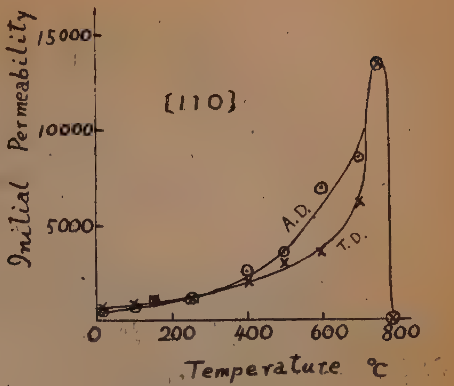

Fig. 3.

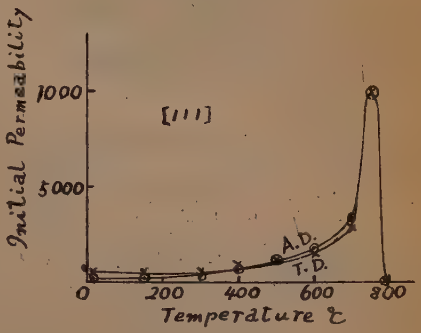

Fig. 4.

T. D.: thermal demagnetisation
A. D.: demagnetisation in alternating field

As for the tension dependence, even at higher temperature the qualitatively same behavior is observed as in Kaya and Taoka's case, that is, initial permeability-tension curve shows the maximum. But specimen [111] at 700°C shows only a monotonous decrease and the maximum is not seen. These maximum values of initial permeability are shown in Fig. 5.

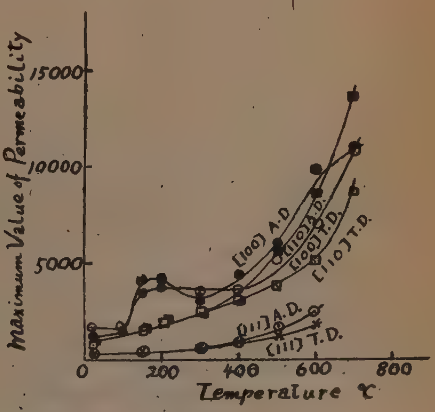

Fig. 5.

σ_m—the external tension corresponding to this maximum value-as show in Fig. 6 decreases rapidly at different temperatures for each specimen, and finally reaches a stationary value. The difference of σ_m due to the demagnetisation method is visible only for [100]. These are illustrated in Fig. 6.

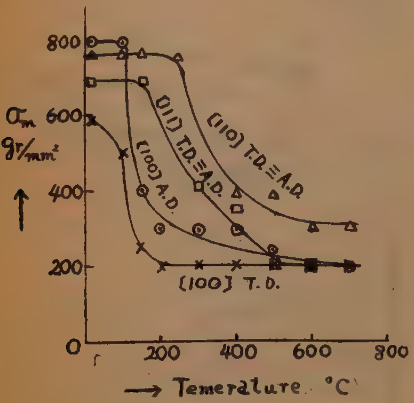

Fig. 6.

§ 4. Discussion.

The above mentioned relation between initial permeability and external tension suggests the followings. The external tension on one side plays a favourable role for magnetisation, but on the other an unfavourable role. At low tension the former effect predominates, but at higher tension the former saturates and only the latter effect appears.

The specimens we used have positive magnetostriction at weak field. For even [111] is not a correct [111]. So the external tension acts in such a way that the volume of magnetic domains directed to the external tension grows at the expense of those orthogonal to the external tension. And when the external tension wholly overcomes the internal force, this increase ceases. This may correspond to the increase of initial permeability. But we can not answer why the increase of domains magnetized to the measuring direction favourably affects the initial magnetisation process.

On the other hand the decrease of permeability by tension becomes more serious as temperature goes higher. Above all, speicmen [111], as seen in Fig. 7, shows no peak at 700°C. From these facts we conclude that the decrease of permeability may be due to the plastic deformation.

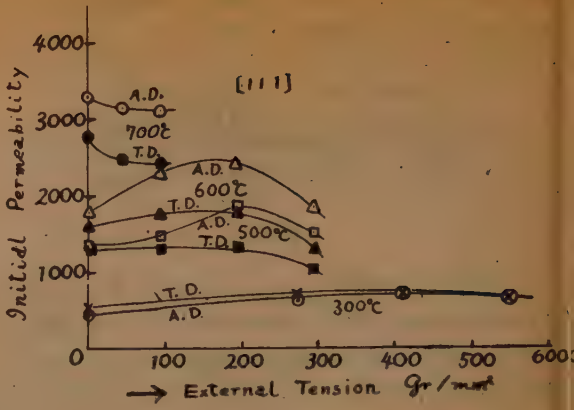

Fig. 7.

σ_m, regarded as the mean value of internal force, rapidly goes down at certain temperature and above that temperature shows almost constant value. From this fact we can say the followings. Near room temperature, a peculiar internal stress, due to the magnetic aging and others, decides the doman distribution, but on the other hand, at higher temperature it is decided by self-consistent force field. We call the force field which is decided by domain distribution itself "self-consistent field", whichever magnetic or elastic force field it may be. The amount of this self-consistent field may be the function of magneto-striction constant, elastic constant and intensity of spontaneous magnetisation. We know, especially on [100] these constants do not so seriously change from 300°C up to 600°C. We can therefore expect, that within this temperature range the strength of the internal force remains nearly constant.

The difference of permeability by demagnetisation method is very much complicated.(6) It needs further investigation.

Closing the paper, we express our thanks to Dr. Kaya who encouraged our researches and to Mr. Taoka who was the designer of magneto-meter.

References.

(1) Kaya, Taoka and Iki: Proc. Phys-Math, Soc. Japan 24 (1942) No. 11.
(2) Becker and Doering: Ferromagnetismus p. 147.
(3) Kaya, Taoka and Iki: loc. cit.
(4) S. Miyahara: Kyozisettairon p. 139.
(5) Y. Simizu: Kinzokugakkaisi 5 (1941) 175.
(6) Webb and Ford: J. I. E. E. Dec., 1934.

On the Theory of Cylindrical Shock Wave.

By Akira SAKURAI.

Electro-Technical College.

(Received August 10, 1948.)

§1. Introduction.

The theory based on the assumption of the adiabatic law is unsatisfactory to explain the occurrence of shock waves in a gas flow through a Laval nozzle or a high speed wind tunnel. On the other hand, usual theories of shock wave cannot give information concerning the entire flow field. Thus it will be of much interest if we can extend the theory so as to be applicable, for example, to the case of radial gas flow in the presence of both viscosity and heat conduction. This is essentially the theory of cylindrical shock wave.

Denoting the velocity and density by u and ρ, the equation for the continuity of mass in polar coordinates can be written as:

$$\rho u r = \text{const} = m, \tag{1}$$

and the equation of steady motion of a viscous gas is

$$\rho u \frac{du}{dr} = -\frac{dp}{dr} + \frac{4}{3}\mu\left(\frac{d^2u}{dr^2} + \frac{1}{r}\frac{du}{dr} - \frac{1}{r^2}u\right),$$

where p is the pressure and μ the coefficient of viscosity. Using m, this equation becomes

$$\frac{4}{3}\mu r^2\frac{d^2u}{dr^2} + \left(\frac{4}{3}\mu - m\right)r\frac{du}{dr} - \frac{4}{3}\mu u = r^2\frac{dp}{dr}. \tag{2}$$

If U is the intrinsic energy of unit mass, T the temperature, and λ the heat conductivity in mechanical unit, the conservation of energy gives

$$\rho u\frac{d}{dr}\left(U + \frac{1}{2}u^2\right)$$

$$= -\frac{1}{r}\frac{d}{dr}\left[ru\left\{p + \frac{2}{3}\mu\left(\frac{u}{r} - 2\frac{du}{dr}\right)\right\}\right]$$

$$+\frac{1}{r}\frac{d}{dr}\left(\lambda r\frac{dT}{dr}\right).$$

Since $\rho u r = m$, this may be integrated to give

$$m\left(U + \frac{1}{2}u^2\right)$$

$$= -ru\left\{p + \frac{2}{3}\mu\left(\frac{u}{r} - 2\frac{du}{dr}\right)\right\} + \lambda r\frac{dT}{dr} + mE,$$

where E is a constant.

The only special case of any importance is that of a perfect gas whose characteristic equations are

$$U = c_v T, \qquad p = c\rho T, \tag{3}$$

where c = (gas constant)/(molecular weight). Then, using the relation: $c_p - c_v = c$, the above equation is reduced to

$$2mc_pT + \left(\frac{4}{3}\mu + m\right)u^2 = 2\lambda r\frac{dT}{dr} + \frac{4}{3}\mu r\frac{du^2}{dr} + 2mE. \tag{4}$$

If we assume, for simplicity, that λ, μ, c_p are constant, the four quantities u, p, ρ, T may be determined by the equations (1)—(4).

§2. Transformation of Equations.

We introduce the local velocity of sound $a = \sqrt{\kappa cT}$, where $\kappa = c_p/c_v$, in place of temperature T, and use non-dimensional constants R and σ, defined by

$$R = \frac{3}{4}\frac{m}{\mu} = \frac{3}{4\sigma}\frac{mc_p}{\lambda},$$

or

$$R = \frac{3}{4}\frac{\rho u r}{\mu}, \qquad \sigma = \frac{c_p\mu}{\lambda}.$$

R is nothing other than the Reynolds number and σ is the Prandtl number.

Introducing these quantities, equations (1)—(4) become respectively

$$\rho u r = m, \qquad \rho a^2 = \kappa p, \tag{5}$$

$$r^2\frac{d^2u}{dr^2} - (R-1)r\frac{du}{dr} - u = \frac{R}{m}r^2\frac{dp}{dr}, \tag{6}$$

$$\frac{2}{\kappa-1}a^2 + \left(1 + \frac{1}{R}\right)u^2 - 2E$$

$$=\frac{3}{4\sigma}\frac{1}{R}\frac{2}{\kappa-1}r\frac{da^2}{dr}+\frac{1}{R}r\frac{du^2}{dr}. \tag{7}$$

Eliminating p and ρ from (5) and (6),

$$r^2\frac{d^2u}{dr^2}-(R-1)r\frac{du}{dr}-u=\frac{R}{\kappa}\left\{r\frac{d}{dr}\left(\frac{a^2}{u}\right)-\frac{a^2}{u}\right\}. \tag{8}$$

By a transformation: $r=e^t$, (7) and (8) are reduced to,

$$\frac{d^2u}{dt^2}-R\frac{du}{dt}-u=\frac{R}{\kappa}\left\{\frac{d}{dt}\left(\frac{a^2}{u}\right)-\frac{a^2}{u}\right\}; \tag{9}$$

$$\frac{2}{\kappa-1}a^2+\left(1+\frac{1}{R}\right)u^2-2E=\frac{1}{R}\frac{d}{dt}\left(\frac{3}{4\sigma}\frac{2}{\kappa-1}a^2+u^2\right). \tag{10}$$

§ 3. The Case of Adiabatic Law.

When the quantities λ and μ in (9) and (10) vanish or $R\to\infty$, the adiabatic process may be expected to take place. In this case, (9) and (10) become respectively

$$\frac{du}{dt}=\frac{1}{\kappa}\left\{\frac{d}{dt}\left(\frac{a^2}{u}\right)-\frac{a^2}{u}\right\}=\frac{e^t}{m}\frac{dp}{dt}, \tag{11}$$

$$\frac{2}{\kappa-1}a^2+u^2-2E=\frac{2\kappa}{\kappa-1}\frac{p}{\rho}+u^2-2E=0. \tag{12}$$

If the velocity of sound corresponding to the fluid at rest is a_0, the integration constant E is determined as

$$E=a_0^2/(\kappa-1).$$

On substituting $\rho ur=\rho ue^t=m$, (11) can be written as:

$$\frac{1}{2}\frac{du^2}{d\rho}=-\frac{1}{\rho}\frac{dp}{d\rho},$$

and eliminating u with the aid of (12), we have

$$\frac{1}{p}\frac{dp}{d\rho}=\frac{\kappa}{\rho},$$

which is integrated to give the adiabatic relation:

$$p=\text{const.}\,\rho^{\kappa}.$$

Next, eliminating a^2 from (11) and (12), we have

$$\left(\frac{2}{\kappa-1}a_0^2-\frac{\kappa+1}{\kappa-1}u^2\right)\frac{du}{dt}+\left(\frac{2}{\kappa-1}a_0^2-u^2\right)u=0, \tag{13}$$

or

$$dt=\frac{dr}{r}=-\frac{1}{u}+\frac{2u}{2a_0^2-(\kappa-1)u^2}.$$

Integrating, in the domain $u\leqq\sqrt{2/(\kappa-1)}\,a_0$, we have the well-known relation:

$$u\left(1-\frac{\kappa-1}{2}\frac{u^2}{a_0^2}\right)^{\frac{1}{\kappa-1}}=\frac{A}{r},$$

A being an arbitrary constant.

§ 4. Integration of Energy Equation.

Though $4\sigma/3$ is assumed to be unity in the usual theory of shock wave, the actual value of it is a little different from unity. If R assumes the special value R_0 given by

$$4\sigma/3=1+1/R_0,$$

the energy equation (10) can be reduced to

$$\frac{2}{\kappa-1}a^2+\left(1+\frac{1}{R_0}\right)u^2-2E$$
$$=\frac{1}{1+R_0}\frac{d}{dt}\left\{\frac{2}{\kappa-1}a^2+\left(1+\frac{1}{R_0}\right)u^2-2E\right\}, \tag{14}$$

which gives, on integration,

$$\frac{2}{\kappa-1}a^2+\left(1+\frac{1}{R_0}\right)u^2-2E=Ce^{(1+R_0)t}=Cr^{1+R_0},$$

where C is a constant.

Now we are concerned with such a case that the state at infinity is uniform; that is, $rdu/dr\to0$, $rda^2/dr\to0$, when $r\to\infty$. Hence C must be equal to zero. Thus we have a relation similar to the Bernoulli equation:

$$\frac{2}{\kappa-1}a^2+\left(1+\frac{1}{R_0}\right)u^2-2E=0.$$

In this case, too, the constant E is determined as $E=a_0^2/(\kappa-1)$, and

$$a^2+\frac{\kappa-1}{2}\left(1+\frac{1}{R_0}\right)u^2-a_0^2=0. \tag{15}$$

From (9) and (15), we have an equation for u (in the special case $R=R_0$)

$$\frac{2\kappa}{\kappa-1}\frac{1}{R_0}u^2\frac{d^2u}{dt^2}+\left\{\frac{2a_0^2}{\kappa-1}-\left(\frac{\kappa+1}{\kappa-1}-\frac{1}{R_0}\right)u^2\right\}\frac{du}{dt}$$
$$+\left\{\frac{2a_0^2}{\kappa-1}-\left(1+\frac{3\kappa-1}{\kappa-1}\frac{1}{R_0}\right)u^2\right\}u=0, \tag{16}$$

which is nothing but the extension of (13) for the case of gas with both viscosity and heat conductivity.

If we measure the velocity u by the maximum velocity:

$$\left(\frac{2}{\kappa-1}\right)^{\frac{1}{2}}\left(1+\frac{3\kappa-1}{\kappa-1}\frac{1}{R_0}\right)^{-\frac{1}{2}}a_0,$$

the above equation becomes

$$\frac{2\kappa}{\kappa-1}\frac{1}{R_0}u^2\frac{d^2u}{dt^2}+\left\{1+\frac{3\kappa-1}{\kappa-1}\frac{1}{R_0}-\left(\frac{\kappa+1}{\kappa-1}-\frac{1}{R_0}\right)u^2\right\}\frac{du}{dt}$$

$$+\left(1+\frac{3\kappa-1}{\kappa-1}\frac{1}{R_0}\right)(1-u^2)u=0,$$

which no more depends on the state at infinity.

Put $du/dt=y$, then

$$\frac{2\kappa}{\kappa-1}\frac{1}{R_0}u^2y\frac{dy}{du}+\left\{1+\frac{3\kappa-1}{\kappa-1}\frac{1}{R_0}-\left(\frac{\kappa+1}{\kappa-1}-\frac{1}{R_0}\right)u^2\right\}y$$

$$+\left(1+\frac{3\kappa-1}{\kappa-1}\frac{1}{R_0}\right)(1-u^2)u=0. \qquad (17)$$

Let us turn to the value of R_0, which is given in the following table:

	σ	$\frac{1}{R_0}=\frac{4}{3}\sigma-1$	R_0
Meyer's theory	0.88	0.17	6
air	0.72	−0.04	−26
H_2O at 100°C	1.06	0.4	2
CO_2	0.80	0.07	15

R_0 is negative in the case of air, and consequently R, which by definition is essentially positive, can never be equal to R_0. But, using R_0 in place of σ, the equation (10) can be rewritten as:

$$\frac{R_0}{R}\frac{1}{1+R_0}\frac{d}{dt}\left\{\frac{2}{\kappa-1}a^2+\left(1+\frac{1}{R_0}\right)u^2-2E\right\}$$

$$-\left\{\frac{2}{\kappa-1}a^2+\left(1+\frac{1}{R_0}\right)u^2-2E\right\}=\left(\frac{1}{R}-\frac{1}{R_0}\right)u^2.$$

This equation is of such property that it can be reduced to (14), if $R^{-1}-R_0^{-1}$ is small. And again the equation (15) would be obtained approximately in the case when the value of R is only slightly different from R_0. Then, combining (9) and (15), we have, in place of (16),

$$\frac{2\kappa}{\kappa-1}\frac{1}{R}u^2\frac{d^2u}{dt^2}+\left\{\frac{2}{\kappa-1}a_0^2-\left(\frac{\kappa+1}{\kappa-1}-\frac{1}{R_0}\right)u^2\right\}\frac{du}{dt}$$

$$+\left\{\frac{2a_0^2}{\kappa-1}-\left(1+\frac{1}{R_0}+\frac{2\kappa}{\kappa-1}\frac{1}{R}\right)u^2\right\}u=0,$$

which holds approximately for the general case of R being not very different from R_0.

§ 5. Solution of Equation and Velocity Distributions.

Let us consider, as an example, the case in which R equals $R_0=6$, as in Meyer's theory, and $\kappa=1.4$, then (17) becomes

$$u^2y\,dy/du+(2-5u)y+2(1-u^2)u=0.$$

This nonlinear equation is solved by a graphical method of isoclines and is shown in Fig. 1. The solution presents different behaviour in the three respective domains (a), (b), (c), and the two boundaries between them are denoted by (d) and (e). On the curves belonging to the domain (a) and (d), $y=r\,du/dr\leqq 0$ and hence u is a monotonely decreasing function of r. In (c) and (e), $y=r\,du/dr\geqq 0$, and consequently u is monotonely increasing. But, in the domain (b), y has a zero and so u must have an extremum there.

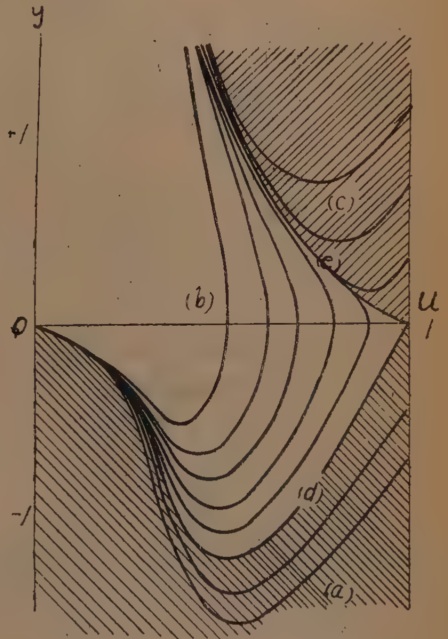

Fig. 1.

By using these integral curves in Fig. 1, velocity distribution curves can also be obtained by the method of isoclines from the equation:

$$y=r\,du/dr,$$

or $u^2d^2u/dt^2+(2-5u^2)\,du/dt+2(1-u^2)u=0,\ r=e^t$. The curves thus obtained are shown in Fig. 2, where we put $u=\sqrt{2/5}$ (which is just the local velocity of sound) at $r=1$ and the letters (a)–(e) correspond to those of Fig. 1.

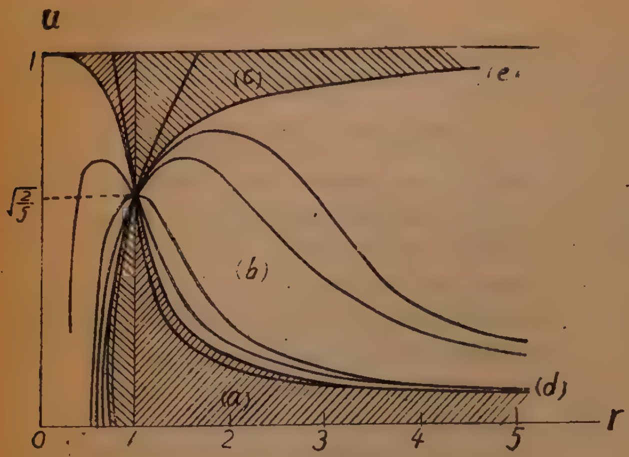

Fig. 2.

The flows represented by the curves in the domain (a) and (d) and those in (c) and (e) in Fig. 2 are respectively sub- and supersonic and are similar to the solutions which appear in adiabatic law theory. On the other hand, in the intermediate region (b), velocity distributions have close resemblance to those of shock waves. Moreover, it will be interesting to note that all these results mentioned above correspond to a definite value of R $(=3m/4\mu)$, and hence to a definite quantity of discharge of mass.

§ 6. Pressure Distribution.

From (5) and (15), we get

$$\frac{\kappa}{m}pur+\frac{\kappa-1}{2}\left(1+\frac{1}{R_0}\right)u^2-a_0^2=0.$$

If we put $p=p_0$, $u=[(\kappa+1)/2-(\kappa-1)/(2R_0)]^{-1/2}$ (which is just the local velocity of sound) at $r=1$, and if we measure u in the manner mentioned before, then

$$\frac{p}{p_0}=\frac{1}{2}\frac{\kappa-1}{R_0-(\kappa-1)}\left\{\left(R_0+\frac{3\kappa-1}{\kappa-1}\right)\left(\frac{\kappa+1}{\kappa-1}R_0-1\right)\right\}^{\frac{1}{2}}$$
$$\times\frac{1}{ur}\left\{1-\frac{(\kappa-1)(R_0+1)}{(\kappa-1)R_0+3\kappa-1}u^2\right\}.$$

When $R_0=6$ and $\kappa=1.4$. this reduces to

$$\frac{p}{p_0}=\frac{\sqrt{10}}{8}\frac{2-u^2}{ur}.$$

Using the values of r and u which are shown in Fig. 2, the above relation between the pressure p and r can be given as shown in Fig. 3. It will be seen that each p/p_0 curve tends to a different value with increase of r, in contrast to the fact that the velocity curves in Fig. 2 all tend to one and the same value zero.

It is a well-known experimental fact that if the pressure at the outlet of a Laval nozzle falls below a certain definite value, a shock wave appears, which moves to the outlet with the fall of the pressure at the outlet, the discharge of mass, the pressure and velocity at the throat remaining constant all the while (the velocity at the throat being always equal to the local velocity of sound). Such a fact is clearly accounted for by the present theory, as may be seen from Fig. 3.

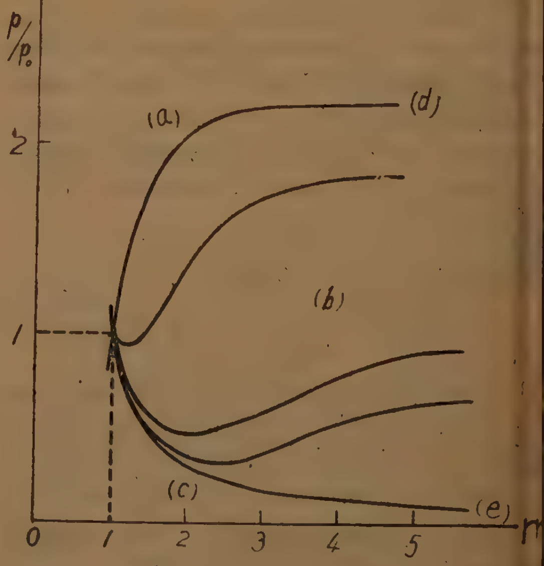

Fig. 3.

In conclusion I wish to express my sincere thanks to Dr. I. Imai for the guidance throughout the present work.

Ionization of Negative Oxygen Ion by Electron Impact. I.

By Masaru WATANABE.

Institute of Applied Mathematics, Second Faculty of Engineering, University of Tokyo.

(Received Nov. 22. 1948.)

The ionization and recombination of negative oxygen ion as the radiative processes have been investigated by Yamanouchi, with the special regard to ionospheric problems. It is also possible, however, that these processes occur through the interaction with the free electrons, existing quite abundantly in the ionoshere. In this paper, the latter processes are treated theoretically, by the group-theoretical method, and the formulae for the cross section are deduced. The numerical results will be published later in separate papers.

1. Negative Oxygen Ion.

Negatively charged ion was first detected by J. J. Thomson in the mass spectrograph, and plays an important rôle in the upper atmosphere, and also in the discharge tube. In the ionosphere, the free electron released from the atom by solar radiation in the daytime, combines with the oxygen atom and forms the negative ion at night.

Hartree and others⁽¹⁾ calculated the wave functions of O^- $(1s)^2$ $(2s)^2$ $(2p)^5$ by the self-consistent field method, including exchange effect and configuration interaction.

The electron affinity of O^- ion has been determined by several authors. Lozier⁽²⁾ gives 2.2 eV. by the experiment which yields O^- ion by electron collision with various gas molecules. (O_2, CO, H_2O etc.) But the other data differ from this value: 3.3 eV. by Milliken,⁽³⁾ and 3.07 eV. by Vier and Mayer.⁽⁴⁾ Perhaps the smallness of the energy difference makes it difficult to decide the value exactly by experiment.

§ 2. Ionization by Electron Impact.

As regard to electron collision, the interesting phenomena has been found out by Yamanouchi.⁽⁵⁾ When the slow electron collides with the oxygen atom, the p-wave which has the angular momentum $l=1$ about the atom, shows anomalous behaviour. The p-function spreads out flately like a "back of whale", and this results to the large excitation probability of the oxygen atom by slow electron impact. Generally speaking, the atom with incomplete shell has a kind of virtual level, and the electron incident with this energy is trapped for a time, so the cross section becomes large. Doesn't the similar effect happen to the O^- ion? If so, to what extent? These questions are not only theoretically interesting, but useful in the application to the ionospheric problem, or discharge phenomena. To begin with, I have worked out the formula for the cross section of the ionization of O^- ion by electron impact.

§ 3. The Transition Probability.

The ionization ocurrs by the following process:

$$(2p)^5\ {}^2P+e\rightarrow(2p)^4\ {}^3P+e'+e'' \qquad (1)$$

Of course, the final state of the oxygen atom may be one of excited states, ${}^1D$ or ${}^1S$. The calculation procedures are almost the same. So we illustrate the method of calculation with the process (1), which is most likely to happen.

Yamanouchi and Kotani⁽⁶⁾ have formulated the excitation cross section of oxygen atom by electron impact:

$$(2p)^4\ {}^3P+e\rightarrow(2p)^4\ {}^1D \text{ or } {}^1S+e'$$

The method can be applied with the modification due to the fact that two electrons out go instead one.

According to their formulation, the collision problem can be treated as $n+1$ body problem, i. e. n electons of the atom plus one colliding electron. To treat many-body problem, the one-body approximation is the only practicable method in present. Owing to the spherical symmetry the wave function is conveniently separated into radial and angular parts.

The wave function of the incident electron with the velocity k in atomic unit,* is decomposed into the partial spherical waves with the angular momenta $l = 0, 1, 2, \cdots$ such as

$$\psi_k(\mathbf{r}) = \sqrt{4\pi}\sum_{l=0}^{\infty}\sqrt{2l+1}\, i^l \exp(i\eta_l) f_{k,l}(r) S_{l,0}(\theta,\varphi) \tag{2}$$

where $S_{l,0}(\theta,\varphi)$ is the normalized spherical harmonic, and $y = krf_{k,l}(r)$ is the solution of the differential equation:

$$\frac{d^2y}{dr^2}+\left\{k^2-2U(r)-\frac{l(l+1)}{r^2}\right\}y = 0 \tag{3}$$

$U(r)$ is the mean field of the O^- ion.

η_l is the phase shift determined by the asymptotic form:

$$y \sim \sin\left(kr-\frac{1}{k}\log 2kr-\frac{l\pi}{2}+\eta l\right) \tag{4}$$

The wave functions of scattered electrons are

$$\psi_{k'l'm'} = f_{k'l'}(r) S_{l'm'}(\theta,\varphi)$$

$$\psi_{k''l''m''} = f_{k''l''}(r) S_{l''m''}(\theta,\varphi) \tag{5}$$

where $y = k'rf_{k'l'}(r)$ satisfies.

$$\frac{d^2y}{dr^2}+\left\{k'^2-2U'(r)-\frac{l'(l'+1)}{r^2}\right\}y = 0 \tag{6}$$

and similar equation for $y = k''rf_{k''l''}(r)$, where $U'(r)$ is the appropriate field hf the oxygen atom. $y_{k'l'}$, $y_{k''l''}$ have the asmptotic forms:

$$y_{k'l'} \sim \sin(kr-l'\pi/2+\eta_{l'}),$$

$$y_{k''l''} \sim \sin(kr-l''\pi/2+\eta_{l''}). \tag{7}$$

Now the transition probability for the process (1) can be expressed as the square sum of the matrix element of the perturbation Hamiltonian operator, such as

$$W = \frac{2\pi}{g}\sum_{\alpha,\alpha'}\left|H_{\alpha}^{\alpha'}\right|^2, \tag{8}$$

where the summation is to be extended for all possible initial states α and final states α' involved in this process and g is the statistical weight of state α. As the partial process $\alpha \rightarrow \alpha'$, we consider the scattering of each elementary spherical wave of the incident electron. The conservation laws exist for the partial process as follows:

(i) spin: $\vec{S}+1/2 = \vec{S'}+1/2+1/2$

As in our case $S = 1/2$ and $S = 1$, the resultant spin is 1 or 0.

(ii) energy:

$$E(0^-)+\frac{1}{2}k^2 = E(0)+\frac{1}{2}k'^2+\frac{1}{2}k''^2$$

$E(0)-E(0^-)$ = electron affinity has not been determined exactly as above mentioned. It may be taken as 0.1 a.u. (2.7 eV.) so as to fasciliate the calculation.

(iii) angular momentum:

$$\vec{P}+\vec{l} = \vec{P}+\vec{l'}+\vec{l''}.$$

This is

$$\{l+1,\ l \text{ or } l-1\}$$

$$= \{l'+l''+1,\ l'+l'',\cdots\cdots \text{or } |l'-l''|+1\}.$$

(iv) parity: l even $\longleftrightarrow$ $l'+l''$ odd,

l odd $\longleftrightarrow$ $l'+l''$ even.

Combining (iii) and (iv), we can tabulate the allowed process $l \leftrightarrow l'$, ll''. as shown in Table III.

(v) z-component of angular momentum;

$$M = M'+m'+m''.$$

M, M' and m', m'' are those of the ion, the atom and the scattered electrons.

Summing up the probabilities of partial processes, we obtain

$$W_{k\rightarrow k',k''} = \frac{16k'k''}{(2L+1)(2S+1)}\sum_{l}\sum_{l'l''}V_l^{l'l''} \tag*{9)}$$

Each factor has its origin:

$$1/2(2L+1), \quad (2S+1)$$

to take average over initial states of the atom and the incident elecron.

$$2k'/\pi, \quad 2k''/\pi$$

to normalize the wave functions of final states with respect to energy.

$$4\pi$$

squared amplitude of the incident partial wave (by series expansion (2)).

Partial cross section $V_l^{l'l''}$ is the sum of tw terms corresponding to the multiplicity of the total spin $S+1/2$ and $S-1/2$.

---

* Atomic units are used exclusively in our calculations.

$$V_l^{l'l''}=(2S+2)\,{}^{S+\frac{1}{2}}U_l^{l'l''}+2S\,{}^{S-\frac{1}{2}}U_l^{l'l''},\qquad(10)$$

where

$${}^{S\pm\frac{1}{2}}U_l^{l'l''}=(2l+1)\sum_{M}\sum_{M'm'm''}\left|{}^{S\pm\frac{1}{2}}H_{Ml0}{}^{M'l'l''m'm''}\right|^2.\qquad(11)$$

Integrating $W_{k\to k',k''}$ above-obtained we get the ionization probability by the electron with the velocity k,

$$W_{k,\,\mathrm{ionization}}=\int_0^{E_k-E_{\mathrm{ion}}}W_{k\to k',k''}dE_{k''}\qquad(12)$$

As the final wave functions are normalized with respect to energy, it does not need the density functions at integration.

If the number of electrons with energy between E and $E+dE$ is N_E per unit volume,

$$W=\int_{E_{\mathrm{ion}}}^{\infty}W_{k,\,\mathrm{ion}}N_EdE\qquad(13)$$

is the probability per unit volume per unit time.

Now as the perturbation potential which causes the transition we consider the Coulomb interaction between incident and ionic electrons $\sum_{i=1}^{n}1/r_{i,n+1}$, where $r_{i,n+1}$ means the distance between the i-th electron of the ion and the colliding electron. If we take account of non-orthogonality of wave functions of the ionic and free electrons, the terms which depend on the one coordinate of only one electron, e. g. radial potential, would have some contribution, which we have neglected in the present calculation.

§ 4. Partial Cross Section.

The matrix element of perturbing Hamiltonian can be calculated by the formula $H=\sum_P U(P)H(P)$, or its modification.(7) The combinations of inital and final sets X and X' for the whole system consisting of the ion or the atom and the free electrons are listed in Table I.

The last orbital marked with asterisk in X and the last two in X' are those of the free electrons. Since the interchange of paired orbitals as a whole does not affect the representation matrix for that part which we need to construct the energy matrix,(8) the first paired oraitals in X can be put the same ones as in X'. Therefore we may use the representation matrix of the symmetric group of the permutation of 4 figures instead of 6.

We construct the energy matrix as usual

$$H_X{}^{X'}=\frac{1}{\sqrt{2^{P(X)+P(X')}}}\sum_P N_PU''(P)H(P/XX')\qquad(14)$$

for both multiplicities, singlet and triplet, of the whole system. That is, $U''(P)$ are those of the representation matrix $R_4{}^1$ or $R_4{}^3$, which are related to the initial and final states, such that the multiplicity of the ion in the initial state be doublet and that of the atom in the final state triplet. They are shown with the shaded regions in Fig. 1.

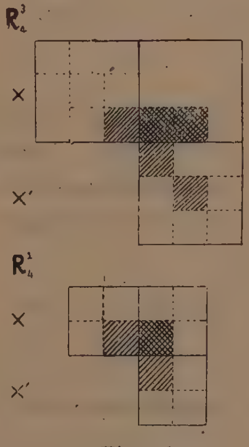

Fig. 1.

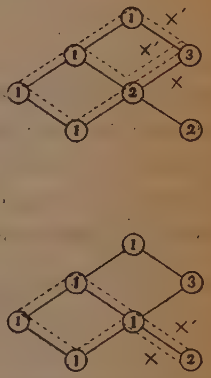

Fig. 2.

Table I.

	M	M'	$m'+m''$	X	X'
(α)	1	1	0	(1100−1; 0*)	(110−1; $m'm''$)
(β)	1	0	1	(1100−1; 0*)	(001−1; $m'm''$)
(γ)	0	1	−1	(11−1−10; 0*)	(110−1; $m'm''$)
(δ)	0	−1	0	(11−1−10; 0*)	(−1−110; $m'm''$)
(ε)	−1	−1	0	(00−1−11; 0*)	(−1−110; $m'm''$)
(ζ)	−1	0	−1	(00−1−11; 0*)	(001−1; $m'm''$)

Also the genetical construction of the representation matrix is indicated by broken lines in the branching diagrams in Fig. 2.

Now in the summation of P in (14), permutations (23) and (24) (23) give essentially non-vanishing components for the combinations (α), (β) and (ε) in Table I, and (13) and (14) (13) for (γ), (δ) and (ζ). $U''(P)$ for these P's are given in Table II. For (13) and (14) (13) the same figures but with opposite sign should be used.

Table II. $U''(P)$

	(23)	(24) (23)
$R_4{}^3$ (2, 1) element	$\sqrt{3/2}$	$-\sqrt{3/2}$
$R_{4\,1}$(3, 1) & (3, 2) elements	$(0, \sqrt{3/2})$	$(\sqrt{6/3}, -\sqrt{3/6})$

Hence we have for the matrix element between X and X'

$$H_X{}^{X'} = \sqrt{2}\left\{\frac{\sqrt{3}}{2}H(23)-\frac{\sqrt{3}}{2}H(24)(23)\right\} \tag{15}$$

for the triplet state in case of (α), (β) and (ε), where

$$H(23) = \iint \bar{\varphi}_{2p,m}(\mathbf{x}_1)\,\bar{\psi}_{k,l,0}(\mathbf{x}_2) \times \frac{1}{|\mathbf{x}_1-\mathbf{x}_2|}\,\phi_{k',l',m'}(\mathbf{x}_1)\,\psi_{k'',l'',m''}(\mathbf{x}_2)\,d\mathbf{x}_1 d\mathbf{x}_2 \tag{16}$$

and $H(23)(24)$ is similar integral obtained by interchanging the index $\{2p, m\}$ and $\{k, l, 0\}$. The integration with respect to the angular parts can be carried out as usual according to the formula worked out by Slater.(9)

$$(m_{2p}, m'; m'', 0^*) = \sum_{\kappa=|m''|} c^{\kappa}(m_{2p}, m')\,c^{\kappa}(m'', 0^*) \times R_{\kappa}(2p, k'l'; k''l'', kl). \tag{17}$$

Here the left-hand side is the abbreviation for the integral (16), and

$$R_{\kappa}(2p, k'l'; k''l'', kl) = \iint_0^{\infty} \frac{r_<{}^{\kappa}}{r_>{}^{\kappa+1}} R_{2p}(r_1) \times f_{k'l'}(r_1) f_{k''l''}(r_2) f_{kl}(r_2)\, r_1{}^2 r_2{}^2 dr_1 dr_2, \tag{18}$$

where $r_<$ or $r_>$ means the smaller or larger one between r_1 and r_2, and R_{2p} is the radial wave function of $2p$-electron in O^- ion.

Now we come to consider the partial process $l \leftarrow\rightarrow l', l''$ for free electrons and at the same time ${}^SL \leftarrow\rightarrow {}^{S'}L'$ for the ion or the atom. Fortunately the ionic sets X with $M = \pm 1$ or 0 represent corresponding $(p^5)\,{}^2p$ state directly, and also the atomic sets X' $(p^4)\,{}^3P$. So it does not require the transformation matrix from M-scheme to L-scheme. To get the partial cross section $U_l{}^{l'l''}$ for a definite multiplicity we must sum up the square of $H_X{}^{X'}$ for all possible combinations of M and (M', m', m''), which are listed in Table I. It is to be noted that for each transition $M \leftarrow\rightarrow M'$ the subsummation should be carried out over all sets (m', m'') that satisfy the relation $m'+m'' = M-M'$. Adding the two $U_l{}^{l'l''}$ corresponding to the total multiplicity, singlet and triplet respectively, with appropriate multiplication factors, we obtain the partial cross section

$$V_l{}^{l'l''} = 12(2l+1) \sum_{m_{2p}=\pm1,0} \sum_{m'+m''=m_{2p}} \{(m_{2p}, m'; m'', 0^*)^2 - (m_{2p}, m'; m'', 0^*)(0^*, m'; m'', m_{2p}) + (0^*, m'; m'', m_{2p})^2\} \tag{19}$$

Inserting the numerical values $c^{\kappa}(m_1, m_2)$, we obtain Table III for $V_l{}^{l'l''}$. Here we use the abbreviation R_{κ} for the double integral involving 4 radial wave functions (18), and $\tilde{R}_{\kappa}$ for the similar integral that is obtained by interchanging $f_{k'l'}$ and $f_{k''l''}$ in (18). Of course, for $l' = l''$, $V_l{}^{l'l''}$ is symmetric with respect to R_{κ} and $\tilde{R}_{\kappa}$, and for $l' \neq l''$ $V_l{}^{l''l'}$ is obtained by interchanging R_{κ} $\tilde{R}_{\kappa}$ and $\tilde{R}_{\kappa} \rightarrow R_{\kappa}$ in $V_l{}^{l'l''}$.

Thus the calulation of the cross section is reduced to that of a large number of double integrals R_{κ} and $\tilde{R}_{\kappa}$, in dependence of energies of the incident electron and one of the scattered electrons.

The writer wishes to take this opportunity of expressing his sincere appreciation to Professor Yamanouchi, under whom this work was done, for helpful guidance and criticism.

References.

(1) Hartree, Hartree and Swirles: Phil. Trans. A, **238** (1939), 229.

(2) Massey: "*Negative Ions*" (1938), I, § 4. 21 and Table I.

(3) Milliken: J. Chem. Phys., **2** (1934), 782.

(4) Vier and Mayer: J. Chem. Phys., **12** (1944), 28.

(5) Yamanouchi, Inui and Amemiya: Proc. Phys-Math. Soc. Japan. **22** (1940), 847.

Table III.

$l-l'l''$	$V_l^{l'l''}$
$s-ps$	$36\left(R_0^2-\frac{1}{3}R_0\tilde{R}_1+\frac{1}{9}\tilde{R}_1^2\right)$
$s-dp$	$8\left(R_1^2-\frac{3}{5}R_1\tilde{R}_2+\frac{9}{25}\tilde{R}_1^2\right)$
$s-fd$	$\frac{108}{125}\left(R_2^2-\frac{5}{7}R_2\tilde{R}_3+\frac{25}{49}\tilde{R}_3^2\right)$
$s-sp$ $s-pd$ $s-df$	similar expressions obtained by interchanging $R_K\to\tilde{R}_K$ and $\tilde{R}_K\to R_K$.
$p-ss$	$4(R_1^2-R_1\tilde{R}_1+\tilde{R}_1^2)$
$p-pp$	$108\left[R_0^2+\frac{4}{125}R_2^2-\left\{\frac{1}{3}R_0\tilde{R}_2+\frac{2}{15}(R_0\tilde{R}+R_2\tilde{R}_0)+\frac{2}{375}R_2\tilde{R}_2\right\}+\tilde{R}_0^2+\frac{4}{125}\tilde{R}_2^2\right]$
$p-dd$	$16\left[R_1^2+\frac{243}{1372}R_3^2-\left\{\frac{1}{10}R_1\tilde{R}_1+\frac{27}{70}(R_1\tilde{R}_3+R_3\tilde{R}_1)+\frac{81}{6860}R_3\tilde{R}_3\right\}+\tilde{R}_1^2+\frac{243}{1372}\tilde{R}_3^2\right]$
$p-ff$	$\frac{972}{125}\left[R_2^2+\frac{2000}{6561}R_4^2-\left\{\frac{1}{21}R_2\tilde{R}_2+\frac{100}{189}(R_2\tilde{R}_4+R_4\tilde{R}_2)+\frac{500}{45927}R_4\tilde{R}_4\right\}+\tilde{R}_2^2+\frac{2000}{6561}\tilde{R}_4^2\right]$
$p-ds$	$8(R_1^2-R_1\tilde{R}_1+\tilde{R}_1^2)$
$p-fp$	$\frac{648}{125}(R_2^2-R_2\tilde{R}_2+\tilde{R}_2^2)$
$p-sd$ $p-pf$	as noted above.
$d-ps$	$8\left(\frac{9}{25}R_2^2-\frac{3}{5}R_2\tilde{R}_1+\tilde{R}_1^2\right)$
$d-dp$	$180\left\{\frac{4}{45}R_1^2+\frac{27}{1715}R_3^2-\left(\frac{2}{15}R_1\tilde{R}_0+\frac{2}{75}R_1\tilde{R}_2+\frac{3}{35}R_3\tilde{R}_0+\frac{6}{1225}R_3\tilde{R}_2\right)+\tilde{R}_0^2+\frac{4}{175}\tilde{R}_2^2\right\}$
$d-fd$	$24\left\{\frac{9}{35}R_2^2+\frac{20}{189}R_4^2-\left(\frac{3}{35}R_2\tilde{R}_1+\frac{16}{81}R_2\tilde{R}_3+\frac{2}{7}R_4\tilde{R}_1+\frac{2}{147}R_4\tilde{R}_3\right)+\tilde{R}_1^2+\frac{6}{49}\tilde{R}_3^2\right\}$
$d-fs$	$12\left(\frac{9}{25}R_2^2-\frac{3}{5}R_2\tilde{R}_1+\tilde{R}_1^2\right)$
$d-sp$ $d-pd$ $d-df$ $d-sf$	as noted above.

---

(6) Yamanouchi and Kotani: ibid., **22** (1940), 14.

(7) Yamanouchi: ibid., **18** (1936), 623.

(8) Yamanouchi: ibid., **22** (1940), 841.

(9) Condon-Shortley: "*Theory of Atomic Spectra*" (1935), Chap. 6.

Ionization of Negative Oxygen Ion by Electron Impact. II

By Masaru WATANABE.

Institute of Applied Mathematics, Second Faculty of Engineering, University of Tokyo.

(Received Jan. 15, 1949.)

§ 1. Introduction.

In the previous reports(1) I have formulated the cross section for ionization of the negative oxygen ion by electron impact. To obtain practical form of the ionization function in dependence of the incident energy, we must compute a number of the double integrals which have the following form

$$R_K = \iint_0^\infty \frac{r_<^K}{r_>^{K+1}} y_{kl}(r_1)P_{2p}(r_2)y_{k'l'}(r_1)y_{k''l''}(r_2)dr_1dr_2, \quad (1)$$

where P_{2p} is the radial wave function (multiplied by r) of $2p$-electron of O⁻ ion, which has been worked out by Hartree and others,(2) and $y_{k'l'}$, $y_{k''l''}$ are those of free electron in the field of the oxygen atom. These are already calculated by Yamanouchi(3) for the another purpose. So there remains y_{kl}, that of free electron in O⁻ ion field, satisfies the following equation:(*)

$$\frac{d^2y}{dr^2}+\left\{k^2-2V(r)-\frac{l(l+1)}{r^2}\right\}y = 0, \quad (2)$$

where $E=\frac{1}{2}k^2$ is the energy of the incident electron, l is the angular mementum and $V(r)$ is the potential of O⁻ ion which is constructed sucn as

$$V(r) = -\frac{8}{r}+\int_0^r \rho(r)\,dr+\int_r^\infty \frac{\rho(r)}{r}\,dr. \quad (3)$$

$\rho(r)$ is the radial charge distribution of ionic electrons between r and $r+dr$, averaged over all directions, and can be expressed in terms of radial wave functions, e. g. given by Hartree and others, such as

$$\rho(r) = 2P_{1s}(r)^2+2P_{2s}(r)^2+5P_{2p}(r)^2.$$

§ 2. Calculations of Wave Functions.

The radial wave functions y_{kl} have been calculated by numerical integration of the equation(2) for several values of k^2, namely

$k^2 = 0.2$, 0.4, 0.6, 0.8, and 1.0 for $l=0$,

and $k^2 = 0.2$, 0.4, 0.6, 0.8, 1.0

1.2, 1.4, 1.6, 1.8 and 2.0 for $l=1$.

For $l \geqq 2$ the wave functions are neglibibly small incide the ion and would not contribute to the cross section.

The procedures of the calculations are similar to the cases of O, O⁺, O⁺⁺ and O⁺⁺⁺.(3) The regular solution, that is physically admissible, can be expanded as

$$r^{l+1}(1+c_1r+c_2r^2+c_3r^3+\ldots), \quad (4)$$

where $c_1, c_2, \ldots.$ are determined successively by substituting the above expansion into (2). This series serves to give the successive three y-values which are needed to start the numerical integration. Then the so-called Störmer-Levy method can be applied, which is the most convenient one now available. The integration has been carried out up to $r=12$. The results are shown in Fig. 1 and 2.

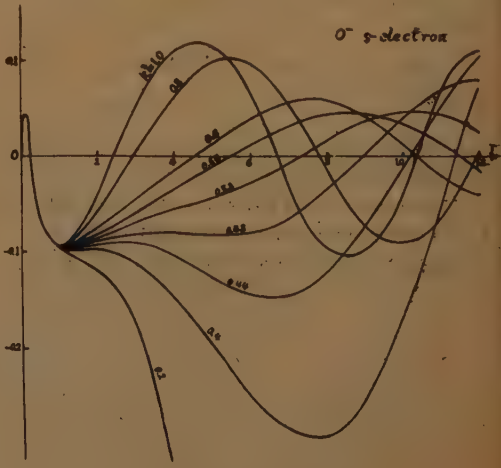

Fig. 1.

(*) All physical quantities are measured in atomic units.

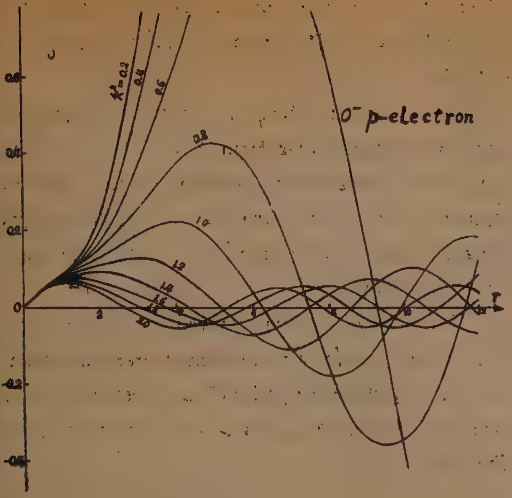

Fig. 2.

§ 3. Normalization of Wave Functions.

For $r \geqq 10$ the electronic wave functions of the negative ion vanish in significant figures, so the ionic field $V(r)$ becomes practically repulsive Coulombic field $1/r$. Hence the equation (2) reduces to

$$d^2y+\left\{k^2-\frac{2}{r}-\frac{l(l+1)}{r^2}\right\}y=0. \tag{5}$$

This is so-called Whittaker's equation.(5) Yost Wheeler and Breit(6) have introduced two independent solutions $F_l(r)$, $G_l(r)$ which have asymptotic forms as follows:

$$\begin{aligned} F_l &\sim \sin\left(\rho-\eta\log 2\rho+\sigma_l-\frac{l\pi}{2}\right), \\ G_l &\sim \cos\left(\rho-\eta\log 2\rho+\sigma_l-\frac{l\pi}{2}\right), \end{aligned} \tag{6}$$

where $\rho=kr$, $\eta=1/k$ and $\sigma_l=\arg\Gamma(l+1+i\eta)$. F_l is regular at $r=0$, but G_l is irregular. These functions can be expressed in terms of confluent hypergometric functions of Whittaker and Watson.(5)

The numerical solution y can be expressed as the linear combination of F_l and G_l,

$$y \sim c_1F_l+c_2G_l\,.$$

c_1, c_2 are determined so that the numerical solutions are jointed smothly to $c_1F_l+c_2G_l$ at $r=10$, that is

$$\begin{aligned} y &= c_1F_l+c_2G_l\,, \\ y' &= c_1F_l'+c_2G_l'. \end{aligned}$$

For the calculation of the cross section, the normalized wave function, that has unit asymptotic amplitude, must be used. For this purpose, the normalization factor $N=1/\sqrt{c_1^2+c_2^2}$ is to be multiplid to the numerical solution.

If we put

$$\frac{c_1}{\sqrt{c_1^2+c_2^2}}=\cos\delta_l\,,\quad \frac{c_2}{\sqrt{c_1^2+c_2^2}}=\sin\delta_l\,, \tag{7}$$

the normalized wave function has the asymptotic form:

$$y \sim \sin\left(\rho-\eta\log 2\rho+\sigma_l-\frac{l\pi}{2}+\delta_l\right) \tag{8}$$

The normalization factors N for s- and p-functions are shown in Fig. 3.

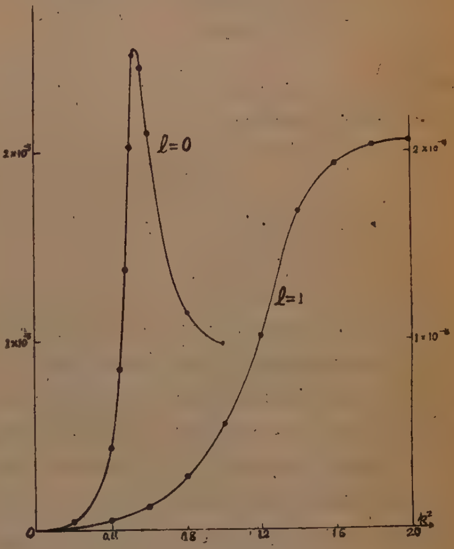

Fig. 3.

§ 4. Calculations of F_l, G_l and F_l', G_l'.

The numerical values of F_l (r), G_l (r) and $F_l'(r)$, $G_l'(r)$ can be calculated by series expansion for small $\rho=kr$, or by asymptotic series for large ρ.

The series expansions are as follows:

$$\begin{aligned} F_l &= C_l\sum_{j=l+1}^{\infty}A_j\rho^j, \\ G_l &= D_l\left\{\sum_{j=-l}^{\infty}a_j\rho^j+(p_l\log 2\rho+q_l)\sum_{j=l+1}^{\infty}A_j\rho^j\right\}, \end{aligned} \tag{9}$$

The formulae of the constants C_l, D_l, p_l and q_l; and the three-terms reccurence formulae for the coefficients A_j's and a_j's are given in Yost, Wheeler and Breit's paper.(6) They have calculated F_l, G_l and their derivatives by these series expansions. But their calculations have not been carried out for large ρ values, which are required in our case.

For large ρ the convergence of the above series are very slow. For example, when $k^2 = 0.6$ and $r = 10$, more than 30 terms are to be summed up. The larger the energy, the more terms are needed. To save superfluous labors, the asymptotic expansions are used effectively. The formulae are already derived in case of attractive field.(7) Sign change in field parameter η will do. We have

$$F_e \sim \sin\theta_l\left\{1+\sum_{n=1}\frac{\alpha_n}{(2\rho)^n}\right\}-\cos\theta_l\sum_{n=1}\frac{\beta_n}{(2\rho)^n}, \quad (10)$$

$$G_e \sim \cos\theta_l\left\{1+\sum_{n=1}\frac{\alpha_n}{(2\rho)^n}\right\}+\sin\theta_l\sum_{n=1}\frac{\beta_n}{(2\rho)^n},$$

where $\theta_l = \rho-\eta\log 2\rho+\sigma_l-\frac{l\pi}{2}$. α_n and β_n satisfy the reccurence formulae:

$$\alpha_n = \left(2-\frac{1}{n}\right)\eta\alpha_{n-1}+\frac{(l+n)(l-n+1)+\eta^2}{n}\beta_{n-1},$$

$$\beta_n = -\frac{(l+n)(l-n+1)+\eta^2}{n}\alpha_{n-1}+\left(2-\frac{1}{n}\right)\eta\beta_{n-1},$$

$$\alpha_0 = 1, \quad \beta_0 = 0. \quad (11)$$

When $\rho \geqq 5$, the asymptotic expansions give five significant figures. Thus for $k^2 \geqq 0.4$, F_l, G_l and F_l', G_l' have been calculated by the asymptotic expansions and their derivatives. For $k^2 = 0.4$ and 0.6 the series expansions have also been used to check the values above obtained.

A slight difficulty occured for $k^2 = 0.2$. In this case $\rho = 4.4721\ldots$ at $r = 10$, where the asymptotic expansion proved to be useless, because it gives only three significant figures. On the other hand, by series expansions we could obtain sufficient figuers for F_l, but did not succeed for G_l. The situation is that, in the series expansion of G_l, two terms, $\sum a_j\rho^j$ and $(p_l\log 2\rho+q_l)\sum A_j\rho^j$ are unfortunately almost same magnitude but have opposite sign, and in their sum several figures drop out. If we want to get five significant figures, both terms must be calculated up to eleven figures.

This requirement can be satisfied for a_j, A_j, and p_l, but not for q_l, because $\Gamma'(-i\eta)/\Gamma(-i\eta)$ in q_l, which is calculated by asymptotic expansion gives only six figures. For $k^2 = 0.2$, C_l is very small, and D_l is large, but G_l is the order of 1. Thus the algebraic sum of the two terms should be very small. This is the situation that makes us fail.

To avoid this difficulty, we may integrate the equation (5) backwards from $r = 10$ to $r = 1$, where the series expansions reserve more significant figures. But it is more convenient to integrate forwards to $r = 20$, where the asymptotic expansion is available.

The convenient recurrence formulae for F_l and G_l are given by the ladder method which is devised originally by Infed(8) and extended to the case of continuous eigenvalues by Yamanouchi.(9) They are.

$$\left.\begin{aligned}\alpha_l F_l &= P_l F_{l-1}-F'_{l-1}\\ \alpha_l F_l' &= P_l F_{l-1}'+Q_l F_{l-1}\end{aligned}\right\} \quad (12)$$

and the same expressions for G_l, G_l', where

$$\left.\begin{aligned}\alpha_l^2 &= k^2+\frac{1}{l^2}, \quad P_l = \frac{l}{r}+\frac{1}{l}\\ Q_l &= k^2-\frac{2}{r}-\left(\frac{l}{r}\right)^2.\end{aligned}\right\} \quad (13)$$

Owing to these formulae we need the series calculation only for $l = 0$. These formulae serve also as powerful check.

$F_l'G_l-F_lG_l' = k$ is used as useful check in all cases.

The results are tabulated in Table I.

§ 5. Effective Potential and Characteristics of Wave Function.

The characteristics of the s-and p-waves, which correspond to $l = 0$ and 1, are interesting. In case of s-wave, the potential curve is shown in Fig. 4.

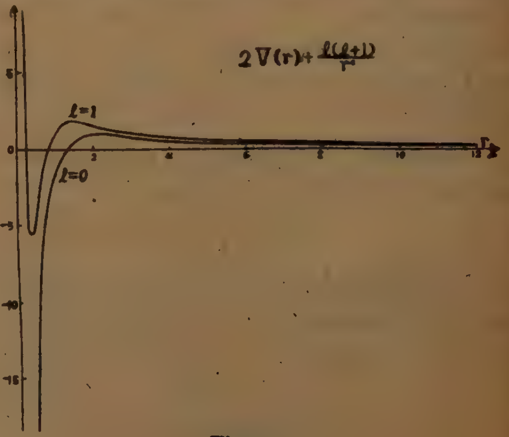

Fig. 4.

Table I. For $k^2=0.2$ values at $r=20$ are given. The others are those at $r=10$. All these values have been calculated by asympotic expansions.

k^2	0.2	0.4	0.6	0.8	1.0
F_0	0.03299	0.8025_0	0.88806	0.75421	0 47757
G_0	-1.1838_3	-0.8659_4	−0.65704	0.76425	0.94288
F_0'	−0.37785	-0.4103_2	−0.40658	0.59897	0.84115
G_0'	0 00305	-0.3454_5	0.57142	0.57897	−0.43327
F_1		1.0928	−0.45082	−1.0648	−0.22336
G_1		-0.5131_8	−1.0231	0.19508	1.0397
F_1'		-0.2526_4	−0.62738	0.15943	0.92102
G_1'		-0.4601_8	0.22432	0.81077	0.18974
$F_0'G_0-F_0G_0'$	0.44721	0.6325_3	0.77460	0.89442	1.0000
$F_1'G_1-F_1G_1'$	0.44721	0.6325_3	0.77458	0.89441	0.99999
k	0.44721	0.6324_6	0.77460	0.89443	1.00000
$(P_1F_0-F_0')/\alpha_1$		1.0928	−0.45085	−1.0648	−0.22332
$(P_1G_0-G_0')/\alpha_1$		-0.5130_8	−1.0231	0.19506	1.0398
$(P_1F_0'+Q_1F_0)/\alpha_1$		-0.2525_9	−0.62738	0.15942	0.92104
$(P_1G_0'+Q_1G_0)/\alpha_1$		-0.4602_0	0.29434	0.81078	0.18970
σ_0	0.3112_2	-0.1248_8	0.2420_0	-0.2850_3	-0.3016_4

k_2	1.2	1.4	1.6	1.8	2.0
F_1	0.78851	1.01211	0.40599	0.41408	0.95739
G_1	0.69570	−0.25363	−0.95474	−0.94637	−0.37837
F_1'	0.68449	−0.28070	−1.12371	−1.18834	−0.50173
G_1'	0.78533	1.0987	0.47301	0.52418	1.2789
$F_1'G_1-F_1G_1'$	1.09544	1.18322	1.26489	1.34166	1.41425
k	1.09545	1.18322	1.26491	1.34164	1 41421
σ_0	0.3070_4	0.3064_6	0.3035_4	-0.2991_3	-0.2939_5

It is attractive near the nucleus, but repulsive far from the ion. In the intermediate region there is a flat potential hill.

Classically speaking, the electrons with energy scarcely enough to pass over the hill, spend a large part of their lapse in the orbital motion around the ion. So the large ionization probability is to be expected. The electrons with smaller incident energy are repelled by the potential barrier, and those with larger energy pass the ion in haste. The critical energy is about $k^2=0.7$ a.u. ($=1.9$ eV.), which is equal to the height of the potential barrier.

The more exact expression is given by wave-mechanical solution. The wave functions with energy near the critical value have large and flat part extending over fairly wide region. It is to be noted that two successive humps like those of a camel appear in some range of energy parameter. (Fig. 1, and 2 in § 2.)

The effective "potential" for p-wave is obtained by adding the centrifugal term $l(l+1)//r^2$. This results to rise up the height of the potential hill as shown in Fig. 4.

The critical value now becomes $k^2=1.3$ a.u. ($=3.5$ eV.) The similar effect as in the case of s-wave happens but at higher energy.

Summing up the two waves, we may foresay on the ionization cross-section as follows. The ionization begins to occur at 3.0 eV. As the incident energy increases, the cross-section curve rises up and has the first maximum due to s-wave. Then it depresses and again ascends to the second maximum, because p-wave becomes effective in turn. Detailed calculation is now in progress and will be reported in the following paper.

As for the ionosphere, the electron temperature is the order of 1000°K. This corresponds to the mean energy 0.1 eV. Thus O^- ion is stable in the night when the solar radiaton is absent. However, if the electrons come from the sun or elsewhere with higher energy, ionization can occur in a considerable extent.

The writer withes to express his sincere thanks to Prof. Yamanouchi for his kind guidance and helpful suggestions. He is also indebted to Miss Ota for her assistance in numerical works.

References.

(1) Watanabe: J. Phys. Soc. Japan, in press.

(2) Hartree, Hartree and Swirles: Phil. Trans. A, **238** (1939), 229.

(3) Yamanouchi: Proc. Phys-Math. Soc. Japan, **22** (1940), 569.
Yamanouchi: Prog. Theor. Phys, **2** (1947), 33.

(4) O reference (3)
O^+ Yamanouchi and Kotani: Proc. Phys-Math. Soc. Japan, **22** (1940), 60.
O^{++} Yamanouchi: ibid., **24** (1942), 351.
O^{+++} Yamanouchi: ibid., **23** (1941), 757.

(5) Whittaker and Watson: "*Modern Analysis*" 4th ed., (1935) Chap. XVI.

(6) Yost, Wheeler and Breit: Phys. Rev., **49** (1936), 174.

(7) Yamanouchi and Kotani: Proc. Phys-Math. Soc. Japan, **22** (1940), 60.

(8) Infeld: Phys. Rev., **59** (1941), 737.

(9) Yamanouchi: Proc. Phys-Math. Soc. Japan, **23** (1941), 764.

Water Jump in the Boundary Layer.

By Itiro TANI.

Department of Physical Technology, Second Faculty of Engineering, University of Tokyo.

(Read October 13, 1948; Received November 27, 1948)

§ 1. When a vertical water jet impinges on a horizontal wall, a thin stream is formed which glides radially along the wall until a standing wave is produced, beyond which the stream increases its thickness considerably. The phenomenon resembles closely to the so-called "water jump", which is frequently observed in the flow in open channels. Closer examination reveals, however, that the thickening of layer is due to the separation of flow, the separated flow getting over a standing vortex ring, as shown in Fig. 1. It seems worth while to study the phenomenon in the light of the boundary layer theory.

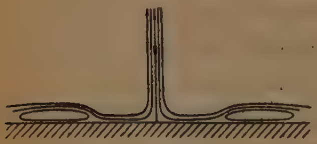

Fig. 1.

§ 2. The layer differs from the usual boundary layer in that it experiences the gravity force and that it has a free surface. The equations of radial flow are

$$\frac{\partial u}{\partial r}+\frac{u}{r}+\frac{\partial w}{\partial z}=0, \tag{1}$$

$$u\frac{\partial u}{\partial r}+w\frac{\partial u}{\partial z}=-\frac{1}{\rho}\frac{\partial p}{\partial r}+\nu\left(\frac{\partial^2 u}{\partial r^2}+\frac{1}{r}\frac{\partial u}{\partial r}+\frac{\partial^2 u}{\partial z^2}-\frac{u}{r^2}\right), \tag{2}$$

$$u\frac{\partial w}{\partial r}+w\frac{\partial w}{\partial z}=-\frac{1}{\rho}\frac{\partial p}{\partial z}-g+\nu\left(\frac{\partial^2 w}{\partial r^2}+\frac{1}{r}\frac{\partial w}{\partial r}+\frac{\partial^2 w}{\partial z^2}\right), \tag{3}$$

where r is the distance measured radially along the wall, z the distance measured normally to the wall, u and w the velocity components in the directions of r and z respectively, p the pressure, g the acceleration due to gravity, ρ the density and ν the coefficient of kinematic viscosity. According to the assumptions accepted in the boundary layer theory, equation (3) reduces to

$$\frac{p}{\rho} = g(h-z), \tag{4}$$

where h is the thickness of the layer. The equation (2) is then simplified to the form

$$u\frac{\partial u}{\partial r}+w\frac{\partial u}{\partial z} = -g\frac{dh}{dr}+\nu\frac{\partial^2 u}{\partial z^2}. \tag{5}$$

The boundary conditions are

$$u = 0,\ w = 0 \quad \text{when} \quad z = 0 \tag{6}$$

for the wall, and

$$u = U,\ \frac{\partial u}{\partial z} = 0 \quad \text{when} \quad z = h \tag{7}$$

for the free surface. Condition of steady state requires that the volume rate of flow

$$Q = 2\pi r\int_0^h u\,dz \tag{8}$$

is constant. Integration of (5) with respect to z gives

$$\frac{d}{dr}\int_0^h u^2 dz = -gh\frac{dh}{dr}-\nu\left(\frac{\partial u}{\partial z}\right)_{z=0}. \tag{9}$$

§ 3. Equation (9) may be used to determine h in terms of r if a reasonable form is assumed for the velocity distribution across the layer. Assuming the simplest form satisfying the conditions (6) and (7)

$$u = U\left(2\frac{z}{h}-\frac{z^2}{h^2}\right), \tag{10}$$

we obtain the differential equation for h:

$$\frac{dh}{dr} = \frac{(5\pi\nu/Q)r^2-h}{r-(10\pi^2 g/3Q^2)r^3h^3}. \tag{11}$$

The isoclines are shown in Fig. 2 for the case $Q = 40\ \text{cm}^3/\text{s}$, $\nu = 0.0114\ \text{cm}^2/\text{s}$, $g = 980\ \text{cm/s}^2$. The integral curves approach in spirals to the point where both the numerator and denominator of (11) vanish. But all the integral curves cannot necessarily have physical significance as lines of free surface. If we start from the point $r = 0$, $h = 0$, the slope of the curve continues to increase, until the isocline with infinite slope is reached. Actually, however, before reaching the infinite slope, the increase in pressure gradient produces separation of flow from the wall and consequently back flow, thus giving explanation for the sudden thickening of the stream.

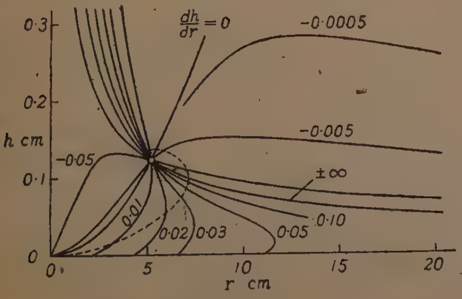

Fig. 2.

The analysis as given here has already been obtained by Prof. Kurihara (1946) in a slightly modified form. The present writer, unawares of that work, developed independently a similar analysis, and came to the conclusion that it would be worth while to put forward another method of solution, in which the change in the form of velocity distribution is taken into account.

§ 4. In order to solve the equation (5) approximately, we assume that the slope of streamline varies linearly with the distance from the wall, i. e.

$$\frac{w}{u} = \frac{dh}{dr}\frac{z}{h}. \tag{12}$$

This assumption is originally due to Prof. Wada (1940), and is used for developing an approximate solution of the usual boundary layer. Since the adequacy of the assumption is justified only in the immediate neighborhood of the wall, the accuracy of the resulting solution has been questioned. In the boundary layer discussed here, however, (12) holds strictly at the wall as well as at the free surface, and the assumption is expected to hold with good approximation throughout the layer.

Substituting (12) into (1) and (5), we have

$$\nu\frac{\partial^2 u}{\partial z^2}+\frac{u^2}{h}\left(\frac{dh}{dr}+\frac{h}{r}\right) = g\frac{dh}{dr}. \tag{13}$$

As shown by Prof. Wada, the equation may be integrated in terms of elliptic functions. We have

$$u = U\wp\left(\alpha\frac{z-z_0}{h};\, g_2,\, g_3\right), \tag{14}$$

where

$$\alpha^2 = -\frac{Uh}{6\nu}\left(\frac{dh}{dr}+\frac{h}{r}\right), \tag{15}$$

$$g_2 = 12\frac{gh}{U^2}\frac{dh/dr}{dh/dr+h/r}, \tag{16}$$

and $\wp$ is the Weierstrassian elliptic function with invariants g_2 and g_3. The constant z_0 is to be determined so as to satisfy the condition (6), $u=0$ at $z=0$. In order that the condition (7) may be satisfied, we require that

$$g_3 = 4-g_2, \tag{17}$$

and

$$\wp(\alpha) = \frac{1}{4}g_2-2. \tag{18}$$

Finally the rate of flow is given by

$$Q = 2\pi r U h\beta, \tag{19}$$

where

$$\beta = -\frac{\zeta(\alpha)+\sqrt{g_2/4-1}}{\alpha}, \tag{20}$$

and $\zeta(\alpha)$ is the Zeta-function.

With the aid of these formulas we can determine the velocity distribution when a definite value is assigned for the invariant g_2. In other words, the velocity distribution is given by a member of the one-parameter family of curves, the parameter of which being g_2. Some of the curves are shown in Fig. 3. It will be seen that $g_2=12$ corresponds to the flow of uniform velocity distribution ($u=U$), $g_2=0$ to the flow of uniform thickness ($dh/dr=0$), and $g_2=4$ to the flow at separation. There is no flow for the values of g_2 lying between 4 and 12. This is to be expected because the assumption (12) excludes the possibility of formation of back flow beyond the separation. The accompanying table contains values of α, β etc. for several values of g_2.

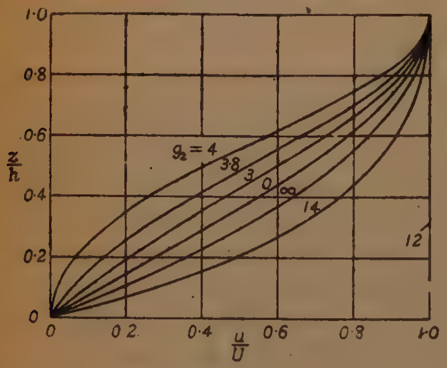

Fig. 3.

g_2	α	β	$\alpha^2\beta$	$g_2\alpha^2/\beta$
12	∞	1.000	∞	∞
14	0.972	0.740	0.698	17.87
16	0.783	0.718	0.440	13.66
19	0.641	0.702	0.289	11.12
28	0.459	0.686	0.145	8.62
±∞	0	0.667	0	6.00
−6	0.493 i	0.643	−0.156	3.02
0	0.701 i	0.615	−0.302	0
2	0.826 i	0.592	−0.405	− 2.31
3	0.936 i	0.569	−0.498	− 4.62
3.8	1.118 i	0.520	−0.650	− 9.14
4	1.311 i	0.457	−0.785	−15.05

§ 5. From equations (15), (16) and (19) we have

$$\alpha^2\beta = -\frac{Q}{12\pi\nu}\frac{1}{r}\left(\frac{dh}{dr}+\frac{h}{r}\right), \tag{21}$$

$$g_2\frac{\alpha^2}{\beta} = -\frac{4\pi g}{\nu Q}rh^3\frac{dh}{dr}. \tag{22}$$

Since α and β are functions of g_2, there is a functional relation between $\alpha^2\beta$ and $g_2\alpha^2/\beta$. This is shown in Fig. 4. With the aid of this relation, the right-hand side of (21) can be connected with the right-hand side of (22), thus giving a functional relation between r, h and dh/dr. This is the differential equation for h.

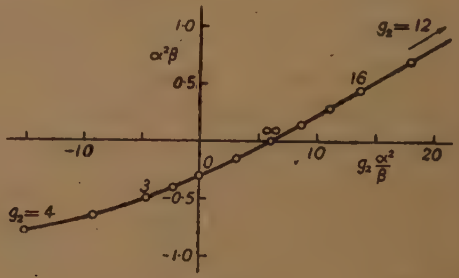

Fig. 4.

The solution of the differential equation can

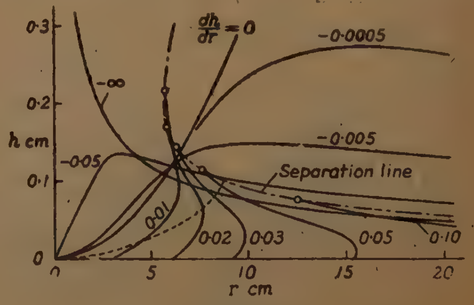

Fig. 5.

only be performed graphically. The isoclines are shown in Fig. 5 for the case $Q = 40\,\mathrm{cm}^3/\mathrm{s}$, $\nu = 0.0114\,\mathrm{cm}^2/\mathrm{s}$, $g = 980\,\mathrm{cm/s}^2$. They resemble closely to those already given in Fig. 2, but the following differences should be noticed. Firstly, some of the isoclines cross each other, so that dh/dr is not a single-valued function of r and h. This is due to the non-linear relation between $\alpha^2\beta$ and $g_2\alpha^2/\beta$. (Indeed, if we assume $\alpha^2\beta = A + Bg_2\alpha^2/\beta$, the differential equation reduces to the form as (11).) Physically, however, no ambiguity arises as to which branch of the curve is to be followed. Secondly, the region of flow of increasing thickness is limited by the "separation line" ($g_2 = 4$), beyond which no isocline exists; therefore there is no isocline with infinite upward slope. This is due to the fact that the value of $g_2\alpha^2/\beta$ cannot decrease beyond a certain limit. On the other hand, $g_2\alpha^2/\beta$ may increase indefinitely, so that we have an isocline with infinite downward slope ($g_2 = 12$), just the same as in Fig. 2.

The integral curve, when started from the point $r = 0$, $h = 0$, continues to increase the slope until the separation line is reached. It is only up to this point that the present analysis describes the state of affairs with good approximation. After the separation occurs, the assumption underlying the analysis can no longer be retained, but the results of analysis may still be used to obtain a rough estimate of the state at such a large radius that the flow has already got over the standing vortex and consequently the back flow has disappeared. Since the value of h in this region is large compared to that before separation, h must continue to decrease as indicated by Fig. 5. If h would have been diminished to such an extent that the isocline with infinite downward slope is reached, the second singularity would arise, as supposed by Prof. Kurihara. Such is not always the case, however, since the slope of the isocline is steeper than that prescribed to it provided h is sufficiently large. (This holds when $h > 0.15$ cm for $r = 20-40$ cm in the case of Fig. 5.)

§ 6. An experiment was performed by allowing a vertical jet of water to impinge on a horizontal glass plate of 35 cm square. The rate of flow Q was varied and the radius r_1 at which the separation occurs was observed. The temperature of water was 16°C. The results are given in Fig. 6, together with the calculated values, which are obtained by assuming $h = 0$ when $r = 0$. (This initial condition seems to be justified because the diameter of jet was less than 0.3 cm.) The calculated radius exceeds the observed one by about 40 per cent. It is not certain why such a discrepancy arises; it may partly be due to the difference in circumstances at large radius between theory and experiment.

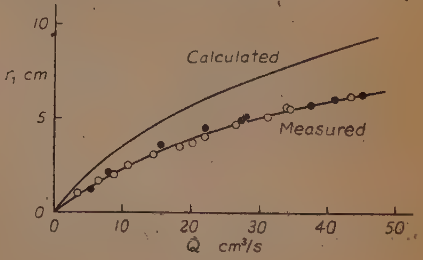

Fig. 6.

References

M. Kurihara, On hydraulic jumps. Report of the Research Institute for Fluid Engineering, Kyusyu Imperial University, Vol, 3, No. 2 (1946), pp. 11-33.

K. Wada, Theory of laminar boundary layer. Report of the Aeronautical Research Institute, Tokyo Imperial University, Vol. 15, No. 196 (1940), pp. 229-306.

On the Theory of Statistical Adjustment of Data. I. Conditions Containing Parameters.

By Wasao SIBAGAKI.

Mathematical Institute, Kyushu University.

(Received Dec. 2, 1948.)

§ 1. Problem of Specification.

Between two measurable quantities (ξ, η) let there exist some functional relation, the state of object under consideration being supposed to be determined by a set of corresponding values (ξ_i, η_i). In one state we measure the quantity ξ several times and let the mean of these measurements be X. In the same state we measure the corresponding quantity η several times and let the mean of these measurements be Y. As a result of these experiments in several states a series of corresponding observed values

$$\begin{matrix} X_1, X_2, \cdots, X_N, \\ Y_1, Y_2, \cdots, Y_N \end{matrix} \tag{1}$$

are obtained. (X_i, Y_i) $(i = 1, 2, \ldots, N)$ is called an *observed point* and we have N observed points. From these observed points suppose that we may infer that the corresponding *true points* (ξ_i, η_i) all lie on a true curve

$$F(\xi, \eta, a_1, a_2, \ldots, a_K) = 0 \tag{2}$$

containing K parameters a_μ $(\mu = 1, 2, \ldots, K)$, whose values are yet not known. The true points (ξ_i, η_i) are, we consider, merely the average values that would result from repeating the experiment a large number of times in state of randomness. Owing to many uncontrollable random errors, observed points, which consider a sample from the parent universe, do not lie on the true curve. Now our problem is to estimate from these data alone the true values (ξ_i, η_i) and the true parameter values a_μ, as accurately as we can. The *estimated values* we designate by

$$(\bar{\xi}_i, \bar{\eta}_i) \quad \text{and} \quad \bar{a}_\mu \tag{3}$$

and require that they satisfy the calculated or *adjusted curve*

$$F(\bar{\xi}, \bar{\eta}, \bar{a}_\mu) = 0, \tag{4}$$

whose form is the same as the true curve, but having different parameter values. It is assumed that if the errors of observation were negligible, the observed coordinates X and Y would satisfy the true curve with true parametric values. Actually, however, the ooserved points do not lie on either the true curve or the calculated curve owing to errors of observation. This problem was treated by several authors,⁽¹⁾ especially by Dr. W. E. Deming,⁽²⁾ who developed for the first time a method for adjusting the observations for the circumstance in which both the x and y coordinates are subject to error. But I found that his idea of introducing the *residuals* at the outset, which are equal to

Observed values—Adjusted values,

is a serious obstacle to a satisfactory development of the theory. So I ventured to give some modifications in the following.

The measurements of ξ_i and η_i are supposed statistically independent and the observed values are supposed to be random variables distributed about the respective true values according to the normal law. Accordingly the means also distribute according to the normal law

$$\left\{\begin{aligned} &\frac{1}{\sqrt{2\pi}\sigma_{xi}} \exp\left[-\frac{(x_i-\xi_i)^2}{2\sigma_{xi}^2}\right] dx_i, \\ &\frac{1}{\sqrt{2\pi}\sigma_{yi}} \exp\left[-\frac{(y_i-\eta_i)^2}{2\sigma_{yi}^2}\right] dy_i, \end{aligned}\right. \tag{6}$$

ξ_i, η_i satisfying the N conditions

$$F(\xi_i, \eta_i, a_\mu) = 0, \quad (i = 1, 2, \ldots, N). \tag{7}$$

Here

$$E(X_i) = \xi_i, \quad E(Y_i) = \eta_i \tag{8}$$

and σ_{xi}, σ_{yi} are respectively the standard deviations (σ_{xi}^2, σ_{yi}^2 the variance) of X_i, Y_i. Now by tne supposed condition of randomness we can to X_i, Y_i respectively the following *weights*

$$w_{xi}' = \sigma_x^2/\sigma_{xi}^2, \quad w_{yi}' = \sigma_y^2/\sigma_{yi}^2, \tag{9}$$

in which σ_x^2 and σ_y^2 are arbitrary proportional factors having respectively the meaning that

$\sigma_x^2 =$ the variance of X-measurement of unit weight,

$\sigma_y^2 =$ the variance of Y-measurement of unit weight.

In general the quantities ξ and η are of different physical dimensions so that we have no theoretical grounds for comparing both variance of unit weight. But practically there must be balancing in precision between both measurements. This point seems to be overlooked by many authors of least squares. By some principle we suppose that the *balancing factor* β (which is in general of same physical dimension) could be determined,) such that

$$\sigma_y : \sigma_x = \beta, \tag{10}$$

then putting $\sigma_x^2 = \sigma^2$ for brevity, we have

$$w_{xi}' = \sigma^2/\sigma_{xi}^2, \quad w_{yi}' = \beta^2\sigma^2/\sigma_{yi}^2. \tag{11}$$

We write for simplicity

$$w_{xi}' \equiv w_{xi}, \quad w_{yi}'/\beta^2 \equiv w_{yi}, \tag{12}$$

then in (6) we can write

$$1/\sigma_{xi}^2 = w_{xi}/\sigma^2, \quad 1/\sigma_{yi}^2 = w_{ys}/\sigma^2. \tag{13}$$

Now the N set of observations being supposed to be independent each other, the simultaneous probability distribution is

$$\frac{\sqrt{w_{xi}\cdots\cdots w_{yN}}}{(2\pi)^N\sigma^{2N}}\exp\left\{-\frac{1}{2\sigma^2}[\sum w_{xi}(x_i-\xi_i)^2\right.$$
$$\left.+w_{yi}(y_i-\eta_i)^2]\right\}.dx_1\cdots\cdots dx_N\,dy_1\cdots\cdots dy_N. \tag{14}$$

But for the possibility of mathematical treatment the problem must be linearized. For that purpose we introduce some approximate values (ξ_i^0, η_i^0) for the true values (ξ_i, η_i) and some approximate values a_{μ_0} for the true parametric values a_μ and denote the small corrections respectively by

$$\xi_i-\xi_i^0 = \Delta_{xi}, \quad \eta_i-\eta_i^0 = \Delta_{yi}, \quad a_\mu-a_\mu^0 = \Delta_\mu. \tag{15}$$

Then the N conditions (7) can be linearixed neglecting small quantities of higher orders and the result is

$$F_i^0+F_{xi}^0\Delta_{xi}+F_{yi}^0\Delta_{yi}+S\mu F_{\mu i}\Delta_\mu = 0, \tag{16}$$

where $\quad F_i^0 \equiv F(\xi_i^0, \eta_i^0, a_\mu^0),$

$$F_{xi}^0 \equiv \partial F(\,''\,)/\partial\xi_i^0, \quad F_{yi}^0 \equiv \partial F(\,''\,)/\partial\eta_i^0,$$
$$F_{\mu i}^0 \equiv \partial F(\,''\,)/\partial a_\mu^0 \tag{17}$$

and S_μ means summation with respect to the index $\mu = 1, 2, \ldots\ldots, K$, while $\sum i$ means summation with respect to the index $i = 1, 2, \ldots\ldots, N$ in the followidg. According to our assumption the ξ_i^0, η_i^0, a_μ are constants, so that all the coefficients (17) are also constants. In practice we may take the actual observed values X_i, Y_i for ξ_i^0, η_i^0 as Dr. Deming did, but theoretically X_i, Y_i are random variables which can take values extending to infinity, so that they can not and must not be taken as approximate values to ξ_i, η_i (which are constants).

Now we introduce new random variables by

$$V_{xi} \equiv X_i-\xi_i^0, \quad V_{yi} \equiv Y_i-\eta_i^0. \tag{18}$$

Then

$$X_i-\xi_i = V_{xi}-\Delta_{xi}, \quad Y_i-\eta_i = V_{yi}-\Delta_{yi}, \tag{19}$$

and the following relations hold.

$$E(V_{xi}) = \Delta_{xi}, \quad E(V_{yi}) = \Delta_{yi}, \quad dX_i = dV_{xi},$$
$$\sigma^2(V_{xi}) = \sigma^2(X_i), \quad \sigma^2(V_{yi}) = \sigma^2(Y_0). \tag{20}$$

Hence the weights of V_{xi}, V_{yi} are also w_{xi}, w_{yi} respectively. The simultaneous probability distribution for V_{xi}, V_{yi} is now

$$\frac{c}{\sigma^{2N}}\exp\left\{-\frac{1}{2\sigma^2}]\sum w_{xi}(V_{xi}-\Delta_{xi})^2+w_{yi}(V_{yi}-\Delta_{yi})^2]\right\}$$
$$\cdot dV_{x1}\cdots\cdots dV_{xN}\,dV_{y1}\cdots\cdots dV_{yN}, \tag{21}$$

where the N conditions (16) hold and

$$c = \sqrt{w_{x1}\cdots\cdots w_{yN}}/(2\pi)^N. \tag{22}$$

§ 2. Problem of Estimation.

Now we estimate the values $\Delta_{xi}, \Delta_{yi}, \Delta_\mu$ and σ^2 according to the *principle of maximum liklihood*, which says that they are the values which maxmizes the liklihood under the N conditions (16), By the introduction of the Lagrange's multipliers k_i the problem becomes

$$(c/\sigma^{2N})\exp\{(-1/2\sigma^2)[\sum w_{xi}(V_{xi}-\Delta_{xi})^2$$
$$+w_{yi}(V_{yi}-\Delta_{yi})^2]\}+\sum k_i(F_i^0+F_{xi}^0\Delta_{xi}+F_{yi}^0\Delta_{yi}$$
$$+SF_{\mu i}^0\Delta_\mu) = \text{stationary}. \tag{23}$$

when the required estimated values are denoted respectively by the barred letters, the respective differentiations give

$$V_{xi} = V_{xi} + \lambda_i F_{xi}^0 / w_{xi}, \tag{24}$$

$$V_{yi} = V_{yi} + \lambda_i F_{yi}^0 / w_{yi}, \tag{25}$$

$$\sum \lambda_i F_{\mu i}^0 = 0, \tag{26}$$

$$F_i^0 + F_{xi}^0 \varDelta_{xi} + F_{\mu i}^0 \varDelta_{yi} + \mathrm{S} F_{\mu i}^0 \varDelta_\mu = 0, \tag{27}$$

$$\sigma^2 = [\sum w_{xi} (V_{xi} - \varDelta_{xi})^2 + w_{yi} (V_{yi} - \varDelta_{yi})^2]/2N, \tag{28}$$

where we put

$$(e^N \sigma^{2N+2}/c)\, k_i \equiv \lambda_i . \tag{29}$$

The equations (24). (25), (26), (27), (28) are $3N+K+1$ equations for the $3N+K+1$ unknowns $\varDelta_{xi}$, $\varDelta_{yi}$, λ_i, $\varDelta_\mu$, σ^2.

Putting the values $\varDelta_{xi}$, $\varDelta_{yi}$ of (24), (25) into (27) we have

$$L_i \lambda_i + \mathrm{S}\, F_{\mu i}^0 \varDelta_\mu = -F_i^0 - F_{xi}^0 V_{xi} - F_{yi}^0 V_{yi}, \tag{30}$$

where we put for brevity

$$L_i \equiv \frac{F_{xi}^0 F_{xi}^0}{w_{xi}} + \frac{F_{yi}^0 F_{yi}^0}{w_{yi}}. \tag{31}$$

The equations (30) with (26) determine λ_i and $\varDelta_\mu$. Further if we put the values λ_i from (30) into (26) we obtain the *normal equations* for our problem, are

$$\mathrm{S}^\nu \varPhi_{\mu\nu} \varDelta_\nu = -\sum_i \frac{F_{\mu i}^0 F_i^0}{L_i} - \sum_i \frac{F_{\mu i}^0 F_{xi}^0}{L_i} - \sum_i \frac{F_{\mu i}^0 F_{yi}^0 V_{yi}}{L_i} \tag{32}$$

where we put

$$\varPhi_{\mu\nu} \equiv \varPhi_{\nu\mu} \equiv \sum_i \frac{F_{\mu i}^0 F_{\nu i}^0}{L_i}. \tag{33}$$

Thus we solve first the normal equations (32) for $\varDelta_\mu$, then we get λ_i by (30), $\varDelta_{xi}$, $\varDelta_{yi}$ by (24), (25) and σ^2 by (28) successively.

Now from the equations (30) and (26) we see that λ_i and $\varDelta_\mu$ are linear functions of V_{xi}, V_{yi}, therefore from (24), (25) $\varDelta_{xi}$, $\varDelta_{yi}$ are also linear functions of V_{xi}, V_{yi}. Accordingly the variables λ_i, $\varDelta_\mu$, $\varDelta_{xi}$, $\varDelta_{yi}$ all distribute according to the normal law. As for the expected values we have

$$E(\lambda_i) = 0, \quad E(\varDelta_\mu) = \varDelta_\mu . \tag{34}$$

Because, by dint of (20) we have from (30), (26)

$$\begin{cases} L_i E(\lambda_i) + \mathrm{S}\, F_{\mu i} E(\varDelta_\mu) = -F_i^0 - F_{xi}^0 \varDelta_{xi} - F_{yi}^0 \varDelta_{yi}, \\ \sum F_{\mu i}^0 E(\lambda_i) = 0. \end{cases} \tag{35}$$

Now by (16) this system of linear equations are evidently satisfied by the values (34), so that by dint of uniqueness of the solution the values appeared in (34) are its only solution. Thus we have the relations (34). Accoadingly by (24), (25) we have also

$$E(\varDelta_{xi}) = \varDelta_{xi}; \quad E(\varDelta_{yi}) = \varDelta_{yi}. \tag{36}$$

As for the variances, since

$$\begin{aligned} \sigma^2(V_{xi}) &= \sigma^2(X_i) = \sigma^2/w_{xi}, \\ \sigma^2(V_{yi}) &= \sigma^2(Y_i) = \sigma^2/w_{yi}, \end{aligned} \tag{37}$$

we see that the variances of λ_i, $\varDelta_\mu$, $\varDelta_{xi}$, $\varDelta_{yi}$ are all proportional to σ^2.

§ 3. Use of 2N-dimensional Vector Space.

Now for the sake of obtaining sampling distributions we simplify the notation by introducing the $2N$-dimensional vector spece which is spred by the following $2N$ normalized orthogonal vectors

$$\begin{aligned} \boldsymbol{i}_1 &= (1, 0, 0, \ldots, 0), \ldots, \\ \boldsymbol{i}_{2N} &= (0, 0, 0, \ldots, 1). \end{aligned} \tag{38}$$

We write

$$\begin{cases} \boldsymbol{x} = \sum \sqrt{w_{xi}}\, \varDelta_{xi}\, \boldsymbol{i}_i + \sum \sqrt{w_{yi}}\, V_{yi}\, \boldsymbol{i}_{i+N}, \\ \boldsymbol{m} = \sum \sqrt{w_{xi}}\, \varDelta_{xi}\, \boldsymbol{i}_i + \sum \sqrt{w_{yi}}\, \varDelta_{yi}\, \boldsymbol{i}_{i+N}, \\ \overline{\boldsymbol{m}} = \sum \sqrt{w_{xi}}\, \varDelta_{xi}\, \boldsymbol{i}_i + \sum \sqrt{w_{yi}}\, \varDelta_{yi}\, \boldsymbol{i}_{i+N}, \\ \boldsymbol{e} = \boldsymbol{x} - \boldsymbol{m} = \sum \sqrt{w_{xi}}\, (X_i - \xi_i)\, \boldsymbol{i}_i \\ \qquad\qquad + \sum \sqrt{w_{yi}} (Y_i - \eta_i) \boldsymbol{i}_{i+N}, \\ \boldsymbol{v} = \boldsymbol{x} - \boldsymbol{m} = \sum \sqrt{w_{xi}}\, (X_i - \xi_i)\, \boldsymbol{i}_i \\ \qquad\qquad + \sum \sqrt{w_{yi}}\, (Y_i - u_i)\, \boldsymbol{i}_{i+N}, \\ \boldsymbol{w} = \overline{\boldsymbol{m}} - \boldsymbol{m} = \sum \sqrt{w_{xi}}\, (\xi_i - \xi_i)\, \boldsymbol{i}_i \\ \qquad\qquad + \sum \sqrt{w_{yi}}\, (\eta_i - \eta_i)\, \boldsymbol{i}_{i+N}. \end{cases} \tag{39}$$

By (20) we have

$$E(\boldsymbol{x}) = \boldsymbol{m}, \quad \therefore \quad E(\boldsymbol{e}) = 0, \tag{40}$$

and

$$\sigma^2(\boldsymbol{x}) = \sigma^2(\boldsymbol{e}) = \sigma^2 \tag{41}$$

The sum of the weighted squares of the residuals S can be written as

$$S = (\boldsymbol{x} - \boldsymbol{m})^2 = \boldsymbol{V}^2. \tag{42}$$

Further we define a set of N constant orthogonal normalized vectors $\boldsymbol{r}_i$ by

$$\boldsymbol{f}_i = \frac{F_{xi}^0}{\sqrt{L_i w_{xi}}} \boldsymbol{i}_i + \frac{F_{yi}^0}{\sqrt{L_i w_{yi}}} \boldsymbol{i}_{i+N}, \quad (i = 1, \ldots, N) \tag{43}$$

which satisfy

$$\boldsymbol{f}_i \cdot \boldsymbol{f}_j = \delta_{ij}. \tag{44}$$

Then another set of constant vectors $\boldsymbol{r}_i$ by

$$\boldsymbol{r}_i = \frac{F_{yi}^0}{\sqrt{L_i w_{yi}}} \boldsymbol{i}_i - \frac{F_{xi}^0}{\sqrt{L_i w_{xi}}} \boldsymbol{i}_{i+N}, \quad (i = 1, \ldots N) \tag{45}$$

which are easily seen to be orthogonal to all $\boldsymbol{f}_i$ and form themselves a set of orthogonal normalized vectors. Therefore our $2N$-dimensional space can also be spread by the system of $2N$ orthogonal normalized vectors $\boldsymbol{f}_i$; $\boldsymbol{r}_i$, which satisfy (44) and

$$\boldsymbol{r}_i \cdot \boldsymbol{r}_j = \delta_{ij}, \quad \boldsymbol{r}_i \cdot \boldsymbol{f}_j = 0. \tag{46}$$

Further we put

$$\Delta_\mu \sim \Delta_\mu = \bar{a}_\mu - a_\mu \equiv e_\mu, \tag{48}$$

$$\sqrt{L_i}\, \lambda_i = \lambda_i'.$$

Then the extremal conditions before obtained can be expressed very simply as follows:

$$\boldsymbol{w} = \boldsymbol{e} + \sum \lambda_i' \boldsymbol{f}_i, \quad (\text{for } (24), (25)) \tag{49}$$

$$\sum \lambda_i' F_{\mu i}^0 / \sqrt{L_i} = 0, \quad (\text{for } (26)) \tag{50}$$

$$\lambda_i' + \boldsymbol{f}_i \cdot \boldsymbol{e} + \mathrm{S}\, F_{\mu i}^0 e_\mu / \sqrt{L_i} = 0. \ (\text{for } (30), (16)) \tag{51}$$

$$\sigma^2 = V^2/2N, \tag{52}$$

$$\boldsymbol{f}_i \cdot \boldsymbol{w} + \mathrm{S}\, F_{\mu i}^0 e_\mu / \sqrt{L_i} = 0, \quad (\text{for } (27), (16)) \tag{53}$$

$$\mathrm{S}\, \Phi_{\mu\nu} e_\nu = -\sum (F_{\mu i}^0 / \sqrt{L_i}) \boldsymbol{f}_i \cdot \boldsymbol{e}, \ (\text{for } (32)) \tag{54}$$

where

$$\Phi_{\mu\nu} \equiv \sum F_{\mu i}^0 F_{\nu i}^0 / L_i.$$

Now let $\varphi_{\mu\nu}$ be the elements of the reciprocal matrix of the matrix $(\Phi_{\mu\nu})$, so that there are the relations

$$\mathrm{S}\lambda\, \Phi_{\mu\lambda} \varphi_{\lambda\nu} = \delta_{\mu\nu}. \tag{55}$$

Then the solved equations for the unknowns e_μ of (54) can be written as

$$e_\mu = \boldsymbol{q}_\mu \cdot \boldsymbol{e}, \tag{56}$$

where we put

$$\boldsymbol{q}_\mu \equiv -\mathrm{S}\nu \sum i (\varphi_{\mu\nu} F_{\nu i}^0 / \sqrt{L_i}) \boldsymbol{r}_i. \tag{57}$$

The vectors $\boldsymbol{q}_\mu$ satisfy

$$\boldsymbol{q}_\mu \cdot \boldsymbol{f}_i = -\mathrm{S}\, \varphi_{\mu\nu} F_{\nu i}^0 / \sqrt{L_i}, \tag{58}$$

$$\boldsymbol{q}_\mu \cdot \boldsymbol{q}_\nu = \varphi_{\mu\nu}. \tag{59}$$

Therefore when $det(\Phi_{\mu\nu}) \neq 0$, $det(\boldsymbol{q}_\mu \cdot \boldsymbol{q}_\nu) \neq 0$ too, thus the vectors $\boldsymbol{q}_\mu$ are a set of linearly independent K vectors in the subspace R_N which are spread by the N vectors $\boldsymbol{f}_i$.

Next from (51) using the expression (56) for e_μ, we have

$$\lambda_i' = \boldsymbol{q}_i \cdot \boldsymbol{e}, \tag{60}$$

where we put

$$\boldsymbol{q}_i \equiv -[\boldsymbol{t}_i + \mathrm{S}\, (F_{\mu i} / \sqrt{L_i}) \boldsymbol{q}_\mu]. \tag{61}$$

The vectors $\boldsymbol{q}_i$ satisfy

$$\boldsymbol{q}_i \cdot \boldsymbol{q}_j = \delta_{ij} - \mathrm{S}\mu, \nu\, \varphi_{\mu\nu} F_{\mu i}^0 F_{\nu i}^0 / \sqrt{L_i L_j}, \tag{62}$$

$$\sum \boldsymbol{q}_i^2 = N - K, \tag{63}$$

$$\boldsymbol{q}_i \cdot \boldsymbol{q}_\mu = 0. \tag{64}$$

From the last relations we see that the N vectors $\boldsymbol{q}_i$ which also belong to the subspace R_N are not linearly independent. Now by using the well-known Schmidt's method of orthogonalization we can introduce $N-K$ mutually orthogonal normalized vectors

$$\boldsymbol{p}_\tau, \ (\tau = 1, \ldots, N-K), \tag{65}$$

which are all orthogonal to the vectors $\boldsymbol{q}_\mu$, such that by the N vectors $\boldsymbol{q}_\mu$ and $\boldsymbol{p}_\tau$ the subspace R_N can be spread. Let the subspace spread respectively by the set $\{\boldsymbol{q}_\mu\}$ or $\{\boldsymbol{p}_\tau\}$ be R_K or R_{N-K}. Then the vectors $\boldsymbol{q}_i$ belong to R_{N-K}. And R_R and R_{N-K} both belong to R_N and are mutually orthogonal. The whole $2N$-space are now spread by the set of $2N$ vectors.

$$\boldsymbol{q}_\mu, \ \boldsymbol{p}_\tau, \ \boldsymbol{r}_i. \tag{66}$$

They satisfy the relations

$$\begin{aligned} &\boldsymbol{q}_\mu \cdot \boldsymbol{q}_\nu = \varphi_{\mu\nu}, \quad \boldsymbol{q}_\mu \cdot \boldsymbol{p}_\tau = 0, \\ &\boldsymbol{p}_\tau \cdot \boldsymbol{p}_\sigma = \delta_{\tau\sigma}, \quad \boldsymbol{q}_\mu \cdot \boldsymbol{r}_i = 0. \\ &\boldsymbol{r}_i \cdot \boldsymbol{r}_j = \delta_{ij}, \quad \boldsymbol{p}_\tau \cdot \boldsymbol{r}_i = 0. \end{aligned} \tag{67}$$

§ 4. Sampling Distributions.

Now by (39) we have

$$\boldsymbol{e} = \boldsymbol{w} + \boldsymbol{V}, \tag{68}$$

and by (49)

$$\boldsymbol{V} = -\sum \lambda_i' \boldsymbol{f}_i. \tag{69}$$

The vectors $\boldsymbol{W}$ and $\boldsymbol{V}$ are orthogonal, because

$$\boldsymbol{W}\cdot\boldsymbol{V} = \mathrm{S}(\textstyle\sum \lambda_i' F_{\mu i}^0/\sqrt{L_i})$$

$$= e_\mu = 0, \text{ (by (53))}. \tag{70}$$

Therefore we have

$$\boldsymbol{e}^2 = w^2 + V^2. \tag{71}$$

By the orthogonal property of the vectors $\boldsymbol{f}_i$, we have

$$V^2 = \textstyle\sum \lambda_i'^2. \tag{72}$$

Now

$$\begin{aligned} E(V^2) &= \textstyle\sum E(\lambda_i'^2) = \sum E(\boldsymbol{q}_i\cdot\boldsymbol{e})^2 \\ &= \textstyle\sum i \sum \alpha\, q_{i\alpha}^2\, E(e\alpha^2), \quad \text{(by (40))} \\ &= \textstyle\sum \boldsymbol{q}_i^2\sigma^2, \quad \text{(by (41))} \\ &= (N-K)\sigma^2. \end{aligned} \tag{73}$$

Therefore we see that the *degree of freedom* of the square sum $\mathrm{S} = V^2$ is

$$n = N-K.$$

Now the vector $\boldsymbol{V}$ which belongs to the space R_N is orthogonal to all $\boldsymbol{q}_\mu$, because

$$\boldsymbol{q}_\mu\cdot\boldsymbol{V} = \mathrm{S}\varphi_{\mu\nu}\textstyle\sum \lambda_i' F_{\nu i}^0/\sqrt{L_i}$$

$$= 0. \text{ (by (58), (50))} \tag{75}$$

Therefore the vector $\boldsymbol{V}$ belongs to the space R_{N-K} spread by the vectors $\boldsymbol{p}_\tau$. Accordingly, since $\boldsymbol{W}$ is orthogonal to $\boldsymbol{V}$, the vector $\boldsymbol{W}$ belongs to the space R_{2N-K} spread by the base-vectors $\boldsymbol{q}_\mu, \boldsymbol{r}_i$. Now introduce the reciprocal system of base-vectors to the old bases (66)

$$\boldsymbol{q}_\mu^*, \quad \boldsymbol{p}_\tau, \quad \boldsymbol{r}_i, \tag{76}$$

which satisfy

$$\boldsymbol{q}_\mu^*\cdot\boldsymbol{q}_\nu = \delta_{\mu\nu}, \quad \boldsymbol{q}_\mu^*\cdot\boldsymbol{p}_\tau = 0, \quad \boldsymbol{q}_\mu^*\cdot\boldsymbol{r}_i = 0, \tag{77}$$

and the relations (67).

The vectors $\boldsymbol{q}_\mu^*$ are determined obviously by the vectors $\boldsymbol{q}_\mu$, only, so that we may put

$$\boldsymbol{q}_\mu^* = \mathrm{S}\, c_{\mu\nu}\,\boldsymbol{q}_\mu.$$

Then by the first relation we have

$$\mathrm{S}\, c_{\mu\lambda}\varphi_{\lambda\nu} = \delta_{\mu\nu}.$$

Comparing this with (55), we see that $c_{\mu\nu} = \Phi_{\mu\nu}$.

$$\therefore\quad \boldsymbol{q}_\nu^* = \mathrm{S}\,\Phi_{\mu\nu}\,\boldsymbol{q}_\nu. \tag{78}$$

It holds

$$\boldsymbol{q}_\mu^*\cdot\boldsymbol{q}_\nu^* = \Phi_{\mu\nu}. \tag{79}$$

Now we can represent the $2N$-dimensional vector $\boldsymbol{e}$ in the following form:

$$\boldsymbol{e} = \mathrm{S}\, w_\mu \boldsymbol{q}_\mu^* + \textstyle\sum v_i \boldsymbol{r}_i + \mathrm{S}\, u_\tau \boldsymbol{p}_\tau, \tag{80}$$

where

$$\boldsymbol{W} = \mathrm{S}\, w_\mu \boldsymbol{q}_\mu^* + \textstyle\sum v_i \boldsymbol{r}_i \equiv \boldsymbol{W}_1 + \boldsymbol{W}_2,$$

$$\boldsymbol{V} = \mathrm{S}\, u_\tau \boldsymbol{p}_\tau.$$

When we use the relations (77), we get

$$\boldsymbol{q}_\mu\cdot\boldsymbol{e} = \boldsymbol{q}_\mu\cdot w = w_\mu$$

$$= e_\mu = \bar{a}_\mu - a_\mu, \tag{81}$$

$$\boldsymbol{r}_i\cdot\boldsymbol{e} = \boldsymbol{r}_i\cdot\boldsymbol{W} = v_i$$

$$= \frac{F_{yi}^0}{\sqrt{L_i}}\sqrt{\frac{w_{xi}}{w_{yi}}}(\hat{\xi}_i - \xi_i)$$

$$-\frac{F_{xi}^0}{\sqrt{L_i}}\sqrt{\frac{w_{yi}}{w_{xi}}}(\hat{\eta}_i - \eta_i), \tag{82}$$

$$\boldsymbol{p}_\tau\cdot\boldsymbol{e} = \boldsymbol{p}_\tau\cdot\boldsymbol{V} = u_\tau. \tag{83}$$

Hence

$$\boldsymbol{e} = \mathrm{S}\, e_\mu \boldsymbol{q}_\mu^* + \textstyle\sum v_i \boldsymbol{r}_i + \mathrm{S}\, u_\tau \boldsymbol{p}_\tau, \tag{84}$$

where v_i and u_τ are given by (82) and (83).

Since $\boldsymbol{W}\cdot\boldsymbol{V} = 0$ and $\boldsymbol{W}_1\cdot\boldsymbol{W}_2 = 0$, we have

$$\boldsymbol{e}^2 = \boldsymbol{W}_1^2 + \boldsymbol{W}_2^2 + V^2, \tag{85}$$

where

$$\begin{aligned} \boldsymbol{W}_1^2 &= \mathrm{S}\,\Phi_{\mu\nu}\, e_\mu e_\nu, \\ \boldsymbol{W}_2^2 &= \textstyle\sum v_i^2 \\ V^2 &= \textstyle\sum u_\tau^2 = 2N\sigma^2. \end{aligned} \tag{86}$$

The simultaneous probability distributions (21) now takes the form

$$J = (2\pi)^{-N}\sigma^{-2N}\exp(-\boldsymbol{W}_1^2/2\sigma^2)\cdot\exp(-\boldsymbol{W}_2^2/2\sigma^2)$$

$$\cdot\exp(-2N\sigma^2/2\sigma^2)\, de_{x1}\ldots de_{yN}, \tag{87}$$

to which we make a transformation of coordinates from $(e_{x1}, \ldots, e_{yN})$ to (e_μ, v_i, u_τ) by the equations

$$\begin{aligned} e_\mu &= \boldsymbol{q}_\mu\cdot\boldsymbol{e}, \quad & \mu &= 1, \ldots, K \\ v_i &= \boldsymbol{r}_i\cdot\boldsymbol{e}, \quad & i &= 1, \ldots, N, \\ u_\tau &= \boldsymbol{p}_\tau\cdot\boldsymbol{e}, \quad & \tau &= 1, \ldots, N-K = n. \end{aligned}$$

Then

$$J = C_1\exp\left\{-\frac{1}{2\sigma^2}\mathrm{S}\,\Phi_{\mu\nu}\, e_\mu e_\nu\right\} de_1\ldots de_K.$$

$$\cdot\prod_{i=1}^{N}\exp\left\{-\frac{1}{2\sigma^2}v_i^2\right\} dv_i$$

$$\cdot\exp\left\{-\frac{2N\sigma^2}{2\sigma^2}\right\} du_1\ldots du_n. \tag{89}$$

where the constant C_1 must be so determined that the J integrated over whole space gives 1.

Now in the subspace R_n of $(u_1, \ldots\ldots u_n)$ we accomplish the integration over the spherical surface

$$\Sigma u_\tau^2 = 2N\sigma^2 \qquad (90)$$

of radius $\sqrt{2N}\sigma$ in order to obtain the sampling distribution for σ^2.

Thus finally we have as the required form of distribution;

$$f(\bar{a}_1, \ldots\ldots, \bar{a}_K)\, d\bar{a}_1 \ldots\ldots d\bar{a}_K$$

$$\cdot \prod_{i=1}^{N} f(v_i)\, dv_i \cdot f(\sigma^2)\, d\sigma^2, \qquad (91)$$

where

$$f(\bar{a}_1, \ldots\ldots, \bar{a}_K)\, d\bar{a}_1 \ldots\ldots d\bar{a}_K$$

$$= (1/(\sqrt{2\pi})^K \sqrt{A}) \exp(-Q/2)\, d\bar{a}_1 \ldots\ldots d\bar{a}_K, \qquad (92)$$

$$Q = \mathrm{S}\mu, \nu\, \Phi_{\mu\nu} (\bar{a}_\mu - a_\mu)(\bar{a}_\nu - a_\nu)/\sigma^2, \qquad (93)$$

$$f(v_i)\, dv_i = (\sqrt{2\pi}\,\sigma)^{-1} \exp(-v_i^2/2\sigma^2)\, dv_i, \qquad (94)$$

$$f(\sigma^2, d\sigma^2 = (2N\sigma^2/2\sigma^2)^{(n-2)/2} \exp(-2N\sigma^2/2\sigma^2)$$

$$\cdot d(2N\sigma^2/2\sigma^2) \Big/ \Gamma\left(\frac{n}{2}\right). \qquad (95)$$

The form (91) shows that the estimated parameters $(\bar{a}_1, \ldots\ldots, \bar{a}_K)$, the estimated coordinates-paar (ξ_i, η_i) and the estimated variance σ^2 have mutually independent distributions. The estimated parameters form a K-dimensional normal universe, having the mean

$$E(\bar{a}_\mu) = a_\mu, \qquad (96)$$

and the variance matrix

$$(A_{\mu\nu}) = (\sigma^2 \varphi_{\mu\nu}), \qquad (97)$$

therefore

$$\sigma^2\varphi_{\mu\mu} = \text{variance of } \bar{a}_\mu, \qquad (98)$$

$$\sigma^2\varphi_{\mu\nu}(\mu \neq \nu) = \text{co-variance of } \bar{a}_\mu \text{ and } \bar{a}_\nu. \qquad (99)$$

The estimated coordinates-paar (ξ_i, η_i) form a one-dimensional normal universe, but, it must be noticed, only with the following linear combination

$$\frac{F_{yi}^0}{\sqrt{L_i}} \sqrt{\frac{w_{xi}}{w_{yi}}}\, \xi_i - \frac{F_{xi}^0}{\sqrt{L_i}} \sqrt{\frac{w_{yi}}{w_{xi}}}\, \eta_i, \qquad (100)$$

As for the estimated variance σ^2, when we put

$$\chi^2 \equiv 2N\sigma^2/\sigma^2, \quad n = N - K, \qquad (101)$$

we see that the χ^2 has the χ^2 distribution of degree of freedom n.

References.

(1). M. Masuyama: Applications of Mathematica Statistics, Kagaku-Sokki (Scientific Instruments, in Japanese) 5 (1945), 33.

(2) W. E. Deming: Statistical Adustment of Data, (1943).

(2) W. E. Deming: Phil. Mag. 11 (1931), 146; 17 (1934), 804; 19 (1935), 389.

Relaxation Phenomena of Polymers III. Motion of Junctions under Stress Relaxation.

By Haruhiko TOHARA.

6th Division, Railway Institute of Technical Research, Tokyo.

(Received Dec. 9, 1948)

§ 1. Thermodynamical Consideration.

We mentioned on the motion of junctions under relaxation in the preceding paper and divided it into the shift, the slip and the liberation of them in view of the relative motion of the joined links (the liberation is not considered for the present)(1). In the shift no relative motion of them is done and they move as one body; in the slip, to the contrary, they once become disjoined and again rejoined where either of the rejoined chains may be different from the one previously joined. Both types of motion are rate processes which have their energies of activation and they tend to increase the configuration entropy of the network.

If one assumes that the viscous segment motion be in equilibrium (it would attain its thermal equilibrium state in much shorter period than the shift or the slip of junctions does), the configuration entropy of the network (Gaussian network is assumed) would be given as follows(2):

$$S = -(3\,k/2\,l^2)\sum_{\text{seg}}(1/N_{\tau\nu})\cdot|\boldsymbol{r}_\tau-\boldsymbol{r}_\nu|^2+S_0 \qquad (1.1)$$

where l denotes the length of a link, $N_{\tau\nu}$ the number of links in (τ, ν) segment, $\boldsymbol{r}_\tau$, $\boldsymbol{r}_\nu$ the positions in space of junctions or fixed points and the summation must be taken for all segments. S_0 is a constant of the network and expressed for the "independent links" model as

$$S_0 = (3k/2)[-\sum_{\text{seg}}\log N_{\tau\nu}+\log(3/2\,\pi l^2)\cdot\sum_{\text{seg}}1]+\text{const.}$$

where $\sum_{\text{seg}} 1$ means the total number of segments in the network and the second term within the bracket varies from model to model. Except in the case of the liberation (it is out of consideration for the present), this term is of no importance in computing the relaxing stress. The last constant no longer concerns to the structure of the network.

When the junctions shift, their positions $\boldsymbol{r}_\iota$, in general, displace with $N_{\tau\nu}$ unchanged and their most probable positions are given by

$$\partial S/\partial x_\iota = \partial S/\partial y_\iota = \partial S/\partial z_\iota = 0 \qquad (1.3)$$

When slip occurs, the number of links in each segment may vary as well as the positions of junctions. One obtains the most probable state from Eqs. (1.3) and the following ones

$$\partial S/\partial N_{\tau\nu} = 0 \qquad (1.4)$$

where the total number of links in the network is held unchanged, that is,

$$\sum_{\text{seg}} N_{\tau\nu} = \text{const.} \qquad (1.5)$$

If only secondary cross-bonds are slippable, one may define a "grand segment" as a part of a chain, the both ends of which terminate at the primary cross-links or fixed points and the condition that the number of links in each grand segment should be held constant must be used in place of Eq (1.5). The slip is accompanied with the shift and it is clear that through the slippage more stable state (of larger entropy) is attained than the case when shift alone is allowed.

The above consideration concerns the final state of relaxation, not the process of relaxation which will be discussed thermodynamically in the following.

As one assumes that, while the shift or the slip of junctions is in progress, the viscous segment motion be held in equilibrium, the relaxing stress would be related to the relaxing entropy

$$\sigma_r(\varepsilon, t, T) = -T[\partial S_r(\varepsilon, t, T)/\partial\varepsilon]_{t, T} \qquad (1.6)$$

where ε is the strain and the relaxing entropy is defined as

$$S_r(\varepsilon, t, T) = S(\varepsilon, t, T)-S(\varepsilon, \infty, T) \qquad (1.7)$$

$S(\varepsilon, \infty, T)$ means the final entropy of the network when the considered relaxation has completed and can be computed by the statistical theory of network. The thermodynamical parameter T may be omitted without confusion, for the temperature will be held constant throughout our consideration.

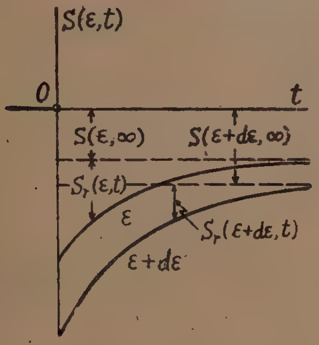

Fig. 1. Entropy as a function of ε and t.

Let one assume that the Tobolsky-Eyring's equation (1.8) hold in the stress relaxation(3), that is,

$$\{1/E(0)\}\cdot(\partial\sigma_r/\partial t)_\varepsilon + A\sinh(B\sigma_r) = 0 \qquad (1.8)$$

where

$$\left.\begin{aligned} A &= 2n\,\lambda(kT/h)\exp(-\Delta F_+/kT) \\ B &= \lambda/2NkT \\ E(0) &= \sigma_r(\varepsilon, 0)/\varepsilon \end{aligned}\right\} \qquad (1.9)$$

and the notations used in Eqs. (1.9) are the same as in Reference 1. Solving Eq. (1.8), one obtains the relaxing stress

$$E(t)\varepsilon = \sigma_r(\varepsilon, t) = (2/B)\,\mathrm{arctanh}\,[D\exp(-t/\tau)] \qquad (1.10)$$

where

$$\left.\begin{aligned} D &= \tanh[(B/2)E(0)\varepsilon] \\ 1/\tau &= A\cdot B\cdot E(0) \end{aligned}\right\} \qquad (1.11)$$

It must be noted in Eq. (1.8) that the Hooke's law is assumed which holds approximately only for a small deformation.

From Eqs. (1.6), (1.8) and (1.10)

$$\partial^2 S_r/\partial t\,\partial\varepsilon = \{A\cdot E(0)/T\}\sinh[B\cdot E(t)\varepsilon] \qquad (1.12)$$

Integrate Eq. (1.12) with respect to ε, and then we obtain

$$\begin{aligned} (\partial S_r/\partial t)_\varepsilon &= \{A\cdot E(0)/T\}\int_0^\varepsilon \sinh[B\cdot E(t)\varepsilon]d\varepsilon \\ &= \{A/BT\}\cdot\{E(0)/E(t)\}\cdot\{\cosh[B\cdot E(t)\varepsilon]-1\} \end{aligned} \qquad (1.13)$$

The integration of Eq. (1.13) with respect to t is carried out elementarily and the relaxing entropy is obtained;

$$S_r(\varepsilon, t) - S_r(\varepsilon, 0) = (\varepsilon/BT)\int_{BE(t)\varepsilon/2}^{BE(0)\varepsilon/2} (\tanh\xi/\xi)d\xi \qquad (1.14)$$

where the instantaneous relaxing entropy is given by

$$S_r(\varepsilon, 0) = -\{E(0)/2T\}\varepsilon^2 \qquad (1.15)$$

This is the stress relaxation considered from the thermodynamical point of view.

2. A New Equation of Stress Relaxation.

We shall state the following consideration with the terms of shift for the sake of simplicity, though the same results hold also for slip with a slight change in terminology.

Each junction has its neighbouring junctions (in general four, these not at all mean the nearest in distance). If the positions of neighbouring junctions were fixed in space, the sub-network, which is consisted of the segments terminated at that junction, would be independent on the other part of the network. The most probable position of it would be uniquely determined by the positions of the fixed neighbours, wherever are the positions of the other junctions. This fact means that each junction may shift in average only when at least one of the neighbours do shift in average. When at first the fixed points are displaced, then the junctions neighbouring to them will shift and the shift will propagate step by step through the network. The relaxing stress at a junction is applied through the segments by the shift of the neighbours, which therefore, in the relaxation process, results in the stress concentration on a fraction of junctions.

A. Tobolsky and H. Eyring assumed in the deduction of their equation that the relaxing stress had been distributed among total junctions throughout the relaxation process(3), but this is not the case. In their notations, N and n denote the numbers of junctions, respectively per unit cross-section area perpendicular to the stress and per unit length parallel to it. They must be, in reality, the numbers of "effective junctions" to which the relaxing stress is applied and these would increase with time, attaining asymptotically to some limiting numbers.

It is convenient to us to take the above unit cross-section area and the unit length in the natural (undeformed) state and therefore to measure the stress for initial cross-section. If junctions are distributed in average isotropically in the natural state, the isotropy would hold in average in the deformed state.

Let one put the number of effective junctions (it is to be noted that this is counted in average) as follows:

$$\left.\begin{aligned} N &= [\nu(t)]^2 \\ n &= \nu(t) \end{aligned}\right\} \qquad (2.1)$$

then A and B in Eq. (1.9) may be written as

$$\left.\begin{aligned} A &= \nu(t)\alpha \\ B &= \beta/[\nu(t)]^2 \end{aligned}\right\} \qquad (2.2)$$

where α and β are independent on time and

$$\left.\begin{aligned} \alpha &= 2\lambda(kT/h)\cdot\exp(-\Delta F_{+}^{+}/kT) \\ \beta &= \lambda/2kT. \end{aligned}\right\} \qquad (2.3)$$

The average rate of plastic flow (shift or slip) of each junction in the stress relaxation may be written as

$$v_f = \alpha \sinh(\beta\sigma/\nu^2) = -(1/\nu E)(d\sigma/dt) \qquad (2.4)$$

Now the function $\nu(t)$ would be determined by the following equation. Let one assume that, on the average, each effective junction introduces per unit time a number of non-effective junctions into effective ones, which is proportional to the rate of flow of the effective one

$$(1/\nu^3)(d\nu^3/dt) = 3p v_f \qquad (2.5)$$

or

$$d\nu/dt = p\nu v_f = -(p/E)(d\sigma/dt) \qquad (2.5')$$

Integrate Eq. (2.5′), then

$$\nu(t) = \nu_\infty - (p/E)\sigma \qquad (2.6)$$

where

$$\nu(t) \rightarrow \nu_\infty \quad (t \rightarrow \infty)$$

Then, an equation of stress relaxation is obtained instead of Eq. (1.8)

$$(1/E)(d\sigma/dt) + \alpha[\nu_\infty - (p/E)\sigma] \cdot \sinh\{\beta\sigma/[\nu_\infty - (p/E)\sigma]^2\} = 0 \qquad (2.7)$$

It is difficult to solve Eq. (2.7) analytically. If one assumes that

$$(p/E)\sigma \ll \nu_\infty \qquad (2.8)$$

(this is ordinarily the case as the result of experiment), then Eq. (2·7) may be expanded as

$$(1/E)\cdot(d\sigma/dt) + \alpha\nu_\infty \sinh(\beta\sigma/\nu_\infty^2)$$
$$+\alpha(p/E)\sigma[2(\beta\sigma/\nu_\infty^2)\cosh(\beta\sigma/\nu_\infty^2) - \sinh(\beta\sigma/\nu_\infty^2)] = 0 \qquad (2.9)$$

Let one put

$$\sigma = \sigma_\infty + \sigma_t \qquad (2.10)$$

and let the further computation be restricted to the case

$$\left.\begin{aligned} \beta\sigma_t/\nu_\infty^2 &\ll 1 \\ \sigma_t &\ll \sigma_\infty \end{aligned}\right\} \qquad (2.11)$$

where σ_∞ satisfies the following equation (Tobolsky-Eyring's equation for $\nu = \nu_\infty$)

$$(1/E)\cdot(d\sigma_\infty/dt) + \alpha\nu_\infty \sinh(\beta\sigma_\infty/\nu_\infty^2) = 0 \qquad (2.12)$$

Replace σ in the third term of Eq. (2.9) (weich is a relatively small correction term) with σ_∞, then the equation for σ_t is obtained

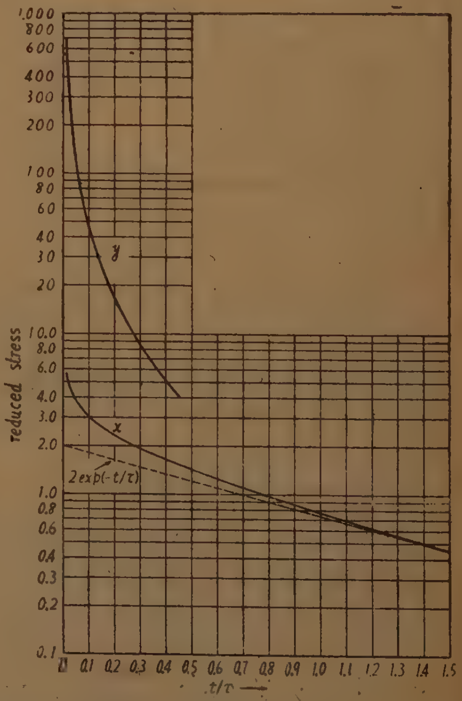

Fig. 2. x and y as functions of t/τ. D and $p\tau\alpha$ are taken to $D = 1.00$, $p\tau\alpha = 1.00$

$$(1/E)\cdot(d\sigma_t/dt)+\alpha\nu_\infty(\beta\sigma_t/\nu_\infty^2)\cosh(\beta\sigma_\infty/\nu_\infty^2)$$
$$=\alpha(p/E)\sigma_\infty[\sinh(\beta\sigma_\infty/\nu_\infty^2)-2(\beta\sigma_\infty/\nu_\infty^2)\cosh(\beta\sigma_\infty/\nu_\infty^2)] \qquad (2.13)$$

Eq. (2.13) can be solved elementarily. Let one put for brevity

$$\left.\begin{aligned} x &= \beta\sigma_\infty/\nu_\infty^2 \\ y &= \beta\sigma_t/\nu_\infty^2 \\ 1/\tau &= \nu_\infty\alpha(\beta/\nu_\infty^2)E \end{aligned}\right\} \qquad (2.14)$$

then the solution of Eq. (2.13) is written as

$$y=p\tau\alpha\left[3\sinh x\cdot\int_0^x(x/\sinh x)dx-2x^2\right] \qquad (2.15)$$

and one rewrites the solution (1.10) of Eq. (2.12)

$$x=2\,\mathrm{arctanh}[D\exp(-t/\tau)] \qquad (2.16)$$

Here, x and y are reduced stresses (dimensionless ones), which enable us to express the stress relaxation with the same equations (2.15) and (2.16). This means that one measures the stress with the unit $\sigma^*(0)/2D$ and the time with τ.

§ 3. Comparison with Experiment.

As mentioned in Reference 1, the relaxing stress, experimentally observed with vulcanized natural rubber at fairly low temperature, deviates from the calculated one which is computed according to Tobolsky-Eyring's equation (the experimentally obtained stress is always above the calculated one). We shall compare this deviation with the one computed in Eq. (2.15), where the parameter $p\tau\alpha$ is to be adjusted to fit with the observed deviation.

The comparison was taken with the reduced stress and their coincidence is always satisfactory, in case $y<1$ as assumed in (2.11).

Examples of this comparison are shown in Fig. 3.

The coincidence of the calculated transient stress with observed one would verify that this is the deviation due to the variation in the number

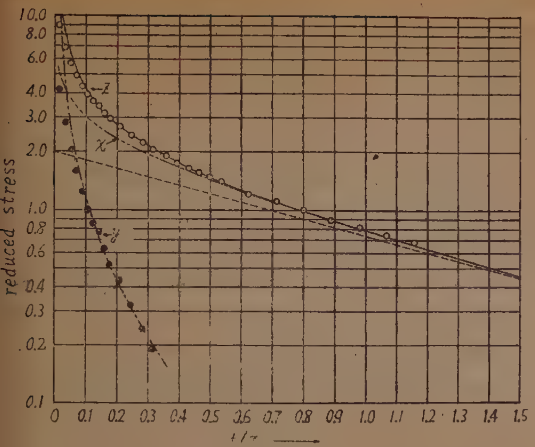

Fig. 3a.

a. $T=-49.5°\mathrm{C}$, $\tau=0.785$ sec, $\sigma^*(0)=2.09$, $p\tau\alpha=0.032$

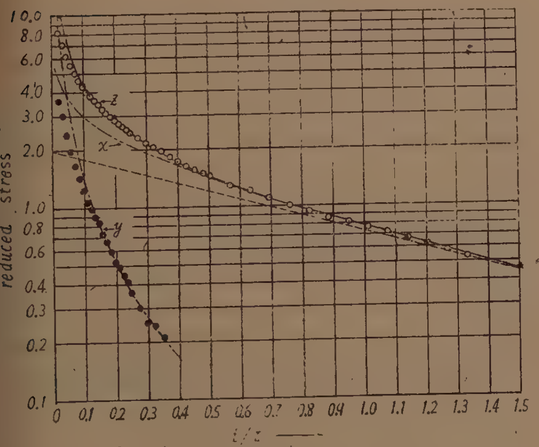

Fig. 3b.

b. $T=-46.0°\mathrm{C}$, $\tau=0.56$ sec, $\sigma^*(0)=1.90$, $p\tau\alpha=0.026$

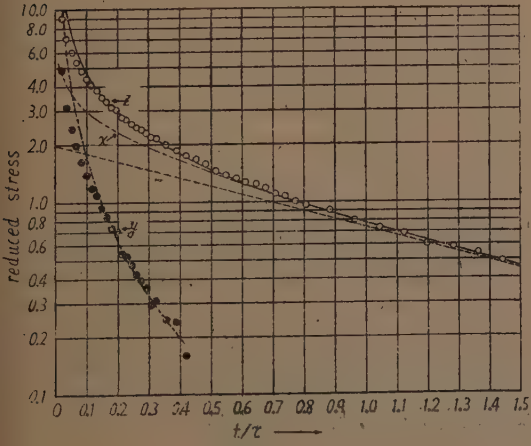

Fig. 3c.

c. $T=-42.5°\mathrm{C}$, $\tau=0.64$ sec, $\sigma^*(0)=2.67$, $p\tau\alpha=0.038$

Fig. 3. Comparison of the observed transient stress y_{obs} with the calculated one y_{cal}. Composition of samples was listed in Table I in Reference 1, $\sigma^*(0)$ is measured with an arbitrary unit.(1)

of effective junctions or, in other words, due to the concentration of the relaxing stress and that its time dependence is expressed fairly well with Eq. (2.6).

Now $p\tau\alpha$ is written

$$p\tau\alpha = 2p\nu_{\infty}(kT/E\lambda) \qquad (3.1)$$

and, according to our experiment, it appears to decrease as temperature rises, to increase with the vulcanization.

§ 4. Motional Unit in the Stress Relaxation.

For not too large deformation, rubber-like molecules behave, in a sense, in the same manner as liquid molecules do. The only difference between the two is that the former are cross-linked three-dimensionally with the primary or other relatively strong junctures. The slip of junctions in the rubber state — especially of secondary nature — corresponds to the viscous flow in the liquid state, whereas the shift of them in the former state has no analogue in the latter state.

According to P. J. Flory the viscosities of several linear polyesters show the energies of activation in the vicinity of 8 kcal/mol.(4). This energy would not vary much for other ordinary long-chain polymers.

On the other hand experiment shows that the energies of activation for viscous flow of long-chain hydrocabons are in general one-quarter of their energies of vaporization, provided they move as the motional unit.(5) Then the energies of vaporization of the motional unit in the viscous flow of long-chain polymers would be about 32 kcal/mol.

From the energies of vaporization of their monomers, the motional unit of them might be concluded to be composed of approximately 30 skeletal atoms.

In our experiment the obtained energies of activation of variously vulcanized rubber are from 15.4 kcal/mol to 16.5 kcal/mol,(1) and therefore the energies of vaporization of their motional unit would be 61 to 66 kcal/mol. The energy of vaporization of isoprene (monomer) is 5.4 kcal/mol (at the boiling point, that is at 38°C)*, and the motional unit of rubber molecules would be composed of about 12 isoprene residues or approximately 60 carbon atoms (including methyl groups) which are nearly twice the number of atoms of of the motional unit in the viscous flow of liquids.

This result suggests a different type of motion of junctions from the one similar to the viscous flow of liquid and it is favourable to the shift of juctions, because it is evident that in the shift the motional unit of them is twice as large as in the slip.

Now, in our experiment, the energy of activation is nearly twice as that of viscous flow of polyester and other long-chain hydrocarbon liquids and this also agrees with the fact that in the shift about two-fold hole would be required as in the slip.

From the above reasoning it is probable that the stress relaxation of rubber-like materials in low temperature or during short period of observation(1) is to be assigned to the shift of junctions.

§ 5. Conclusion.

The observed stress relaxation in our experiment (that is observed at low temperatures or during short periods of observation) would be probably due to the shift of junctions rather than to the slip of them ; the wide-range spectrum of relaxation time, however, would be necessary for its final decision.

A new equation (2.7) of stress relaxation which takes the transient concentration of relaxing stress into account agrees fairly well with the observation.

The Author expresses his sincere thanks to Prof. T. Sakai, Assist Prof. R. Kubo, to Dr. S. Oka, Mr. A. Ookawa for their good theoretical

---

* The heat of vaporization of isoprene and that of isoprene residue would be nearly equal ; the refered value is the heat of the former.

isoprene : $CH_2 = C(CH_3)-CH = CH_2$
isoprene residue : $-CH_2-C(CH_3) = CH-CH_2-$

This is suggested, for instance, by the fact that the heats of vaporization of isoprene and normal pentane are respectively 6.27 kcal/mol and 6.22 kcal/mol at 25°C, and whether there is a double bond or not, and whether a group is attached as side-group or as skeleton affect little the heat of vaporization.

advices and also to Prof. S. Kambara for his advices in the chemical aspects.

References.

(1) H. Tohara: J. Phys. Soc. Japan **4** (1947).
(2) H. M. James: J. Chem. Phys. **15** (1947), 651.
(3) A. Tobolsky, H. Eyring: J. Chem. Phys. **11** (1943), 125.
(4) P. J. Flory: J. Am. Chem. Soc. **62** (1940), 1057.
Grasstone, Laidler & Eyring: Theory of Rate Processes (1941), 500 (McGraw-Hill Book Co.)
(5) F. Eirich & B. Shimho: J. Chem. Phys. **17** (1939), 116; Grasstone, Laidler & Eyring: ibid, 493.

Multiple Scattering of Fast Electrons, Part II. Comparison with Experiments.

By Ken-ichi SHINOHARA, Kenzo INOUE* and Nobuko HIROHATA.

Faculty of Science, Kyushu University.

(Received Dec. 14, 1948)

Abstract.

A cloud chamber measurement was made of the scattering of electrons of kinetic energy between 1.5 and 5.8 Mev. by a lead foil of thickness 0.115 mm. The result was in an approximate agreement with the result of a similar measurement made by Sheppard and Fowler. This result as well as the results by various other authors were compared with the theory of williams and also with the theory given in the previous paper. It is shown that the latter is, generally, in a better agreement.

§ 1. Introduction.

A calculation on the multiple scattering of electrons, based on the assumption that the electrons are diffracted by minute crystals in the scattering foil has been given in the previous paper.(1) As in the theory of Williams,(2) the angle of scattering projected on a plane containing the initial direction of the electrons, has been assumed to have a Gaussian distribution, which is written as

$$F(W\alpha)=\frac{2}{\pi W\alpha_M}\exp\left(-\frac{W^2\alpha^2}{\pi W^2\alpha^2_M}\right).$$

where W is the total energy of the electrons. The value of α_M, the arithmetic mean angle of the distribution was found to be smaller than in the case of the theory of Williams or of Goudsmit and Saunderson,(3) The interference between the electrons scattered by the neighbouring atoms is not considered in either of these theories.

There are several experimental results to be compared with the theories. In the experiments using lead foils as scatterers, the experimental scattering was generally, smaller than that predicted by the theories. When light materials, such as aluminium or carbon, are used as scatterers, results approximately agreeing with the theories are obtained. However, the accuracy of the experiments do not seem to be very high and there are, also serious discrepancies in the results between various experiments. Because of this fact, we have tried to make a new series of measurement using lead as a scatterer,

§ Description of the Experiment.

A large number of cloud chamber pictures,** obtained in the gamma ray measurement on $F+{}_1H^1$ were examined. Numerous secondary electrons of the monochromatic gamma rays of 6

---

* Now at the Institute of Science and Technology, Tokyo University.

** The pictures were taken, in collaboration with Mitio Hatoyama and ZiroYuhara, at the Institute of Physical and Chemical Research, in Tokyo.

Mev. quantum energy, originating in the chamber walls and surroundings traversed the chamber. The scattering foil was a lead sheet of 0.115 mm placed in the chamber. Kinetic energy of the electrons ranged from 1.5 to 5.8 Mev.

As the electrons entered the lead foil at various angles of incidence, only those electrons making a projected angle less than 10° with the normal to the foil, on the side of incidence, has been measured, in order to secure nearly normal incidene.

The cloud chamber has been placed in a magnetic field of about 1600 gauss in order to measure the energy of the electrons. Only the electrons having a track length of more than 6 cm in the illuminated region, on the emergent side, and more than 4,5 cm on the side of incidence, were chosen for the measurement. The strength of the magnetic field was measured at each expansion.

The pictures were taken stereoscopically, but only the projected angle of deflection was measured.

There is a small energy loss of the electrons in traversing the foil. Therefore, the arithmetic mean of the energies before entering and after leaving the foil has been taken as the energy of the electrons. In some cases, the energy could be measured with certainty, only after leaving the foil. In such a case, an approximate loss of enegy in the foil has been estimated and half of its value has been added to the energy to get an approximate mean energy of the electron.

§ 3. Result of the Measurement.

237 electron tracks were measured, The result is shown in Table I, together with other experi-

Table. I.

Scattering by lead.

Authors			Sheppard and Fowler	Sheppard and Fowler	Olson, Chao, Halpern, and Crane	Present	Sheppard	Kulchitsky and Latyshev
Method			cloud chamber	cloud chamber	cloud chamber	cloud chamber	G-M counters	G-M counters
Total energy of electrons W (Mev)			5—17	5—17	2—8	2.0—6 3	Electrons from B^{12}. Mean eungy 6.2Meq.	2.76
Thickness (cm)			0.015	0.038	0.0064	0.0115	0.0103	0.00070
$W\alpha_M$ (Mev-deg.)	Experiment		47	106	45*	37	64	14.6
	Theory	Williams	95	160	58**	81	76	14.8**
		Present	81	143	46	70	61	12.0

* Includes single scattering tail.

** Calculated from the expression given by Sheppard and Fowler,(4)

Table. II.

Scattering by aluminium

Authors			Sheppard and Fowler	Kulchitsky and Latyshev
Method			cloud chamber	G-M counters
Total energy of Electrons W (Mev)			5—17	2.76
Thickness (cm)			0.118	0.0099
$W\alpha_M$ (Mev-deg.)	Experiment		50	14
	Theory	Williams	60	13.7*
		Present	48	10.8

* Calculated from the expression given by Shappard and Fowler(4)

ments(4), (5), (6), (7) on lead and compared with the theory of Williams and the theory given in the previous paper. Our result of measurement is nearly the same as that of Sheppard and Fowler.(4)

§ 4. Discussions.

Table I shows that all the cloud chamber measurements on lead result in a far smaller scattering than that predicted by the theory of Williams. The theory of Coudsmit and Saunderson will only slightly improve this point, as was pointed out by them and also shown in the provious paper. The theory given in the previous paper predicts a smallest scattering and agrees best with the experiments, but still is not very satisfactory.

In the case of scattering by aluminium, the theory of Williams is already in a fairly good agreement with the colud chamber measurement of Sheppard and Fowler (Table II), but our calculation snows a still better agreement.

Experiments using Geiger-Müller counters seem to give slightly different results. Sheppard(6) used a set of Geiger-Müller coincidence counters and instead of measuring the distribution of the scattering from a single scatterer, compared the scattering by a lead foil with the scattering by a carbon plate, In this way, the ratio of α_M for lead and carbon scatterers was found, experimentally, to be 0.7, whereas the theory of Williams predicted the value of 0,8, He, therefore, concluded that, since the scattering by a light material such as carbon is supposed to agree with the theory of Williams, the scattering by lead also agrees roughly with the same theory, and doubted the adequacy of using cloud chambers in this kind of work, If, now, the scattering by carbon was assumed to agree exactly with the theory of Williams, the experimental ratio of 0.7 requires 64 Mev,-degrees as the value of $W\alpha_M$ for lead (Table II), The theoretical values of the same quantity are, respectively, 75 Mev,-degrees and 61 Mev.-degrees, A much better agreement is obtained with our calculation, The experiment made by Kulchitsky and Latyshev(7) which also uses two Geiger-Müller coincidence counters, gives the result agreeing quite well with the theory of Williams, and not with our calculation, both in the case of lead and aluminium. But, as the scatterers used in their experiment were very thin, it is doubtful if our calculation can be applied rigorously to their experiment.

Our calculation, thus, improves the agreement with the experimental results of varions authors, as a whole, but still predicts a larger scattering than is required by experiments.

References.

(1) K. Shinohara: J. Phys. Soc. Japan, in the press.

(2) E. J. Williams: Proc. Roy. Soc., A, **169** (1939), 531; Phys. Rev., **58** (1940), 292.

(3) S. Goudsmit and J. L. Saunderson; Phys. Rev., **57** (1940), 24; **58** (1940), 36,

(4) C. W. Sheppard and W. A. Fowler; Phys. Rev., **57** (1940), 273.

(5) N. L. Olson, K. T. Chao, J. Halpern and H. R. Crane: Phys. Rev., **56** (1939), 482; **56** (1939), 1171,

(6) C. W. Sheppard: Phys, Rev., **62** (1942), 313.

(7) L. A. Kulchitsky and G. D. Latyshev: Phys, Rev,, **61** (1942), 254.

On the Excitation of H_2O Molecule by Impact of Fast Electron.

By Kazuo NIIRA.

Physics Department, Tokyo Institute of Technology.

(Read May 21, 1948; Received Jan. 28, 1949)

§ 1. Introduction.

In the vacuum discharge of water vapour the H_2O molecule is excited by electron impact to the unstable electronic state and dissociates into OH radical and H atom. Thus produced OH is in the excited state $^2\Sigma^+$ and makes transition to the ground state $^2\Pi$ emitting a system of bands in ultraviolet. It is observed by many workers(1) that the OH bands thus excited exhibit "abnormal rotation", i. e. intensity distribution among lines in each band has a strong maximum about the rotational quantum number $J = 20$ besides $J = 5$. It means that some parts of OH radicals, which arise from the H_2O molecules in thermal rotation, rotate with abnormally high speed (corresponding to the temperature of 8000 °K) while the greater parts of them do with ordinary thermal energies. The ratio between them appears to be nearly 3 to 1 from intensity distribution. The D_2O molecule shows similar behavior, too.(2)

The H_2O molecule has an equilibrium form of an isosceles triangle, two H atoms bonding with an O atom at nearly right angle. If in an unstable excited state one of the two H atoms flies apart into the direction transverse to the line of the inital position and the O atom, the other has to rotate about O atom by reaction. As it is the electronic energies that plays role of the potential to the H atom which moves along the valley in it, abnormal rotation should occur when the valley runs in the transverse direction above mentioned. We have shown it by calculating excited electronic states of H_2O molecule with atomic oribital approximation.(3)

As the result of it, it turns out that there are just two different unstable excited states which dissociate into H (1s) and OH ($^2\Sigma^+$) under consideration, and one of them gives normally rotating OH ($J = 5$) and the other causes abnormal rotation. The former corresponds to the representation A_1 of the point group C_{2v} (we call this $^1A_1{}^*$) and is a singlet one which may be excited by both of direct and exchange collisions of electrons, and the latter is a triplet one of B_1 type (indicated by $^3B_1{}^*$) excited only by exchange collisions. By taking account of interactions between states of different types (say, A_1 and B_1) which arise from deformation of the H_2O triangle into scalene one at dissociation it turns out that in both states H atom flies apart in the transverse direction. But as the dissociation energy is not sufficient to excite abnormal rotation in $^1A_1{}^*$, it may take place only in $^3B_1{}^*$.

These results may not be considered as conclusive because of approximate nature of our the calculations. And there is another qualitative explanation called "paired electron theory"(4) which ascribes the abnormal rotation to excitation of a singlet state and the normal to a triplet one, and both states arise from transition of a $2p$ electron of the O atom into the $3s$ orbit. Therefore, according to this theory abnormal rotation does occur only by direct collisions. In order to decide between two theories it may be useful to work with the incident electron of specified energy, for at high energies one exchange collision will take place so scarcely that intensities of rotational lines (either normal or abnormal) in bands should be influenced greatly. Recent observation by Horie(5) seems to support our interpretation.

In the following, we will estimate probabilities for excitation of above both states (i. e. excitation functions) by collisions of fast electrons, according to our theory.

§ 2. Excited States of H_2O.

We assume that the Franck-Condon principle holds at excitation by electron impact, i. e. nuclei are in their initial equilibrium positions immediately after exciation, as may be plausible.

We choose our z axis perpendicular to the plane of the molecule and x and y axes toward each H atom (one of them we indicate by H′) from O atom. In the ground state which is shown to be of ${}^1A_1$ type the electronic configuration of H_2O molecule is approximated to

$$\mathrm{O}:\ (2p\,\sigma_z)^2\ (2p\,\sigma_x)\ (2p\,\sigma_y)$$

$$\mathrm{H}:\ (1s)\qquad \mathrm{H}':\ (1s),$$

in which by spin pairs $2p\,\sigma_x$ couples with the electron H : (1s) and $2p\,\sigma_y$ with H′ : (1s), respectively. And according to our theory, for excited states under consideration

$$\mathrm{O}:\ (2p\,\sigma_z)^2\ (2p\,\sigma_x)^2,\ \text{or}\ (2p\,\sigma_z)^2\ (2p\,\sigma_y)^2$$

$$\mathrm{H}:\ (1s)\qquad \mathrm{H}':\ (1s),$$

approximately. Thus, $2p\,\sigma_y$ in the ground state makes transition into $2p\,\sigma_x$ (or vice versa. $2p\,\sigma_x$ into $2p\,\sigma_y$) which loses any ability to combine with H : (1s) and repels H atom to make dissociation. From this electronic configuration arise two molecular states of ${}^3B_1{}^*$ and ${}^1A_1{}^*$, and relative orientation of spins between H : (1s) and H′ : (1s) is parallel in the former and antiparallel in the latter. ${}^3B_1{}^*$ is excited only by exchange collision of incident electron. Level of ${}^3B_1{}^*$ is rather higher than ${}^1A_1{}^*$ merely on account of interaction between two H atoms, and if we neglect it both are estimated to be nearly equal to 9 eV, while excitation potentials for these states are 10±2 eV experimentally.(6)

§ 3. Calculation of Excitation Functions.

Then we will calculate excitation functions for the processes under consideration, assuming the Franck-Condon principle as mentioned before. For the electronic wave function of the ground state we assume the paired orbital function such as

$$\Psi_{\mathrm{I}} = \psi_{\sigma z}(1)\,\psi_{\sigma z}(2)\cdot\frac{1}{\sqrt{2}}\{\psi_{\sigma x}(3)\,\psi_{H}(4)+\psi_{H}(3)\,\psi_{\sigma x}(4)\}$$

$$\cdot\frac{1}{\sqrt{2}}\{\psi_{\sigma y}(5)\psi_{H'}(6)+\psi_{H'}(5)\psi_{\sigma y}(16)\}.$$

where $\psi_{\sigma x}$, $\psi_{\sigma y}$ and $\psi_{\sigma z}$ are atomic orbitals for $2p\,\sigma_x$, $2p\,\sigma_y$ and $2p\,\sigma_z$ electrons respectively, and ψ_H and $\psi_{H'}$ for H : (1s) and H′ : (1s). The figures in parenthesis represent spatial coordinates, and the closed shells of 1s and 2s of O atom are omitted. We multiply this function by spin functions and then construct the antisymmetrized wave function for the molecule.

For both excited states under consideration (${}^1A_1{}^*$ and ${}^3B_1{}^*$) the orbital functions are approximated to

$$\Psi_{\mathrm{II}} = \psi_{\sigma z}(1)\,\psi_{\sigma z}(2)\cdot\frac{1}{\sqrt{2}}\{\psi_{\sigma x}(3)\,\psi_{\sigma x}(4)+\psi_{\sigma y}(3)\,\psi_{\sigma y}(4)\}$$

$$\cdot\frac{1}{\sqrt{2}}\psi_{H}(5)\,\psi_{H'}(6).$$

From this and suitable spin functions we get the antisymmetrized function for each excited state.

We indicate wave functions of incident and scattered electrons by φ and χ, respectively. The differential cross sections $Q(\delta)$ for the processes may be calculated by the non-stationary method of perturbation. For ${}^1A_1{}^*$ we get

$$Q^s(\delta) = \frac{2\pi m^2}{h^4}\frac{k'}{k}\mathbf{A}\Big|\int\psi_{\sigma x}{}^*(1)\,\varphi^*(2)\,V\,\psi_{\sigma y}(1)\,\chi(2)\,d\tau_1 d\tau_2$$

$$+\int\psi_{\sigma y}{}^*(1)\,\varphi^*(2)\,V\,\psi_{\sigma y}(1)\,\chi(2)\,d\tau_1\,d\tau_2$$

$$-\frac{1}{2}\int\psi_{\sigma x}{}^*(1)\,\varphi^*(2)\,V\chi(1)\,\psi_{\sigma y}(2)\,d\tau_1\,d\tau_2$$

$$-\frac{1}{2}\int\psi_{\sigma y}{}^*(1)\,\varphi^*(2)\,V\chi(1)\,\psi_{\sigma x}(2)\,d\tau_1\,d\tau_2\Big|^2,$$

and for ${}^3B_1{}^*$

$$Q^t(\delta) = \frac{2\pi m^2}{h^4}\frac{k'}{k}\mathbf{A}\,\frac{3}{4}\Big|\int\overset{*}{\psi}_{\sigma x}(1)\,\varphi^*(2)\,V\chi(1)\psi_{\sigma y}(2)d\tau_1 d\tau_2$$

$$+\int\overset{*}{\psi}_{\sigma y}(1)\,\varphi^*(2)\,V\chi(1)\,\psi_{\sigma x}(2)\,d\tau_1\,d\tau_2\Big|^2,$$

where

δ: angle of scattering,

$V = \dfrac{e^2}{|r_1-r_2|}$, and r_1 and r_2 are vectors for each position of electrons,

$\mathbf{A}$: the operation averaging over relative orientations of the molecule to the direction of incident electron,

k, k': wave numbers of incident and scattered electrons. respectively.

Here, all the terms containing nuclear coordinates disappear on account of our assumption that atomic orbitals are orthogonal with each other. Further, the overlap integral between wave functions of nuclei in the initial and the final state was put equal to unity.

In the following we proceed with the usual Born approximation which is suitable for high energy impact and assume φ and χ to be plane waves:

$$\varphi = \exp(i\boldsymbol{k}\cdot\boldsymbol{r}), \quad \chi = \exp(i\boldsymbol{k}'\cdot\boldsymbol{r}),$$

$$k^2 - k'^2 = \frac{8\pi^2 m E_e}{h^2},$$

E_e: excitation potential.

The third and fourth terms in Q^s and each of Q^t represent the effect of exchange collision which may not be remarkable except for low energy electron and we ignore them. Then, they become

$Q^t(\delta) = 0,$

$$Q^s(\delta) = \frac{128\pi^3 m^2 e^4}{h^4}\frac{k'}{k}\frac{1}{K^4}\mathbf{A}|D|^2$$

$$= \frac{8}{\pi a_0^2}\frac{k'}{k}\frac{1}{K^4}A|D|^2,$$

where

$$D = \int \psi_{\sigma x}^*(1)\,\psi_{\sigma y}(2)\exp(i\boldsymbol{K}\cdot\boldsymbol{r}_1)\,d\tau_1,$$

a_0: radius of Bohr orbit (0.528×10^{-8} cm),

$\boldsymbol{K} = \boldsymbol{k} - \boldsymbol{k}'$.

The direction of K is indicated by Θ and Φ in the polar coordinate around the O atom.

Putting

$$\left.\begin{matrix}\psi_{\sigma x}\\ \psi_{\sigma y}\end{matrix}\right\} = R(r)\left\{\begin{matrix}\dfrac{x}{r}\\[2ex] \dfrac{y}{r}\end{matrix}\right.,$$

$$D = -\frac{2\pi}{K}\sin^2\Theta\sin 2\Phi\int_0^\infty r^2\left\{\frac{3\sin Kr}{(Kr)^2} - \frac{3\cos Kr}{Kr} - \sin Kr\right\}R^2(r)\,dr.$$

For $R(r)$ we choose the form of the radial part of $2p$ wave function of O atom such as

$$R(r) = \frac{r}{\sqrt{N}}\exp\left(-\frac{\lambda}{2}r\right),$$

where the parameter λ is so adjusted to approximate $R(r)$ to the Hartree $2p$ function for O atom.(7) N is a normalisation factor equal to $32\pi/\lambda^5$. Then we have

$$D = -\frac{96\pi\lambda K}{N(\lambda^2+K^2)^4}\sin^2\Theta\sin 2\Phi.$$

As the average value of $\sin^4\Theta\sin^2 2\Phi$ over molecular orientations is 4/15,

$$Q^s(\delta) = \frac{96}{5\pi a_0^2}\frac{k'}{k}\frac{\lambda^{12}}{(\lambda^2+K^2)^8}.$$

From it we get total cross section, i. e. excitation function as

$$Q^s = \int_0^\pi Q^s(\delta)\sin\delta\,d\delta$$

$$= \frac{48}{35\pi a_0^2}\frac{\lambda^{12}}{k^2}\left\{\frac{1}{[\lambda^2+(k-k')^2]^7} - \frac{1}{[\lambda^2+(k+k')^2]^7}\right\}.$$

It is seen that Q^s varies inversely proportional to k^2 or the energy of incident electron E at large value of E, for $k-k'$ in the first term becomes negligible and the second can also be ignored. Putting $\lambda = 5/a_0$ and $E_e = 10$ eV (experimental value), we can plot Q^s as in the Figure 1.

G. Hayakawa(6) measured relative intensities of band spectra of OH*($^2\Sigma^+ \rightarrow {}^2\Pi$) with (0−0) and (1−0) transitions emitted by dissociations of water vapour in the triode tube against electronic energies. As intensities are considered to be proportional to excitation functions, we compare them with our result suitably adjusted at 100 eV. The agreement may not be said so good but we remark that if be worked under the condition of constant space densities of incident electrons, it is just kQ^s

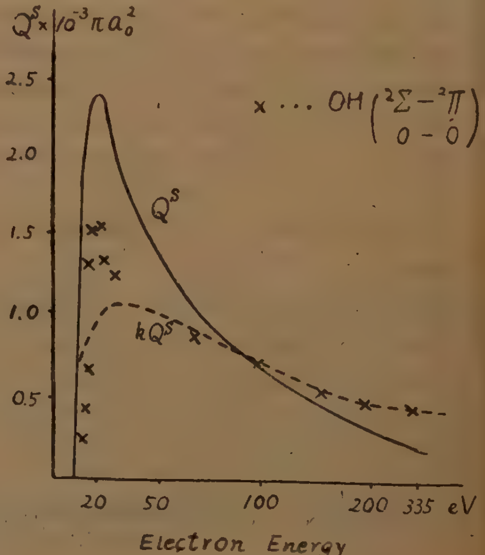

Fig. 1.

In the figure kQ^s is suitably adjusted so that agreement is obtained at 100 eV with experiment.

which ought to be compared and this varies inversely proportional to $\sqrt{E}$ at large E in accordance with observation.*

Since ${}^1A_1{}^*$ has the same type as the ground state (${}^1A_1$) and ${}^3B_1{}^*$ is a triplet one, both are forbidden to optical excitation. And besides both the above, there are many excited states arising from the ground electronic configurations of O atom and two H atoms, but all of them are not excited by direct collisions of electrons.

The author expresses his sincere thanks to Professor M. Kotani, Assistant Professor T. Horie, Mr. M. Ninoniya and Mr. H. Shōgenji for their valuable discussions and kind suggestions in the course of this work.

This work is indebted to the Ministry of Education for research grant.

---

* This remark owes to M. Watanabe, but we cannot ascertain experimental conditions in detail because of his death of Hayakawa.

References.

(1) K. F. Bonhoffer and T. G. Pearson: Zeits. f. phys. Chemie **14** (1931) 1.
I. O. Oldenberg: Phys. Rev. **46** (1934) 210.
E. R. Lyman: Phys. Rev. **53** (1938) 379.
H. Wakeshima: Proc. Phys.-Math. Soc. Japan **24** (1942) 367; J. Phys. Soc. Japan **2** (1947) 12.
T. Horie: J. Phys. Soc. Japan **1** (1946) 6.
For the general review, see T. Horie: Ōyō Butsuri **15** (1946) 26.
(2) M. Ninomiya: Unpublished.
(3) K. Niira: Busseiron Kenkyū **11** (1948) 1.
(4) T. Horie: Unpublished.
(5) T. Horie: in the paper prepared to the Memoir of Osaka University. This will serve to review our topics.
(6) G. Hayakawa: Private communication.
(7) D. R. Hartree and M. Black: Proc. Roy. Soc. **A 139** (1933) 311.
(8) G. Hayakawa: Proc. Phys.-Math. Soc. Japan **26** (1944) 78.

Notes on Statistical Thermodynamics of Solutions and Gaseous Mixtures I.

By Yosio MUTŌ.

Yokohama National University, Japan.

(Received Dec. 4, 1948.)

The method used by J. E. Mayer in the theory of condensation was extended by K. Fuchs, W. G. McMillan and J. E. Mayer to the case of a multi-component system. So there may be nothing essentially new to study in this field. But a special integral which is named semi-reducible integral in the paper seems to play some important rôle in the theory.

Facilities will be afforded by this conception especially when the fugacities or the chemical potentials of some of the components and the number densities of molecules of the remaining components are given. Therefore this is useful in treating some chemical equilibria. We may also consider a hypothetical system enclosed in a bag of semipermeable membrane so that the fugacities of the permeable components are given by the outer conditions only. In such a case we can define a thermodynamic function which corresponds to the osmotic pressure of a solution and becomes the partial pressure in the case of perfect gases.

As we assume that the chemical potentials of some of the components are given, some similarity exists between the case of such a gasseous mixture and a solution in which the chemical potential of the solvent is given. Therefore in part I of the paper we begin with the study of the latter in § 1 and define thermodynamically a function which might be called the relative free energy of the solute molecules in the solvent of given chemical potential. In § 2 this function is interpreted statistical mechanically.

In part II, which will be published a little later in this journal and contains § 3 and 4, we consider statistical mechanics of gaseous mixtures. In decomposing the cluster integrals we go step by step with respect to the kinds of molecules. Semi-reducible integrals appear in this stage. The final results are the same as obtained by K. Fuchs.

The components whose fugacities are given may be treated together as a continous medium in which move the molecules of the components whose densities are given. Therefore something which might be called the free energy of these molecules in such a medium is considered and this corresponds to the relative free energy mentioned above.

In part III relations to McMillan and Mayer's theory will be considered.

§ 1. Thermodynamic Introduction, the Theory of Solutions.

Let us consider at first a solution containing only one kind of solute molecules. The free energy of this solution of volume V in which N_0 solvent molecules and N_1 solute molecules are contained will be denoted by $F(T, V, N_0, N_1)$.

When N_1 varies, with the chemical potential of the solvent μ_0 fixed at a constant value, N_0 changes as a function of μ_0, T, V and N_1,

$$N_0 = \varphi(\mu_0, T, V, N_1). \qquad (1)$$

Hence free energy is also a function of μ_0, T, V and N_1.

In the following, as T nda μ_0 are assumed to be constant, we often drop these variables.

Now the pressure of the system P is given by

$$P = -\left(\frac{\partial F}{\partial V}\right)_{T, N_0, N_1}. \qquad (2)$$

This is a function of T, V, N_0 and N_1, that is, $P(T, V, N_0, N_1)$. Substituting (1) into this function we can express the pressure as a function of V and N_1 (μ_0 and T being constant)

Osmotic pressure of a solution is the pressure of the solution minus the pressure of the pure solvent at the same value of μ_0. In the following this will be denoted by $P^{\dagger}$, hence

$$P^{\dagger} = P\{T, V, \varphi(V, N_1), N_1\} - P\{T, V, \varphi(V, 0), 0\}$$
$$= P^{\dagger}(V, N_1). \qquad (3)$$

Then a function $F^{\dagger}(V, N_1)$ will be defined by

$$F^{\dagger}(V, N_1) = -\int_{V_0}^{V} P^{\dagger}(x, N_1)\,dx + \int_0^{N_1} \mu_1(V_0, n)\,dn, \qquad (4)$$

where $\mu_1(V, N_1)$ is the chemical potential of the solute,

$$\mu_1 = \left(\frac{\partial F}{\partial N_1}\right)_{T, V, N_0}, \qquad (5)$$

expressed as a function of μ_0, T, V and N_1 by (1).

Let us consider some properties of this function $F^{\dagger}$.

At first we obtain

$$\left(\frac{\partial F^{\dagger}}{\partial V}\right)_{N_1} = -P^{\dagger}(V, N_1). \qquad (6)$$

This relation corresponds to the one between free energy and pressure in a one-component system.

In order to examine the relation between the derivative $\partial F^{\dagger}/\partial N_1$ and μ_1, Eq. (3) will be substituted into (4), giving

$$F^{\dagger}(V, N_1) = \int_{V_0}^{V} [F_V\{x, \varphi(x, N_1), N_1\}$$
$$- F_V\{x, \varphi(x, 0), 0\}]\,dx + \int_0^{N_1} \mu_1(V_0, n)\,dn,$$

in which F_V denotes $\partial F/\partial V$ at constant T, N_0 and N_1. Then we get

$$\left(\frac{\partial F^{\dagger}}{\partial N_1}\right)_V = \int_{V_0}^{V} (F_{VN_0}\varphi_{N_1} + F_{VN_1})\,dx + \mu_1(V_0, N_1) \qquad (7)$$

in which partial derivatives are derived from F as a function of T, V, N_0 and N_1.

Now differentiating (5) partially with respect to V at constant μ_0, we get

$$\frac{\partial \mu_1(V, N_1)}{\partial V} = F_{N_1 V} + F_{N_1 N_0}\varphi_V = F_{VN_1} + F_{N_0 N_1}\varphi_V. \qquad (8)$$

On the other hand we get

$$F_{N_0 V} + F_{N_0 N_0}\varphi_V = 0$$

and

$$F_{N_0 N_1} + F_{N_0 N_0}\varphi_{N_1} = 0$$

by partially differentiating $\mu_0 = F_{N_0} =$ const with respect to V and N_1 respectively at constant μ_0 and T. We then obtain

$$F_{N_0 V}\varphi_{N_1} = F_{N_0 N_1}\varphi_V. \tag{9}$$

On account of Eq. (9), Eq. (8) becomes

$$\frac{\partial\mu_1(V,N_1)}{\partial V} = F_{VN_1} + F_{VN_0}\varphi_{N_1}$$

and the right-hand side is equal to the integrand of (7), hence

$$\left(\frac{\partial F^\dagger}{\partial N_1}\right)_V = \mu_1(V,N_1). \tag{10}$$

(6) and (10) express the meaning of the function $F^\dagger$, which might be called the relative free energy of the solute molecules in the medium of the solvent whose chemical potential is fixed at μ_0.

We can also define the same function by another formula,

$$F^\dagger(V,N_1) = F\{V,\varphi(V,N_1),N_1\} - \varphi(V,N_1)\mu_0$$

$$-F\{V,\varphi(V,0),0\} + \varphi(V,0)\mu_0 \tag{11}$$

$$= N_1\mu_1(V,N_1) - P^\dagger(V,N_1)V. \tag{11'}$$

(11′) is the result of substituting

$$F(T,V,N_0 . N_1) = N_0\mu_0 + N_1\mu_1 - PV$$

into (11). It would be quite easy to ascertain the agreement of (11) or (11′) and (4) by differentiating partially, for $F^\dagger$ vanishes with N_1/V.

In the preceding paragraphs we have considered some thermodynamic properties of the function $F^\dagger$ defined by (4). In the following sction we shall study further from the standpoint of statistical mechanics, and before doing so some relations between the potentials of average forces and $F^\dagger$ will be outlined.

It was shown by McMillan and Mayer(1) that the osmotic pressure $P^\dagger$ can be expressed as a power series in concentration $c = N_1/V$, hence according to (4) $F^\dagger$. too, except for the term $N_1 k \times T \log c$. But we shall consider from a little different point of view, although we are treating the same phenomena essentially.

For this purpose we shall take the following step.

A function $\phi^\dagger(\mu_0 . T)$ will be defined by the equation

$$\lim_{N_1\to 0}\frac{N_1}{V}\exp\frac{-\mu_1(V,N_1)}{kT} = \phi^\dagger. \tag{12}$$

This function may be interpreted as the usual partition function for one molecule without the V-factor, deformed by the presence of solvent molecules.

As we have for an infinitely diluted solution $P^\dagger V = N_1 kT$ evidently, we get from (11′) and (12)

$$F^\dagger(V,N_1) = N_1 kT(-1+\log c) - N_1 kT \log\phi^\dagger.$$

For a concentrated solution this does not hold. In this case the interactions between a solute mole- and the solvent will be influenced by other molecule cules in the neighborhood. Then the V-factor thatappear raised to the power N_1 in the expression of the relevant partition function $\exp(F^\dagger/kT)$ in the case of infinite dilution must be replaced by a sort of configuration integral.

In other words such influences or interactions will be represented by the so-called average forces that take place between the solute molecules distributed among the solvent molecules, whose momentary positions are not fixed but instead the chemical potential μ_0 or the fugacity z_0 (Reference (1), § 6).

So we consider the potentials of the average forces between N_1 solute molecules distributed in the solveut of volume V and fugacity z_0 (or chemical potential μ_0). Then a distribution function will be constructed and we can define the partition function $f_a{}^\dagger$ and the free energy $F_a{}^\dagger$ for the average forces by integrating the distribution function with respect to the coordinates of the N_1 molecules.

According to Mayer, Kahn and Uhlenbeck, or McMillan and Mayer, such functions are expressible as power series in concentration with the irreducible integrals $B^\dagger{}_k$ as coefficients:

$$f_a{}^\dagger = \frac{V^{N_1}}{N_1!}\exp(VG^\dagger), \tag{13}$$

$$F_a{}^\dagger = N_1 kT(-1+\log c) - VkTG^\dagger, \tag{14}$$

$$G^\dagger = \sum_{k\geq 2} B^\dagger{}_k c^k, \qquad c = N_1/V. \tag{15}$$

In the irreducible integral $B^\dagger{}_k$, the integrand is not only the sum of products of functions for the pairs generally. We shall discuss on this point a little more in detail in the next section.

Using this function $F_a{}^\dagger$, the free energy $F^\dagger$ will be expressed as

$$F^\dagger = F_a{}^\dagger - N_1 kT \log\phi^\dagger, \tag{16}$$

and the chemical potential μ_1 as

$$\mu_1 = \partial F_a{}^{\dagger}/\partial N_1 - kT\log\phi^{+}. \qquad (17)$$

A thermodynamic interpretation of this relation may be obtained by the following considerations.

Let us assume that there are two solutions each of which contains N_1 solute molecules. The one has the volume V and the other V_0. Then dN_1 solute molecules will be transferred from the latter to the former. We assume that the chemical potential of the solvent is kept constant and equal in both solutions, hence certain amount of solvent molecules must be transferred simultaneously. The increase in free energy in the system composed of both solutions will be the sum of two terms, the one is caused by the actions of solute molecules,

$$\left\{\frac{\partial F_a{}^{\dagger}}{\partial N_1} - \left(\frac{\partial F_a{}^{\dagger}}{\partial N_1}\right)_{V=V_0}\right\} dN_1,$$

the other by the transference of solvent molecules,

$$\left\{\frac{\partial \varphi}{\partial N_1} - \left(\frac{\partial \varphi}{\partial N_1}\right)_{V=V_0}\right\} \mu_0 dN_1.$$

On the other hand we can express this in terms of $F(T, V, N_0, N_1)$ as follows:

$$\left\{\frac{\partial F}{\partial N_1} + \frac{\partial F}{\partial N_0}\frac{\partial \varphi}{\partial N_1} - \left(\frac{\partial F}{\partial N_1} + \frac{\partial F}{\partial N_0}\frac{\partial \varphi}{\partial N_1}\right)_{V=V_0}\right\} dN_1.$$

Accordingly we obtain

$$\frac{\partial F_a{}^{\dagger}}{\partial N_1} - \left(\frac{\partial F_a{}^{\dagger}}{\partial N_1}\right)_{V=V_0} = \frac{\partial F}{\partial N_1} - \left(\frac{\partial F}{\partial N_1}\right)_{V=V_0}$$

because of $\partial F/\partial N_0 = \mu_0 = \text{const}$, and then

$$\mu_1 = \frac{\partial F}{\partial N_1} = \frac{\partial F_a{}^{\dagger}}{\partial N_1} + [*]$$

where $[*]$ is independent of N_1/V, depending only on μ_0 and T.

Substituting (14) and considering the case of infinite dilution, we get $[*] = -kT\log\phi^{\dagger}$, hence Eq. (17).

we get also from (16)

$$P^{\dagger} = -\partial F_a{}^{\dagger}/\partial V. \qquad (18)$$

§ 2. The Potentials of Average Forces and the Free Energy F^{+}.

Let us consider a little more in detail the course in deriving the equations (13), (14) and (15), although essentially these are already given by McMillan and Mayer.

The same symbols are used as in Mayer's and McMillan and Mayer's papers(1)(2)(3), and the distribution function $F_N(z_0, \{N\})$ is defined by the statement that in a solution of infinite extent the probability that N solute molecules be at $\{N\}$ in the element of configuration space $d\{N\}$ is proportional to $F_N(z_0, \{N\})\, d\{N\}$, the normalization condition being

$$\lim_{V\to\infty} \frac{1}{V^N}\int\!\!\int_V \cdots \int F_N(z_0, \{N\})\, d\{N\} = 1. \qquad (19)$$

The fugacity of the solvent is taken to be fixed at z_0.

The functions defined by

$$W_N(z_0, \{N\}) = -kT\log F_N(z_0, \{N\}) \qquad (20)$$

are called the potentials of the average forces between N solute molecules in an infinite system of solvent with the fugacity z_0. That this naming is adequate was explained by McMillan and Mayer (§ 6).

This function can be developed into the sum

$$W_N(z_0, \{N\}) = \Sigma_{\{n\}_N} w_n(z_0, \{n\}_N) \qquad (21)$$

of the component potentials w_n, for which the inverse relation

$$w_n(z_0, \{n\}) = \Sigma_{\{N\}_n} (-1)^{n-N}\, W_N(z_0, \{N\}_n) \qquad (21')$$

holds.

Therefore we can write

$$F_N(z_0, \{N\}) = \exp\left\{-\frac{W_N(z_0, \{N\})}{kT}\right\}$$

$$= \Pi_{\{n\}_N} \exp\left\{\frac{w_n(z_0, \{n\}_N)}{kT}\right\}, \qquad (22)$$

and if we define another set of functions by

$$f_n(z_0, \{n\}) = \exp\left\{-\frac{w_n(z_0, \{n\})}{kT}\right\} - 1 \qquad (23)$$

we get

$$F_N(z_0, \{N\}) = \Pi_{\{n\}_N}[1 + f_n(z_0, \{n\}_N)]. \qquad (24)$$

This formula gives the connection between f_n and $g_n(z_0, \{n\})$ defined by

$$F_n(z_0, \{N\}) = \Sigma_{\{k\{n_i\}_N\}_n} \prod_{i=1}^{k} g_{n_i}(z_0, \{n_i\}_N). \qquad (25)$$

which states that

$$g_n(z_0, \{n\}) = \Sigma_{\{\{\nu_i\}_n\}_n} \prod_i f_{\nu_i}(z_0, \{\nu_i\}_n). \qquad (26)$$

In the right-hand side the summation runs over all connected sets of the subsets $\{\nu_i\}_{l,n}$, and the products over all subsets i. This product corresponds to a cluster of connected molecules.

The cluster integral $b^{\dagger}_l(z_0)$ is defined by

$$b^{\dagger}_l(z_0)=\frac{1}{l!\,V}\iint_V\cdots\int g_l(z_0,\{l\})\,d\{l\}$$

$$=\frac{1}{l!\,V}\iint_V\cdots\int\Sigma_{\{\{n_i\}_l\}_c}\prod_i f_{n_i}(z_0,\{n_i\}_l)\,d\{l\},\qquad(27)$$

which is assumed to be independent of V in the present paper.

We can also define the irreducible integral $B^{\dagger}_l(z_0)$ by

$$B^{\dagger}_l(z_0)=\frac{1}{l!\,V}\iint_V\cdots\int\Sigma_{\{\{n_i\}_l\}_{ir}}$$
$$\prod_i f_{n_i}(z_0,\{n_i\}_l)\,d\{l\},\qquad(28)$$

where the summation runs over all such connected sets of the subsets $\{n_i\}_l$ that in the corresponding diagram all the molecules are more than singly connected. For example we have

$$B^{\dagger}_2(z_0)=\frac{1}{2V}\iint_V f_2(z_0,(i)(j))\,d(i)\,d(j),$$

$$B^{\dagger}_3(z_0)=\frac{1}{6\nu}\iiint_V[f_2(z_0,(i)(j))f_2(z_0,(i)(k))f_2(z_0,(j)(k))$$
$$+f_3(z_0,(i)(j)(k))\{1+f_2(z_0,(i)(j))+f_2(z_0,(i)(k))$$
$$+f_2(z_0,(j)(k))+f_2(z_0,(i)(j))f_2(z_0,(i)(k))$$
$$+f_2(z_0,(i)(j))f_2(z_0,(j)(k))+f_2(z_0,(i)(k))f_2(z_0.(j)(k))$$
$$+f_2(z_0,(i)(j))f_2(z_0,(i)(k))f_2(z_0,(j)(k))\}]$$
$$d(i)\,d(j)\,d(k).$$

It can be readily shown that the relations between $b^{\dagger}_l(z_0)$'s and $B^{\dagger}_k(z_0)$'s are just the same as those between b_l's and B_k's $(B_k=\beta_{k-1}/k)$:

$$b^{\dagger}_l(z_0)=\frac{1}{l^2}\sum\prod_{k\geq 2}\frac{\{lkB^{\dagger}_k(z_0)\}^{n_k}}{n_k!}\qquad(29)$$

$$\sum_{k\geq 2}(k-1)\,n_k=l-1.$$

Now from the meaning of $W_N(z_0,\{N\})$ we see that

$$\frac{\iint_V\cdots\int W_N(z_0,\{N\})F_N(z_0,\{N\})\,d\{N\}}{\iint_V\cdots\int F_N(z_0,\{N\})\,d\{N\}}=W^{\dagger}_N(z_0)\qquad(30)$$

represents the average of the potential of the average force or the average of the energy of interactions between N solute molecules distributed in the solvent of volume V with the fugacity z_0. Thus

$$\frac{1}{N!}\iint_V\cdots\int F_N(z_0,\{N\})\,d\{N\}=\Omega^{\dagger}(z_0,T,V,N)\qquad(31)$$

may be interpreted as the partition function for this potential. Evidently this can be expressed in terms of the cluster integrals as

$$\Omega^{\dagger}(z_0,T,V,N)=\sum_{m_l}\prod_l\frac{\{Vb^{\dagger}_l(z_0)\}^{m_l}}{m_l!}\qquad(32)$$

$$\sum_l lm_l=N.$$

From this relation (13), (14) and (15) will be soon derived because of $F_a^{\dagger}=-kT\log\Omega^{\dagger}$.

References.

(1) W. G. McMillan, J. E. Mayer: J. Chem. Phys. **13** (1945), 276.

(2) J. E. Mayer, E. Montroll: J. Chem. Phys. **9** (1941), 2.

(3) J. E. Mayer: J. Chem. Phys. **10** (1942), 629.

Notes on Statistical Thermodynamics of Solutions and Gaseous Mixtures II.

By Yosio Mutō.

(Received Dec. 4, 1948.)

In part I of the present paper⁽¹⁾ some properties of a solution were treated by considering a quantity called the relative free energy. In the present part a similar quantity is derived in the case of a gaseous mixture. At first a quanity called the semireducible integral is defined and its property is used to derive the relative free energy. With the use of this integral, any thermodynamic function can be expressed in terms of the fugacities of some of the components and the number densities of molecules of the remaining ones. Such functions are mainly power series not only in the number densities but also in the fugacities.

As, on the other hand, the relative free energy can be expressed in terms of the irreducible integrals concerning the potentials of the average forces, the relation between these irreducible integrals and semi-reducible integrals is obtained.

3. Semi-reducible Integrals in Multi-component Systems.

In the following it is assumed for the sake of simplicity that molecules have only Cartesian coordinates of the centers of mass and that the potential energy of the system may be written as the sum of the mutual potentials of the pairs. Rapid disappearance of these with the growing distance is also assumed.

Consider that there are σ types of molecules, $1, 2, \ldots, \sigma$. Positive integers p, r, and t take on the values with the limitations $1 \leqq r \leqq \sigma$, $1 \leqq p <$ or $\leqq r$, $r <$ or $\leqq t \leqq \sigma$.

The functions f_{ij} are defined as usual by

$$f_{ij} = \exp(-u_{ij}/kT) - 1, \tag{33}$$

u_{ij} being the potential energy of the pair i and j. Then the cluster integral b_l will be defined by

$$b_l = \frac{1}{l_1!\, l_2! \ldots l_\sigma!\, V} \iint_V \cdots \int \sum_{\text{cluster}} \Pi f_{ij}\, d\tau \tag{34}$$

where the integrand is the sum over all the products connecting l_1 molecules of type 1, l_2 of type 2, ..., l_σ of type σ. In the following such letters as l or k mean the sets of numbers as $l_1, \ldots, l_\sigma$ or $k_1, \ldots, k_\sigma$. $d\tau$ means the product of volume elements for the l molecules.

The irreducible integral B_k can be defined similarly. The integrand is the sum of all the products such that all the molecules are more than singly connected by f_{ij}. The relations between b_l and B_k were studied by K. Fuchs.

Besides these integrals we use in this paper some special integrals which we shall call semi-reducible integrals.

The r-semi-reducible integral $b_{(r)l}$ will be defined by

$$b_{(r)l} = \frac{1}{l_1! \ldots l_\sigma!\, V} \iint_V \cdots \int \sum^{(r)} \Pi f_{ij}\, d\tau \tag{35}$$

in which the integrand is the sum over all the products connecting $l_1, \ldots, l_\sigma$ molecules such that any of the corresponding diagrams can be dissociated into irreducible frames by removing some of the molecules of types $r, r+1, \ldots, \sigma$, any of the molecules of types $1, 2, \ldots, r-1$ neverbelonging to more than one frame. Such diagrams are called to be r-semi-reducibly connected.

We can find pretty simple relations between r-semi-reducible integrals and $r+1$-semi-reducible integrals.

As in dissociating an r-semi-reducible figure into its component $r+1$-semi-reducible figures only some suitable molecules of type r are necessary and sufficient to be removed, it is rather easy to ascertain that $b_{(r)l}$ is expressed as the sum of products of $b_{(r+1)k}$, each raised to the power n_k, where n_k satisfies the relations

$$\sum_k k_p n_k = l_p, \quad \sum_k k_t n_k = l_t, \quad \sum_k k_r n_k = l_r - 1, \tag{36}$$

with $p = 1, \ldots, r-1$ and $t = r+1, \ldots, \sigma$. This is only a slight generalization of the case of a one component system.

The coefficients are also easily found. As we must take into account the distribution into the $r+1$-semi-reducible figures of molecules other than those of the r'th kind too, we find as the final formula

$$l_r^2 b_{(r)\,l} = \sum_{n_k}{}_{(36)} \prod_{k} \frac{\{l_r k_r b_{(r+1)\,k}\}^{n_k}}{n_k!}. \tag{37}$$

Summation should be carried out with respect to n_k satisfying the relations (36).

The right-hand side of Eq. (37) can be expressed in the form of a complex integral

$$l_r^2 b_{(r)\,l} = \frac{1}{(2\pi i)^\sigma} \int\int \cdots \int \exp\Big[\sum_k l_r k_r b_{(r+1)\,k} \times \prod_{p=1}^{r-1} (\zeta_p)^{k_p} (\zeta_r)^{k_r-1} \prod_{t=r+1}^{\sigma} (\zeta_t)^{k_t}\Big]$$
$$\times \prod_{p=1}^{r-1} (\zeta_p)^{-l_p-1} (\zeta_r)^{-l_r} \prod_{t=r+1}^{\sigma} (\zeta_t)^{-l_t-1}\, d\zeta_1 \ldots d\zeta_\sigma. \tag{38}$$

Then we can state also that when z_r is a function of σ variables $\zeta_1, \ldots, \zeta_r, z_{r+1}, \ldots, z_\sigma$ such that

$$z_r = \zeta_r \exp \Big[-\sum_k k_r b_{(r+1)\,k} \prod_{p=1}^{r-1} (\zeta_p)^{k_p} (\zeta_r)^{k_r-1} \prod_{t=r+1}^{\sigma} (z_t)^{k_t}\Big], \tag{39}$$

the relations

$$\sum_l l_r^2 b_{(r)\,l} \prod_{p=1}^{r-1} (\zeta_p)^{l_p} (z_r)^{l_r} \prod_{t=r+1}^{\sigma} (z_t)^{l_t}$$
$$= \frac{\zeta_r}{1-\sum_k k_r(k_r-1) b_{(r+1)\,k} \prod_{p=1}^{r-1} (\zeta_p)^{k_p} (\zeta_r)^{k_r-1} \prod_{t=r+1}^{\sigma} (z_t)^{k_t}}, \tag{40}$$

$$\sum_l l_r b_{(r)\,l} \prod_{p=1}^{r-1} (\zeta_p)^{l_p} (z_r)^{l_r} \prod_{t=r+1}^{\sigma} (z_t)^{l_t} = \xi_r, \tag{41}$$

and

$$\sum_l b_{(r)\,l} \prod_{p=1}^{r-1} (\zeta_p)^{l_p} (z_r)^{l_r} \prod_{t=r+1}^{\sigma} (z_t)^{l_t}$$
$$= \zeta_r - \sum_k (k_r-1) b_{(r+1)\,k} \prod_{p=1}^{r-1} (\zeta_p)^{k_p} (\zeta_r)^{k_r} \prod_{t=r+1}^{\sigma} (z_t)^{k_t} \tag{42}$$

are simultaneously satisfied. (41) and (42) are obtained by multiplying the preceding equations by

$$\frac{dz_r}{z_r} = \Big[1-\sum_k k_r(k_r-1) b_{(r+1)\,k} \prod_{p=1}^{r-1} (\zeta_p)^{k_p} (\zeta_r)^{k_r-1} \prod_{t=r+1}^{\sigma} (z_t)^{k_t}\Big] \frac{d\zeta_r}{\zeta_r} \tag{43}$$

and integrating. (43) is the result of differentiating (39) with respect to ζ_r at constant $\zeta_1, \ldots, \zeta_{r-1}, z_{r+1}, \ldots, z_\sigma$.

Such rather complicated formulas can be expressed in far more simple form when we denote by $H_{(r)}(\zeta, z)$ the σ'ple power series in $\zeta_1, \ldots, \zeta_{r-1}, z_r, \ldots, z_\sigma$ with coefficients $b_{(r)\,l}$. We also denote the partial derivatives as follows:

$$\left.\begin{aligned} \partial H_{(r)}/\partial \zeta_p &= H_{(r),\,p} \\ \partial H_{(r)}/\partial z_t &= H_{(r),\,t} \end{aligned}\right\} \tag{44}$$

The relations (39), (41) and (42) become

$$z_r = \zeta_r \exp[-H_{(r+1),\,r}] \tag{45}$$

$$\zeta_r = z_r H_{(r),\,r} \tag{46}$$

$$H_{(r)} = H_{(r+1)} + \zeta_r - \zeta_r H_{(r+1),\,r}. \tag{47}$$

We can also derive more convenient formulas. For this purpose we first show that for any fixed number x the relation

$$H_{(r+1),\,r} = H_{(x+1),\,r} \tag{48}$$

holds with an arbitrary number r satisfying $x \geqq r$. (48) is proved when the equation

$$H_{(x+1),\,r} = H_{(x+2),\,r} \tag{49}$$

is proved to be valid.

Now let us write $x+1$ instead of r in Eq. (47) and then differentiate partially with respect to ζ_r at constant $\zeta_1, \ldots, \zeta_{r-1}, \zeta_{r+1}, \ldots, \zeta_x, z_{x+1}, \ldots, z_\sigma$. Then as on the right-hand side $H_{(x+2)}$ contains the variable ζ_{x+1} which can not remain constant but varies with ζ_r, we get

$$H_{(x+1),\,r} = H_{(x+2),\,r} - \zeta_{x+1} H_{(x+2),\,x+1,\,r}$$
$$+ \{1-\zeta_{x+1} H_{(x+2),\,x+1,\,x+1}\} \zeta_{x+1,\,r} \tag{50}$$

where $\zeta_{x+1,\,r}$ means the partial derivative of ζ_{x+1} with respect to ζ_r at constant $\zeta_1, \ldots, \zeta_{r-1}, \zeta_{r+1}, \ldots, \zeta_x, z_{x+1}, \ldots, z_\sigma$.

On the other hand we get

$$0 = \exp\{-H_{(x+2),\,x+1}\}$$
$$\times [\{1-\zeta_{x+1} H_{(x+2),\,x+1,\,x+1}\} \zeta_{x+1,\,r} - \zeta_{x+1} H_{(x+2),\,x+1,\,r}]$$

when we write $x+1$ instead of r in Eq. (45) and then differentiate partially with respect to ζ_r at constant $\zeta_1, \ldots, \zeta_{r-1}, \zeta_{r+1}, \ldots, \zeta_x, z_{x+1}, \ldots, z_\sigma$. Then we see that the second and the third member in the right-hand side of (50) cancel and we get (49) and (48).

We can also derive the relation

$$H_{(r),r} = H_{(1),r} \tag{51}$$

as follows. It is sufficient to prove the equation

$$H_{(p+1),r} = H_{(p),r} \tag{52}$$

for $p < r$.

Now from Eq. (47) we get

$$H_{(p+1)} = H_{(p)} - \varsigma_p \{1 - H_{(p+1),p}\},$$

and as $-H_{(p+1),p} = \log z_p - \log \varsigma_p$ according to (45), we can write

$$H_{(p+1)} = H_{(p)} - \varsigma_p (1 + \log z_p - \log \varsigma_p).$$

Differentiating this partially with respect to z_r at constant $\varsigma_1, \ldots\ldots \varsigma_p, z_{p+1}, \ldots z_{r-1}, z_{r+1}, \ldots\ldots, z_\sigma$, we get

$$H_{(p+1),r} = H_{(p),r} + \{H_{(p),p} - \varsigma_p/z_p\} \partial z_p/\partial z_r,$$

and as the second member on the right-hand side vanishes because of (46) we see that (52) is correct.

Because of these results which may be resumed as

$$\left.\begin{aligned} H_{(1),r} &= H_{(2),r} = \ldots\ldots = H_{(r),r} \\ H_{(r+1),r} &= H_{(r+2),r} = \ldots\ldots = H_{(\sigma+1),r} \end{aligned}\right\} \tag{53}$$

Eq. (45), (46) and (47) become

$$z_r = \varsigma_r \exp\{-H_{(x+1),r}\} \tag{54}$$

$$\varsigma_r = z_r H_{,r}, \tag{55}$$

$$H_{(r)} = H_{(r+1)} + \varsigma_r \{1 - H_{(x+1),r}\} \tag{56}$$

with $r \leqq x \leqq \sigma$. H is the power series in $z_1, \ldots\ldots, z_\sigma$ having the ordinary cluster integrals (34) as coefficients.

Especially when we put $x = \sigma$, $H_{(x+1)}$ becomes the power series in $\varsigma_1, \ldots\ldots, \varsigma_\sigma$, having the ordinary irreducible integrals B_k as coefficients. Thus we can write

$$\begin{aligned} H = H_{(1)} &= G(z, b) \\ &= \sum_l b_l (z_1)^{l_1} \ldots\ldots (z_\sigma)^{l_\sigma}, \end{aligned} \tag{57}$$

$$\begin{aligned} H_{(\sigma+1)} &= G(\varsigma, B) \\ &= \sum_k B_k (\varsigma_1)^{k_1} \ldots\ldots (\varsigma_\sigma)^{k_\sigma}. \end{aligned} \tag{58}$$

For the sake of simplicity we often use the letter G to express the function $G(\varsigma, B)$. (54) and (56) then become

$$z_r = \varsigma_r \exp(-G_{,r}) \tag{59}$$

and

$$H_{(r)} = H_{(r+1)} + \varsigma_r (1 - G_{,r}), \tag{60}$$

and from the latter we get

$$H = G + \sum_{r=1}^{\sigma} \varsigma_r (1 - G_{,r}). \tag{61}$$

The relations

$$H = H_{(r+1)} + \sum_{r=1}^{r} \varsigma_p (1 - G_{,p}) \tag{62}$$

$$= H_{(r+1)} + \sum_{p=1}^{r} \varsigma_p \{1 - H_{(r+1),p}\} \tag{62'}$$

also follows. Eq. (61) corresponds to Eq. (65) in McMillan and Mayer's paper.(2)

§ 4. Some Thermodynamic Functions of Gaseous Mixtures.

Let us derive some thermodynamic relations from the results given above.

For this purpose we must consider as usual the configurational partition function of $N_1 + \ldots\ldots + N_\sigma$ molecules in a volume V, which will be written as

$$\Omega(T, V, N) = \sum_{m_l}{}_{(64)} \prod_l \frac{(Vb_l)^{m_l}}{m_l!} \tag{63}$$

where the sum is taken over the sets of m_l satisfying

$$\sum_l l_r m_l = N_r \quad (r = 1, \ldots\ldots, \sigma). \tag{64}$$

N also means the set $N_1, \ldots\ldots, N_\sigma$.

The absolute activity of the r'th component will be denoted by λ_r, and the partition function of an isolated molecule of the r'th kind without the V-factor by ϕ_r. Then the fugacity will be given by

$$z_r = \lambda_r \phi_r \tag{65}$$

and the pressure by

$$P = kT \sum b_l (z_1)^{l_1} \ldots\ldots (z_\sigma)^{l_\sigma} \tag{66}$$

$$= kTH(z, b). \tag{66'}$$

For the system where the fugacity set, the absolute activity set or the chemical potential set is given, the average number of molecules of type r is determined by

$$N_r = \frac{\partial \log \Xi}{\partial \log \lambda_r} = \frac{\partial VH(z, b)}{\partial \log z_r}$$

where Ξ is the grand partition function. Accordingly the number density ρ_r satisfies the relation

$$\rho_r = \frac{N_r}{V} = \frac{\partial H(z, b)}{\partial \log z_r} = z_r H,_r \tag{67}$$

which is the same as (55).

Then on account of (61) and (66′) pressure will be expressed as a power series in ρ_r

$$P = kT\left\{G(\rho, B) + \sum_r \rho_r(1 - G,_r)\right\}, \tag{68}$$

and the free energy as

$$\begin{aligned} F &= \sum_r N_r \mu_r - PV \\ &= -\sum_r N_r kT(1 - \log \rho_r + \log \phi_r) - VkTG(\rho, B). \end{aligned} \tag{69}$$

The latter can be also expressed in terms of fugacities as

$$F = VkT\sum_r z_r H,_r(\log z_r - \log \phi_r) - VkTH. \tag{70}$$

These expressions are useful when the densities of all the components or else the fugacities of all the components are given. But it will sometimes occur that the fugacities of some of the components and the densities of the remaining components are given. Suppose that the latter were named 1, 2, $\ldots$, r and the former $r+1, \ldots, \sigma$. Then the free energy must be a function of $\rho_1, \ldots, \rho_r, z_{r+1}, \ldots, z_\sigma$. This will be obtained by substituting the relations such as (54), (55), (62) and (53) into (70) with the result

$$\begin{aligned} F = &-\sum_{p=1}^{r} N_p kT(1 - \log \rho_p + \log \phi_p) \\ &+ VkT \sum_{t=r+1}^{\sigma} z_t H_{(r+1),t}(\log z_t - \log \phi_t) \\ &- VkTH_{(r+1)}. \end{aligned} \tag{71}$$

Correspondingly pressure is given by

$$P = kT\left\{H_{(r+1)} + \sum_{p=1}^{r} \rho_p(1 - H_{(r+1),p})\right\}. \tag{72}$$

Now we have defined the relative free energy $F^\dagger$ for the solute in a solution. This conception can be extended to the present case if we treat the components 1, 2, $\ldots$, r as solutes and the other ones as solvents. Thus we get

$$\begin{aligned} &F^\dagger(z_{r+1}, \ldots, z_\sigma, T, V, N_1, \ldots, N_r) \\ &= F(T, V, N_1, \ldots, N_r, z_{r+1}, \ldots, z_\sigma) - \sum_{t=r+1}^{\sigma} N_t \mu_t \\ &\quad - F(T, V, 0, \ldots, 0, z_{r+1}, \ldots, z_\sigma) + \sum_{t=r+1}^{\sigma} (N_t)_0 \mu_t \end{aligned} \tag{73}$$

where N_t is the average number of molecules of type t at given $N_1, \ldots, N_r, z_{r+1}, \ldots, z_\sigma$ and $(N_t)_0$ at $N_1 = \ldots = N_r = 0$ with the same values of $z_{r+1}, \ldots, z_\sigma$.

Because of (71) and

$$Vz_t H_{(r+1),t} = N_t, \quad \log z_t - \log \phi_t = \mu_t/kT$$

we soon obtain

$$\begin{aligned} &F^\dagger(z_{r+1}, \ldots, z_\sigma, T, V, N_1, \ldots, N_r) \\ &= -\sum_{p=1}^{r} N_p kT(1 - \log \rho_p + \log \phi_p) \\ &\quad - VkT\{H_{(r+1)} - (H_{(r+1)})_0\}. \end{aligned} \tag{73′}$$

For the pressure we get

$$\begin{aligned} -\frac{\partial F^\dagger}{\partial V} &= P(T, V, N_1, \ldots, N_r, z_{r+1}, \ldots, z_\sigma) \\ &\quad - P(T, V, 0, \ldots, 0, z_{r+1}, \ldots, z_\sigma) \\ &= P^\dagger(z_{r+1}, \ldots, z_\sigma, T, V, N_1, \ldots, N_r). \end{aligned} \tag{74}$$

Another equation

$$\partial F^\dagger/\partial N_p = \mu_p \tag{75}$$

also follows. $P^\dagger$ is something resembling the osmotic pressure of solutions.

Now we can write (73′) in the form

$$\begin{aligned} &F^\dagger(z_{r+1}, \ldots, z_\sigma, T, V, N_1, \ldots, N_r) \\ &= -\sum_{p=1}^{r} N_p kT(1 - \log \rho_p + \log \phi^\dagger_p) \\ &\quad - VkT\left[H_{(r+1)} - \{H_{(r+1)}\}_0 - \sum_{p=1}^{r} \rho_p \log \phi^\dagger_p/\phi_p\right], \end{aligned} \tag{73′′}$$

and put

$$\begin{aligned} &H_{(r+1)} - \{H_{(r+1)}\}_0 - \sum_{p=1}^{r} \rho_p \log \phi^\dagger_p/\phi_p \\ &= \sum\nolimits_{k_1, \ldots, k_r} B^\dagger_{k_1 \ldots k_r}(z_{r+1}, \ldots, z_\sigma)(\rho_1)^{k_1} \ldots (\rho_r)^{k_r} \end{aligned} \tag{76}$$

$$= G(\rho_1, \ldots, \rho_r; B^\dagger(z_{r+1}, \ldots, z_\sigma)). \tag{77}$$

Comparing Eq. (73) with (14) and (16)[1] we can see that the coefficients in (77) may be interpreted as the irreducible integrals for the molecules of types 1, $\ldots$, r in the medium of other types of molecules at the given values of $z_{r+1}, \ldots, z_\sigma$. (Cf. the next section). Their relation to the semi-reducible integrals is evidently

$$\begin{aligned} &B^\dagger_{k_1 \ldots k_r}(z_{t+1}, \ldots, z_\sigma) \\ &\quad \sum\nolimits_{k_{r+1}, \ldots, k_\sigma} b_{(r+1)k_* \ldots k_\sigma}(z_{r+1})^{k_{r+1}} \ldots (z_\sigma)^{k_\sigma} \end{aligned} \tag{78}$$

with the exception of $B^\dagger_{00\cdots0}(z_{r+1},\ldots,z_\sigma)=0$ and

$$B^\dagger_{10\cdots0}(z_{r+1},\ldots,z_\sigma) = B^\dagger_{01\cdots0}(z_{r+1},\ldots,z_\sigma)=\cdots=0.$$

From the last equations we get the relations necessarily fulfilled by $\phi^\dagger_p$:

$$\log\frac{\phi^\dagger_1}{\phi_1} = \sum_{k_{r+1},\ldots,k_\sigma} b_{(r+1)10\cdots0k_{r+1}\cdots k_\sigma}(z_{r+1})^{k_{r+1}}\cdots(z_\sigma)^{k_\sigma},$$

$$\cdots\qquad\cdots\qquad\cdots$$

$$\log\frac{\phi^\dagger_r}{\phi_r} = \sum_{k_{r+1},\ldots,k_\sigma} b_{(r+1)00\cdots1k_{r+1}\cdots k_\sigma}(z_{r+1})^{k_{r+1}}\cdots(z_\sigma)^{k_\sigma}.$$

References.

(1) Y. Mutō: J. Phys. Soc. Jap. **4** (1949), 233.

(2) W. G. McMillan, J. E. Mayer: J. Chem. Phys. **13** (1945), 276.

Notes on Statistical Thermodynamics of Solutions and Gaseous Mixtures III.

By Yosio Mutō.

(Received Dec. 4, 1948)

In part I of the present paper⁽¹⁾ some properties of a solution were treated by considering a quantity called the relative free energy. A relation to the potentials of the average forces was also considered. In part II⁽²⁾ a gaseous mixture was studied after introducing the conception of semi-reducible integrals. Then the relative free energy for any arbitrary part of the components was expressed in terms of these integrals.

Now we are going to examine some relations between the present theory and McMillan and Mayer's one. For this purpose we begin with a modification of the grand partition function. In the last sections relations between cluster integrals for the potentials of average forces and semi-reducible integrals are obtained.

§ 5. A Modification Grand Partition Function.

Suppose that there are a large number M of compartments each of volume V. Molecules of types from $r+1$ to σ are able to pass through the boundaries between these compartments each of which contains $N_1,\cdots,N_r$ molecules of the remaining components. Total number of molecules of any type is given as well as the total energy.

The number of quantum states of a system of volume V and numbers of molecules $N_1,\cdots,N_r,N_{r+1},\cdots,N_\sigma$, having the energy value E_l, will be denoted by ω.

Then for the whole system the total number of possible states in which m of the compartments are in some of the quantum states mentioned above is denoted by $\Omega(m)$. The maximum of this quantity or the corresponding value of entropy $S(m)=k\log\Omega(m)$ will be gained when m satisfies the relation

$$\frac{m}{M\omega}=\exp\left\{\left(-PV+\sum_{x=1}^{\sigma}N_x\mu_x-E_l\right)/kT\right\}.$$

This formula is obtained by a quite similar argument as was carried by McMillan and Mayer. Difference lies in the fact that in the present case the set $N_1,\cdots,N_r$ and $\mu_{r+1},\cdots,\mu_\sigma$ is fixed instead of the set $\mu_1,\cdots,\mu_\sigma$. Indeed this is the probability for finding just N_{r+1} molecules of type $r+1,\cdots,N_\sigma$ of type σ in a box of volume V in which N_1 molecules of type $1,\cdots,N_r$ of type r are confined, with the condition that the quantum state for all of these molecules together belong to the level E_l. This will be denoted by

$\mathfrak{P}(l,N_{r+1},\cdots,N_\sigma;V,N_1,\cdots,N_r)$, hence

$$\mathfrak{P}(l, N_{r+1}, \cdots, N_\sigma;\ V, N_1, \cdots, N_r)$$
$$= \exp\left\{\left(-PV + \sum_{p=1}^{r} N_p\mu_p + \sum_{t=r+1}^{\sigma} N_t\mu_t - E_l\right)\Big/kT\right\}. \tag{79}$$

This quantity $\mathfrak{P}$ must evidently satisfy the relation

$$\Sigma_{N_{r+1}, \cdots, N_\sigma} \sum_l \mathfrak{P}(l, N_{r+1}, \cdots, N_\sigma;\ V, N_1, \cdots, N_r) = 1$$

and as

$$\sum_l \exp(-E_l/kT) = Q(T, V, N_1, \cdots, N_\sigma)$$

is the partition function, we get

$$\exp(-PV/kT)\exp\left(\sum_{p=1}^{r} N_p\mu_p/kT\right)$$
$$\times \Sigma_{N_{r+1}, \cdots, N_\sigma} \exp\left(\sum_{t=r+1}^{\sigma} N_t\mu_t/kT\right)$$
$$\times Q(T, V, N_1, \cdots, N_\sigma) = 1. \tag{80}$$

In fact μ_p depends upon $N_{r+1}, \cdots, N_\sigma$, for the given quantities are $N_1, \cdots, N_r$ and $\mu_{r+1}, \cdots, \mu_\sigma$. But as the change in $\exp(N_p\mu_p/kT)$ is small compared with that in $\exp(N_t\mu_t/kT)$ for a given change in $N_{r+1}, \cdots, N_\sigma$, we can put the factor $\exp(\Sigma N_p\mu_p/kT)$ before the summation symbol.*

If absolute activity is used (80) may be written as

$$\Sigma_{n_{r+1}, \cdots, n_\sigma} (\lambda_{r+1})^{n_{r+1}} \cdots (\lambda_\sigma)^{n_\sigma}$$
$$\times Q(T, V, N_1, \cdots, N_r, n_{r+1}, \cdots, n_\sigma)$$
$$= \exp\left\{\left(PV - \sum_{p=1}^{r} N_p\mu_p\right)/kT\right\}. \tag{81}$$

Now McMillan and Mayer proved the equation

$$\left\{\frac{\rho(z)}{z}\right\}^N F_N(z, \{N\}) = \exp\left\{-\frac{VP(z)}{kT}\right\}$$
$$\times \sum_n \frac{z^n}{n!} \int\!\!\int_V \cdots \int F_{N+n}(0, \{N+n\})\, d\{n\}, \tag{82}$$

where we use the abbreviations

z for $z_1, \cdots, z_\sigma$

$\left\{\frac{\rho(z)}{z}\right\}^N$ for $\left\{\frac{\rho_1(z)}{z_1}\right\}^{N_1} \cdots \left\{\frac{\rho_\sigma(z)}{z_\sigma}\right\}^{N_\sigma}$

$\frac{z^n}{n!}$ for $\frac{(z_1)^{n_1}}{n_1!} \cdots \frac{(z_\sigma)^{n_\sigma}}{n_\sigma!}$.

Then let us consider the special case where $z_1 = \cdots = z_r = 0$ and $N_{r+1} = \cdots = N_\sigma = 0$. We get

$$\left\{\frac{\rho(z)}{z}\right\}^N = \prod_{p=1}^{r} \left(\frac{\phi^\dagger_p}{\phi_p}\right)^{N_p}, \tag{83}$$

where $\phi^\dagger_p$ is defined by

$$\lim_{N_1, \cdots, N_r \to 0} \frac{N_p}{V} \exp\frac{-\mu_p}{kT} = \phi^\dagger_p \tag{84}$$

in which the set $\mu_{r+1}, \cdots, \mu_\sigma$ is kept constant. This equation corresponds to Eq. (12).(1)

The integral

$$\frac{1}{N_1! \cdots N_r!} \int\!\!\int_V \cdots \int F_N(z, \{N\})\, d\{N\}$$
$$= \Omega^\dagger(z, T, V, N_1, \cdots, N_r) \tag{85}$$

can be interpreted as the configurational partition function or the partition function for the average forces of the molecules of types $1, \cdots, r$ distributed among the molecules of types $r+1, \cdots, \sigma$ at the given fugacity set $z_{r+1}, \cdots, z_\sigma$. Thus integrating (82) we get

$$\prod_{p=1}^{r} \left(\frac{\phi^\dagger_p}{\phi_p}\right)^{N_p} \Omega^\dagger(z, T, V, N_1, \cdots, N_r)$$
$$= \exp\left\{\frac{-VP(z)}{kT}\right\} \Sigma_{n_{r+1}, \cdots, n_\sigma} \prod_{t=r+1}^{\sigma} (z_t)^{n_t}$$
$$\times \Omega(T, V, N_1, \cdots, N_r, n_{r+1}, \cdots, n_\sigma), \tag{86}$$

in which z means the set $z_{r+1}, \cdots, z_\sigma$ only and

$$\frac{1}{N_1! \cdots N_\sigma!} \int\!\!\int_V \cdots \int F_N(0, \{N\})\, d\{N\}$$
$$= \Omega(T, V, N_1, \cdots, N_\sigma)$$

for the general set $N_1, \cdots, N_\sigma$.

Multiplying both sides of (86) by the factor

$$\prod_{p=1}^{r} (\phi_p)^{N_p}$$

and remembering the relation between the ordinary partition function $Q(T, V, N_1, \cdots, N_r, n_{r+1}, \cdots, n_\sigma)$ and the ordinary configurational partition function $\Omega(T, V, N_1, \cdots, N_r, n_{r+1}, \cdots, n_\sigma)$,

$$\Omega(T, V, N_1, \cdots, N_r, n_{r+1}, \cdots, n_\sigma)(\phi_1)^{N_1} \cdots (\phi_\sigma)^{n_\sigma}$$
$$= Q(T, V, N_1, \cdots, N_r\, n,_{r+1}, \cdots, n_\sigma),$$

---

* Such a treatment is not allowed when phase change occurs.

and also the relation

$$z_\iota = \lambda_\iota \phi_\iota ,$$

we get

$$\Omega^\dagger(z, T, V, N_1, \cdots\cdots, N_r) \prod_{p=1}^{r} (\phi^\dagger{}_p)^{N_p}$$

$$= \exp \frac{-VP(z)}{kT} \Sigma_{n_{r+1}, \cdots, n_\sigma} (\lambda_{r+1})^{n_{r+1}} \cdots (\lambda_\sigma)^{n_\sigma}$$

$$\times Q(T, V, N_1, \cdots\cdots, N_r, n_{r+1}, \cdots\cdots, n_\sigma).$$

Substituting Eq. (81) into the right-hand side we obtain at last

$$\Omega^\dagger(z, T, V, N_1, \cdots\cdots, N_r) \prod_{p=1}^{r} (\phi^\dagger{}_p)^{N_p}$$

$$= \exp\left\{ \left(P^\dagger V - \sum_{p=1}^{r} N_p \mu_p \right) \Big/ kT \right\}, \tag{87}$$

for $P(z)$ means the pressure when molecules of types $1, \cdots\cdots, r$ are not contained in the system corresponding to $z_1 = \cdots\cdots = z_r = 0$.

If we put

$$F^\dagger = -kT \log \Omega^\dagger - \sum_{p=1}^{r} N_p kT \log \phi^\dagger{}_p \tag{88}$$

we get

$$F^\dagger = -P^\dagger V + \sum_{p=1}^{r} N_p \mu_p$$

and regain the Eq. (73)⁽²⁾.

§ 6. Relations between cluster integrals and semi-reducible integrals.

As it was explained in § 2⁽¹⁾, we can express $\Omega^\dagger$ or $F^\dagger$ in terms of cluster or irreducible integrals containing the fugacity set $z_{r+1}, \cdots\cdots, z_\sigma$ as parameters. Of course extension of the method to the multicomponent system is necessary. Thus an irreducible integral $B^\dagger{}_l(z)$ will be defined by

$$B^\dagger{}_l(z) = \frac{1}{l!\,V} \iint_V \cdots\cdots \int \Sigma_{\{\{n_i\}_l\}_{ir}}$$

$$\prod_i f_{n_i}(z, \{n_i\}_l) d\{l\} \tag{90}$$

and a cluster integral by

$$b^\dagger{}_l(z) = \frac{1}{l!\,V} \iint_V \cdots\cdots \int \Sigma_{\{\{n_i\}_l\}_c}$$

$$\prod_i f_{n_i}(z, \{n_i\}_l) d\{l\}, \tag{91}$$

where we use the abbreviations

l for $l_1, \cdots\cdots, l_r$

z for $z_{r+1}, \cdots\cdots, z_\sigma$

n for $n_1, \cdots\cdots, n_r$

$l!$ for $l_1! \cdots\cdots l_r!$.

Moreover for the sake of brevity we must use the quantity

$$z^\dagger{}_p = z_p \phi^\dagger{}_p / \phi_p$$

and a function $H^\dagger$ which is the power series in $z^\dagger{}_p$ with the cluster integrals $b^\dagger{}_l(z)$ as coefficients.

Then $F^\dagger$ is expressed as

$$F^\dagger = VkT \sum_{p=1}^{r} z^\dagger{}_p H^\dagger{}_{,p} (\log z^\dagger{}_p - \log \phi^\dagger{}_p) - VkTH^\dagger \tag{92}$$

$$= -\sum_{p=1}^{r} N_p kT (1 - \log \rho_p + \log \phi_p) - VkTG^\dagger(\rho, B^\dagger). \tag{93}$$

On the other hand we have got (73′)⁽²⁾. Therefore we know that $B^\dagger{}_l$ defined by (76) or (78)⁽²⁾ is the same as (90).

A similar relation between $b^\dagger{}_l(z)$ and the cluster integrals defined by (34)⁽²⁾ is obtained by comparing the expressions for the pressure $P^\dagger$. We get at first from (66)⁽²⁾

$$P^\dagger = kT \Big\{ \sum_l b_{l_1 \cdots l_\sigma} (z_1)^{l_1} \cdots\cdots (z_\sigma)^{l_\sigma}$$

$$- \Sigma_{l_{r+1}, \cdots, l_\sigma} b_{0 \cdots 0\, l_{r+1} \cdots l_\sigma} (z_{r+1})^{l_{r+1}} \cdots\cdots (z_\sigma)^{l_\sigma} \Big\} \tag{94}$$

On the other hand when we use the cluster integrals (91) defined from the distribution functions $F(z_{r+1}, \cdots\cdots, z_\sigma, \{N_1, \cdots\cdots, N_r\})$, we get

$$P^\dagger = kT \sum b^\dagger{}_{l_1 \cdots l_r} (z_{r+1}, \cdots\cdots, z_\sigma) (z^\dagger{}_1)^{l_1} \cdots\cdots (z^\dagger{}_r)^{l_r}. \tag{95}$$

Thus we can derive the relation

$$b^\dagger{}_{l_1 \cdots l_r} (z_{r+1}, \cdots\cdots, z_\sigma) \left(\frac{\phi^\dagger{}_1}{\phi_1} \right)^{l_1} \cdots\cdots \left(\frac{\phi^\dagger{}_r}{\phi_r} \right)^{l_r}$$

$$= \Sigma_{l_{r+1}, \cdots, l_\sigma} b_{l_1 \cdots l_\sigma} (z_{r+1})^{l_{r+1}} \cdots\cdots (z_\sigma)^{l_\sigma}, \tag{96}$$

with the exception of $b^\dagger{}_{00 \cdots 0} = 0$.

The expression of $\phi^\dagger{}_p$ was given in the last paragraph of § 4⁽²⁾ which may be resumed as

$$\log \frac{\phi^\dagger{}_p}{\phi_p} = \Sigma_{k_{r+1}, \cdots, k_\sigma} b_{(r+1)[p] k_{r+1} \cdots k_\sigma} (z_{r+1})^{k_{r+1}}$$

$$\cdots\cdots (z_\sigma)^{k_\sigma}, \tag{97}$$

where $[p]$ means the set $k_1, \cdots, k_r$ with $k_1 = \cdots = k_{p-1} = k_{p+1} = \cdots = k_r = 0$, $k_p = 1$. But this can also be obtained from (96), for $b^{\dagger}{}_l(z)$ must be unity when one of the numbers $l_1, \cdots, l_r$ is equal to one and others zero. Thus

$$\frac{\phi^{+}{}_p}{\phi_p} = \sum_{l_{r+1},\cdots,l_\sigma} b_{[p]l_{r+1}\cdots l_\sigma}(z_{r+1})^{l_{r+1}}\cdots(z_\sigma)^{l_\sigma} \tag{98}$$

Substituting (98) into (96) $b^{\dagger}{}_l(z)$ will be completely expressed in terms of $b_{l_1\cdots l_\sigma}$ and ${}_{r+1}z, \cdots, z_\sigma$.

We get also the relation

$$\sum_{l_{r+1},\cdots,l_\sigma} b_{[p]l_{r+1}\cdots l_\sigma}(z_{r+1})^{l_{r+1}}\cdots(z_\sigma)^{l_\sigma}$$

$$= \exp\Big[\sum_{k_{r+1},\cdots,k_\sigma} b_{(r+1)[p]k_{r+1}\cdots k_\sigma}(z_{r+1})^{k_{r+1}}\cdots (z_\sigma)^{k_\sigma}\Big]. \tag{99}$$

But we can prove this directly from the nature of the semi-reducible integrals.

References.

(1) Y. Mutō: J. Phys. Soc. Jap. **4** (1949), 233.
(2) Y. Mutō: J. Phys. Soc. Jap. **4** (1949), 238.
(3) W. G. McMillan, J. E. Mayer: J. Chem. Phys. **13** (1945), 276.
(4) J. E. Mayer, E. Montroll: J. Chem. Phys. **9** (1941), 2.
(5) J. E. Mayer: J. Chem. Phys. **10** (1942), 629.

A Mathematical Analysis of the C. M. Witcher's Beta-Ray Spectrometer of a Type Using Helical Orbit.

By Yujiro Koh.

Department of Physics, Faculty of Science, Osaka University.

(Received Dec. 20, 1948.)

In 1941, C. M. Witcher⑴ has constructed a beta-ray spectrometer of an electron lens type, which utilized the uniform magnetic field by a long Hermholtz's solenoid and its focussing action for charged particles moving with helical orbits. He pointed out the advantages of such a type compared with the conventional type as follows: 1) The relatively higher efficiency, or the solid angle at the source to be utilized without sacrifice of resolving power*. 2) Source material can be distributed over the surface of much larger area. It is thus possible for this type to furnish data on materials whose activity cannot be concentrated sufficiently for use in the usual type. 3) The source can be located relatively far from any scattering material except that of the source holder itself. 4) The relatively large distance between source and detector, together with the large amount of absorbing material interposed by a central baffle system, would practically eliminate background by gamma-ray.

But a marked defect of this type of spectrometer is that positron and electron could not be resolved without a particular device for the baffle system⑶. The author thinks, however, the fact that the structure of this type is much more simple and symmetrical than the others and the field by the long solenoid is made easily as uniform as desired enables us to add another advantage: 5) It is easy to calculate mathematically the optimum geometrical condition for the source, baffle and detector system in order to obtain the largest luminosity and resolving power. And, furtheremore even the calculation of a form of the luminosity

---

* Recently, S. Frankel⑵ has called our attention to the fact that this type should be more appreciated owing to the advantage of both the remarkably larger solid angle and resolving power.

vs. particle's momentum curve (the transmission factor) will be expected to be not impossible.

Under such presumptions the author intended to construct an instrument of this type, but recently it was determined to give up this plan for an unavoidable reason. Thus, only several results of the calculation in the course of design of the spectrometer will be represented here.

General Consideration.

As well known, a particle of charge e projected into a uniform magnetic field H, with a momentum p in a direction making an angle α to H, has the path whose form is the circular helix of radius

$$(p/He)\sin\alpha \qquad (1)$$

and pitch

$$(2\pi p/He)\cos\alpha. \qquad (2)$$

It z denotes the displacement of particle from the initial position in the direction of H and σ its displacement perpendicular to H,

$$\sigma = D\sin\alpha\sin(z/D\cos\alpha), \qquad (3)$$

introducing a parameter $D = 2p/He$ which is equal to the diameter of the circular path of particle when projected perpendicularly to H. Apparently the form of path is dependent upon the values of p and H, but the variation of path with p and H is included in its variation with D. So we can replace the variation of p and H simply by the variation of a parameter D.

As α increases from 0 to $\pi/2$, the value of σ on a plane $z = z_0$ and for a particle of constant $D = D_0$ starts from 0 and oscillates. The zeros of $|\sigma|$ are at α_n, for which

$$Z_0/(D_0\cos\alpha_n) = n\pi,\ O < \alpha_n < \pi/2,$$

$$n = n_0,\quad n_0+1,\quad n_0+2,\quad n_0+3, \ldots \text{and}$$

$$n_0 = \lim_{\alpha\to 0}\left(\begin{array}{c}\text{The number of rotations before the}\\ \text{particle arrives at the plane } z = z_0.\end{array}\right)$$

From (3) it can be seen that σ is able to be either positive or negative, which means physically no more than that the number of above-mentioned rotations is odd or even.

The Optimum Geometrical Condition for Baffle System.

Apertures in baffles are, of course, assumed to be of a ring shape for brevity and arranged such that they have a axis of rotational symmetry. In order to obtain the optimum condition, it will be enough for us to investigate only the case when a point source exists on the axis of symmetry, because position and shape of source will vary on each meassurement and they could be treated as small corrections. The luminosity is given as the solid angle divided by 4π, subtended at a source point by the detector's window without being prevented by intermediate baffles in the case of given D, and depends, therefore, upon the position $z = l_i$ of each baffle and the outer and inner radii R_i, r_i of annular aperture in each baffle. We must decide all of l_i, R_i and r_i, such that the form of the luminosity *vs.* D curve becomes as high and sharp as possible in the given maximum point D_m of that curve.

The Witcher's condition may be ranked as a first approximation, in which only the dependency upon the outer radius R_d and the position l_d of detector's window is considered. He makes R_d equal to $|\sigma_{ext}|$, one of the extremum values of the curve (3) for given l_d and D_m, and inner radius r_d equal to $|\sigma_{ext}|-d\sigma$.* Other intermediate baffles are arranged such that the solid angle for D_m subtended by the detector's window

$$2\pi(\sin\alpha)_{\sigma_{ext}}\left\{\left|\frac{d\alpha}{d\sigma}\right|_{\sigma_{ext}-0}\times d\sigma+\left|\frac{d\alpha}{d\sigma}\right|_{\sigma_{ext}+0}\times d\sigma\right\}$$

is not shaded and decreased by them. As $\lim\limits_{\sigma\to\sigma_{ext}}|d\alpha/d\sigma| = +\infty$, the solid angle determined in such a manner becomes extremely larger than the one determined otherwise, even in the case of small $d\sigma$ for the attainment of large resolving power.

One can see, however, by taking into account of the simultaneous variation of more parameters l_i R_i and r_i, it may be possible to obtain a better condition as a stage of next approximation. In order to consider a number of parameters at the same time, it is convenient to use a graphical method as follows.

---

* In the Witcher's condition, consequently, the detector's window must be of a annular shape, not of a circular shape, in order to obtain the large resolving power.

Introducing

$$D\cdot\sin\alpha = s \quad D\cdot\cos\alpha = c, \tag{4}$$

then

$$s^2+c^2 = D^2 \tag{5}$$

and, from (3), for s and c which give a special value to $|\sigma|$ at z

$$s = |\sigma|/\sin(z/c) \tag{6}$$

The projection angle α_i, with which a particle of given D arrives at $|\sigma| = R_i$ (or r_i) on the plane $z = l_i$, is obtained from cross points (s', c') of curve (5) and (6) as shown in Fig. 1. The curve of (6) has many branches, corresponding to the number of rotations before arrival at $z = l_i$. And as each branch has generally two cross points with circle (5), there are two α_i. The larger is the projection angle in the case when $|\sigma|$ decreases as α increases, and the smaller is it in the inverse case.

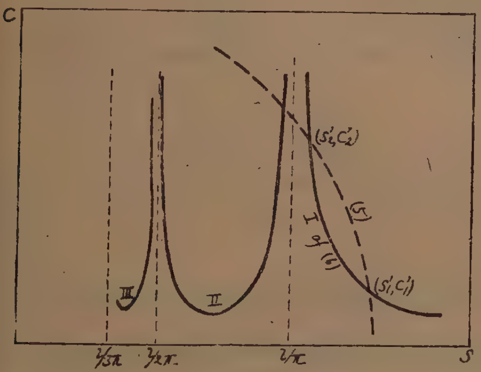

Fig. 1.

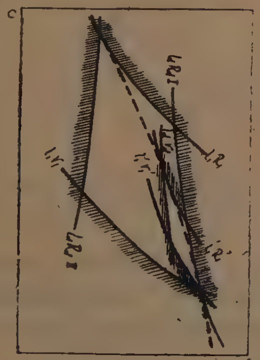

Fig. 2. (*i*) when the detector's window is a circle; $l_1R_1r_1$ l_dR_d, (*ii*) when it is an annular ring. $l_1'R_1'r_1'$ $l_dR_dr_d$

If the curve (6) touches tangentially to the circle (5) in one point, the corresponding α_i is just a extremum point of the curve (3) as used in the Witcher's condition. However many baffles may be set up, we can calculate geometrically for each D the interval of α, in which a particle can fly without being stopped by any baffles. Draw the curve (6) for l_i R_i r_i of each aperture and shade the regions corresponding to $R_i < |\sigma|$ and $|\sigma| < r_i$, as shown in Fig. 2, then the arc of circle (5) for each D cut off by the unshaded region represents the required interval. The solid angle subtended by the baffle system is given by

$$2\pi\{\cos\alpha_l(D) - \cos\alpha_u(D)\}^{\dagger} \tag{7}$$

provided that $\alpha_l(D)$ and $\alpha_u(D)$ represent respectively lower and upper limits of the above-mentioned interval.

From these considerations we can conclude the optimum geometrical condition for baffle system as follows; 1) The radius and position of the circular apertures in the baffles should be decided such that, as shown in Fig. 2, the unshaded region has a shape like a rhombus one diagonal of which is the circle (5) for D_m, the value of D for maximum solid angle given arbitrily by us.* 2) The shorter is the another diagonal compared with the D_m diagonal, the larger is the resolving power. A large resolving power can be obtained in a case, when two right-upper sides of the rhombus touch tangentially to the D_m diagonal.‖ 3) The conditions 1) and 2) can be realized by two pairs of outer and inner baffles or one pair and only one outer baffle of the detector's window. Other intermediate baffles are, of course, necessary to prevent particles from entering the detector after more than two rotations or to stop particles scattered anomalously.

But it is enough, and even better for simplicity, to make the sides of unshaded region be determin-

---

† In special case the circle (5) may be cut off into more than one part, then the formula (7) must be modified accordingly.

* In order to materialize these conditions, the restriction that the apertures are of a ring shape is unnecessary, rather too close. The outer and inner baffles might not always be on a same plane.

‖ In Witcher's condition R_d only satisfies this condition.

ed by the least number of baffles or two baffles, as described in the condition 3), and make curves (6) corresponding to other baffles be in the shaded region at a considerable distance from the sides of the unshaded. Because unnecessarily many baffles near the path of particles increase undesirable scattering.

Fig. 3 are examples of the luminosity *vs.* D curves of the baffle system, which satisfy these conditions.† The maximum values of these curves are larger by one order or two than the conventional type's of the comparable resolving power.

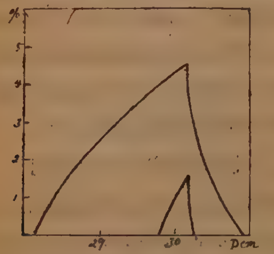

Fig. 3. (*i*) The maximum luminosity 4.5 %, the half-intensity windth 4.7 %; $l_1 = 66.3\,cm$, $R_1 = 8.7\,cm$, $r_1 = 5.9\,cm$, $l_d = 86\,cm$, $R_d = 1.5\,cm$. (*ii*) The maximum luminosity 1.7 %, the half-intensity width 0.9 %; $l_1 = 77.8\,cm$, $R_1 = 4.1\,cm$, $r_1 = 3.5\,cm$, $l_d = 86\,cm$, $R_d = 1.5\,cm$, $r_d = 10\,cm$.

In this study, we neglect the thickness of each baffle. When we take it into account, we must use envelopes of the curves (6) as the sides of unshaded region. But, as the thickess is usually very small in comparison with l_i of each baffle, it will be able to be neglected without appreciable error.

An Attempt to the Analytical Method of Calculation for General Case

When sources are distributed in a region which can not be regarded as a point, or even in a case of a point source deviated from the axis of symmetry, the calculation of the luminosity *vs.* D curve by the graphical method as described in the preceding section is practically impossible. So it seems to be not meaningless to attempt the calculation in a case of a deviated point source by the analytical method on trial. According to the preceding section, let us consider a case of only tw baffles and take the xyz-axes as shown in Fig. 4. The distance $\omega(z)$ of a charged particle from the z-axis, which starts from a deviated point source $(\rho,\ \varphi,\ 0)$ and has flown a distance z along the z-axis, is

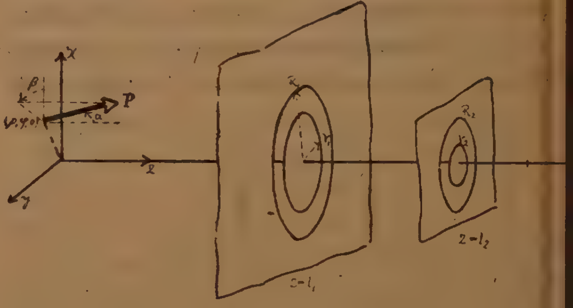

Fig. 4

$$\omega(z) = \{\rho^2 + \sigma(z)^2 - 2\rho|\sigma(z)| \cos(\pm z/D \cos\alpha \mp \varphi - \beta + \pi)\}^{1/2}, \tag{8}$$

where $\pm$ corresponds to positive and negative charge respectively. Then, the solid angle S subtended by two annular apertures is a function of $l_1 R_1 r_1$, $l_2 R_2 r_2$, ρ, D and can be expressed

$$S_{l_1,\ R_1,\ r_1;\ l_2,\ R_2,\ r_2;\ \rho}(D) = \int_{\alpha=0}^{\alpha=\pi/2} 2\pi \sin\alpha\, d\alpha \int_{\beta=0}^{\beta=2\pi} f(\omega,\ R_1) \times \{1 - f(\omega_1,\ r_1)\} f(\omega_2,\ R_2)\{1 - f(\omega_2,\ r_2)\} \frac{d\beta}{2\pi}. \tag{9}$$

provided that

$$\omega_1 = \omega(l_1) \quad \omega_2 = \omega(l_2)$$

and

$$f(x,\ y) = y\int_0^\infty J_0(xt) J_1(yt)\, dt = \begin{cases} 0 & x > y \\ 1/2 & x = y \\ 1 & x < y \end{cases}$$

where $J_0(t)$, $J_1(t)$ are the Bessel function of order 0, 1 and $f(x,\ y)$ is the Weber-Schafheitlin's discontinuous integral. From the relation

$$f(x,\ y_1)\{1 - f(x,\ y_2)\} = f(x,\ y_1) - f(x,\ y_2)$$

The integral $\int d\beta$ in (9) is able to be deformed by changing the order of integration

---

† These values are of the same order as the evaluations given recently in short notes by several authors.(2) (4) But the detalied comparison with these is impossible as the meaning of resolving power or half-intensity width are not defined in these notes.

$$\int_0\int^{\infty}\{R_1J_1(R_1t)-r_1J_1(r_1t)\}\{R_2J_1(R_2u)-r_2J_1(r_2u)\}dt\,du \times\int_0^{2\pi}J_0(\omega_1t)\cdot J_0(\omega_2u)d\beta.$$

By Neumann's addition theorem

$$J_0(\omega_it)=\sum_{n=0}^{\infty}\varepsilon_nJ_n(\rho t)\cdot J_n(|\sigma_i|t)\cos n\{\pm l_i/(D\cos\alpha)+\varphi+\pi-\beta\},$$

where $\sigma_i=\sigma(l_i)$ and $\varepsilon_n=1$ when $n=0$, $=2$ when $n\neq0$. So

$$\int_0^{2\pi}J_0(\omega_1t)\cdot J_0(\omega_2u)d\beta=2\pi\sum_{n=0}^{\infty}\varepsilon_nJ_n(\rho t)\cdot J_n(|\sigma_1|t)\cdot J_n(\rho u)\cdot J_n(|\sigma_2|u)\cos\cdot\frac{n(l_1-l_2)}{D\cos\alpha},$$

Thus, we must calculate the integral of the form

$$\int_0^{\infty}rJ_1(rt)\cdot J_n(\rho t)\cdot J_n(\sigma t)dt$$

$$r\geqslant0,\ \rho\geqslant0,\ \sigma\geqslant0,\ n=0,1,2,3,\ldots.$$

Such a integral is calculated by H. M. Macdonald(5) and the result is

$$=\begin{cases}0\\ 2/\pi\cdot\sin(A_i/2)\cdot{}_2F_1(1/2+n,\,1/2-n\,;\,3/2\,;\,\sin^2A_i/2)\\ 1\text{ when }n=0,\quad=0\text{ when }n=1,2,3,\ldots.\end{cases}$$

$$\text{corresponding to}\quad\begin{matrix}r^2\leqslant(\sigma-\rho)^2\\ (\sigma-\rho)^2\leqslant r^2\leqslant(\sigma+\rho)_2\\ (\sigma+\rho)^2\leqslant r^2.\end{matrix}$$

where $A_i=\mathrm{Cos}^{-1}(\rho^2+\sigma_i^2-r_i^2)/(2\rho|\sigma_i|)$ and ${}_2F_1$ is the Gauss' hypergeometeric function, which can be simplified, multiplied by the factor $2/\pi\cdot\sin(A_i/2)$, such that

$$2/\pi\cdot\sin(A_i/2)\cdot{}_2F_1=\begin{cases}A_i/\pi & n=0\\ (\sin nA_i)/(n\pi) & n=1,2,3,\ldots.\end{cases}$$

as confirmed easily by the expansion of each side into infinite series. Introducing

$$\mathrm{I}_n(\alpha)=\int_0^{\infty}\{R_1J_1(R_1t)-r_1J_1(r_1t)\}J_n(\rho t)\cdot J_n(|\sigma_1|t)dt \tag{10}$$

$$\mathrm{II}_n(\alpha)=\int_0^{\infty}\{R_2J_1(R_2u)-r_2J_1(r_2u)\}J_n(\rho u)\cdot J_n(|\sigma_2|u)du, \tag{11}$$

we obtain

$$S=\int_0^{\pi/2}\left\{\sum_{n=0}^{\infty}\varepsilon_n\cos\frac{n(l_1-l_2)}{D\cos\alpha}\,\mathrm{I}_n(\alpha)\cdot\mathrm{II}_n(\alpha)\right\}\cdot2\pi\sin\alpha d\alpha. \tag{12}$$

Unfortunately, functions $\mathrm{I}_n(\alpha)$ and $\mathrm{II}_n(\alpha)$ are not simple functions of α and the interval of α must be divided in a complex manner as shown in Table 1, in order that they are expressed as elementary functions.

For example, the integrand of (12) in the case of

$$l_1=45\quad R_1=12.5\quad r_1=7.2\qquad\rho=1.0\quad D=31.0$$

$$l_2=86\quad R_2=1.5\quad r_2=1.0$$

are

$$2\pi\sin\alpha(1-a_1/\pi)(A_2/\pi-a_2/\pi)+4\pi\sin\alpha\sum_{m=1}^{\infty}\cos\frac{41\cdot m}{31\cos\alpha}\left(-\frac{\sin ma_1}{m\pi}\right)\times\left(\frac{\sin mA_2}{m\pi}-\frac{\sin ma_2}{m\pi}\right)\qquad\alpha_{1a}\leqq\alpha\leqq\alpha_{2b},$$

$$2\pi\sin\alpha(1-a_1/\pi)\cdot A_2/\pi+4\pi\sin\alpha\sum_{m=1}^{\infty}\cos\frac{41\cdot m}{31\cos\alpha}\left(-\frac{\sin ma_1}{m\pi}\right)\frac{\sin mA_2}{m\pi}\qquad\alpha_{2b}\leqq\alpha\leqq\alpha_{1c},$$

$$2\pi\sin\alpha.\ A_2/\pi\qquad\alpha_{1c}\leqq\alpha\leqq\alpha_{2d},$$

$$2\pi\sin\alpha.\ (A_2/\pi-a_2/\pi)\qquad\alpha_{2d}\leqq\alpha\leqq\alpha_{1e},$$

$$2\pi\sin\alpha\cdot A_1/\pi\cdot(A_2/\pi-a_2/\pi)+4\pi\sin\alpha\sum_{m=1}^{\infty}\cos\frac{41\cdot m}{31\cos\alpha}\frac{\sin mA_1}{m\pi}\times\left(\frac{\sin mA_2}{m\pi}-\frac{\sin ma_2}{m\pi}\right)\qquad\alpha_{1e}\leqq\alpha\leqq\alpha_{2f},$$

wher

$$A_i=\mathrm{Cos}^{-1}(\rho^2+\sigma_i^2-R_i^2)/(2\rho|\sigma_i|)$$

$$a_i=\mathrm{Cos}^{-1}(\rho^2+\sigma_i^2-r_i^2)/(2\rho|\sigma_i|)$$

and

$\tan\alpha_{1a}=0.2034$ $\tan\alpha_{2b}=0.2230$

$\tan\alpha_{1c}=0.2726$ $\tan\alpha_{2d}=0.3711$

$\tan\alpha_{1e}=0.3992$ $\tan\alpha_{2f}=0.4841$

are boundary points of α intervals in Table 1, arranged in their order of magnitude, and have been derived by the graphical calculation as shown in Fig. 1.

Infinite series of the form

$$\sum_{m=1}^{\infty}\cos mX(\sin mY)/(m\pi)\cdot(\sin mZ)/(m\pi)$$

in the integrand can be summed easily

$$=\sum_{m=1}^{\infty}(2\pi m)^{-2}\cos m(X+Y-Z)+\sum_{m=1}^{\infty}(2\pi m)^{-2}\cos m(X-Y+Z)-\sum_{m=1}^{\infty}(2\pi m)^{-2}\cos m(X+Y+Z)-\sum_{m=1}^{\infty}(2\pi m)^{2}\cos m(X-Y-Z)$$

Table I. The form of functions $I_n(\alpha)$ in each interval of α, whose boundary points are determined by the relative dimensions of $\sigma_1(\alpha)$, R_1, r_1, ρ. The arrow showes the length of $\sigma_1(\alpha)$. $A_1=\cos^{-1}(\rho^2+\sigma_1^2-R_1^2)/(2\rho|\sigma_1|)$. $a_1=\mathrm{Cos}^{-1}(\rho^2+\sigma_1^2-r_1^2)/(2\rho|\sigma_1|)$. $n=0, 1, 2, 3, \ldots.$ $m=1, 2, 3, \ldots.$ All the same for $II_n(\alpha)$, $\sigma_2(\alpha)$, R_2, r_2.

<table>
<tr><td colspan="7">When $\rho\leqq r_i$</td><td>$r_i<\rho$</td></tr>
<tr><td>When
$2\rho\leqq$
R_i-r_i</td><td>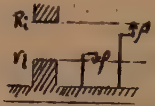 </td><td></td><td>When
$\rho\leqq R_i-r_i$
$\leqq 2\rho$</td><td>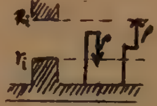 </td><td></td><td>When
R_i-r_i
$\leqq\rho$</td><td></td></tr>
<tr><td>$I_n=0$
$\cos a_i=-1$
$I_0=1-\frac{a_i}{\pi}$
$I_m=-\frac{\sin ma_i}{m\pi}$
$\cos a_i=+1$
$I_0=1$
$I_m=0$
$\cos A_i=-1$
$I_0=\frac{A_i}{\pi}$
$I_m=\frac{\sin mA_i}{m\pi}$
$\cos A_i=+1$
$I_n=0$</td><td>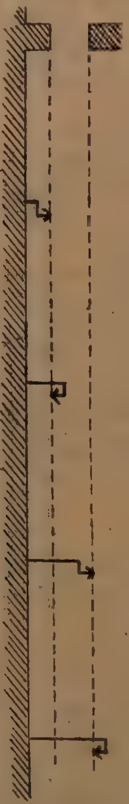</td><td>$\sigma_i(\alpha)=$
$r_i-\rho$
$r_i+\rho$
$R_i-\rho$
$R_i+\rho$</td><td>$I_n=0$
$\cos a_i=-1$
$I_0=1-\frac{a_i}{\pi}$
$I_m=-\frac{\sin ma_i}{m\pi}$
$\cos A_i=-1$
$I_0=\frac{A_i}{\pi}-\frac{a_i}{\pi}$
$I_m=\frac{\sin mA_i}{m\pi}-\frac{\sin ma_i}{m\pi}$
$\cos a_i=+1$
$I_0=\frac{A_i}{\pi}$
$I_m=\frac{\sin mA_i}{m\pi}$
$\cos A_i=+1$
$I_n=0$</td><td>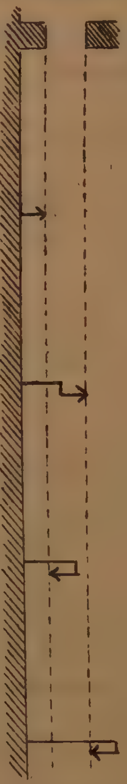</td><td>$\sigma_i(\alpha)=$
$r_i-\rho$
$R_i-\rho$
$r_i+\rho$
$R_i+\rho$</td><td>Same as the case of $\rho\leqq R_i-r_i\leqq 2\rho$.</td><td>Abbreviated.</td></tr>
</table>

and

$$\sum_{m=1}^{\infty}(2\pi m)^{-2}\cos m\pi\theta=\begin{cases}1/16\cdot\{\theta^2-2|\theta|\}+1/24 & -1\leqq\theta\leqq+1\\ 1/16\cdot\{(\theta-2)^2-2|\theta-2|\}+1/24 & +1\leqq\theta\leqq+3\\ \cdots\cdots\cdots\cdots\cdots\cdots & \\ 1/16\cdot\{(\theta-2q)^2-2|\theta-2q|\}+1/24 & (2q-1)\leqq\theta\leqq(2q+1)\end{cases}$$

It is difficult for us to integrate these functions except by the method of graphical integration. But we can check easily this analytical calculation, without carrying through the tedious graphical integration, by ascertaining that $S_{l,\,R,\,r;\,\rho}(D)$, the solid angle in the case of only one baffle, is equal to $S_{l_1,\,R_1,\,r_1;\,l_2,\,R_2,\,r_2;\,\rho}(D)$, provided R = the smaller of R_1 and R_2, r = the larger of r_1 and r_2; $l=l_1=l_2$.

As the final results we can conclude: The analytical expression (12) can be deformed to a finit integral, which contains no infinite series and is integral function of $A_i(\alpha)$, $a_i(\alpha)$ and $1/\cos\alpha$. Bu its integration with respect to α is difficult excep by the graphical method, because of the necessit of complex division of the integrating interval a well as the complex form of functions $A_i(\alpha)$ an $a_i(\alpha)$. Although the graphical integration is als not easy for the same reason, it seems to be use ful and not impossible if the exact luminosity v D curve is indispensable. When more than tw baffles are set up in order to stop the particles which have rotated more than two times etc., as described in the preceding section, the integrating interval of α should be reduced according to them.

Conclusion.

In this type of spectrometer, we can obtain, for example, the luminosity of 4.5 % and the half-intensity width of 4.7 %. It will also be easy to use the more larger projection angle without decrease of the resolving power, and therefore to make the efficiency more larger. The method of analytical calculation as given in this paper is, though exact rigorously, not able to be utilized for the practical purposes (e. g. the design or the approximate evaluation for the source of unneglisible dimension), as the introduction of approximation is difficult because of the use of peculiar integral, which becomes divergent nearly always when deformed approximately. We must device another method of approximate investigation for the sake of practical purposes. But the possibility to calculate the exact luminosity *vs. D* curve makes this type fit for the exact measurement, together with the facility to increase the exactness of the uniform magnetic field.

Finally the author expresses his sincere thanks to Prof. Y. Watase and Prof. J. Itoh for their kind guidance and helpful criticism.

References.

(1) C. M. Witcher: Phys. Rev. **60** (1941), 32.
(2) S. Frankel: Phys. Rev. **73** (1948), 804 (L).
(3) C. S. Wu, W. W. Havens, Jr., R. Albert and G. Grimm: Phys. Rev. **73** (1948), 1259 (A).
(4) E. Perisco: Phys. Rev. **73** (1948), 1475 (L).
(5) H. M. Macdonald: Proc. London Math. Soc. (2) **7** (1909), 142.

On the Magnetic Scattering of Fast Electrons in the Ferromagnetic Crystal.

By Toshinosuke MUTO, Kenzo INOUE and Ichie WATANABE.

Institute of Science and Technology, University of Tokyo.

(Received December 27, 1948)

§ 1. Introduction.

As well-known, the polarization of electron waves has been attempted to observe by many experimental investigators through the elastic scattering process by the electrostatic fields of atoms involved in the crystal, but all the experiments still remain unsuccessful or unconfirmative. In view of the electron polarization being closely connected with the electron spin and its proper magnetic moment, however, it may be conceivable in principle for the experimental observation of the electron polarization to make use of the magnetic scattering of electrons in the Weiss molecular field within the ferromagnetics, although the considerable electromagnetic disturbance of Lorentz's force upon the phenomena under consideration seems generally to make it quite difficult to observe the electron polarization in contradistinction to the case of the magnetic scattering of slow neutrons which has no net electric charge but the proper magnetic moment. In view of the present situation that all the experiments to observe the electron polarization by the electrostatic scattering process have still been insufficient to confirm the effect despite of all the efforts of the experimenters, it will be worth while to examine in more detail whether the observable influence of the electron spin upon the mentioned magnetic scattering makes its appearance, to an appreciable amount, compared with the disturbance due to Lorentz's force, or not for some appropriate electron energies. In this connection, it should be mentioned that Meyer and Cox⁽¹⁾ have attempted actually to observe the magnetic scattering of β-rays emitted from Radium passing through two sheets of ferromagnetic iron metals but without success. Their experimental accuracy, however, seems not to be sufficiently great to observe such minute effect of the electron spin upon the magnetic scattering. On the other hand, Weizsäcker⁽²⁾ has discussed qualitatively the passage of high speed cosmic ray particles through the ferromagnetic materials in connection with the experimental observation of Rossi, Mott-Smith and Millikan and Anderson, but he has not attempted to work out theoretically the magnetic scattering of the charged particles in the ferromagnetics, whose detailed theoretical discussion remains unattacked quantitively so far. Moreover, on a purely theoretical viewpoint, it is quite interesting and instructive to make clear the characteristic difference between the magnetic scatterings of fast electrons and slow neutrons⁽⁴⁾ in the ferromagnetics. For the reasons given above, both theoretical and experimental, we have, in the present note, worked out theoretically the magnetic scattering of Dirac's electrons in the ferromagnetics in order to clarify the effect of electron spin on the phenomena under consideration.

§ 2. The Electromagnetic Influence on the Incoming Dirac's Electron within the Ferromagnetics.

According to Dirac, the Hamiltonian of an electron is given by

$$H=(\vec{\alpha}\vec{p})+\beta\mu+e(-\phi(\vec{r})+\vec{\alpha}\vec{A}(\vec{r})), \tag{1}$$

where e and $\mu=mc^2$ mean the electronic charge and the rest energy of an electron respectively, $\vec{p}$ its momentum multiplied by c (light velocity), $\vec{\alpha}$ and β the spin operators, $\phi(\vec{r})$ and $\vec{A}(\vec{r})$ the scalar and vector potentials due to the electro- and magneto static field within the ferromagnetic crystal. Since the Born approximation may be considered to be valid for the fast electron scattering, we have, for the unperturbed Hamiltonian H_0,

$$H_0=(\vec{\alpha}\vec{p})+\beta\mu, \tag{2}$$

and, for the unperturbed wave functions⁽¹⁾ of an incoming electron,

$$\psi_0=u(i)\exp i(\vec{p}_0\vec{r}/\hbar c-E_0t/\hbar)\cdot/\sqrt{V},\ E_0^2=p_0^2+\mu^2, \tag{3}$$

$$\left.\begin{array}{lll} & (\uparrow) & (\downarrow) \\ u(1)= & 1, & 0, \\ u(2)= & 0, & 1, \\ u(3)= & p_{0z}/(\mu+E_0), & (p_{0x}+ip_{0y})/(\mu+E_0) \\ u(4)= & (p_{0x}-ip_{0y})/(\mu+E_0), & -p_{0z}/(\mu+E_0) \end{array}\right\} \cdot(1+p_0^2/(\mu+E_0)^2)^{-1/2}, \tag{4}$$

respectively, where E_0 and $\vec{p}_0/c$ represent the energy and momentum of an electron, the symbols ↑ and ↓ denote each of the two spin states of an electron and V the total volume of the crystal. We have omitted in (4) the wave functions belonging to the negative energy ($E_0<0$), which do not concern us here for the scattering process to a first approximation.

For the perturbing term, therefore, it follows

$$\delta H=-e\phi(\vec{r})+e\vec{\alpha}\cdot\vec{A}(\vec{r}). \tag{5}$$

The scalar potential $\phi(\vec{r})$ within a single Fe crystal of a body centered cubic may be given by

$$\phi(\vec{r})=\Sigma(\vec{g})\cdot\phi'_{\vec{g}}\left\{\exp\frac{i}{2}\vec{g}(\vec{a}_1+\vec{a}_2+\vec{a}_3)+1\right\}e^{i\vec{g}\vec{r}} \tag{6}$$

and

$$\phi'_{\vec{g}}=\frac{4\pi}{g^2}\frac{e}{a^3}(Z-F(\vec{g}));\quad F(\vec{g})=\int_{\tau_0}\rho(r')e^{-i\vec{g}\vec{r}'}d\tau', \tag{7}$$

using the well-known Fourier theorem, respectively, where $\vec{a}_1$, $\vec{a}_2$ and $\vec{a}_3$ represent each of the primitive translation vectors of the cubic lattice, $\vec{g}\left(\frac{2\pi}{a}n_1, \frac{2\pi}{a}n_2, \frac{2\pi}{a}n_3\right)$ a vector specifying each lattice point in the reciprocal lattice (n_1, n_2, n_3 = integers), Z the atomic number of Fe atom, $e\rho(r)$ the density of electronic charge distribution within a single Fe atom. The expression contained in the curved bracket of the equation (6) is easily seen to become 2 for the even number of $(n_1+n_2+n_3)$ while 0 for its odd number respectively.

The vector potential $\vec{A}(\vec{r})$ due to the magnetostatic field within the ferromagnetic crystal of Fe may be expanded, for the saturated state of magnetization, into the following Fourier series.

$$\vec{A}(\vec{r})=\sum_{\vec{g}}\vec{A}'_{\vec{g}}\left\{\exp\frac{i}{2}\vec{g}(\vec{a}_1+\vec{a}_2+\vec{a}_3)+1\right\}e^{i\vec{g}\vec{r}}. \tag{8}$$

Similary, we have, for the density of saturation value $\vec{M}(\vec{r})$ of magnetization,

$$\vec{M}(\vec{r}) = \sum_{\vec{g}} \vec{M}'_{\vec{g}} \left\{ \exp \frac{i}{2} \vec{g}(\vec{a}_1 + \vec{a}_2 + \vec{a}_3) + 1 \right\} e^{i\vec{g}\vec{r}} \tag{9}$$

and

$$\vec{M}'_{\vec{g}} = \frac{1}{a^2} \int \vec{M}'(\vec{r}) e^{-i\vec{g}\vec{r}} d\tau = \vec{\mu}_a / a^3 \cdot F_d(\vec{g}), \tag{10}$$

where

$$\vec{M}'(\vec{r}) = \vec{\mu}_a \rho_m(\vec{r}), \quad F_d(\vec{g}) = \int_{\tau_0} e^{-i\vec{g}\vec{r}} \rho_m(\vec{r}) d\tau, \tag{11}$$

since the continuous distribution of magnetic moment may be considered, on the average, to be realized with the crystal period in the saturated state of magnetization of the crystal. τ_0 denotes the volume of an elementary cell, $\vec{\mu}_a$ the magnetic moment per atom, $\rho_m(r)$ the density of 3d electrons within a single Fe atom, and $M_0 = \frac{2}{a^3}\mu_a$ represents the observable intensity of magnetization in the saturated state. In order to express the vector potential by the intensity of magnetization directly observed, we have to find the relation between both coefficients in the expansion of the mentioned qnantities.

According to the classical theory of electromagnetism, it follows

$$-\Delta \vec{A} = 4\pi \operatorname{curl} \vec{M}. \tag{12}$$

Putting the expansions of both vector potential and intensity of magnetization (8) and (9) into the relation (12), the following important relation for our purpose has been obtained by comparing the coefficients of both sides of the equation.

$$\vec{A}'_{\vec{g}} = \frac{4\pi i}{g^2}(\vec{g} \times \vec{M}'_{\vec{g}}) = \frac{4\pi i}{g^2} \cdot \frac{1}{a^3} F_d(\vec{g}) \cdot (\vec{g} \times \vec{\mu}_a), \tag{13}$$

using the equation (9), which shall be made use of in the next chapter.

§ 3. Effective Cross Section for Elastic Scattering.

According to the general theory of quantum mechanics, we have, for the transition probability of elastic scattering of an electron from $\vec{p}_0$ to $\vec{p}(p_0 = p,\ E_0 = E)$,

$$\Delta W = \frac{2\pi}{\hbar} \rho(E) \,|\, (i \,|\, \delta H \,|\, f) \,|^2 \tag{14}$$

and

$$\rho(E) = \frac{pE}{(2\pi\hbar c)^3} V d\Omega, \tag{15}$$

where $d\Omega$ denotes the solid angle around the direction of scattered electron, i and f refer to the initial and final states respectively.

Substituting (6)—(13) into (5) and, further, using (3) and (4), the matrix elements of the perturbation term δH are easily shown to take the following form, for the elastic scattering of electrons without spin change,

$$|(i|\delta H|f)|^2 = \frac{1}{V^2} \sum_{\vec{g}} \left| \left[-e\phi_{\vec{g}} \begin{Bmatrix} (\overset{1}{u}_i\ \overset{1}{u}_f) \\ (\overset{\iota}{u}_i\ \overset{\iota}{u}_f) \end{Bmatrix} + e\vec{A}_{\vec{g}} \begin{Bmatrix} (\overset{1}{u}_i\ \vec{\alpha}\ \overset{1}{u}_f) \\ (\overset{\iota}{u}_i\ \vec{\alpha}\ \overset{\iota}{u}_f) \end{Bmatrix} \right] \left(\exp \frac{i}{2} \vec{g}(\vec{a}_1 + \vec{a}_2 + \vec{a}_3) + 1\right) \right|^2 \prod_{xyz} \frac{2\left(1 - \cos\left(g_x + \frac{p_{0x} - p_x}{\hbar c}\right)L\right)}{\left(g_x + \frac{p_{0x} - p_x}{\hbar c}\right)^2} \tag{16}$$

since each of Laue spots on the diffraction pattern may be assumed not to overlap with respect to each other, which situation may be taken to be satisfied quite well in the ordinary experimental observation. $\overset{1}{u}_i$ and $\overset{1}{u}_f$ refer to the initial and final spin eigenfunctions belonging to the positive direction of spin, while $\overset{\iota}{u}_i$ and $\overset{\iota}{u}_f$ to those belonging to the negative direction of spin respectively.

In order to get the total probability for the elastic scattering of electrons, we have to sum up the contributions from both spin states to the transition probabilities and, further, to integrate them over all directions of scattering, in which the replacement of Laue terms in (16) with Dirac's δ-functions will be approximately permitted to be made for carrying out the integration analytically.

Namely,

$$\frac{1-\cos\left(g_x+\frac{p_{0x}-p_x}{\hbar c}\right)L}{\left(g_x+\frac{p_{0x}-p_x}{\hbar c}\right)^2}\sim\pi L\delta\left(g_x+\frac{p_{0x}-p_x}{\hbar c}\right),\ \text{etc.,} \tag{17}$$

Thus, it follows, for the total probability of elastic scattering without spin change,

$$W=\int\Delta W=\frac{2\pi}{\hbar}\cdot\frac{pE}{(2\pi\hbar c)^3}\cdot 8\pi^3\sum_{\vec{g}}\int|V_{\vec{g}}|^2\delta\left(\frac{p}{\hbar c}\frac{x}{R}\right)\delta\left(\frac{p}{\hbar c}\frac{y}{R}\right)\delta\left(\left|\vec{g}+\frac{\vec{p}_0}{\hbar c}\right|-\frac{p}{\hbar c}\frac{z}{R}\right)\frac{dS}{R^2}, \tag{18}$$

the polar axis being supposed to lie along the direction of $\left(\vec{g}+\frac{\vec{p}_0}{\hbar c}\right)$ and the surface element to be $dS=\frac{R}{z}dx\,dy (R=\sqrt{x^2+y^2+z^2})$, from which we obtain

$$W=\frac{2\pi}{\hbar^2 c}\cdot\frac{E}{p}\sum_{\vec{g}}|V_{\vec{g}}|^2{}_{p_x=p_y=0,\,p_z=p}\,\delta\left(\frac{p}{\hbar c}-\left|\vec{g}+\frac{\vec{p}_0}{\hbar c}\right|\right), \tag{19}$$

by the use of the well-known properties of δ-function, with

$$V_{\vec{g}}=\left[-e\phi_{\vec{g}}\begin{Bmatrix}(\overset{\uparrow}{u_i}\ \overset{\uparrow}{u_f})\\(\overset{\downarrow}{u_i}\ \overset{\downarrow}{u_f})\end{Bmatrix}+e\vec{A}_{\vec{g}}\begin{Bmatrix}(\overset{\uparrow}{u_i}\ \vec{\alpha}\ \overset{\uparrow}{u_f})\\(\overset{\downarrow}{u_i}\ \vec{\alpha}\ \overset{\downarrow}{u_f})\end{Bmatrix}\right]\left(\exp\frac{i}{2}\vec{g}(\vec{a}_1+\vec{a}_2+\vec{a}_3)+1\right) \tag{20}$$

Evaluating the matrix element of α by using (4) and putting the results obtained above into (20), we get finally, after some process of manipulations,

$$V_{\vec{g}}=\left\{-\left[\frac{8\pi}{g^2}\frac{e^2}{a^3}(Z-F(g))\left(1+\frac{\vec{p}\vec{p}_0}{(\mu+E)^2}\right)\pm\frac{8\pi}{g^2}\frac{e}{a^3}F_a(g)\frac{1}{\mu+E}\left((\vec{g}\vec{\mu}_a)(\vec{p}-\vec{p}_0)\vec{\mu}_a\frac{1}{\mu_a}+\mu_a\vec{g}(\vec{p}-\vec{p}_0)\right)\right]\right.$$
$$\left.\mp i\left[\frac{8\pi}{g^2}\frac{e^2}{a^3}(Z-F(g))\frac{(\vec{p}_0\times\vec{p})\vec{\mu}_a}{(\mu+E)^2\mu_a}\mp\frac{8\pi}{g^2}\frac{e}{a^3}F_a(g)\frac{1}{\mu+E}(\vec{p}_0+\vec{p})(\vec{g}\times\vec{\mu}_a)\right]\right\}\left(1+\frac{p^2}{(\mu+E)^2}\right)^{-1}, \tag{21}$$

where the double signs correspond to each of the two possible directions of electron spins respectively.

For the case of polycrystal, used in the ordinary scattering experiments, we have to take the average, over all orientations of the crystal, of the total probability obtained above, which procedure is equivalent to the averaging process with respect to the directions of $\vec{g}$.

Then, we have

$$\begin{aligned}\overline{W}&=\frac{2\pi}{\hbar^2 c}\frac{E}{p}\sum_{\vec{g}}\left(|V_{\vec{g}}|^2{}_{p_x=p_y=0,\,p_z=p}\,\delta\left(\frac{p}{\hbar c}-\left|\vec{g}+\frac{\vec{p}_0}{\hbar c}\right|\right)\right)_{Av}\\&=\frac{2\pi}{\hbar^2 c}\frac{E}{p}\sum_{\vec{g}}\frac{1}{4\pi g}\int_0^{\pi}d\varphi\int_0^{\pi}|V_{\vec{g}}|^2{}_{p_x=p_y=0,\,p_z=p}\,\delta\left(\frac{\hbar cg}{2p}+\cos\theta\right)\sin\theta\,d\theta\\&=\frac{1}{2\hbar^2 c}\frac{E}{p}\sum_{g<2p/\hbar c}\frac{1}{g}\int_0^{2\pi}d\varphi|V_{\vec{g}}|^2{}_{p_x=p_y=0,\,p_z=p}\left(\cos\theta=-\frac{\hbar cg}{2p}\right),\end{aligned} \tag{22}$$

On account of (21), we obtain finally

$$\overline{W}=\frac{16\pi^3}{a^6}\cdot\frac{e^4}{\hbar^2 c}\cdot\frac{(E+\mu)^2}{Ep}\sum_{g<2p/\hbar c}\frac{(Z-F(g))^2}{g^5}\left\{\left[1+\frac{E-\mu}{E+\mu}\left(1-2\left(\frac{\hbar cg}{2p}\right)^2\right)\right]^2+2\left(\frac{E-\mu}{E+\mu}\right)^2\left(\frac{\hbar cg}{2p}\right)^2\left(1-\left(\frac{\hbar cg}{2p}\right)^2\right)\sin^2\theta\right\}$$
$$+\frac{32\pi^3}{a^6}\frac{e^4}{\hbar^2 c}\frac{\mu_a^2}{e^2}\frac{E^2-\mu^2}{Ep}\sum_{g<2p/\hbar c}\frac{F_a(g)^2}{g^3}\left\{\left(1-\left(\frac{\hbar cg}{2p}\right)^2\right)\sin^2\theta+\left(\frac{\hbar cg}{2p}\right)^6 2\cos^4\theta+\left(\frac{\hbar cg}{2p}\right)^2\left(1-\left(\frac{\hbar cg}{2p}\right)^2\right)\right.$$
$$\left.\times\frac{3}{4}\sin^4\theta+\left(\frac{\hbar cg}{2p}\right)^4\left(1-\left(\frac{\hbar cg}{2p}\right)^2\right)6\sin^2\theta\cos^2\theta\right\}$$

$$\mp\frac{16\pi^3}{a^6}\frac{e^4}{\hbar^2 c}\frac{\hbar c}{e}\mu_a\frac{E+\mu}{Ep}\sum_{g<2p/\hbar c}\frac{(Z-F(g))F_d(g)}{g^3}\Big\{2\Big(\frac{\hbar cg}{2p}\Big)^2\Big(1+\frac{E-\mu}{E+\mu}\Big(1-2\Big(\frac{\hbar cg}{2p}\Big)^2\Big)\Big)$$

$$+\Big[1-3\Big(\frac{\hbar cg}{2p}\Big)^2-\frac{E-\mu}{E+\mu}\Big(1+3\Big(\frac{\hbar cg}{2p}\Big)^2-6\Big(\frac{\hbar cg}{2p}\Big)^4\Big)\Big]\sin^2\theta\Big\} \tag{23}$$

where θ denotes the angle between the direction of the intensity of magnetization and that of incoming electron beam.

Dividing the equation (23) by the current density of incoming electrons

$$j=\frac{2cp}{\sqrt{2E(E+p)}}\cdot\frac{1}{V}$$

$$\Big(V=\frac{1}{2}a^3N,\ N=\text{number of atoms in }V\Big)$$

we get, for the effective cross section per atom of the mentioned scattering process by the polycrystal of iron,

$$\sigma=\sigma_e+\sigma_m\mp\sigma_{em},$$

$$\sigma_e=\frac{4\sqrt{2}\pi^3}{a^3}\Big(\frac{e^2}{\hbar c}\Big)^2\frac{\sqrt{E+\mu^3}}{(E-\mu)\sqrt{E}}\sum_{g<2p/\hbar c}\frac{(Z-F(g))^2}{g^5}\Big\{\Big[1+\frac{E-\mu}{E+\mu}\Big(1-2\Big(\frac{\hbar cg}{2p}\Big)^2\Big)\Big]^2+2\Big(\frac{E-\mu}{E+\mu}\Big)^2\Big(\frac{\hbar cg}{2p}\Big)^2$$

$$\times\Big(1-\Big(\frac{\hbar cg}{2p}\Big)^2\Big)\sin^2\theta\Big\}, \tag{25}$$

$$\sigma_m=\frac{8\sqrt{2}\pi^3}{a^3}\Big(\frac{e^2}{\hbar c}\Big)^2\frac{\mu_a^2}{e^2}\sqrt{\frac{E+\mu}{E}}\sum_{g<2p/\hbar c}\frac{F_d^2(g)}{g^3}\Big\{\Big(1-\Big(\frac{\hbar cg}{2p}\Big)^2\Big)\sin^2\theta+2\Big(\frac{\hbar cg}{2p}\Big)^6\cos^4\theta+\frac{3}{4}\Big(\frac{\hbar cg}{2p}\Big)^2$$

$$\times\Big(1-\Big(\frac{\hbar cg}{2p}\Big)^2\Big)\sin^4\theta+6\Big(\frac{\hbar cg}{2p}\Big)^4\Big(1-\Big(\frac{\hbar cg}{2p}\Big)^2\Big)\sin^2\theta\cos^2\theta\Big\}, \tag{26}$$

$$\sigma_{em}=\frac{4\sqrt{2}\pi^3}{a^3}\Big(\frac{e^2}{\hbar c}\Big)^2\frac{\hbar c}{e}\mu_a\frac{\sqrt{E+\mu}}{(E-\mu)\sqrt{E}}\sum_{g<2p/\hbar c}\frac{F_d(g)(Z-F(g))}{g^3}\Big\{2\Big(\frac{\hbar cg}{2p}\Big)^2\Big[1+\frac{E-\mu}{E+\mu}\Big(1-2\Big(\frac{\hbar cg}{2p}\Big)^2\Big)\Big]+$$

$$+\Big[1-3\Big(\frac{\hbar cg}{2p}\Big)^2-\frac{E-\mu}{E+\mu}\Big(1+3\Big(\frac{\hbar cg}{2p}\Big)^2-6\Big(\frac{\hbar cg}{2p}\Big)^4\Big)\Big]\sin^2\theta\Big\}, \tag{27}$$

where $\frac{2p_0}{\hbar c}=\frac{2\pi}{\lambda}$ (λ = de Broglie wave length of an electron), $g=\frac{2\pi}{a}\sqrt{n_1^2+n_2^2+n_3^2}$

and

$$F(g)=4\pi\int_0^\infty\frac{\sin gr}{gr}\rho(r)r^2dr,\quad F_d(g)=4\pi\int_0^\infty\frac{\sin gr}{gr}\rho_m(r)r^2dr.$$

The relative increase of the transmission power for unpolarized beam of the magnetized iron crystal in saturation compared with that of the unmagnetized ones becomes of the following form, provided that the elastic scattering takes place without spin change.

$$\Delta T=\cosh(\sigma_{em}xN)-1, \tag{28}$$

where x denotes the thickness of the material along the incident direction.

On a similar way to the above computations, we get, for the scattering cross section associated with the spin change,

$$\sigma_{\uparrow\downarrow}=\frac{8\pi^3}{a^3}\Big(\frac{e^2}{\hbar c}\Big)^2\frac{\sqrt{2}(E-\mu)}{\sqrt{E(E+\mu)}}\sum_{g<2p/\hbar c}\frac{(Z-F(g))^2}{g^5}\Big(\frac{\hbar cg}{2p}\Big)^2\Big(1-\Big(\frac{\hbar cg}{2p}\Big)^2\Big)(1+\cos^2\theta)$$

$$+\frac{16\pi^3}{a^3}\Big(\frac{e^2}{\hbar c}\Big)^2\frac{\mu_a}{e}\sqrt{\frac{2(E-\mu)}{E}}\sum_{g<2p/\hbar c}\frac{F_d(g)(Z-F(g))}{g^4}\Big(\frac{\hbar cg}{2p}\Big)^2\Big(1-\Big(\frac{\hbar cg}{2p}\Big)^2\Big)^{1/2}(\sin^2\theta-\cos^2\theta)$$

$$+\frac{2\pi^3}{a^3}\left(\frac{e^2}{\hbar c}\right)^2\left(\frac{\mu_a}{e}\right)\sqrt{\frac{2(E+\mu)}{E}}\sum_{g<2p/\hbar c}\frac{F_d(g)^2}{g^3}\left(\frac{\hbar cg}{2p}\right)^2\left\{\left(27\left(\frac{\hbar cg}{2p}\right)^4-22\left(\frac{\hbar cg}{2p}\right)^2+3\right)\sin^2\theta\cos^2\theta\right.$$

$$\left.+4\left(\frac{\hbar cg}{2p}\right)^2\left(1-\left(\frac{\hbar cg}{2p}\right)^2\right)(\sin^4\theta+\cos^4\theta)+\left(1-\left(\frac{\hbar cg}{2p}\right)^2\right)\left(5\left(\frac{\hbar cg}{2p}\right)^2-1\right)\cos^2\theta+\left(1-\left(\frac{\hbar cg}{2p}\right)^2\right)^2\right\}, \tag{24}$$

after some process of manipulations.

§ 4. Discussions of the Results.

For the observation of electron polarization by using the change with magnetizatien of the transmission power of electron beam through the iron sheet, it is essentially required to prepare the experimental condition in which $|\sigma_{em}|$ becomes large as possible and simultaneously the stopping power of the iron sheet due to elastic scattering, ionization, excitation, Bremsung and pair creation and, further, the disturbing effect due to the stray magnetic field outside the crystal for incoming electrons are suitably depressed not to mask the observed magnetic effect. It, therefore, should be carefully analyzed from both experimental and theoretical viewpoints whether such favourable conditions to give measurable magnetic scattering may be realized or not for some appropriate values of the electron energies. For this purpose, we have estimated, as seen Table I, the order of magnitude of the various cross sections for a number of electron energies in which the atom form factors $F(g)$ and $F_d(g)$ have been numerically evaluated with the eigenfunctions constructed by Slater's method of shielding constants (Fig. 1).

Table I

$E-\mu$	σ_e(cm²)	$\lvert\sigma_{em}\rvert$(cm²)	σ_m(cm²)	$\sigma^{\uparrow\downarrow}$(cm²)
10^6 ev	$10.8\cdot10^{-17}$	$0.74\cdot10^{-22}$	$4.90\cdot10^{-23}$	$1.25\cdot10^{-22}$
10^7 ev	$7.7\cdot10^{-17}$	$1.20\cdot10^{-24}$	$4.34\cdot10^{-23}$	$3.77\cdot10^{-24}$
10^8 ev	$7.6\cdot10^{-17}$	$1.28\cdot10^{-26}$	$4.24\cdot10^{-23}$	$4.10\cdot10^{-26}$

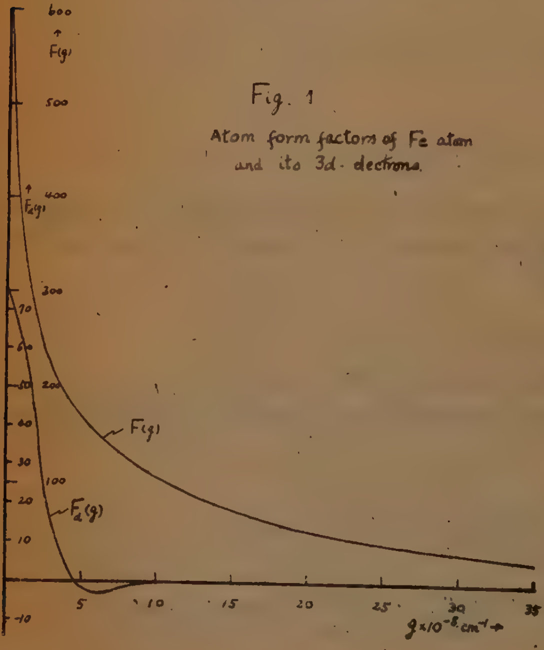

Fig. 1

Atom form factors of Fe atom and its 3d-electrons.

As far as the magnetic scattering with spin change are neglected, the relative change of transmission with magnetization ΔT in (28) will be expected to become of the measurable order of magnitude for the mentioned electron energies unless the transmitted intensity of electron beam becomes extremely small owing to the electrostatic scattering and the similar phenomena mentioned above. Table I, however, shows that the situation is not the case since the magnetic scattering cross sections without spin change $|\sigma_{em}|$ are of comparable order of magnitudes to those with spin change $\sigma^{\uparrow\downarrow}$, the redistribution of electron spins due to the former being expected to be completely disturbed by the latter.

Table II

($E-\mu = 10^7$ ev)

x	ΔT
0.5 cm	2.10^{-3}
1.0 cm	4.10^{-3}
1.5 cm	1.10^{-2}
2.0 cm	2.10^{-2}

In order to get a provisional information of the phenomena in question, we have estimated roughly the relative change of transmission with magnetization of iron sheet, using the non-relativistic formula due to Halpern and Holstein(6) which takes account the magnetic scattering with spin change. Since the electron energies in Table II lie well within the relativistic region, the mentioned values of the relative change of transmission are to be attached much physical significance but may be considered to show a qualitative tendency of the mentioned process with electron energies.

Finally it should be remarked that our theoretical discussions will be available for the magnetic analysis of the soft component of cosmic ray particles.

The authors are indebted to Special Research Committee of Theoretical Physics, National Research Council of Education Ministry for financial aid.

References.

(1) Meyer and Cox: Phys. Rev. **34** (1929) 1069.
(2) Weizsäcker; Ann. d. Phys. **19** (1933) 869.
(3) Halpern and Holstein: Phys. Rev. **59** (1941) 960.
(4) Heitler: The Quantum Theory of Radiation, 1936.
(5) Slater: Phys. Rev. **36** (1930) 57.
(6) Halpern and Helstein: loc. cit.

Anomalous Dielectric Behavior of Rochelle Salt. (I)

By Hidetosi TAKAHASI and Sigeyosi HARA.

Institute of Science and Technology, University of Tokyo.

(Read May 23, 1948; Received Dec. 28, 1948.)

§ 1. Introduction.

The anomalous dielectric behavior of Rochelle salt, summarized by the word "ferroelectricity" on account of its analogy to ferromagnetism, has called attention of many physicists, and experimental investigation has been made by numerous workers. Yet the phenomenon is so complicated that there are many points requiring further study. In particular, there are great discrepancies between the results of different authors using the same as well as different methods. Apart from those discrepancies that can be ascribed to the difference in external conditions, especially humidity,(1) a great difference is reported to exist between the dielectric constant measured by a. c. and that measured by a ballistic method.(2) This may be accounted for by the presence of dielectric after-effect,(3) which has been also directly observed and can also be anticipated from the presence of dispersion in a. c. measurements.(4) (5) Since this phenomenon is related to the process of reorientation of dipoles in the crystal, which may perhaps proceed by the shift of the boundaries between oppositely polarized domains, it is of interest to make further observations on the behavior of polarization as function of time under appropriately varied field.

The following measurements attempt to obtain a precise knowledge of the polarization vs. electric-field relation, i. e. hysteresis loop taken with *stepwise* varied field. The result shows clearly, that the dielectric after-effect is very large in Rochelle salt and not a subsidiary phenomenon as in ordinary dielectrics and also in ferromagnetics.

Some measurements were made using the same method to investigate the behavior of Rochelle salt under varying temperature, with special reference to the appearance and disappearance of spontaneous polarization at the Curie point.

§ 2. Experimental Method.

The principle of the method employed is illustrated in the schematic diagram (Fig. 1). The sample condenser C is a Rochelle salt crystal cut in rectangular plate ($^1/_2$ cm × 2 cm × 4 cm) with larger faces perpendicular to a-axis and foiled with silver on both sides by anhydrous alcohol, and is enclosed in a glass vessel and dried by $CaCl_2 \cdot 6H_2O$ to a relative humidity of about 25–35%. The vessel is immersed in a water bath, whose temperature can be raised by introducing steam from separate boiler. Direct heating by electric current was discarded in order to avoid the induction effect to the circuit.

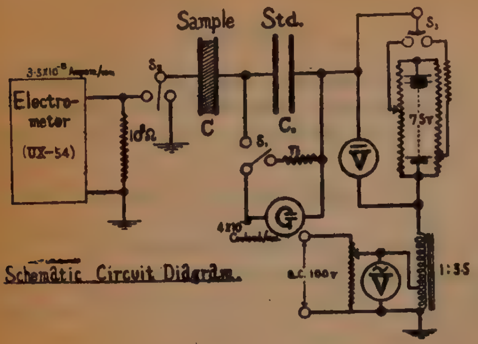

Fig. 1.

The condenser C is charged or discharged through anothor condenser C_0, which can eventually be discharged through the galvanometer G by closing the switch S_1 momentarily. C_0 is a mica condenser of capacity 1μF, which is not impregnated with paraffine and is dried with P_2O_5. In our experiment the capacity of C_0 does not affect the measurement primarily, but dielectric after-effect and leakage of C_0 will alter the result completely, so that a mica condenser was employed, whose after-effect charge and leakage in an hour was less than a few percent of the total charge. A slight existence of paraffine will increase the absorption so that we had to wash out the paraffine several times by xylol from an ordinary mica condenser, which had been impregnated with paraffine to avoid humidity. The capacity C_0 is so large compared with C, that the voltage across C is practically equal to the voltage across the voltmeter. This voltage can be varied stepwise in any desired manner by two potentiometers across the battery and a changeover switch S_3.

The charge in the condenser C_0 is measured by the ballistic stroke of the galvanometer on each discharge of C_0 by momentary closing of S_1. It should be recalled that, for this measurement to be accurate, C_0 should not be too large, otherwise a fraction of the charge in C_0 will be left in it. This is explained by the counter-electromotive force, which is generated in the galvanometer coil by the rotational velocity instantly created by the current pulse. In this respect, a galvanometer can be regarded as equivalent to a condenser C_g. (A precise equivalent circuit for a galvanometer is a parallel circuit of capacity, resistance, and inductance.) The value of C_g, which is calculated from the mechanical and electrical constants of the galvanometer, was about 50μF in our experiment (Fig. 2). Accordingly a fraction 1/50 of the charge in C_0 was left in C_0 in every discharge and was added to the subsequent discharge.

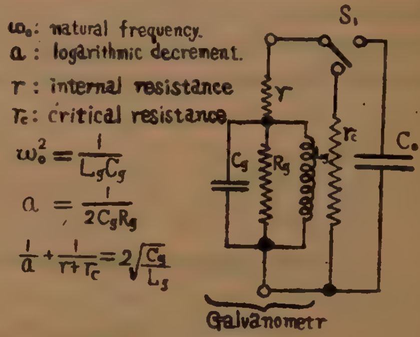
ω_0: natural frequency.
a : logarithmic decrement.
r : internal resistance
r_c: critical resistance
$\omega_0^2 = \frac{1}{L_g C_g}$
$a = \frac{1}{2C_g R_g}$
$\frac{1}{a} + \frac{1}{r+r_c} = 2\sqrt{\frac{C_g}{L_g}}$
S₁
r
C_g
R_g
r_c
C₀
Galvanometr

Fig. 2.

Equivalent Circuit of galvanometer.

All the following measurements were made by successive addition of the quantities of electricity, discharged through the galvanometer by closing of the switch S_1. Most data are therefore obtained by the summation of hundreds of individual readings, so that one false reading in a series of measurements will affect all the data after (or before) it. In this respect, the precision of the following measurement is to be regarded excellent.

The advantages of this procedure are the following;

(1) A better precision in the integrating process can be achieved compared to the integration of the readings of current itself. The latter process leads to great error especially when the current change is abrupt or irregular, a situation to be expected when the *dielectric Barkhausen effect** is present.

(2) Compared to the method of direct measurement of the voltage across a condenser by an electrometer,⁽³⁾ this method has the advantage of the freedom from the effect of the leakage of the condenser, because C_0 can be discharged before it acquires a considerable voltage.

(3) The measurement is extremely insensitive to a. c. disturbances. This feature is essential in

---

* To be reported in a later paper.

the observation of depolarization by a. c. field.

A vacuum tube electrometer (UX-54) with a high resistance of 10^8 ohms was inserted in the opposite side of C to enable a continuous measurement of the current. The reading of the current was confirmed to be consistent with the ballistic measurement when the current was stationary.

§ 3. Hysteresis Loops.

The hysteresis curve ($P-E$) of Rochelle salt was obtained by stepwise variations of the voltage, in contrast to the ordinary sinusoidal variations. The after-effect presents itself as a continuous current flow in the period that the voltage is kept constant. It was first intended to wait until the current almost vanishes, that is, the polarization is almost constant. It was soon found that such a stable state can not be attained in some minutes or even hours. So the measurements were all made by waiting 15 minutes at every value of E, taken in 10 V steps. Fig. 3 and Fig. 4 show results taken at 17.6°C and 21.6°C respectively. The vertical parts of the lines represent the variation of polarization by after-effect, whereas the tilted parts correspond to momentary polarization, by which is meant the charge obtained by discharging C_0 as soon as the voltage is changed. It corresponds approximately to discharge time of 1/5 second.

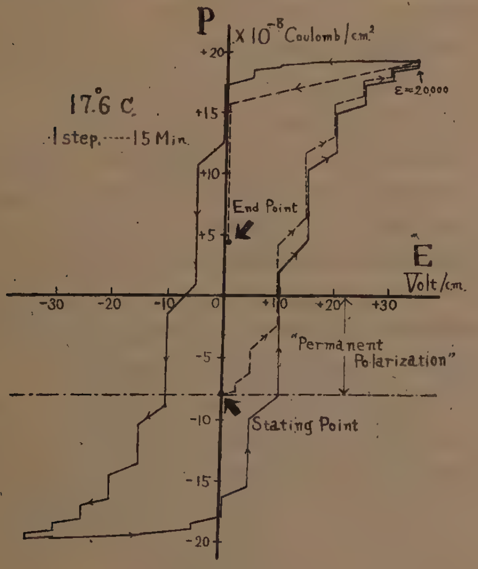

Fig. 3.
$P-E$ relation at 17.6°C.

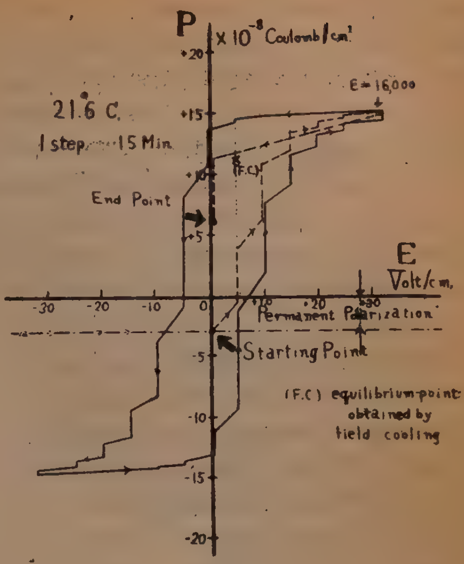

Fig. 4.
P—E relation at 21.6°C.

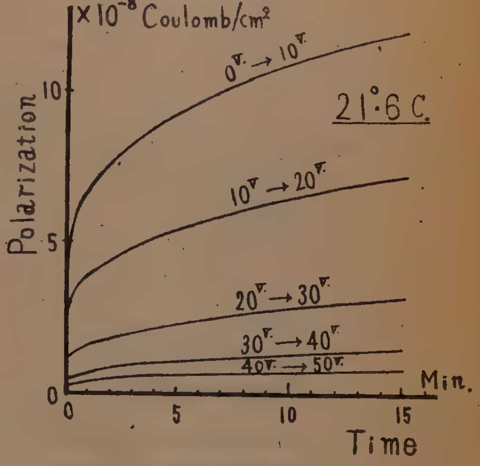

Fig. 5.
Time dependence of polarization on each step.

The time dependences of polarization on each step are shown in Fig. 5. You may note here that (1) the polarization is very gradual and does not tend to an ultimate value in measurable time. (2) For low field, the after-effect is very large and comprises the main part of polarization, while the instantaneous polarization is very small. The stronger the field, the after-effect becomes the less marked. (3) With the same voltage on the crystal, the curve corresponding to rising voltage and that corresponding to lowering voltage (two branches in the hysteresis loop) can be imagined to tend to a common limiting value. Thus a true equilibrium value for the polarization may exist for every field strength, which may be represented by a single curve lying inside the hysteresis loop (Cf. § 6, (a) Part II). The slower the speed with which we vary the voltage up and down, the nearer the hysteresis loop to the limiting curve. This ideal curve is, however, never obtained practically. Yet our experiment confirms that the breadth of the loop depends strongly on the rate of change of the field strength.

Practically no after-effect was observed at temperatures well above the Curie point, where all ferroelectric properties are absent (Fig. 6). This speaks definitely in favor of the assumption that the after-effect of Rochelle salt is a true dielectric after-effect due to the time lag in the re-polarization of spontaneously polarized domains.

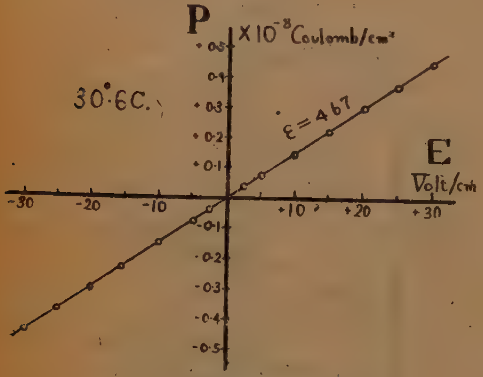

Fig. 6.

P—*F* relation at 30.6°C.

All these data were, as mentioned before, obtained by addition of successive differences of polarization. The measurement of polarization *P* necessitates in any way an integration of this sort, because we have no means of measuring directly the polarization *P*. (A true charge attached externally on the surface cannot be distinguished from the polarization charge.) We can indeed get informotion on the polarization by measuring the piezoelectric shearing strain, but precise measurement of this seems rather difficult.

A primary cause of error in such integrating measurements is the current of other origin than polarization, the leakage current. Drying with $CaCl_2 \cdot 6H_2O$ might not be sufficient for excluding this, so we shall have to provide with some means of check. One of the checks is the fact that the hysteresis curve so obtained closes. If some leakage were present, it would not have closed. This test is however, not unobjectionable, since it is possible that the leakage has been just canceled for the whole cycle. We are nevertheless convinced, on the ground mentioned below, that conduction current is negligible in our experiment.

§ 4. Permanent Polarization.

We notice in Fig. 3 and Fig. 4. that the loop is asymmetric regarding to upper and lower sides, if we take the starting point as origin. It is however more reasonable to move the line $D = 0$ (Note that D is only measured with unknown additive constant.), since the magnitude of saturation polarization must be equal in both directions on account of crystal symmetry. Thus a Rochelle salt crystal must have some spontaneous polarization or "permanent polarization" in the absence of electric field and external stress. (The existence of permanent polarization was also referred to by J. Valasek(6))

Rochelle salt loses its polarization if heated to above the Curie point. A crystal with non-vanishing polarization will gradually discharge its polarization charge as it is heated up to the Curie point. The absolute polarization of a crystal after the measurement of hysteresis loop, which corresponds therefore to the remanence point, was measured thus, and the point for the polarization above Curie point coincided very accurately with the middle point of both saturations. This may be another evidence for the smallness of leakage current.

Anomalous Dielectric Bahavior of Rochelle Salt. (II)

By Hidetosi TAKAHASI and Sigeyosi HARA.

Institute of Science and Technology, University of Tokyo.

(Read May 23, 1948. Received Dec. 28, 1948.)

§ 5. Behavior of Permanent Polarization under Varying Temperature.

The following observations are concerned with the behavior of permanent polarization under temperbture variation, and direct and alternating field.

The non-vanishment of polarization in absence of field is interpreted as the difference in the volumes of domains of each polarization. Since the polarization of each domain decreases in proportion as the temperature is raised, the resultant polarization will also decrease in the same proportion, until it would vanish altogether at Curie point, where the domain structure would disappear. If the temperature is then lowered, domains will appear at the Curie point. It might be expected that domains of both polarizations are formed in equal volume, or if this is not the case, yet the sense of resultant polarization may be quite independent of the previous sense of polarization. The result of the experiment was as follows, however:

(1) The temperature dependence of polarization depends strongly on the heating rate, but in no case does the polarization vanish at the Curie point 23°C, but persists though small up to nearly 28°C. Above 28°C, polarization vanishes perfectly, and no anomalous effects nor after-effect are observable (Fig. 7.).

(2) On lowering temperature, in the absence of field, a polarization spontaneously appears at about 23°C. The sense is always the same as the natural polarization before heating (Fig. 8). The absolute value of polarization become always less by each run of heating and cooling (Fig. 7).

Thus, the "permanent polarization", although not an absolutely invariable property, is due to a definite trend, in any way persistent and causing the formation of the domains of one polarization in preference to the domains of other polarization.

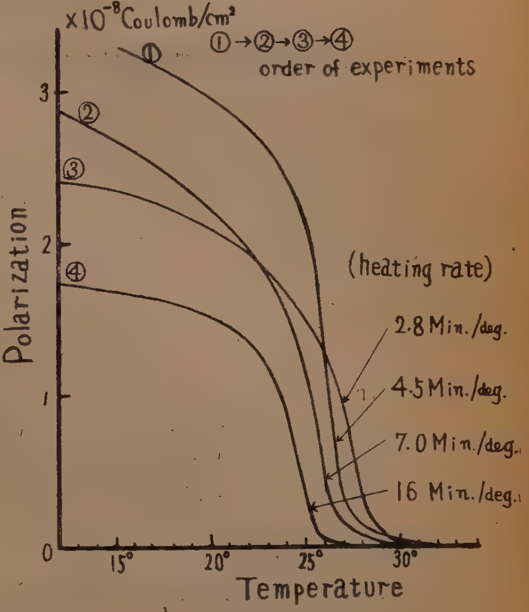

Fig. 7.
Temperature dependence of polarization by heating.

This effect has been also described by Mueller.(7)

The following experiments will further exhibit the persistence of this "permanent polarization" against external conditions.

(a) *Effect of d. c. field.*

If we apply a large field at room temperature in the direction which would reverse the original permanent polarization, the remanent polarization is of course that determined by external field. If, however, we heat the crystal after removal of field, the polarization decreases gradually, until the sign is changed and the crystal polarizes in the sense of its natural permanent polarization. On further heating, the polarization decreases again and vanishes. The reversal of polarization indicates a strong tendency of the crystal to be polarized in a definite direction (Fig. 8).

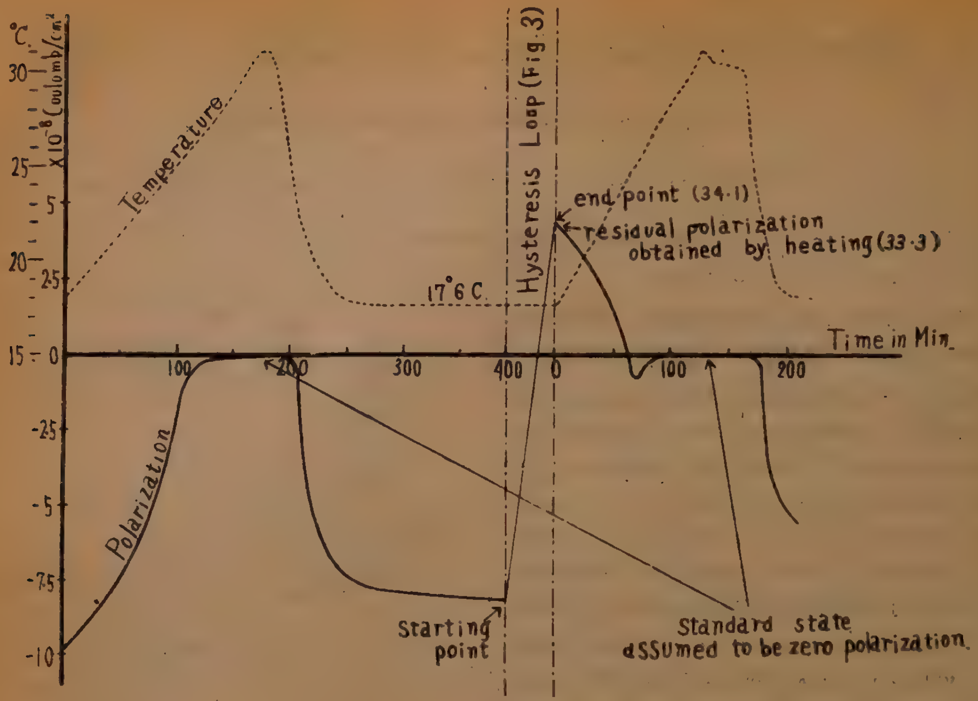

Fig. 8.
Disappearance and appearance of "permanent polarization" by heating and cooling. (before and after the hysteresis loop measurement).

(b) *Effect of a. c. field.*

Suggested by the demagnetization of a magnet by an alternating magnetic field, an a. c. voltage of 350 V_{eff} was applied to the crystal for 30 min. in an attempt to depolarize the crystal. The polarization measured subsequently showed indeed a slight decrease, but it began to increase again, tending to restore the value before depolarization (Fig. 9).

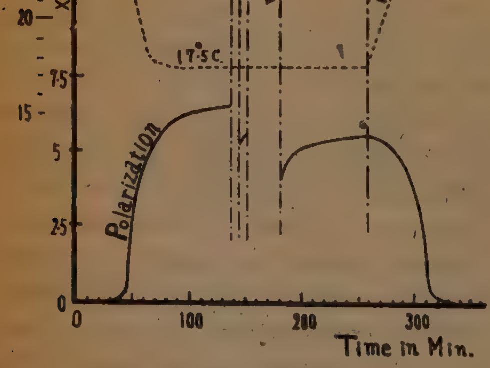

Fig. 9.
Effect of a. c. field at 17.5°C.

Since it was supposed that the permanent polarization might be especially unstable between the Curie point 23°C and the true vanishing point

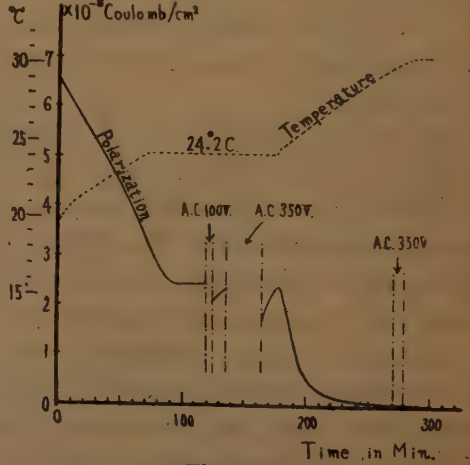

Fig. 10.
Effect of a. c. field at 24.2°C.

of spontaneons polarization, a. c. field was applied at 24°C. The result was, however, similar as below 23°C. Thus the permanent polarization is stable also against large a. c. field (Fig. 10).

(c) *Polarization above* 23°C.

It may be assumed that the remaining of polarization above 23°C might correspond to an unstable state, coexisting with a stable unpolarized state. To examine this hypothesis, the temperature was raised above 23°C, and then stopped for 3 hours at 24°C.

The polarization was observed, however, not to change a slightest as long as the temperature is constant. It even increased as the temperature was lowered accidentally. The same was observed at 25°7C. Thus the polarized state above Curie point is a really stable state (Fig. 11).

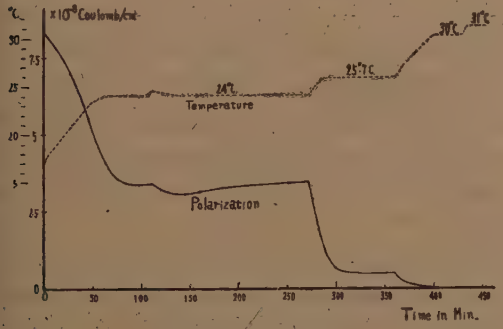

Fig. 11.

Depolarization by stepwise heating.

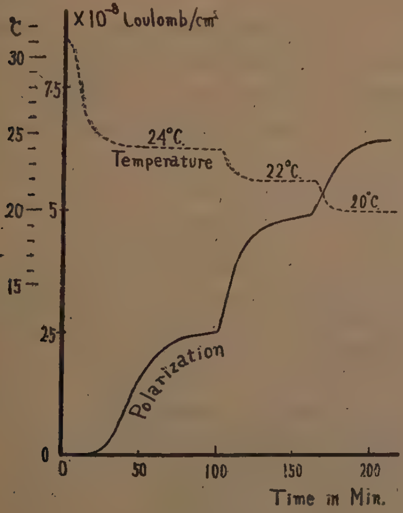

Fig. 12.

Polarization by stepwise cooling.

The reappearance of polarization as the temperature is lowered seemed to commence at about 23°C. It turned out, however, that it began to take place really at 26°C, though the rate of the increase in polarization was very low at high temperature (Fig. 12).

To summarize, it was confirmed by these experiments that the "permanent polarization" might indeed be due to an internal stress caused by a slight imperfection in the crystal, but it is very persistent and cannot be affected by thermal or electrical influences. It was also confirmed that the so-called Curie point 23°C, with which is ordinarily identified the peak point of the dielectric constant measured by a. c., cannot be associated with temperature of perfect disappearance of spontaneous polarization. In fact, the disappearance of domains seems to take place much more gradually, perhaps owing to internal stresses, so that the Curie point should have to be considered as a temperature range extended perhaps from about 20°C to about 28°C, although the 23°C would correspond to the temperature, at which most of the domains loses its spontaneous polarization.

§ 6. Miscellaneous Experiments.

(a) *Field cooling.* An experiment analogous to the magnetic cooling of ferromagnetic materials were made. The crystal was heated above the Curie point, aud a small d. c. potential (10 V) was applied, and then the crystal was cooled down to room temperature (21.6°C) under the field. This procedure was expected to realize a state which is much closer to the absolute equilibrium state mentioned in section 3 than is obtained at lower temperature. The polarization thus obtained corresponds really to a reasonable point inside the hysteresis loop (Fig. 4). It was also noticed incidentally that this procedure increases the permanent polarization contrary to the simple heating and cooling (Fig. 13).

(b) *Effect of large field applied for a long time.* Although at first sight the ultimate state of complete saturation seems to be rapidly attained at larger field, this is not the case. D. c. voltage which is much greater than the minimum voltage for saturation was applied to the crystal and the

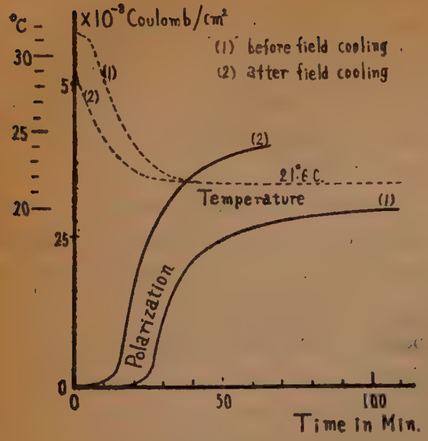

Fig. 13.

Effect of field cooling.

current was observed for several hours. The current followed strictly the empirical formula

$$i \propto t^{-n} \ (n \simeq 1) \quad \text{or} \quad P = P_0 + At^p \quad (1 > p > 0)$$

for all t measured (Fig. 14). The last value of the current observed was 3×10^{-12} amp. corresponding to $t = 6 \times 10^3$ seconds. The leakage, if present, must be still smaller. This sets the upper limit of specific conductivity at 3.6×10^{-16} mho cm^{-1}; Rochelle salt will be classified among the pretty good insulators!

The total polarization of the crystal polarized for a long time was measured by discharging at room temperature and subsequent heating above Curie point. The polarization thus obtained, 694 e.s.u. at 17.5°C, was higher than the saturation ordinarily obtained from hysteresis loop of 15 min. steps, 585 e.s.u. Thus the ordinary value of saturation obtained from hysteresis loop is not a true saturation corresponding to perfect alignment of all domains.

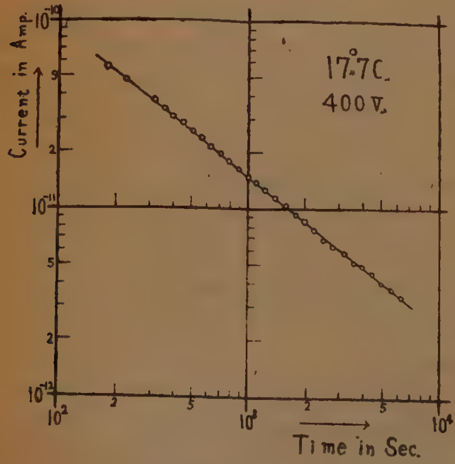

Fig. 14.

Time dependence of after-effect current.

§ 7. Summary.

(1) Our results show that the form of the hysteresis loop is dependent on the velocity of the variation of field (the frequency), and the loop becomes thinner as the velocity is decreased, but it never collapses entirely. The coercive force is therefore not a sharply defined constant. The dielectric after-effect is especially large in weak fields.

(2) A real crystal of Rochelle salt always possesses a non-vanishing polarization in virgine state, that is, when it is cooled down from above the Curie point in the absence of field. This spontaneous polarization is quite stable against external field (direct and alternating) and has always the same sense each time it is cooled from above the Curie point.

(3) The Curie point, defined as the temperature of the vanishment of spontaneous polarization, is not a sharply defined point located at 23°C, but is distributed rather broadly between about 20°C. and 28°C.

In conclusion, we wish to express our hearty thanks to Dr. H. Kawai of the Kobayasi Institute of Physical Research, who was always ready to give us the samples, as well as helpful technical advices.

References.

(1) H. Kawai: J. Phys. Soc. Jap. **3**, (1948) 105.
(2) J. Valasek: Phys. Rev. **17**, (1921) 476; **24**, (1924) 560.
(3) I. Kurtschatow: Phys. Zeits. d. Sowj. **7**, (1935) 631.
(4) R. D. Schulwas-Sorokin & M. V. Posnov. Phys. Rev. **47**, (1935) 166.
(5) H. Kawai: J. Phys. Soc. Jap. **3**, (1948) 8.
(6) J. Valasek: Phys. Rev. **17**, (1921) 476.
(7) H. Mueller: Phys. Rev. **47**, (1935) 185.

A Statistical Mechanical Treatment of Conduction Electrons. An Attempt to the Theory of the Superconductivity.

By Hiroshi ICHIMURA.

Physical Institute, Faculty of Science, Tokyo University.

(Recieved Jan. 13, 1949)

§ 1. Introduction.

The properpties of the conduction electron in the metal have been treated by Sommerfeld(1) using the Fermi-Dirac statistics, and with the appropriate quantum mechanical suppliments this theory could explain very well the experimental facts concerning the ordinary electrical condution, the magnetic susceptibility and the thermal properties of the system. Inspite of these success, however, the phenomena of the superconductivity which occurs in some metals at extemly low temperatures could not be predicted by this Sommerfeld theory. On the other hand, the main role of the conduction electron in this phenomena has little to be doubted considering various experimental facts(2) and their theoretical analyses.(3)

The origin of this discrepancy may be attributed to the nature of the approximations made in the Sommerfeld theory, as has been pointed out by many authers. It is essentialy the one-body approximation and the couplings between the electrons are taken into account to the Hartree-approximation. Many attempts(4) have been made to improve this point, but on account of unsurmountable difficulties in the treatment of the many body problems, we have no definite solutions of this problem up to the present time.

In this article*, we give a theoretical attack to this problem along a line somewhat different from those of previous authers. We modify the ordinary Fermi distribution function by introducing 'the cooperative interaction in the momentum space' between the electrons near the Fermi surface of their normal distribution. By a statistical reasonig, we get a special state for the electron system, which is stable below some specified temperature. We consider this state as the superconducting state of conduction electrons and calculate the jump of the specific heat of this system at the transition temperature. The formula for this jump of the specific heat is essentially equal to that which has been derived by Kok from phenomenological standpoint and agrees very well with the experimental data. We can not enter here in the trasport properties of our system, but the treatment of the magnetic susseptibility with our model will be given in the next paper.

§ 2. The Partition Function of the System of conduction Electrons.

a) Energy states. In the one-body approximation, the wave function of the conduction electron in a metal has the following form

$$\psi_{\boldsymbol{k},n}(\boldsymbol{r}) = \exp(i\boldsymbol{k}\boldsymbol{r})u_{\boldsymbol{k},n}(\boldsymbol{r}) \qquad (2.1)$$

where $\boldsymbol{r}$ is the position vector (x, y, z) and $\boldsymbol{k}$ is a wave number vector (k_x, k_y, k_z). $\boldsymbol{k}$ may be defined in terms of the reciprocal lattice of the crystal if the Born-von Karman boundary conditions are used in determining the function (2.1). $u_{\boldsymbol{k},n}$ has the periodicity of the lattice, and indicates the atomic energy state from which the conduction level are originated.

The functions (2.1) are the plane waves modulated by $u_{\boldsymbol{k},n}$, which extend all over the metal specimen (we take its volume as V in the following), so the electron has no localizability in the configuration space, and we must designate it in the momentum space, or in the same sence, in the wave number space. The energy of these waves depends upon $\boldsymbol{k}$,

$$\varepsilon_n = \varepsilon_n(\boldsymbol{k}) \qquad (2.2)$$

---

* See also the authers preliminary treatment, Jornn. of Phys. Soc. Japan 2 (1947), 184.

Actually these expressions are obtained by the so-called Wigner-Seitz(6) method or by the method of Herring,(7) but all of these methods will be insufficient in the acuracy for such a subtle problem as the superconductivity.

In the simplest case, $u_{k,n}$ is a constant, so that we get a free-electron-type wave function for which the energy is expressed as

$$\varepsilon(\boldsymbol{k}) = \frac{\hbar^2}{2m}k^2, \qquad k = |\boldsymbol{k}|$$

where $\hbar$ is Plank's constant divided by 2π and m is the mass of the electron. The Sommerfeld theory corresponds to this case, and, owing to the Pauli principle the states of electrons at 0°K fill the sphere of the radious $r_f = \left(\frac{3N}{8\pi N}\right)^{1/3}$ in the wave number space. To the next approximation the effective mass $m^*(=\partial^2\varepsilon/\partial k^2)$ of the electron is usually used instead of m. m^* is essentially the function of k but its precise form will be very difficult to obtain, so in the following treatment we assume rather arbitrarily a certain values for this m^*.

b) *The specification of the model.* The metals which become superconducting at sufficiently low temperatures are all multivalent, so it may be considered that in these case the overrapping of the Brillouin zones will occur and the dependence of the energy on $\boldsymbol{k}$ will be very complicated near the zone boundaries.

Now we assume that for these metals the Fermi surface of the distribution is situated in these complicated domain and some inter-electronic interactions are more decidedly important for the electron having their energy states outside a certain critical surface ($|\boldsymbol{k}| = \text{const.}$) near the Fermi surface, than for the electrons in the other part of the Fermi sphere. With these assumptions we proceed as follows.

c) *The partition function of the system.* The partition function of the system of the N free electrons may be written in the following form,

$$e^{-\beta\Phi} = \sum_{N_1,\cdots N_l,\cdots,} \Pi \frac{\Delta_l!}{N_l!(\Delta_l - N_l)!} e^{-\beta N_l \varepsilon_l}$$

$$\beta = 1/kT \tag{2.3}$$

$$\sum_l N_l = N \tag{2.4}$$

where Ψ is the free energy of the system, N_l is the number of the particles in the state ε_l, Δ_l is the level density, k is the Boltzmann's constant and the summation is to be taken over all possible values of N_l's under the restriction of (2.4). From this partition function we can derive the usual Fermi distribution for the equilibrium values $\bar{N}_l$ of N_l.

In the present case, we modify (2.3) as

$$e^{-\beta\Phi} = \sum\left\{\prod_l^{l^+-1} \frac{\Delta_l!}{N_l!(\Delta_l - N_l!)} e^{-\beta N_l \varepsilon_l}\right.$$

$$\times \prod_{\lambda=l^+}^{\infty} \frac{\Delta_\lambda!}{N_\lambda!(\Delta_\lambda - N_\lambda)!} e^{-\beta N_\lambda \varepsilon_\lambda - \beta U_\lambda(N_{l^+},\cdots\cdots)} \tag{2.5}$$

$$\sum^{l^+-1} N_l + \sum_{l^+} N_\lambda = N \tag{2.6}$$

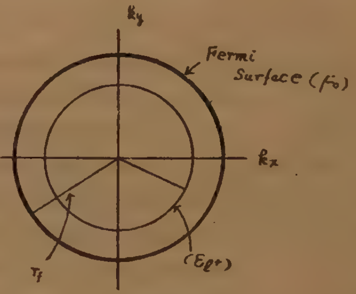

Fig. 1

corresponding to the assumptions above mentioned. Here we have devided the system into two parts in the momentum space, in one of which ($0-l^+-1$) the electrons may be assumed to be approximated by the Sommerfeld model but in the other part ($l^+-\infty$) some interactions between them become more important. This interaction term is expressed by $U_\lambda(N_{l^+},\cdots\cdot)$, whereby another approximation is made that it is determined by the number of the electrons which is in the neighbouring states in the momentum space. The critical ε_{l^+} value is chosen to be closely near the Fermi surface for present purposes. Proceeding in the usual manner, we get the following distribution,

$$\bar{N}_l = \frac{\Delta_l}{1+\exp(\alpha+\beta\varepsilon_l)} \tag{2.7}$$

$$\bar{N}_\lambda = \frac{\Delta_\lambda}{1+\exp(\alpha+\beta\varepsilon_\lambda+\beta\partial U_\lambda/\partial N_\lambda)} \tag{2.8}$$

$$\alpha = -\zeta/kT \tag{2.9}$$

where ζ is the thermodynamic potential per electron of the system. In the following, we write N_l instead of $\bar{N}_l$ without the fear of the confusion. Using the ordinary level density formula of the free electron for Δ_l, we get

$$N=\frac{3}{2}N\left(\frac{kT}{\mu_0}\right)^{\frac{3}{2}}\int_0^{\varepsilon_{l+}/kT}\frac{x^{\frac{1}{2}}dx}{1+\exp(x-\zeta/kT)}+\sum_\lambda N_\lambda \tag{2.10}$$

where

$$\mu_0=\frac{h^2}{8m}\left(\frac{3N}{\pi V}\right)^{\frac{2}{3}}$$

and setting

$$N_s=\sum_\lambda N_\lambda,\ N_r=\frac{3}{2}N\left(\frac{kT}{\mu_0}\right)^{\frac{3}{2}}\int_{\varepsilon_{l+}/kT}^{\infty}$$

$$\times\frac{x^{\frac{1}{2}}dx}{1+\exp(x-\zeta/kT)} \tag{2.11}$$

we can write (2.10) as

$$N-(N_s-N_r)=\frac{3}{2}N\left(\frac{kT}{\mu_0}\right)^{\frac{3}{2}}\int_0^\infty\frac{x^{\frac{1}{2}}dx}{1+\exp(x-\zeta/kT)} \tag{2.12}$$

Because of our assumptions, we may consider as $N\gg N_s-N_r$ and $\zeta\gg kT$. This means that the Fermi degeneracy of the conduction electrons has not been affected seriously by our special modification. So we can expand the right hand side of (2.12) as in the Sommerfeld theory and get for ζ,

$$\zeta=\left(\mu_0-\frac{\pi^2}{12}\frac{k^2T^2}{\mu_0}\right)-\frac{2}{3}\mu_0\frac{N_s-N_r}{N} \tag{2.13}$$

the first term of this equation is the thermodynamic potential of the usual Fermi gas and the next term is the correction term due to our modification.

Now we make a rather arbitrary assumption that in (2.8) we can put

$$\frac{\partial U_\lambda}{\partial N_\lambda}=\left\langle\frac{\partial U}{\partial N}\right\rangle_{Av} \tag{2.14}$$

for all λ and

$$\left\langle\frac{\partial U}{\partial N}\right\rangle_{Av}=-\psi\frac{N_s-N_r}{N} \tag{2.15}$$

where ψ is the proportionality constant.

Assumption (2.15) means that the interaction assumed here is of the nature of the coorperative interaction and its energy per one electron is proportional to the excess number of electrons occupying these special levels over the normal Fermi distribution. This will correspond to the Bragg-Williams approximation in the theory of alloys and $(N_s-N_r)/N$ plays the role of the order-disorder parameter in that theory.

So it results from (2.13)

$$\xi=\mu_0\left(\frac{kT}{\mu_0}\right)^{\frac{3}{2}}\times$$

$$\delta\left\{\int_c^\infty\left[\frac{1}{1+\exp\left(x-\left\{\zeta_f+\left(\frac{3}{2}\psi/\mu_0-1\right)\xi\right\}\Big/kT\right)}\right.\right.$$

$$\left.-\frac{1}{1+\exp(x-\{\zeta_f-\xi\}/kT)}\right]x^{\frac{1}{2}}dx \tag{2.16}$$

where

$$\zeta_f=\mu_0-\frac{\pi^2}{12}\frac{k^2T^2}{\mu_0},\quad \xi=\zeta_f-\zeta,\quad c=\varepsilon_{l+}/kT,$$

and expressions in (2.7) (2.8) and (2.15) are used. The parameter δ is introduced to take into account that the effective mass** of the electron in our special state is different from m in the expression of μ_0, δ is a function of the en rgy as remarked previously and in our case it may be considered to change its value with the degree of the excess occupation of the special states, since the energy of these levels change with the number of the electrons which enter into them. We set $\delta=\delta_0$ when there is no excess occupation and $\delta=\delta_*$ in the case of maximum occupation at absolute zero of the temperature. Concerning ε_{l+}, we set as

$$N_s=N_s{}^*\text{ and }N_r=0\text{ at }T=0,$$

corresponding to our assumptions, so we get from (2.8)

$$N_s{}^*=\frac{3}{2}\left(\frac{kT}{\mu_0}\right)^{\frac{3}{2}}\delta^*\int_{\varepsilon_{l+}}^{\mu_0+\left(\frac{3}{2}\psi/\mu_0-1\right)\cdot\frac{2}{3}\mu_0\frac{N_s{}^*}{N}}\varepsilon^{\frac{1}{2}}d\varepsilon$$

$$\therefore\quad \varepsilon_{l+}=\mu_0+\mu_0\frac{N^*}{N}\left\{\left(\frac{\psi}{\mu_0}-\frac{4}{3}\right)+\frac{2}{3}\left(1-\frac{1}{\delta_*}\right)\right\} \tag{2.17}$$

It is to be noticed here that the above effective masses of the electron may be regarded to differ from the effective mass which is estimated from the electronic specific heat formula for the metals. This may be seen when we consider the approximational method used in deriving that formula.

** If we write this effective mass as md, δ is equal to $d^{\frac{3}{2}}$.

By (2.16), we can determine ξ as the function of the temperature, consequently ζ may be given as the function of the temperature. From ζ all thermodynamic properties of the system are calculated using the formulas of thermodynamics.

§ 3. The Transition Point.

It will easily be seen that Eq. (2.16) has the solution for all temperatures. Below a certain temperature, the non-zero solution for ξ is obtained, that is to say, there exists a branch-point-singurarity for ζ at that temperature. Since the state which corresponds to this non-zero ξ has the lower thermodynamic potential as may be seen from (2.13), we can expect a phase change at this critical temperture. In the following we call the new stable state with $\xi \neq 0$ as s-state and the state with $\xi = 0$ as n-state.

To show these circumstances approximately, we expand the right hand side of (2.16) in the neighbourhood of $\xi = 0$ as follows,

$$\left(\frac{\xi}{kT}\right) = \left(\frac{\xi}{kT}\right)\frac{3}{2}\frac{\psi}{\mu_0}\delta_0\left(\frac{kT}{\mu_0}\right)^{\frac{1}{2}} \int_c^\infty \frac{\exp(x-\zeta_f/kT)}{[1+\exp(x-\zeta_f/kT)]^2} x^{\frac{1}{2}} dx$$
$$+\frac{1}{2}\left(\frac{\xi}{kT}\right)^2 \frac{3}{2}\frac{\psi}{\mu_0}\left(\frac{3}{2}\frac{\psi}{\mu_0}-2\right)\delta_0\left(\frac{kT}{\mu_0}\right) \cdot \int_c^\infty \frac{\exp(x-\zeta_f/kT)\,[\exp(x-\zeta_f/kT)-1]}{[1+\exp(x-\zeta_f/kT)]^3} x^{\frac{1}{2}} dx$$
$$+\cdots \qquad (3.1)$$

If we neglect the higher terms than the second order of $\left(\frac{\xi}{kT}\right)$, (3.1) gives the quadratic equation for $\left(\frac{\xi}{kT}\right)$. So the condition for the double root at $\xi = 0$, i. e., the condition for the branching of the thermodynamic potential ζ is given by

$$\frac{3}{2}\frac{\psi}{\mu_0}\delta_0\left(\frac{kT}{\mu_0}\right)^{\frac{1}{2}} \int_c^\infty \frac{\exp(x-\zeta_f/kT)}{[1+\exp(x-\zeta_f/kT)]^2} x^{\frac{1}{2}} dx = 1. \qquad (3.2)$$

From this the critical temperature T_c is determined. Partially integrating, it becomes

$$\frac{3}{2}\frac{\psi}{\mu_0}\delta_0\left(\frac{kT}{\mu_0}\right)^{\frac{1}{2}} \left\{ \left.\frac{-x^{\frac{1}{2}}}{1+\exp(x-\zeta_f/kT)}\right|_c^\infty + \frac{1}{2}\int_c^\infty \frac{x^{-\frac{1}{2}}dx}{1+\exp(x-\zeta_f/kT)} \right\} = 1$$

where the second term in the bracket may be negrected on account of our assumptions for the valaes of ε_{l^+} and ζ_f. Hence we have

$$\frac{\mu_0}{kT_c}\frac{N_s^*}{N}\left\{\left(\frac{\psi}{\mu_0}-\frac{4}{3}\right)+\frac{2}{3}\left(1-\frac{1}{\delta *}\right)\right\}+\frac{\pi^2}{12}\frac{kT_c}{\mu_0} = \log\left(\frac{3}{2}\frac{\psi}{\mu_0}\delta_0-1\right) \qquad (3.3)$$

For our present purposes we need further the condition for the phase change of the second order in the thermodynamical sence. This is expressed as

$$\left(\frac{\partial\xi}{\partial T}\right)_{T_c-0} = 0$$

And we get

$$\frac{\mu_0}{kT_c}\frac{N_s^*}{N}\left\{\left(\frac{\psi}{\mu_0}-\frac{4}{3}\right)+\frac{2}{3}\left(1-\frac{1}{\delta_*}\right)\right\} = \frac{\pi^2}{12}\frac{kT_c}{\mu_0} \qquad (3.4)$$

This is the condition for the continious change of the entropy at the transition point.

From (3.3) (3.4) the parameters N_s^* and ψ are expressed by T_c and δ_0, δ_*.

$$\frac{N_s^*}{N} = \frac{\pi^2}{8}\left(\frac{kT_c}{\mu_0}\right)^2 \frac{\delta_0\delta_*}{2\delta_*-\delta_6-2\delta_*\delta_0}$$
$$\qquad (3.5)$$
$$\psi\frac{N_s^*}{N} = \frac{\pi^2}{12}\frac{(kT_c)^2}{\mu_0}\frac{\delta_0\delta_*}{2\delta_*-\delta_0-2\delta_*\delta_0}$$

§ 4. The Discontinuity ofthe Specific Heat.

The phase change of the second order the means the discontinuous change of the second derivatives of the thermodynamic function with respect to independent variables. In our case, the analysis shows that at T_c the following relations between the s-state and n-state are introduced.

$$\varDelta\zeta = \zeta_s - \zeta_n = 0$$

$$\varDelta S = S_s - S_n = \varDelta\left(\frac{\partial\zeta}{\partial T}\right) = -\left(\frac{\partial\xi}{\partial T}\right)_{T_c-0} = 0$$

where S is the entropy of the system. The discontinuity appears in the specific heat and we can calculate this by the formula

$$\varDelta C = C_s - C_n = \varDelta\left(-T\frac{\partial^2\zeta}{\partial T^2}\right) = T_c\left(\frac{\partial^2\xi}{\partial T^2}\right)_{T_c-0} \qquad (3.6)$$

The difference between C_v and C_p can be neglected. By lengthy but straightforward calculations we get from (3.1) and (3.6)

$$\Delta C \doteqdot \frac{\pi^2}{3} \frac{k^2 T_c}{\mu_0} \frac{\delta_0}{1-\delta_0} \qquad (3.7)$$

and

$$\left(\frac{\partial C_s}{\partial T}\right)_{T_c} = \left(\frac{\partial^2 \xi}{\partial T^2}\right)_{T_c-0} \doteqdot \frac{\pi^2}{6} \frac{k^2 T_c}{\mu_0} + \frac{\pi^2}{3} \frac{k^2}{\mu_0} \frac{\delta_0}{1-\delta_0} \qquad (3.8)$$

So we get the solid curve in Fig. 2., this may be considered to correspond to the experimental curve shown in Fig. 3.. The entire relationship between C and T cannot be obtained from our approximate treatment.

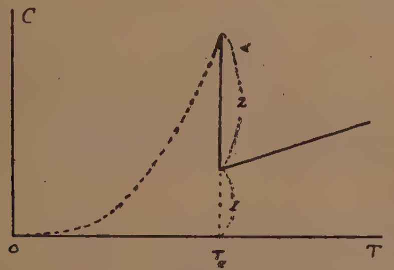

Fig. 2.

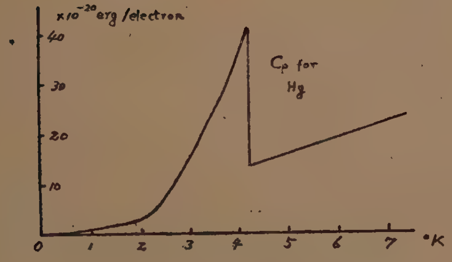

Fig. 3.

If we set $\delta_0 \doteqdot \frac{1^*}{2}$ in (3.7), the factor $\frac{\delta_0}{1-\delta_0}$ becomes 1, so we get

$$\Delta C = \frac{\pi^2}{3} \frac{k^2 T_c}{\mu_0} = 2\gamma T_c, \quad \left(\frac{\partial C_s}{\partial T}\right)_{T_c} = 5\gamma \qquad (3.9)$$

where γ is the constant which appears in the electronic specific heat formula in the Sommerfeld theory, that is

$$C = \frac{\pi^2}{6} \frac{k^2 T}{\mu_0} = \gamma T, \quad \frac{\partial C}{\partial T} = \gamma$$

The first of the formulae in (3.9) has been obtained by Kok(5) from a phenomenological reasoning different from ours. This agrees very well with the experimental data as shown in Table I.

Table I.

	ΔC obs cal/mol	ΔC by (3.9)	μ_0 erg/molec	T_c K°
Hg	0.0035	0.0037	0.831×10^{-12}	4.17
In	0.0020	0.0026	1.116	3.37
Sn	0.0024	0.0023	1.444	3.69
Pb	0.0083	0.0117	0.5557	7.26
Tl	0.0014	0.0018	1.2043	2.38
Ta	0.0104	0.0193	0.2048	4.38
Nb	0.144	0.1248	0.0660	9.2

From (3.5) the order of the magnitude of the number of electrons in s-states and of the interaction energy assumed to operate in the s-tate, can be determined. The former is the order of 10^{15}/cm^3 and the latter is 10^{-8}eV or 10^{-19} erg. Both do not contradict to our assumptions made in the caluculation and are not unreasonable values.

From this value of the interaction energy, we may imagine that the origin of this interaction is the usually neglected terms in the interaction operator between two electrons(8). It will go too further, however, to enter here into this problem.

§ 5. Conclusion.

Our present treatment follows along the line of the idea in the theory of the collective electron ferromagnetism presented by Stoner and Hirone-Miyahara, and uses the conception of the local field in the theory of the order-disorder phenomena in the alloy. We think that our simple model for the special state of the electron system can explain the long range order in the momentum space which is considered to exist in the system of the electrons when it is in the superconducting state as shown in F. London's recent paper(9). Our model will also be convenient for the explanation of the super-transfer process in the superconducting state, but its treatment will be left in future, since the more precise calculation of the energy state of the electron in the metal will be neccessary for this purpose(10). In the next paper we intend to calculate the magnetic behavior of our system.

Finally, the auther expresses his hearty thanks to Professor T. Sakai for the kind guidance in the research and to his friends Mr. R. Kikuchi, A. Mi-

---

* This means that the effective mass here assumed is about 1/2.8 of that which is used in μ_0.

yake and N. Hashizume for their valuable discussions and suggestions.

References.

(1) A. Sommerfeld: Zeits. f. Physik **47** (1928) 1.

(2) E. F. Burton, H. G. Smith & J. O. Wilhelm: "Phenomena at the Temperature of Liquid Helium" (1940).

(3) C. J. Gorter and H. Casimir: Physica **1** (1934), 281.

(4) R. de L. Kronig: Zeits. f. Physik **78** (1932), 744; **80** (1932), 203. A. Papapetrou: Zeits. f. Physik **111** (1937), 318. J. C. Slater: Phys. Rev. **51** (1937), 195; **52** (1937), 214; H. Welker: Zeits. f. Physik **114** (1939), 525.

(5) J. A. Kok: Physica **1** (1934), 1103.

(6) E. Wigner and F. Seitz: Phys. Rev. **43** (1933), 804; **46** (1934), 509.

(7) C. Herring: Phys. Rev. **57** (1940), 1167.

(8) G. Breit: Phys. Rev. **34** (1929), 553.

(9) F. London: Phys. Rev. **74** (1948), 562.

(10) O. Klein and J. Lindhard: Rev. Mod. Phys. **17** (1945), 305.

A Study on Corrosion of Iron by Electron Diffraction.

By Hide YOSHIOKA.

Physical Institute, Nagoya University.

(Received, Jan. 21, 1949)

§ 1. Introduction.

The method of electron diffraction has been applied, ever since the days of its discovery, to the study of corrosion of iron immersed in salt solution(1). The detailed research, however, was performed by S. Miyake several years later(2). His results were as follows: The brown rust which was produced as a thick layer on the surface of iron was $\gamma\text{-Fe}_2\text{O}_3\cdot\text{H}_2\text{O}$, and had the same crystal structure as the mineral lepidocrocite. This rust was easily washed off in a water jet. The underlying substance which remained adhered to the surface varied with the period of immersion. At the initial stage of corrosion the diffraction pattern consisted of two strong rings besides which only very faint and obscure ones were present. This pattern was inferred by Miyake to be due to an intermediate substance between $\gamma\text{-Fe}_2\text{O}_3\cdot\text{H}_2\text{O}$ and its anhydride $\gamma\text{-Fe}_2\text{O}_3$, and he denoted this substance by the "two ring substance (T. R. S.)" for convenience. The product after a longer period of immersion was identified with $\gamma\text{-Fe}_2\text{O}_3$. Finally after a still longer immersion, a composite of several kinds of products was observed.

The above studies dealt with the corrosion of *pure* iron. As regards the corrosion of *cast* iron, a similar experiment as Miyake's was lately performed in our laboratory(3). The brown rust in this case was also $\gamma\text{-Fe}_2\text{O}_3\cdot\text{H}_2\text{O}$. The examination of the products adhered to the surface, however, showed two kinds of patterns which occurred separately in some cases, and simultaneously in others, by chance. One of them was T. R. S., while the other was unknown either in cathode-ray or X-ray analysis. The latter consisted of very sharp rings, so it was conveniently denoted by the "sharp-ring substance (S. R. S.)".

The present research was performed to find the nature of S. R. S. and to clarify the relations between S. R. S. and other corrosion products of iron.

§ 2. The Green Rust Produced in an Immersion Experiment.

Three possible answers were considered to the question in what condition S. R. S. is formed: (1) S. R. S. is produced also in the case of *pure* iron under certain conditions; (2) it is peculiar to the case of *cast* iron; or (3) it is due to the impurities contained in the cast iron specimen. In order to determine which is the case, pure iron specimens were subjected to corrosion under the same condition as in the case of cast iron.

The specimens used in the experiment were prepared from the electrolytic iron which had the purity of 99.98% Fe. They were small discs of 4 mm in diameter and 1.5 mm in thickness, having surfaces abraded with an emery cloth "Riken Collundum BO". They were placed at the bottom of a test tube, whose diameter was about 1 cm, and which was filled with an aqueous 1% NaCl solution to a height of 1 cm. The temperature during the immersion was 25°–29°C. After a certain period of immersion, they were taken out and washed vigourously in a water jet to remove the brown rust which covered the surface, and desiccated as rapidly as possible to be examined by the diffraction method.

Table I. The substance on the surface removed of brown rust.

Immersion period / Substance	0.5—3 h	3—25 h	25—50h	more than 50 h
T. R. S.	③	②	1	0
γ-Fe_2O_3	0	1	③	1
Composite	0	0	1	1
S. R. S.	0	2	0	0

The diffraction apparatus employed in this experiment was of a horizontal type (Kikuchi type) having the camera length of 30 cm. The accelerating voltage of about 30 KV was applied to electrons.

In total, 15 specimens were examined. The results are summarized in Table I, in the same manner as in Miyake's paper. The column on the left represents the substance on the surface. The numbers in it identify specimens on which the corresponding substance was formed after an immersion of corresponding period. This table shows the same trend as Miyake's result except in the last row, where two specimens showed the pattern of S. R. S. Along the edge of one of them a crescent-shaped area covered with a green rust was observed. The very pattern of S. R. S. was obtained from this portion. Afterwards, it was noticed that in most specimens the green rust was formed on the lower surface, which almost contacted the bottom of the vessel, after one day's immersion. The diffraction pattern of this green rust was that of S. R. S. in every case. Thus, S. R. S. was concluded to be the green rust of iron and neither peculiar to cast iron nor due to impurities.

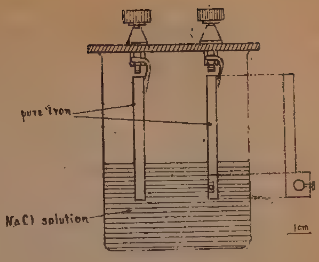

Fig. 1.

This rust was converted to γ-$Fe_2O_3 \cdot H_2O$ in a few hours when kept in open air without drying. According to a literature(4), the green rust is formed when the corrosion takes place in an oxygen-poor condition. Its formation on the lower surface of specimens might be due to this fact. In this connection it must also be noted that our vessel employed for immersion was a test tube while Miyake's was a shallow vessel. In order to check this property, specimens were immersed in an oxygen-poor salt solution which had been boiled previously to diminish the content of the dissolved oxygen and whose surface was covered with liquid paraffin to prevent the intrusion of oxygen. The specimens corroded under this condition showed the pattern of S. R. S. in most cases, though the green rust was not observed on their surfaces by naked eyes. Thus the formation of the green rust in an oxygen-poor condition is well confirmed.

§ 3. The Rust Formed by Electrolysis.

According to the general conclusion of a great number of studies, the process of corrosion of iron is an electrochemical one, in which electric currents pass between different parts of a metallic surface. Such currents may be generated by local differences of physical and chemical properties in the metal, although they are frequently connected with differences in the oxygen-supply to different parts of the metal. However, the exact method of the generation of currents does not seem to affect the formation of corrosion products seriously. Therefore, in order to simplify the complicated circumstance, the corrosion accompanying electrolysis was examined. The equipment used for electrolysis is shown in Fig. 1. Electrodes made of pure iron were immersed in an aqueous 1% NaCl solution which was contained in a beaker. The anode had a hole in the middle of its plate-shaped portion, in which a specimen for electron diffraction was inserted. The latter was prepared in the same way as in § 2 except the finishing with a finer emery paper (00). After electrolysis it was washed in a water jet, dried with filter paper and brought into the diffraction apparatus as soon as possible.

The corrosion product adhering to the anode surface varied with the current densities. This is shown in Table II: At small current densities 2–4 mA/cm^2, the rust was mainly T. R. S., and sometimes a trace of γ-$\mathrm{Fe_2O_3\cdot H_2O}$ was observed. On the other hand, at large current densities 20–45 mA/cm^2, it was S. R. S., i. e. the green rust in almost every case. A faint pattern of T. R. S. overlapped on it generally. No noticeable change of the pattern was observed, although the period of attack was varied between 0.5 and 10 min. The two species of rusts, i. e. T. R. S. and the green rust, obtained in this experiment, are the same as those described in § 1 concerning cast iron. It is important that the formation of the two species was controled by giving the current density in the present experiment, while it was by chance in the immersed cast iron.

During the electrolysis, besides that adhering to the anode surface, rust was produced as precipitates in the solution. At the first stage a greenish white colloidal substance appeared in the space between the electrodes. It rapidly became green, and settled down slowly at the bottom of the beaker. This rust was also identified with S. R. S. by the diffraction method.

Table II. Corrosion product adhered to the anode surface.

Current density / Substance	2–4 mA/cm^2	5–6 mA/cm^2	20–45 mA/cm^2
T. R. S.	1	1	0
T. R. S. +small Amt. of γ-$\mathrm{Fe_2O_3\cdot H_2O}$	②	0	0
S. R. S. +small Amt. of γ-$\mathrm{Fe_2O_3\cdot H_2O}$	0	②	2
S. R. S.	0	0	③

§ 4. Oxidation and Dehydration of the Green Rust.

The precipitate described at the end of the last section was very voluminous and accumulated in a great mass when electrolysis was continued. The upper part of the green precipitate turned yellowish brown after an elapse of time, the converted rust being proved to be γ-$\mathrm{Fe_2O_3\cdot H_2O}$ in accordance with the result of § 2. This conversion to brown rust extended to the whole precipitate, when the amount of the latter was small. However, when the amount was comparatively large, the lower part of the precipitate became more compact and darker in colour on standing, and finally produced a black granular substance at the bottom. This was proved to be $\mathrm{Fe_3O_4}$ or γ-$\mathrm{Fe_2O_3}$ by the diffraction method. Although they cannot be distinguished by spacing, it is surely $\mathrm{Fe_3O_4}$, because γ-$\mathrm{Fe_2O_3}$ usually has a reddish colour.

The green rust remains unchanged in vacuo at least for several hours. It turns into the T. R. S., when it is dried perfectly in vacuo and then exposed to air.

Since the green rust is considered to be an earlier product of corrosion than the brown rust γ-$\mathrm{Fe_2O_3\cdot H_2O}$, it seems to be a hydrate of some kind of oxide. In order to find the corresponding anhydride a dehydration experiment was carried out. A simple vacuum furnace made of silica tube was used to prevent the oxidation of the specimen. The pressure in the tube was reduced to 10^{-3}–10^{-4} mmHg. An iron specimen whose surface had been proved by the diffraction method to be covered with the green rust was heated in the furnace. After 10 minutes' heating at 150°C the diffraction pattern revealed only three rings, preserving none of S.R.S. Furthar heating at 350°C for 15 min. made the pattern sharper and increased the number of rings. These spacings and intensities are shown in Table III. Comparing them with the X-ray data, which are also shown in the table, it is concluded that the substance is mainly FeO, though the observed lattice constant is a little smaller. This decrease of the lattice constant is inferred to be due to the presence of γ-$\mathrm{Fe_2O_3}$. This result suggests that the anhydride corresponding S.R.S. is not a simple oxide such as $\mathrm{Fe_3O_4}$, but a mixture of FeO and γ-$\mathrm{Fe_2O_3}$.

Table III. The substance formed by dehydration of S. R. S.

obs. 150°C. 10 min.		FeO (X-ray)			γ-Fe_2O_3 (X-ray)		
Int.	$1/d$	Int.	Index	$1/d$	Int.	Index	$1/d$
V.S.	0.406	V.S.	(111)	0.404	V.S. W.	(311) (222)	0.396 0.414
S.	0.485	V.S.	(200)	0.468	M.	(400)	0.478
V.S.	0.678	V.S.	(220)	0.660	V.S.	(440)	0.676
obs. 350°C. 15 min.		FeO (X-ray)			γ-Fe_2O_3 (X-ray)		
V.W.	0.347	—	—	—	M.	(220)	0.338
S.	0.404	V.S.	(111)	0.404	V.S. W.	(311) (222)	0.397 0.414
V.S.	0.478	V.S.	(200)	0.468	M.	(400)	0.478
W.	0.628	—	—	—	S.	(511)	0.621
V.S.	0.674	V.S.	(220)	0.660	V.S.	(440)	0.676
W.	0.784	M.	(311)	0.774	W.M. V.V.W.	(533) (622)	0.783 0.793
M.	0.829	M.	(222)	0.808	V.W.	(444)	0.828
W.	0.965	W.	(400)	0.935	W.	(800)	0.957
W.M.	1.072	W.	(420)	1.043	V.W.	(840)	1.070
W.M.	1.175	W.M.	(422)	1.145	W.M.	(844)	1.171

§ 5. Discussion.

The green rust already attracted the interest of several chemists who studied the corrosion of iron. However, owing to its instability, its chemical formula has remained uncertain till now. As it is considered to be a ferroso-ferric body, A. Girard(5) assumed it to be simply $Fe_3O_4 \cdot H_2O$, but this assumption contradicts our result of the dehydration experiments.

Among other opinions, that proposed by E. Deiss and G. Schikorr(6) seems to us most reasonable. They explained the oxidation of $Fe(OH)_2$, the primary corrosion product of iron, as follows. When $Fe(OH)_2$ is oxidized, $Fe(OH)_3$ is formed as a direct product. This $Fe(OH)_3$ crystallizes as the α-form of $Fe_2O_3 \cdot H_2O$ (goethite); Schikorr(7) confirmed it when the oxidation occurred rapidly. However, in the case of slower oxidation, i.e. a poor supply of oxygen, they inferred that, when a part of $Fe(OH)_2$ is converted to $Fe(OH)_3$, it reacts with the remaining $Fe(OH)_2$, since the former is basic, whereas the latter is strongly acidic. This process can be separated to two steps owing to the two valencies of $Fe(OH)_2$. The first step is

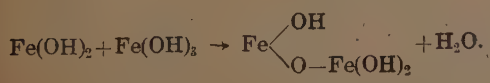

$$Fe(OH)_2+Fe(OH)_3 \rightarrow Fe\begin{array}{l}\diagup OH\\ \diagdown O-Fe(OH)_2\end{array}+H_2O.$$

The product of this reaction, a basic ferrous ferrite, was considered to correspond to the green rust. As the content of combined water in this compound was uncertain, they inferred it to be $2FeO \cdot Fe_2O_3 \, nH_2O$.

The second step takes place in two ways. In the first way, it turns directly to two molecules of $Fe(OH)_3$. This $Fe(OH)_3$ crystallizes as the γ-form of $Fe_2O_3 \cdot H_2O$ (lepidocrocite) in this case in contrast to the case of direct oxidation. In the second way, it changes to the neutral ferrous ferrite, namely magnetite, Fe_3O_4, according to the following equation.

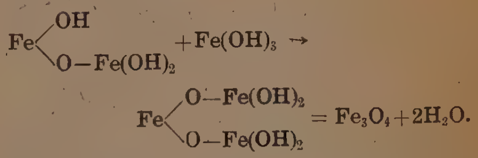

$$Fe\begin{array}{l}\diagup OH\\ \diagdown O-Fe(OH)_2\end{array}+Fe(OH)_3 \rightarrow$$
$$Fe\begin{array}{l}\diagup O-Fe(OH)_2\\ \diagdown O-Fe(OH)_2\end{array}=Fe_3O_4+2H_2O.$$

Which of these two ways occurs is determined by the concentration of dissolved oxygen in the solution. The first occurs when it is plentiful, and the second when it is poor.

The above processes of oxidation of $Fe(OH)_2$ may be summarized in the following form.

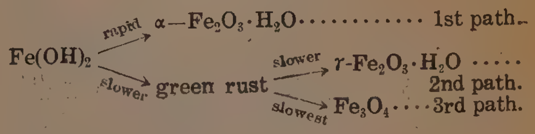

Deiss and Schikorr were unable, because of experimental difficulties, to secure analytical proof that the green rust had the composition $2FeO \cdot Fe_2O_3 \cdot nH_2O$. Their scheme, however, is very suited to account for our observation on the oxidation of the green rust.

The composition assumed by them is well supported by our dehydration experiment which showed that the corresponding anhydride is a mixture of FeO and γ-Fe_2O_3. This formula, when n was taken as 1, was ascertained correct by the consideration of the crystal structure of the green rust, which will be reported in the next paper.

The oxidation of the green rust in open air and in wet state gives γ-$Fe_2O_3 \cdot H_2O$ as described in § 2. This observation corresponds to the second path of oxidation in Deiss and Schikorr's scheme. Also, our observation in the electrolysis experiment, that the upper part of the green precipitate converted to γ-$Fe_2O_3 \cdot H_2O$, corresponds to this kind of oxidation.

The observation in § 3 that the lower part of the green rust converted black magnetite is in accordance with the third path in Deiss and Schikorr's scheme. This change is evidently due to the slow rate of diffusion of oxygen to that portion.

Although Miyake inferred the substance formed on the surface of immersed iron to be γ-Fe_2O_3, it seems better to regard this substance as Fe_3O_4 which is produced through the third path. For the brown rust was stable, without changing either to γ-Fe_2O_3 or to T.R.S., when it was kept by itself in the solution even for a week. On the other hand, the circumstance is very favourable for the formation of Fe_3O_4, since Fe^{++} ions may be abundant close to the surface and the brown rust over it prevents the supply of oxygen.

T.R.S. was inferred by Miyake to be the substance which is formed intermediately when γ-$Fe_2O_3 \cdot H_2O$ dehydrates to γ-Fe_2O_3. This may mean, in our opinion, a small crystallite of γ-Fe_2O_3 including a certain imperfection. Now, since Fe_3O_4 has the almost same structure as γ-Fe_2O_3, T.R.S. is also capable of being interpreted as the small imperfect crystal of Fe_3O_4. In the case of immersion the latter interpretation seems to be reasonable according to Deiss and Schikorr's scheme.

The change of the green rust to T.R.S., when it is exposed to air after a perfect desiccation, is incapable of explanation by Deiss and Schikorr's scheme, because it occurs in a dry state, whereas their scheme deals with reactions in solution. Our result seems to indicate that, when the green rust is in perfect desiccation, the oxidation simultaneously causes decompositions to small crystallites of γ-Fe_2O_3 or Fe_3O_4. To which of the two the observed T.R.S. corresponds cannot be determined in this case.

The result of the experiment of electrolysis, that S.R.S. and T.R.S. are produced corresponding to large and small current densities, is explained as follows. The primary product $Fe(OH)_2$ increases with current density, whereas the oxygen-supply to the solution is constant. This causes the deficiency of oxygen at high current densities, allowing only the first step of oxidation, i.e. the formation of the green rust. When the current decreases, the relative amount of oxygen increases so that the next step of oxidation occurs, resulting in the production of Fe_3O_4. The observed T.R.S. seems to be the small imperfect crystal of Fe_3O_4 as in the case of immersion. When the oxygen content of the solution is more plentiful, the formation of γ-$Fe_2O_3 \cdot H_2O$ may also be possible, a trace of which is really observed in the experiment.

This explanation of the electrolysis experiment gives some information on the peculiar behaviour of cast iron described in § 1, i.e. the existence of the green rust. In cast iron, the graphite flakes seem to function as the cathodic parts of local cells,(8) so that the scale of the cell is much smaller than in the case of pure iron, in which the distribution of anodic and cathodic parts is determined by the differential aeration principle.(9) This may cause high current density if the electromotive forces are of the same order. In addition, since the rust is formed close to the metal and remains adhered to the skeleton of undissolved graphite, forming a compact layer over the surface, the supply of oxygen is much hindered. These facts are considered to prevent the complete oxidation, allowing the existence of the green rust on the surface.

§ 6. Summary.

The unknown substance S.R.S. which was found in the corrosion of cast iron was identified with the green rust of iron. It is an unstable substance in the presence of oxygen. Its chemical changes in wet state, in dry state and in vacuo at high temperatures were traced by means of electron diffraction. The results agreed well with the assumption of Deiss and Schikorr on the oxidation of $Fe(OH)_2$. Above all, the chemical formula $2FeO \cdot Fe_2O_3 \cdot H_2O$ is supported.

The corrosion accompanying electrolysis was also examined. From its result a possible explanation of the peculiarity of the corrosion of cast iron was also given.

In conclusion, the author wishes to express shi sincere thanks to Prof. R. Uyeda for his kind guidance and Prof. S. Nishikawa and Dr. S. Miyake for their helpful advices and encouragements.

References.

(1) G.P. Thomson, Proc. Roy. Soc. A, **128**, (1930), 641.; J. Cate, Trans. Faraday Soc., **29**, (1933), 823.

(2) S. Miyake, Sci. Pap. I. P. C. R., **36**, (1939), 363.

(3) R. Uyeda and H. Yoshioka, Proc. Acad. Japan, **21**, 340.

(4) U.R. Evans, Metallic Corrosion Passivity and Protection (1937), p. 171.

(5) A. Girard and Chaudron, Comp. Rend., **200**, (1935), 127.

(6) E. Deiss and G. Schikorr, Zeits. anorg. allgem. Chem., **172**, (1928), 32.

(7) G. Schikorr, Ibid. **191**, (1930), 322.

(8) U. R. Evans, loc. cit. p. 432.

(9) U. R. Evans, loc. cit. p. 167.

On the Abnormal Intensity Distribution of OH Band.

By Masayoshi NINOMIYA.

Faculty of Science, University of Tokyo.

(Received Jan. 22, 1949.)

§1. Introduction.

It has been well known since K. F. Bonhoeffer and T. G. Pearson's experiment,(1) that the relative intensities of the rotational lines of the OH band excited by the discharge through water vapour do not correspond to the Boltzmann distribution of the rotational energy, but show the existence of more molecules in the higher rotational states than expected. Oldenberg(2) has interpreted this phenomenon as arising from the simultaneous occurring of the dissociation of H_2O and the excitation of the produced OH by an electron impact and the change of a part of the dissociation energy of H_2O into the rotational energy of the excited OH. Indeed, the intensity of the band is roughly proportional to the discharge current(3) and not to the square. Recently Horie(4) has stated that the intensity distribution of the OH band in the ring discharge can be expressed aproximately as due to the emission of the mixture of two molecular groups in the thermal equilibrium at 600°K and at 8000°K respectively. Horie and Nīra(5) have pointed out by calculation that there are two possible mechanisms of the simultaneous dissociation and excitation in regard to the electronic transition, namely,

$$H_2O \xrightarrow{e} H_2O^*(^1A_1) \rightarrow OH^*(^2\Sigma)+H(1^2S) \qquad \text{(I)}$$

and

$$H_2O \xrightarrow{e} H_2O^*(^3B_1) \rightarrow OH^*(^2\Sigma)+H(1^2S) \qquad \text{(II)}$$

in the former OH molecules being turned mostly into lower rotational states and in the latter, into higher ones. For the confirmation of this theory, however, a further experimental evidences are desirable. The author has investigated the intensity distribution of the OH band excited by the impact of electrons with known velocities and also the intensity distribution of OH and OD band excited by discharge through H_2O and D_2O respectively. In this paper his result and explanation of the intensity distribution of OH band will be given.

§ 2. Experiments.

a) *Electron Impact.*

As Nīra(5) has stated, the process (II) can occur only by the exchange of impinging and bound electron and hence has the probability only in low-velocity collisions, while the process (I) has considerable probabilities in the wider range of velocity of electrons. We can then expect, that the intensity distribution changes with the velocity of electrons, as in slow collisions the intensities of the rotational lines relating to higher rotational quantum number, K, are relatively strong and in fast collisions, those relating to lower rotational quantum number are intense.

In the discharge tube, which is provided with an oxide-coated cathode, a cylindrical grid with the bottom of Ni gauze and a Faraday cage, water vapour was let flow at pressure of 0.002–0.005 mm Hg. The distance between the cathode and the grid was made 2 mm so as to be shorter than the mean free path of electrons. The light emitted in the portion near the grid on the anode side free from electric field, was focussed on the slit of the Hilger EI spectrograph. The time of exposure was 4–8 hours.

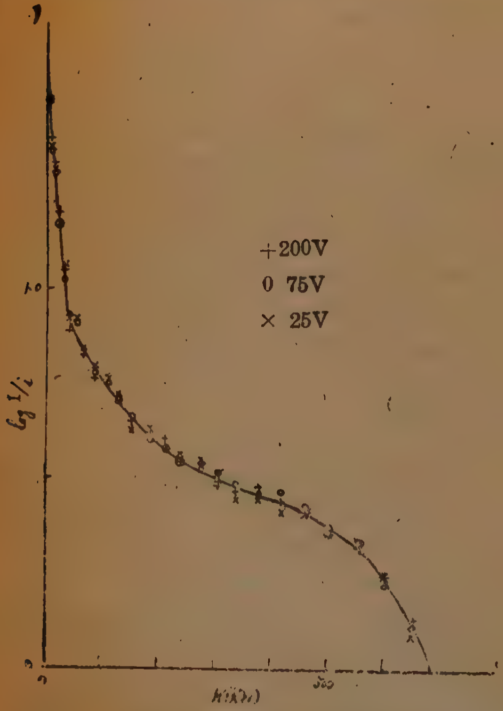

Fig. 1. log $I/i \sim K(K+1)$ for electron impact.

Under he conditions above-mentioned, the results in various electron energies are plotted in a log $I/i \sim B'K'(K'+1)$ diagram, Fig. 1, where I means intensity, i, the theoretical intensity factor(6) and K', the rotational quantum number of the upper state. Because the value of log I/i for six principal branches must be equal, as indicated by Lyman(7), the mean value for the unoverlapped lines among Q_1, Q_2, P_1, P_2 branches are plotted. The relation is not linear and it is shown that the intensity distribution in rotational lines does not change with the energy of colliding electrons. Thus it is difficult to consider that two mechanisms (I) and (II) take place and contribute to the intensity in the same extent. It seems unnecessary to consider the mechanism II, besides I, as Nīra has indicated that the relation between the transition probability of (I) and electron energy obtained by theoretical calculation agrees almost with Hayakawa's experimental curve.

The number of molecules OH in K′ state, n, does not vary with K′ from K′ 6 to 20, as shown in Fig. 2, since $(2J'+1)I/i$ is equal to n. This relation was also indicated by Wakeshima(8), but in his data the lower limit of unvaried region was 13 instead of 6. This reason will b discribed below.

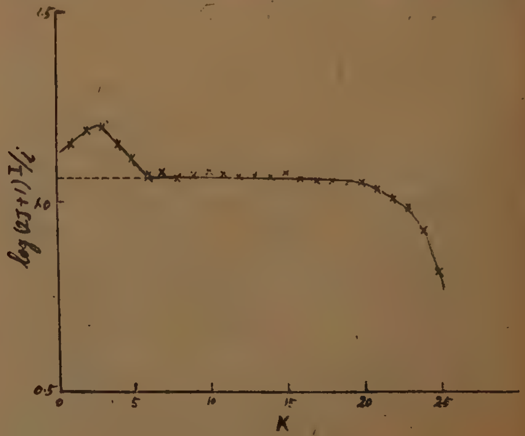

Fig. 2. log $(2J'+1)I/i \sim K'$ for electron impact

The band intensity against electron current as obtained in a different experiment by the use of small quartz spectrograph, is linear, but the intensity of the Balmer lines is proportional to $c^{\frac{3}{2}}$, not linear as concluded by Hayakawa⁽⁹⁾. They are shown in Fig. 3.

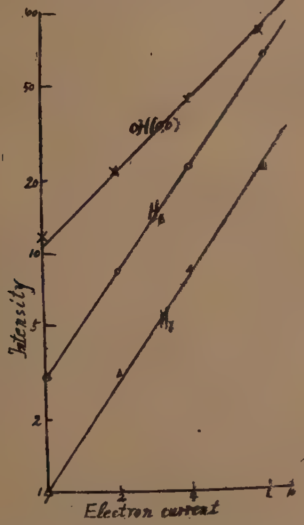

Fig. 3. Intensity ~ Current in electron impact.

b) *High frequency discharge through H_2O and D_2O.*

The source of the spectrum was furnished by the discharge in a silica tube of 6 mm diameter and provided with two external electrodes. For the excitation a short wave oscillator was used ($\lambda = 5$ m).

The water vapour was let flow through the discharge tube and the pressure was controlled to be at 0.07 mm Hg. by cooling a bulb containing water. The (0.0) bands of H and OD were photographed in the 3rd order of a 21-feet concave grating (dispersion 0.8 A/mm).

The relations $\log(2J'+1)I/i \sim B'K'(K'+1)$ of the (0.0) band both for OH ane OD are shown in Fig. 4. Between $K' \doteqdot 13$–20 for OH and $K' = 18$–29 for OD, n changes scarcely, and the distributions for OH and OD are shown in one curve at

$$B'K'(K'+1) \gtrsim 3000\,\text{cm}^{-1}.$$

At smaller K′, n are not the same for OH and OD, but the relations.

$$\log\frac{[(2J'+1)I/i]-[(2J'+1)I/i]_{dtr.}}{(2J'+1)} \sim B'K'(K'+1)$$

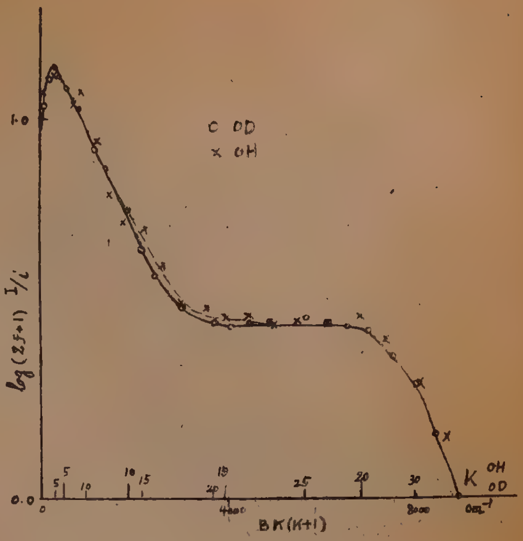

Fig. 4. Number of molecules ~ $B'K'(K'+1)$ in discharge experiment

where $[(2J'+1)I/i]_{dtr.}$ means the constant value at large K, are linear and parallel with each other under the same conditions of the discharge (Fig. 5). This indicates that the number which is remainder subtracted the constant amount from the number of molecules at every K state makes a distribution of the Boltzmann's type and the corresponding temperature is about 650°C. This value of temperature is not unreasonable, since the temperature determined from the intensty distribution of the N_2 band (λ3805A) at the same pressure and power was 550°C.

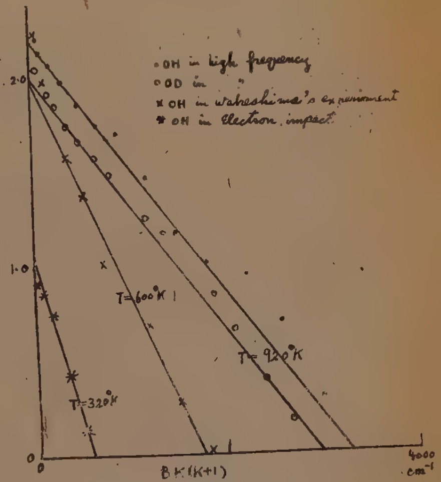

Fig. 5.

$$\log\frac{[(2J+1)I/i)]-[(2J+1)I/i]_{dtr.}}{(2J+1)} \sim BK(K+1)$$

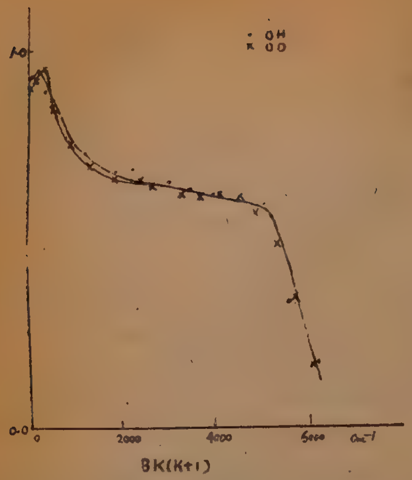

Fig. 6. $\log(2J+1)I/i \sim BK(K+1)$ for (1.0) band

For the (1,0) band of OH and OD these regularities were obtained also, but the intensty begins to fall down steeply at K = 17 for OH and K = 23 for OD (Fig. 6).

§ 3. Discussion.

As mentioned above, $(2J'+1)I/i$ in a region of large K is constant and the lower limit of this region is smaller in the experiment of electron impact than in the high frequency discharge. Since in the former the electron current is weak and the free OH molecules are few, it seems that the intensity of the OH band is more contributed by the direct bombardment on H_2O than in the latter case. We consider in general that the number of excited OH is the sum of the number of molecules which are excited at the time of the dissociation of H_2O and that excited from existing OH in the ground state. We shall designate the former as direct and the latter as indirect excitation. Perhaps the OH molecules in the ground state are almost in the thermal equilibrium(9), so $\log(I/i)_{ind.}$ contributed from the indirect excitation might be proportional to $-\frac{BK(K+1)}{kT}$ and at large K $(I_k)_{ind.}$ should be negibly small compared with $(I_k)_{dir.}$ due to the direct excitation. But at small K $(I_k)_{ind.}$ might be comparable to $(I_k)_{dir.}$, as the density of free OH is relatively large. Then it does not seem unreasonable to assume that $(n_k)_{dir.}(= (2J+1)I_k/i)$ is constant between K = $0 \sim 21$ for OH and K = $0 \sim 29$ for OD. This assumption is confirmed by the linear relation of $\log(I/i)_{ind.} \sim BK(K+1)$, as shown in Fig. 5,

Besides the reason mentioned in section II a., the simple aspect of the rotational distribution of OH molecules produced by the direct excitation indicates also that only the process (I) should take place. How many molecules are produced in every K state, is determined by the potential surface of the unstable $H_2O^*(^1A_1)$ and the initial motion of the dissociated H atom. The angular momentum $K\hbar$ of OH is given by the equation.

$$\frac{(K\hbar)^2}{2Ma^2}\left(1+\frac{a^2}{p^2}\right)=E,$$

where E means the dissociation energy, p the collision parameter, a the distance between O and H, M the mass of the hydrogen atom. In order that OH is to be produced in $K=20$, E must be larger than 0.8 eV. while Nira's calculation gave $E=$ 0.5 eV. This discrepancy may be due to insufficient approximation of the calculation.

In order that the OH is produced in the higher vibrational states, the initial conditions of the dissociated H atom should be restricted in narrower domain than in the case of the zero vibrational states according to the symmetry, and thus the lowering of the upper limit of K of constant n_k is understood.

A part of the thermal rotational energy of H_2O changes into the rotational energy of OH*. So even at $K'=21$ the intensity is not zero, and in fact it is stronger according to the temperature becomes higher as is seen in Wakeshima's work.

When the intensities of the rotational lines consist of the two parts, direct and indirect, the relation between the intensity and the discharge current should not be linear. Because the density of the free OH molecules, [OH], increases in proportion to current density, C, and to the vapour pressure, $[H_2O]$, and decreases by triple collisions, as pointed out by Frost and Oldenberg(10), hence

$$\frac{d[OH]}{dt}=aC[H_2O]-b[OH]^2[H_2O],$$

since $\frac{d[OH]}{dt}=0$ in case of stationary discharge,

$$[OH]=\sqrt{\frac{a}{b}C},$$

and then the intensities of the band lines are give by

$$I = A[H_2O]C + B[OH]C$$
$$= A'C + B'C^{3/2},$$

Therefore, at large K, where only the first term corresponding to the direct excitation is effective, the intensity should be proportional to the current, but at small K is not so. Since in Wakeshima's data $[(2J+1)I/i]_{dir}$. is equal to about $[(2J+1)I/i]_{ind}$. at K = 4 and $C = 22$ mA, then $A' \times 22$ is equal to $B' \times (22)^{3/2}$ and so

$$I_c = I_{22} \times \frac{1}{2}\left[\left(\frac{C}{22}\right) + \left(\frac{C}{22}\right)^{3/2}\right] = xI_{22}.$$

When C is 43, 63 and 81 mA, x is 2.34, 3.85 and 5.37 respectively and concides to his experimental values 2.2, 3.9 and 5.4. In his report the values at large K are not in table, but he has stated that the increase of the intensity against the current at large K is slower than at small K. In our experiment of the electron impact where are a little amount of free OH, concerned, the intensity of the band head is proportional to the current.

If we assume that the excitation probabilities of H_2O and OH are equal to each other, the ratio of the number of OH to H_2O is given by

$$\sum_K[(2J+1)I/i]_{ind} \cdot / \sum_K[(2J+1)I/i_{\,dir}.$$

and is 0.04, 0.4 and 1.2 in the case of the electron impact, Wakeshima's data and the high frequency discharge respectively. In the high frequency discharge the ratio is very large, but not unreasonable, as investigated by Rodebush and his collaborators,⁽¹¹⁾ because the life time of OH is long and the current density is large.

Since the density [OH] does not change with the pressure of H_2O approximately in comparatively low density, as indicated by above introduced equation, the ratio of the intensity by the indirect excitation to that by the direct excitation should be larger under the lower pressure. Therefore, Lyman's experiments⁽⁷⁾ are understood qualitatively too.

§ 4. Conclusion.

The intensity of the OH band excited by the electric discharge through water vapour is contributed by two processes,

$$H_2O \xrightarrow{e} H_2O^*(^1A_1) \rightarrow OH^* + H \qquad (I)$$

and

$$OH \xrightarrow{e} OH^* \qquad (II)$$

and the abnormality of the intensity distribution is owing to (I). The proportion of (I) and (II) taking place, determined by the conditions of the discharge, determines the aspect of the intensity distribution.

In conclusion, the author takes his oppotunity with pleassure to express his sincere thanks to Prof. T. Tanaka and Prof. M. Kiuti for their interest and encouragement through this work. He wishes also to thank to assist. Prof. T. Horie and assist. Prof. K. Nīra for their kind discussions.

References.

(1) K. F. Bonhoeffer and T. G. Peareon : Zeits. für Phys. Chem. **14** (1931) 3.
(2) O. Oldenberg : Phys. Rev. **46** (1934) 210.
(3) H. Wakeshima : Proc. Phys.-Math. Soc. Japan **24** (1942) 367.
(4) T. Horie : J. Phys. Soc. Japan **1** (1945) 8.
(5) K. Nīra : "Busseiron Kenkyu" (in Japanese).
(6) L. T. Earls : Phys. Rev. **48** (1935) 423.
(7) E. R. Lyman : Phys. Rev. **53** (1938) 379.
(8) H. Wakeshima : J. Phys. Soc. Japan **2** (1947) 12.
(9) G. Hayakawa : Proc. Phys.-Math. Soc. Japan **26** (1944) 78.
(10) A. A. Frost and Oldenberg : Journ. Chem. Phys. **4** (1936) 642.
(11) W. H. Rodebush, C. W. Wende and R. W. Campell : J. Amer. Chem. Soc. **59** (1937) 1924.

On the Relation between Compressibility and Molal Volume of Organic Liquids.

By Yasaku WADA.

First Faculty of Engineering, University of Tokyo.

(Received Feb. 16. 1949)

§ 1. Relation between compressibility and density.

If the product of density ρ and n-th root of iso-thermal compressibility β of an organic liquid, $\rho\beta^{\frac{1}{n}}$, is independent of temperature, the ratio of $1/\beta\cdot\partial\beta/\partial t$ to $-1/\rho\cdot\partial\rho/\partial t$ is expected to be a constant n. The result of calculations shows that the constant n is nearly equal for many organic liquids with a mean value of 6,5. Similarly, if $\rho\beta^{\frac{1}{n}}$ is independent of pressure, the ratio of $1/\beta.\ \partial\beta/\partial p$ to $-1/\rho\cdot\partial\rho/\partial p$ will be also n. In the latter case the average value of n is 7,3 for several organic liquids.

As shown later, n is expected to be the same in both cases, and hence it seems plausible to take n as 7 in common. In Table I are listed two examples of numerical values of $\rho\beta^{\frac{1}{7}}$ as a function of temperature and pressure. The units of density and compressibility are taken as g/cm^3 and 10^{-12} cm/dyne respectively in this paper.

As Rao(1) has already pointed out, the product of density and 7-th root of adiabatic compressibility α, $\rho\alpha^{\frac{1}{7}}$, is highly independent of temperature. From the analogy of the case of isothermal compressibility above mentioned, $\rho\alpha^{\frac{1}{7}}$ is expected to be independent also of pressure. The data of adiabatic compressibility under high pressure are, however, too scarce to prove it.

Table I. Temperature- and pressure-independence of $\rho\beta^{\frac{1}{7}}$

(1) Toluene (1 atm.)

Temp. (°C)	ρ	β(10^{-12}cm^2/dyne)	$\rho\beta^{\frac{1}{7}}$
0	0,8845	78	1,648
10	0,8754	84	1,648
20	0,8664	90	1,648
30	0,8573	96	1,645
40	0,8484	103	1,645
50	0,8396	111	1,645
60	0,8309	120	1,647
70	0,8222	129,5	1,647

(2) Acetone (20°C)

Press. (atm.)	ρ	β(10^{-12}cm^2/dyne)	$\rho\beta^{\frac{1}{7}}$
1000	0,8529	55,9	1,515
2000	0,8952	42,5	1,530
3000	0,9288	32,1	1,525
4000	0,9554	25,5	1,517
5000	0,9778	21,7	1,518
6000	0,9978	19,2	1,522
7000	1,0160	17,3	1,527

§ 2. Molecular Compressibility.

As related above, the functions $\rho\beta^{\frac{1}{7}}$ and, most likely $\rho\alpha^{\frac{1}{7}}$ also, are independent of both temperature and pressure and are characteristic functions of each organic liquid. Moreover the ratios of the molecular weight M to $\rho\beta^{\frac{1}{7}}$ and $\rho\alpha^{\frac{1}{7}}$ are both additive of the molecular constitution. In other words, the two characteristic functions of a liquid, $B = M/\rho\beta^{\frac{1}{7}}$ and $A = M/\rho\alpha^{\frac{1}{7}}$, which the author chooses to call "Molecular isothermal compressibility" and "Molecular adiabatic compressibility" respectively, can be computed by summing increments assigned to constituting atmos or atomic bonds.

The additivity was proved for all liquids for which the data were available, namely sixty kinds of liquids for B, and more than one hundred and twenty for A, including the liquids of such complicated molecules as tetraline, citral, adipic diethyl ester, etc.. Among the liquids for which B or A was calculated, only one liquid for B and seven for A show appreciable discrepancies between experimental and calculated values, some of which seem to be ascribed to errors of data or misprints in an original table and others to peculiar constitutions as in cases of pinene, etc..

In Table III are recorded some examples, where β is the extrapolated value to atmospheric pressure(2) and α is calculated from the supersonic velocity(3). In this table calculated values are computed as the sum of bond increments given in Table II, but it is also possible to compute them as that of atomic increments. The calculated values in brackets have large discrepancies from the experimental values.

(Examples of calculations)

Ether: $10(C-H)+2(C-C)+2(C-O)$

Quinoline: $4(C=C)+(C=N)+5(C\ \ C)+(C-N)$
$+7(C-H)+2(\text{Ring})$

Table II. Bond increments.

Bonds	*B*	*A*	Bond	*B*	*A*
C–C	1,07	–1,10	O–H	5,07	4,64
C–O	2,78	2,05	N–H	5,00	5,57
C–S	—	5,43	C = C	6,36	5,68
C–N	0,24	0,40	C = O	9,08	9,93
C–H	4,16	5,10	C = S	—	16,83
C–F	6,57	—	C = N	—	7,60
C–Cl	12,55	12,91	N = O	8,28	8,17
C–Br	15,33	15,54	C≡N	—	14,13
C–I	—	19,65	Ring	–0,43	4,80

Table III. Molecular compressibility.

Liquids	*B* (exp.)	*B* (calc.)	*A* (exp.)	*A* (calc.)
Hexane (*n*)	64,2	63,6	65,9	65,9
Decane (*n*)	100,7	101,1	—	—
Pentadecane	148,5	148,1	—	—
2, 4-dimethyl pentane	—	—	74,4	75,0
Benzene	46,7	46,8	49,0	49,1
Xylene (*m*)	65,7	65,6	67,7	67,4
Mesitylene	—	—	76,5	76,5
Ethyl benzene	64,6	65,6	67,2	67,3
Tetraline	—	—	78,6	79,0
Inden	—	—	66,4	66,5
Pinene	—	—	88,9	(85,9)
Carbontetrachloride	50,6	50,2	52,5	51,6
Chloroform	41,8	41,8	44,0	43,8
Methylen bromide	48,1	48,4	41,4	41,3
Ethylen tetrachloride	55,5	56,6	57,2	57,3
Chlorobenzene	55,5	55,2	56,4	57,0
Dichlorobenzene (*o*)	—	—	65,0	64,8
Bromonaphthalene	—	—	83,6	82,6
Butyl alcohol (*n*)	48,2	48,5	49,9	49,3
Propyl alcohol (*iso*)	39,4	39,1	40,6	40,2
Glycol	33,5	33,4	—	—
Glycerine	46,8	46,5	47,2	(43,4)
Cresol (*m*)	59,8	59,9	—	—
Cyclohexanol	59,4	59,6	62,4	61,0
Palmitic acid	158,6	161,2	—	—
Methyl acetate	41,0	40,7	42,6	43,6
Ethyl propionate	59,3	59,5	61,7	61,7
iso-Butyl acetate	68,8	68,8	—	—
Ethyl caprylate	—	—	107,3	107,2

Liquids	B (exp.)	B (calc.)	A (exp.)	A (calc.)
Ethyl carbonate	—	—	65,3	66,9
Adipic diethyl ester	—	—	113,3	112,2
Geranyl acetate	—	—	119,0	118,6
Ethyl phthalate	—	—	116,5	(123,1)
Thio-diglycolic diethyl ester	—	—	105,9	105,9
Ether	—	—	51,4	52,9
Cresol methyl ether (p)	—	—	70,9	72,5
Resorcin monomethyl ether	—	—	65,8	65,1
Anisole	—	—	63,5	63,5
Diethyl ketone	55,0	55,0	57,6	57,6
Citral	—	—	96,8	95,3
Salicyl aldehyde	—	—	61,9	59,6
Acetal	—	—	95,2	96,3
Cyclopentanone	—	—	50,9	50,0
Aniline	53,0	52,9	55,6	55,6
Toluidine (o)	61,5	62,3	64,6	64,7
Quinoline	—	—	71,5	70,5
Picoline (α)	—	—	56,0	56,5
Phenyl mustard oil	—	—	69,5	68,9

§ 3. Theory of Molecular Compressibility.

The molal volume of liquids, M/ρ, is the sum of the molal volume of close-packed state V_0 and the free volume per mole v Hence

$$M/\rho = V_0 + v = V_0(1+k), \tag{1}$$

where $k = v/V_0$ (fractional free volume).

From the above-mentioned experimental fact that $\rho\beta^{\frac{1}{7}}$ is independent of temperature and pressure, follows the relation

$$\beta = \beta_0(1+k)^7, \tag{2}$$

where V_0 and β_0 are assumed to be independent of temperature and pressure. Combining (1) with (2), it follows

$$B = M/\rho\beta^{\frac{1}{7}} = V_0/\beta_0^{\frac{1}{7}} \tag{3}$$

Since V_0 is of course additive of constituting atoms or bonds, B is expected to be also additive, provided that β_0, the compressibility in the close-packed state, is equal for every organic liquid. This assumption seems reasonable since the compressibility of various liquids under high pressure does not differ each other so much as under atmospheric pressure(4). The independence of β_0 on the kinds of liquids is also shown in Table IV, where $\beta_0^{\frac{1}{7}}$ was calculated for several liquids as the ratio of V_0 to B, using the molecular radii taken from Schaaffs.(5).

Table IV. Numerical values of $\beta_0^{\frac{1}{7}}$ as the ratio of V_0 to B.

Liquids	Mol. Rad. (Å)	V_0 (cm^3/mole)	B	V_0/B
Carbontetrachloride	2,033	21,2	50,6	0,419
Choroform	1,900	17,3	41,8	0,414
Benzene	1,990	19,9	46,7	0,425
Toluene	2,107	23,6	56,5	0,418
Xylene (m)	2,216	27,45	65,8	0,417
Chlorobenzene	2,080	22,7	55,5	0,409

§ 4. Relation to Molecular Sound Velocity.

" Molecular sound velocity ", defined by Rao⁽⁶⁾ as

$$R = Mv^{\frac{1}{3}}/\rho, \qquad (4)$$

is a constant independent of temperature and is an additive function of constituting atoms⁽⁶⁾ or bonds⁽⁷⁾. As the velocity of sound v is related to density and adiabatic compressibility by the relation

$$v = 1/(\rho\alpha)^{\frac{1}{2}}, \qquad (5)$$

it follows

$$R = M/\rho^{\frac{7}{6}} \cdot \alpha^{\frac{1}{6}}. \qquad (6)$$

Therefore it is not probable that R and the molecular adiabatic compressibility, $A = M/\rho\alpha^{\frac{1}{7}}$, are both additive at the same time. Perhaps the former may be an approximate function of the latter on account of following reasons: (1) the additivity can be explained reasonably in the case of molecular compressibility, (2) compressibility is the more direct property of a liquid than sound velocity.

In conclusion, the author wishes to acknowledge kind advices given by Professor Yoshio Suge.

References.

(1) M.R. Rao: J. Chem. Phys. **14** (1946) 699.
(2) The data were compiled from Int. Crit. Tab. Vol. 3.
(3) The data are edited by E. Hiedemann in the appendix of " Glundlagen und Ergebnisse der Ultraschallforschung (1939) ".
(4) P. W. Bridgman: Int. Crit. Tab. **3** p. 40–42.
(5) W. Schaaffs: Zeits. f. Phys. **114** (1939) 110.
(6) M.R. Rao: Ind. Journ. Phys. **14** (1940) 109.
(7) R. T. Lagemann & J. E. Correy: J. Chem. Phys. **10** (1942) 759.

The Model Experiment of " The Phenomenon of Sea-snake ".

By Michika MIYANISHI.

Hiroshima Technical College.

(Received Feb. 28, 1949.)

The temperature of the air near a sea-surface is usually different from that of the sea water. When the difference is great, heating or cooling of the air takes place remarkably, and in consequence its density changes discontinuously. In the air medium the extraordinary refraction of light is given. There are many examples of phenomena due to such as refraction as just above mentioned. Among of them vince, mirage and Fata-morgana are famous in the world, and in our country Shinkiro and Siranui are well known, the fomer being studied by Fujiwara⁽¹⁾ and the latter by the present writer⁽²⁾. In the study of us, the phenomenon of " The Great Billow ", which was named by us, was also investigated.

A new phenomenon i.e. " The Phenomenon of Sea-snake " was observed in the Pacific Ocean, and it was studied by means of a model experiment by us. The experiment and its result are given below.

Experimental Arrangement.

In the preliminary experiment, the experimental arrangement used in our model experiment of Siranui⁽²⁾ was utilized. The upper water-tank was removed and the length of the base metal plate was increased 1 m. Thus the iron plate of 3.5 m in length and 25 cm in width was obtained. The surface of the plate was covered with asbestos and was bent along its length the radius of curvature being 60 m. A light source was placed at one end of the plate, and a camera having a lens of 30 cm focus was set at a place detouched 1 m from the other end. The lens had a horizontal slit of 1 cm width in front of it.

Then the metal plate was heated with coal gas flames and the extraordinary refraction of light given at the horizontal line of the model was observed. When wind was sent to the surface of the model with a fan in the direction parallel to its longer side, a phenomenon similar to that of the Sea-snake observed in the Pacific Ocean was given.

In order to investigate the effect of winds of different directions on the phenomenon, a model having a wide surface was constructed. A virtical section of it is shown in Figure 1. In the figure *K* and *S* were made of concrete, and have a form of a large box with a cover of spherical surface whose radius of curvature being 60 m. The thickness of the base and side wall is 10 cm, and that of the ceiling of the cover is 2 cm. The ceiling is reinforced with a metal net inlaid in it. The length of the model is 180 cm and the width 120 cm. The height of the inner hollow space is 30 cm at the maximum, and it is reduced to about 7 cm, sand being placed in it. Twelve nichrome wires of 0.5 KW are placed on the sand with equal interval, they being parallel connected, and an electric current is passed through them. With this heater the temperature of the air touched to the surface was raised up to 140°C.

As a back ground of the model, a white screen was placed, and on its surface black parallel lines of 180 cm in lengh were drawn in the interval of 5 mm. The distance between the one end of the model and the screen was 260 cm, and that between the other end and the camera lens mentioned above 300 cm. The height of the camera was varied by means of rotation of a screw provided for its stand. This height was indicated by a scale placed near the lens. In Fig. 1 the letters A, B, C, ····, I show the positions of the lens at different height respectively. The straight line drawn from the higher position *D* to the surface touches at its far end as shown in the figure. A wind was sent by a fan from the front, the side or the intermediate position of them. The photographs of the horizontal line of the model were taken on Fuji panchromatic plates with exposures of 1/30 sec.

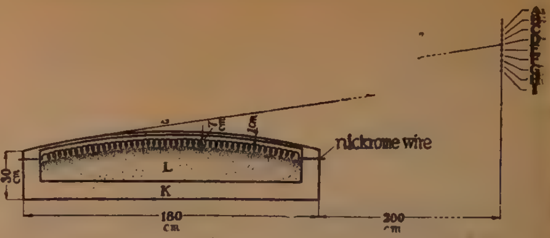

Fig. 1.

The Method of Measurement of the Temperature of the Air near the Surface of the Model.

As already explained the surface was heated by the electric heater. If a mercury thermometer is placed near the surface its glass part will absorb the heat radiation from the surface. The thermometer, therefore, will not show the true temperature of the air. In an object to reduce this effect, a thermometer consisted of nickel and copper thermojunction was constructed as shown in the Figure 2.

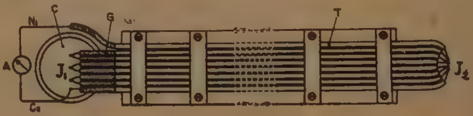

Fig. 2.

Eight glass tubes *T* of 55 cm in length and 5 mm in diameter were arranged side by side and fixed on a wooden plate by means of metal bands. Nickel wires and copper ones were put into them alternately, and their ends connected in series. The joints J_2 at the ends of the tubes were arranged closely. At the other ends of the tubes the length of the wires was about 25 cm and they were put into gum tubes *G* respectively. Both ends of wires thus connected in series were fixed to terminals of a voltmeter *A* respectively, and joint J_1 was put in to a Dewer vessel *C* containning ice and water. By means of a lever the joint J_2 was raised or down gradually at the surface of the model and its height from the surface was varied.

The junction J_2 and mercury standard thermometers were immersed in transformer oil, and the oil was warmed gradually. Then the reading of the scale of the voltmeter and that of mercury thermometer were compared. The result was represented by a temperature and voltage diagram. Using this diagram the junction was used as a thermometer to measure the temperature of hot air near the heated surface of the model. In the mesurement the height of the junction J_2 was varied as 1, 2, 4, 6, 8, 10, 15, 20, 25, 30, 40, 50, 60, and 70 mm. The velocities of the wind were $v = 0$, 1.1, 1.75, 2.65 and 3.1 m/sec. respcctively. A result obtained in the case of $v = 3.1$ m/sec. is indicated diagrammatically in Figure 3. As is seen in the figure the curve is nearly hyperbola. This will be shows that a mirage phenomenon is given in the air by the refraction of light. The curvatures such as that of the curve as above mentioned become flat gradually in accordance with the velocity decrease.

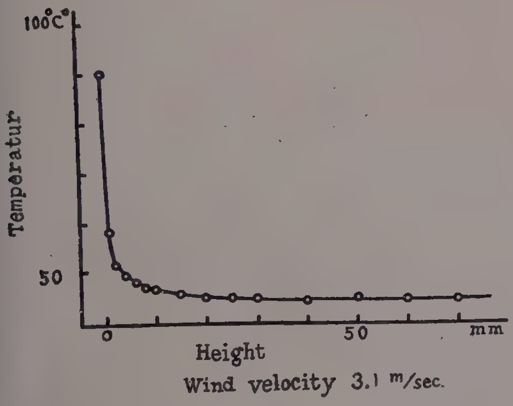

Fig. 3.

Result.

The photographs taken with the camera whose position being C, D and E, under the various conditions of the wind are shown in the Figures 4. The temperature of the air at the height 1 mm was 140°C when the velocity of the wind $v = 0$. As already communicated in the report “the model experiment of Siranui”, when the sea level of a model was observed through cellular vortex of the air its appearance became a regular wavy form. While in this experiment when it was observed through air mentioned above, the appearance became a irregular wavy form. It seemed, therefore, as if sea-snakes were swimming on the sea level. Thus a phenomenon quite similar to that observed in the sea near Japan in the Pacific Ocean was obtained. We named it “The Phenomenon of Sea-Snake”. As is shown in the Fig. 4 the phenomenon was influenced by the direction of the wind. And it was most remarkable when the wind was sent from the front. On the contrary when the wind was sent from the side the wavy form became very flat. The phenomenon was remarkable when it was observed at C, D and E, while became faint at A, B, F and G, and disappeared at I. From this result and the nature of the temperature gradient, it was found that this phenomenon was due to the mirage of a sea surface near horizon. The direct and inverted images of it formed thick or thin lines due to irregular distribution of the air temperature on the surface. The distribution varied more remarkably when the wind was sent from the front. Consequently the form of the mirage also changed showing the phenomenon of Sea-snake.

The envelope of the wavy form is slightly lower than the true horizon. Using a comparator the difference detected in the photographs was measured the scale drawn on the back ground being taken as a comparison scale. The values thus obtained are shown in Table I.

As is show in the table the differences are very small. Generally they increased in the order of C, D and E. The more the position becomes low, the more the difference increases, and also the more the phenomenon becomes faint. At the lowest position I the phenomenon disappears and an apparent horizon is seen. When there was a body higher than the true level, its direct and inverted images appeared above the apparent sea level showing its mirage.

The phenomenon of Sea-snake is a mirage phenomenon of the sea surface near the sea level. The difference between the higher points in the former and the latter varied from 0.10 to 0.3 mm. If we represent the difference by an angle $\delta\theta$, the distance between the lens and the image by r and the difference given in the above table by ds, the following relation will be obtained. $\delta\theta = ds/s$. The valu $\delta s = 0.2$ mm taken as a mean value, and that $r = 30$ cm are put into this equation, we obtain

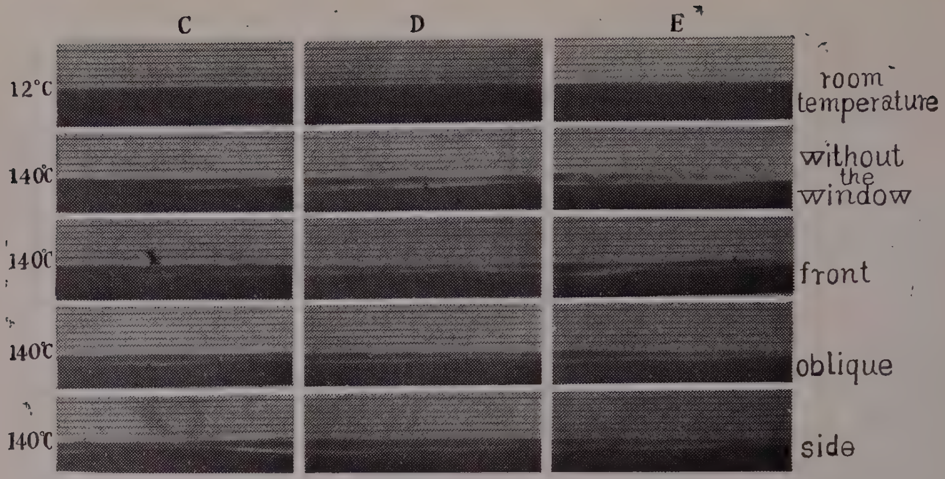

Fig. 4.

Table I.

position of the camera		C				D				E			
direction of the wind		$v=0$	front	oblique	side	$v=0$	front	oblique	side	$v=0$	front	oblique	side
	No. 1	0.18	0.18	0.28	0.11	0.25	0.22	0.04	0.14	0.29	0.36	0.33	0.36
difference (mm)	No. 2	0.18	0	0.27	0.18	0.14	0.33	0.28	0.14	0.33	0.26	0.36	0.33
	No. 3	0	0.08	0.27	0.08	0.04	0.22	0.28	0.07	0.18	0.29	0.14	0.18
mean		0.12	0.09	0.27	0.12	0.14	0.26	0.23	0.12	0.27	0.30	0.28	0.29

$$\delta\theta = \frac{1}{1500} \text{ (radian)}.$$

$$\therefore \quad \delta\theta \fallingdotseq 0.^\circ 037 \fallingdotseq 2'.2.$$

There is necessity occasinally to measure the height of stars from the sea level in an ocean. The phenomenon of sea snake appears in winter most remarkably in the Black Current in the Pacific Ocean. If the height of a star is measured the highest point of it, errors in the order of the value mentioned above will be given.

Summary.

1. A model experiment of "the phenomenon of sea-snake", was carried out.
2. In order to measure the air temperature near the heated surface of the model, a thermo-junction was constructed.
3. With this junction the air temperature just above mentioned was measured.
4. The phenomenon at the various conditions was photographed, and it was found that the phenomenon was a mirage of the sea surface near sea level.
5. The distance between the true sea level and the envelope of the the phenomenon was measured.

References.

(1) S. Fujiwara, T. Oomori and K. Taguti: The Geophysical Magazine, Vol. **4**, No. 4 (1931), 317.
(2) M. Miyanishi: Sc. Pap. I.P.C.R., **36** (1939), 198.
(3) M. Miyanishi: Sc. Pap. I.P.C.R., **39** (1942), 279.

X-ray and Thermal Studies on the Phase Transitions of Cuprous Sulphide Cu_2S.

By Ryuzo Ueda.

Department of Applied Phisics, Waseda University, Tokyo, and Kobayashi Institute of Physical Research, Tokyo.

(Read May 23 1948; Received Feb. 28 1949).

§ 1. Introduction.

Cuprous sulphide Cu_2S, or mineral chalcocite, has been investigated minerallogically and crystallographically from early years. Recently, Hirahara⁽¹⁾ has measured many physical constants of this substance as a function of temperature and found a new anomaly in the neigbourhood of 450°C in addition to the phase change at about 110°C already known,⁽²⁾ and showed that there exist the remarkable ionic conductivity between these two transtion points.

X-ray studies of this substance were already performed by Ramsdell, Rahlfs, Kurz, Alsen and others.⁽³⁾ In the recent studies on the single crystal of chalcocite and Cu_2S-CuS system, M.J. and N.W. Buerger found the existence of a superstructural relation between 'high' and 'low' chalcocite above and below 105°C, and the existence of a cubic phase $Cu_{1.8}S$ as the mineral digenite. The simple relations of lattice constants between two modifications of chalcocite were found as follows:- (Table I).

Table I. (Buerger).

	Low-Chalcocite (γ)	High-Chalcocite (β)
Space group	C_{2v}^{15}	D_{6h}^{4}
Lattice Const. (Å)	$a = 11.90$ $b = 27.28$ $c = 13.41$	$a' = 3.09$ $b' = 6.68$
Z	96	2

$$a = 5a', \ b = \sqrt{3}\,a', \ c = 2c', \ z = 2z' \times 3 \times 4 \times 2 = 96$$

The definite atomic arrangements, however, have not been determined.

The present auther, at Hirahara's request, tried to reveal the structural relations among these three solid phases by x-ray and calorimetric methods.

For the convenience of the description we will use the following phase names for the three temperature intervals.

←— 115°C	←→	450°C —→
γ-phase	β-phase	α-phase

§ 2. X-ray Analysis.

A) The measurements on chalcocite single crystals.

At first, single crystals of mineral chalcocite, from Cornwall, England, were used. Crystals are black needles and have metallic lustre. Their dimensions are about $0.5 \times 0.5 \times 3mm^3$. The lattice periode along c-axis is determined by the rotation photographs. That is $c = 13.41$Å. Assuming the space group C_{2v}^{15}, the lattice constants can be know by (600) and (346) spectra. They are: $a = 11.79$Å, $b = 27.28$Å. These values coincide with the results given by Buerger.

Of reflection spectra in the rotation photograph with [001] as the rotation axis, ones on odd layer lines are weak, and ones on even layer lines are strong in general. It is found, however, that X-ray spectra are readily damaged by cutting or polishing the sample, and its Laue pattern loses the characteristic spots, showing a few diffuse rings, on which some intense spots are distributed. Examining other specimens more than ten, we could obtain no other specimen which give regular good spectra. The analysis, therefore, mainly depended upon the powder samples as described below.

B) Power X-ray photographs

The specimens I and II were prepared by Hirahara and the specimen III was prepared by the present author in the manner formerly described by Hirahara. Samples made synthetically are more or less solid solutions of chalcocit and digenite $Cu_{1.8}S$ as proved by X-rays. Sample II is found to be purest among them. The density measured by a pycnometer is 5.81 (at 15°C) which agrees with the values formerly reported 5.79–5.99, and with 5.79 (γ-phase) and 5.09 (β phase) calculated from X-ary data. Being found that the sample is attacked chemically by the air as described later, it was necessary to seal it into the pyrex glass capirally, especially in vaccum when used above 350°C. The sample rod is inserted into a small furnace placed in an X-ray camera. Temperature fluctuation is controlled within ± 1°C below 200°C, ±2°C between 200° and 300°C, and ±3°C above 350°C. The temperature is measured by copper-constantan thermocouple, which is placed in close contact with the sample. Wave length used is CuK_α, voltage 40KV, current 10 mA, exposure 4–6 hours.

Fig. 1 schematically reproduce the Debye photogramms under various conditions. The assignment of the orthorhombic index to the powder lines of γ-phase is possible by referring the relation between two reciprocal lattices $C_{2v}^{15} \rightleftarrows D_{3h}^{4}$ (Fig. 2). It is easier to assign the hexagonal indeces to the lines of the β phase, only if we avoid the confusion due to digenite lines. In α-phase (above 450°C), there are observed only two lines, which seem to correspond to (220) and (311) in digenite phase.* X-ray analysis of digenite is also shown in diagramm No. 6 of Fig 1. By keeping the sample three months in air, however, it was found that it transformed into a different pattern, giving the new line shown by two arrows in diagramm No. 7. This fact suggests the instability of this substance. The heating effect in air above 150°C can be seen in diagramm No. 8, increasing the number of the lines due to oxidation.

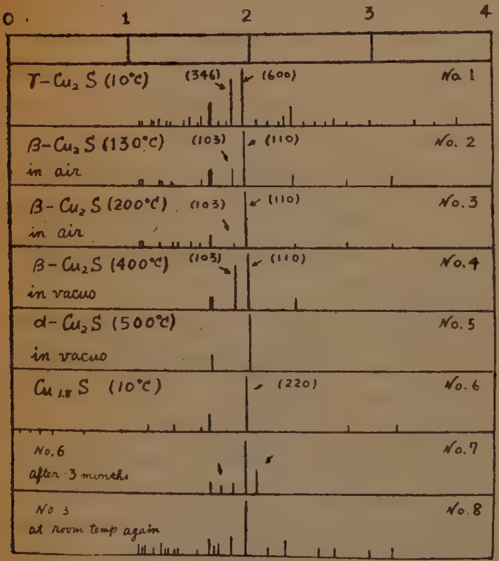

Fig. 1.

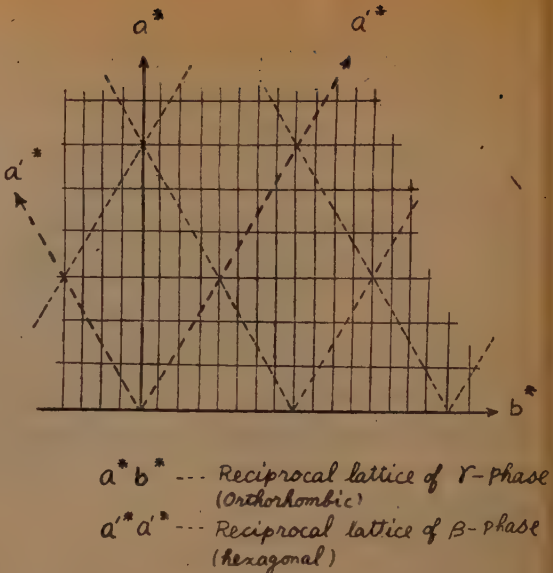
a*
a'*
a'*
b*
a* b* --- Reciprocal lattice of γ-phase (Orthorhombic)
a'* a'* --- Reciprocal lattice of β-phase (hexagonal)

Fig. 2.

We will now investigate the temperature variation of lattice constants in each phase up to 500°C, and the intensity change when the sample was heated in air below 150°C. Some remarks upon the structural relations of three solid phases of this substance will be discussed in the last paragraph.

i) *Temperature variations of lattice constants.*

The temperature variation of lattice constants are shown in Fig. 3, 4 and 5. In γ-phase, the elongation along b axis is largest and those along the other axes smaller. The lattice constants begin to increase gradually in the neighbourhood of 70°C and the phase transformation completes at 115°C, losing the superstructural lines.

---

* The tables of measured and calculated lattice spacings for Debye lines in each phase are omitted out of space consideration.

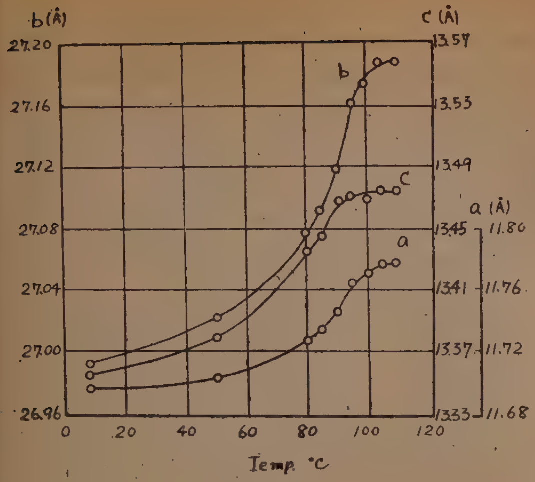

Fig. 3.

It is noticable that there exist fluctuations of lattice constants for three different sample rods, which are prepared by pulverizing the same cuprous sulphide block. This fact, presumably corresponding to the difference of the chemical compositions of the samples, shows the complicated properties of this substance and probably correlates to the time variation of electrical and thermal characteristics as observed by Posnjak, Hirahara and others.

Fig. 4 shows the temperature variation of lattice constants a' and c' ($a/6$ and $c/2$ in γ-phase), which is calculated from the lattice spacings of (600)—(110) and (346)—(103). The change of the lattice constants in the neighbourhood of 115°C is considerable but without discontinuity, and is considered to be a kind of phase transformation of second order. a' and c' in β-phase increase linearly with temperature, and the line (103) disappear at 500°C. A Debye pattern at 500°C resembles that of digenite $Cu_{1.8}S$.

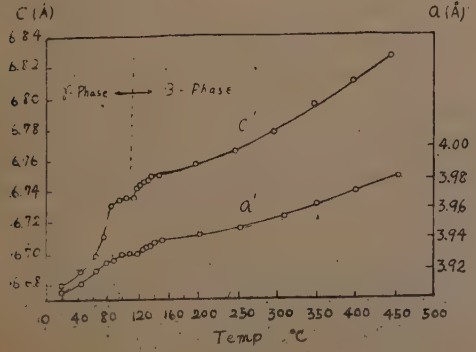

Fig. 4.

It is remarkable that the lattice spacings of (600) in γ-phase, (110) in β-phase, and (220) in α-phase or in $Cu_{1.8}S$ coincide with each other (taking account of the thermal expansions). The intensity of these lines is strongest compared with the other lines in every photograms. This fact is considered to suggest that there exist close relations among the crystal structures of the three phases of cuprous sulphide and digenite phase.

The change of cell volume calculated from lattice constants is shown in Fig. 5. The lattice volume in β-phase is 1/48 of that of the orthorhombic γ-cell. Coefficients of thermal expansion obtained are :—

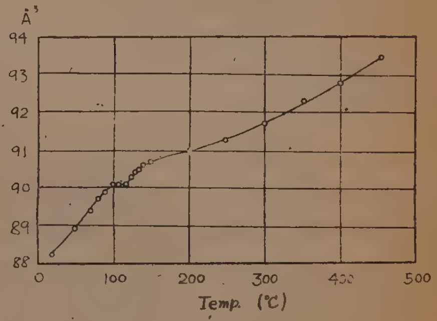

Fig. 5.

$2.08\times10^{-4}/°C$ (γ—Cu_2S)

$0.96\times10^{-4}/°C$ (β—Cu_2S)

The difference in thermal expansion between two phases is rather small.

ii) Intensity changes.

The relative intensity of Debye lines is largely affected by heating the sample in air (Fig. 1). Fig. 6 shows the temperature variation of the intensity ratio of (346) and (600) in γ-phase. In this figure, the open and solid circles correspond to the specimens which differ with each other in their lattice constants. At room temperatures, the intensity ratio I (346)/I(600) is nearly equal to 9:10, but it decreases with temperature gradually near 70°C, reaching 3:10 at 150°C. These intensity changes are reversible if the heating is confined below 150°C. The initiation of the intensity change of Debye lines at 70°C means the beginning of changes of internal structure. This fact may correlate to the change of the lattice constants as described above and of the specific heat and the thermal expansion in the same temperature region as will be described latter.

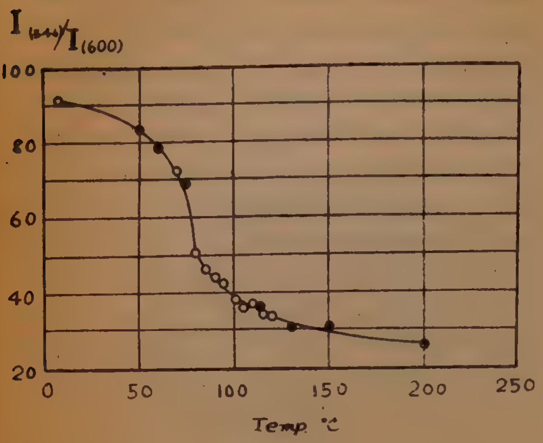

Fig. 6.

If the temperature exceeds 150°C, the sample in air receive the irreversible change of the structure. This intensity variation seems to depend mainly upon the oxidation of the sample. As Buerger suggested, at higher thmperatures the complete reversibility can not be obtained without sealing the sample in the capirally in vaccum.

§ 3. Specific Heat and Thermal Expension.

The differential calorimetry of this substance was performed by Posnjak and Hirahara, the latter found new anomaly at 450°C. The present author measured the absolute value of specific heat by using an adiabatic calorimeter. A thin walled copper vessel containing about 5 cc of sample powder is kept adiabatically at elevated temperatures. The constant energy (about 0.1 watt) is introduced into the vessel by electric heating, the heating rate being about 1°C per three minutes. The absolute value of specific heat is calibrated by quartz powder. The measurements were made in air.

At first, we studied on the mixture of the sample I and II, in order to obtain the sufficient quantity of the sample. The result is shown in Fig. 7A. There exist small humps at 60° and 70°C, and two farely large peaks at 97° and 105°C in the specific heat temperature curve. These double peaks are ascribed to the mixing of two kinds of samples which differ in the transitional temperature with each other on account of the difference of the chemical composition. The result obtained on the sample III is shown in Fig. 7B. In this case, a small hump and a single large peak at 90°C are observed. The lowering of the temperature of anomaly may also due to the deviation of chemical composition from stoichiometric ratio. (X-ray analysis confirmed it.)

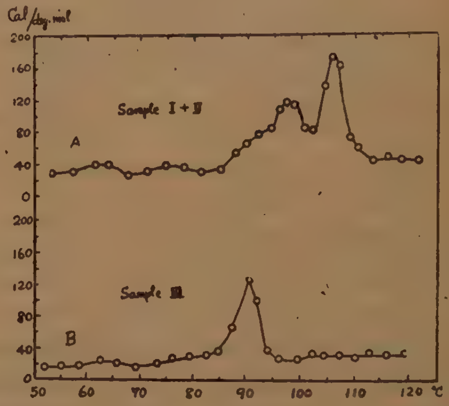

Fig. 7.

The transitional energy ΔQ, and entropy change ΔS in the transition are given by :—$\Delta Q_1 = 896$ cal/deg. mol., $\Delta S_1 = 1.8R$ (R = *gas const.*) These values are considered to be reasonable for the transformation of this kind. The energy change at the transition $\beta \rightleftarrows \alpha$ could not be measured by means of the present apparatus. We can, however, estimate it by utilizing the differential calorimetry curve obtained by Hirahara. That is $\Delta Q_2 = 90$ cal/deg. mol.

We performed the dilatometry by using a glass capirally and a bulb containing the sample of about 6gr. to ascertain the gradual transition at about 115°C**. The method used is the same as formerly described in the case of $BaTiO_3$ by the present author.(6) Heating rate is about 1°C per five minutes. The result is shown in Fig. 8, in which the ordinate represents the total expansion read by the cathetometer: That is the total sum of thermal expansions of the sample itself, glass and paraffine oil. The expansion beins at about 70°C

** Hirahara reported the discontinuous change in thermal expansion at 110°C. (Annual Meeting of the Physical Society of Japan, held at Kyoto, May, 1948).

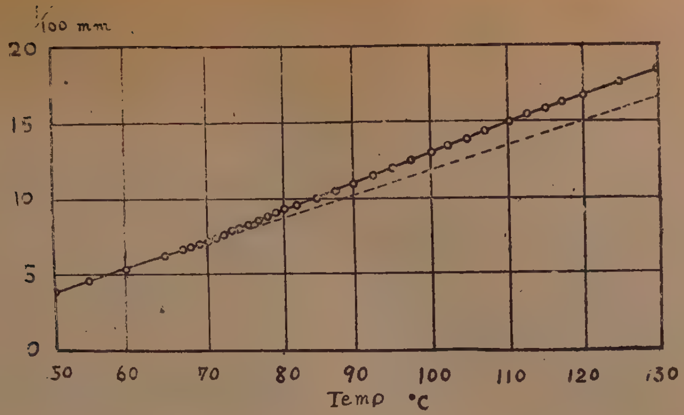

Fig. 8.

gradually and saturates at about 110°C. This result agrees with the change of the lattice volume measured by X-ray method as indicated above.

§ 4 General Discussions.

X-ray powder analysis revealed the two phase changes of cuprous sulphide. In $\gamma \rightleftarrows \beta$ transformation, the change of the lattice volume is continuous and the anomaly in specific heat is so-called λ-type, showing no latent heat. We will now discuss these phase changes from the structural standpoint. We can not, however, touch the complicated structure of γ-phase in detail by using the above X-ray results only, which is concerned with the powder samples. Therefore, the following discussions will be confined to more simple β-and α-phases.

According to Rahalfs, crystal structure of digenite $Cu_{1.8}S$ is cubic antifluorite type, the sulpher atoms in the face-centred positions and the copper atoms in some statistical distribution. In that structure, the spacing d (220) is equal to an half of S-S distance. On the one hand, the fact that d (220) in $Cu_{1.8}S$ and d (110) in β-Cu_2S coincide with each other suggest the existence of the same S-S distance in β-Cu_2S as in digenite. Taking the space group D_{6h}^4 and $Z=2$, the positions of sulpher atoms in β-phase may take one of the following four special positions, each of which satisfy such a S-S distance.

(a) $000,\ 00\frac{1}{2}$　　(b) $00\frac{1}{4},\ 00\frac{3}{4}$

(c) $\frac{1}{3}\frac{2}{3}\frac{1}{4},\ \frac{2}{3}\frac{1}{3}\frac{3}{4}$　　(d) $\frac{1}{3}\frac{2}{3}\frac{3}{4},\ \frac{2}{3}\frac{1}{3}\frac{1}{4}$.

The columus I-IV in the Table II show the calculated |F| -values by assuming that the two sulpher atoms take one of the above four positions and four copper atoms the remaining probable special positions. The column Obs. of the Table II shows the observed |F|-values, which is obtained from the measured line intensity by the relation

$$I \propto p \cdot F^2 \frac{1+\cos^2 2\theta}{\sin^2\theta\cos\theta}$$

where θ is the Bragg angle, p the multiplicity of reflections. The cases, in which two sulpher atoms take one of the four positions (a), (b), (c) and (d), and four copper atoms partly or wholly twenty-four general positions with various parameter values, are also considered. In any case, the agreements were unsatisfactory.

Table II.

Calculated |F| values in β—Cu_2S

(hkl)	Obs.	I	II	III	IV	V	VI
(102)	3	7	2	8	8	11	5
(110)	10	10	10	10	10	10	10
(103)	7	0	0	0	0	0	8
(200)	5	2	2	0	0	9	4
(112)	4	9	6	0	0	9	4
(201)	3	0	0	0	0	0	7
(203)	3	0	0	0	0	0	6
(210)	4	2	2	0	0	6	3
(114)	4	8	8	8	8	6	6
(300)	6	8	8	8	8	5	5
(30)	4	4	7	8	0	5	5

Lastly, if the distribution of copper atoms is completely disorder, the diffraction of X-ray is considered to be mainly due to sulpher atoms. That is:—

(*V*) $2S$ in (*a*) or (*b*)

(*VI*) $2S$ in (*c*) or (*d*)

Columns V and VI in the table 2 correspond to such cases. It is interesting to see that the agreements are fairly good in the case of VI. In these cases, the appropriate temperature factor is taken in calculating the intensity. The complete result, however, cannot be expected by using the powcer samples. It may be interesing to perform the Fourier synthesis on such an "averaged structure" for single crystals.

β-Cu_2S transforms into α-Cu_2S at about 450°C, and Debye pattern becomes similar to that of digenite (Fig. 1). If α-phase belong to the cubic closest packing, the transition $\beta \rightarrow \alpha$ may be due to the lattice transformation $D_{6h}^{4} \rightarrow O_h^{5}$, accompanied with the small transitional heat. In α-phase, the copper ions have the regular stable state again, so that the conductivity may be mainly due to the large mean free paths of electrons.

As we can see from above description, it is not reasonable to explain the phase changes of this substance by Hirahara's model, which assumes the regular and irregular arrangements of two kinds of antifluorite lattice. These two states of antifluorite lattice are the same one to each other, so that we can not expect any transformation by this model.

In conclusion, the author wishes to express his sincere thanks to Dr. S. Miyake (Kobayashi institute) for his valuable discussions and encouragements throughout this study, and also to Prof. T. Muto (Tokyo University) and Mr. E. Hirahara (Hiroshima Technical College) for their interests in this work. Mr. H. Toda kindly helped the author in the experimental works.

References.

(1) E. Hirahara: J. Phys. Soc., Japan **2** (1947) 211.

(2) Posnjak, Allen and Merwin: Econ. Geol. **10** (1915) 491.

(3) L. Ramsdell: Amer, Min. **13** (1928) 115.
P. Rahlfs: Z. Phys. Chem. (B) **31** (1936) 157.
W. Kurz: Z. Krist. **92** (1935) 408.
N. Alsen: Geol. Fareningens I (Stockholm Far.) **53** (1931) 111.

(4) N. W. Buerger: Amer. Min. **27** (1942) 712; Econ. Geol. **36** (1942) 19.
M. J. and N. W. Buerger: Amer. Min. **27** (1942) 216, **29** (1944) 56.

(5) R. Ueda: J. Phys. Soc., Japan. (in press).

On the Magnetic Moment of Complex Ions. (I)

By Masao KOTANI.

Physics Department, Faculty of Science, University of Tokyo.

(Read on April 28, 1946; Received Feb. 28, 1949)

§ 1. Introduction.

Experimentally the effective magnetic moment μ of paramagnetic ions in salts is obtained from observed susceptibilities χ of these salts according to Curie's formula

$$\chi = \frac{N\mu^2}{3kT} + (\text{diamag. term}). \qquad (1)$$

Now, it is well known that the values of the effective magnetic moment μ of some complex ions are quite different from its values found in case of simple salts containing the same metallic ions. For example, the magnetic moment of the ion $\mathrm{Fe(CN)_6}^{---}$ is about 2.3β, where β denotes Bohr magneton, and is considerably smaller than the magnetic moments of ferric ion in most simple salts. According to Pauling,(1) this low value of magnetic moment is explained in the following way. Since two orbitals $d\gamma$ belonging to $3d$ are employed to form sp^3d^2 hybridized orbitals, which are occupied by electrons forming six equivalent covalent bonds between Fe^{---} and CN, the remaining five $3d$ electrons of Fe^{+++} have to be housed in three $d\varepsilon$ orbitals. Hence the spins of two pairs of electrons cancel each other, and the ion shows magnetic moment corresponding to one electron spin

$$\mu = \beta\sqrt{4s(s+1)}_{s=\frac{1}{2}} = 1.73\,\beta \qquad (2)$$

Van Vleck(2) has shown that the same result may be obtained also on the assumption of the ionic bond if the crystalline (or rather intraionic) electric field to which the central ion Fe^{+++} is subjected is sufficiently strong, and called our attention to the fact that the low value of magnetic moment of complex ions cannot be regarded as direct evidence for the covalent nature of bonds between central atom and ligands. Namely, under the influence of electric field of cubic symmetry $3d$ level splits into 2 sublevels, doubly-degenerate $d\gamma$ and triply degenerate $d\varepsilon$, and if the six ligands are electronegative and are arranged at six corners of regular octahedron as in case of $\mathrm{Fe(CN)}^{3-}$ $d\varepsilon$ is lower than $d\gamma$. If the electric field due to ligands is sufficiently strong, the level $d\gamma$ is shifted so high that five d-electrons of Fe^{+++} are housed solely in $d\varepsilon$-orbitals, and the same reasoning as in case of Pauling leads to the formula (2) for the magnetic moment.

According to either interpretation, magnetic moments of these complex ions are regarded as due to the electron configurations $(d\varepsilon)^n$, and if we take spins only into account, their magnitudes are given as follows:

$$\left.\begin{array}{lll} \text{In case of } (d\varepsilon)^1 \text{ and } (d\varepsilon)^5 & & \mu = 1.73\,\beta \\ \quad ,, \quad (d\varepsilon)^2 \text{ and } (d\varepsilon)^4 & & \ 2.83\,\beta \\ \quad ,, \quad\quad\quad\ (d\varepsilon)^3 & & \ 3.87\,\beta \end{array}\right\} \qquad (3)$$

Now, comparing these results with experimental values of magnetic moments of several complex ions shown in Table I, we notice that although in case of $(d\varepsilon)^3$ the observed values are in fair agreement with $3.87\,\beta$ predicted in (3), in cases of $(d\varepsilon)^4$ and $(d\varepsilon)^5$ the observed values are considerably higher than the spin only values given in (3). These additional moments are regarded as due to the contributions of orbital magetic moments which are partly still alive in $d\varepsilon$-orbitals; in fact, Howards(3) have calculated the principal susceptibilities of the single crystal of $\mathrm{K_3Fe(CN)_6}$ successfully on this idea. In the present paper, it is attempted to the derive theoretical formulae for magnetic moments due to electron configurations $(d\varepsilon)^n$, for all possible values of n, $1 \leqq n \leqq 5$.

Table I

Electron configuration	Substance	Observed value	Observer	Spin-only value	Calculated value
$(d\varepsilon)^3$	$K_2[Mn(IO_3)_6]$	3.82 β	Goldenberg (1940)	3.87 β	3.87 β
	$K_3[Cr(CN)_6]$	3.74 β	Welo (1928)		
	$[Cr(NH_3)_6]I_3$	3.80 β	Leiterer (1937)		
	$[Cr(NH_3)_6]Br_3$	3.77 β	,,		
	$[Cr(OC(NH_2)_2)_6]Cl_3$	3.64 β	,,		
	$[Cr(OH_2)_6]Cl_3$	3.78 β	Welo (1928)		
$(d\varepsilon)^4$	$K_3[Mn(CN)_6]$	3.25 β	Goldenberg (1940)	2.83 β	3.60 β
	,,	3.61 β	Blitz (1928)		
	,,	2.95 β	Ray, Bhar (1928)		
	,,	3.40 β	Szego, Ostinelli (1930)		
	$K_4[Cr(CN)_6]$	3.3 β			3.56 β
$(d\varepsilon)^5$	$K_4[Mn(CN)_6]\cdot 3H_2O$	2.11 β	Ray, Bhar (1928)	1.73 β	2.49 β
	,,	2.04 β	Szego, Ostinelli (1930)		
	,,	1.97 β	Freed, Casper (1930)		
	,,	2.18 β	Goldenberg (1940)		
	$K_3[Fe(CN)_6]$	2.2 β	Ishiwara (1914)		2.46 β
	,,	2.36 β	Blitz (1928)		
	,,	2.33 β	Coryell, Stitt, Pauling (1937)		
	Ferrihemoglobin cyanide	2.50 β	,,		(2.46 β)
	Ferrihemoglobin hydrosulfide	2.26 β	,,		
	$Na_2Fe(CN)_5NH_3\cdot 2H_2O$	2.38 β	Welo (1928)		
	$Na_3Fe(CN)_5NO_2\cdot 2H_2O$	2.26 β	,,		

§ 2. Calculation of Effective Magnetic Moment.

The general basic formula for the magnetic susceptibility is well known,(4) which is applicable to cases when exchange coupling between magnetic ions is negligible and we have effectively "one ion problem". It expresses molar susceptibility in the following form:

$$\chi_{\text{mol}} = L\,\frac{\sum\limits_{n,m}\left\{\dfrac{(E_{nm}^{(1)})^2}{kT}-2E_{nm}^{(2)}\right\}e^{-\frac{E_n^{(0)}}{kT}}}{\sum\limits_{n} g_n\, e^{-\frac{E_n^{(0)}}{kT}}} \qquad (4)$$

where $E_n^{(0)}$ means energy levels under no applied magnetic field, and $E_{nm}^{(1)}$ and $E_{nm}^{(2)}$ denote coefficients of 1st and 2nd order Zeeman displacements of levels respectively, defined by the relation

$$E_{nm} = E_n^{(0)} + E_{nm}^{(1)}H + E_{nm}^{(2)}H^2 + \cdots \qquad (5)$$

Magnetic field removes in general g_n-fold degeneracy of level n, and these sub levels are specified by magnetic quantum number m. Equating (4) to (1) effective magnetic moment μ is obtained immediately. We have to bear in mind that μ thus obtained is in general a function of temperature.

In order to apply this general procedure to the case of 6-coordinated complex ions of the type $[MX_6]^{-n}$, we take the following Hamiltonian for the central ion

$$H = H^0 + V_{\text{cubic}} + A\sum l_i s_i + \beta H\cdot(L+2S) \qquad (6)$$

in which the last term denotes energy due to applied magnetic field H, $A\sum\limits_i l_i s_i$ denotes spin-orbit interaction, and $H^0 + A\sum l_i s_i$ is the Hamiltonian of the free metallic ion. V_{cubic} denotes intramolecular (and possibly part of crystalline) electrostatic energy, mainly due to six ligands (CN in the example referred to above), and is assumed to have cubic symmetry. Moreover, we assume that V_{cubic} is so strong that the level $d\gamma$ lies sufficiently high above $d\varepsilon$, and hence the central ion has the electron configuration $(d\varepsilon)^n$ only. (According to

Pauling's interpretation the same electron configuration is realized because $d\gamma$-orbitals are employed in forming bonding orbitals.) We give in the following our results for each value of n separately.

(i) $(d\varepsilon)^1$

Including spin, level $(d\varepsilon)^1$ is sixfold degenerate. Spin-orbit interaction splits this into two levels, and magnetic field splits further each of these levels into two. The energy values of these levels can be obtained as the roots of secular equations: we omit the details of their construction and give the formulas ef these levels. Up to the second order of magnetic field intensity they are given by

$$\left.\begin{array}{ll} A+\beta H+\dfrac{4}{3}\dfrac{\beta^2}{A}H^2; & \\ A-\beta H+\dfrac{4}{3}\dfrac{\beta^2}{A}H^2, & \\ -\dfrac{1}{2}A & \text{(doubly degenerate)} \\ -\dfrac{1}{2}A-\dfrac{4}{3}\dfrac{\beta^2}{A}H^2 & (\qquad ,, \qquad) \end{array}\right\} \quad (7)$$

These levels are shown diagrammatically in Fig. 1. Six-fold degenerate level $d\varepsilon$ shown in (a) splits into two levels as shown in (b) when spin-orbit interaction is taken into account, and (c) shows further splitting caused by the magnetic field (Zeeman splitting).

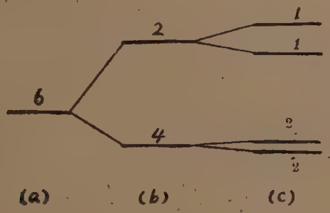

Fig. 1

On substituting these results into (5), we find for the effective number of Bohr magneton $n_{\text{eff}}=\dfrac{\mu}{\beta}$ the following formula:

$$n_{\text{eff}}^2=\frac{8+(3x-8)e^{-\frac{3}{2}x}}{x(2+e^{-\frac{3}{2}x})}, \qquad (8)$$

where $x=\dfrac{A}{kT}$.

(ii) $(d\varepsilon)^5$

Since there are three independent $d\varepsilon$ orbitals, $(d\varepsilon)^6$ is a closed-shell configuration. Hence energy level structures arising from $(d\varepsilon)^n$ and $(d\varepsilon)^{6-n}$ are closely related. Especially, as long as operators which are expressible as sums of quantities depending on coordinates and momenta of single electrons, such as $A\sum l_i s_i$ are concerned, level diagram for $(d\varepsilon)^{6-n}$ is just the inverted one of that for $(d\varepsilon)^n$. In case of $(d\varepsilon)^5$, therefore, energy levels, which are obtained by taking spin-orbit interaction and magnetic field into account, are expressed by formulae (7) in which A is replaced by $-A$, and are represented graphically by turning Fig. 1 upside-down. With the use of this result the magnetic moment can be calculated as in the former case; and we find

$$n_{\text{eff}}^2=\frac{3x+8-8e^{-\frac{3}{2}x}}{x(1+2e^{-\frac{3}{2}x})}. \qquad (9)$$

This formula may be obtained from (8) simply by substituting $-x$ for x.

(iii) $(d\varepsilon)^2$

Two electron system $(d\varepsilon)^2$ gives rise to triplet and singlet states. Since Hund's rule will hold in the present case, the ground state will belong to the triplet. Now, as triplet states arising from $(d\varepsilon)^2$ we have only one level (excluding spin-orbit interaction) ${}^3T_1$, which has nine-fold degeneracy. If we take spin-orbit interaction and magnetic energy into account the degeneracy is completely removed, and we have following levels

$$\left.\begin{array}{l} A+12\dfrac{\beta^2}{A}H^2 \\ \dfrac{A}{2}+\dfrac{1}{2}\beta H+\dfrac{9}{4}\dfrac{\beta^2}{A}H^2 \\ \dfrac{A}{2}\qquad\quad -9\dfrac{\beta^2}{A}H^2 \\ \dfrac{A}{2}-\dfrac{1}{2}\beta H+\dfrac{9}{4}\dfrac{\beta^2}{A}H^2 \\ -\dfrac{A}{2}+\beta H \\ -\dfrac{A}{2}+\dfrac{1}{2}\beta H-\dfrac{9}{4}\dfrac{\beta^2}{A}H^2 \\ -\dfrac{A}{2}\qquad\quad -3\dfrac{\beta^2}{A}H^2 \\ -\dfrac{A}{2}-\dfrac{1}{2}\beta H-\dfrac{9}{4}\dfrac{\beta^2}{A}H^2 \\ -\dfrac{A}{2}-\beta H \end{array}\right\} \quad (10)$$

(See Fig. 2).

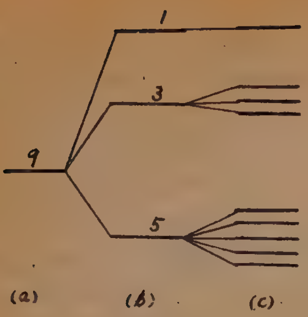

Fig. 2.

Using (10), (5) and (1), we obtain following formula for n_{eff}:

$$n_{\mathrm{eff}}^2 = \frac{3\left\{\frac{5}{2}x+15+\left(\frac{x}{2}+9\right)e^{-x}-24e^{-\frac{3}{2}x}\right\}}{x\left(5+3e^{-x}+e^{-\frac{3}{2}x}\right)}. \tag{11}$$

(iv) $(d\varepsilon)^4$

Energy level diagram is just that of Fig. 2 turned upside down. Formula for n_{eff} is obtained simply by changing x into $-x$ in (11)

$$n_{\mathrm{eff}}^2 = \frac{3\left\{24+\left(\frac{x}{2}-9\right)e^{-\frac{1}{2}x}+\left(\frac{5}{2}x-15\right)e^{-\frac{3}{2}x}\right\}}{x(1+3e^{-\frac{1}{2}x}+5e^{-\frac{3}{2}x})}. \tag{12}$$

(v) $(d\varepsilon)^3$

In this case the ground state is expected to be quartet. Now, $(d\varepsilon)^3$ gives only one quartet level, which has no orbital degeneracy. Hence the orbital motion of electrons makes no contribution to the magnetic moment, and n_{eff} has the constant, spin-only value $\sqrt{15} = 3.87$ independent of temperature.

§ 3. Discussion of Results and Comparison with Experiment.

The behavior of n_{eff} given by (8), (9), (11), (12) is represented graphically in figs. 3 and 4, in which abscissa is chosen as $\frac{1}{x} = \frac{kT}{A}$, or the temperature measured in unit of $\frac{A}{k}$. In cases of $(d\varepsilon)^1$ and $(d\varepsilon)^4$, the lowest level shows no 1st order Zeeman effect, so that n_{eff} tends to zero as the temperrture approaches the absolute zero. In cases of $(d\varepsilon)^2$ and $(d\varepsilon)^5$, however, n_{eff} tends to finite values $\sqrt{\frac{3}{2}} = 1.22$ and $\sqrt{3} = 1.73$ respectively as the temperature is lowered unlimitedly. In the limit of high temperature n_{eff} converges to $\sqrt{5} = 2.24$ in both cases $(d\varepsilon)^1$ and $(d\varepsilon)^5$, while it converges to $\sqrt{10} =$

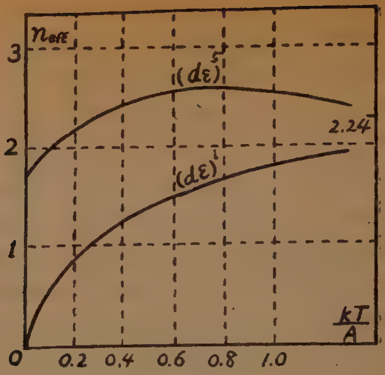

Fig. 3

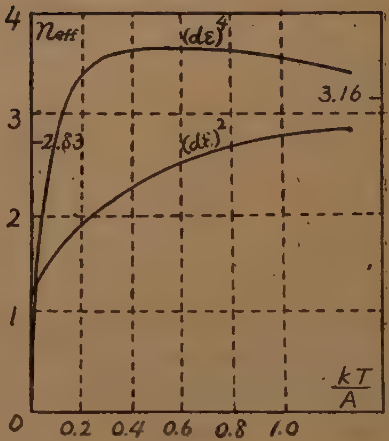

Fig. 4

3.16 in cases $(d\varepsilon)^2$ and $(d\varepsilon)^4$. As the result of calculation we find that in cases $(d\varepsilon)^4$ and $(d\varepsilon)^5$ n_{eff} has board maximum in the range $x = 0.4 \sim 1.0$, and these maximum values 2.52 and 3.64 are considerably higher than the spin-only values 1.73 and 2.83. This means that the orbital motion of electrons gives appreciable contribution to the magnetic moment over large range of temperature so long as the intramolecular electric field is assumed to have nearly cubic symmetry. Especially, although n_{eff} tends to zero with T in case $(d\varepsilon)^4$ as remarked above, it rises steeply, reaches spin-only value already at $T \fallingdotseq 0.12\frac{A}{k}$, and is always larger than the latter value at higher temperatures. Contrary to this, in cases $(d\varepsilon)^1$ and $(d\varepsilon)^2$ n_{eff} increases monotonously with T, and reaches spin-only values firstly at temperatures of the order of $\frac{A}{k}$.

As experimental values which may be compared with our results we give observed values of n_{eff} of several complex ions of the type $[MX_6]$ in Table I. Data for complex ions which correspond to electron configurations $(d\varepsilon)^1$ and $(d\varepsilon)^2$ are not available, as far as the author is aware of. Corresponding to $(d\varepsilon)^3$ we have complex salts with Cr^{+++} and Mn^{++++} as central atoms. In these complex salts n_{eff} is fairly close to the spin-only value 3.87. This is in satisfactory agreement with our theoretical result that the orbital motion does not contribute to n_{eff} in case of $(d\varepsilon)^3$. In cases of complex salts whose central ions have $(d\varepsilon)^4$ or $(d\varepsilon)^5$ configuration, observed n_{eff} is fairly larger than the spin-only value, but is not so high as to exceed the theoretical maximum value mentioned above. Thus theory and experiment agree also in these respects. Further, in order to make quantitative comparison we have to know the values of characteristic temperature $\frac{A}{k}$ for individual ions. Spectroscopy gives following values for them:

	Cr^{++}	Mn^{+++}	Mn^{++}	Fe^{+++}
A (cm^{-1})	226	341	(395)	(440)
A/k (°K)	326	492	(570)	(635)

With the use of these values n_{eff} has been calculated for room temperature and is shown in the last column of Table I. (Values tentatively calculated for ferrihemoglobin cyanide and ferrihemoglobin hydrosulfide are given in parenthesis because six ligands are not completely equivalent in these complex ions so that it seems necessary to assume intramolecular electric field of symmetry lower than the cubic.) Although the agreement of these calculated values with observation is in general fairly good, we must refrain ourselvee from placing too much weight in the quantitative agreement on the following grounds. Firstly, most observations were made on powdered crystals, and for each individual crystallite the central magnetic ion is probably subjected to electric field of lower symmetry. Secondly, Jahn-Teller effect will distort to some extent the octahedron formed by six ligands even without the action of mor distant atoms. Relatively large disagreement in case of $K_3[Mn(CN)_6]\cdot 3H_2O$ might probably be explained by taking these effects into account. These considerations indicate that there is room for several refinements in our theory. However, the available experimental data are not enough to encourage us to develop these refined and elaborate theories; we should emphasize that the measurements of paramagnetic anisotropy for single crystals of complex salts, especially the measurements over wide range of temperature, are very desirable. Our main purpose of the present note is to show that the deviation of n_{eff} of some complex ions from Pauling's spin-only values may be explained satisfactorily as contributions from the magnetic moment due to orbital motion of electrons.

Though another possibility remains that these excess of n_{eff} is explained on the assumption that besides $(d\varepsilon)^n$, $(d\gamma)(d\varepsilon)^{n-1}$ or $(d\gamma)^2(d\varepsilon)^{n-2}$ is included in some percentage in the ground state, this interpretation does not appear attractive to us, since salts corresponding to $(d\varepsilon)^6$ are diamagnetic, as $K_4Fe(CN)_6$. However, we intend to study these points with the use of molecular orbitals, and hope to obtain at the same time clearer insight into the nature of intramolecular bonds in complex ions.

Several Experiments on the Permalloy Problem.

Yuzo TOMONO.

Physical Department, Faculty of Science, University of Tokyo.

(Received March 18, 1949)

§ 1. Introduction.

We mean by "the permalloy problem" the followings: a) Ni–Fe alloy with similar composition to the permalloy, when quenched from 600°C, shows very high initial permeability. b) The same alloy, tempered or cooled in the magnetic field, has high maximum permeability, small coercive force and small magneto-striction.

Previously some researchers⁽¹⁾ said that a) was due to the rapid cooling which prevented the impurity precipitation and b) due to the plastic deformation which fixed the magnetic domains to the field direction. But recently the existance of superlattice phase Ni_3Fe was discovered by O. Dahl⁽²⁾ and verified at Dr. Kaya's laboratory⁽³⁾ by various experimental methods. Since then this problem has been investigated from the viewpoint of superlattice transformation.

Our experiments stand on this point of view. And it is our question when internal stress grows larger on the cource of superlattice formation. If these alloys are quenched before the internal stress grows larger, they will show high initial permeability and if they are cooled in the magnetic field as the internal stress is growing, we shall see field cooling effect. At present stage, it is imagined that this growth of internal stress may be due to the lattice contraction in the process of superlattice formation.

§ 2. Investigation on the Field Cooling Effect.

Our specimens are Ni–Fe alloys whose iron contents are 10-60 %. These are annealed at 1000 °C for 2 hours and cooled slowly, the magnetic field of 50 Oe. being applied from various temperatures to 20°C.

Fig. 1 and 2 show respectively maximum permeability and saturation magneto-striction versus

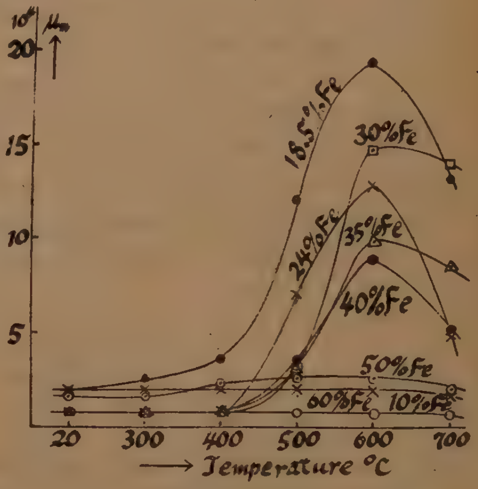

Fig. 1.

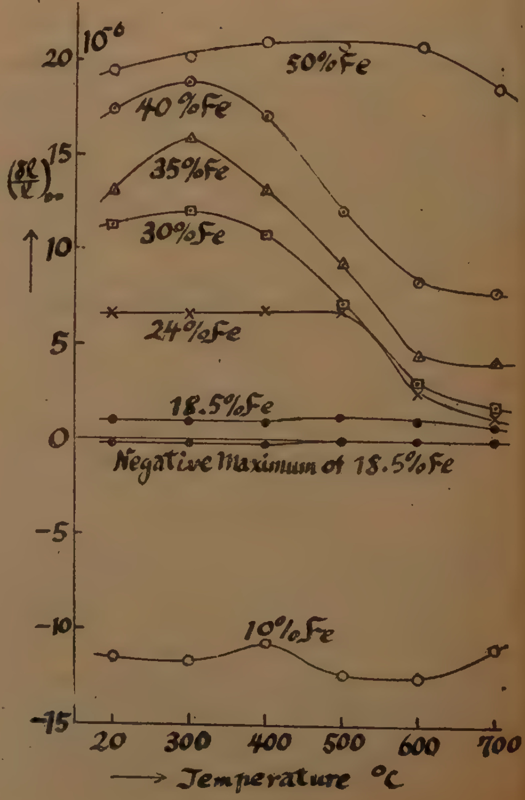

Fig. 2.

temperature from which the field is applied.

They show that field cooling effect is remarkable on specimens whose compositions are near Ni_3Fe and which are cooled in the field above 500°C. As the critical temperature of Ni_3Fe is 490°C, these are the expected results.

But we are interested in the peculiar effect between 500°C and 600°C. Therefore, we performed the following experiments.

We take two specimens whose iron contents are 24.5 and 30 %, which are most sensible to the field cooling. As cooling them after annealing at 1000°C for 2 hours, the magnetic field of 20 Oe. is applied for every 30°C temperature interval near 500°C. Then they are cooled slowly to room temperature without the field.

Saturation magneto-striction versus temperature interval where the magnetic field was applied is shown in Fig. 3. On both specimens, above 490°C, especially between 510°C and 540°C, the field cooling effect is most interesting. This temperature range is a little higher than the critical temperature, where the nuclei of Ni_3Fe may appear.

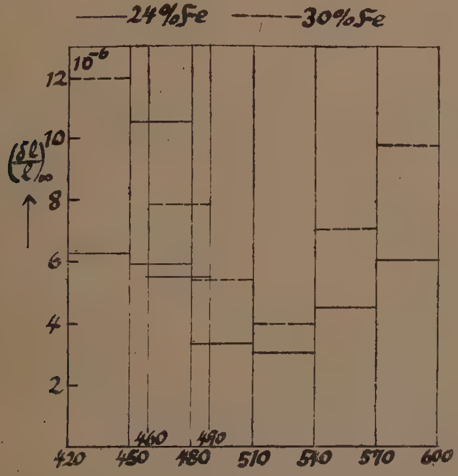

Fig. 3.

§ 3. Investigations on the Permalloy Effect.

We used three specimens whose iron contents are 21.5, 24.5 and 30 %. After annealing at 1050°C for 1 hour, they are cooled slowly to some temperature, kept there for 30 minutes, and rapidly cooled on the cold copper plate. These temperature versus initial permeability curves are illustrated in Fig. 4.

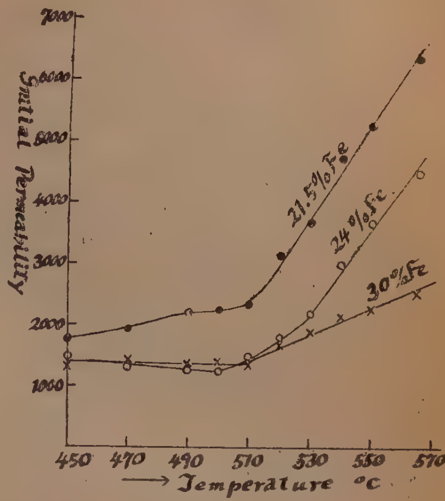

Fig. 4.

Very high values at 600°C decrease rapidly down to 510°C, below which they do not change so peculiarly as above.

§ 4. Summary.

We have found from the two experiments that a little above 490°C the internal stress grows enough to fix the magnetic domains and utterly decrease initial permeability. The same initial permeability decrease was observed by Dr. Kaya and others when specimens, quenched from 600°C, were kept at 490°C for a few minutes. In this case too, we can expect only nuclei of superlattice may exist. Now we know from our experiments that the magnetic domains are also fixed at the same stage of superlattice formation.

The term "internal stress" we used above is a vague word. We mean by it the force or atom arrangement which minimize the free energy of the magnetic domain with regard to some special direction. But theoretical relation between internal stress and initial permeablity is not clear. The theories of R. Becker and others are not reliable in this case, because they are based on some special conditions.

Closing this short paper we want to express sincere thanks to Dr. Kaya and members of his laboratory for their encouragement and support.

References.

(1) Bozorth, Dillinger and Kelsal. Phys. Rev. **45** (1934) 742. Kussman, Scharnow and Steinhaus: Heraeus-Vakuumschmelze Fest Band, Hanau (1933) 310.

(2) O. Dahl, Z. Metallkde: **24** (1932) 107, **28** (1938) 133.

(3) S. Kaya, J. Fac. Hokkaido Univ. Ser. 2, **2** (1938) 29 S. Kaya, H. Sato and Y. Kumassaka: Kinzoku-gakkaisi 6 (1937).

On the Grid Emission.

By Tetsuya ARIZUMI and Shin-ichiro NARITA.

Kawanishi Machine Works Ltd.

(Received Mar. 28, 1949)

§ 1. Introduction.

The grid in a vacuum tube with the oxide coated cathode is contaminated by some kind of substances, evaporated from the cathode and sometimes it turns into a new source of thermionic emission, when it is heated by the thermal radiation or by electron bombardment. The "grid emission" increases the tube noise, limits the amplification ratio and has some unfavorable effect upon the tube characteristics.

Up to the present time, however, little has been known on the grid emission. Only two papers by C. Davisson and A. Pidgeon⑴ and by G. L. Tawney⑵ have been published without any agreement and conclusive discussion. In the present paper, the thermionic emission from several kinds of metals contaminated by evaporated substances from the oxide coated cathode have been pursued in details, to find out the effect of activity of the cathode upon the grid emission and to make clear how the contaminated layer is being built up.

§ 2. Experimental Procedure.

The experimental tube is shown in Fig. 1. A movable plate with a window was mounted around an oxide coated cathode and one or two fine metal wires or sleeves (designated by *G*-metal in the following) were mounted outside the plate. Only when the window of the plate is faced perpendicularly to the front of the cathode, evaporated materials go through the window to the *G*-metal. When the thermionic emission from the contaminated *G*-metal (designated by *G*-emission) is measured, the plate is moved to a opposite side and the cathode is cooled. The emission from the cathode is able to be measured at the same condition, if necessary. The *G*-emission was always measured at 750°K by a galvanometer with the sensitivity of 10^{-10} ampere per millimeter. During evaporation the cathode was kept at 1250°K and the *G*-metal at the cold state except several special cases. Evaporation and emission measurement were carrid out alternatively.

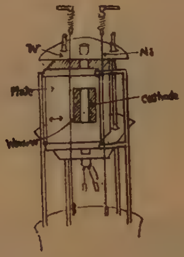

Fig. 1.

For determing the work function of the contaminated *G*-metal, both the cathode and the *G*-metal in a ordinary tube were replaced by cathode sleeves of rectangular section, because they are convenient for exact determination of temperature for which a Ni—W thermo-couple, previously calibrated, was weld to the sleeve.

All experimental tubes were evacuated by a three stage oil diffusion pump backed by a Cenco-type Megavac pump. After the glass baking, degassing of all metal parts and the activation of the cathode, the getter was flashed and the tube was tipped off.

The final pressure attainable was below 10^{-} m.m. Hg.

§ 3. Work Function.

As the amount of contamination on the *G*-metal becomes larger, the *G*-emission current increases rapidly at first and then it is followed by a gradual increase. Fig. 2 (a) and (b) shows the change of the *G*-emission from contaminated tungsten and molybdenum. Both curves are different from the activation curve of thorium on tungsten in which the emission becomes to saturate as the formation of the mono-molecular layer of thorium, suggesting that the contamination on the *G*-metal has a different structure.

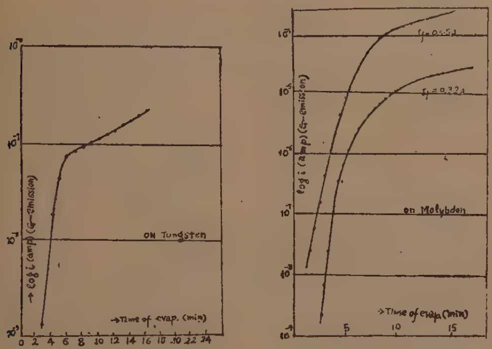

(a) (b)

Fig. 2.

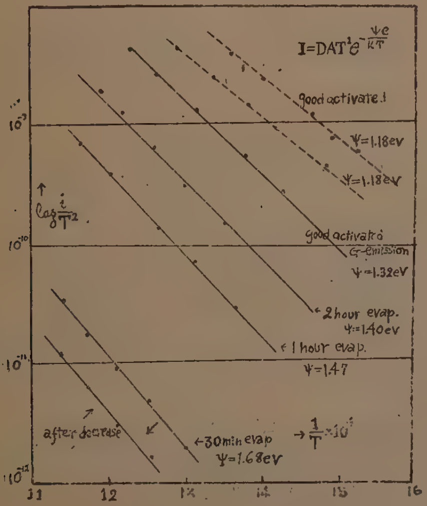

Fig. 3.

Fig. 3 shows Richardson lines for the contaminated nickel sleeve in which the work function approaches gradually to that of the oxide coated cathode, shown in a dotted line, as the amount of contamination increases. The result shows that the contamination has almost similar structure as the oxide coated cathode.

X-ray and electron diffraction studies on the the oxide coated cathode(3) have revealed that surface of the cathode after a long run is covered by SrO only, giving the direct evidence that BaO evaparates chiefly from the oxide coated cathode. Thus the most part of contamination on the *G*-metal is supposed to be BaO. The result in Fig. 2 suggests that BaO condensed on to the *G*-metal does not form the mono-molecular layer, but aggregates to tiny crystals.

§ 4. Evaporation of Barium from the Cathode.

Small amount of excess barium is always contained in the activated oxide coated cathode. If they are evaporated from the cathode together with BaO the *G*-emission must have a close dependency upon the activity of the cathode. The relation is shown in Fig. 4.

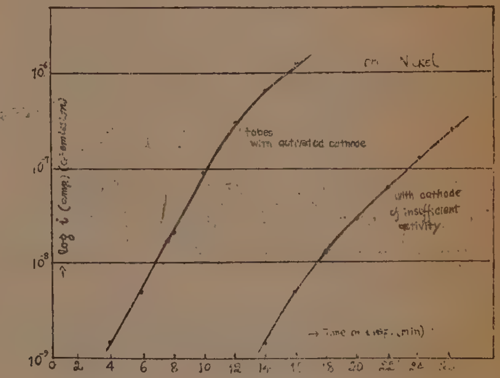

Fig. 4.

In one tube with the activated cathode the *G*-emission becomes measurable much earlier than in the other tube with the cathode of insufficient activity. As the cathode in the latter tube becomes to be activated gradually during the evaporation of several minutes, the inclinations of both curves are almost equal. Similar results are also shown in Fig. 5, in which time changes of *G*-emissions are

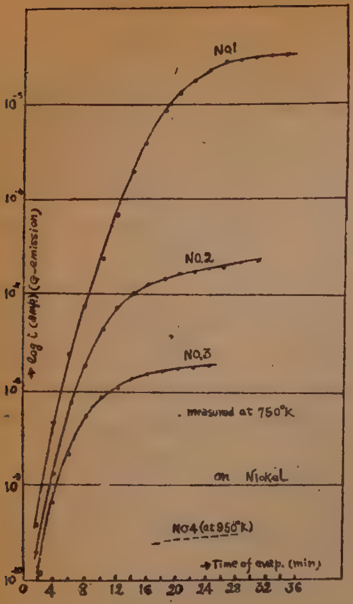

Fig. 5.

plotted with the parameter being the cathode emission at 650°K. From these results some quantity of excess barium is found to evaporate from the oxide coated cathode.

Table I.

Tube number	No. 1	No. 2	No. 3	No. 4
Cathode activity (at 650°k) (ma)	8.0	0.52	0.17	1×10^{-6}
Saturation value of *G*-emission (at 750°k) (ma.)	6.10^{-2}	48.10^{-4}	4.10^{-5}	—

The amount of *G*-emission is almost proportional to the square value of the thermionic emission current from the cathode, which is, in general, represented(4) by

$$i_0 = ADN_0^{1/2}T^{4/5}\exp\left\{\frac{-(E/2+\phi)e}{KT}\right\}, \cdots\cdots\cdots\cdots(1)$$

as seen in Fig. 5 and table 1. Evaporation of free barium from the cathode will be written in the form,

$$n = K_1N_0e^{-F/RT}\backsim i_0^2, \cdots\cdots\cdots\cdots\cdots(2)$$

Thus the above experimental result shows that the *G*-emission should obey the emission formula(5)

$$i = A'D'n_0T^2\exp\left\{\frac{-(E+\phi)e}{KT}\right\}\backsim i_0^2 \cdots\cdots\cdots\cdots(3)$$

As the evaporation energy of free barium in the oxide coated cathode is smaller than that of barium oxide, the relative amount of barium in the contamination on the *G*-metal should be larger than in the cathode. Neverthless, the *G*-emission is represented by (3), which is applicable to a deactivated cathode. This strange result suggests that the behavior of barium atoms and barium oxide molecules are quite different.

§ 5. Effect Temperature.

Throughout above-mentioned experiments, the *G*-emission was measured at 750°K for at higher temperature a gradual change of the *G*-emission was observed even during the emission measure-

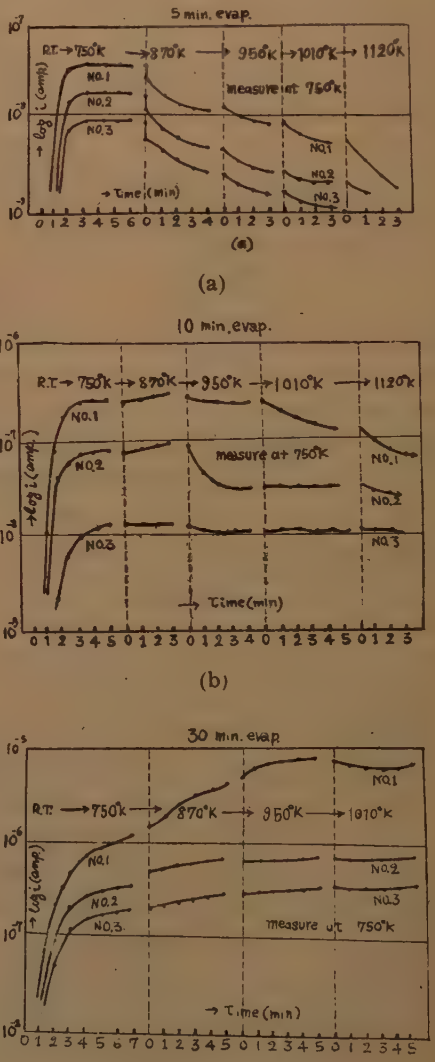

(a)

(b)

(c)

Fig. 6.

ment. For studying the effect of temperature on the G-emission the following procedure was used: The contaminated G-metal was kept at a higher temperature for several minutes without evaporation and then it was cooled to the measuring temperature 750°K. Although contaminated barium oxide may evaporate above 1200°k, it is perhaps negligible in the temperature range in the experiments.

The obtained results are presented in Fig. 6, (a) (b) and (c), each of which corresponds to 5, 10 and 30 minutes evaporation respectively. It is seen in the figure that the G-emissiou from the contaminated nickel decreases in the case of thin contamination while it begins to increase as the amount of contamination increases. Almost Similar results were obtained for the G-emission from the contaminated tungsten.

There are several possibilities to explain such behaviour of the G-emission: the crystal growth of contaminated barium oxide, the chemical reaction of barium and barium oxide with the base metal, the evaporation of barium from the G-metal and so on.

The first hypothesis, however, fails to explain the increase of the G-emission in the thick contamination, while the second also fails to explain the silimar thermal effects on the G-emission in nickel and tungsten. Thus only the third hypothesis is mainly responsible for the results shown in Fig. 6 and 7. From the standpoint of this hypothesis, the decrease of the G-emission is proportional to the amount of evaporation of barium atoms from the contaminated G-metal, which is represented by the similar formula as (2). In Fig. 8, $\log (i_0-i)/i_0$, where i_0 is a initial and i is the G-emission st any time, is plotted with the abscissa $1/T$, from the data in Fig. 7. As the inclination of each curve gives the energy of evaporation of barium atoms, Fig. 8 shows that the evaporation of barium becomes difficult as the amount of the contamination increases.

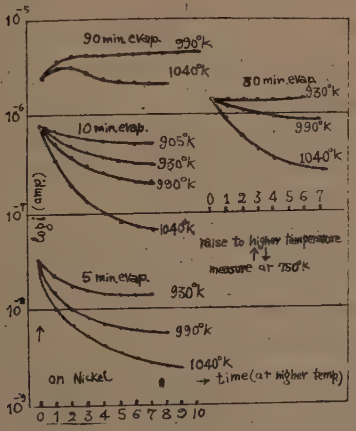

Fig. 7.

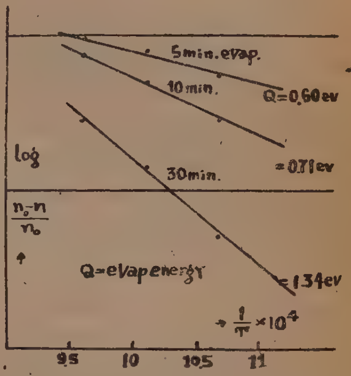

Fig. 8. Evap. energy of Ba.

§ 6. Effects of the G-metal.

For studying the effects of the base metal upon the G-emission, two kinds of G-metals were mounted at equal distances apart from the cathode and G-emissions from both metals were measured. In Fig. 9 G-emissions from tungsten and nickel are shown. The initial increase of the G-emission in tungsten

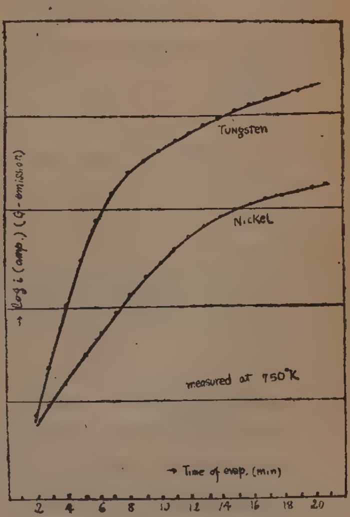

Fig. 9

is much steeper than that in nickel showing that the behaviours of barium and barium oxide on both metals are different. This assumption is supported by the following experiment: the temperatures of G-metals with same thick contamination were kept at 820°k for two minutes and then their temperatures were lowered to 750°k to measure the G-emissions. The results are shown in Fig. 10, in which the increase of the G-emission in the tungsten is observed to be much more rapid than in the case of nickel. Only in the case of thin contamination, however, the change of the G-emissions in both metals are almost similar.

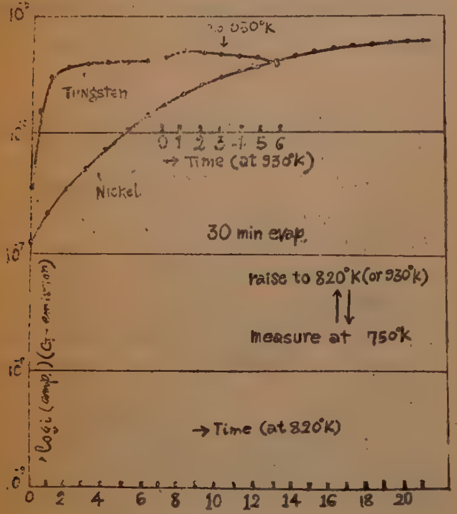

Fig. 10.

If the contaminated G-metal is kept at 970°k and then cooled to 750°k, the G-emission decreases. Then the G-metal is exposed to evaporation from the cathode for two minutes to increase the G-emission. By alternation of both processes, the results presented in Fig. 11, (a) and (b) were obtained in which the dotted lines represent the G-emission when the G-metal is exposed to evaporation continuously. Two curves for nickel and tungsten are almost similar, but in the case of nickel the curve takes an almost same locus as that of continuous evaporation, while it is not so in the case of tungsten. Both results in the preceeding and this paragraphs seem to give evidences that the behaviours of barium are not so different in the thin contamination. Moreover, the final results deny the mono-molecular structure of the contamination. If the mono-molecular structure is assumed, the decrease of the G-emission is almost equal to the increase because the change of the emission is directly proportional to the covering area of the mono-molecular layer.

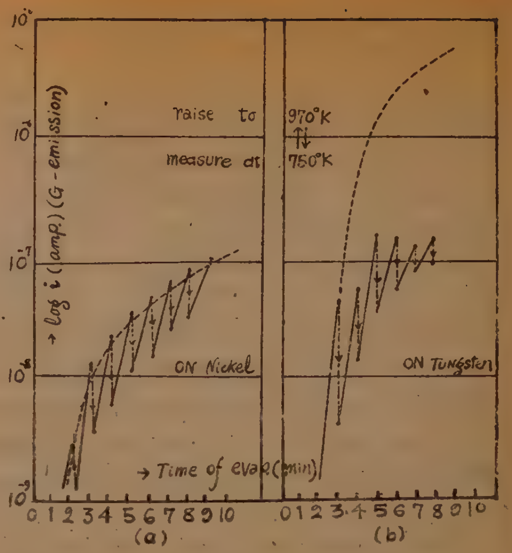

Fig. 11.

§ 7. Discussion.

It has been pointed out in previous sections that both barium and barium oxide evaporate from the oxide coated cathode and the contaminated substances does not form the mono-molecular layer. The contaminated barium and barium oxide, perhaps co-agulates together into fine crystals. The measured G-emission should be a thermionic emission from these fine crystals, for the emission of barium on G-metal is much smaller than that of these crystals. Thus the evaporation from contaminated G-metal, described in § 5, means that some amount of barium evaporates from these co-agulated fine crystals.

The relative amount of barium in the contamination is larger than that in the original oxide coated cathode, because the energy of evaporation of barium is less than that of barium oxide itself. Barium oxide in the contamination does not evaporate easily, but it is not the case with barium atoms. One part of barium atoms evaporates, the other part diffuses into the G-metal, the third part remains on the surface and the fourth co-agulates together with barium oxide into fine crystals. Only the last part has a main effect upon the G-emission, but its ratio to total barium seems to be very small so long as the amount of the contamination is still small. This is verified by the fact that the *G*-emission obeys the emission formula (3) in spite of the activity of the original cathode.

Both experimental results that *G*-emission increases gradually to saturate when the temperature is held at 750°k and that it takes longer time for the saturation of the *G*-emission as the contamination becomes thicker, show that co-agulated crystal sizes differ in both cases. Probably larger crystals are formed in the thicker contamination, and thus the work function of the contaminated *G*-metal approaches gradully to the original oxide coated cathode as shown in Fig. 3.

Moreover the result in Fig. 8 that the energy of evaporation becomes larger as amount of the contamination increases shows that the evaporation of barium is easier from fine crystals than from larger stable ones. The phenomena observed in the heat-treatment of the *G*-metal are well explained by this hybothesis; when the amount of the contamination and crystal size are still small, barium evaporates easily and thus the *G*-emission decreases by a slight heat-treatment, while it does not decrease without severe treatment in the thick contamination.

The velocity of co-agulation of barium and barium oxide on nickel differs from that on tungsten, resulting in the difference of the activation curves in both cases, as shown in Figs. 9 and 10.

The difficulty of the activation on nickel is probably due to the larger affinity of barium to nickel. The neglisibly small *G*-emission, observed in gold, silver and carbon may be caused by similar effect, whose results will be published in future. The evaporation of barium from co-agulated crystals, however, must be similar independent of the used metals. Both the decrease of the *G*-emission by the heat treatment and the similar behaviour in nickel and tungsten observed in the case of alternative evaporation and heat treatment is also understood.

§ 8. Conclusion.

Main results obtained are as followed.

(1) The *G*-emission increases rapidly at first, followed by a gradual increase.

(2) The work function of the contaminated *G*-metal approaches gradually to that of the original oxide coated cathode.

(3) The *G*-emission is dependent upon the activity of the original cathode, showing that both barium and barium oxide evaporate from the cathode. It is almost proportional to the square value of the cathode emission.

(4) When the contaminated *G*-metal is heated at higher temperature, the *G*-emission decreases or increases as to whether the amount of contamination is small or large respectively.

(5) The kind of *G*-metal has a close dependency upon the *G*-emission. In the case of tungsten the contaminated *G*-metal is activated more easily than in the case of nickel.

These phenomena are well explained by th hypothesis; (1) the contamination coagulates together into small crystals, (2) evaporation of barium from fine crystals is easier than that from stable larger crystals, and (3) the velocity of coagulation depends upon the kind of *G*-metal.

In conclusion we acknowledge all members is our laboratory for their sincere discussions.

References.

(1) C. Davisson and N. A. Pidgeon: Phys. Rev. **15** 553.

(2) Refer to J. P. Blewett: J. App. Phys. **10** (1939) 668.

(3) M. Benjamin and H. P. Rooksby: Phil. Mag. **15** (1933) 810. **16** (1933) 519.
J.A. Darbyshire: Proc. Phys. Soc. **50** (1938) 635.
A. Eisenstein: J. App. Phys. **17** (1946). Aug.

(4) R. H. Fowler: Proc. Roy. Soc. **A 140** (1933) 505.

(5) B. R. A. Nijboer: Proc. Roy. Soc. **51** (1939) 575.

Liquid Rise in a Capillary Tube.

By Yoshiro IKEDA and Teruko SOEYA.

Department of Physics, Faculty of Science, Hokkaido University.

(Received April 4, 1949).

§ 1. Solution of Brittin's Differential Equation.

W. E. Brittin(1) has investigated theoretically the motion of a liquid in a capillary tube. In his paper a differential equation for the motion of the liquid in the tube was set up, and a method of solution was discussed. The results of his calculation were compared with the experimental data by Decharme and Rense, and the agreement be tween theory and experiment was satisfactory in almost all domain except the neighbourhood of the initial point.

In this paper the differential equation is exactaly solved even in a domain near the initial point and it is proved that the agreement between theory and experiment is satisfactory in all domain from 0 to infinity. But E. J. Le Grand and W. A. Rense(2) published new experimental data. In order to explain the result some modification of Brittin's differential equation is inevitable. By solving the modified equation, it is proved that the equation is sufficient enough to give satisfactory agreement between calculation and experiment.

A capillary tube of radius r is toached to the surface of a liquid of density ρ, surface tension σ, and viscosity μ at time $t=0$.

Let Z be the extent of rise of the surface of the liquid measured to the bottom of the meniscus at time $t \geqq 0$, and α the angle that the axis of the tube makes with the horizontal. The problem is then to determine the extent of rise Z, as a function of the time t; $Z=Z(t)$. According to the paper by W. E. Brittin, it is assumed that the same force acts on the liquid when it is in an accelerated state as when it is in a steady state. The amount of the liquid above the bottom of the meniscus is neglected which enables one to write $\pi r^2\rho Z\frac{dZ}{dt}$ for the momentum of the liquid in the tube. The Poiseuille's viscous force for stream line flow is $-8\pi\mu Z\frac{dZ}{dt}$ and the component of the weight along the tube is $-\pi r^2\rho g Z\sin\alpha$ where g is the gravitational force per unit mass. The surface tension force which is responsible for the rise is given by $2\pi r\sigma\cos\vartheta$ where ϑ, the average angle of contact between the liquid and the wall of the tube, is assumed constant. The end of the tube, assumed flat, gives rise to some turbulent flow in the neighbourhood of the opening which produces additional drag force on the liquid. The end-effect drag will be taken to be of magnitude $n\pi r^2\rho\left(\frac{dZ}{dt}\right)^2$ for the liquid entering the tube. Newton's second law of motion yields the following differential equation for the motion of the liquid in the capillary tube.

$$Z\frac{d^2Z}{dt^2}+(n+1)\left(\frac{dZ}{dt}\right)^2+bZ\frac{dZ}{dt}+cZ+d=0 \qquad (1)$$

where

$$b=\frac{8\mu}{\rho r^2},\quad c=g\sin\alpha,\quad \text{and}\quad d=-\frac{2\sigma\cos\vartheta}{\rho r}$$

According to Brittin's paper, n = 1/4, but from the experimental data given by Le Grand and Rense n is not necessarily constant, and b is not always a constant which is assumed to be due to Poiseuille's force alone.

§ 2. Solution of Non-linear Differential Equation.

Assume that a non-linear differential equation which is to be solved can be transformed into the following integral equation by some suitable method;

$$Z=U(t)+\int_0^t F(t,\ Z)dt.$$

If $F(t, Z)$ satisfies the Lipschitz's condition, that is

$$|F(t,\ Z_1)-F(t,\ Z_2)|<k|Z_1-Z_2|$$

in a domain

$$|Z-Z_0| < a, \quad |t-t_0| < b$$

and $|F(t,\ Z)| < M$ in that domain, M and k being positive finite constants, then the equation can be solved by successive approximation and in order that the series obtained by successive approximation may converge quickly, it is desirable that k and M are small.

Now the initial condition is

$$Z(0) = 0 \qquad (2)$$

The initial velocity can be obtained directly from the original differential equation by setting $Z_0 = 0$;

$$\left(\frac{dZ}{dt}\right)_0 = Z_0' = \sqrt{\frac{-d}{n+1}} \qquad (3)$$

The terminal velocity is assumed zero as it must be physically and thus Z_∞ is obtained from equation (1) by setting $Z_\infty' = 0$.

$$Z_\infty = -\frac{d}{c} \qquad (4)$$

By putting

$$\left(\frac{dZ}{dt}\right) = \left(\frac{dZ}{dt}\right)_0 e^{-\lambda t} X \text{ or } Z = Z_0' \int_0^t e^{-\lambda t} X dt \qquad (5)$$

eqnation (1) will be transformed into

$$X' = (\lambda-b)X + (n+1)\left[\frac{e^{\lambda t}-e^{-\lambda t}X^2}{\int_0^t e^{-\lambda t}Xdt} - \frac{Z_0'}{Z_\infty}e^{\lambda t}\right] \qquad (6)$$

It is supposed that Z' decreases gradually and tends to zero with increasing t, but X does not decrease necessarily. If the value of λ is taken suitably, X may decrease gradually and tends to zero with increasing t.

Since

$$\int_0^t e^{-\lambda t} X dt$$

$$= \int_0^\infty e^{-\lambda t} X dt - \int_t^\infty e^{-\lambda t} X dt = \frac{Z_\infty}{Z_0'} - \int_t^\infty e^{-\lambda t} X dt,$$

equation (6) at $t = \infty$ reduces to

$$\lambda(\lambda-b) + (n+1)\left(\frac{Z_0'}{Z_\infty}\right)^2 = 0 \qquad (7)$$

If b is sufficiently large, the quadratic equation has two real roots. In order that the last term in the brace of (6) may be small, the smaller root will be more convenient. From equation (5), it follows $X(0) = 1$. Hence by putting $X = 1+f$ in (6), it follows

$$f' + \Big\{(b-\lambda)$$
$$+ 2(1+n)\lambda \frac{e^{-\lambda t}}{1-e^{-\lambda t}}\Big\} f = (\lambda-b) + (1+n)\lambda(e^{\lambda t}+1)$$
$$-(1+n)\frac{Z_0'}{Z_\infty}e^{\lambda t}$$
$$+(n+1)\left[\frac{e^{\lambda t}-e^{-\lambda t}(1+f)^2}{\int_0^t (1+f)e^{-\lambda t}dt} - \frac{e^{\lambda t}-e^{-\lambda t}(1+2f)}{\frac{1}{\lambda}-e^{-\lambda t}/\lambda}\right] \qquad (8)$$

Hence

$$f = c \exp\left[-\int_0^t \left\{b-\lambda+2(n+1)\frac{\lambda e^{-\lambda t}}{1-e^{-\lambda t}}\right\}dt\right]$$
$$+\int_0^t \left[\lambda-b+(1+n)\lambda(e^{\lambda\tau}+1)-(n+1)\frac{Z_0'}{Z_\infty}e^{\lambda\tau}\right]$$
$$\times \exp\left[-\int_\tau^t \left\{(b-\lambda)+\frac{2(n+1)\lambda e^{-\lambda t}}{1-e^{-\lambda t}}\right\}dt\right]d\tau$$
$$+(n+1)\int_0^t \left[\frac{e^{\lambda\tau}-e^{-\lambda\tau}(1+f)^2}{\int_0^\tau (1+f)e^{-\lambda t}dt} - \lambda\frac{e^{\lambda\tau}-e^{-\lambda\tau}(1+2f)}{1-e^{-\lambda\tau}}\right]$$
$$\times \exp\left[-\int_\tau^t \left\{b-\lambda+\frac{2(n+1)\lambda e^{-\lambda t}}{1-e^{-\lambda t}}\right\}dt\right]d\tau \qquad (9)$$

From $X(0) = 1$, $f(0) = 0$, therefore $c = 0$ and since

$$\int_0^t \left[b-\lambda+2(1+n)\frac{\lambda e^{-\lambda t}}{1-e^{-\lambda t}}\right]dt$$
$$= (b-\lambda)t + 2(1+n)\log(1-e^{-\lambda t})$$

equation (9) reduces to

$$f = \int_0^t \Big[\lambda-b+(1+n)\lambda(e^{\lambda\tau}+1)$$
$$-n\frac{Z_0'}{Z_\infty}e^{-\lambda\tau}\Big]\left(\frac{1-e^{-\lambda\tau}}{1-e^{-\lambda t}}\right)^{2(1+n)} e^{-(b-\lambda)(t-\tau)}d\tau$$
$$+(1+n)\int_0^t \Big[\frac{e^{\lambda\tau}-e^{-\lambda\tau}(1+f)^2}{\int_0^\tau (1+f)e^{-\lambda t}dt}$$
$$-\lambda\frac{e^{\lambda\tau}-e^{-\lambda\tau}(1+2f)}{1-e^{-\lambda\tau}}\Big]\left(\frac{1-e^{-\lambda\tau}}{1-e^{-\lambda t}}\right)^{2(1+n)} e^{-(b-\lambda)(t-\tau)}d\tau \qquad (10)$$

This integral equation can be solved by successive approximation in all domain $t \geqq 0$. When f is small, the series obtained by the second and third approximations give sufficiently exact values of f. As f is rapidly increasing function of t, X decreases to a small value. Then for such value of f the series obtained by the successive approximation converges very slowly. In this case it is preferable to take another method. Write equation (1) as the following

$$Z' = a\left(\frac{Z_\infty}{Z}-1\right) - \frac{(1+n)}{b}\frac{Z'^2}{Z} - \frac{Z''}{b} \qquad (11)$$

where

$$a = \frac{g}{b}$$

Now b is assumed to be very large, hence $1/b$ is a small quantity and denoted by ε. For the first approximation, place

$$Z' = a\left(\frac{Z_\infty}{Z}-1\right) \tag{12}$$

Then

$$Z'' = -a\frac{Z_\infty}{Z^2}Z' = -a^2\frac{Z_\infty}{Z^2}\left(\frac{Z_\infty}{Z}-1\right).$$

For the second approximation

$$Z' = a\left(\frac{Z_\infty}{Z}-1\right)\left\{1-\varepsilon a\left[n\frac{Z_\infty}{Z^2}-\frac{(1+n)}{Z}\right]\right\} \tag{13}$$

Hence

$$Z+(Z_\infty-\varepsilon a)\log(Z_\infty-Z)-\varepsilon an\log Z = at+c$$

or

$$Z-Z_a$$
$$+(Z_\infty-\varepsilon a)\log\frac{Z_\infty-Z}{Z_\infty-Z_a}-\varepsilon an\log\frac{Z}{Z_a} = -a(t-t_a) \tag{14}$$

where $Z_a = Z(t_a)$.

§ 3. Numerical Calculation.

As an example, the data given by Decharme will be investigated. Now

$$n = \frac{1}{4},\quad \frac{8\mu}{r^2} = 258.64,$$

$$Z_0' = 80.117,\quad Z_\infty = 11.70 \quad\text{and}\quad r = 0.00117$$

From equation (7) $\lambda = 0.23$. Hence $e^{\lambda t} = e^{-\lambda t} = 1$ $1-e^{-\lambda t} = \lambda t$ Z is calculated from $t = 0$ to $t = 0.$ by equation (10). As the first approximation, we have

$$f_1 = \left[\lambda-b+\frac{5}{4}\lambda+\frac{5}{4}\left(\lambda-\frac{Z_0'}{Z_\infty}\right)\right]\int_0^t\left(\frac{\tau}{t}\right)^{\frac{5}{2}}e^{-(b-\lambda)(t-\tau)}d \tag{15}$$

As the second approximation, we have

$$f_2 = f_1+(n+1)$$
$$\times\int_0^t\left[\frac{e^{\lambda\tau}-e^{-\lambda\tau}(1+f_1)^2}{\int_0^\tau(1+f_1)e^{-\lambda t}dt}-\lambda\frac{e^{\lambda\tau}-e^{-\lambda\tau}(1+2f_1)}{1-e^{-\lambda\tau}}\right]\left(\frac{\tau}{t}\right)$$
$$\times e^{-(b-\lambda)(t-\tau)}d\tau \tag{16}$$

As the third approximation, we obtain f_3 by putting f_2 instead of f_1 in (16). It will be seen that f is nearly equal to f_2. Thus we obtain

$$Z(0.1) = 2.38 \quad Z(0.2) = 3.09 \quad Z(0.3) = 3.37$$

By equation (14), $Z(0.4)$, ... will be calculated and agreement between calculation and experiment will be shown in Table I.

§ 4. Modification of Brittin's Equation.

Though the calculation in the preceding paragraph agrees with the experimental data obtained by Decharme, it is not sufficient to explain the results obtained by Le Grand and Rense. There

Table I.

t (sec)	Exp. by Decharme (cm)	Calc. by auther (cm)	Calc. by Brittin (cm)	t (sec)	Exp. by Decharme (cm)	Calc. by auther (cm)	Calc. by Brittin (cm)
0.1		2.38		2.5		8.36	
0.2		3.09		3.0	8.80	8.82	8.52
0.3		3,73		4.0	9.46	9.59	9.36
0.4		4.24		5.0	9.98	10.09	9.94
0.5		4.67		6.0	10.36	10.44	10.36
0.6		5.05		7.0	10.65	10.70	10.61
0.7		5.37		8.0	10.85	10.90	10.91
0.8		5.68		9.0	11.05	11.04	11.09
0.9		5.93		10.0	11.20	11.19	11.23
1.0	6.20	6.17	4.96	12.0	11.40	11.36	11.43
1.2		6.61		14.0	11.54	11.50	11.55
1.4		6.99		16.0	11.62	11.60	11.62
1.6		7.30		18.0	11.66	11.65	11.67
1.8		7.57		20.0	11.70	11.67	11.70
2.0	7.87	7.82	7.22				

are many factors which must be considered to derive the differential equation of motion of liquid rise in a capillary tube, but according to Le Grand and Rense the most important factors are the following:

"(1) The rise involves a non-steady-state condition, and, at least in the earlier stage is impulsive. The fact that a mass of liquid is in motion below as well as above the opening to the capillary must be considered.

(2) The vital factor in effecting the rise is surface tension. However, the question of angle of contact is very partinent. Does this remain constant during the accelerating rise, or does it vary in a predictable, regular way?

(3) The possible presence of turbulence over some of the column of liquid can not be ignored despite low values of Reynolds number. If the meniscus assume a concave shape, how can the upward speed of flow be greatest at the center without an adjustment at the boundary? Likewise, on entering the tube itself, the liquid must adjust suddenly to new conditions of flow, and turbulence may arise.

(3) Viscosity contributes in producing frictional force, probably in the same sense as in ordinary stream line flow. Slipping along the wall of the tube should be considered."

Brittin's equation (1) will be written as

$$Z' = -\frac{d+gZ}{bZ} - \frac{(n+1)Z'^2}{bZ} - \frac{Z''}{b} \qquad (17)$$

Now Z, Z' and Z'' can be obtained from the experimental data. In order to derive the modified equation, b, n and d are assumed to be variable at first, though they are defined as constants in Brittin's equation. According to the remark (2), d may be a variable. According to the last part of remark (3) the contribution due to the turbulence at the entrance of the capillary tube must be a decreasing function of t. Indeed it may be expressed by $n_0 e^{-\alpha t}$. Remark (3) and (4) mean that the coefficient of the frictional term b is not only due to the Poiseuille's force b_0, but also to the frictional force of slipping b_1.

In order to explain the results of the experiments obtained by Le Grand and Rense, there are three ways disposable, that is, (1) b is assumed as constant and d variable, (2) d is assumed as constant and b variable, and (3) b and d are both variable. It is very fortunate that we may put b and d as constants at least for the first approximation.

§ 5. Solution of the Modified Equation.

When t is small, equation (10) will be used by placing

$$(1+n_0 e^{-\alpha t})(1+\bar{f})^2$$

instead of $(1+n)(1+f)^2$ in the second integral of the right hand side of the equation. Calculation will be carried out in the same way as before. When t is large, $(1+n_0 e^{-\alpha t})$ reduces to 1, and Z'^2 reduces to a small quantity. Hence calculation needs no change in the first approximation.

For example, we take a data given by Le Grand and Rense, where

$$n_0 = 8,\ \alpha = 27.72,\ b = 148.4 \text{ and } Z_\infty = 5.06$$

consequently $\lambda = 1.317$

The result of the calculation is illustrated in Fig. 1 by the smooth curve. The deviation between

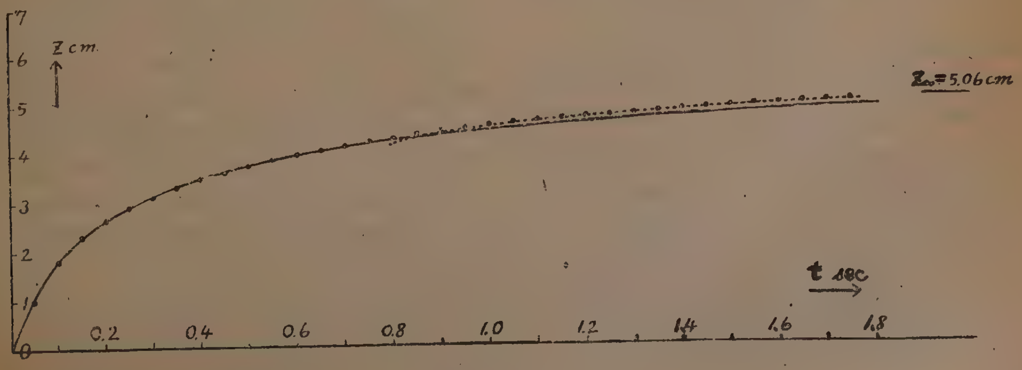

Fig. 1.

calculation and experiment appears only where t is large enough, but even in such a case, if we put $b_0 = \frac{8\mu}{r^2} = 88.4$ instead of $b = 148.4$, the agreement will be perfect as shown in Fig. 1 by the broken line. Judging from the result, it may be concluded that at first the effect of frictional force is due to the Poiseuille's viscous force and that of slipping, and then through some unstable state, it reduces to the one due to, the Poiseuille's force alone.

§ 6. Discussion.

For the tube with very thin radius, Brittin's equation is sufficient as shown in Table 1, but for the tube with larger radius, the equation must be modified. The effect due to turbulence at the entrance of the tube is conspicuous at first and soon reduces to zero. The amount of the effect may be depend perhaps on the carefullness of the experiment and smoothness of the end of the tube. The angle of contact remains nearly constant and the coefficient due to the frictional force is a decreasing function of time. The question whether the angle of contact remains strictly constant or not, and how the coefficient due to the frictional force varies during the accelerating rise can be determined, if the experiments can be carefully repeated and radius of the capillary tube is more exactly measured. Especially uniformity of the bore should be strictly examined. It may be concluded that the modified equation is sufficient to explain the water rise for the first approximation.

References.

(1) Wesley E. Brittin. J. App. Phys. 17, 37 (1946).

(2) E. J. Le Grand and W. E. Rence. J. App. Phys. 16, No. 12 (1945).

The Theory of Thermoelectromotive Force in Semiconductors.

By Jiro YAMASHITA.

Institute of Science and Technology, University of Tokyo.

(Received April 5, 1949)

§ 1. Introduction.

The theory of thermoelectromotive force in semiconductors has been worked by some investigators(1) on the basis of Sommerfeld's free electron model. The proposed theory, however, is too simple to elucidate the detailed behaviours of the thermoelectromotive force with temperatures, though it may give roughly the right order of the phenomena in question. In order to improve the mentioned qualitative treatment, the distribution functions of electrons in a semiconductor on the basis of the quantum theory of solids are essentially required on account of which the internal electric field caused by the temperature gradient in a semiconductor is easily evaluated. For such an attempt to improve the simple theory, it is necessary for us to have the thorough knowledge about the structure of energy bands, i. e., the quantum states of conduction electrons and the interaction between electrons and lattice vibrations. For our lacking of the detailed knowledges about the electronic structure of semiconductors, however, we are forced to adopt tentatively in the present computation the following plausible assumptions that the free electron-like wave functions are valid for conduction electrons and Fröhlich-Mott's interaction type(2) for that between electrons and lattice vibrations in semiconductors. On the basis of the above assumptions we have calculated the thermoelectromotive force in semiconductors quantumtheoretically. As shown in the last chapter, we shall be able to interpret theoretically some experimental facts, which the previous simple theory failed to derive, so we are sure that our improvement of the theory proceeds in the right way.

§ 2. Fundamental Equation.

In Boltzmann-Bloch's integral equation(3) to determine the electronic distribution function in conduction band the characteristic differences between metals and semiconductors are to be taken into account. Namely, electrons in metals obey Fermi-Dirac statistics, while those in ionic crystals obey Maxwell-Boltzmann statistics, for the electron number being very few except for the case of very high temperature. Further, in metals the interaction bntween the electron and the lattice vibrations is of Bloch-Bethe type (quadripole interaction), while in ionic crystals it is of Fröhlich-Mott type (dipole interaction) except for the case of extremely low temperature. For conduction electrons we adopt the free-electron like approximation, which may be justified for electrons near the top or bottom of energy bands approximately. Using the above assumptions the fundamental integral equation of conduction electrons under the combined influence of both electrostatic field and temperature gradient is reduced to:

$$\int\frac{dq}{q}\frac{1}{e^{\xi}-1}\Big[\{c(\varepsilon+\xi)-c(\varepsilon)\}+e^{\xi}\{c(\varepsilon-\xi)-\varepsilon(\varepsilon)\}$$

$$-\left(\frac{q^2-k_\nu^2}{2K^2}\right)c(\varepsilon+\xi)-\left(\frac{q^2+k_\nu^2}{2K^2}\right)e^{\xi}\,c(\varepsilon-\xi)\Big]$$

$$=\frac{2Ma^3h^3\nu}{e^4m^2}K\left(-eF+kT\frac{\partial\log A}{\partial x}+\frac{E}{T}\frac{\partial T}{\partial x}\right),\quad(1)$$

where

q: wave number of lattice vibration, $\xi=h\nu/kT$,

ν: frequency of lattice vibration, $\varepsilon=E/kT$,

K: wave number of electron, $E=h^2K^2/2m$ (energy of conduction electron),

e: electronic charge, m: electronic mass

h: Planck's const./2π,

M: reduced mass of two ions,

k: Boltzmann constant, F: intensity of electrostatic field, $2a^3$: volume of unit cell in the crystal lattice, T: absolute temperature, x: space coordinate in the direction of temperature gradient.

In the equation (1) the distribution function $f(E)$ is assumed to be of the same form as in metals.

$$f(E)=f_0(E)\left(1+\frac{K_x}{kT}C(E)\right),$$

in which $f_0(E)$ is given by

$$f_0(E)=Ae^{-\frac{E}{kT}},\text{ and } A=\text{const. }T^{-\frac{3}{4}}\,e^{-\frac{\Delta W}{2kT}}$$

ΔW being the energy difference between the impurity level and the bottom of the conduction band.

§ 3. The Solution of the Integral Equation.

Now we shall solve the fundamental integral equation (1) according to Kroll's method, which has been used in the thermoelectromotive force in metals. Since the right hand side of Eq. (1) consists of two parts, that is, the one not containing E and the other linear in E, we are permitted to divide also the left hand side into two parts:

$$\int\frac{dq}{q}\frac{1}{e^{\xi}-1}\Big[\{\alpha(\varepsilon+\xi)-\alpha(\varepsilon)\}+e^{\xi}\{\alpha(\varepsilon-\xi)-\alpha(\varepsilon)\}$$

$$-\left(\frac{q^2-k_\nu^2}{2K^2}\right)\alpha(\varepsilon+\xi)-\left(\frac{q^2+k_\nu^2}{2K^2}\right)e^{\xi}\alpha(\varepsilon-\xi)\Big]$$

$$=\frac{2Ma^3h^3\nu}{e^4m^2}K\left(-eF+kT\frac{\partial\log A}{\partial x}\right)\qquad(2\text{—}1)$$

$$\int\frac{dq}{q}\frac{1}{e^{\xi}-1}\Big[\{\beta(\varepsilon+\xi)-\beta(\varepsilon)\}+e^{\xi}\{\beta(\varepsilon-\xi)-\beta(\varepsilon)\}$$

$$-\left(\frac{q^2-k_\nu^2}{2K^2}\right)\beta(\varepsilon+\xi)-\left(\frac{q^2+k_\nu^2}{2K^2}\right)e^{\xi}\beta(\varepsilon-\xi)\Big]$$

$$=\frac{2Ma^3h\nu}{e^4m^2}K\frac{E}{T}\frac{\partial T}{\partial x}.\qquad(2\text{—}2)$$

Here the limits of integrals are determined by the law of conservation of energy and momentum of the total system.

$$q_{\max}=\sqrt{K^2+k_\nu^2}+K,\quad q_{\min}=\sqrt{K^2+k_\nu^2}-K.$$

(i) For the case of $E<h\nu$ (i. e. $\varepsilon<\xi$), in which electrons can only absorb the lattice quantum, and then the terms involving the emission of lattice quantum in Eq. (2) vanish in accordance with the conservation law of energy. Consequently Eqs. (2) become of

$$\int\frac{dq}{q}\Big[\{\alpha(\varepsilon+\xi)-\alpha(\varepsilon)\}-\left(\frac{q^2-k_\nu^2}{2K^2}\right)\alpha(\varepsilon+\xi)\Big]$$

$$=\frac{2Ma^3h\nu^3}{4^4m^2}(e^{\xi}-1)\left(-eF+kT\frac{\partial\log A}{\partial x}\right),\qquad(3\text{—}1)$$

$$\int\frac{dq}{q}\left[\{\beta(\varepsilon+\xi)-\beta(\varepsilon)\}-\left(\frac{q^2-k_\nu^2}{2K^2}\right)\beta(\varepsilon+\xi)\right]$$

$$=\frac{2Ma^3\nu h^3}{e^4m^2}(e^{\xi}-1)K\frac{E}{T}\frac{\partial T}{\partial x}. \qquad (3-2)$$

According to the method of solution of successive approximation, we put

$$\alpha(\varepsilon)=\alpha_0(\varepsilon)+\alpha_1(\varepsilon)+\cdots\cdots$$

As the first approximation we are allowed to assume

$$\alpha(\varepsilon+\xi)=\alpha(\varepsilon)\doteqdot\alpha_0(\varepsilon)$$

and inserting it into Eq. (3—1), we obtain

$$\alpha_0(\varepsilon)=B\left(-eF+kT\frac{\partial\log A}{\partial x}\right)k_\nu S^{\frac{3}{2}}$$

$$\left[2\sqrt{S(S+1)}-\log\frac{\sqrt{1+S}+\sqrt{S}}{\sqrt{1+S}-\sqrt{S}}\right]^{-1}, \qquad (4)$$

where S and B are given by

$$S=E/h\nu,\quad B=4Ma^3\nu h^3(e^{\xi}-1)/e^4m^2,$$

When S is small, we have

$$\alpha_0(\varepsilon)\backsim(1+3\varepsilon/10+\cdots\cdot),$$

which leads to the result that $\alpha_0(\varepsilon)$ does not depend upon ε strongly, the assumption $\alpha_0(\varepsilon+\xi)\doteqdot\alpha_0(\varepsilon)$ being fulfilled approximately. As the second approximation we put

$$\alpha(\varepsilon)=\alpha_0(\varepsilon)+\alpha_1(\varepsilon)$$

and

$$\alpha(\varepsilon+\xi)=\alpha_0(\varepsilon+\xi)+\alpha_1(\varepsilon+\xi).$$

Assuming $\alpha_1(\varepsilon+\xi)=\alpha_1(\varepsilon)$, we obtain the following expression:

$$\alpha_1(\varepsilon)=Bk_\nu\left(-eF+kT\frac{\partial\log A}{\partial x}\right)$$

$$\cdot\left[\frac{2S\log\dfrac{\sqrt{1+S}+\sqrt{S}}{\sqrt{1+S}-\sqrt{S}}}{2\sqrt{S(1+S)}-\log\dfrac{\sqrt{1+S}+\sqrt{S}}{\sqrt{1+S}-\sqrt{S}}}-1\right]$$

$$\times\left[\frac{(1+S)^{\frac{3}{2}}}{2\sqrt{(1+S)(2+S)}-\log\dfrac{\sqrt{2+S}+\sqrt{1+S}}{\sqrt{2+S}-\sqrt{1+S}}}\right.$$

$$\left.-\frac{S^{\frac{3}{2}}}{2\sqrt{S(1+S)}-\log\dfrac{\sqrt{1+S}+\sqrt{S}}{\sqrt{1-S}+\sqrt{S}}}\right] \qquad (5)$$

Since $\alpha_0(\varepsilon+\xi)$ is nearly equal to $\alpha_0(\varepsilon)$ as shown above, $\alpha_1(\varepsilon)$ is seen to be much smaller than $\alpha_0(\varepsilon)$ on account of which the convergence of our sucsessive approximation is justified.

Similarly we may solve Eq. (3—2), by putting

$$\beta=\beta_0(\varepsilon)+\beta_1(\varepsilon)+\cdots\cdots,$$

the results of which are

$$\beta_0(\varepsilon)=Bk_\nu\frac{h\nu}{T}\frac{\partial T}{\partial x}S^{\frac{5}{2}}\left[2\sqrt{S(1+S)}\right.$$

$$\left.-\log\frac{\sqrt{1+S}+\sqrt{S}}{\sqrt{1+S}-\sqrt{S}}\right]^{-1} \qquad (4')$$

$$\beta_1(\varepsilon)=Bk_\nu\frac{h\nu}{T}\frac{\partial T}{\partial x}$$

$$\times\left[\frac{2S\log\dfrac{\sqrt{1+S}+\sqrt{S}}{\sqrt{1+S}-\sqrt{S}}}{2\sqrt{S(1+S)}-\log\dfrac{\sqrt{1+S}+\sqrt{S}}{\sqrt{1+S}-\sqrt{S}}}-1\right]$$

$$\times\left[\frac{(1+S)^{\frac{5}{2}}}{2\sqrt{(1+S)(2+S)}-\log\dfrac{\sqrt{2+S}+\sqrt{1+S}}{\sqrt{2+S}-\sqrt{1+S}}}\right.$$

$$\left.-\frac{S^{\frac{5}{2}}}{2\sqrt{S(1+S)}-\log\dfrac{\sqrt{1+S}+\sqrt{S}}{\sqrt{1+S}-\sqrt{S}}}\right]. \qquad (5')$$

As seen in the equation (4′) and (5′), $\beta_0(\varepsilon)$ is roughly proportional to ε, the relation $\beta_0(\varepsilon+\xi)=\beta_0(\varepsilon)$ being unfulfilled, and consequently $\beta_1(\varepsilon)$ becomes greater than $\beta_0(\varepsilon)$. $\beta_1(\varepsilon)$, however, does not depend upon ε as a first approximation and the relation $\beta_1(\varepsilon+\xi)=\beta_1(\varepsilon)$ is satisfied approximately. By the similar consideration to the case of α- evaluation, therefore, we may easily be justified to neglect $\beta_2(\varepsilon)$ which is much smaller than $\beta_1(\varepsilon)$.

(ii) For the case $E>h\nu$ we may solve Eq. (2—1) and Eq. (2—2) formally by the same method. It, however, should be noticed that the interaction form Fröhlich-Mott type is certainly not a good approximation when E is nearly equal to $h\nu$. In the range of $E\gg h\nu$, $\alpha_1(\varepsilon)$ and $\beta_1(\varepsilon)$ become very small in comparison with $\alpha_0(\varepsilon)$ and $\beta_0(\varepsilon)$ respectively, in which case the approximate solution of Eq. (2) makes quite feasible to be carried out. In the case of $E\sim h\nu$, however, the solutions are obtained by the interporation method from the results valid in both cases of $E<h\nu$ and in $E>h\nu$.

§ 4. Thermoelectromotive Force in Semiconductors.

By the use of the distribution function $C(E) = \alpha(E)+\beta(E)$ computed above, the internal electric field is given by

$$eF = k\left(T\frac{\partial \log A}{\partial x}+\frac{h\nu}{kT}\frac{A_2}{A_1}\frac{\partial T}{\partial x}\right) = eF_1+eF_2, \quad (6)$$

where

$$A_1 = \int_0^\infty(\alpha_0(s)+\alpha_1(s))y^{\frac{3}{2}}e^{-y}dy, \quad y = E/kT, \quad (7)$$

and

$$A_2 = \int_0^\infty(\beta_0(s)+\beta_1(s))y^{\frac{3}{2}}e^{-y}dy, \quad s = E/h\nu. \quad (7)$$

Now we may stress that the electric field consists of two parts F_1 and F_2 as seen in (6).

(i) Thermoelectromotive force due to F_2 is given as follows:

$$\theta_2 = -\int_A^B F_2dx = \frac{k}{(-e)}\int_A^B\frac{h\nu}{kT}\frac{A_2}{A_1}\frac{\partial T}{\partial x}dx$$

$$= \frac{k}{(-e)}\int_{T_1}^{T_2}\frac{h\nu}{kT}\frac{A_2}{A_1}dT$$

and

$$\frac{d\theta_2}{dT} = \frac{k}{(-e)}\frac{h\nu}{kT}\frac{A_2}{A_1} = \frac{k}{(-e)}\frac{\theta}{T}\frac{A_2}{A_1}. \quad (8)$$

The previous simple theory gives merely constant term $2k/(-e)$ instead of (8). Eq. (8) depends upon temperature in some complicated way through A_1 and A_2. Since the term A_2/A_1 is not expressed by simple analytic functions of temperatures, the numerical evaluations have been adopted, which results are shown in Fig. 1. In the temperature range of $T < \theta$, $d\theta_2/dT$ decreases roughly proportional $1/T$ and in the temperature range of $T > \theta$ it increases with temperature so slowly that we may consider it nearly constant. We may roughly understand the mentioned situation through the following simple considerations. For the rather small electron energy of $E < h\nu$, $\alpha_0(E)$ is larger than $\alpha_1(E)$, $\alpha_0(E)$ being nearly constant, while $\beta_1(E)$ is larger than $\beta_0(E)$, $\beta_1(E)$ also being nearly constant as before. In the lower temperature range, where the mean electron energy is smaller than $h\nu$, therefore, $h\nu A_2/kTA_1$ becomes $\theta/T\times$const. On the contrary, for the larger electron energy of $E \gg h\nu$, $\alpha_0(E) \backsim E^{\frac{1}{2}}$ becomes larger than $\alpha_1(E)$ and $\beta_0(E) \backsim E^{\frac{3}{2}}$ does larger than $\beta_1(E)$. In the higher temperature range, where the greater part of electrons have larger energies, therefore, A_2/A_1 approaches the limiting value

$$\int_0^\infty E^3e^{-\frac{E}{kT}}dE\Big/\int_0^\infty E^2e^{-\frac{E}{kT}}dE = 3kT$$

and then $d\theta_2/dT$ becomes nearly constant.

(ii) Thermoelectromotive force due to F_1 is already obtained by the previous simple theory. When there is only one kind of impurity level in a semiconductor, θ_1 has been obtained as follows.

$$\theta_1 = -\int_A^B F_1dx = \frac{k}{(-e)}\int_A^B T\frac{\partial \log A}{\partial x}dr$$

$$= \frac{k}{(-e)}\left\{[T\log A]_A^B-\int_A^B\log A\frac{\partial T}{\partial x}dx\right\}$$

$$= \frac{k}{(-e)}\left[\frac{\varDelta W}{2k}\log\frac{T_2}{T_1}-\frac{3}{4}(T_2-T_1)\right]$$

$$\frac{d\theta_1}{dT} = \frac{k}{(-e)}\left(\frac{\varDelta W}{2kT}-\frac{3}{4}\right) \quad (9)$$

When two kinds of impurity happen to take parts in the phenomena, and, further, their energy distances and the number of impurity centres are given by $\varDelta W_1$, $\varDelta W_2$, N_1 and N_2 respectively, we may easily derive the following formula by a simple consideration.

$$\frac{d\theta_1}{dT} = \frac{k}{(e-)}\left(\frac{N_1\varDelta W_1e^{-\frac{\Delta W_1}{kT}}+N_2\varDelta W_2e^{-\frac{\Delta W_2}{kT}}}{2kT(N_1e^{-\frac{\Delta W_1}{kT}}+N_2e^{-\frac{\Delta W_2}{kT}})}-\frac{3}{4}\right) \quad (10)$$

which is reduced to (9) for $N_2 = 0$.

§ 5. Comparison with Experiments and the Discussion of the Results.

The sign of thermoelectromotive force becomes minus or plus according to the current carriers

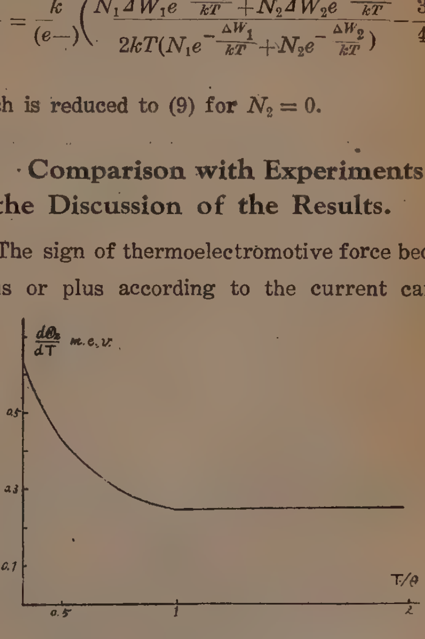

Fig. 1. Theoretical $d\theta_2/dT$.

being electrons or positive holes, as seen in Eq. (8) and Eq. (9), which contain the electronic charge e linearly. For example, ZnO belongs to the former and Cu_2O to the latter. As for the temperature behaviours of thermoelectromotive force, $d\theta_1/dT$ is nearly proportional to $\Delta W/T$, while $d\theta_2/dT$ is proportional to $1/T$ in the low temperature region and nearly constant in the high temperature one. When a material has large value of ΔW and consequently $d\theta_1/dT \gg d\theta_2/dT$, its thermoelectromotive force is to be nearly proportional to $1/T$. On the other hand, if ΔW is small and thus $d\theta_2/dT \gg d\theta_1/dT$, the thermoelectromotive force will behave with temperature as shown in Fig. 1. The mentioned types of temperature behaviours of the thermoelectromotive force in semiconductors have been actually observed experimentally. For example, WO_2 belongs to the former and ZnO belongs to the latter. The thermoelectromotive force of ZnO has been measured by Fritsch⁽⁵⁾ the temperature behaviours of which are similar for all specimens, being of the form shown in Fig. 1, though each of its absolut values is rather scattered according to the preparation of each of the sample. As ΔW of ZnO is comparatively small, the above observed fact is in accord with the one expected from our theory. Moreover, for one of the specimens ($\Delta W = 0.056$ ev) the calculated values are quantitatively in good accord with the observed ones, but the previous simple theory fails to give the observed behaviours as shown in Fig. 2. The thermoelectromotive force of Cu_2O has been measured by the various investigators⁽⁶⁾, but their results are at variance with one another. Although the measured values are distributed from 0.6 m.e.v. to 1.2 m.e.v. at room temperature, the observed temperature-variations are seen clearly to behave as expected from our theory. The experimental result of Vogt and some of Okada's observations are in good agreement with our theory quantitatively as shown in Fig. 3 and Fig. 4, but the results of Mönch and the other one of Okada's show that the observed values are always larger than our theoretical values. The simple theory, however, is found to give smaller values than all the observed data. Although Mönch pointed out the fact that the boundary layer between Cu_2O and Cu had some effect for thermoelectromotive force, we shall not concern this problem here in view of the experimental data at variance with each other. In Cu_2O semiconductors, $\log\sigma$ (σ : electronic conduc-

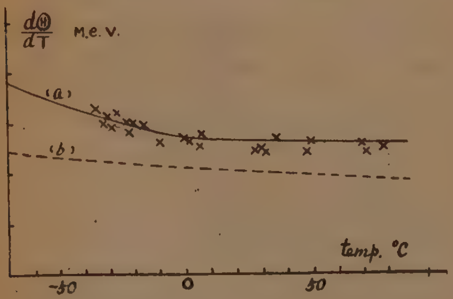

Fig. 2. ZnO.

× Fritsch'e observation.
(a) our theory ($\Delta W = 0.056$ ev, $\theta = 280$)
(b) previous theory. ($\Delta W = 0.056$ ev).

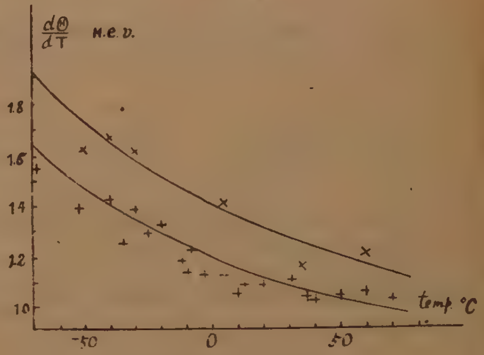

Fig. 3. Cu_2O.

+, × Vogt's observation.
——— our theory. ($\theta = 300$).
(a) $\Delta W = 0.66$ ev. observed.
(b) $\Delta W = 0.556$ ev. ,,

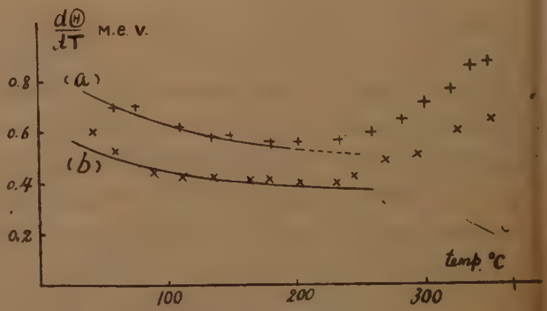

Fig. 4. Cu_2O.

× Okada's observation.
——— our theory. ($\theta = 400$).
(a) $\Delta W = 0.34$ ev. observed.
(b) $\Delta W = 0.2$ ev. ,,

tivity) and log R (R : Hall coefficient) plotted against $1/T$ in the usual way are found experimentlly to show a kink separating two straight lines. If the crystal is supposed to contain two kinds of impurity centres with different activation energies in view of the mentioned observations, we have to use Eq. (10) instead of Eq. (9) in order to examine the behaviours of thermoelectromotive force near the kink point. Since $d\Theta_1/dT$ will turn upwards with temperatures at the kink point in accordance with (10), the total thermoelectromotive force is expected theoretically to behave as in Fig. 5 (a), when the temperature of kink point is rather low and $d\Theta_2/dT$ decreases as proportionately to $1/T$. On the other hand, it behaves as in Fig. 5 (b), when the temperature of kink point is rather high and $d\Theta_2/dT$ is nearly constant. According to the observations of electrical conductivity and Hall coefficient of Cu_2O, Engelhard(7) obtained

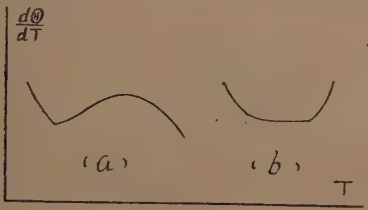

Fig. 5. The possible behaviours of thermoelectromotive force, which is xpected theoretically for the case of two kinds of impurity levels.

$$n = 2\times10^{20}\,e^{-\frac{0.35}{kT}} + 10^{16}\,e^{-\frac{0.20}{kT}}\ ,$$

for number of conduction electrons of his sample. Using his data, the thermoelectromotive force of the sample will be expected theoretically to behave as in Fig. 6, since the temperature of the kink point is sufficiently low (−70°C). Unfortunately, our theoretical expectation is not yet checked since the observation of thermoelectromotive force for the same sample was not carried out. Schweickelt, however, observed experimentally the thermoelectromotive force for another sample of Cu_2O (kink point at −72°C), the result of which is shown in Fig. 7, being in agreement with our theroretical results. The expected behaviour in Fig. 5 (b) seems to be realized in Okada's experimental observation as shown in Fig. 4.

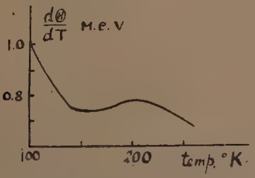

Fig. 6. Theoretical results for t. e. m. f. near the kink point.

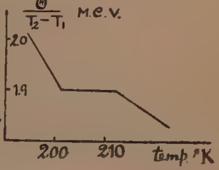

Fig. 7. Schweickelt's observation.

Finally it may be concluded that the comparison of our theory with the experimental observations is quite satisfactory, despite of the assumptions concerning the electronic behaviours of semiconductors in view of the present situation that we have not yet sufficiently reliable experimental data to be discussed theoretically owing to the sensitive dependency of the physical properties of semiconductors upon the method of preparations.

The author takes great pleasure in thanking Professor T. Muto for his suggestion of the problem and his helpful advice throughout this work.

References.

(1) Bronstein: Phys. Zeits. Sowj. **2** (1932) 40.
Fowler: Proc. Roy. Soc. **A 140** (1933) 505.
Mönch: Zeits. f. Phys. **83** (1933) 247; Ann. d. Phys. **26** (1936) 481; **34** (1939) 265.
(2) Fröhlich: Proc. Roy. Soc. **A 160** (1937) 230.
Fröhlich and Mott: Proc. Roy. Soc. **A 171** (1939) 496.
(3) Bloch: Zeits. f. Phys. **52** (1928) 555.
Wilson: Proc. Roy. Soc. **A 133** (1931) 458; **134** (1931) 277.
(4) Kroll: Zeits. f. Phys. **77** (1932) 322.
(5) Fritsch: Ann. d. Phys. **22** (1935) 375.
(6) Vogt: Ann. d. Phys. **7** (1930) 183.
Mönch: Ann. d. Phys. **26** (1936) 481.
Schweickert: Ann. d. Phys. **34** (1939) 250.
Rohde: Ann. d. Phys. **34** (1939) 259.
Okada: Reported at the Meeting of Physical Society Japan (1946),
(7) Engelhald: Ann. d. Phys. **17** (1933) 501.

Statistical Theory of the Ferromagnetic Superlattice
Part III. Elastic Scattering of Slow Neutrons.

By Toshinosuke MUTO.

Institute of Science and Technology, University of Tokyo.

(Received April 5, 1949)

§ 1. In part I and II,⁽¹⁾ the statistical theory of ferromagnetic superlattice has been developed in a close connection with the anomalous specific heat and the spontaneous magnetization of the mentioned superlattice, using the Ising's model and Bethe's theory of order-disorder transformation, and has been found to be in qualitative agreements with the available experimental observations. In such ferromagnetic superlattice the intimate correlation between both orderings of component atoms and molecular magnets situated at each lattice point has been observed to exist, which influences upon the various physical properties of ferromsgnetic superlattice are to be expected to appear in the experimental observations. In the present note, therefore, we shall work out theoretically the elastic scattering of slow neutrons in the ferromagnetie superlattice, while the mentioned scattering process for the non-magnetic superlattice has been already treated theoretically by Honda⁽²⁾ on the basis of Bragg-Williams' theory of order-disorder transformation. Nix, Pegram and Dunning⁽³⁾ have observed experimentally the elastic scattering of slow neutrons through ferromagnetic alloy $NiFe_3$ in order to detect the degree of ordering by the neutron scattering instead of X-rays one, allowing for the simillar electronic structure of constituent atoms mentioned above. In the following computation, however, we have adopted, for simplicity, a simple cubic or a body-centred cubic lattice in order to make use of the numerical results obtained in Part I and II, and further, to find quantitatively the characteristic behaviours of the mentioned phenomena.

§ 2. As for the interaction potential between a neutron and the ferromagnetic superlattice, we shall take the following form,

$$V(\vec{r}) = \sum_i \Big\{ v_i \delta(|\vec{R}_i - \vec{r}|) + \frac{(\vec{\mu}_{ai} \cdot \vec{\mu}_n)|\vec{R}_i - \vec{r}|^2 - 3(\vec{\mu}_{ai} \cdot \vec{R}_i - \vec{r})(\vec{\mu}_n \cdot \vec{R}_i - \vec{r})}{|\vec{R}_i - \vec{r}|^5} \rho(|\vec{R}_i - \vec{r}|) \Big\}, \tag{1}$$

in which the summation extends over all atoms situated at each lattice point of the crystal, the the first and second terms in the curved bracket represent the nuclear and magnetic interactions respectively. In (1) use has been made of the trick of replacing the actual nuclear potential by a fictitions potential suitable for the application of Born approximation method in collision problem. $\vec{\mu}_{ai}$ and $\vec{\mu}_n$ are magnetic moments of a molecular magnet and a neutron respectively. Further $\vec{r}$ and $\vec{R}_i$ represent the position vectors of a neutron and a lattice point designated by a suffix i, and $\rho(r)$ the space density of 3d electrons within a single Fe or Ni atom responsible for the ferromagnetism, which has been computed by wave functions constructed by Slater's shielding constants method.

The matrix elements of (1) responsible for the elastic scattering of neutron without spin change are written as

$$(\vec{K}, \sigma | V(\vec{r}) | \vec{K}_0, \sigma) = \sum_j \frac{1}{\Omega} (v_j + w_j) e^{i(\vec{K} - \vec{K}_0)\vec{R}_j}, \tag{2}$$

in which

$$w_j = \pm \mu_n \mu_{aj} w \tag{3}$$

$$w = \frac{256}{45} \pi \beta^2 (1 - 3\cos^2\theta) \frac{|\vec{K} - \vec{K}_0|^2 + 3\beta^2}{|\vec{K} - \vec{K}_0|^2 (|\vec{K} - \vec{K}_0|^2 + 4\beta^2)^2}, \tag{4}$$

$$\beta = \frac{1}{a_H} \times \frac{1}{2} (2.52 + 2.08), \quad a_H = \text{Bohr's radius}, \tag{5}$$

The double sign stands for whether the magnetic moments of incoming neutron are oriented parallel or antiparallel to the direction of the saturation magnetization of the crystal, and θ denotes the angle between the directions of the saturation magnetization and $\vec{K}-\vec{K}_0$. Further, v_j is evaluated from the elastic scattering cross sections σ_j of a single nucleous j for slow neutron as follows.

$$v_j = [(\pi\sigma_j)^{1/2}\hbar/m]\exp(i\delta_j), \tag{6}$$

where δ_j denotes the phase shift in the collision process.

§ 3. In order to obtain the observable scattering cross section σ, the mean square of the scattering matrix elements (2) has to be taken according to the statistical distribution of component atoms and molecular magnets situated at each lattice point in the crystals using the relative probabilities of the mentioned distributions computed in Part I and II, and further the obtained differential cross section has to be integrated over all directions of the scattered neutrons.

Thus, we have

$$\sigma = \frac{4m^2\rho}{\pi h^4}\left\{F(T) \pm \frac{4\pi}{45}\beta^6\mu_n\mu_A G(T)\,(K_1+K_2\sin^2\Theta)\right\}, \tag{7}$$

in which m denotes a neutron mass, ρ the density of crystal in atomic number and Θ the angle between the incident direction of neutron and that of the saturation magnetization. Further, we have

$$K_1 = \frac{6}{\beta^2 K_0^2}J - 6\left(\frac{4}{K_0^4}+\frac{1}{\beta^2 K_0^2}\right)\log\left(1+\frac{K_0^2}{\beta^2}\right) + 2\frac{1+3\beta^2/K_0^2}{\beta^2(\beta^2+K_0^2)}, \tag{8}$$

$$K_2 = \frac{-9}{\beta^2 K_0^2}J + 9\left(\frac{4}{K_0^4}+\frac{1}{\beta^2 K_0^2}\right)\log\left(1+\frac{K_0^2}{\beta^2}\right) - 3\frac{1+3\beta^2/K_0^2}{\beta^2(\beta^2+K_0^2)}, \tag{9}$$

and

$$J = \int_0^2 dv/v. \tag{10}$$

J is a logarithmically divergent integral, which depends sensively upon the magnetic moment distribution within a region of a neutron radius and may be made finite, at the present stage of the theory, by a suitable mathematical technique of using the appropriate converging factor g, i.e.,

$$J = \lim_{\varepsilon\to 0}\int_0^2 g(\varepsilon v)\frac{dv}{v},\quad g(0)=1$$

or by a construction of the wave packet of incident neutron wave. $F(T)$ and $G(T)$ are dependent upon the nuclear potential v_A, v_B, the molecular magnetic moments, and the relative probabilities of both atomic and molecular magnet distribution which are the functions of temperature of the crystal, the bond and exchange energies of the component atoms of the crystal.

$$F(T) = v_A^2+v_B^2-[v_A(\overset{\uparrow}{r}+\overset{\downarrow}{r})+v_B(\overset{\uparrow}{w}+\overset{\downarrow}{w})]^2 - [v_A(\overset{\uparrow}{w}+\overset{\downarrow}{w})+v_B(\overset{\uparrow}{r}+\overset{\downarrow}{r})]^2, \tag{11}$$

and

$$G(T) = \left(v_A+v_B\frac{\mu_B}{\mu_A}\right)(\overset{\uparrow}{r}-\overset{\downarrow}{r}+\overset{\uparrow}{w}-\overset{\downarrow}{w}) - [v_A(\overset{\uparrow}{r}+\overset{\downarrow}{r}) + v_B(\overset{\uparrow}{w}+\overset{\downarrow}{w})]\left[\overset{\uparrow}{r}-\overset{\downarrow}{r}+\frac{\mu_B}{\mu_A}(\overset{\uparrow}{w}-\overset{\downarrow}{w})\right] - [v_A(\overset{\uparrow}{w}+\overset{\downarrow}{w}) + v_B(\overset{\uparrow}{r}+\overset{\downarrow}{r})]\left[\overset{\uparrow}{w}-\overset{\downarrow}{w}+\frac{\mu_B}{\mu_A}(\overset{\uparrow}{r}-\overset{\downarrow}{r})\right], \tag{12}$$

in which $\overset{\uparrow}{r}$, $\overset{\downarrow}{r}$, $\overset{\uparrow}{w}$ and $\overset{\downarrow}{w}$ represent the various kinds of relative probabilities of the mentioned distributions as shown in Part I and II.

As seen in (7), the maximum value of the magnetic scattering is obtained for the case of $\Theta=0$, i.e., the incident direction of neutron being parallel to that of the saturation magnetization, taking into account of $K_2 \sim \frac{-9}{\beta^2 K_0^2}J$. Although the detailed discussion of σ is not yet possible owing to the divergent integral J at present, the characteristic variations with temperatures of the nuclear part $F(T)$ and the magnetic one $G(T)$ of the total cross section have been computed numerically by the use of the results obtained in Part I and II, in which

$$v_A = 1.5\cdot 10^{-19},\quad v_B = \pm 2.0\cdot 10^{-19}$$

(corresponding to $\delta_B-\delta_A = 0$ or π)

$\mu_A = 2.2\,\beta_B$ and $\mu_B = 0.6\,\beta_B$ (β_B = Bohr mngneton) are taken tentatively in the numerical evaluations. The results are described in the accompanying figures which show the peculiar variations of both $F(T)$ and $G(T)$ below and above the atomic and magnetic Curie points, which behaviours may be considered to be observed experimentally in the

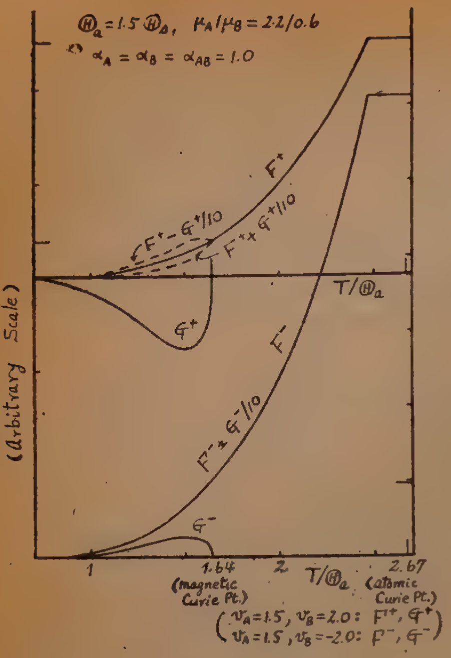

Fig. 1.

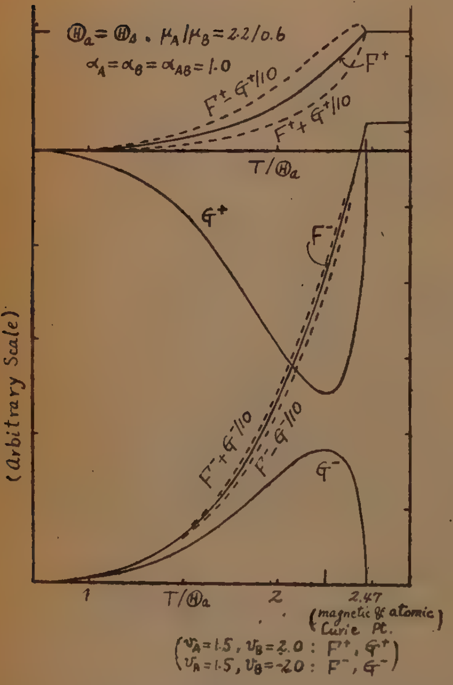

Fig. 2.

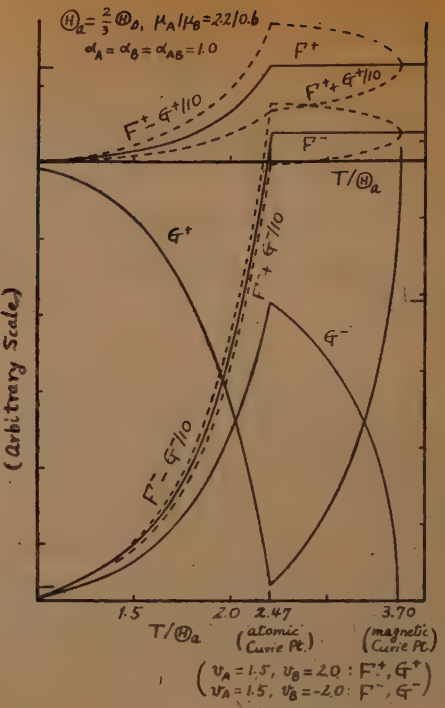

Fig. 3.

scattering of slow neutron by the ferromagnetic superlattice.

The author is indebted to Special Research Committee of Theoretical Physics, National Research Council of Education Ministry for financial aid.

References.

(1) T. Muto, T. Eguchi and M. Shibuya: J. Phys. Soc. Japan, **3**, (1948) 277; 264.

(2) Y. Honda: Subutsu-Kaishi (in Japanese), **16**, (1942) 148.

A. A. Smirnow and S. N. Vonsovsky: J. Phys. USSR. **5**, (1941) 263.

(3) F. C. Nix. H. G. Pegram and J. R. Dunning: Phys. Rev. **58**, (1940) 1031.

Statistical Theory of Linear Polymers V.
Paraffine-like Chain.

By Ryogo KUBO.

Department of physics, Faculty of Science, University of Tokyo.

(Received April 8, 1949)

Introduction.

While the statistical treatments of polymeric substances have brilliantly succeeded to explain the general features of physical properties of such substances, most of them failed to take into account the characteristic structures of molecules owing to their over-simplified models. Theories must be developed in future along such a line as to give the reasonable explanation of peculiarities of materials. Of course there are some such efforts(1), but they are not very satisfactory.

In view of these circumstances the writer has tried to develope as far as possible a general method for treating the intramolecular statistics of chain molecules, the general results of which are summarized in the preceding papers I and IV(2). Here I want to give the rigorous expressions for the long paraffine-like chain, which is often considered as a typical model of the flexible chain molecules. The notations are the same as used in IV.

§ 1. The Transformation Matrices.

The formulae (50) and (57), IV, show that we need only to know the average transformation matrices K_1 and K_2 so long as we content ourselves with the approximation to the power s^2, that is the Gaussian approximation.

For the sake of simplicity only the correlation of three neighboring skeletal bonds is considered, though it is also possible in principle to take into account the correlation between any number of bonds by our method. The zig-zag form of the chain is characterized by the rigid bond angle α and the angles between the planes determined by two neighboring bonds, which define the coordinate system S ($\boldsymbol{e}_1$, $\boldsymbol{e}_2$, $\boldsymbol{e}_3$) as shown in Fig. 1. There the unit vector $\boldsymbol{e}_3$ is chosen parallel to AB, $\boldsymbol{e}_2$ perpendicular to AB in the plane ABC, and finally $\boldsymbol{e}_1$ normal to $\boldsymbol{e}_2$ and $\boldsymbol{e}_3$. As one proceeds along the chain from ABC to BCD, the system S is transformed into S′ which is defined similarly by the bonds BC and CD. The angle ϕ between $\boldsymbol{e}_1$ and $\boldsymbol{e}_1'$ is a measure of internal rotation. ϕ is zero in the cis-form, and π in the trans-form.

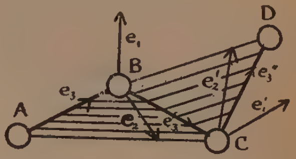

Fig. 1.

For brevity we put

$$\sin\alpha = \sigma, \quad \cos\alpha = \gamma, \quad \sin\phi = s, \quad \cos\phi = c. \tag{10}$$

The transformation D which leads S to S′ is shown to be

$$D(\phi) = \begin{bmatrix} c & -\gamma s & \gamma s \\ s & \gamma c & -\sigma c \\ 0 & \sigma & \gamma \end{bmatrix}. \tag{2}$$

The average transformation K_1 is given by

$$K_1 = \overline{D(\phi)} = \int D(\phi) e^{-E(\phi)/kT} d\phi \Big/ \int e^{-E(\phi)/kT} d\phi, \tag{3}$$

where $E(\phi)$ is ths hindering potential. For simplicity we assume hereafter

$$E(\phi) = E(-\phi) \tag{4}$$

so that

$$\bar{s} = \frac{\int \sin\phi e^{-E/kT} d\phi}{\int e^{-E/kT} d\phi} = 0 \tag{5}$$

$$\overline{cs} = \frac{\int \sin\phi\cos\phi e^{-E/kT}d\phi}{\int e^{-E/kT}d\phi} = 0$$

and

$$K_1 = \begin{bmatrix} \bar{c} & 0 & 0 \\ 0 & \gamma\bar{c} & -\sigma\bar{c} \\ 0 & \sigma & \gamma \end{bmatrix}. \tag{6}$$

For chain molecules with unsymmetrical side groups the assumption (4) will not be rigorously satisfied. In such cases calculations are very cumbersome though not impossible.

The average transformation matrix K_2 which belongs to the representation $\mathfrak{D}_2$ of the rotational group can be obtained from Eq. (38) and Table II in the paper IV (it must be noted here there are some misprints in the Table), that is

$$(K_2)_{\rho\sigma} = \sum_{ijkl} T_{\rho ij}\overline{D_{ik}D_{jl}}T_{kl\sigma}^{-1},\ \rho,\ \sigma = 1, 2, \cdots 5.$$

The explicit form is shown to be

$$K_2 = \begin{vmatrix} 1-\frac{3}{2}\sigma^2 & -\frac{\sqrt{2}}{3}\sigma^2 & \sqrt{3}\gamma\sigma & 0 & 0 \\ \frac{\sqrt{3}}{2}\sigma^2 f & -\frac{1}{2}(1+\gamma^2)f & -\gamma\sigma f & 0 & 0 \\ -\sqrt{3}\gamma\sigma\bar{c} & -\gamma\sigma\bar{c} & (\gamma^2-\sigma^2)\bar{c} & 0 & 0 \\ 0 & 0 & 0 & \gamma\bar{c} & \sigma\bar{c} \\ 0 & 0 & 0 & \sigma f & -\gamma f \end{vmatrix}, \tag{7}$$

where

$$f = \overline{s^2} - \overline{c^2}.$$

§ 2. Average of the Square of the Length.

The average $<r_n^2>$ of the square of the length is given by Eq. (5). IV, which takes the explicit form

$$<r_n^2> = na^2\frac{(1+\gamma)(1-\bar{c})}{(1-\gamma)(1+c)} \tag{8}$$

saymptotically for large n for every value of $\bar{c}$. This expression has already derived by Oka.(3) Exact expression of $<r_n^2>$ valid for all n can be derived without difficulty from Eqs. (50) or (52), IV, if necessary. It is interesting to note that it approaches to the asymptotic value (8) sometimes smoothly and sometimes oscillating in zig-zag with the increase in n.

As Oka has remarked, $<r_n^2>$ takes exactly the same asymptotic value as that of freely rotating chain molecule if the hindering potential is assumed to have several minima which are symmetrical and of equal depth, for then we have $\bar{c}=0$.

Here we assume three minima at $\phi=\pi$, and $\pm\frac{\pi}{3}$ as shown in Fig. 2, and take the partition functions near the minima as ε at $\phi=\pi$ and 1 at $\phi=\pm\frac{\pi}{3}$. The partition functions are assumed suitably normalized, so that ε can be written as

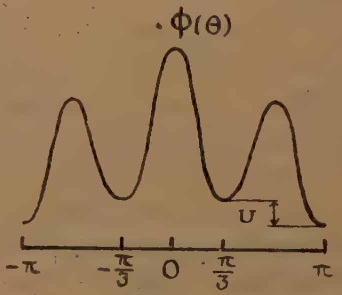

Fig. 2.

$$\varepsilon = \exp(U/kT) \tag{9}$$

where U is the difference of the free energies at the minima involving the contributions from rotational vibrations and other modes of internal motion. Assuming deep minima and low temperatures we have

$$\bar{c} = \frac{1-\varepsilon}{\varepsilon+2} \tag{10}$$

and

$$<r_n^2> = na^2\frac{1+\cos\alpha}{1-\cos\alpha}\cdot\frac{2\varepsilon+1}{3}. \tag{11}$$

For the tatrahedral angle $\alpha = 180°-109°$, $\gamma = 1/3$, Eq. (11) becomes

$$<r_n^2> = \frac{4}{3}na^2\left(e^{U/kT}+\frac{1}{2}\right) \tag{12}$$

(cf. Eq. (38), I).

The elastic stress of an amorphous rubberlike solid composed of such linear polymers as we have discussed will be given by

$$X_0 = \frac{dRT}{m}\rho_0^2\frac{3}{4}\frac{\left(A-\frac{1}{A^2}\right)}{e^{U/kT}+2}. \tag{13}$$

for simple elongation (cf. (59), IV, (14) and (39), II), provided that the junctions of the network are tight and not very concentrated. If U is positive the chains prefer the elongated forms at low temperatures, and the elastic response will show a maximum at some temperature. For large value of $U(U \gg kT)$ it will decrease with the increase of temperature near the room temperature in contradiction to the characteristic curve of the ideal rubber. In this case, however, the index of curling of chains (the mean fractional extension) will not be small but very near to 1, and the approximation of the Gassian network cannot be justified. More detailed insights on the network structure is required.

For small U the above mentioned maximum will appear near the room temperature or even at lower. In this case we have the simple rubber-like elasticity which is familiar to us.

Why certain polymeric materials show the rubber-like elasticity and not the others? Answer to this question are not yet complete. The molecular cohesion of the polymers and the flexibility play the main role, and further the activation energy for the internal rotation. Discussion on this problem are left to another occasion.

§ 3. Elastic Double Refraction.

Next let us consider the effect of internal rotation on the elastic double refraction. For simplicity we assume that the coordinate system S coincides with the principal axes of polarizability tensor α so that $\alpha_{23} = \alpha_{31} = \alpha_{12} = 0$. Put the expressions (6), (7), and $\boldsymbol{a} = (0, 0, a)$ into (57) and (62), IV, we get

$$\frac{\Delta n}{X} = \frac{n_{11} - n_1}{X}$$

$$= \frac{2\pi}{15}\frac{(n_0^2+2)^2}{n_0 kT}\left[\left\{\frac{2}{3}G + \frac{\gamma - \frac{\sigma^2}{2} - \bar{c}(1+\gamma)(1+2\gamma)+\gamma\bar{c}^2}{(1-\gamma^2)(1-\bar{c}^2)}\right\}\right.$$

$$\left.\left(\alpha_{33} - \frac{\alpha_{11}+\alpha_{22}}{2}\right) - \frac{1}{6}\left(\frac{\overline{c^2-s^2}}{\overline{s^2}} + \frac{3\overline{c^2}}{1-\overline{c^2}}\right)(\alpha_{11}-\alpha_{22})\right] \tag{14}$$

where

$$G = \left[\left\{1 - \frac{1}{2}(1+\gamma^2)(\overline{c^2-s^2})\right\}\{1-(\gamma^2-\sigma^2)\bar{c}\}\right.$$

$$\left. + \sigma^2\gamma^2\bar{c}(\overline{c^2-s^2})\right][3\sigma^2\overline{s^2}(1+\bar{c})]^{-1} \tag{15}$$

after some lengthy calculations.

Assuming the three minima and the tetrahedral angle as before, this becomes

$$\frac{\Delta n}{X} = \frac{(n_0^2+2)^2}{n_0 kT}\left[\frac{2\pi}{45}\frac{3}{2\varepsilon+1}\left\{\frac{(\varepsilon+2)(2\varepsilon+1)}{9}\left(1+\frac{3}{2(\varepsilon+2)}\right)\right.\right.$$

$$\left. + \frac{(\varepsilon+2)^2}{36}\left(22 - \frac{78}{\varepsilon+2} + \frac{27}{(\varepsilon+2)^2}\right)\right\}\left(\alpha_{33} - \frac{\alpha_{11}+\alpha_{22}}{2}\right)$$

$$\left. - \frac{\pi}{135}\frac{(\varepsilon-1)(7\varepsilon-1)}{2\varepsilon+1}(\alpha_{11}-\alpha_{22})\right] \tag{16}$$

Particularly for the case $\varepsilon = 1$, $\alpha_{11} = \alpha_{22}$,

$$\Gamma = \frac{\Delta n}{X}\frac{n_0 kT}{(n_0^2+2)^2} = \frac{\pi}{18} \tag{17}$$

and for the case $\varepsilon \gg 1$, $\alpha_{11} = \alpha_{22}$

$$\Gamma = \frac{\pi}{36}e^{U/kT} \tag{18}$$

the former being exactly the same as that for freely rotating molecule (cf. Eq. (45), III). Eq. (18) is the exact value of Γ whose approximate one was given by Eq. (47), III.

Polymers such as polyethylene $\alpha_{11} - \alpha_{22} = 0$, while for polystylene, for example, it is clea that $\alpha_{11} - \alpha_{22} \neq 0$. In the latter case, however, Eq. (14) is only a certain approximation, because the hindering potential may cease to be symmetrical. These unsymmetrical molecules require more elaborate calculations.

The ratio $\Delta n/X$ is independent of ρ_0 and consequently of the concentration of the junctions in the network provided only that the junctions are not too densely distributed. Even if junctions due to the secondary bonds are being generated or destroyed in the course of temperature variation, this remains true. Thus $\Delta n/X$ seems to give direct information on the internal structures of the molecules, while the elastic forces and the double refraction themselves may show somewhat complicated behaviour due to the changes in the structure of the network.

For this reason it seems very desirable that experiments will be carried out on the elastic forces and the double refraction of polymeric materials at the same time at various temperatures. Of course the effect of crystallization and that of the creep may be superimposed on the orientation effect treated here and in III. Our results, however, will remain useful for the analysis of such experiments.

References.

(1) For example, E. Mack: J. Amer. Chem. Soc. **56**, (1934) 2757.

(2) R. Kubo: J. Phys. Soc. Japan **2**, 47, **3**, (1948) 119.

(3) S. Oka: Proc. Phys-Math. Soc. Japan **24**, (1942) 657.

(4) R. Kubo: J. Phys. Soc. Japan. **2**, (1947) 51.

(5) R. Kubo: J. Phys. Soc. Japan, **2**, (1947) 84.

Interaction between Electrons and Ions in Semiconductors. II.

By Ryogo KUBO.

Physical Department, Faculty of Science, University of Tokyo.

(Received April 8, 1949).

Introduction.

In ionic crystals the wave functions of electrons are strongly affected by the polarization of the lattice. This strong coupling is the most important key to clarify the mechanism of electronic processes in ionic crystals. In the preceding paper.(1) I have shown the general principle for the treatment of stationary states of electrons in polar crystals and have discussed the ground states of an electron trapped by a defect with positive charge, where by the lattice was roughly replaced by a dielectric continuum and the defect by an extra positive change embedded in it. We shall call this the continuum model.

The F-centre of alkali-halides crystals has been proved to be a centre formed by an electron trapped in a negative ion vacancy in the lattice. Tibbs(2) was the first who treated theoretically this model of the F-centre suggested by de Boer.(3) More recently detailed calculations have been undertaken by Muto,(4) Nagamiya(5), Inui(6) and their callaborators. These workers aim to give a satisfactory estimation for the energy of the F-absorption. The effect of the displacement of ions is not, or insufficiently, taken into account.

In this paper the writer does not aim at such a quantitative computation of the electronic levels in real crystals, but he wishes to give a fairly detailed discussion of the continuum model mentioned above. Such a discussion will be helpful for us to get deeper insights on such electronic processes in alkali-halides and other polar crystals that has been very elegantly described by Mott and Gurney in their excellent book.(7)

§ 1. General Treatment of the Continuum Model.

In our continuum model, the displacement of ions is represented by the polarization field $\mathbf{P}_i(\mathbf{r})$, the divergence of which gives the space charge $\rho_i(\mathbf{r})$ due to the polarization. By polarization we mean here exclusively that caused by the displacement of ions. The deformability of ion cores is taken into account by the dielectric constant κ_0. The displacement of ions is caused by the electric forces due to the charge cloud ρ_- of electrons and to the defect point-like extra change $+ze$ embedded in the medium. (Throughout the present work we shall not consider the "hole model".)

As we have shown in I (eq. (3)), the energy of the total system, the electrons, ions, and the defect, consists of two parts. The first is the polarization energy U_p which is the work required to construct the polarization field. The second is the average Hamiltonian $\bar{H}$ of the trapped electrons, which is the sum of the kinetic term, the coulombic interaction term between the electrons and finally $\hat{U}_e$ or the average of the potential energy of the electron due to the presence of the defect and the polarization charge.

As far as we are concerned with s-state of the electrons, the distributions of the trapped electrons and of the polarization field are spherically symmetric. For simplicity, we assume that the polarization field is always described by the charge distribution of the form.

$$\rho_i(r) = -\left(1-\frac{\kappa_0}{\kappa}\right)ze\delta(r)+\left(1-\frac{\kappa_0}{\kappa}\right)n_i e\frac{\beta^3}{8\pi}e^{-\beta r} \qquad (1)$$

so that

$$p_i(r) = \frac{1}{e}\int_0^r \rho_i 4\pi r^2 dr = -\left(1-\frac{\kappa_0}{\kappa}\right)(z-n_i g(\beta r)), \qquad (2)$$

where

$$g(\beta r) = 1-\{1+\beta r+\frac{1}{2}\beta^2 r^2\}e^{-\beta r} \qquad (3)$$

Naturally we have

$$\lim_{r\to 0} p_i(r) = -z\left(1-\frac{\kappa_0}{\kappa}\right).$$

for the defect charge ze is always shielded off by the factor κ_0/κ owing to the ionic polarization in the immediate neighborhood of the defect.

The polarization energy U_p is given by (cf. Eqs. (21), (22) and (23))

$$U_p = \frac{e^2}{2\kappa_0}\left\{\frac{1}{c}\int_0^\infty \frac{p_i^2}{r^2}dr+\int_0^\infty \frac{2zp_i}{r^2}dr\right\}. \qquad (4)$$

where for brevity we have put

$$c = 1-\frac{\kappa_0}{\kappa}. \qquad (5)$$

Assuming the distribution of Eq. (1), this expression becomes

$$U_p = \frac{e^2 c}{2\kappa_0}n_i^2\times\frac{5}{16}\beta+\text{const.}, \qquad (6)$$

the first term of which is the polarization energy measured from the standard state in which the medium is polarized only by the central defect charge (i. e. n = 0).

Let

$$p_- = -\frac{1}{e}\int_0^r 4\pi\rho_- r^2 dr. \qquad (7)$$

where ρ_- is the charge density of the trapped electrons. Then the average of the potential is

$$U_e = -\kappa_0\int_0^r \{(z+p_i)p/r^2\}dr. \qquad (8)$$

by Eq. (26), I. If we assume the s-functions for the electrons, we have

$$\rho_- = n\alpha^3 e^{-\alpha r}/8\pi \qquad (9)$$

weere n (= 1, or 2) is the number of the trapped electrons at the centre. Then Eq. (8) becomes

$$U_e = -\frac{ne^2}{2\kappa_0}\left[\{z+c(n_i-z)\}\alpha-cn_i\frac{\alpha^3(\alpha+2\beta)}{(\alpha+\beta)^3}\right] \qquad (10)$$

When two electrons are trapped at the centre, we have to take into account their coulombic interaction energy U_{int}, which is given by

$$U_{\text{int}} = \frac{1}{\kappa_0}\iint\frac{e^2}{r_{12}}|\Psi(\mathbf{r}_1\mathbf{r}_2)|^2 d\mathbf{r}_1 d\mathbf{r}_2\,. \qquad (11)$$

On the assumption of the s-functions, this is transformed into

$$U_{\text{int}} = (5/16)e^2\alpha/\kappa_0\,. \qquad (12)$$

Finally the average of the kinetic energy of the electrons is given by

$$K = n(\hbar^2/2m)(\alpha^2/4). \qquad (13)$$

For brevity we put

$$x = \kappa_0 a_0\alpha/2, \quad y = \kappa_0 a_0\beta/2. \quad R' = R/\kappa_0^2 \qquad (14)$$

where a_0 is the radius of the hydrogen atom and R the Rydberg constant. The total energy of the centre is written down as

$$\begin{aligned}\bar{E} = nR'\Big[&x^2-2\{(1-c)z+cn_i-(5/16)\delta_{n2}\}x\\&+2cn_i\frac{x^3(x+2y)}{(x+y)^3}+\frac{5}{8}\frac{cn_i^2}{n}y\Big]\end{aligned} \qquad (15)$$

where $\delta_{n2} = 0$ when $n = 1$ and $\delta_{n2} = 1$ when $n = 2$. The average of Hamiltonian of the electron is naturally

$$H = \bar{E}-(5/8)cn_i^2 R'y. \qquad (16)$$

These expressions are valid for $n = 1$ and 2.

Let

$$\left.\begin{aligned}&A = (1-c)z+cn_i-(5/16)\delta_{n2}\,,\\&K = cn_i/A, \quad R'' = nR'A^2,\\&\lambda = y/A, \quad \lambda = x/y\end{aligned}\right\}. \qquad (17)$$

Then the above formulae are transformed into

$$\bar{E}(\lambda,\ \eta) = R''\left[(\lambda\eta-1)^2-1+2K\frac{\lambda^3(\lambda+2)}{(\lambda+1)^3}\eta+\frac{5}{8}\frac{n_i}{n}K\eta\right]. \qquad (18)$$

$$H(\lambda,\ \eta) = R''\left[(\lambda\eta-1)^2-1+2K\eta\frac{\lambda^3(\lambda+2)}{(\lambda+1)^3}\right] \qquad (19)$$

The stationary state of the electrons is determined by the condition

$$\frac{\partial H}{\partial \lambda} = \frac{\partial \bar{E}}{\partial \lambda} = 0 \tag{20}$$

or

$$(\lambda\eta - 1) = K\{(\lambda+4)(\lambda+1)^{-4} - 1\} \tag{21}$$

for every fixed value of η. Thus we have the stationary electronic energy

$$H(\eta) = H(\lambda(\eta), \eta). \tag{22}$$

and the total energy

$$E(\eta) = \bar{E}(\lambda(\eta), \eta). \tag{23}$$

as functions of η which describes the polarization state of the dielectric medium.

By Eqs. (23), (20) and (18) we have

$$\frac{dE(\eta)}{d\eta} = \left(\frac{\partial \bar{E}}{\partial \eta}\right)_{\lambda} = 2R''\left[\lambda(\lambda\eta - 1) + \frac{K\lambda^3(\lambda+2)}{(\lambda+1)^3} + \frac{5}{8}\frac{n_i}{n}K\right]$$
$$= 2R''K\left\{\alpha\left\{\frac{\lambda+4}{(\lambda+1)^4} + \frac{\lambda^2(\lambda+2)}{(\lambda+1)^2} - 1\right\} + \frac{5}{8}\frac{n_i}{n}\right] \tag{24}$$

which becomes equal to zero at $\lambda = 1$ if we put $n = n_i$. Thereore if $n = n_i$ there exists a stable stationary state of the centre which is given by

$$\eta = 1 - (11/16)K,$$
$$E(\eta)_{\min.} = -R''\left(1 - \frac{11}{16}K\right)^2. \tag{25}$$

In this stable configuration we have $\lambda = 1$, and $\alpha = \beta$, so that $\rho_i(r) = -c\rho_-$, which must be true as shown in I (Eq. (13)). Eq. (25) are also derived from the minimum condition of $\bar{E}$ (1, η).

Though the equality $n = n_i$ has to be satisfied in the stable configuration, it may not necessarily be true for some unstable configuration. Consider, for example, the case in which a surplus electron is suddenly captured by a centre containg only one electron. Immediately after the capture the configuration of lattice ions is preserved in its initial state which is the stable configuration for one electron but not for two electrons. Including the case $n \neq n_i$ these stable configurations are also considered. In the Table I the various types of centres are listed corresponding to various values of z, n, and n_i. F and F′ are the analogues of F- and F′- centre of colored crystals in our model. They are formed of a monovalent positive defect ($z = 1$). F⁻ means a centre formed from F by sudden capturing of a surplus electron, and F′⁺ the F′-centre from which an electron is suddenly taken away. Thus F⁻ and F′⁺ are unstable states of F′-and F-centres respectively.

Table I.

	z	n	n_i	A	K
F	1	1	1	1	c
F′	1	2	2	$\frac{11}{16}+c$	$\frac{2c}{c+11/16}$
F⁻	1	2	1	$1+c$	$\frac{2c}{(1+c)}$
F′⁺	1	1	2	$\frac{11}{16}$	$\frac{16}{11}c$
F_{ex}	1	1	1	—	—

	z	n	n_i	A	K
D′	2	2	2	27/16	$32c/27$
D	2	1	1	$2-c$	$c/(2-c)$
D′⁺	2	1	2	$27/16-c$	$c/\left(\frac{27}{16}-c\right)$
D⁻	2	2	1	2	c
S	0	1	1	c	1

Divalent centres ($z = 2$) are denoted by the symbol D. D involes only one electron, and D′ two electrons, so that D′ is the usual form of the centre. D⁻ and D′⁺ are analogous to F⁻ and F′⁺, and are unstable formes of D′ and D. Finally S means the centre formed by an electron which has fallen into a trapped state by digging its own hole.

In the table F_{ex} means the excited state of F-centre. If the F-centre is excited photoelectrically, the electron goes up to 2-p level. Keeping the configuration of ions in that of 1-s state, the 2-p level can be calculated in a similar way as before. Assuming the wave function

$$\Psi \doteq (\alpha^5/32\pi)^{1/2}e^{-\alpha r/2}r\cos\theta.$$

the average of the Hamiltonian is shown to be

$$H = R'[x^2 - x + cx^5(x+3y)(x+y)^{-5}] \tag{26}$$

where x, y, and R' are those defined in (14). Minimizing the expression we obtain the electronic energy. Adding the polarization energy U_p to H, the total energy of F_{ex}. can be expressed as a function of y.

§ 2. The Energy-Configuration Diagram for the Continum Model.

The electronic levels of centres in polar crystals are considerably affected by the positional configuration of the neighboring ions. This situation is often expressed by the "energy-configuration diagram" in which the levels are plotted against some configurational coordinate appropriate to describe the configuration of ions. This diagram is proved very useful to explain the various properties of colored crystals, semiconductors, and especially those of certain phosphors. The construction of the diagram, however, is not generally an easy task.

In our crude continuum model, the configuration of ions has been assumed to be described by the polarization field of Eq. (1), so that we may be granted to choose the parameter β or its equivalent y for a configurational coordinate. Then the total energy E(y) of the centre gives at once the desired diagram which demonstrates the behaviour of the centres in our model.

Before the discussion of the diagrams we must add here some remarks. Our diagrams are based 1. On the crude continuum model, and 2. on the approximate wave function of the type.

$$\Psi(r_1, r_2) = (\alpha^3/8\pi)e^{-\alpha(r_1+r_2)/2} \tag{27}$$

for the two electron system. These approximations require two kinds of improvement.

A. If we consider the atomic structure of the lattice, the levels will be considerably lowered below those calculated from the above formulae, so that the F-absorption frequency must coincide with the observed value. We may, however, expect that the relative values of the levels are not too much changed. But it is also probable that the lowering will be somewhat greater for the ground state than for the excited state, and also be greater for one-electron centres than for two-electron centres.

B. As well known, the type of the approximation (27) leads to the result that the H$^-$ ion has a negative electron affinity of -0.0547 R, while the better approximation of Hylleraas(8) which includes the correlation beween the electrons gives the positive affinity of 0.052 R. Thus for the two-electron centres we have possibly underestimated the absolute values of the electronic energies by about 10%. (In our calculation, the zero of the energy is taken as that of the state in which the electrons are at rest at infinite separation from the centre, so that the energy of the stabel state of two electron system is given as -0.94531 R', while in higher approximation it becomes equal to -1.052 R'.)

These two corrections are of opposite sign for the two-electron centres with respect to the relative positions of the levels.

In the next paper we shall give some tentative discussions about the energy-configuration diagram of the centres.

References.

(1) R. Kubo: J. Phys. Soc. Japan **3**, (1948) 254.
(2) S. R. Tibbs: Trans. Faraday Soc. **35**, (1939) 1471.
(3) de Boer: Receuil des Trav. Chim. d Pay-Bas **56**, (1937) 301.
(4) T. Muto: Progress of Theo. Phys. **4** 181, 243, (1949)
(5) T. Nagamiya: unpublished.
(6) T. Inui: unpublished.
(7) Mott and Gurney: Electronic Processes in Ionic Crystals. (1940).
(8) Hylleraas: Zeits. f. Phys. **60**, (1930) 624.

Interaction between Electrons and Ions in Semiconductors. III.

By Ryogo Kubo.

Physical Department, Faculty of Science, University of Tokyo.

(Received April, 8, 1949)

Introduction.

In the preceding paper II[1] the general formulae were obtained which give the energy of centres in polar crystals as functions of the configuration of lattice ions based on the continuum model. Though the model is very crude, it seems worth while to give some discussions on the energy-configuration diagrams of the centres thus obtained, since such diagrams are not easily derived theoretically in general.

Figs. 1—4 show the diagrams for the centres listed in the Table I of the paper II, where we have assumed the value

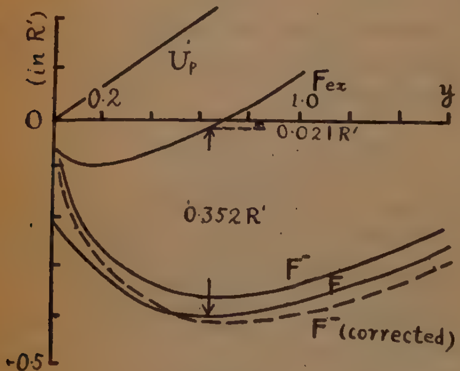

Fig. 1.

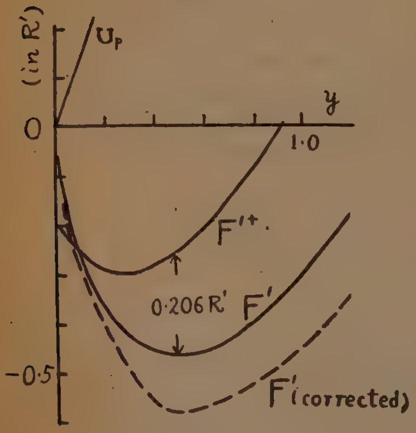

Fig. 2.

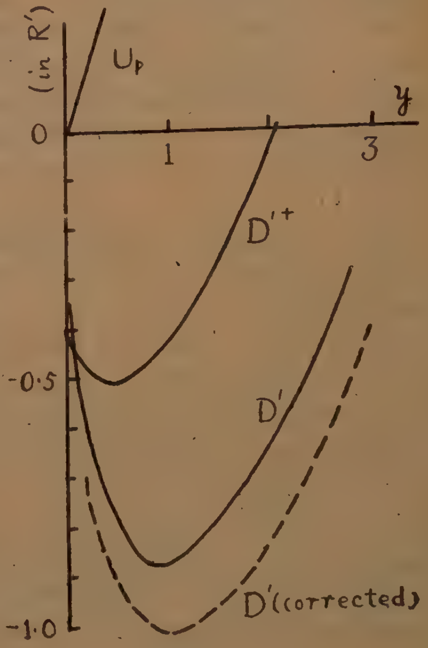

Fig. 3.

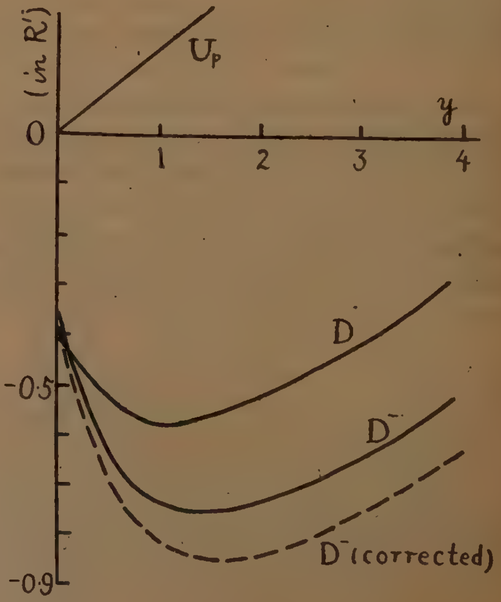

Fig. 4.

$$c = 0.55 \text{ or } \kappa_0/\kappa = 0.45$$

which corresponds to the typical case of KCl crystal. By these diagrams we are able to get some information about the behaviour of colored crystals and some semiconductors, which is the subject of the following sections. It must be noted here that the levels of two-electron centres are lowered about 10% below the curves calculated from Eq. (23), II because of the correction B (cf. § 2, B, II). In the figures the dashed durves are the corrected curves in this sense.

§ 1. F- and F′-centres.

In Figs. 1. and 2, the minima of the levels are as follows:

F : $E[F]_{\min} = -0.387\,R'$ at $y = 0.622$,

F^- : $E[F^-]_{\min} = -0.352\,R'$ at $y = 0.689$,

F' : $E[F']_{\min} = -0.463\,R'$ at $y = 0.481$,

F'^+: $E[F'^+]_{\min} = -0.308\,R'$ at $y = 0.255$.

1) The F-absorption is attributed to the excitation of F-centre to F_{ex}. From the figure we obtain the energy of the F-absorption as

$$h\nu_F = 0.366R',$$

for the F_{ex}-level is $E = +0.021\,R'$ at $y = 0.622$. If we put $\kappa_0 = 2.13$ corresponding to KCl crystal, we get

$$h\nu_F \sim 1.1 \text{ ev}.$$

This is only about one-half of the actually observed value of KCl which is about 2.3 ev(2). This discrepancy is naturally to be expected, for the consideration of the atomic structure will lower the levels. Expecting the relative behaviour of the levels in actual crystals to be essentially the same as that in our crude model, we may take

$$R' \sim 6 \text{ ev}.$$

instead of $R' \sim 3$ ev. Thus we try in the following to estimate various energies concerning some electronic processes in KCl crystals.

2) The excited F-centre or F_{ex} is expected to throw out the electron into the conduction band if the additional energy of $0.021\,R'$ is supplied by thermal agitation. This energy amounts to 0.12 ev. in our estimation. This is in rough agreement with the experiments of photoconduction of colored crystals, though it seems somewhat too high.(3) For the reason stated in § 2, II, the value $R' \sim 6$ ev. may be too large for the excited levels, so that we have to say the above energy is less than 0.12 ev.

3) The difference $E_F - E_{F^-} = A_F$ is the electron affinity of F-cetre in the case when the configuration is frozen in that of the F-centre. When an electron approaches the F-centre so rapidly that the lattice ions have not sufficient time to rearrange themselves, it can be captured giving out the energe A_F as radiation. In the rough approximation, however, A_F is negative as seen in Fig. 1, so that the capture can take place only with absorption of energy, if this estimation is true. But it seems more probable that A_F is actually positive in a higher approximation, which is shown schematically by the dashed curve in Fig. 1. If the latter is the case, the F-centre has a positive affinity to electron. On the other hand, from the figure it is seen that the unstable F^--centre can go back to F giving out the surplus electron back to the free state when supplied with an activation energy of about $0.03\,R'$, that is 0.2 ev. or less.

4) The stable state of F'-centre is as low as $-0.463\,R'$. Thus the unstable F^--centre will be stabilized by the rearrangement of ions giving out the energy of $0.05\,R'$ as heat waves into the lattice. The thermal ionization of F^--centre (unstable) competes with this stabilization process. Discussion about the rate of these processes would be of great interest.

5). The level of F'-centre meets with that of F'^+ as seen in Fig. 2. Hence the F'-centre can be ionized thermally to go back to F-centre. But in this case the activation energy is much greater than that for the F^--centre. It amounts probably to $0.3\,R'$ or about 2 ev. or less. Thus the stabilized F'-centre seems very stable.

6) The F'-absorption is believed to be attributed to the photoionization of the F'-centre. Therefore it corresponds to the transition from F' to F'^+ in Fig. 2. If we take the uncorrected curve of F', the energy of this absorption is estimated to be

$$h\nu_{F'} = -0.257\,R'+0.463R' = 0.206\,R',$$

which is smaller than that of the F-absorption. This is in agreement with the experimental fact(2). If the correction B in § 2, II, is considered, this energy may be somewhat larger.

7) The F-absorption is broadened to a band by thermal agitation. We can easily estimate the width of the band in our model. Near the minimum the F-curve is approximated by the parabola

$$E_F(y) = -R'\left(1-\frac{11}{16}c\right)^2+\frac{3}{8}R'\frac{c}{1-5\,c/16}(y-y_0)^2$$

$$= E_F(y_0)+\frac{1}{2}E_F''(y-y_0)^2$$

($y_0 = 0.622$) and the F_{ex}-level by the straight line

$$E_{F\mathrm{ex}}(y) = E_{F\mathrm{ex}}(y_0)+R'c$$

$$\left\{\frac{5}{8}-\frac{2\,\lambda^5(1+6\,\lambda)}{(1+\lambda)^6}\right\}(y-y_0)$$

$$= E_{F\mathrm{ex}}(y_0)+E'_{F\mathrm{ex}}(y-y_0)$$

where λ is given from the minimum point of the expression (26), II.

Though the parameter y is not a normal coordinate of the lattice vibration, we may approximately assume that the F-centres are distributed by the law

$$N(y)dy \propto \exp\left[-\frac{E''_F}{2kT}(y-y_0)^2\right]dy \qquad (1)$$

at the temperature T. Then the F-band will be broadened in proportion to the square root of T. Inserting the numerical values we get

$$h\Delta\nu_F \sim 1.00\sqrt{h\nu_F kT},$$

which formula has already been suggested by Mott and Gurney(4). We have given here a plausible estimation of the numerical factor.

Similary, the breadth of the F'-band is also estimated. It is shown to be

$$(h\Delta\nu)_{F'} \sim 1.4\sqrt{h\nu_{F'}kT}$$

which is somewhat larger than that of the F-band. In fact the F'-band is broader than the F-band.

8) The maximum of the F-band is observed to shift to red with the rise of temperature(5). Near the minimum of the F-level the transition probability P from 1-s to 2-p state varies with the configuration. It is roughly estimated by the trial function used in II. It is approximated by

$$P = p_0\exp\{-\gamma(y-y_0)\}.$$

where

$$\gamma = \left[\frac{d}{dy}\log\{x_F{}^3x_F{}^5{}_{\mathrm{ex}}(x_F+x_{F\mathrm{ex}})^{-10}\}\right]_{y=y_0}$$

Inserting the numerical values we get

$$p = P_0\exp[-0.603(y-y_0)]$$

The shift of the maximum is given by the formula

$$(h\Delta\nu)_{\mathrm{shift}} = -\gamma kTE'_{F\mathrm{ex}}/E_F'',$$

which becomes in our case

$$(h\Delta\nu)_{\mathrm{shift}} = -0.36\,kT$$

Thus the shift is estimated here to be about 0.3×10^{-4} ev/deg. to red, while it amounts to 3×10^{-4} ev./deg. in experiments. The calculated value is only one-tenth of the observed. It is not certain how this discrepancy depends on the rough approximation of our model, or the shift is essentially to be attributed to some other effect. The latter case seems more probable. (In fact, according to Inui and Uemura(6) the shift is explained by the thermal expansion of the crystal.)

§ 2. Divalent Centres.

Figs. 3 and 4 are the energy-configuration diagrams of divalent centres. For these centres the experimental data are not yet so complete as those for the monovalent centres.

1. The photoelectrical ionization of D'-centres requires the energy $E_{D'+}-E_{D'} = \phi_{\mathrm{ph}}$, which is the socalled (internal) photoelectric work function. For the case $c = 0.55$, this becomes

$$\phi_{\mathrm{ph}} = -0.88\,R'+1.73\,R' = 0.85\,R',$$

which is about 2 ev., if we assume $\kappa_0 = 2.16$ (as in the case of BaO).

2. By thermal ionization D'-centre is transformed into the stable D-centre. This requires the energy

$$\phi_{\mathrm{th}} = (E_D)_{\mathrm{min}}-(E_{D'})_{\mathrm{min}}$$

$$= -1.15\,R'+1.73\,R' = 0.58\,R',$$

which is about 7/10 of ϕ_{ph}. This internal thermal work function is about 1.4 ev. for $c = 0.55$ and $\kappa_0 = 2.16$. This is near to the observed value of BaO(7).

3. The difference between the curves D and D^- is the electron affinity of the D-centre or the stable ionized divalent centre. From Fig. 4 it is seen to be fairly large.

As seen above the estimated internal work functions are of the same order in magnitude as those observed for BaO, for instance. It seems likely that our continuum model is more appropriate for divalent centres than for monovalent ones.

§ 3. Landau's Self-Trapped Electron.

It was suggested by Landau⁽⁸⁾ that an electron can be immobilized in ionic crystal by digging its own hole. If the electron has a chance to stay at a positive ion for some time, the ions would rearrange themselves to stabilize the electron. This self-trapped electron of Landau was once supposed to be the *F*-centre, but now this hypothesis is decidedly abandoned. Though the existence of such a state has not been realized by experiments, it is possible that the trapping process plays some role in the complicated behaviour of ionic crystals.

The energy of this self-trapped electron in our continuum model is easily obtained from Eq. (25), II, namely

$$(E_s)_{\min} = -\frac{25}{256}\left(1-\frac{\kappa_0}{\kappa}\right)^2 \frac{R}{\kappa_0^2}.$$

which gives, for instance, $(E_s)_{\min} = -0.06$ ev. if we put $\kappa_0/\kappa = 0.45$, and $R/\kappa_0^2 \sim 3$ ev. This energy is far smaller than that of *F*-absorption. But it is large enough to affect the mobility of conduction electrons in ionic crystals.

After the preparation of this paper I had a chance to read the work of J. J. Markham and F. Seitz,⁽⁹⁾ who have treaed the same problem taking into account the atomic structure of the lattice. Their final value of the energy of the self-trapped electron is 0.13 ev, which is larger than the value above mentioned. As was stated in § 2, II, this is naturally to be expected. But I have some doubt about their method of the calculation, for it corresponds to minimize the Hamiltonian of the electron not that of the whole system including the lattice. Moreover, it is to be noticed that the kinetic term of lattice vibration is neglected from the Hamiltonain both in their method and in this paper. In fact the nature and origin of the self-trapped state becomes clear only when this term is included in the theory. On this point we shall give further discussions in another article.

Conclusion.

The above discussion was necessarily qualitative so far as real crystals are concerned. The theory must be extended to include proper consideration of the atomic structure of the crystals. In principle it goes on the same line. It must also be noticed that we have not taken here the lattice vibration into account. The customary way to consider the lattice vibration is the perturbation method, which proves sometimes inadequte in polar crystals for it leads to too short mean free paths of the conduction electrons as shown by Mott and Fröhlich.⁽¹⁰⁾ There is a hope to clarify this situation by the crude continuum model.

References.

(1) R. Kubo: J. Phys. Soc. Japan **4**, (1949) 322.
(2) H. Pick: Ann. d. Phys. **31**, (1938) 365, R.W. Pohl: Proc. Phys. Soc. **49**, (Extra Vol.) (1937) 11.
(3) Mott and Gurney: Electronic Processes in Ionic Crystals, Chap. IV, 6.1.
(4) Mott and Gurney: ibid, Chap. IV, § 3.
(5) R.W. Pohl: Proc. Phys. Soc. **49** (Extra Vol.) 3. (1937).
(6) Private Communication.
(7) E. Nishibori, H. Kawamura, and K. Hirano: Proc. Phys-Math. Soc. Japan **23**, (1941) 37.
(8) L. Landau: Phys. Zeits. Sowjet. **3**, (1933) 664.
(9) J.J. Markham and F. Seitz: Phys. Rev. **74**, (1948) 1014.
(10) H. Frönlich: Proc. Roy. Soc. **160**, (1937) 230. H. Fröhlich and N.F. Mott: ibid, **71**, (1939) 496.

Electron Diffraction Studies on Oxide Films Formed on Metals and Alloys

Part 1. Oxidation of Pure Copper.

By Goro HONJO.*

Kobayashi Institute of Physical Research. Kokubunji, Tokyo, Japan.

(Received April 14, 1949)

§ 1. Introduction.

The identification of oxide products formed on metals and alloys at higher temperatures is one of the best fitted applications of the electron diffraction method. Among many works which have been reported on this subject, a series of studies on Cu, Fe, Cr, Ni and their alloys by Miyake(1) and on Fe by Iimori(2) should especially be mentioned here in relation to the present work. The determinant factors for the formation of oxide films at the uppermost surfaces of metals and alloys are temperature and oxygen pressure. The works of Miyake, being carried out on the oxidation at various temperatures in the atmospheric air, left many problems open which are desirable to be clarified by performing further experiments in various oxygen pressures. Iimori controlled the two factors in an evacuable furnace, by changing the air pressure from 10^{-5} to 750 mmHg. and temperature from 150°C to 1000°C.

The present author carried out the experiments to extend the Miyake's work with the procedure of oxidation adopted by Iimori. In the present article the results for pure copper will be presented.

Besides the usually known oxides, Cu_2O and CuO, the so-called "three ring substance" (CuO′), has been reported by Murison by the electron diffraction method, and since then, has been considered to be an intermediate oxide between Cu_2O and CuO(3). It is interesting, therefore, to determine the conditions for the formation of these various oxides at the uppermost surface and to make clear the nature of CuO′.

§ 2. Experimental Method.

Our method of preparation of oxidized specimens was similar to that of Iimori. Namely, the specimens of about $3\times3\times3$ mm³ in dimension, cut from larger blocks, polished with emery paper of 000 and then washed by water jet, were placed in an evacuable quartz tube and were heated beforehand up to desired temperature (from 200°C to 1000°C) in the highest vacuum attainable ($5\times10^{-}$[illegible] mmHg. of air). And then a volume of air was let in the tube through a leak cock to obtain the desired pressure (from 760 mmHg. to 5×10^{-5} mmHg. of air). In the condition thus obtained the oxidizing treatments were carried out for several minutes. After this treatment the specimens were cooled rapidly down to room temperature by pouring water around the quartz tube. This method can define the oxidation conditions very well, because the relaxation times of heating up and cooling down are shortened very much. The oxidized specimens were then subjected to the electron diffraction analysis by reflection method with camera length 15 cm.

§ 3. Experimental Results.

Iimori(2), in his work on iron, drew a temperature-pressure diagram for the purpose to summarize his experimental results and divided the diagram into regions in each of which one of four oxides of iron would be produced.

Our main results can also be represented in the "*temperature pressure diagram*" as is shown in Fig. 1, in which the temperature and the air pressure corresponding to the oxidizing condition are taken as abscissa and ordinate respectively and the kinds of the surface oxide products, which were

---

* Present Address: Tokyo Institute of Technology, O-okayama, Meguroku, Tokyo.

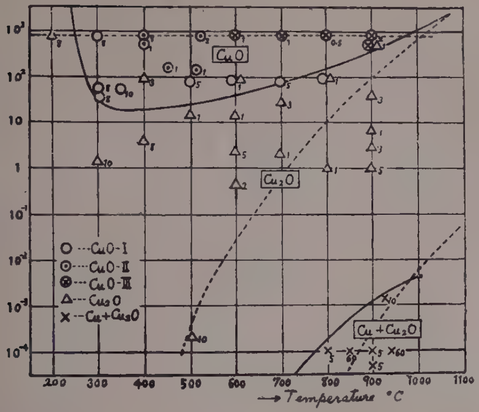

Fig. 1.

identified by the electron diffraction method, are discriminated by different marks. The numeral attached to each mark represents the time of oxidation in minute. The circles and the triangles represent CuO and Cu_2O respectively. The surface of the specimens treated in the conditions with lowest air pressures and the highest temperatures showed mixed patterns of pure Cu and Cu_2O, which are shown in Fig. 1 by the crosses. The diagram, therefore, can be divided into the following three regions having the boundaries shown by the full lines.

1) CuO—Region.

In this region, the uppermost surface products are further classified into three types. Those which are represented by plain circles, CuO-I, showed the diffraction rings of normal intensity distribution as expected from the structure of the tenorite determined by Tunell and others⁽⁴⁾ (Fig. 2). The products represented by the dotted circles, CuO-II, and the crossed circles, CuO-III, showed the patterns as Fig. 3 and Fig. 4 respectively. The rings of CuO-II CuO-III clearly agree with that of the tenorite in their spacings, but differ considerably from the latter in their apparent intensity distributions. The CuO-II showed the "*three ring pattern*" with the characteristic three innermost strong rings of almost equal intensity. The CuO-III, showing new type of pattern, has been failed to be caught in the former works because of the higher temperature of its appearence. For, after the usual method of oxidation performed throughout in open air, the oxidation proceeds too

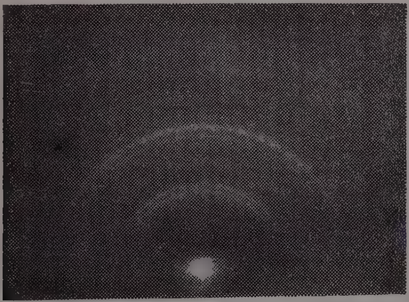

Fig. 2. CuO-I formed at 500°C, 10^2 mmHg.

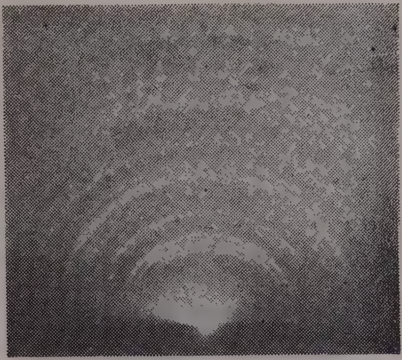

Fig. 3. CuO-II formed at 400°C, 760 mmHg.

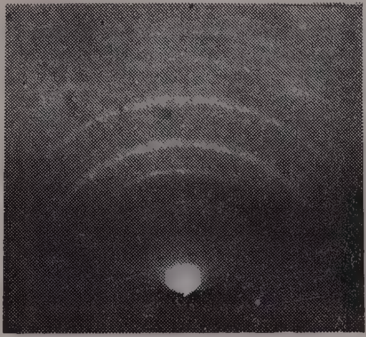

Fig. 4. CuO-III formed at 700°C, 760 mmHg.

Fig. 5. $Cu+Cu_2O$ formed at 900°C, 10^{-4} mmHg.

vigorous in the longer relaxation time for heating up and cooling down, that the surface becomes too rough to give good patterns.

These products which show the three types of the patterns were identified altogether to the tenorite structure from the reason discussed in § 4.

2) Cu_2O—Region.

In this region the surface products were clearly identified with Cu_2O. The products at lower temperatures showed continuous rings of uniform intensity distribution. The patterns of the products formed at temperature higher than 600°C, showed spots having tails directed downward nearly perpendicular to the shadow edge.

3) $(Cu+Cu_2O)$—Region.

The diffraction patterns from the specimens treated under the conditions corresponding to this region were composed of several striations and weak continuous rings of Cu_2O (Fig. 5). The striations, strong in intensity and small in number, having their heads at the positions of Debye rings of Cu, were elongated considerably downward nearly perpendicular to the shadow edge. Under this conditions, the main features of the pattern were not changed even after prolonged treatment (for about an hour).

§ 4. Discussion of the Results.

1) Three types of the patterns of CuO and *identification of the "three ring substance"*.

From the following consideration the present author reached the conclusion that the all three kinds of the surface products which appeared in CuO-region of Fig. 1, including the three ring substance, should be identified altogether to normal CuO, having the well-established structure of the tenorite, and that the apparent differences among them about the intensity distribution in their diffraction rings merely arise from the different crystalline orientations. The fact that the anomalous intensity distribution in CuO-III is due to the preferred orientation of normal CuO making (010)-plane parallel to the specimen surface, can easily be understood by inspecting its pattern. The case of the "three ring substance", CuO-II, which is also concluded to be CuO having another preferred orientation making (110)-plane parallel to the specimen surface, was not so obvious at the first glance in the pattern. The three strong rings, characteristic in the diffraction patterns due to CuO-II, correspond respectively to (110) and the unresolved doublet rings $\{(\bar{1}11), (002)\}$ and $\{(111), (200)\}$. The innermost (110)-ring, which normally possesses moderate intensity becomes especially much enhanced as the result of (110)-orientation. The origin of the confusion which failed Murison to catch the orientation effect and made him erroneously assume the substance as being an intermediate oxide between Cu_2O and CuO seems to lie in the following facts. The electron diffraction rings of lager intensity from the tenorite structure are correspond to the unresolved doublet rings such as $\{(\bar{1}11), (002)\}$, $\{(111), (200)\}$, $\{(022), (\bar{3}11)\}$ and $\{(113), (220)\}$. On account of the doublet structure, they appear as continuous rings with comparatively uniform intensity distribution even after the orientation in question, without showing the arcing characteristic in usual fibrous orientation. This fact may be understood from the diagram of perfect fibrous pattern of this orientation. (Fig. 6). The arcing of rings by the effect of this orientation can be observed in singlet rings of medium intensity such as $(\bar{2}02)$, (020), (202) and $(\bar{1}13)$.

The conclusion that the pattern is not due to any intermediate oxide between CuO and Cu_2O, but merely caused by the preferred orientation of CuO itself, is substanciated also by the following facts. Firstly, the appearence of them was not favoured by reducing the oxygen pressure. Secondly, they were never observed in Shirai's experiments(5) which were carried out with the transmission method on thin films oxidized from the evaporated Cu films. The present author studied similar film by reflection method and also could not observe the three ring pattern.

The fact that the different types of orientation appear according to various temperature is interesting. It is very much conceivable that the various type of orientations may be caused by the differences of velocity of the crystal growth along various crystallographic directions, which in turn may be determined by the velocity of migration of copper

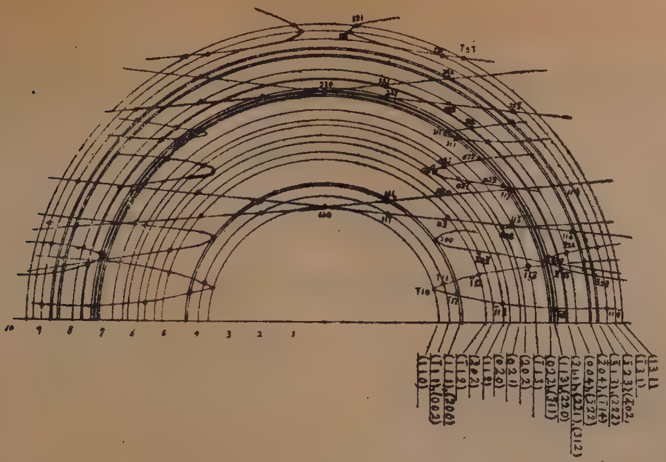

Fig. 6.

ions towards the surface through the oxide film. The observation that one more other type of preferred orientation, making (111)-plane parallel to the specimen surface, appeared on the surface of 40% Ni–Cu alloy oxidized in open air at 600°C, should be mentioned here.

2) According to the theory of the oxidation of metals, the theory of the "Anlaufvorgänge" by Wagner and others, the oxide at the uppermost surface should be determined by the temperature and the partial pressure of oxygen. Therefore, the temperature-pressure diagram like Fig. 1 should be divided into three regions, each of which corresponds to one of CuO, Cu_2O and Cu. And the boundaries among these regions should be represented by the relation giving the dissociation pressure:

$$\log p = -\frac{Q}{4.57}\frac{1}{T}+1.75\log T+2.8$$

with the value of Q, 52.4 Kcal for the reaction $4CuO = 2Cu_2O+O_2$, and 81.6 Kcal for the reaction $2Cu_2O$ $4Cu+O_2$. The boundaries thus calculated are shown in Fig. 1 with dotted lines.

The apparent discrepancy between the theoretical and the experimental boundaries for CuO—Cu_2O, being especially conspicuous at lower temperatures, shows the fact that the assumed chemical equilibrium at the uppermost surface in the theory fails to hold at these temperatures. The co-existence of Cu and Cu_2O at the surface of the specimens treated in the conditions corresponding to the experimental Cu—Cu_2O region (even after prolonged treatment for an hour) also indicates the failure of the simple assumption in the theory. The trend of the experimental boundary for CuO—Cu_2O to approach the theoretical shows that the assumption comes to hold at higher temperatures than about 1000°C.

Summary.

The oxidation products at the uppermost surface of copper formed in dry air of various temperatures and pressures were studied by the electron diffraction method. The results were summarized in the temperature—pressure diagram (Fig. 1), which is divided into three regions, CuO–, Cu_2O– and Cu+Cu_2O-regions. The "three ring pattern", which has been attributed to an intermediate oxide between Cu_2O and CuO by Murison, was concluded to be a fibrous pattern of normal CuO. The boundary-lines of the regions was discussed in relation to the theory of the Anlaufvorgänge.

In conclusion, the author wishes to express his sincere thanks to Dr. S. Miyake and Prof. R. Ueda for their kind advices and encouragements.

References.

(1) S. Miyake: Sci. Pap. I. P. C. R. **29** (1936) p. 167, **31** (1937) p. 161.

(2) T. Iimori: Sci. Pap. I. P. C. R. **34** (1937) p. 60.

(3) C. A. Murison: Phil. Mag. **17** (1934) p. 96. cf. G. P. Thomson and W. Cochrane: Theory and Practise of Electron Diffraction. (1939) p. 177.

(4) G. Tunell, E. Posnjak and C. J. Ksanda: J. Washington Acd. Sci. **23** (1933) p. 195.

(5) S. Shirai: J. Phys. Soc. Jap. **2** (1947) p. 81.

On the Upper and Lower Bounds of Eigenvalues.

By Tosio KATO.

Physics Department, University of Tokyo.

(Received April 25, 1949)

§ 1. Introduction.

As is well known, the approximate solution of eigenvalue-problems based on the Ritz variational principle always leads to upper bounds of eigenvalues, but does not provide us with their lower bounds. Thus it does not allow us to estimate the error of the approximate values, and the method must be regarded as incomplete from the theoretical point of view. We know only empirically that the results are usually in good agreement, at least for the lowest eigenvalue, with experimental values or with exact values obtained by other methods.

On the other hand, there are other methods which can be used to estimate lower bounds of eigenvalues theoretically. But these methods are discovered rather recently and different authors(1) propose different formulas, so that their real character and mutual relations have not been fully discussed from a systematic point of view.

These formulas are of various kinds and some of them are incorrect. Evidently we cannot discuss the relative merits of any two of them if the underlying data are different for them. But detailed study shows that most of these formulas are based on the same data and are essentially of the same character in spite of their apparent difference. They can be regarded as a variational method of higher order, and can be treated as a direct application of the spectral theorem for self-adjoint operators in the abstract Hilbert space. If we reexamine them from this general standpoint, we can make them free from special external forms or unnecessary assumptions so that their mutual relations become clear. As the result, it turns out that the formula given by Temple* is the most precise one among them notwithstanding that it was the oldest as well as the simplest one.

But all these formulas are restricted to the lowest eigenvalue which is, moreover, assumed to be non-degenerate. In the present paper, we will treat the problem under more general conditions and extend the Ritz-Temple formula to the case of degenerate eigenvalues of operators which are not necessarily half-bounded. The main purpose of our investigation lies in its application to a rigorous foundation of the perturbation theory as an approximate method for calculating eigenvalues. This application will be treated in a subsequent paper.

At this point we will make a remark on the method of derivation and the validity of formulas of this sort, for there seems to be some confusion about them. They are usually derived in the case of differential operators, using the expansion theorem or the Green function, and some authors(2) regard the use of the expansion theorem as non-rigorous. But the expansion theorem is equivalent to the spectral theorem and is valid for all self-adjoint operators of the Hilbert space, while non-self-adjoint operators are so rare in application that we may always assume that the operators under consideration are self-adjoint, even when it is not explicitly proved. For this reason, the use of the expansion theorem is not a fault in deriving the formulas; on the contrary it is to be regarded as more general and more pertinent to the problem than e.g. the use of the Green function which is restricted to differential operators.

---

* The original formulas of Temple are concerned with the error of each stage of approximation in the so-called iteration method applied to the lowest eigenvalue of an operator with *positive* lower bound. Out of these formulas we take up only the one for the first approximation, which is, however, shown to be valid for more general operators. In the following the Temple formula is referred to always in this sense.

Of course the expansion theorem stated here retains its general validity only when interpreted in the sense of strong convergence in the Hilbert space (convergence in the mean!). It is important, however, to notice that the expansion in this sense is quite sufficient for our purpose, for the expansion itself is not our final end but only a means to reach the result.†

2. Generalization of the Ritz-Temple Formula.

Let H be a self-adjoint⁽³⁾ (or hypermaximal Hermitian)⁽⁴⁾ operater in the Hilbert space. The spectral representation of H is given by

$$H=\int_{-\infty}^{+\infty}\lambda dE(\lambda), \tag{1}$$

where $E(\lambda)$ is the so-called resolution of the identity belonging to H. We make no further assumptions on H; in particular, H need not be bounded below.

We assume that for a normalized vector w ($||w||=1$) in the domain of H the following quantities are calculated:

$$(Hw,\ w)=\eta,\quad ||(H-\eta)w||=\varepsilon. \tag{2}$$

We have

$$||Hw||^2=\eta^2+\varepsilon^2, \tag{3}$$

so that it comes to the same thing if we calculate $||Hw||$ in place of ε.

Lemma 1. For every α such that $\alpha<\eta$ ($\alpha=-\infty$ is permitted), the interval $(\alpha,\ \zeta]$* contains a point of the spectrum,** where ζ is defined by

$$\zeta=\eta+\frac{\varepsilon^2}{\eta-\alpha}. \tag{4}$$

In general*** the interval $(\alpha,\ \zeta]$ cannot be replaced by smaller one.

Proof. If the interval $(\alpha,\ \mu)$ for a $\mu>\alpha$ contains no point of the spectrum, the quadratic expression

$$(\lambda-\alpha)(\lambda-\mu)=\lambda^2-(\alpha+\mu)\lambda+\alpha\mu \tag{5}$$

is not-negative when λ changes over the spectrum.**** The same is true if we multiply (5) by $d(E(\lambda)w,\ w)$ (≥ 0) and integtate. Since

$$\left.\begin{aligned}\int\lambda^2 d(E(\lambda)w,\ w)&=||Hw||^2=\eta^2+\varepsilon^2,\\ \int\lambda d(E(\lambda)w,\ w)&=\eta,\end{aligned}\right\} \tag{6}$$

we have

$$\varepsilon^2+\eta^2-(\alpha+\mu)\eta+\alpha\mu\geqq 0,$$

that is

$$\mu\leqq\eta+\frac{\varepsilon^2}{\eta-\alpha}=\zeta. \tag{7}$$

In other words, the interval $(\alpha,\ \mu)$ contains a point of the spectrum if $\mu>\zeta$. Since the spectrum is a closed set, the same is true with the interval $(\alpha,\ \zeta]$.

When α and μ are eigenvalues of H and w is a linear combination of the associated eigenvectors, the equality holds in (7). Moreover, we can assign $\eta=(Hw,\ w)$ arbitrarily provided that $\alpha\leqq\eta\leqq\mu=\zeta$. In other words, there is, for each value of α, η, and ε, a case in which the theorem is false if $(\alpha,\ \zeta]$ is replaced by a smaller interval.

Corollary.‡ There is a point of the spectrum within the distance ε from η.

Proof. We have only to put $\alpha=\eta-\varepsilon$ in Lemma 1.

Similarly we can prove

Lemma 2. For every β such that $\beta>\eta$ ($\beta=+\infty$ is permitted), the interval $[\xi,\ \beta)$ contains a point of the spectrum, where ξ is defined by

$$\xi=\eta-\frac{\varepsilon^2}{\beta-\eta}. \tag{8}$$

---

† If we forget this simple fact, it would be difficult not to feel uneasy about such a procedure as expanding a function of several variables into a series of eigenfunctions, differentiating it term by term, multlplying it by a function and integrating term by term, etc. But the result of these operations is completely justified from the standpoint of spectral analysis in the abstract Hilbert space.

* We denote by $(\alpha,\ \beta)$ the open interval $\alpha<\lambda<\beta$, by $[\alpha,\ \beta]$ the closed interval $\alpha\leqq\lambda\leqq\beta$. $(\alpha,\ \beta]$ means the half-closed interval $\alpha<\lambda\leqq\beta$.

** The spectrum means that of H, if the contrary is not stated.

*** As to the precise meaning, see the proof.

**** If $\alpha=-\infty$ replace (5) by $\lambda=\mu$.

‡ This theorem is sometimes ascribed to Weinstein.

In general the interval $[\xi, \beta)$ cannot be replaced by smaller one.

Combining these two lemmas, we obtain

Theorem. We assume that the interval (α, β) contains no point of the spectrum except at most a non-degenerate eigenvalue, and that for a w, η and ε are calculated and satisfy

$$\varepsilon^2 < (\eta-\alpha)(\beta-\eta). \tag{9}$$

Then the interval (α, β) certainly contains one and only one eigenvalue λ_0 such that

$$\eta-\frac{\varepsilon^2}{\beta-\eta} = \xi \leqq \lambda_0 \leqq \zeta = \eta+\frac{\varepsilon^2}{\eta-\alpha} \tag{10}$$

In general (10) cannot be replaced by more precise formula if we know only the four quantities η, ε, α and β, whatever these quantities may be.

If we denote by u_0 the normalized eigenvector associated with the eigenvalue λ_0, we have

$$1-|(w, u_0)|^2 \leqq \left\{\left(\eta-\frac{\alpha+\beta}{2}\right)^2+\varepsilon^2\right\} \Big/ \left(\frac{\beta-\alpha}{2}\right)^2 \tag{11}$$

If either $\zeta \leqq \frac{\alpha+\beta}{2}$ or $\xi \geqq \frac{\alpha+\beta}{2}$ holds, we have more precisely

$$1-|(w, u_0)|^2 \leqq \begin{cases} \dfrac{\varepsilon^2}{(\eta-\alpha)^2+\varepsilon^2} & \left(\zeta \leqq \dfrac{\alpha+\beta}{2}\right), \\[2ex] \dfrac{\varepsilon^2}{(\beta-\eta)^2+\varepsilon^2} & \left(\xi \geqq \dfrac{\alpha+\beta}{2}\right). \end{cases} \tag{12}$$

Proof. According to Lemmas 1 and 2, each of the intervals $(\alpha, \zeta]$ and $[\xi, \beta)$ contains a point of the spectrum. Since (9) means that $\zeta < \beta$ and $\xi > \alpha$, we conclude that the interval $[\xi, \zeta]$ contains an eigenvalue λ_0. These lemmas show that there is in general no formula more precise than (10).

To derive (11) we note that the quadratic expression

$$(\lambda-\alpha)(\lambda-\beta) = \lambda^2-(\alpha+\beta)\lambda+\alpha\beta$$

is not-negative, except at $\lambda = \lambda_0$, when λ changes over the spectrum. If we multiply it by $d(E(\lambda)w, w)$ and integrate, noting (6) and $((E(\lambda_0)-E(\lambda_0-0))w, w) = |(w, u_0)|^2$, we have

$$\varepsilon^2+\eta^2-(\alpha+\beta)\eta+\alpha\beta \geqq (\lambda_0-\alpha)(\beta-\lambda_0)|(w, u_0)|^2. \tag{13}$$

But as

$$(\lambda_0-\alpha)(\beta-\lambda_0) = \left(\frac{\beta-\alpha}{2}\right)^2-\left(\lambda_0-\frac{\alpha+\beta}{2}\right)^2, \tag{14}$$

we can replace the factor $(\lambda_0-\alpha)(\beta-\lambda_0)$ by $\left(\frac{\beta-\alpha}{2}\right)^2$ and obtain (11). This replacement is, however, in some cases not advantageous. $(\lambda_0-\alpha)(\beta-\lambda_0)$ is maximum for $\lambda_0 = \frac{\alpha+\beta}{2}$ and diminishes monotonously when λ_0 departs from $\frac{\alpha+\beta}{2}$, so that we can replace λ_0 by ζ if $\zeta \leqq \frac{\alpha+\beta}{2}$. Thus we obtain the first inequality of (12). The case $\xi \geqq \frac{\alpha+\beta}{2}$ can be treated similarly.

We will add some remarks on this theorem.

1. Our theorem is symmetric with respect to upper and lower bounds, as it should be. The asymmetry in the Ritz-Temple formula results from the fact that here the lowest eigenvalue is considered (see 2. below).

2. If $\alpha = -\infty$, λ_0 is the lowest eigenvalue, and since $\zeta = \eta$, η is an upper bound of λ_0 (the Ritz formula). In this case $\lambda_0 \geqq \xi$ is nothing but the Temple formula.* According to our theorem, it is evident that *in this case there can be no formula more precise than that of Temple.* Therefore all other formulas given by the authors cited above(1) are worse than the Temple formula, unless at best identical with the latter.**

3. When the approximate eigenvector w is not completely preassigned but contains some free parameters, it is advantageous to choose them once so as to make ξ maximum and then so as to make ζ minimum, independently for both cases (see the example below).

4. If we take the same w for both ξ and ζ, the error of the approximate eigenvalue is of the order ε^2 and very small when ε is small. The factors of ε^2 are $1/\eta-\alpha$ and $1/\beta-\eta$, and these are small when the eigenvalues are widely separated from each other as in the case of classical ordinary differential operators. In the case of partial dif-

---

* See the footnote on page 2.

** In particular the complicated formulas of Trefftz and Newing are superfluous, inasmuch as the Temple formula is better and yet much simpler. Of course this can be verified directly, but it is rather tedious owing to the complicated form of their formulas. The reader will easily verify that all numerical restlts in their examples are improved by using Temple's formula. Though the improvement in the final results is not very remarkable, the labor of calculation is cut down almost to nothing.

On the other hand, Weinstein's formula (see the corollary to Lemma 1, is nearly as simple as Temple's, but is much less precise.

ferential operators of many variables, the eigenvalues are rather crowded and the above formula does not always give satisfactory results. It is partly for this reason that the Hylleraas approximate eigenfunction of He ground state gave only rough lower bound(5).

5. It can easily be shown from (11) and (12) that $||w-u_0|| = O(\varepsilon)$ if u_0 is properly normalized. Thus the approximate eigenvector is not necessarily so precise as the approximate eigenvalue calculated with itself.

6. If we know the exact value of λ_0, we have naturally better estimation of $|(w, u_0)|^2$. It follows from (13)

$$1-|(w, u_0)|^2 \leqq \frac{\varepsilon^2+(\eta-\lambda_0)(\eta+\lambda_0-\alpha-\beta)}{(\lambda_0-\alpha)(\beta-\lambda_0)}.$$

If in particular λ_0 is the lowest eigenvalue ($\alpha = -\infty$), we have

$$1-|(w, u_0)|^2 \leqq \frac{\eta-\lambda_0}{\beta-\lambda_0}.$$

7. Our theorem assumes that we know an upper bound α for the next lower eigenvalue and a lower bound β for the next upper eigenvalue to λ_0. Thus it cannot be applied unless we know, by some method or other, rough estimate of eigenvalues (0-th approximation). This is a common defect for all formulas of this sort. In some cases this inconvenience is avoided by using Lemma 1 or 2 directly.

Example. By way of illustration let us cite a simple example. Consider the eigenvalue-problem:

$$\frac{d^2u}{dx^2}+(\lambda-x^4)u = 0, \quad (-\infty < x < +\infty).$$

As an approximate eigenfunction for the first (lowest) eigenvalue λ_1, we take

$$w = \pi^{-\frac{1}{4}} p^{\frac{1}{4}} \exp\left(-\frac{1}{2}px^2\right), \quad (p>0).$$

η and ε are easily calculated to be

$$\eta = \frac{1}{2}p+\frac{3}{4}p^{-2}, \qquad \varepsilon^2 = \frac{1}{2}p^2-3p^{-1}+6p^{-4}.$$

Further we need β, for which we can take a rough lower bound of the *third* eigenvalue λ_3, for we can restrict ourselves to *symmetric* functions. For this purpose, we note that the eigenvalues of $\frac{d^2u}{dx^2}+(\lambda-\gamma^2x^2)u = 0$ are given by $(2n-1)\gamma$ ($n = 1, 2, \cdots\cdots$) and that the inequality $x^4 \geqq \gamma^2x^2-\frac{1}{4}\gamma^4$ holds for arbitrary γ. Thus we have $\lambda_n \geqq (2n-1)\gamma-\frac{1}{4}\gamma^4$, and taking $\gamma = (2n-1)^{\frac{1}{3}}$ to make the right-hand side maximum, we obtain a rough estimate $\lambda_n \geqq \frac{3}{4}(2n-1)^{\frac{4}{3}}$. In particular $\lambda_3 \geqq \frac{3}{4}\cdot 5^{\frac{4}{3}} = 6.41$ and we can take $\beta = 6.41$.

Putting these values and $\alpha = -\infty$ into (10), we have

$$\frac{1}{2}p+\frac{3}{4}p^{-2}-\frac{\frac{1}{2}p^2-3p^{-1}+6p^{-4}}{6.41-\frac{1}{2}p-\frac{3}{4}p^{-2}} \leqq \lambda_1 \leqq \frac{1}{2}p+\frac{3}{4}p^{-2}.$$

The minimum of the right-hand side occurs for $p = 3^{\frac{1}{3}} = 1.442$ and is 1.082 (Ritz's method!), while the maximum of the left-hand side occurs for about $p \doteq 1.70$ and is 1.034. Thus we have

$$1.034 \leqq \lambda_2 \leqq 1.082.$$

In the same way the simple function $w = \text{const.}\, x \exp\left(-\frac{1}{2}px^2\right)$ leads to

$$3.74 \leqq \lambda_2 \leqq 3.85.$$

Higher eigenvalues λ_n can be treated similarly, taking for β the rough lower bound of λ_{n+2} obtained above and for α the upper bound of λ_{n-2} already calculated.

§ 3. Degenerate Eigenvalues.

The theorem of the preceding section is not applicable to degenerate eigenvalues and, even for non-degenerate ones, the error is large when they are densely crowded. In this section we will attempt to remove these restrictions and derive similar formula for upper and lower bounds of a group of eigenvalues simultaneauoly.

We assume that the interval (α, β) contains (at most) m eigenvalues $\lambda_1 \leqq \lambda_2 \leqq \cdots\cdots \leqq \lambda_m$ but no other point of the spectrum, and that m approximate eigenvectors $w_1, \cdots\cdots, w_m$ are so chosen that the matrices (Hw_i, w_j) and (w_i, w_j) are diagonal:

$$(Hw_i, w_j) = \eta_i\,\delta_{ij}, \quad (w_i, w_j) = \delta_{ij}, \quad (i, j = 1, 2, \cdots\cdots, m), \tag{15}$$

and that

$$\alpha < \eta_1 \leqq \eta_2 \leqq \cdots\cdots \leqq \eta_m < \beta. \tag{16}$$

Further we assume that

$$\|(H-\eta_i)w_i\| = \varepsilon_i, \quad (i = 1, 2, \cdots, m) \tag{17}$$

are calculated.

Let $u_i (i = 1, 2, \cdots, m)$ be the eigenvectors associated with the eigenvalues λ_i, and let M_k be the k-dimensional linear manifold determined by $u_1, \cdots, u_k$. We put

$$w = \sum_{i=1}^{k} \gamma_i w_i \,, \tag{18}$$

and choose the coefficients γ_i so that

$$\|w\|^2 = \sum_{i=1}^{k} |\gamma_i|^2 = 1,$$

$$w, u_i) = 0 \quad (i = 1, 2, \cdots, k-1). \tag{19}$$

If we put

$$(Hw, w) = \eta, \; \|(H-\eta)w\| = \varepsilon, \tag{20}$$

we can apply Lemma 1 and conclude that the interval $(\alpha, \zeta]$ contains a point of the spectrum, where ζ is defined by (4) with (20). By virtue of (19) w belongs to the orthogonal manifold $N_{k-1} = \overset{\perp}{M}_{k-1}$ to M_{k-1}. Since u_i are eigenfunctions of H, M_{k-1} and N_{k-1} reduce H so that Hw also belongs to N_{k-1}. Hence we can regard H as an operator in the Hilbert space N_{k-1} so long as the vector w is concerned. Considered in N_{k-1}, however, the spectrum of H contains no longer $\lambda_1, \cdots, \lambda_{k-1}$. Hence the point of the spectrum contained in $(\alpha, \zeta]$ stated in Lemma 1 must coincide with the eigenvalue λ_k. Thus we have

$$\lambda_k \leqq \zeta = \eta + \frac{\varepsilon^2}{\eta-\alpha} = \frac{\eta^2+\varepsilon^2-\alpha\eta}{\eta-\alpha}. \tag{21}$$

We have only to express the right-hand side of (21) with the aid of the given quantities η_i and ε_i. Since

$$\eta^2+\varepsilon^2 = \|Hw\|^2 = \sum \gamma_i \bar{\gamma}_j (Hw_i, Hw_j),$$

$$(Hw_i, Hw_j) = ((H-\eta_i)w_i, (H-\eta_j)w_j) + \eta_i^2 \delta_{ij},$$

we have by (17)

$$\eta^2+\varepsilon^2 \leqq (\sum \varepsilon_i |\gamma_i|)^2 + \sum \eta_i^2 |\gamma_i|^2.$$

Further we have

$$\eta = (Hw, w) = \sum \eta_i |\gamma_i|^2,$$

so that (21) becomes

$$\lambda_k \leqq \frac{(\sum \varepsilon_i |\gamma_i|)^2 + \sum \eta_i (\eta_i-\alpha) |\gamma_i|^2}{\sum (\eta_i-\alpha) |\gamma_i|^2}, \tag{22}$$

where summation is to be taken $i = 1$ to k. As we do not know the exact values of γ_i, we eliminate γ_i from (22) as follows. According to the Schwarz inequality, we have

$$(\sum \varepsilon_i |\gamma_i|)^2 \leqq \sum x_i^2 |\gamma_i|^2 \sum \frac{\varepsilon_i^2}{x_i^2}, \tag{23}$$

where x_i^2 are coefficients to be determined by

$$\sum \frac{\varepsilon_i^2}{x_i^2} = 1, \tag{24}$$

$$\frac{x_i^2 + \eta_i(\eta_i-\alpha)}{\eta_i-\alpha} = \rho, \quad (i = 1, \cdots, k). \tag{25}$$

Then we have by (22), (23), (24) and (25)

$$\lambda_k \leqq \rho. \tag{26}$$

ρ satisfies the equation obtained from (24) and (25) by eliminating x_i^2:

$$\sum_{i=1}^{k} \frac{\varepsilon_i^2}{(\rho-\eta_i)(\eta_i-\alpha)} = 1. \tag{27}$$

It is easily seen that $x_i^2 > 0$ can really be chosen to satisfy (24) and (25) if the largest root of (27) is larger than η_k. If this is not the case, we can easily show that $\lambda_k \leqq \eta_k$. Thus we have obtained an upper bound of λ_k:

$$\lambda_k \leqq \mathrm{Max}(\eta_k, \rho_k), \; (k = 1, \cdots, m) \tag{28}$$

where ρ_k denotes the largest root of (27).

From (27) it follows that

$$\rho_k - \eta_k \leqq \sum_{i=1}^{k} \frac{\varepsilon_i^2}{\eta_i-\alpha}, \tag{29}$$

so that we have a simple estimation

$$\lambda_k \leqq \eta_k + \sum_{i=1}^{k} \frac{\varepsilon_i^2}{\eta_i-\alpha}, \; (k = 1, \cdots, m). \tag{30}$$

It will be noted that the denominators do not contain such quantities as $\eta_i - \eta_j$, which may be small or even zero. In some cases (30) is not precise and the original estimation (28) should be preferred. If in particular $\lambda_1, \lambda_2, \cdots$ are the lowest eigenvalues, we can put $\alpha = -\infty$ and (30) reduces to $\lambda_k \leqq \eta_k$. This result is a generalization of the Ritz formula and is well known.

In the same way we can obtain a lower bound of λ_k:

$$\lambda_k \geqq \mathrm{Min}(\eta_k, \sigma_k), \; (k = 1, \cdots, m) \tag{31}$$

where σ_k is the smallest root of the equation

$$\sum_{i=k}^{m} \frac{\varepsilon_i^2}{(\beta-\eta_i)(\eta_i-\sigma)} = 1. \qquad (32)$$

In particular, we have, corresponding to (30),

$$\lambda_k \geqq \eta_k - \sum_{i=k}^{m} \frac{\varepsilon_i^2}{\beta-\eta_i}, \quad (k=1, \cdots, m). \qquad (33)$$

In conclusion we will notice that the above formulas for upper and lower bounds of λ_k are not the unique ones, contrary to the non-degenerate case.

The writer wishes to express his cordial thanks to Professor Ochiai for his continued interest in this work.

References.

(1) G. Temple: Proc. Lond. Math. Soc. **29** (1928), 257; Proc. Roy. Soc. **119** (1928), 276;
D. H. Weinstein: Phys. Rev. **40** (1932), 797; **41** (1932), 839; Proc. Nat. Acad. Sci. **20** (1934), 529,
F. Trefftz: Math Ann. **108** (1933), 595.
J. K. L. MacDonald: Phys. Rev. **46** (1934), 828.
W. Romberg: Phys. Zs. Sowjetu. **8** (1935), 516; **9** (1936), 546.
R. A. Newing: Phil. Mag. **24** (1937), 114.
A. F. Stevenson: Phys. Rev. **53** (1938), 199.
G. Horvay: Phys. Rev. **56** (1939), 214.
L. Collatz: Z. A. M. M. **19** (1939), 224; 297.
E. Kamke: Math. Z. **45** (1937), 788.
G. Temple and W. G. Bickley: Rayleigh's Principle and its Applications to Engineering, London, 1933.
(2) For instance, see Collatz, reference (1).
(3) M. H. Stone: Linear Transformations in Hilbert Space, New York, 1932, Chap. V.
(4) J. v. Neumann: Mathematische Grundlagen der Quantenmechanik, Berlin, 1932. p. 88.
(5) Weinstein, see (1).

Note added in proof: Although this work was originally intended for the rigorous foundation of the perturbation method, it turned out to be very useful for direct solution of eigenvalue problems of various kinds. These applications will be treated elsewhere.

Non Reflective Dielectrics.

By Tokio Sakurai.

Electrical Communications Laboratory, Ministry of Telecommunications.

(Received March 26, 1949).

§ 1. Sandwich Type Dielectric.

By cutting wedge teeth stripes on the surface of dielectric substances, we can diminish the reflection of electromagnetic waves at the surface. In order to explain this phenomenon we first consider *sandwich type dielectric* as shown in Fig. 1., which is constructed by piling up two *elementary dielectric plates* alternately. One elementary plate has dielectric constant ε_1, permeability μ_1, and the thickness b_1, while another has ε_2, μ_2, and b_2. Rectangular x, y, z-coordinates are taken so that x-axis is perpendicular to elementary plates. In addition we take x_1 and x_2 coordinates along x-axis so that an elementary plate with the thickness b_1 lies between $x_1 = 0$ and $x_1 = b_1$, and neighbouring elementary plate with the thickness b_2 lies between $x_2 = 0$ and $x_2 \doteq b_2$. Now we investigate the electromagnetic wave propagating in z-direction in the sandwiches type dielectrics. Since electrom-

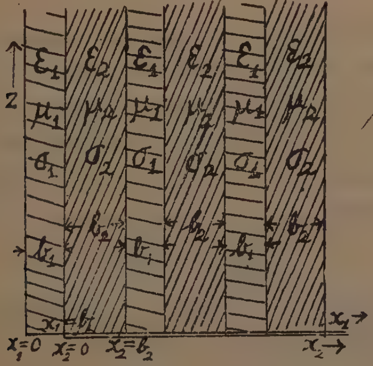

Fig. 1. Sandwich Type Dielectric.

agnetic phenomena in elementary plates of the same sort are similar to each other, it is sufficient to consider the phenomena in two elementary plates lying between $x_1 = 0$, $x_1 = b_1$ and between $x_2 = 0$, $x_2 = b_2$.

We first investigate the case of E incidence, that is, the case when the electric field of incident wave is perpendicular to plates of sandwiches type dielectric. It is easily seen that the fields in plates lying between $x_1 = 0$, $x_1 = b_1$ and between $x_2 = 0$, $x_2 = b_2$ are expressed by $\Pi_z^{(1)}$ and $\Pi_z^{(2)}$ respectively, where $\Pi_z^{(1)}$ and $\Pi_z^{(2)}$ are z-components of Hertz vectors of electric type written as follows:

$$\Pi_z^{(1)} = (A_1 \sin \gamma_1 x_1 + B_1 \cos \gamma_1 x_1) e^{-jhz} e^{j\omega t}, \tag{1}$$

$$\Pi_z^{(2)} = (A_2 \sin \gamma_2 x_2 + B_2 \cos \gamma_2 x_2) e^{-jhz} e^{j\omega t}, \tag{2}$$

where

$$\gamma_1^2 = k_1^2 - h^2, \quad k_1^2 = \omega^2 \varepsilon_1 \mu_1, \tag{3}$$

$$\gamma_2^2 = k_2^2 - h^2, \quad k_2^2 = \omega^2 \varepsilon_2 \mu_2. \tag{4}$$

The field components are evaluated from (1) and (2) as follows:

$$\left.\begin{aligned} E_z^{(1)} &= \gamma_1^2 (A_1 \sin \gamma_1 x_1 + B_1 \cos \gamma_1 x_1) e^{-jhz} e^{j\omega t} \\ H_y^{(1)} &= -j\omega\varepsilon_1 \gamma_1^2 (A_1 \cos \gamma_1 x_1 - B_1 \sin \gamma_1 x_1) e^{-jhz} e^{j\omega t} \\ E_y^{(1)} &= 0, \quad \text{etc.} \end{aligned}\right\} \tag{5}$$

$$\left.\begin{aligned} E_z^{(2)} &= \gamma_2^2 (A_2 \sin \gamma_2 x_2 + B_2 \cos \gamma_2 x_2) e^{-jhz} e^{j\omega t} \\ H_z^{(2)} &= -j\omega\varepsilon_2 \gamma_2 (A_2 \cos \gamma_2 x_2 - B_2 \sin \gamma_2 x_2) e^{-jhz} e^{j\omega t} \\ E_y^{(2)} &= 0, \quad \text{etc.} \end{aligned}\right\} \tag{6}$$

since $x_1 = b_1$ and $x_2 = 0$ express a boundary of two elementary plates, and since tangential electric and magnetic components must be continuous through this boundary, we have by (5) and (6)

$$\left.\begin{aligned} \gamma_1^2 A_1 \sin \gamma_1 b_1 + \gamma_1^2 B_1 \cos \gamma_1 b_1 &= \gamma_2^2 B_2, \\ \varepsilon_1 \gamma_1 A_1 \cos \gamma_1 b_1 - \varepsilon_1 \gamma_1 B_1 \sin \gamma_1 b_1 &= \varepsilon_2 \gamma_2 A_2. \end{aligned}\right\} \tag{7}$$

Since the field at $x_1 = 0$ is equal to the field at $x_2 = b_2$ owing to the periodicity of the field, and since tangential electric and magnetic components must be continuous through the boundary at $x_2 = b_2$, we have by (5) and (6)

$$\left.\begin{aligned} \gamma_2^2 A_2 \sin \gamma_2 b_2 + \gamma_2^2 B_2 \cos \gamma_2 b_2 &= \gamma^2 B_1, \\ \varepsilon_2 \gamma_2 A_2 \cos \gamma_2 b_2 - \varepsilon_2 \gamma_2 B_2 \sin \gamma_2 b_2 &= \varepsilon_1 \gamma_1 A_1. \end{aligned}\right\} \tag{8}$$

Elimininating constants A_1, B_1, A_2, B_2 from four equations (7) and (8), we have

$$\begin{vmatrix} \gamma_1 \sin \gamma_1 b_1 & \gamma_1 \cos \gamma_1 b_1 & 0 & -\gamma_2 \\ \varepsilon_1 \cos \gamma_1 b_1 & -\varepsilon_1 \sin \gamma_1 b_1 & -\varepsilon_2 & 0 \\ 0 & -\gamma_1 & \gamma_2 \sin \gamma_2 b_2 & \gamma_2 \cos \gamma_2 b_2 \\ -\varepsilon_1 & 0 & \varepsilon_2 \cos \gamma_2 b_2 & -\varepsilon_2 \sin \gamma_2 b_2 \end{vmatrix} = 0. \tag{9}$$

If we solve (9), we get the values of propagation constant h. But since it is difficult to get the values of h in general case, we shall only discuss the case when thicknesses of elementary plates are small compared with wave length. In this case $\gamma_1 b_1$ and $\gamma_2 b_2$ are small compared with unity, and (9) becomes approximately

$$\begin{vmatrix} \gamma_1^2 b_1 & 1 & 0 & -1 \\ \varepsilon_1 & -\varepsilon_1 b_1 & -\varepsilon_2 & 0 \\ 0 & -1 & \gamma_2^2 b_2 & 1 \\ -\varepsilon_1 & 0 & \varepsilon_2 & -\varepsilon_2 b_2 \end{vmatrix} = 0. \tag{10}$$

If we solve (10) combinig with (3) and (4), we get

$$h^2 = \frac{(b_1/\varepsilon_1) k_1^2 + (b_2/\varepsilon_1) k_2^2}{b_1/\varepsilon_1 + b_2/\varepsilon_2}. \tag{11}$$

This result shows that propagation constant h is the mean value of the propagation constants k_1 and k_2 of both elementary plates in propotion of b_1/ε_1 and b_2/ε_2.

If the plane electromagnetic wave is incident with its magnetic field perpendicular to elementary plates of sandwich type dielectric, we call this case H incidence. In this case the fields in elementary plates are deduced from z-components of Hertz vectors of magnetic type which are exactly expressed in the same formulas as (1) and (2). Proceeding in exactly the same manner as from (1) to (11), we get

$$h^2 = \frac{(b_1/\mu_1) k_1^2 + (b_2/\mu_2) k_2^2}{b_1/\mu_1 + b_2/\mu_2} \tag{12}$$

as the expression of propagation constant in sandwich type dielectric in H incidence.

Even when the elementary plates are made of conducting materials with conductivities σ_1 and σ_2 respectively, the above arguments hold still, if we replace ε_1 and ε_2 by

$$\bar{\varepsilon}_1 = \varepsilon_1 - j\sigma_1/\omega, \quad \bar{\varepsilon}_2 = \varepsilon_2 - j\sigma_2/\omega \tag{13}$$

respectively. In this case k_1, k_2 defined by (3) and (4) become

$$k_1^2 = \omega^2 \mu_1 (\varepsilon_1 - j\sigma_1/\omega), \quad k_2^2 = \omega^2 \mu_2 (\varepsilon_2 - j\sigma_2/\omega). \tag{14}$$

Consequently h's given by (11) and (12) become

$$\bar{h}^2 = \frac{(b_1/\bar{\varepsilon}_1)k_1^2+(b_2/\bar{\varepsilon}_2)k_2^2}{b_1/\bar{\varepsilon}_1+b_2/\bar{\varepsilon}_2}, \qquad (15)$$

$$\bar{h}^2 = \frac{(b_1/\mu_1)k_1^2+(b_2/\mu_2)k_2^2}{b_1/\mu_1+b_2/\mu_2}. \qquad (16)$$

§ 2. Macroscopic Boundary.

We shall now investigate the non-reflective dielectric on the bases of the results obtained in the foregoing section. We consider the dielectric surface so carved that many equally wedge-shaped stripes are arranged over the surface. We call this dielectric the *wedge-teeth dielectric* and its lateral section is shown in Fig. 2. Let the electromagnetic constants of the space be denoted by ε_1, μ_1 and those of wedge teeth dielectric by ε_2, μ_2, σ_2. Rectangular x, y, z-coordinates are so chosen that xy-plane contacts on the summits of wedges and z-axis is directed perpendicularly inwards the dielectric.

Suppose we cut the teeth of dielectric by a *plane* parallel to xy-plane, which is shown by the dotted line in Fig. 2. This line is divided by surface of wedges in pieces so that its pieces in each space between neighbouring wedges are of length b_1, while those contained in each dielectric wedge are of length b_2. If the wedges are sharp, both surfaces of each wedge may be regarded parallel to yz-plane, Therefore, the state of propagation of electromagnetic wave through this imaginary plane is approximately equal to that of electromagnetic wave through the *sandwich type dielectric* shown in Fig. 1. Hence the propagation constants h's or $\bar{h}$'s at the plane are approximately equal to the results (11) and (12) or (15) and (16). Let the height of teeth be denoted by l, and the space between two parallel planes $z=0$ and $z=l$ be called *teeth space*. Since b_1 and b_2 are slowly varying functions of z which expresses the ordinate of imagined surface, the values of h's or $\bar{h}$'s vary slowly from $z=0$ to $z=l$. Since no sudden change occurs in the values of h's or $\bar{h}$'s, there is no reflection in electromagnetic wave in passing through the teeth space of dielectric. Therefore, electric wave propagates into or out of the wedge teath dielectric without reflelection.

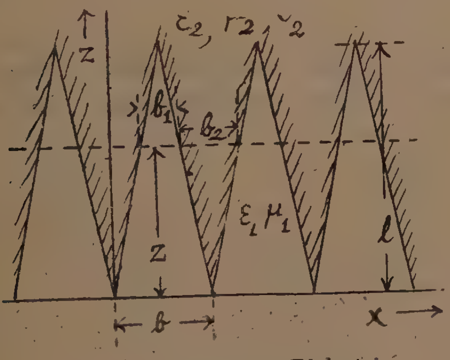

Fig. 2. Wedge-Teeth Dielectric.

Supposing that the dielectric is not conductive, we consider the physical meanings of the equation

$$\int_0^l h dz = \int_0^a k_1 dz + \int_a^l k_2 dz. \qquad (17)$$

The left hand side expresses the phase change as the dielectric wave passes through the teeth space. In order to explain the physical meaning of right hand side of (17) we consider a *pile of two layers*. The first layer with ε_1, μ_1 lies between $z=0$ and $z=a$, the second layer with ε_2, μ_2 lies between $z=a$ and $z=l$. Since the propagation constants in first and second layer are k_1 and k_2 respectively, the right hand side expresses the phase change of plane electromagnetic wave when it passes through this pile of two layers. Since ε_1, μ_1 are equal to electromagnetic constants of the space outside the wedge teeth dielectric and ε_2, μ_2 are equal to electromagnetic constants of the dielectric, if we replace the teeth space of the wedge teeth dielctric by the pile of two layers, the plane $z=a$ becomes the boundary of two domains with ε_1, μ_1 and ε_2, μ_2. We call this boundary the *macroscopic boundary* of wedge teeth dielectric.

In practical cases, such as designation of lenses, the phase change is the most important quantity to be calculated. But on account of complicated structures of the teeth space, the calculation of phase change in this space is difficult. Therefore, it is convenient to replace teeth space by the pile of two layers mentioned above and to reduce wedge teeth dielectric to the dielectric of equivalent phase change which is bounded by macroscopic boundary.

When the dielectric is conductive, it is evident by (13) and (14) that $\bar{h}$ given by (15) ann (16) becomes complex value. In this case we consider

$$\Im\left\{\int_0^l \bar{h}dz\right\} = \Im\left\{\int_a^l \bar{k}_2 dz\right\} \qquad (18)$$

in place of (17), where $\Im$ means the imaginary part of the right quantity, Since imaginary part of $\bar{h}$ means the attenuation constant of teeth space, the left hand side of (18) expresses the total attenuation quantity through the teeth space. Since $\Im\{\bar{k}_2\}$ means the attenuation constant of the second layer of the pile already mentioned the right hand side of (18) expresses the total attenuation quantity of the second layer. Hence $z = \bar{a}$ in (18) expresses the boundary of the secend layer of the same attenuating power as the teeth space of conductive wedge-teeth dielectric, and we call $z = \bar{a}$ the *macroscopic boundary* in the conductive case. The conductive wedge-teeth dielectric is good absorber of electromagnetic wave, because the electromagnetic wave transmits without reflection into the dielectric and attenuates away.

Let us now calculate the position of macroscopic boundary of wedge teeth dielectric whose orthogonal section is shown in Fig. 2, when the permeability of the dielectric is assumed to be non-conductive. In this case (11) and (12) becomes

$$h^2 = \mu_1\omega^2 \frac{b_1+b_2}{b_1/\varepsilon_1+b_2/\varepsilon_2}, \quad (E \text{ incidence}) \qquad (19)$$

$$h^2 = \mu_1\omega^2 \frac{b_1\varepsilon_1+b_2\varepsilon_2}{b_1+b_2}, \quad (H \text{ incidence}) \qquad (20)$$

respectively. If b is the summit distance of two neighbouring wedges, there exists the relations $b_1+b_2 = b$ and $b_2 = zb/l$, whatever the value of the ordinate z of the imagined plane may be. Making use of these relations, (19) and (20) become

$$h = k_1 \Big/ \sqrt{1-\frac{z}{l}\left(1-\frac{\varepsilon_1}{\varepsilon_2}\right)}, \quad (E \text{ incidence}) \qquad (21)$$

$$h = k_1 \sqrt{1+\frac{z}{l}\left(\frac{\varepsilon_2}{\varepsilon_1}-1\right)}, \quad (H \text{ incidence}) \qquad (22)$$

respectively. Hence

$$\int_0^l hdz = \frac{2k_1 l}{1+\sqrt{\varepsilon_1/\varepsilon_2}}, \quad (E \text{ incidence}) \qquad (23)$$

$$\int_0^l hdz = \frac{2k_1 l/3}{\varepsilon_2/\varepsilon_1-1}\left\{\left(\frac{\varepsilon_2}{\varepsilon_1}\right)^{3/2}-1\right\}, \quad (H \text{ incidence}) \qquad (24)$$

On the other hand

$$\int_0^a k_1 dz + \int_a^l k_2 dz = k_1\left\{a+\frac{\varepsilon_2}{\varepsilon_1}(l-a)\right\}. \qquad (25)$$

By substituting (23), (24) and (25) into (17) we get

$$a = \frac{l}{\varepsilon_2/\varepsilon_1-1}\left\{\frac{\varepsilon_2}{\varepsilon_1}-\frac{2}{1+\sqrt{\varepsilon_1/\varepsilon_2}}\right\}, \quad (E \text{ incidence}) \qquad (26)$$

$$a = \frac{l}{\varepsilon_2/\varepsilon_1-1}\left\{\frac{\varepsilon_2}{\varepsilon_1}-\frac{2}{3}\frac{(\varepsilon_2/\varepsilon_1)^{3/2}-1}{\varepsilon_2/\varepsilon_1-1}\right\}, \quad (H \text{ incidence}) \qquad (27)$$

(26) and (27) express the ordinates of the macroscopic boundary in E and H incidences respectively.

On Araki's Theory of Inverted Alkali Doublets.

Ta-You Wu.

Department of Physics, Columbia University, New York.

(Received Aug. 8, 1949).

Abstract.

The explanation of Araki that the inversion of doublets in certain alkali spectra is due to the spin-orbit interactions between the valence electron and the core electrons has been examined more closely. It is found that his "good agreement" between theory and observation is the result of unjustified approximations and that the proposed interactions are entirely inadequate for the explation of the observed inversion.

The explanation of White[1] for the inversion of certain doublets in the alkali-like spectra of some elements, namely, that it is due to the interaction between the doublet in question and another inverted doublet arising from a configuration in which one electron in a closed shell of the core is excited, has been generally accepted. More recently another theory for the inversion of doublets has been proposed by Araki,[2] according to which the inversion is due to an "over-screening" of the valence electron by the spin-orbit interaction between the valence and the core electrons resulting in a negative effective field for the valence electron. He claims an agreement of the calculated separation -4.0 cm^{-1} with the observed -3.6 cm^{-1} in the case of the $4f\,^2F$ of Cu I. The purpose of this note is to examine his calculations more closely. It is shown that his good agreement is obtained through unjustified approximations and that the proposed interactions when correctly calculated are far too small to account for the observed inversion.

To facilitate discussion, let us outline Araki's procedure. Consider an atom or ion with one valence electron $(n,\ l,\ m_l,\ m_s) = (n,\ l,\ M \mp 1/2,\ \pm 1/2)$ outside a closed-shell core of N electrons, and introduce the perturbation

$$H = \sum_{1}^{N+1} \overset{(1)}{\Lambda}(k) + \sum_{k=1}^{N+1} \sum_{j=k+1}^{N+1} \left(\overset{(2)}{\Lambda}(kj) + \overset{(3)}{\Lambda}(kj)\right), \qquad (1)$$

where

$$\overset{(1)}{\Lambda}(k) = \frac{2\mu^2 z}{r_k^3}(\boldsymbol{l}_k \cdot \boldsymbol{s}_k)$$

$$\overset{(2)}{\Lambda}(k,\ j) = -\frac{2\mu_2}{r^3_{kj}}\{(\boldsymbol{K}_{kj} + 2\boldsymbol{K}_{jk},\ \boldsymbol{S}_k) + (\boldsymbol{K}_{jk} + 2\boldsymbol{K}_{kj},\ \boldsymbol{S}_j)\} \qquad (2)$$

$$\overset{(3)}{\Lambda}(k, j) = \frac{4\mu^2}{r^3_{kj}}\left\{(\boldsymbol{s}_k \cdot \boldsymbol{s}_j) + \frac{3}{r^2_{kj}}(\boldsymbol{r}_{kj} \cdot \boldsymbol{s}_k)(\boldsymbol{r}_{jk} \cdot \boldsymbol{s}_j)\right\}$$

$i\boldsymbol{l}_k = [\boldsymbol{r}_k \times \nabla_k]$; $i\boldsymbol{K}_{kj} = [\boldsymbol{r}_{kj} \times \nabla_k]$, $\mu =$ Bohr magneton. $\overset{(1)}{\Lambda}$ is the spin-orbit interaction of the separate electrons; $\overset{(2)}{\Lambda}$ is the interaction between the spin of one and the orbit of another electron; and $\overset{(3)}{\Lambda}$ is the spin-spin interaction. Araki finds that $H^{1)}$ is diagonal with respect to M, and is given by

$$\begin{vmatrix} M - \frac{1}{2} & -\sqrt{\left(l - M + \frac{1}{2}\right)\left(l + M + \frac{1}{2}\right)} \\ -\sqrt{\left(l - M + \frac{1}{2}\right)\left(l + M + \frac{1}{2}\right)} & -\left(M + \frac{1}{2}\right) \end{vmatrix} (z - \sigma)\mu^2 \overline{\frac{1}{r^3}} \qquad (3)$$

from which it follows that doublet separation is, in term values,

$$^2L_{l-\frac{1}{2}} - {}^2L_{l+\frac{1}{2}} = (2l+1)(z-\sigma)\mu^2 \overline{\frac{1}{r^3}}\,. \qquad (4)$$

Here, for a $4f$ electron in Cu,

$$\sigma = \sum_{n=1}^{3} \sum_{l=0}^{h-1} 2(2l+1)(\zeta_{nl,\,43} + 3\tilde{\zeta}_{nl,\,43}) \qquad (5)$$

and

$$\zeta_{nl,\,43} = -\frac{1}{\overline{r^{-3}}} \int_0^\infty \int_0^\infty \frac{1}{r_2}\frac{\partial a_0}{\partial r_2} \left[R_{nl}^{(1)} R_{43}^{(2)}\right]^2 r_1^2 dr_1 r_2^2 dr_2, \quad \text{etc.} \qquad (6)$$

$$\overline{\frac{1}{r^3}} = \int_0^\infty \frac{1}{r^3} R^2_{43} r^2 dr, \quad a_0 = \frac{1}{r_1},\ r_1 > r_2; \quad = \frac{1}{r_2},\ r_1 < r_2 \qquad (7)$$

Araki evaluates the integrals in $\zeta_{nl,\,43}$, $\overline{\frac{1}{r^3}}$ etc. in (6) using hydrogenic wave functions and finds $\sigma=30.21$ so that $\sigma-z=1.21$. To obtain the doublet separation, he evaluates $\overline{\frac{1}{r^3}}$ in (3) using hydrogenic wave function with an effective nuclear charge $29-21.4=76$ on the following ground[2]: "Araki and Noma calculated the screening constant of $\overline{\frac{1}{r^3}}$ for $4p$ of Cs using the Hartree function. The result is 21.4. That for $4p$ of Cu may be smaller than it, for Z is smaller and there is no outer shell. That for $4f$ of Cu may be larger than this value. It may be therefore not very different from that for $4p$ of Cs. Thus we can assume that the screening constant for $4f$ of Cu is 21.4". Thus he finds $\overline{\frac{1}{r^3}}=0.163$ in atomic units for $4f$ of Cu, and finally

$$^2F_{\frac{5}{2}}-{}^2F_{\frac{7}{2}}=-4.0\,\mathrm{cm}^{-1} \tag{8}$$

compared with the observed value $-3.6\,\mathrm{cm}^{-1}$

(i) We shall first show that the above "agreement" is achieved chiefly through the unjustified assumption that the screening constant for $4f$ of Cu is 21.4. It is clear from the above quotation that there is really no argument for any specific value such as 21.4 at all. Granting for the moment that all the rest of the calculations are correct, we need now evaluate the matrix element of $\frac{1}{r^3}$ of the $4f$ electron of Cu. Now, reference to the energy states of the $nf\,^2F$ series of Cu I and a Rydberg table shows that the $nf\,^2F$ are practically hydrogenic, the quantum defects being of the order 0.01. It follows that the wave functions of the nf electrons in Cu are to a very good approximation hydrogenic, with an effective charge equal to unity instead of $29-21.4=7.6$ as assumed by Araki. This leads to a value for $\overline{\frac{1}{r^3}}$ which is $(1/7.6)^3=1/440$ times that of Araki's i.e.,

$$\overline{\frac{1}{r^3}}=0.00037 \text{ in atomic units.}$$

It is obvious that this will lead to an exceedingly small separation, namely, $\sim -0.01\,\mathrm{cm}^{-1}$ if Araki's values for the $\zeta_{nl,\,43}$'s are taken to be correct, instead of $-4.0\,\mathrm{cm}^{-1}$ as found by Araki.

(ii) In evaluating the $\zeta_{nl,\,43}$'s, Araki employs hydrogenic wave functions for the $4f$ and the core electrons, the argument being that the error so introduced will be small since the $\zeta_{nl,\,43}$'s are the ratios of two integrals containing these wave functions. It is seen, however, that while the $4f$ wave function does appear quadratically in both integrals, the wave function of the core electron n, l appears only in the integral in the numerator. As an uncertainty of only 4 per cent in the values of the $\zeta_{nl,\,43}$'s alone would give rise to an uncertainty of 1.2 unit in σ and hence an uncertainty of 100 per cent in $(Z+\sigma)$, it is seen that great accuracy must be employed in calculating the $\zeta_{nl,\,43}$'s. Instead of hydrogenic wave functions, a much better approximation would be to employ the correctly "screened" wave functions such as given by Slater on the basis of the Hartree field.[3] Thus with the radial wave functions

$$R(1s)\sim e^{-\alpha r} \qquad \alpha=28.7,$$

$$R(2p)\sim re^{-\beta r}+cre^{-\gamma r} \qquad \beta=14.7,\ \gamma=10.1$$

$$R(3d)\sim r^2(e^{-\delta r}+de^{-\varepsilon r}+fe^{-\chi r})$$

$$\delta=63,\ \varepsilon=2.65,\ \lambda=1.25,$$

$$R(4f)\sim r^3e^{-\varphi r} \qquad \varphi=0.25,$$

one certainly would obtain different values for the $\zeta_{nl,\,43}$'s. The calculation has not been carried out here because no agreement with the experimental result can be expected on account of the smallness of the factor $\overline{\frac{1}{r^3}}$, as pointed out in (i) above.

(iii) Incidentally, a recalculation of the $\zeta_{nl,\,43}$'s with hydrogenic wave functions, as done by Araki, leads to quite different values for some of the $\zeta_{nl,\,43}$'s, as shown in the following table. It is then seen that these correct $\zeta_{nl,\,43}$'s give for σ the value 19.773 so that Z-σ is positive and there is no over-screening in this case.[4]

$\zeta_{nl,\,43}$	Araki's value	Recalculated here
$1s$, $4f$	0.9988	0.9988
$2s$, $4f$	0.8779	0.8779
$2p$, $4f$	0.9234	0.9234
$3s$, $4f$	0.9772	0.386
$3p$, $4f$	0.9793	0.4384
$3d$, $4f$	0.9843	0.594

Without further calculations, one can see that for a valence electron with high azimuthal quantum number l' for which the $\zeta_{nl,\,n'l'}$'s are large, the value of the matrix element $\overline{\frac{1}{r^3}}$ for the valence electren is small. On the other hand, for low azimthal quantum number l' of the valence electron, the $\overline{\frac{1}{r^3}}$ is large, but then the $\zeta_{nl,n'l'}$'s will be small.5) In the latter case, there will be normal doublets, as is observed in paratically all cases. In the former case, even if there is any "over-screening" due to the spin-orbit interaction between the valence and the core electrons, the theoretical value for the doublet separation will be too small to account for the actually observed inverted doublets, as shown in (i) above.

References.

(1) H. E. White: Phys. Rev. **40**, 316 (1932); M. Phillips, ibid **44**, 644, (1933).

(2) G. Araki: Proc. Phys.-Math. Soc. Japan **21**, 508 (1939); **19**, 592, (1937).

(3) J. C. Slater: Phys. Rev. **42**, 33 (1932). The 1*s*, 2*p*, 3*d* wave functions employed here are Slater's functions for CuII, but the wave functions of the core electrons are in general not greatly modified by changing or even removing the valence electron.

(4) Araki's values for the $\zeta_{nl,43}$ are taken here. They have not been recalculated since their contribution to σ is comparatively small.

(5) Compare the table of $\zeta_{nl,n'l'}$ of Araki, Proc. Phys.-Math. Soc. Japan **20**, 746 (1938).

A Remark on Ta-You Wu's Criticism on the Theory of Inverted Alkali Doublets.

By Gentaro ARAKI.

Department of Industrial Chemistry, Kyoto University.

(Received September 3, 1949)

Introduction.

Ta-You Wu(1) made a critical remark on my theory of inverted alkali doublets.(2) His criticism consists of three parts (i), (ii) and (iii) as follows: (i) the estimated value of $\overline{r^{-3}}$ is too large; (ii) the hydrogen eigenfunction is too rough to obtain the accuracy in calculating $\zeta_{n'l',43}$; (iii) the evaluation of parameters involves some mistakes. As for (ii) and (iii) he is quite right whereas I have a slightly different opinion on (i) and even on a part of the argument mentioned in (ii). According to my recalculation it seems that the theory has no need of changing its essential conclusion. The result of the recalculation and some remarks will be accounted for in the present note.

§ 1. Effective Charge of Valence Orbital.

The quantum defects of the $nf\,^2F$ of Cu are of the order 0.01. This does not necessarily mean that the effective charge of the nf orbital is equal to unity contrary to Wu's argument. We can derive this effective charge from the spectral term in the following way. For this purpose we write the spectral term of an alkali atom in the form

$$nl\,^2L = Z^{*2}/(2n^2) \quad \text{atomic units} \tag{1.1}$$

where n is equal to $l+1$ and Z^* is an effective charge of the spectral term.

If the nl orbital of the valence electron is hydrogen-like its radial part is given by

$$R_{nl}(r) = cr^l \exp\{-(Z-s)r/n\} \tag{1.2}$$

where $Z-s$ is the effective charge of the orbital and c is the normalization constant. If we neglect the dependence of core orbitals on n and l, a relation between Z^* and s can be easily found by reducing the energy integral which is calculated by using the determinantal eigenfunction of the atom. The result is given by

$$Z^{*2} = (Z-s_1)^2-(s_1-s)^2 \tag{1.3}$$

where s_1 is the screening constant due to the electrostatic interaction between the valence electron and core electrons and it is defined by

$$s_1 r^{-1} = \sum_{\text{core}} \iint \phi_{\text{val}}^*(1)\phi_{\text{core}}^*(2) r_{12}^{-1}$$

$$\{\phi_{\text{val}}(1)\phi_{\text{core}}(2) - \phi_{\text{core}}(1)\phi_{\text{val}}(2)\} \qquad (1.4\text{a})$$

$$\overline{r^{-1}} = \int r^{-1} |\phi_{nl}|^2 \qquad (1.4\text{b})$$

It follows from Eq. (1.3) that Z^* and $Z-s$ are the same only in case of $s \overset{?}{=} s_1$ but they are generally different. Thus we see that Wu's argument is not necessarily correct. The numerical examples for $4f\,^2F$ of Na and Cu are shown in Tables I and II. We see that $Z-s$ amounts to 7 when $Z-s_1$ is between 3 and 4. In order to get a more definite estimation we have to evaluate $Z-s_1$.

Table I

Atom	Z	$4f\,^2F$ in cm^{-1} (obs.)(3)	Z^{*2} (obs.)	$Z-s_1$ (calc.)	$Z-s$
Na	11	6860.37	1.00026	1.033	1.292
Cu	29	6880.3	1.00317	2.256	4.279

Table II

$Z-s_1$	$Z-s$	
	Na	Cu
1.1	1.56	1.55
1.2	1.85	
1.4	2.38	
1.6	2.85	
2	3.73	
3	5.83	
4	7.87	
5	9.90	

Carrying out the angular integration we can write $Z-s_1$ as follows:

$$Z-s_1 = 1 + \sum_{n'l'} (2l'+1)(2A_{n'l'} + B_{n'l'}) \qquad (1.5\text{a})$$

where the summation is to be extended over all shells in the core, $A_{n'l'}$ is given by

$$\overline{r^{-1}} A_{n'l'} = \int_0^\infty [rR_{nl}(1)]^2\, dr_1 \int_{r_1}^\infty \left(\frac{1}{r_1} - \frac{1}{r_2}\right) [rR_{n'l'}(2)]^2 dr_2 \qquad (1.5\text{b})$$

and $B_{n'l'}$ is the exchange term. We shall estimate the order of magnitude of $Z-s_1$ by hydrogen radial functions. The calculated values of $A^{n'l'}$ are shown in Table III. The values of $Z-s_1$ calculated from these parameters neglecting $B_{n'l'}$ are shown

Table III

A_{10}	0.00001	A_{30}	0.1047
A_{10}	0.00001	A_{30}	0.1047
A_{20}	0.00621	A_{31}	0.08625
A_{21}	0.00339	A_{32}	0.04964

in the fifth column of Table I. From these values of $Z-s_1$ and Z^{*2} given in the fourth column we obtain the values of $Z-s$ which are shown in the sixth column. We see that the effective charge is not equal to 1 but 4.3 for Cu $4f$. In fact $Z-s_1$ is larger because we neglect $B_{n'l'}$ which is positive. The inaccuracy of the hydrogen function may compensate partly this error. The above mentioned values of $Z-s$ may thus be smaller than the correct values.

A more accurate valence orbital would involve two or three exponentials instead of (1.2).(4) This may give rise to a much larger difference between $Z-Z^*$ and a screening constant of $\overline{r^{-3}}$.

Another way of estimating the effective charge of the $4f$ orbitals is given by the inter- or extrapolation from hitherto known values on the basis of the method of the self-consistent field. In the previous paper(2) this was crrried out from orbitals of different n and l.

Numerical expressions of $4f$ orbitals of W and Hg were calculated by Manning and Millman(5) and Hartree and Hartree(6) respectively. We can easily obtain the effective charges of the orbitals from their results assuming the analytical expressions given by (1.2) for the orbitals. The result of a rough estimation is as follows: $Z-s=41$ for W $4f(Z=74)$; $Z-s=47$ for Hg $4f(Z=80)$. From these values of effective charges we obtain $s=33$ as the value of the screening constant for both cases.

If we consider this screening to be due to 46 electrons in the Cu core and $4s^2 4p^6 4d^{10}$ shells, the mean screening per an electron is equal to 33/46. The screening of the Cu core is equal to $33 \times 28/46 = 20$. This value may be smaller than the correct value because the screening per an electron in the Cu core must be larger than that in the N shell. The neglect of the effect due to outer electrons may partly compensate this error. The previously estimated value(2) $s=21.4$ for the Cu core is thus justified to some extent. At any rate it seems probable that the effective charge of $\overline{r^{-3}}$ is not equal to unity but of the order 5∼9 probably 7.

§ 2. Values of $Z-\sigma$ and $\zeta_{n'l',43}$.

At first sight $Z-\sigma$ seems to be a small difference of two large numbers and it may be imagined that a small percentage error of σ is enlarged in $Z-\sigma$. But this is not the case because $Z-\sigma$ can be written in the following form:

$$Z-\sigma=1+\sum_{n'l'}2(2l'+1)(\xi_{n'l',nl}-3\tilde{\zeta}_{n'l',nl}) \quad (2.1a)$$

where

$$\overline{r^{-3}}\xi_{n'l',nl}=\int_0^\infty r_1{}^{-3}[r_1R_{nl}(1)]^2dr_1\int_{r_1}^\infty[r_2R_{n'l'}(2)]^2dr_2 \quad (2.1b)$$

The parameter $\zeta_{n'l,nl}$ is given by $1-\xi_{n'l',nl}$.

My previous values(2) of $\zeta_{30,43}$, $\zeta_{31,43}$ and $\zeta_{32,43}$ were incorrect as was pointed out by Wu.(1) A factor 3^3 was omitted from $\xi_{3l,43}$ by mistake. The recalculated values of them using hydrogen functions are shown in the third column of Table IV.* However these values are inaccurate because interactions between electrons are not taken into account. Better values would have been obtained by employing adequate screening constants for each of orbitals.(7) A much better approximation would be to employ Slater's analytical expressions of self-consistent functions as was pointed out by Wu.(1)

Table IV. Calculated Values of $\zeta_{n'l',43}$

	Without screening		With self-consistent screening constant
$n'l'$	Wu's values	Recalculated here	
$3s$	0.386	0.3853	0.99998
$3p$	0.4384	0.4423	0.99967
$3d$	0.594	0.5873	0.99605

As an approximation of the above mentioned Slater function we replace the atomic number of hydrogen-like functions by effective charges which are determined for each of orbitals from self-consistent functions according to Slater's method, where the exponential of the lowest power of r and the inner exponential are adopted.(4) These effective charges for Cu are as follows: 21.62×3 for $3s$; 12.32×3 for $3p$; 6.29×3 for $3d$. As the effective charge for $4f$ the value given in Table I. namely 1.07×4, is presumably adopted.

The values of parameters evaluated using these screening constants are shown in the fourth column of Table IV. We see that these values are very close to unity. Consequently it seems that our previous conclusion on the inverted doublet $4f\,^2F$ of Cu has still no need of changing. The $4f\,^2F$ of Na is also expected to be inverted though the experimental evidence has not yet been obtained. In order to obtain the more definite conclusion it is necessary to evaluate all the parameters by employing the self-consistent functions. This will be carried out in near future.

References.

(1) Ta-You Wu, J. Phys. Soc. Japan, **4** (1949).
(2) G. Araki, Proc. Phys. Math. Soc. Japan, **21** (1939), 508.
(3) R. F. Bacher and S. Goudsmit, Atomic Energy States, (1932).
(4) J. C. Slater, Phys. Rev., **42** (1932), 33.
(5) M. F. Manning and J. Millman, Phys. Rev., **49** (1936), 848.
(6) D. R. Hartree and W. Hartree, Proc. Roy. Soc. London A, **149** (1935), 210.
(7) G. Araki, Proc. Phys. Math. Soc. Japan, **19** (1937), 592.
S. Tutihasi, J. Phys. Soc. Japan, 3 (1948), 137.

---

* My new values are slightly different from Wu's. I think the formers are correct because they quite agree with those independently calculated by Mr. Tutihasi.

Short Notes

Theory of Elasticity for Finite Displacement, II.

By Sinsuke SUGAMOTO.

(Read March 28, 1948; Received Jan. 20, 1949).

In the previous paper I.,(1) we have dealt with the strain components, which can be considered as thermodynamical state-variables. Here we shall rewrite the equation of motion and the boundary condition with other two kinds of strain components, which generally are not considered as thermodynamical state-variables, but are useful in a special case. Let $\mathfrak{i}, \mathfrak{j}, \mathfrak{k}$ be unit vectors in three directions of axes of Cartesian coordinates, $\mathfrak{r}_0$ be $\xi\mathfrak{i}+\eta\mathfrak{j}+\zeta\mathfrak{k}$, the operator ∇_0 be $\mathfrak{i}\frac{\partial}{\partial\xi}+\mathfrak{j}\frac{\partial}{\partial\eta}+\mathfrak{k}\frac{\partial}{\partial\zeta}$, and define the components of finite strain from the (L′) and (E′) stand-points as follows:

$$\text{(L}'\text{)}\quad \begin{cases} (\nabla_0 x\cdot\nabla_0 x) = 1+2\sigma_{\xi\xi}, & (\nabla_0 y\cdot\nabla_0 y) = 1+2\sigma_{\eta\eta}, \\ (\nabla_0 z\cdot\nabla_0 z) = 1+2\sigma_{\zeta\zeta}, & (\nabla_0 y\cdot\nabla_0 z) = \sigma_{\eta\zeta}, \\ (\nabla_0 z\cdot\nabla_0 x) = \sigma_{\zeta\xi}, & (\nabla_0 x\cdot\nabla_0 y) = \sigma_{\xi\eta}; \end{cases}$$

$$\text{(E}'\text{)}\quad \begin{cases} \left(\frac{\partial\mathfrak{r}_0}{\partial x}\cdot\frac{\partial\mathfrak{r}_0}{\partial x}\right) = 1-2\sigma_{xx}, & \left(\frac{\partial\mathfrak{r}_0}{\partial y}\cdot\frac{\partial\mathfrak{r}_0}{\partial y}\right) = 1-2\sigma_{yy}, \\ \left(\frac{\partial\mathfrak{r}_0}{\partial z}\cdot\frac{\partial\mathfrak{r}_0}{\partial z}\right) = 1-2\sigma_{zz}, & \left(\frac{\partial\mathfrak{r}_0}{\partial y}\cdot\frac{\partial\mathfrak{r}_0}{\partial z}\right) = -\sigma_{yz}, \\ \left(\frac{\partial\mathfrak{r}_0}{\partial z}\cdot\frac{\partial\mathfrak{r}_0}{\partial x}\right) = -\sigma_{zx}, & \left(\frac{\partial\mathfrak{r}_0}{\partial x}\cdot\frac{\partial\mathfrak{r}_0}{\partial y}\right) = -\sigma_{xy}, \end{cases}$$

then $\epsilon_{\xi\xi}, \ldots, \epsilon_{\xi\eta}$ and $\epsilon_{xx}, \ldots, \epsilon_{xy}$ are linear functions of $\sigma_{\xi\xi}, \ldots, \sigma_{\xi\eta}$ and $\sigma_{xx}, \ldots, \sigma_{xy}$ respectively, whose coefficients are products of components of $\partial\mathfrak{r}/\partial\xi$, $\partial\mathfrak{r}/\partial\eta$, $\partial\mathfrak{r}/\partial\zeta$ and $\nabla\xi$, $\nabla\eta$, $\nabla\zeta$. When we assume these coefficients to be constant in differentiating W with respect to $\sigma_{\xi\xi}$, etc., the Eqs. (L) and (E) can be rewritten as follows.

The equation of motion:

$$\text{(L}'\text{)}\quad \rho_0\frac{d\mathfrak{V}}{dt} = \rho_0\mathfrak{K}+\left(\frac{\partial}{\partial\xi}, \frac{\partial}{\partial\eta}, \frac{\partial}{\partial\zeta}\right) \left\{ \begin{pmatrix} \frac{\partial x}{\partial\xi}, & \frac{\partial y}{\partial\xi}, & \frac{\partial z}{\partial\xi} \\ \frac{\partial x}{\partial\eta}, & \frac{\partial y}{\partial\eta}, & \frac{\partial z}{\partial\eta} \\ \frac{\partial x}{\partial\zeta}, & \frac{\partial y}{\partial\zeta}, & \frac{\partial z}{\partial\zeta} \end{pmatrix} \begin{pmatrix} \frac{\partial W}{\partial\sigma_{\xi\xi}}, & \frac{\partial W}{\partial\sigma_{\xi\eta}}, & \frac{\partial W}{\partial\sigma_{\zeta\xi}} \\ \frac{\partial W}{\partial\sigma_{\xi\eta}}, & \frac{\partial W}{\partial\sigma_{\eta\eta}}, & \frac{\partial W}{\partial\sigma_{\eta\zeta}} \\ \frac{\partial W}{\partial\sigma_{\zeta\xi}}, & \frac{\partial W}{\partial\sigma_{\eta\zeta}}, & \frac{\partial W}{\partial\sigma_{\zeta\zeta}} \end{pmatrix} \begin{pmatrix} \mathfrak{i} \\ \mathfrak{j} \\ \mathfrak{k} \end{pmatrix} \right\},$$

$$\text{(E}'\text{)}\quad \rho\frac{d\mathfrak{V}}{dt} = \rho\mathfrak{K}+\left(\frac{\partial}{\partial x}, \frac{\partial}{\partial y}, \frac{\partial}{\partial z}\right) \left\{ \frac{\partial(\xi,\eta,\zeta)}{\partial(x,y,z)} \begin{pmatrix} 1-2\sigma_{xx}, & -\sigma_{xy}, & -\sigma_{zx} \\ -\sigma_{xy}, & 1-2\sigma_{yy}, & -\sigma_{yz} \\ -\sigma_{zx}, & -\sigma_{yz}, & 1-2\sigma_{zz} \end{pmatrix} \begin{pmatrix} \frac{\partial W}{\partial\sigma_{xx}}, & \frac{\partial W}{\partial\sigma_{xy}}, & \frac{\partial W}{\partial\sigma_{zx}} \\ \frac{\partial W}{\partial\sigma_{xy}}, & \frac{\partial W}{\partial\sigma_{yy}}, & \frac{\partial W}{\partial\sigma_{yz}} \\ \frac{\partial W}{\partial\sigma_{zx}}, & \frac{\partial W}{\partial\sigma_{yz}}, & \frac{\partial W}{\partial\sigma_{zz}} \end{pmatrix} \begin{pmatrix} \mathfrak{i} \\ \mathfrak{j} \\ \mathfrak{k} \end{pmatrix} \right\}.$$

The boundary condition:

$$\text{(L}'\text{)}\quad \mathfrak{T}_\mathfrak{n} = \frac{1}{\frac{\partial(x,y,z)}{\partial(\xi,\eta,\zeta)}}(\mathfrak{i}, \mathfrak{j}, \mathfrak{k}) \begin{pmatrix} 1+2\sigma_{\xi\xi}, & \sigma_{\xi\eta}, & \sigma_{\zeta\xi} \\ \sigma_{\xi\eta}, & 1+2\sigma_{\eta\eta}, & \sigma_{\eta\zeta} \\ \sigma_{\zeta\xi}, & \sigma_{\eta\zeta}, & 1+2\sigma_{\zeta\zeta} \end{pmatrix} \begin{pmatrix} \frac{\partial W}{\partial\sigma_{\xi\xi}}, & \frac{\partial W}{\partial\sigma_{\xi\eta}}, & \frac{\partial W}{\partial\sigma_{\zeta\xi}} \\ \frac{\partial W}{\partial\sigma_{\xi\eta}}, & \frac{\partial W}{\partial\sigma_{\eta\eta}}, & \frac{\partial W}{\partial\sigma_{\eta\zeta}} \\ \frac{\partial W}{\partial\sigma_{\zeta\xi}}, & \frac{\partial W}{\partial\sigma_{\eta\zeta}}, & \frac{\partial W}{\partial\sigma_{\zeta\zeta}} \end{pmatrix} \begin{pmatrix} (\mathfrak{n}\cdot\mathfrak{i}) \\ (\mathfrak{n}\cdot\mathfrak{j}) \\ (\mathfrak{n}\cdot\mathfrak{k}) \end{pmatrix},$$

$$\text{(E}'\text{)}\quad \mathfrak{T}_\mathfrak{n} = \frac{\partial(\xi,\eta,\zeta)}{\partial(x,y,z)}(\mathfrak{i}, \mathfrak{j}, \mathfrak{k}) \begin{pmatrix} 1-2\sigma_{xx}, & -\sigma_{xy}, & -\sigma_{zx} \\ -\sigma_{xy}, & 1-2\sigma_{yy}, & -\sigma_{yz} \\ -\sigma_{zx}, & -\sigma_{yz}, & 1-2\sigma_{zz} \end{pmatrix} \begin{pmatrix} \frac{\partial W}{\partial\sigma_{xx}}, & \frac{\partial W}{\partial\sigma_{xy}}, & \frac{\partial W}{\partial\sigma_{zx}} \\ \frac{\partial W}{\partial\sigma_{xy}}, & \frac{\partial W}{\partial\sigma_{yy}}, & \frac{\partial W}{\partial\sigma_{yz}} \\ \frac{\partial W}{\partial\sigma_{zx}}, & \frac{\partial W}{\partial\sigma_{yz}}, & \frac{\partial W}{\partial\sigma_{zz}} \end{pmatrix} \begin{pmatrix} (\mathfrak{n}\cdot\mathfrak{i}) \\ (\mathfrak{n}\cdot\mathfrak{j}) \\ (\mathfrak{n}\cdot\mathfrak{k}) \end{pmatrix};$$

These results as summarized above seem to be an extension in more general form of the theories of Kappus,(2) Biot(3) and Murnaghan.(4)

References.

(1) S. Sugamoto: J. Phys. Soc. Japan, **3** (1948), 90.
(2) R. Kappus: Z. A. M. M., **19** (1939), 271.
(3) M. A. Biot: Phil. Mag., Sec. 7, **27** (1939/4), 468.
(4) F. D. Murnaghan, Am. J. Math., LIX (1937), 235.

Probe Measurements for High Frequency Discharge.

By Shoji Kojima and Kazuo Takayama.
Tokyo University of Literature and Science.

(Received Feb. 15, 1949.)

The electrical probe is used as a valuable method for the studies of d. c. discharges, but it is not applied for high frequency electrodeless discharges. For the latter case it has no return circuit. Then we have tried to use a pair of probes. Characters of such probes have been studied and it is found that the electron temperature in h. f. discharge is determined.

Experimental apparatus are shown in Fig. 1. A h. f. field about 200 mc/sec is applied between the parallel electrodes, in which discharge tubes are put. Discharge tubes contain argon gas at the pressure of 1∼10 mm Hg and have two or three probes (one is reserved). The probes are set in the neutral position of high frequency field as shown in Fig. 1. XX′. The probe current is measured altering the d. c. voltage between the pair of probes. A typycal result is indicated as the dotted curve in Fig. 2. It shows that the probe current is symmetric to the applied voltage and that it reaches to a saturated value for sufficiently positive or negative voltage.

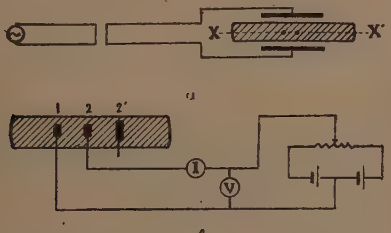

Fig. 1.

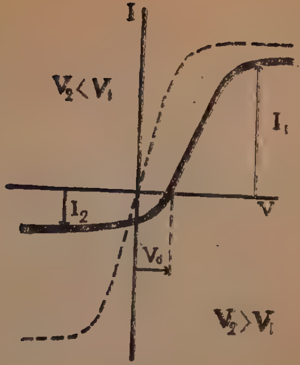

Fig. 2.

When the probes are not arranged in neutral position, the probe current has no symmetrical nature and often some current flows at the zero voltage. This phenomena is known as "the rectifying action of discharge tubes" which comes from the difference of high frequency potentials at the position of two probes. In this report we shall not discuss this phenomena further. In the following measurements the probes are always in the neutral position. To test the neutral position of the probes we may try to touch the probe circuit by a wire. If the position is not neutral, the probe current is disturbed by such operation.

We have measured the probe current characters using various discharge tubes. It is found that the saturation current depend only on the area of the probe which has negative voltage. For example, either pair probes 1—2 or 1—2′ in Fig. 1 show the same saturation current when the probe 1 is negative. In the case of d. c. discharges the saturation phenomena of the negative probe is well known. That mechanism may be applied in the present case. Then the saturation current I is expressed by(1)

$$I = (1/4)\, eN_{+} w_{+} S \qquad (1)$$

where e, N_+ and w_+ are the charge, density and mean velocity of positive ions respectively and S is the area of the negative probe.

It appears interesting character when the probes are displaced near the periphery of plasma maintaining neutral position. The probe current obtained at such position is shown in Fig. 2 as the full curve. The values of saturation are not same in both sides, for the density of ions is different. The ratio of saturation currents I_2/I_1 gives the ratio of positive-ion densities N_2/N_1 provided the same area of probes.

The characteristic curves shows that some d. c. current flows at zero voltage or that some d. c. electromotive force appears. This e. m. f. is measured by the voltage which is just sufficient to stop the probe current.

The sign of the e. m. f. V_d is such that the probe inserted in less ionized part is positive. The origin of this e. m. f. seems to be due to the diffusion of electrons. When the density of ionization in plasma is not uniform, it needs some electric force to prevent its diffusion. Since the electron has sufficiently large mobility comparing with the positive ion, we count the motion of electrons only. The electric field E necessary to prevent the diffusion of electrons is determined with the relation that the diffusion current is compensated by the drift current. Then

$$b_-NE = D_-dN/dx \qquad (2)$$

where b_- is the mobility, N is the dencity, D_- is the diffusion coefficient. Integrating E we obtain the e. m. f. as:

$$V_d = -\int_1^2 E\,dx = -\frac{D_-}{b_-}\log\frac{N_2}{N_1} \qquad (3)$$

Using the Einstein's relation it follows

$$V_d = -\frac{kT}{e}\log\frac{N_2}{N_1} \qquad (4)$$

where k is Boltzmann's constant e is the charge of the electron and T is the electron temperature. If we assume the plasma that the density of electrons is same as that of positive ions, N_2/N_1 is measured by the ratio of saturation currents. So we can determine the electron temperature by the probe measurements. When motion of positive ions is not negleected, equation (3) replaced by

$$V_d = -\frac{D_- + D_+}{b_- + b_+}\log\frac{N_2}{N_1} \qquad (5)$$

In usual condition this equation reduce to (3).

One example of measurements of the electron temperature for the argon filled tube with 7 mm Hg is given in Fig. 3. The saturation currents I_1 and I_2, and electromotive force V_d, are measured when the position of pair probes is altered on XX'. The calculated electron temperatures from those data lie in $(2.5 \sim 2.8) \times 10^4$ °K, which are distributed in narrow region compared to the value of V_d as $0 \sim 4\,V$. To hold the equation (4) it must be assumed that the contact potential between the probe and plasma does not differ for any position. Above results suggest that this assumption is satisfied.

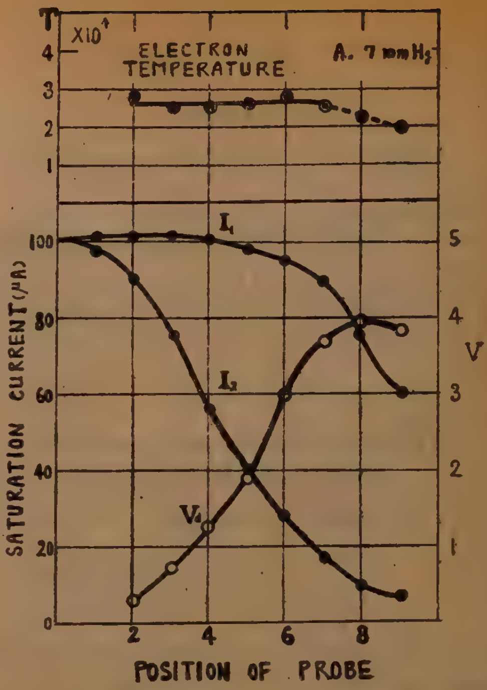

Fig. 3.

We have determined also electron temperature at various intensity of high frequency field. It shows that the temperature rises with field strength. For strong field, however, the probe measurements are disturbed by the secondary emission from the probes.

We are indebted to the Ministry of Education for the research grant.

Reference.

(1) Leonard B. Loeb. Fundamental Processes of Electrical Discharge in Gases. John Wiley & Sans, Inc. 1939, p. 238.

On the Inner Photo-Effect of Cuprous Oxide.

By Toshihiro OKADA and Ryosei UNO.

Physical Institute, Faculty of Science,
Kyushu University.

(Received March 2, 1949.)

There are several researches(1), (2), (3) about the inner photo-effect of cuprous oxide and it is reported that the spectral sensitivity curve has maxima at 0.25, 0.63, 0.8 and 2.0 μ. The authors investigated on the temperature-dependency of the spectral sensitivity and the influences of tempering of samples between the wave length of 0.5 and 1.0 μ.

The apparatus for the measurement is the same as Schönwald's(2); the sample is exposed to the light of about 500 cycles per sec., and the change of resistance of the sample is detected by means of an a. c. amplifier of four-stages and an oscilograph with Braun tube. The monochrometer used is the Hilger's quartz monochrometer (" Wordsworth,, type), and its slit is broden to 0.1~0.2 mm.

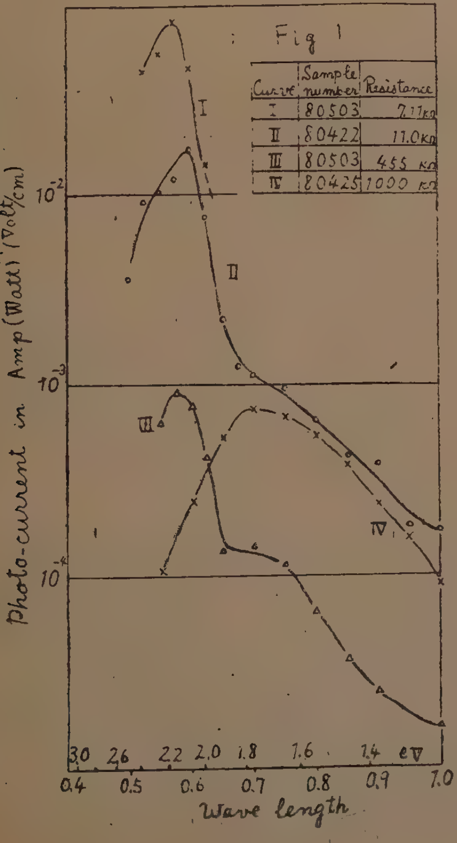

Fig. 1.

Experimental results are as follows:

(1) The influence of tempering.

Fig. 1 shows the spectral dependency of the photo-conductivity per unit incident energy of light for various samples. The peak value of the photo-conductivity for 0.6 μ becomes larger, when the dark-conductivity increases by heating and annealing in oxygen-gas (The curves I and II). Then, if the sample is heated and annealed in vacuum, both the dark-conductivity and the photo-conductivity for 0.6 μ are reduced, while the photo-conductivity for 0.8 μ becoming remarkable (The curve III). And if tempered in oxygen-gas again, the photo-conductivity for 0.8 μ increases and so on.

Some samples, which were tempered at 900°C in vacuum (10^{-3} mm Hg) for the hours and quenched to the room temperature, have the peak of the photo-conductivity only at 0.8 μ (The curve IV).

(2) The temperature-dependency of the peak values of the spectral sensitivity curve.

Results are shown in Fig. 2. In this measurement we used the samples having only one peak of 0.6 μ or 0.8 μ respectively. At high temperature the measurement is unavailable because of the large noise.

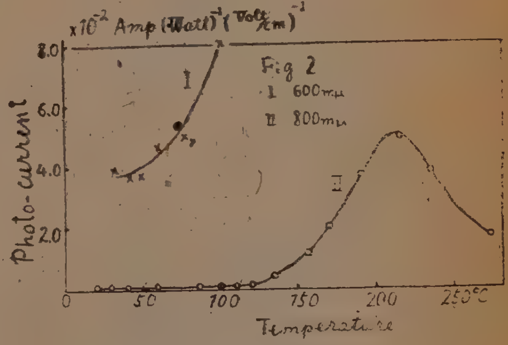

Fig. 2.

According to our results, it seems probable that the peak of the photo-conductivity at 0.6 μ may correspond to the transition of electrons from the full band to impurity levels in the semi-conductor, not to the conduction band.

We are indebted to the Ministry of Education for the research grant.

References.

(1) A. H. Pfund: Phys. Rev. **7** (1916) 289.
(2) B. Schönwald: Ann. d. Phys. **15** (1932) 395.
(3) A. W. Joffe and A. Th. Joffe: Phys. ZS. USSR. **11** (1937) 241.

On the Anomalous Structures of Silicon Carbide.

By Goro Honjo.*

Kobayashi Institute of Physical Research, Kokubunji, Tokyo, Japan.

(Received March 8, 1949.)

On silicon carbide, SiC, there have been reported five modifications.(1) We can take for all of them hexagonal lattices built of the identical basal atomic planes, which themselves are two-dimensional net works composed of tetrahedral units of Si—C. (Fig. 1) As is well known, the atomic planes like these are classified into three species A, B and C, when they are stacked with each other. The discrimination among the five modifications merely arises from the order of the sequences of these species of the atomic planes in the direction of c-axis. In SiC-IV, it is ABCA, in SiC-III, ABACA and so forth. (Table I)

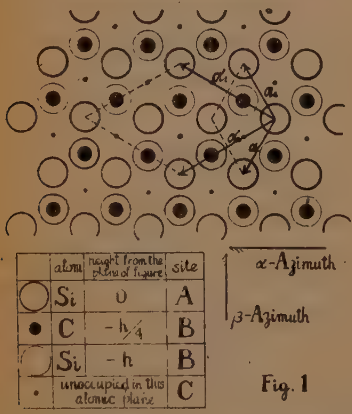

Fig. 1

The present author found two kinds of anomalous structure of silicon carbide by X-ray and electron diffraction methods. The one is the anomaly due to the *stacking disorder* of the above mentioned atomic planes. The Laue photographs for a number of specimens showed strong continuous radial streaks and diffuse spots, which are apparently corresponding to the disordered structure of this kind.

The other anomaly found for some specimens, which was revealed by the reflection method of electron diffraction, is that due to a super structure. The electron diffraction patterns obtained for the natural surface (parallel to the basal plane (0001)), with the incident electrons in α-azimuth $[1\bar{1}00]$ (Fig. 1), showed layer lines of the periodicity identical to that of the normal structure in the direction of $[11\bar{2}0]$. Whereas the patterns for the electrons in β-azimuth $[11\bar{2}0]$ showed the periodicity one third of that of normal structure in the direction of $[1\bar{1}00]$, which manifests the existence of a super structure. The evidence of the one third periodicity is also favoured by the following observations. Generally in electron diffraction patterns of single crystals, there appear arrays of spots which lie on circular Laue zones corresponding to the interference due to the lattice row on the surface nearly parallel to the incident beam. In the diffraction patterns of the α-azimuth of specimens with the super structure, two additional circular Laue zones appear between the first two Laue zones corresponding to the normal structure.

In order to explain these observations we must assume a_1' and a_2' axes as the fundamental translations in the basal plane, instead of a_1 and a_2 which correspond to the normal structure of SiC. (Fig. 1) The lattice period in the direction of the c-axis, however, is kept the same in the both structure. This super structure means that there takes place occasionally a structural anomaly *in the basal atomic planes themselves.*

Though the specimens showing the superstructural anomaly are comparatively rare — found three instances out of twenty samples from different origins —, this structure seems to exist in this substance usually. It was observed the fact that even for a specimen showing the anomalous pattern, the super structure was formed only in a restricted region of the surface. Moreover, the structure is supposed to be restricted only in thin layer of the uppermost surface. This is inferred

---

* Present Address, Physics Department, Tokyo Institute of Technology, Oh-okayama, Tokyo, Japan.

Table I.

SiC	Original Representation	Hexagonal Representation*			Stacking Order
		a	c	Z	
I	Rhombohedral a = 12.78, α = 13°55′, Z = 5	3.076	37.68 = 2.511×15	15	ABCBABCACBCABACA
II	Hexagonal a = 3.095, c = 15.17, Z = 6	3.076	15.06 = 2.511× 6	6	ABCACBA
III	Hexagonal a = 3.095, c = 10.10, Z = 4	3.076	10.04 = 2.511× 4	4	ABACA
IV	Cubic a = 4.348, Z = 4	3.076	7.53 = 2.511× 3	3	ABCA
V	Rhombohedral a = 43.15, α = 4°6′ Z = 17	3.076	128.0 = 2.511×51	51	········

* Recalculated with the more accurate value⁽²⁾ of $a = 3.076 + 0.003$ using the relation $c = h \times Z$, $h = \sqrt{2}/\sqrt{3} \times a$ = height of Si—C tetrahedron.

from the facts that the one third periodicity above mentioned can not be observed in the Kikuchi band even for the electrons of β-azimuth, and that in the rotation photograph for this azimuth the Bragg reflections coming from the supper structure disappear when their glancing angles exceed about 4° for the electrons of 35 K.e.V.

References.

(1) R. W. Wyckoff: The Structure of Crystals (1931) p. 222.

(2) G. Borrmann and H. Seyfarth: Zeit f. Krist. **86** (1933) p. 472.

Absorption of Flare-Type Cosmic Rays.

By Yataro SEKIDO and Teitiro YAGI.

Institute of Physics, Faculty af Science, Nagoya University.

(Received March 9, 1949.)

At the time of the cosmic-ray flare which occurred on March 7, 1942, the absorption of this increased radiation was measured by Ishii et al.⁽¹⁾ in Tokio. On March 7, when three chambers were in operation in a wooden thermostatic chamber, another one in the basement of the building (roofed with concrete about 80 cm thick), each of them recorded the unusual increases of intensities. Using the maximum of twenty minutes' running-average (Fig. 1), the increment was 8±0.6% on the ground and 4±1.5% underground. We checked whether this observed absorption could be explained or not by assuming that the absorption of the extra radiation (presumably coming from the sun and hence called *S*-rays hereafter) is of the same nature as that of ordinary rays.

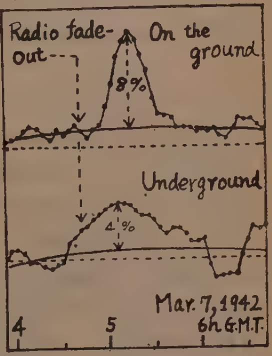

Fig. 1. Cosmic-ray flare observed at Tokio on March 7, 1942 (upper curve is the average of intensities of three chambers, lower that of one chamber).

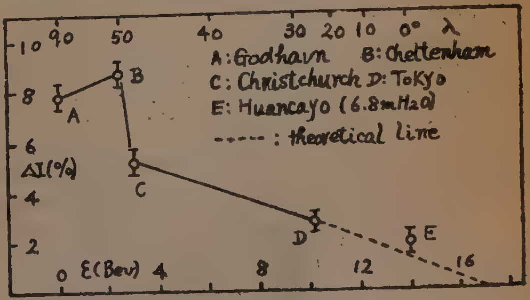

Fig. 2. Latitude effect of Cosmic-ray flare on March 7, 1942.

This increment shows a marked latitude effect(1), (2) as in Fig. 2. According to Johnson,(3) the absorption of the field sensitive ray ΔI at atmospheric depth h is given by

$$(\Delta I/I)_h + 1 = (h/h_0)^{-\delta}, \qquad (1)$$

where I is the total intensity and h_0 and δ are constants. We shall assume that a similar equation to (1) holds also for slightly higher energies than the field-sensitive range. Then, if the range h_0 of S-rays is known, its absorption can be calculated.

The range h_0 for tne field-sensitive rays ($\varepsilon_{\max.} =$ 14 Bev), which will be a function of the maximum energy ε of the primary rays, is 16.8 ± 1.4 m H_2O including the lead shield, when Compton-Turner's result $\Delta I/I = 6.5\%$ at sea level and Johnson's result $\delta = 0.16 \pm 0.05$ are applied to eq. (1). On the other hand, the knee ($\varepsilon = 6.6 \pm 0.6$ Bev) of latitude effect at sea level is thought to be correspond to $h_0 =$ 10 m H_2O + shield.(4) From these two points, the $\varepsilon - h_0$ relation can be otained, if it is assumed to be linear.

Assuming the integral spectrum of S-rays as linear beyond the incident energy at Tokio, and taking the inclination of its line so that the absorption of S-rays in air at the equator(4) can be just accounted for by a similar equation to (1) and the above mentioned $\varepsilon - h_0$ relation, we get $\varepsilon_{\max.} = 17$ Bev i. e. $h_0 = 19$ m H_2O for the S-rays on March 7.

In Fig. 3 point $B_{\rm obs}$, shows the observed value underground, which appears to be a little smaller than the theoretical value $B_{\rm th.}$. Furthermore, eq. (1) represents the absorption in air, while $B_{\rm obs.}$ that in a dense material. Hence, if the absorption of S-rays in air had been observed, the result would have deviated even more from the theoretical value than $B_{\rm obs.}$ does. Thus, the absorption of S-rays presumably tends to be larger than that of ordinary cosmic rays, but this does not necessarily preclude the possibility that the S-ray is of the same nature as ordinary cosmic says, for the experimental uncertainty(6) is considerably large.

On the other hand, from the existense of the latilude effect of S-rays in some latitudes higher than the knee of ordinary cosmic rays, such S-rays that reached the high latitudes seem to be more penetrating than ordinary cosmic rays.

However, a more detailed knowledge will be necessary of the latitude effect of charged particles approaching the earch from a certain direction, before we can conclude that S-rays and ordinary rays are of different nature.

In conclusion the authors wish to express their cordial thanks to each of the cosmic-ray group of Nishina Laberatory of the Science Research Institute for their kind cooperation in this work.

References.

(1) C. Ishii, Y. Sekido and Y. Miyazaki: Shortly to be published elsewhere.

(2) S. E. Forbush: Terr Mag., **47**, (1942), 331.

(3) T. H. Johnson: Rev. Mod. Phys., **10**, (1938), 230.

(4) According to the measuments of Millikan et al., the soft component at high altitudes shows latitude effect up to about 60° lat.. Furthermore, Swann et al. recently found that the knee of hard component exist at 48° lat. in the high altitudes from 25,000 ft. to 33,000 ft. (W. F. G. Swann and P. A. Morris: Phys. Rev., **71**, (1947), 462 A.) From these facts, the knee of the latitude effect at sea level is considered to be due to absorption rather than due to the cut-off of the sun's magnetic field, at least in the vicinity of 40° lat..

(5) This increase occurred also at the equator. See reference (1).

(6) not only of $B_{\rm obs.}$, but also of $B_{\rm th.}$, which is really a semi-empirical value.

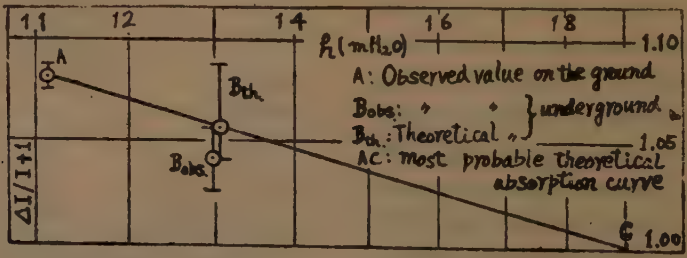

Fig. 3. Absorption of flare-type comic rays ΔI at atmospheric depth.

Induced Discharge Phenomena on the Central Wires of Multiple Geiger Counters.

By Kazuzi HASHIMOTO and Heiichi HAGIWARA.

The Hitachi Central Laboratory.

(Received April 5, 1949.)

In the self-quenching multiple Geiger counters the experimental facts show that every central wire does not play the individual counter, and some spurious counts occur at the special central wire being affected by the counts of adjacent one.⁽¹⁾⁽²⁾

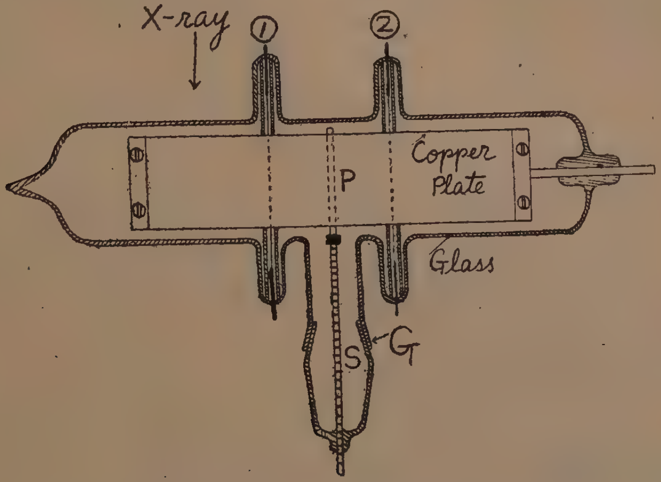

Fig. 1. Schematic and lateral cross section of test plate-type counter.
G: Ground joint, P: Partition, S: Support.

In order to determine the cause of spurious counts a special parallel-plate type counter has been constructed as shown in Fig. 1.

Two central electrodes consist of two parallel wires; and parallel copper plates sandwitch the central wires. The ground joint *G* (see Fig. 1) is used in order to open or close the ebonite, glass or quartz partition *P* as to screen the openings among two central electrodes. (see Fig. 2 *A*, *B*.)

Let the notation ①, ②, (see Fig. 1.) be the counting rate observed from each individual central wire No. 1, and No. 2; and notation $②_1$ with suffix means the counting rate of No. 2 central wire when No. 1 are in counting condition. Then the percentage of induced discharge probability of No. 2 wire that is caused by the discharge of adjacent wire No. 1 may be computed as follows.

$$\frac{②_1 - ②}{①} \times 100\%$$

These experiments have been carried out by the certain narrow *X*-ray beam which is striking a suitable point near the central wire No. 1.

Using the quartz plate, the probability of induced discharge is 4.2% when the plate is closed and 5% when it is opened, (see Fig. 2 *A*, *B*) indicating a small difference between two conditions of the quartz plate.

On the contrary when we use the soda glass plate as a partition instead of quartz, the probability of induced discharge is reduced remarkably.

Fig. 2.

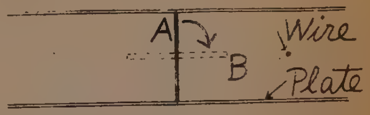

Fig. 3.

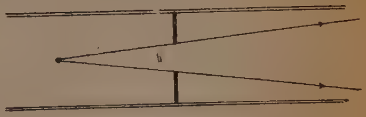

Fig. 4.

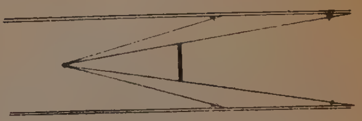

Fig. 2, 3, 4. Schematic cross section of test counter showing the position of partition and electrodes. The elctrode wires are perpendicular to the cross section.

It was 0.25% when the partition is closed and 4.5% when it is opened.

From these experimental results it was ascertained that the spurious count will be caused by incomplete absorption of the photons which are produced by every avalanche. Fig. 3 and Fig. 4 show the diaphragms of ebonite which controll the photon transmission coming from one central wire to the other. In Fig. 3 the photons produced at the surroundings of one central wire will reach the vicinity of the other. On the contrary in Fig. 4 these photons from one central wire will strike only the cathode metal in front of the other.

The value of probability in condition as shown in Fig. 4 was nearly equal to 5% which was the percentage obtained in the lack of diaphragm. Nevertheless the value of probability in case as shown in Fig. 3 was nearly zero and equal to the value when the partition is complete.

From these experiments, the following fact will be evolved that even in the self-quenching counter many photons will be produced in every count and some of them will reach adjacent cathode metal. These photons will strike cathode metal of the counter and liberate the photoelectrons which initiate the avalanche in the other.

References.

(1) K. Hashimoto; J. Phys. Soc. Japan. **3** (1948) 151.
(2) W. H. Chamber; R. S. I. **19** (1948) 467.

Abnormal Absorption of Sound Waves in Water.

By Yoshihito Takesada.

Institute of Geophysics, Kyoto University.

(Received April 11, 1949.)

In this report the behaviour of abnormal absorption of the high power sound waves radiated into the water will be stated. Let ρ_m, ρ_1, ρ_2 and v be the mean density of water, the density of small non-resonant air-bubbles generated in water by impinging sound wave, the density of clear water, and the specific volume of the air, respectively. Then we have $\rho_m = v\rho_1+(1-v)\rho_2$ and for the mean elasticity $E_m = E_1 E_2/vE_2+(1-v)E_1$. Therefore, we get

$$\rho_m C_m = \sqrt{\{\rho_1 v+\rho_2(1-v\} E_1E_2/vE_2+(1-v)E_1},$$

where C_m, E_1 and E_2 represent the mean velocity, elasticity of the air-bubbles and the water, respectively. When a sound wave transmits to the pure liquid from the mixed medium, the percentage of reflected power is given by $\{(\rho_m C_m-\rho_2 C_2)/(\rho_m C_m+\rho_2 C_2)\}^2$, where C_2' is the velocity of sound in the clear water. We shall denote by $(1+\Delta\rho)$ the density of dense medium, and by $(1-\Delta\rho)$ that of rare medium. The latter is induced by the dissociation of water. It may also be interpreted as has been generated by air hole of $\Delta\rho$ per unit volume, so v becomes the value of $\Delta\rho$. Gradient of sound wave is $\Delta\rho/\rho_0$, where ρ_0 is the original density. Hence, if the original density of water is equal to 1, we can use $\Delta\rho/\rho_0'$ instead of v. The reflection coefficient may be taken as the power loss of sound. The percentage of the power transmitted from the bubbly water to pure liquid is plotted as the func-

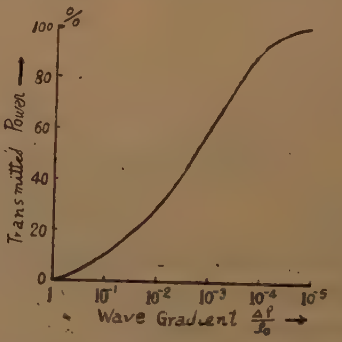

Fig. 1.

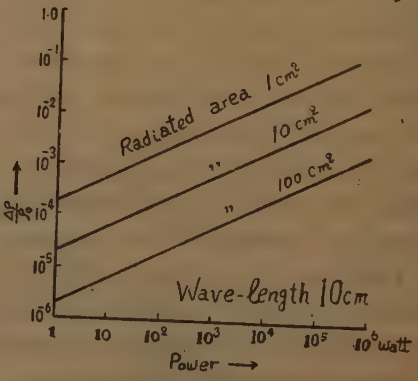

Fig. 2.

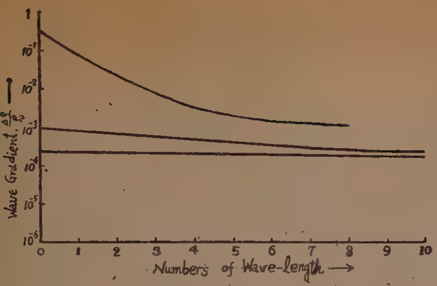

Fig. 3.

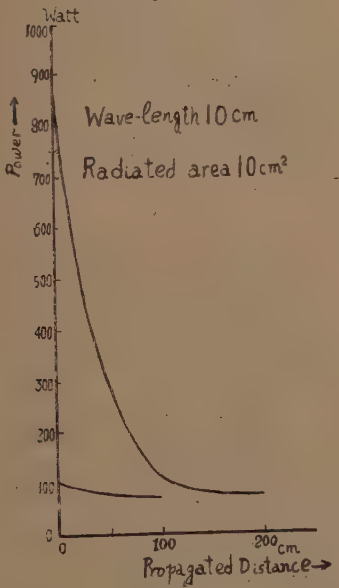

Fig. 4.

tion of $\Delta\rho/\rho_0$ at Fig. 1. The relation between mean power and sound gradient may be obtained by the relation $W = 1/2\cdot\rho C\pi\cdot F^2w^2/\lambda^2$, where F is the area of vibrating surface and w is the maximum velocity amplitude. Employing this relation, we obtain the curve shown in Fig. 2. When the high power sound waves are propagated through the water, it generates the bubbles inside the medium, and is attenuated by these bubbles themselves. These circumstances are shown in Fig. 3 which is constructed from Fig. 1 and Fig. 2. These curves illustrate that the gradient of sound wave is decreased abnormally near the sound source. For example, $F = 10\,\text{cm}^2$, $\lambda = 10\,\text{cm}$ and the sound power is 1000 Watt, the behaviour of abnormal attenuation will become as is shown in Fig. 4. It is also constructed by the aid of Fig. 2 and Fig. 3.

On the Modification of Boltzmann's Equation.

By Naruo TAKETA.

Faculty of Engineering, University of Nagoya.

(Read May 22, 1948; Received May 11, 1849.)

We can express the so-called Boltzmann's equation of continuity in the form of an integral equation, which is useful for the treatments of the phenomena not in thermal equilibrium.

we take an ensemble of similar elements (e. g. molecules) and let the variable q denote the properties of each element (e. g. position, x, y, z and velosity, v_x, v_y, v_z). Then the change of distribution function $f(q, t)$ with time may be expressed as follows according to Boltzmann:

$$\frac{df(q,t)}{dt} = \frac{\partial f}{\partial t} + \frac{dq}{dt}\frac{\partial f}{\partial q} = b(q,t) - a(q,t), \tag{1}$$

where $b(q,t)$ denotes the number of elements changed from the other states to the state q per unit time by interaction between elements and $a(q,t)$ denotes that from the state q to the others. Here we can say that the function $f(q,t)$ which satisfies the following integral equation also satisfies equation (1).

$$f(q,t) = \int_0^\infty t\{q(t-\tau), t-\tau)$$

$$\exp\left\{-\int_0^\tau \frac{a\{q(t-\tau), t-\tau\}}{f\{q(t-\tau), t-\tau\}}d\tau\right\}d\tau \quad (a/f \neq 0) \tag{2}$$

By differentiating equation (2), and by making use of the relation $-d/dt = d/d\tau$, the above-mentioned result may be easily obtained as follows.

$$\frac{df}{dt} = \int_0^\infty \frac{db}{dt}\exp\left\{-\int_0^\tau \frac{a}{f}d\tau\right\}d\tau$$

$$-\int_0^\infty b\int_0^\tau \frac{d}{dt}\left(\frac{a}{f}\right)d\tau \exp\left\{-\int_0^\tau \frac{a}{f}d\tau\right\}d\tau$$

$$= -\int_0^\infty \frac{d}{d\tau}b\cdot\exp\left\{-\int_0^\tau \frac{a}{f}d\tau\right\}d\tau$$

$$+\int_0^\infty b\cdot\int_0^\tau \frac{d}{d\tau}\left(\frac{a}{f}\right)d\tau\cdot\exp\left\{-\int_0^\tau \frac{a}{f}d\tau\right\}d\tau$$

$$= \left[-b\cdot\exp\left\{\int_0^\tau \frac{a}{f}d\tau\right\}\right]_0^\infty - \left(\frac{a}{f}\right)f = b - a$$

$$(a/f \neq 0).$$

In equation (2) a/f is the probability that an element will be scattered per unit time. Therefore, the physical meaning of the equation will be evident. Namely, the integrand in the right-hand side expresses the number of the elements which, starting from the state $q(t-\tau)$ at time $t-\tau$, reach the state $q(t)$ after the time τ without being scattered. Therefore, this equation expresses a generalization of the treatment which Meyer adopted in his theory of heat conduction⑴

We can apply this equation (2) to the phenomena not in thermal equilibrium, the so-called transport phenomena and others. The method was indicated by Toyoki Koga.⑵

Reference.

(1) J. H. Jeans: The Dynamical Theory of Gases. 4 th edition (1925) p. 291.
(2) T. Koga: Journal of the Physical Society of Japan. (1949) Vol. 4. No. 1.

Theory of Recrystallization of Cold-Worked Metals.

By Ryukiti HASIGUTI.

Faculty of Engineering, University of Tokyo.

(Received May 28, 1949.)

The rate of crystal growth in the case of recrystallization of cold-worked metals was treated theoretically. At the interface between a newly formed crystal and the strained old matrix, atoms in the latter move a little and rearrange themselves according to the crystal lattice of the new crystal grain. This is the elementary process of crystal growth. A unit of process is generally not a single atom, but it is a group of atoms. As the number of atoms in an unit of process seems to be very large, it may be improbable that all the atoms in a unit move simultaneously across a potential barrier in one jump. The atoms will jump across a barrier one by one, but successively one after another with very short intervals, like so to speak a chain reaction or an avalanche of reactions. A chain or an avalanche makes an elementary process. If we advance the considerations along these lines, we get the following equations:

$$G = (b\lambda_0 S^2/\tau RT)\exp\{-(E+E_1)/RT\}, \qquad (1)$$

$$\lambda = \lambda_0 \exp(-E_1/RT), \qquad (2)$$

where G is the rate of crystal growth, b a constant, S the strain produced during cold-working, τ the time of relaxation for the movements of groups of atoms, R the gas constant, T the absolute temperature, E the activation energy of the process, and λ the length of atomic group measured parallelly to the direction of crystal growth. λ_0 and E_1 are constants which determine the value of λ as a function of temperature according to the equation (2).

When temperature is kept constant, the equation (1) reduces to the form

$$G = G_1 S^2, \qquad (3)$$

where G_1 is a constant. Plotting G against S^2 at constant temperatures using the experimental data obtained by Anderson and Mehl,⑴ we get straight lines, which coincide very well with the equation (3). As we can get the values of G_1's for various temperatures from the slopes of these lines, we can make the $\log G_1$ versus reciprocals of absolute temperatures plotting, which gives a straight line. This straight line yields an activation energy ($E+E_1$) of 58,500 cal./mol. If we assume $E = E_1 =$ = 29,250 cal./mol., we can calculate the values of λ from the equation (2). The numerical calculation shows that its value is for instance 320 Å. at 400°K. It is a very striking feature that the atomic group has considerable length, and therefore it contains a good many atoms.

The detail of this paper will be published later in this journal.

Reference.

(1) W. A. Anderson, R. F. Mehl, Trans. Amer. Inst. Min. Met. Engr., **161** (1945), 140.

On the Thermo-elastic Effect.

By Akira NOMOTO.

First Faculty of Engineering, University of Tokyo.

(Read May 1, 1949; Received May 11, 1949).

Thermo-elastic effects have ever been treated as problems for mathematical physics by several investigators, and its participations to the internal friction etc. were thoroughly clarified. The author treates the general relations about the thermo-elasticity of an isotropic homogeneous solid. Thermal and elastic equilibrium of a solid is expressed by the theories of elasticity and conduction of heat as

$$(\lambda+2\mu)\nabla^2\Delta-\rho p^2\Delta=\alpha\nabla^2 T, \qquad (1)$$

$$\mu\nabla^2\tilde{\omega}-\rho p^2\tilde{\omega}=0, \qquad (2)$$

$$\kappa\nabla^2 T-pT=\beta p\Delta, \qquad (3)$$

where λ, μ, κ and ρ are isothermal Lame's constant, rigidity, thermal diffusivity and density respectively, and p represents the differentiation with respect to time, *viz.* $\partial/\partial t$. T, Δ and $\tilde{\omega}$ are temperature, dilatation and rotation by which the state of the solid shall be decided. α and β are thermo-elastic constants derived from thermodynamic relations as $\alpha=\left(\lambda+\frac{2}{3}\mu\right)\eta$ and $\beta=\left(\lambda+\frac{2}{3}\mu\right)\eta T/C$, where η is coefficient of expansion and C is specific heat without any deformation. From (1) and (3), we get for Δ and T the equation

$$[\kappa(\lambda+2\mu)\nabla^4-\{(\lambda+2\mu)p+\kappa\rho p^2\}\nabla^2-\rho p^3]\left(\begin{matrix}\Delta\\ T\end{matrix}\right)=0. \qquad (4)$$

For the quasi-static equilibrium, in which the inertia force is negligible, solution for (4) shows us that the dilatation Δ and the temperature T should be composed of three separate terms respectively—namely the term about the cooling by dilatation for which $T_1=-\beta\Delta_1$ and $\nabla^2 T_1=0$, term about the expansion by heating for which $T_2=(\lambda+2\mu)\Delta_2/\alpha$ and $\kappa'\nabla^2 T_2=pT_2$ and finally the stationary term T_3 and Δ_3. Diffusivity for the second term κ' is less than κ, namely $\kappa'=\kappa\{1-\alpha\beta/(\lambda+2\mu+\alpha\beta)\}$.

By the thermo-elastic effect, the velocity of the dilatational wave becomes a function of the frequency. Equation (4) are able to be factorized formally as

$$\left(\nabla^2-\frac{p^2}{c^2}\right)\left(\nabla^2-\frac{p^2}{c'^2}\right)\left(\begin{matrix}\Delta\\ T\end{matrix}\right)=0, \qquad (5)$$

where

$$\frac{1}{c^2}\&\frac{1}{c'^2}=\{(\lambda+2\mu+\alpha\beta+\kappa\rho p)$$
$$\pm\sqrt{(\lambda+2\mu+\alpha\beta+\kappa\rho p)^2+4\kappa\rho p(\lambda+2\mu)}\}$$
$$/2\kappa(\lambda+2\mu)p. \qquad (6)$$

c and c' are the velocities of dilatational waves. Putting $\sqrt{(\lambda+2\mu)/\rho}=v$, $p=i\omega$ and $(1/c)\&(1/c')=(n-ik)/v$, we get

$$(n-ik)^2=\{(x-i)\pm\sqrt{(x^2-1)+2i(1-2\delta)x}\}/(2x), \qquad (7)$$

where $x=\kappa\rho\omega/(\lambda+2\mu+\alpha\beta)$ and $\delta=\alpha\beta/(\lambda+2\mu+\alpha\beta)$. n corresponds to the index of refraction, and $\theta=2\pi k/n$ the coefficient of absorption, for the amplitude of the plane wave diminishes as $\exp(-r\theta/\Lambda)$, where Λ is its wave length. Complex wave velocities c and c' are inferred by Fig. 1, which expresses (7) in terms of x and δ. Fig. 1 shows us that dilatational wave resolves itself into two branches [1] and [2]. Wave expressed on the branch [1] is almost the same as that without any consideration to the conduction of heat, but always having the velocity larger than $v=\sqrt{(\lambda+2\mu)/\rho}$, and absorbed most between the extreme cases $x=0$ (isothermal) and $x=\infty$ (adiabatic). Wave on the branch [2] is highly dispersive, and corresponds to the slow progress of the temperature and the dilatation as the conduction of heat, but they diminish barely less than the case for the conduction of heat.

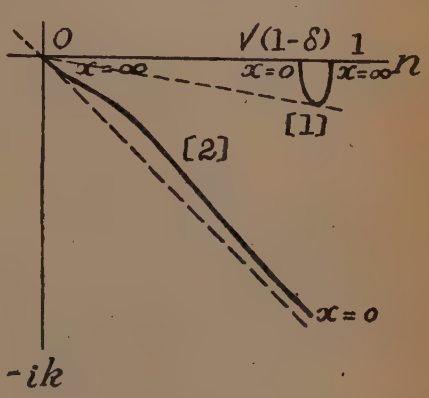

Fig. 1.

The author wishes to thank Prof. G. Nishimura for his kind guidance.

References.

(1) C. Zener: Proc. Phys. Soc. 52, I (1940), 289, 152. Phys. Rev. **52** (1937), 230; **53** (1938), 90, 100, 582.
(2) A. Kneser: Die Integralgleichungen und ihre Anwendungen in der mathematischen Physik, Braunschweig, 1922, S. 199.

On the Mechanisms of the Grid Emission.

By Ken-ici Noga and Yoshitarō Okada.

Mazda Research Laboratory, Tokyo Shibaura Electric Co., Kawasaki.

(Received, June 18, 1949).

It is known that most part of the evaporating materials from an oxide coated cathode are BaO molecules, which have the heat of evaporation of 2.9 e.V.[1] As the heat of evaporation of the excess Ba atoms is known to be 2.5 e.V.[2], the concentration of excess Ba atoms in the beam of BaO molecules evaporating from a hot cathode heated at 1200°K, is about fifty times of that in the orignal oxide cathode. These evaporating materials deposited on the grid wire of a vacuum tube may cause the thermionic emission, which we call the "grid emission".

When these materials evaporating from a cathode are deposited on a tungsten filament held at 800°K, the thermionic emission from the filment increases with time as shown by curve I in Fig. 1. The change of the work function of the filament obtained by the contact potential method is also shown by curve II. Both curves have distinct knicks at the point A. After stopping the deposition at the point B in Fig. 1, the filament was heated at 1000°K. Then the steep decrease in the emission was found but the work function obtained by the method of Richardson Plot remained unchanged. In the case of smaller fraction θ of the surface covered with BaO molecules than the covering at the point A, the steep increase in the emission may be attributed to the lowering of the work function by the dipole moments of the BaO molecules. As θ increases beyond A, the interaction between the BaO molecules becomes appreciable and then they coagulate to small BaO crystals, in which case the thermoelectrons will be emitted from the BaO crystals as in the usual oxide cathodes, composed of thick layers of BaO.

In Fig. 1, the farther deposition causes the slow increase in emission, but when the thickness of the layers becomes more than twenty molecular layers, the influence of the thickness on the emission becomes negligiblly small. The thermionic emission from such thick layers decreases irreversibly by the heat-treatment at temperatures higher than 800°K as shown in Fig. 2. This decrease in emission may be due to the disappearance of the excess Ba atoms by evaporation or by diffusion into the base metal and also to the growth of the BaO crystals.

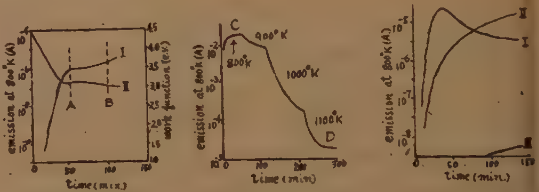

Figs. 1–3.

After the sufficiently long heat-treatment at 1100°K we obtain the stable state (D in Fig. 2) whose activity changes reversibly with temperature. Though the activity of this state is very low, it shows almost the same behaviors as an usual oxide cathode. Therefore this state seems to be very similar to a sintered oxide cathod of coarse grains[2].

Such processes of the change in activity as shown in Fig. 2 are also observed in the case whe other metals used as grid material. But it is very remarkable that the activities of BaO layers are very sensitive to the base metals. For instance, in the case of tungsten the thermionic emission at state C (in Fig. 2) is of the same order of magnitude with that from an usual oxide cathode, but for nickel it is about 10^{-2} times and for gold 10^{-5} times of that from an ordinary cathode. Thus it will be concluded that these facts are caused by the difference in the diffusion velocities of free Ba atoms into the different grid materials. It is impossible to suppose that the barium oxide may be reduced by base metals at a temperature lower than 800°K because it is so stable. It is also unreasonable to suppose that the rate of evaporation of the free Ba atoms depends on the grid materials. Thus we have tried the following experiments to confirm these considerations.

When the Ba atoms are deposited on tungsten, nickel or gold held at 900°K, the thermionic emissions from them rise as shown in Fig. 3. Here we used the "Batalum getter" as the barium source. In the case of tungsten the curve has an obvious maximum (curve I) but in the case of nickel there is no maximum (curve II). As the rate of evaporation is negligible at temperatures lower than 1000°K, these results show the possibility of the diffusion of Ba atoms into nickel. In the case of gold, the diffusion of Ba atoms into it is more remarkable as shown in curve III.

Hence, if we use as the grid materials the metals into which the diffusion of Ba atoms occurs very easily, the concentration of the excess Ba atoms, which act as the emission centers in the deposited BaO layers, diminishes by diffusion and thus the decrease in the activity results.

References

(1) H. Kawamura; J. Phys. Soc. Jap. **1**, (1946) 8.
(2) H. Kawamura, A. Shinohara and K. Takahashi; J. Phys. Soc. Jap. **3**, (1948) 301.

On Eigenvalues of Incompletely Reducible Matrix.

By Seiichi SUEOKA.

Second Facutly of Engineering, University of Tokyo.

(Read October 14, 1948; Received May 27, 1949.)

In the theory of atomic spectra, the energy values are usually determined as the eigenvalues of Hamiltonian matrix referring to some finite number of bases. This treatment is certainly correct when the full matrix is reducible completely to some sub-matrices corresponding to each system of bases. But even when this condition is not satisfied, the above treatment serves as the starting point of approximation. In order to obtain eigenvalues in higher order approximation, it is necessary to take larger matrix, taking a few numbers of the system of bases together. This makes often the calculation difficult, on account of enlarged dimensions of matrix.

To avoid this difficulty, we intend to generalize the results obtained by Brillouin, in which only one base is added to the original bases.[1] Making use of the method of hypermatrix[2] we get to the general formula to obtain the eigenvalues, without increasing the dimension. The problem of such a kind may be found frequently in atomic spectra, for examples, configuration interaction, spin-orbit interaction, Stark effect in strong electric field[3] and perturbation phenomena of hyperfine structures.

Let H_n and H_m represent the Hamiltonian matrices referred to systems of bases $\varphi_1, \varphi_2, \ldots\ldots, \varphi_n$ and $\phi_1, \phi_2, \ldots\ldots, \phi_m$ respectively and assume that the full matrix of Hamiltonian be reducible to sub-matrices, H_n, H_m approximately. This corresponds to the fact that the matrix elements between the bases of φ_i $(i = 1, 2, \ldots\ldots, n)$ and ϕ_j $(j = 1, 2, \ldots\ldots, m)$ are small. Then the matrix H_{n+m}, in which φ_i and ϕ_j are taken as the bases together, has the form

$$H_{n+m} = \begin{pmatrix} H_n, & A \\ \tilde{A}, & H_m \end{pmatrix}, \tag{1}$$

where A is a rectaugular matrix of n rows and m columns and corresponds to the interaction between the φ_i's system and ϕ_j's system. $\tilde{A}$ represents the transposed conjugate matrix of A.

The eigenvalues of H_n and H_m which are supposed known are denoted as λ_i $(i = 1, 2, \ldots\ldots, n)$ and λ_j $(j = 1, 2, \ldots\ldots, m)$. Thus, we may find the unitary transformation matrices U_n and U_m that make H_n and H_m transform into diagonal form as,

$$U_n^{-1} H_n U_n = ((\lambda_i \delta_{ij})), \quad U_m^{-1} H_m U_m = ((\lambda_i' \delta_{ij})). \tag{2}$$

Making use of U_n and U_m, we can compose a transformation matrix of $n+m$ dimensions U_{n+m} as follows

$$U_{n+m} = \begin{pmatrix} U_n, & 0 \\ 0, & U_m \end{pmatrix}$$

which makes H_{n+m}

$$U_{n+m}^{-1} H_{n+m} U_{n+m} = \begin{pmatrix} \Lambda_n, & B \\ \tilde{B}, & \Lambda_m \end{pmatrix} = H'_{n+m}, \tag{3}$$

where Λ_n and Λ_m are the diagonal matrices and B

is a rectangular matrix, namely $\Lambda_n = ((\lambda_i\delta_{ij}))$, $\Lambda_m = ((\lambda_i'\delta_{ij}))$ and $B = U_n^{-1}AU_m$.

The eigenvalue λ of H_{n+m} may be obtained from the following equation, in which $\boldsymbol{x}$ is a $n+m$ dimensional vector:

$$H'_{n+m}\boldsymbol{x} = \lambda E_{n+m}\boldsymbol{x}, \qquad (4)$$

where E_{n+m} represents a unit matrix of $n+m$ dimensions. Regarding (3) as a hypermatrix whose elements are two square matrices and two rectangular matrices, we suppose that $\boldsymbol{x}$ also consists of two parts, $\boldsymbol{x}_1$ of n dimensions and $\boldsymbol{x}_2$ of m dimensions. Then the equation (4) is separated into two matrix-equations:

$$\Lambda_n\boldsymbol{x}_1 + B\boldsymbol{x}_2 = \lambda E_n\boldsymbol{x}_1\,; \quad \widetilde{B}\boldsymbol{x}_1 + \Lambda_m\boldsymbol{x}_2 = \Lambda E_m\boldsymbol{x}_2 \qquad (5)$$

where E_n and E_m re unit matrices of n and m dimensions respectively. Or we may transform (5) into

$$(\lambda E_n - \Lambda_n)\boldsymbol{x}_1 = B\boldsymbol{x}_2\,; \quad \widetilde{B}\boldsymbol{x}_1 = (\lambda E_m - \Lambda_m)\boldsymbol{x}_2\,; \qquad (6)$$

If we assume H'_{n+m} does not contain λ_i $(i = 1, 2, \ldots\ldots, n)$ as eigenvalue, then

$$\det\{\lambda E_n - \Lambda_n\} \neq 0. \qquad (7)$$

On account of this condition, there exists a inverse matrix of $\lambda E_n - \Lambda_n$ and from (6) we obtain

$$\boldsymbol{x}_1 = (\lambda E_n - \Lambda_n)^{-1}B\boldsymbol{x}_2.$$

Substituting this into the latter of (6), we obtain the following matrix-equation of m dimensions:

$$\{\lambda E_m - \Lambda_m - \widetilde{B}(\lambda E_n - \Lambda_n)^{-1}B\}\boldsymbol{x}_2 = 0.$$

In order that there exists a solution $\boldsymbol{x}_2 \neq 0$, following determinantal equation is obtained in place of usual secular equation,

$$\begin{vmatrix} \lambda-\lambda_1'-\sum\limits_{k=1}^{n}\dfrac{|b_{k1}|^2}{\lambda-\lambda_k}, & -\sum\limits_{k=1}^{n}\dfrac{b_{k1}\bar{b}_{k2}}{\lambda-\lambda_k}, & \ldots\ldots, & -\sum\limits_{k=1}^{n}\dfrac{b_{k1}\bar{b}_{km}}{\lambda-\lambda_k} \\ -\sum\limits_{k=1}^{n}\dfrac{b_{k2}\bar{b}_{k1}}{\lambda-\lambda_k}, & \lambda-\lambda_2'-\sum\limits_{k=1}^{n}\dfrac{|b_{k2}|^2}{\lambda-\lambda_k}, & \ldots\ldots, & -\sum\limits_{k=1}^{n}\dfrac{b_{k2}\bar{b}_{km}}{\lambda-\lambda_k} \\ \cdots\cdots & \cdots\cdots & \cdots\cdots & \cdots\cdots \\ -\sum\limits_{k=1}^{n}\dfrac{b_{km}\bar{b}_{k1}}{\lambda-\lambda_k}, & -\sum\limits_{k=1}^{n}\dfrac{b_{km}\bar{b}_{k2}}{\lambda-\lambda_k}, & \ldots\ldots, & \lambda-\lambda_m'-\sum\limits_{k=1}^{n}\dfrac{|b_{km}|^2}{\lambda-\lambda_k} \end{vmatrix} = 0. \qquad (8)$$

Or briefly

$$\det\left\{(\lambda-\lambda_i')\delta_{ij}-\sum_{k=1}^{n}\frac{b_{ki}\bar{b}_{kj}}{\lambda-\lambda_k}\right\}_{i,j\leq n} = 0, \qquad (9)$$

where b_{ij} represents the i, j element of B and $\bar{b}_{ij}$ is the conjugate complex of b_{ij}.

Noting the symmetry of (9), we obtain also the following equation instead of (9), provided $\det\{\lambda E_m - \Lambda_m\} \neq 0$ be assumed.

$$\det\left\{(\lambda-\lambda_i)\delta_{ij}-\sum_{k=1}^{m}\frac{b_{ik}\bar{b}_{jk}}{\lambda-\lambda_k'}\right\}_{i,j\leq m} = 0. \qquad (10)$$

In the particular case $m = 1$, the equation (9) may be reduced to the following equation

$$\lambda-\lambda_1'-\sum_{k=1}^{m}\frac{|b_{k1}|^2}{\lambda-\lambda_k} = 0.$$

This is the very equation obtained by Brillouin¹⁾.

In conclusion, the author expresses his cordial thanks to Prof. T. Yamanouchi for his valuable advices and encouragement given to this work.

References.

(1) Brillouin: J. de phys, 3 (1932), 379 or Condon and Shortly: The Tneory of Atomic Spectra, p. 37.

(2) M. Born and P. Jordon: Elementare Quantenmechanik, p. 28.

(3) The calculation of strong perturbation energy of Stark effect of He, taking the matrix elements between the states of different principal quatum numbers into account, will appear in a later issue of this Journal.

On the Noise of Rochelle Salt.

By Shoji **Kojima** and Kiyoe **Kato**.

Tokyo University of Literature and Science.

(Received June 13, 1949)

In the case of ferroelectric substances a noise analogous to the Barkhausen effect of ferromagnetism is expected. Such noise was studied by Schönfeld⁽¹⁾ and Mueller⁽²⁾ with Rochelle salt. However, Schönfeld⁽³⁾ found by the subsequent experiment that his observed noise was due to a surface effect. We have studied noises of Rochelle salt with a high gain amplifier and observed some noise besides Schönfeld's one.

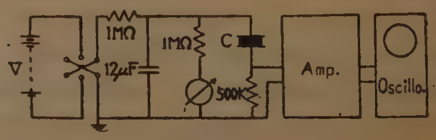

Fig. 1.

Noise measurements have been performed with the arrangement shown in Fig. 1. The field strength in the crystal C is varied slowly and continuously with the aid of a condenser and resistances. The time required for the voltage change from −300 to +300 V is about 30 sec. The amplifier works in the range of frequency from 200 to 20,000 c/s with a gain of 120 db. Noise is observed by a cathode-ray oscilloscope. Hysteresis loops operated by 50 c/s are also observed with a cathode-ray oscilloscope by a Mueller arrangement.

When the voltage applied to the crystal is sweeped from −300 to +300 V repeatedly, many noise pulses are observed as shown in Fig. 2a. At first with respect to heights of pulses these noises are grouped in two: the large noise and the small noise. The pulses of the large noise have about 10~100 fold heights of the small one. The large noise appears mostly on the saturation region of the hysteresis loops. When the voltage is changed as shown in Fig. 2b, this noise does not appear on the region indicated by R. Since this character agrees with Schönfeld's observation this noise is due to a surface effect.

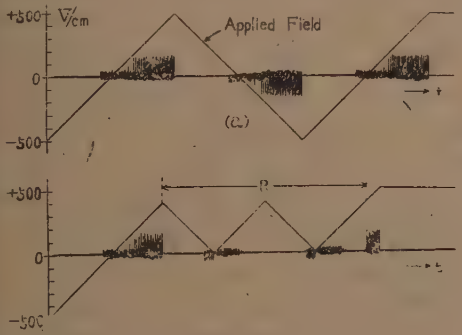

Fig. 2.

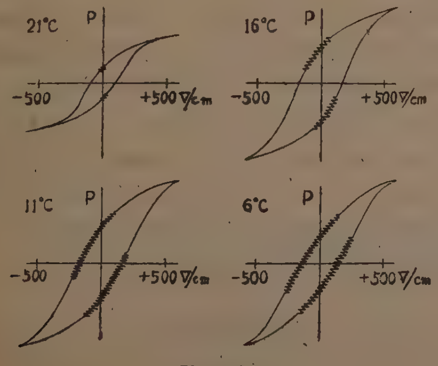

Fig. 3.

The small noise appears always at low voltage regions as shown in Fig. 2, which corresponds to the steep parts of the hysteresis loops as Fig. 3. This noise can not be eliminated by the method of the voltage change as Fig. 2b. This character is useful in experiments to distinguish them from the Schönfeld noise.

The small noise seems to originate in the Barkhausen effect.

Some rough observation of the forms of pulses by the cathoder-ay oscilloscope showed that the charge of the pulses were $10^{-13}\sim10^{-14}$ coulomb and that the time of polarization was $10^{-3}\sim10^{-4}$ sec.

Temperature dependence of the noise has been studied between 6°~40°C. It is obtained that the voltage range for the Barkhausen noise and the heights of the pulses increase with decreasing temperature, and that the noise can not be observed till the upper Curie point when the temperature is lowered gradually from 40°C.

The mostly used crystal is 2 cm by 2 cm by 0.5 cm thick. The heights of pulses are decreased by smaller dimension of crystals. The noise is also affected by humidity. When surface leakage is lower than 10^{-6} mho, the leakage noise predominate.

We wish to express our sincere thanks to Dr. Y. Kakiuchi and Dr. H. Kawai who kindly prepared for us Rochelle salt crystals.

References.

(1) H. Schönfeld: Ann. d. Phys. **19** (1934), 733.
(2) H. Mueller: Phys. Rev. **47** (1935), 175.
(3) H. Schönfeld: Ann. d. Phys. **22** (1935), 53.

On the Electrostrictive Effect of Barium Titanate.

By Yutaka TAKAGI and Etsuro SAWAGUCHI.

Tokyo Institute of Technology, Oh-okayama, Meguro-ku, Tokyo.

(Received June 30, 1949)

In a recent paper,(1) Mason has reported the electrostriction of $BaTiO_3$ ceramic estimated from the electromechanical vibration. Now, by making use of a Michelson's interferometer, we have succeeded in observing statically the transverse electrostrictive effect in a thin plate of $BaTiO_3$ ceramic prepared in our laboratory.

The specimen was 22 mm by 3 mm by 0.5 mm thick and was silvered on the 22 mm by 3 mm faces. Then it was suitably attached to one mirror of the interferometer to measure the striction parallel to the 22 mm edge. The polarizing d.c. field was applied between the silver plated faces. It was increased step by step to its maximum values, 10 kv/cm, 20 kv/cm and 30 kv/cm in three experiments. Always it was changed by a constant jump of each 2 kv/cm, and then at each stage retained unaltered for about one minute. Immediately before the field intensity was altered, the striction was measured.

As might be expected, indeed, the transverse electrostrictive effect was found to be a contraction. The strain *vs.* field strength curve is shown in Fig. 1. Evidently there is at first remarkable hysteresis character. But after the polarity of the field is reversed several times it is seen that the residual strain increases, and besides, the strain curve becomes approximately reproducible. The result in these final states are shown in Fig. 2. The order of magnitude of the value obtained is in agreement with Mason's value.

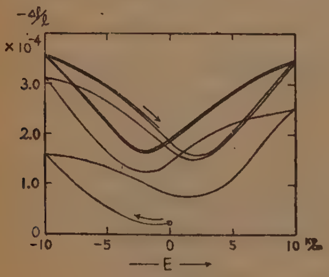

Fig. 1 Successive shift of strain hysteresis curve accompanying with several cycles of biasing field.

It will be seen in Fig. 2, that there is a saturation tendency as might be expected from the hysteresis loop. However, it is noteworthy that in the case of large amplitude of field strength, such as 30 kv/cm, the maximum amplitude of strain cycle is rather smaller than that in the case of 20 kv/cm. To explain this fact, it should be necessary to investigate the manner how the twin structure(2),(3) rearranges during the change of dielectric polarization.

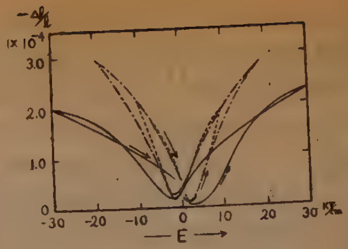

Fig. 2. Electrostrictive contraction as a function of biasing field. ----- for 10 kv/cm maximum strength; -·-·-· 20 kv/cm maximum strength; ——— 30 kv/cm maximum strength.

In relation with the electrostrictive effect, the dielectric constant in the same direction as that of d.c. field was measured with the same specimen; the results are shown in Fig. 3. The measurement was carried out under the similar condition except that an a.c. field of 1103 kc/sec, less than 20 v/cm, was superposed. The curve clearly shows a decrease of permittivity with increasing field intensity. Particularly, the decrease is more conspicuous during the period of increasing field than in the period of decreasing field. Moreover, there is remarkable diversity between the tendency of hysteresis curves of electrostriction and curves of the permittivity, so it should be noted that the decrease of permittivity is not to be completely explained by the alignment of domains only.

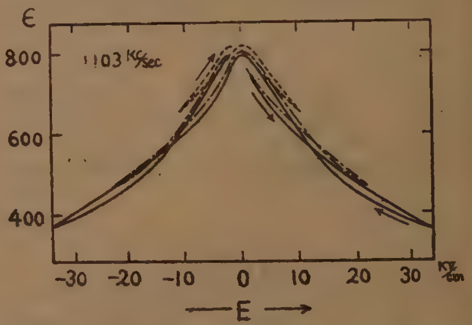

Fig. 3. Dielectric constant as a function of biasing field. ----- for 10 kv/cm. maximum strength; -·-·-· 20 kv/cm maximum strength; ——— 30 kv/cm maximum strength.

References.

(1) W. P. Mason, Phys. Rev. **74** (1948) 1134.

(2) H. F. Kay, Acta. Cryst. **1** (1948) 229.
(3) B. Matthias and A. von Hippel, Phys. Rev. **73** (1948) 1378.

Anomalous Specific Heat and Molecular Rotation in Solid Normal Hexadecyl Alcohol.

By Yoshinobu KAKIUCHI and Tosio SAKURAI.

Institute of Science and Technology, University of Tokyo.

(Received July 30, 1949).

Normal hexadecyl alcohol (cetyl alcohol) is well known to have a phase transition in solid state,(1) and its anomalous dielectric behaviors are often attributed to molecular rotation.(1), (2) We have investigated the diffraction of X-rays(3) by *n*-hexadecyl alcohol and reached to the conclusion that the molecules rotate around their long axis as A. Müller(4) has found in case of paraffines.(5)

Recently we have measured the specific heat and found its anomaly at exactly the same temperature where the lattice transformation sets in.

The calorimeter is made of copper, containing equally spaced thin copper disks which facilitates the heat conduction. Its total weight is about 54 grams and the entire surfaces are nickel plated for the purpose of preventing the chemical reaction between the sample and copper. The moltea sample weighing about 13 grams is poured into the calorimeter and then solidified. The heat capacity is measured by a continuous method resembling to that of Sykes'.(6)

One of the results is shown in Fig. 1, the sample being the same as was used in our X-ray studies (curve A). The anomaly is clearly seen at about 20°C, the temperature at which molecules begin to rotate. The curve is rather bell shaped than of λ-type, showing that nearly half a number of the total molecules are still librating at the transformation point.

The heat of transformation sometimes reaches to nearly half the value of the heat of fusion. The results are, however, greatly affected by the thermal history, and it is nescessary to cool the sample well below the transformation temperature, otherwise the specific heat anomaly almost disappears, because of the tendency that the molecular rotation persists for a long time at the temperature just below the transformation point. The transformation is also greatly affected by the purity of the sample. The more the sample pure, the higher the transformation point becomes (See Fig. 1). Although our sample is not perfectly pure, the essential point of our results is believed to be correct. Further purification is now in progress.

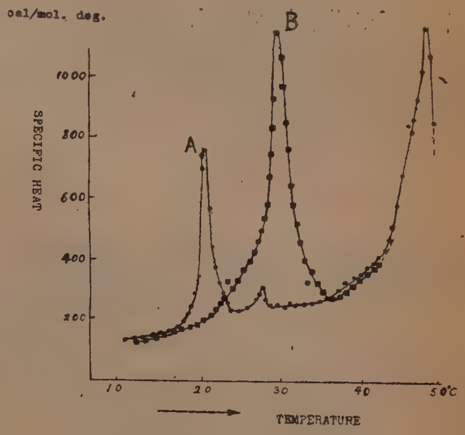

Fig. 1.

Measurement was done, by raising temperature.

Curve A: The sample same as former X-ray studies.

Curve B: The sample purified by destillating the above.

Dielectric properties of this substance were already studied by various investigaters.(1), (2) Recently Hoffman and Smyth(7) have reported the extensive study of the dielectric properties of normal higher alcohols and attributed the anomaly to the molecular rotation, where the proton transfer and molecular rotation mechanism as was suggested by Eyring in case of anomalous electric conductivity of ice is considered to be responsible for the larger values of low frequency dielectric constant. We have also started the dielectric measurement(8) along exactly the same line, and the results will be published in near future.

A part of the expense of our experiment was defrayed from the Ministry of Education.

References.

(1) K. Higasi and M. Kubo: Sci. Pap. I.P.C.R. **36** (1939) 286.

(2) O. Baker and C. P. Smyth: J. Am. Chem. Soc. **60** (1938) 1229.

(3) K. Sano and Y. Kakiuchi: J. Phys. Soc. Japan, in press.

(4) A. Müller: Proc. Roy. Soc. London **A138** (1932) 514.

(5) J.D. Bernal: Nature **129** (1932) 870.

(6) Sykes and Jones: J. Inst. Metal **12** (1936) 257.

(7) Hoffman and C. P. Smyth: J. Am. Chem. Soc. **71** (1949) 431.

(8) Presented to the annual meeting of the chemical society of Japan, April, 1949 and the 4th regular meeting of the Institute of Science and Technology, University of Tokyo, June, 1949.

Calculation of the Reflectivity of Multi-layers of $\lambda/4$ Thickness.

By Kōzō ISHIGURO.

Physical Institute, University of Tokyo.

(Received July 30, 1949)

Let us adopt the recurrence formula of W. Weinstein⁽¹⁾ as the starting point. Then, if one more layer of thickness h_k is added on the $k-1$ parallel layers on the glass surface, the following equations are proved

$$x_{k+1}^{+} = \{(u_{k+1}+u_k)\exp(-iv_kh_k)x_k^{+} + (u_{k+1}-u_k)\exp(iv_kh_k)x_k^{-}\}/2u_{k+1} \tag{1}$$

$$x_{k+1}^{-} = \{(u_{k+1}-u_k)\exp(-iv_kh_k)x_k^{+} + (u_{k+1}+u_k)\exp(iv_kh_k)x_k^{-}\}/2u_{k+1}$$

and

$$\begin{aligned} x_1^{+} &= (u_1+u_0)x_0^{+}/2u_1 \\ x_1^{-} &= (u_1-u_0)x_0^{+}/2u_1 \end{aligned} \tag{2}$$

The reflectivity R_k and transmissivity T_k are given by

$$R_k = |x_k^{-}/x_k^{+}|^2, \quad T_k = 1-R_k \tag{3}$$

The notations are the same as in Weinstein's paper.

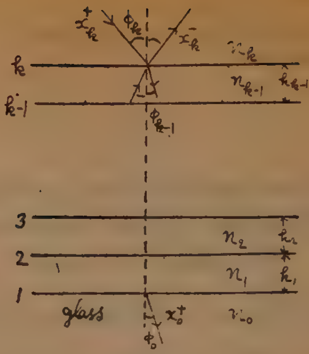

Fig. 1.

It is convenient to introduce the following transformation*:

$$\begin{aligned} x_k^{+} + x_k^{-} &= a_k \\ x_k^{+} - x_k^{-} &= ib_k \end{aligned} \tag{4}$$

Then (1) is easily transformed into

$$\begin{aligned} a_{k+1} &= \Theta_k a_k - \Psi_k b_k \\ b_{k+1} &= (u_k/u_{k+1})(\Psi_k a_k + \Theta_k b_k) \end{aligned} \tag{5}$$

where

$$\begin{aligned} \Theta_k &= \cos v_kh_k \\ \Psi_k &= -\sin v_kh_k \end{aligned} \tag{6}$$

The fact that the coefficients of (5) do not involve imaginary quantity is one of the advantage of such transformation.

In the case of the so-called $\lambda/4$ layer in the generalized sense, we have

$$v_kh_k = (2\pi/\lambda)n_kh_k\cos\phi_k = \pi/2 \text{ or } n_kh_k\cos\phi_k = \lambda/4 \tag{7}$$

Hence $\Theta_k = 0$, $\Psi_k = -1$ and (5) becomes

$$a_{k+1} = b_k, \quad b_{k+1} = -(u_k/u_{k+1})a_k \tag{8}$$

Using (8), (4) and (2), it is easily shown that

$$\begin{aligned} x_k^{\pm} = (-1)^{(k-1)/2}\{&(u_1u_3\cdots\cdots u_{k-2})^2u_k \\ &\pm u_0(u_2u_4\cdots\cdots u_{k-1})^2\}x_0^{+}/(2u_1u_2\cdots\cdots u_k) \end{aligned}$$

$k = \text{odd}$

$$\begin{aligned} x_k^{\pm} = (1/i)(-1)^{k/2-1}\{&u_0(u_2u_4\cdots\cdots u_{k-2})^2u_k \\ &\pm(u_1u_3\cdots\cdots u_{k-1})^2\}x_0^{+}/(2u_1u_2\cdots\cdots u_k) \end{aligned}$$

$k = \text{even}$

From (3), the reflectivity and transmissivity are given by

$$\begin{aligned} R_k &= |x_k^{-}/x_k^{+}|^2 = \{(A_k-B_k)/(A_k+B_k)\}^2, \\ T_k &= 1-R_k \end{aligned}$$

(9

where

$$\left.\begin{aligned} A_k &= (u_1 u_3 \cdots\cdots u_{k-2})^2 u_k \\ B_k &= u_0 (u_2 u_4 \cdots\cdots u_{k-1})^2 \end{aligned}\right\} k = \text{odd}$$

or

$$\left.\begin{aligned} A_k &= u_0 (u_2 u_4 \cdots\cdots u_{k-2})^2 u_k \\ B_k &= \quad (u_1 u_3 \cdots\cdots u_{k-1})^2 \end{aligned}\right\} k = \text{even}$$

Of course, the thickness h_k of every layer must satisfy the condition (7).

According to Weinstein's definition of u_k, it must be taken that, in the case of normal incidence of light, we have $u_k = n_k =$ the refractive index of the k th layer, while, in the case of oblique incidence of angle ϕ_k, we have $u_k = n_k / \cos\phi_k$ (electric vector of incident light//plane of incidence), or

$u_k = n_k \cos\phi_k$ (electric vector of incident light $\perp$ plane of incidence).

From (9) it can be seen that the condition of zero reflection is

$$A_k = B_k$$

which involves the condition of zero reflection of R. L. Mooney⁽²⁾, P. King⁽³⁾, A. Vašiček⁽⁴⁾ etc., as special cases, that the condition to increase the reflection is to make the difference between A_k and B_k large as possible and that the existence of $\lambda/2$ layer is equal to the existence of two successive $\lambda/4$ layers of the same refractive index and has no influence on the reflection.

Finally, it should be remarked that the transmissivity $T_k = n_0 |E_0{+}|^2 / n_k |E_k{+}|^2$ $(= (n_0 \cos^2\phi_k / n_k \cos^2\phi_0) |x_0{+}/x_k{+}^2$ or $(n_0/n_k)|y_0{+}/y_k{+}|^2)$ in Weinstein's paper is to be corrected to $T_k = n_0 \cos\phi_0 |E_0{+}|^2 / n_k \cos\phi_k |E_k{+}|^2$

References.

(1) W. Weinstein: J. O. S. A. **37** (1947), 576.
(2) R. L. Mooney: J. O. S. A. **35** (1945), 574.
(3) P. King & L. B. Lockhart: J. O. S. A. **37** (1947), 689.
(4) A. Vašiček: J. O. S. A. **37** (1947), 623.

---

* The author's original calculation did not use such transformation and was more complicated. The method in this paper owes mainly to Toshio Kato of our institute.

CONTENTS

(Vol. 4)

Page

No. 1

Ryoichi KIKUCHI: Theory on the Crystallization and Melting of Unvulcanized Rubber, Part I. 1

Ryoichi KIKUCHI: Theory on the Crystallization and Melting of Unvulcanized Rubber, Part II. 7

Masataka MIZUSHIMA: On the Ammonia Molecule, I. 11

Akiya OOKAWA: Crystallite Theory of Liquid, III. The Viscous Flow. 14

Giiti IWATA: La Théorie du Champ Unitaire et la Théorie Quantique. 21

Yoshiaki TINO: On Thermal Hysteresis in Irreversible Iron-Nickel Alloys. 24

Koreo KINOSHITA, Mitsuo SUMI & Takashi OWAKI: On the Physical Cleaning of Surface, I. Spectra of Gliding Sparks on Contaminated Glass Surfaces. 30

Toyoki KOGA: On States not in Thermal Equilibrium (Introduction of the Equation of Motion of Gas). 34

Hiroo KUMAGAI, Koichi SHIMODA, Iwao OGAWA, Yasuo TORIKAI & Teisuke KODAMA: Discharge Mechanism in Geiger-Müller Counters
Part I. 39
Part II. 44
Part III. 48

Shozo SAWADA & Gen SHIRANE: Specific Heat and Thermal Expansion of Barium Titanate. 52

No. 2

Yutaka SHIGEMITSU: On the Laminar Sub-Layer in the Turbulent Boundary Layer, I. 61

Masao KOTANI & Hidetoshi TAKAHASHI: Theoretical Determination of Proper Frequencies of the Resonant Circuit of the Cavity Magnetrons. 65

Masao KOTANI & Hidetoshi TAKAHASHI: Numerical Tables of Functions useful for the Calculation of Resonant Frequencies of a Cavity Magnetron. 73

Ken-ichi SHINOHARA; Toshihiro OKADA & Susumu MORITA: Determination of the Cross Section for the Photo-Disintegration. 77

Isaaki YOKOTA: Thomas-Fermi-Dirac Equation for Incompletely Degenerate Electron Gases. 82

Nobuhiko SAITÔ: Viscosity of High Polymer Solutions, I. Rigid Skein Model. 85

Nobuhiko SAITÔ: Viscosity of High Polymer Solutions, II. Influence of Rubber Elasticily. 88

Heiji KAWAI & Masakazu MARUTAKE: The Dispersion of the Piezoelectric Modulus of Rochelle Salt. 91

Shuzo MIYAKE; On the Mean International Electric Units. 93

Akio KOBAYASHI & Kenzi ARITA: The Patch Effect of Crystal Rectifiers. 96

Yutaka TAKAGI: Statistical Theory of Binary Alloys, (IV). 99

Tsugihiko SATÔ D Syû ONO: The Second Report on the Hole Theory of Liquid. 103

Makoto TANIFUJI: On the Internal Conversion in M-Shell and the Isomer Analysis. 107

Takehiko OGUCHI, Yutaka TAKAGI & Gen SHIRANE: Tentative Explanation on the Hysteresis Loops of Rochelle Salt. 112

No. 3

Yutaka SHIGEMITSU: On the Laminar Sub-Layer in the Turbulent Boundary Layer, II. 123

Yutaka SHIGEMITSU: On the Laminar Sub-Layer in the Turbulent Boundary Layer, III. 129

Haruhiko TOHARA: Relaxation Phenomena of Polymers, I. Stress Relaxation of Vulcanized Rubber (Part I.). 136

Haruhiko TOHARA: Relaxation Phenomena of Polymers, II. Stress Relaxation of Vulcanized Rubber (Part II.). 139

Ken-ichi SHINOHARA: Multiple Scattering of Fast Electrons, Part I. Theoretical Considerations. 144
Itiro TANI: On the Solution of the Laminar Boundary Layer Equations. 149
Kazutake KOHRA & Ken-ichi SHINOHARA: On the Anomalies of the Small Angle Reflection of Cathode Rays from the Surface of a Single Crystal, Part I. The Usual Dinamical Treatment. 155
Kazutake KOHRA & Ken-ichi SHINOHARA: On the Anamalies of the Small Angle Reflection of Cathode Rays from the Surface of a Single Crystal, Part II. The Investigation on the Causes of the Anomalies. 160
Takasi HUZIMURA & Tatsuya KATAYAMA: On the Velocity of Displacement of Magnetic Domain Boundary. 164
Seitaro NAKAMURA, Soei SIMA & Minoru KOBAYASHI: Probabilities of Beta Decay and Orbital Electron Capture for the Forbidden Transitions. 166
Gen SHIRANE & Takehiko OGUCHI: On the Transition in KH_2PO_4. 172

No. 4~6

Tosio AOKI: On the Diffraction of Electromagnetic Waves by Screens and Holes of Perfect Conductors, (I). On a Dual Relation between the Diffractions of Electromagnetic Waves by Screens and that by Holes of Perfect Conductors. 183
Tosio AOKI: On the Diffraction of Electromagnetic Waves by Screens and Holes of Perfect Conductors, (II). Approximate Formulas and their Applications. 185
Masataka MIZUSHIMA: On the Ammonia Molecule, (II). 191
Yuzo TOMONO: The Temperature Dependence of Initial Permeability of Iron Single Crystal under External Tension. 196
Akira SAKURAI: On the Theory of Cylindrical Shock Wave. 199
Masaru WATANABE: Ionization of Negative Oxygen Ion by Electron Impact, (I). 203
Masaru WATANABE: Ionization of Negative Oxygen Ion by Electron Impact, (II). . . . 208
Itiro TANI: Wave Jump in the Boundary Layer. 212
Wasao SHIBAGAKI: On the Theory of Statistical Adjustment of Data, (I). 216
Haruhiko TOHARA: Relaxation Phenomena of Polymers, (III). Motion of Junctions under Stress Relaxation. 222
Ken-ichi SHINOHARA, Kenzo INOUE & Nobuko HIROHATA: Multiple Scattering of Fast Electrons, Part II. Comparison with Experiments. 227
Kazuo NIIRA: On the Excitation of H_2O Molecules by Impact of Fast Electron, ... 230
Yoshio MUTO: Notes on Statistical Thermodynamics of Solutions and Gaseous Mixtures, (I) 233
Yoshio MUTO: Notes on Statistical Thermodynamics of Solutions and Gaseous Mixtures, (II). 238
Yoshio MUTO: Notes on Statistical Thermodynamics of Solutions and Gaseous Mixtures, (III). 242
Yujiro KOH: A Mathematical Analysis of the C. M. Witcher's Beta-Ray Spectrometer of an Type Using Helical Orbit. 245
Toshinosuke MUTO, Kenzo INOUE & Ichie WATANABE: On the Magnetic Scattering of Fast Electrons in the Ferromagnetic Crystal. 251
Hidetosi TAKAHASI & Sigeyosi HARA: Anomalous Dielectric Behavior of Rochelle Salt, (I) 257
Hidetosi TAKAHASI & Sigeyosi HARA: Anomalous Dielectric Behavior of Rochelle Salt, (II) 261
Hiroshi ICHIMURA: A Statistical Mechnical Treatment of Conduction Electrons; An Attempt to the Theory of the Superconductivity. 265
Hide YOSHIOKA: A Study of Corrosion of Iron by Electron Diffraction. 270
Masayoshi NINOMIYA: On the Abnormal Intensity Distribution of OH Band. 275
Yasaku WADA: On the Relation between Compressibility and Molal Volume of Organic Liquid. 280

Michika MIYANISHI: The Model Experiment of "the Phenomena of Sea-Snake". 283
Ryuzo UEDA: X-Ray and Thermal Studies on the Phase Transitions of Cuprous Sulphide Cu_2S. 287
Masao KOTANI: On the Magnetic Moment of Complex Ions. 293
Yuzo TOMONO: Several Experiments on the Permalloy Problem. 298
Tetsuya ARIZUMI & Shin-ichiro NARITA: On the Grid Emission. 300
Yoshiro IKEDA & Teruko SOEYA: Liquid Rise in a Capillary Tube. 306
Jiro YAMASHITA: The Theory of Thermoelectromotive Force in Semiconductors. 310
Toshinosuke MUTO: Statistical Theory of Ferromagnetic Superlattice, Part III. Electric Scattering of Slow Neutrons. 316
Ryogo KUBO: Statistical Theory of Linear Polymers, V. Paraffin-Like Chain. 319
Ryogo KUBO: Interaction between Electrons and Ions in Semiconductors, II. 322
Ryogo KUBO: Interaction between Electrons and Ions in Semiconductors, III. 326
Goro HONJO: Electron Diffraction Studies on Oxide Films Formed on some Metals and Alloys, Part I. Oxidation of Pure Copper. 330
Toshio KATO: On the Upper and Lower Bounds of Eigenvalues. 334
Tokio SAKURAI: Non-Reflective Dielectrics. 339
Ta-you WU: On ARAKI's Theory of Inverted Alkali Doublet. 343
Gentaro ARAKI: A Remark on Ta-you WU's Criticism on the Theory of Inverted Alkali Doublets. 345

SHORT NOTES

No. 1

Yoichi UCHIDA, Masayasu UETA & Yoshio NAKAI: A New Absorption Band in Colored Rock-Salt Crystal. 57
Akio KOBAYASHI & Kenzi ARITA: Variation of the Capacity of Crystal Rectifiers with Bias. 58

No. 2

Etsuro SAWAGUCHI & Tetsuo AKIOKA: Dielectric Residual Polarization of Barium Titanate Ceramics. 117
Yasuhiro DOI: On the Mechanism of Coloring of Oxidized Copper. 118
Shoichiro NOMURA & Shozo SAWADA: On the Hysteresis Loops of $BaTiO_3$ Ceramics. 120

No. 3

Kazuzi HASHIMOTO, Munemaru IMAI & Heiichi HAGIWARA: Further Experiments on the Parallel Wire-and-plate Tpye Counter. 176
Kenzo SANO & Yoshinobu KAKIUCHI: X-ray Studies on Cetyl Alcohol. 178
Shigeki SUWA: A New Type of Fine Structure in the Spectrum of NeII. 179
Shin-ya MIYATANI: On the Precipitation in Single Crystals of Berillium-Copper Alloy. . 181
Hazimu KAWAMURA, Akira SHINOHARA & Yoshio EMOTO: Micro-second Decay of the Thermionic Emission from Oxide Cathode. 182

No. 4 ~ 6

Shinsuke SUGAMOTO: Theory of Elasticity of Finite Displacement, II. 348
Shoji KOJIMA & Kazuo TAKAYAMA: Probe Measurements for High Frequency Discharge. 349
Toshihiro OKADA & Ryosei UNO: On the Inner Photo-Effect of Cuprous Oxide. 351
Goro HONJO: On the Anomalous Structures of Silicon Carbide. 352
Yataro SEKIDO & Teitiro YAGI: Absorption of Flare-Type Cosmic Ray. 353
Kazuji HASHIMOTO & Heiichi HAGIWARA: Induced Discharge Phenomena on the Central Wires of Multiple Geiger Counters. 355
Yoshihito TAKESADA: Abnormal Absorption of Sound Waves in Water. 356
Naruo TAKETA: On the Modification of Boltzmann's Equation. 357
Ryukiti HASIGUTI: Theory of Recrystallization of Cold-Worked Metals. 358
Akira NOMOTO: On the Thermo-elastic Effect. 359

Ken-ichi Noga & Toshitaro Okada: On the Mechanisms of the Grid Emission 360
Seiichi Sueoka: On Eigenvalues of Incompletely Reducible Matrix 361
Shoji Kojima & Kiyoe Kato: On the Noise of Rochelle Salt 362
Yutaka Takagi & Etsuro Sawaguchi: On the Electrostrictive Effect of Barium Titanate 363
Yoshinobu Kakiuchi & Tosio Sakurai: Anomalous Specific Heat and Molecular Rotation in Solid Normal Alcohol. 365
Kozo Ishiguro: Calculation of the Reflectivity of Multi-Layers of $\lambda/4$ Thicknees 366

AUTHOR INDEX

Page
Akioka T.
E. Sawaguchi & ———: Dielectric Residual Polarization of Barium Titanate Ceramics 117
Araki G.: A Remark on Ta-you Wu's Criticism on the Theory of Inverted Alkali Doublets.......... 345
Arita K.
A. Kobayashi & ———: Variation of Capacity of Crystal Rectifiers with Bias .. 58
A. Kobayashi & ———: The Patch Effect of Crystal Rectifiers.......... 96
Arizumi T.
——— & S. Narita: On the Grid Emission.......... 300
Aoki T.: On the Diffraction of Electromagnetic Waves by Screen and Holes of Perfect Conductors, (I). On a Dual Relation between the Diffraction of Electromagnetic Waves by Screens and that by Holes of Perfect Conductors 183
On the Diffraction of Electromagnetic Waves by Screen and Holes of Perfect Conductors, (II). Approximate Formulas and their Applications 185
Doi Y: On the Mechanism of Coloring of Oxidized Copper 118
Emoto Y.
H. Kawamura, A. Shinohara & ———: Micro-second Decay of the Thermionic Emission from Oxide Cathode 182
Hagiwara H.
K. Hashimoto, M. Imai & ———: Further Experiment on the Parallel Wire-and-Plate Type Counter 176
K. Hashimoto & ———: Induced Discharge Phenomena on the Central Wire of Multiple Geiger Counters.......... 355
Hara S.
H. Takahashi & ———: Anomalous Dielectric Behavior of Rochelle Salt, (I). 257
H. Takahashi & ———: Anomalous Dielectric Behavior of Rochelle Salt, (II) ... 261
Hashiguti R.: Theory of Recrystallization of Cold-Worked Metals 358
Hashimoto K.
———, M. Imai & H. Hagiwara: Further Experiments on the Parallel Wire-and-Plate Type Counters.......... 176
———, H. Hagiwara: Induced Discharge Phenomena on the Central Wire of Multiple Geiger Counters.......... 355

HIROHATA N.
K. SHINOHARA, K. INOUE & ———: Multiple Scattering of Fast Electrons, Part II. Comparison with Experiments 227
HONJO G.: Electron Diffraction Studies on Oxide Films Formed on some Metals and Alloys, Part I. Oxidation of Pure Copper........ 230
On the Anomalous Structure of Silicon Carbide........ 352
HUZIMURA T.
——— & T. KATAYAMA: On the Velocity of Displacement of Magnetic Domain Boundary 164
ICHIMURA H.: A Statistical Mechanical Treatment of Conduction Electrons; An Attempt to the Theory of the Superconductivity........ 265
IKEDA Y.
——— & T. SOEYA: Liquid Rise in a Capillary Tube........ 306
IMAI M.
K. HASHIMOTO, ——— & H. HAGIWARA: Further Experiments on the Parallel Wire-and-Plate Type Counters 176
INOUE K.
K. SHINOHARA, ——— & N. HIROHATA: Multiple Scattering of Fast Electrons, Part II. Comparison with Experiments........ 227
T. MUTO, ——— & K. WATANABE: On the Magnetic Scattering of Fast Electrons in the Ferromagnetic Crystal 251
ISHIGURO K.: Calculations of the Reflectivity of Multi-Layers $\lambda/4$ Thickness........
IWATA G.: La Thèorie du Champ Unitaire et la Thèorie Quantique 21
KAKIUCHI Y.
K. SANO & ———: X-ray Studies on Cetyl Alcohol........ 178
——— & TOSHIO SAKURAI: Anomalous Specific Heat and Molecular Rotation in Solid Normal Alcohol 365
KATAYAMA T.
T. HUJIMURA & ———: On the Velocity of Displacement of Magnetic Domain Boundary 164
KATO K.
S. KOJIMA & ———: On the Noise of Rochelle Salt 362
KATO T.: On the Upper and Lower Bounds of Eigenvalues 334
KAWAI H.
——— & M. MARUTAKE: The Dispersion of the Piezoelectric Modulus of Rochelle Salt........ 91
KAWAMURA H.
———, A. SHINOHARA & Y. EMOTO: Micro-second Decay of the Thermionic Emission from Oxide Cathode 182
KIKUCHI R.: Theory on the Crystallization and Melting of Unvulcanized Rubber, Part I .. 1
Part II . 7
KINOSHITA K.

————, M. SUMI & T. OWAKI: On the Physical Cleaning of Surface, I. Spectra of Gliding Sparks on Contaminated Glass Surfaces 30

KOBAYASHI A.
———— & K. ARITA: The Patch Effect of Crystal Rectifiers 96
———— & K. ARITA: Variation of Capacity of Crystal Rectifiers with Bias 58

KOBAYASHI M.
S. NAKAMURA, S. SIMA & ————: Probabilities of Beta Decay and Orbital Electron Capture for the Forbidden Transitions 166

KODAMA T.
H. KUMAGAI, K. SHIMODA, I. OGAWA, Y. TORIKAI & ————: Discharge Mechanism in Geiger-Müler Counters, Part I 39
,, Part II 44
,, Part III 48

KOGA T.: On States not in Thermal Equilibrium (Introduction of the Equation of Motion of Gas) 34

KOH Y.: A Mathematical Analysis of the C. M. Witcher's Beta-Ray Spectrometer of an Type Using Helical Orbit 245

KOHRA K.
———— & K. SHINOHARA: On the Anomalies of the Small Angle Reflection of Cathode Rays from a Surface of a Single Crystal, Part I. The Usual Dynamical Treatment 155
———— & K. SHINOHARA: On the Anomalies of the Small Angle Reflection of Cathode Rays from the Surface of a Single Crystal, Part II. The Investigation on the Causes of the Anomalies 160

KOJIMA S.
& K. TAKAYAMA: Probe Measurements for High Frequency Discharge 351
& K. KATO: On the Noise of Rochelle Salt 362

KOTANI M.
———— & H. TAKAHASHI: Theoretical Determination of Proper Frequencies of the Resonant Circuit of the Cavity Magnetron 65
& H. TAKAHASHI: Numerical Tables of Functions useful for the Calculation of Resonant Frequencies of a Cavity Magnetron 73
————: On the Magnetic Moment of Complex Ions 293

KUBO R.: Statistical Theory of Linear Polymers, V. Paraffin-like Chain 319
Interaction between Electrons and Ions in Semiconductors, II 322
,, ,, ,, III 326

KUMAGAI H.
————, K. SHIMODA, I. OGAWA, Y. TORIKAI & T. KODAMA: Discharge Mechanism in Ceiger-Müler Counters, Part I 39
————, K. SHIMODA, I. OGAWA, Y. TORIKAI & T. KODAMA: Discharge Mechanism in Geiger-Müler Counters, Part II 44

———, K. SHIMODA, I. OGAWA, Y. TORIKAI & T. KODAMA: Discharge Mechanism in Geiger-Müler Counters, Part III 48

MARUTAKE M.

H. KAWAI & ———: The Dispersion of the Piezoelectric Modulus of Rochelle Salt. 91

MIYAKE S.: On the Mean International Electrical Units 93

MIYANISHI M.: The Model Experiment of "the Phenomena of Sea-Snake" 283

MIYATANI S.: On the precipitation in Single Crystals of Berillium Copper Alloy 181

MIZUSHIMA M.: On the Ammonia Molecule, I 11

" " II 191

MORITA S.

K. SHINOHARA, T. OKADA & ———: Determination of the Cross Section for the Photo-Disintegration 77

MUTO T.

———, K. INOUE & I. WATANABE: On the Magnetic Scattering of Fast Electrons in the Ferromagnetic Crystal 251

———: Statistical Theory of Ferromagnetic Superlattice, Part III. Electric Scattering of Slow Neutrons 316

MUTO Y.: Notes on Statistical Thermodynamics of Solutions and Gaseous Mixtures, (I).. 233

" " (II).. 238

" " (III).. 242

NAKAMURA S.

———, S. SIMA & M. KOBAYASHI: Probabilities of Beta Decay and Orbital Electron Capture for the Forbidden Transitions 166

NARITA S.

T. ARIZUMI & ———: On the Grid Emission 300

NIIRA K.: On the Excitation of H_2O Molecules by Impact of Fast Electron 230

NINOMIYA M.: On the Abnormal Intensity Distribution of OH Band 275

NOGA K.

——— & T. OKADA: On the Mechanisms of the Grid Emission 360

NOMOTO A.: On the Thermo-Elastic Effect 359

NOMURA S.

——— & S. SAWADA: On the Hysteresis Loops of $BaTiO_3$ Ceramics 120

OGAWA I.

H. KUMAGAI, K. SHIMODA, ———, Y. TORIKAI & T. KODAMA: Discharge Mechanism in Ceiger-Müler Connters, Part I 39

" " Part II 44

" " Part III 48

OGUCHI T.

———, X. TAKAGI & G. SHIRANE: Tentative Explanation on the Hysteresis Loops of Rochelle Salt 112

G. SHIKANE & ———: On the Transition in KH_2PO_4 172

Okada Toshihiro
———, K. Shinohara, & S. Morita: Determination of the Cross Section for the Photo-Disintegration 77
——— & R. Uno: On the Inner Photo-Effect of Cuprous Oxide 351

Okada Toshitaro
K. Noga & ———: On the Mechanisms of the Grid Emission 360

Ono S.
T. Sato & ———: The Second Report on the Hole Theory of Liquid 103

Ookawa A.: Crystallite Theory of Liquid, III. The Viscous Flow 14

Saito N.: Viscosity of High Polymer Solutions, I. Rigid Skein Model 85
,, ,, II. Influence of Rubber Elasticity 88

Sakurai A.: On the Theory of Cylindrical Shock Wave 199

Sakurai Tokio: Non-Reflective Dielectrics 339

Sakurai Tosio
Y. Kakiuchi & ———: Anomalous Specific Heat and Molecular Rotation in Solid Normal Alcohol 365

Sano K.
——— & Y. Kakiuchi: X-ray Studies on Cetyl Alcohol 178

Sato T.
——— & S. Ono: The Report on the Hole Theory of Liquid 103

Sawada S.
——— & G. Shirane: Specific Heat and Thermal Expansion of Barium Titanate. 52
S. Nomura & ———: On the Hysteresis Loops of $BaTiO_3$ Ceramics 120

Sawaguchi E.
——— & T. Akioka: Dielectric Residual Polarization of Barium Titanate Ceramics 117
Y. Takagi & ———: On the Electrostrictive Effect of Barium Titanate 363

Seikido Y.
——— & T. Yagi: Absorption of Flare-Type Ceramic Ray 353

Sibagaki W.: On the Theory of Statistical Adjustment of Data, (I) 216

Shigemitsu Y.: On the Laminar Sub-Layer in the Turbullent Boundary Layer, I 61
II 123
III ... 129

Shimoda K.
H. Kumagai, ———, I. Ogawa, Y. Torikai & T. Kodama: Discharge Mechanism in Geiger-Müller Counters, Part I 39
,, ,, Part II 44
,, ,, Part III 48

Shinohara A.
H. Kawamura, ——— & Y. Emoto: Micro-second Decay of the Thermionic Emission from Oxide Cathode 182

SHINOHARA K.
 ———, T. OKADA & S. MORITA: Determination of the Cross Section for the Photo-Disintegration........ 77
 ———: Multiple Scattering of Fast Electrons, Part I. Theoretical Considerations. 144
 K. KOHRA & ———: On the Anomalies of Small Angle Reflection of Cathode Rays from the Surface of a Single Crystal, Part I. The Usual Dynamical Treatment. 155
 K. KOHRA & ———: On the Anomalies of Small Angle Reflection of Cathode Rays from the Surface of a Single Crystal, Part II. The Investigation of the Causes of Anomalies........ 160
 ———, K. INOUE & N. HIROHATA: Multiple Scattering of Fast Electrons, Part II. Comparison witn Experiments........ 227
SHIRANE G.
 S. SAWADA & ———: Specific Heat and Thermal Expansion of Barium Titanate. 52
 T. OGUCHI, Y. TAKAGI & ———: Tentative Explation on the Hysteresis Loops of Rochelle Salt........ 112
 ——— & T. OGUCHI: On the Transition in KH_2PO_4........ 172
SIMA S.
 S. NAKAHARA, ——— & M. KOBAYASI: Probabilities of Beta Decay and Orbital Electron Crpture for the Forbidden Transitions........ 166
SOEYA T.
 Y. IKEDA & ———: Liquid Rise in a Crpillary Tube........ 306
SUGAMOTO S.: Theory of Elasticity of Finite Displacement, II. 348
SUEOKA S.: On Eigenvaleus of Incompletely Reducible Matrix........ 361
SUWA S.: A New Type of Fine Structure in the Spectrum of NeII........ 179
TAKAGI Y.
 ———: Statistical Theory of Binary Alloys, (IV)........ 99
 T. OGUCHI, ——— & G. SHIRANE: Tentative Explanation of Hystsresis Loops of Rochelle Salt........ 112
 ——— & E. SAWAGUCHI: On the Electrostrictive Effect of Barium Titanate..... 363
TAKAHASHI H.
 M. KOTANI & ———: Theoretical Determination of Proper Frequencies of the Resonant Circuit of the Cavity Magnetrons........ 65
 M. KOTANI & ———: Numerical Tables of Functions useful for the Calculations of Resonant Frequencies of a Cavity Magnetron........ 73
 ——— & S. HARA: Anomalous Di lectric Behavior of Rochelle Salt, (I)........ 257
 ——— & S. HARA: Anomalous Dielectric Behavior of Rochelle Salt, (II) 261
TAKAYAMA K.
 S. KOJIMA & ———: Probe Measurements for High Frequency Discharge........ 349
TAKESADA Y.: Abnormal Absorption of Sound Waves in Water........ 356
TAKETA N.: On the Modification of Boltzmann's Equation........ 357
TANI I.: On the Solution of the Laminar Boundary Layer Equations........ 149
 Wave Jump in the Boundary Layer 212

Tanifuji M.: On the Internal Conversion in M-shell and the Isomer Analysis.......... 107
Tino Y.: On the Thermal Hysteresis in Irreversible Iron-Nickel Alloys................ 24
Tohara H.: Relaxation Phenomena of Polymers, I. Stress Relaxation of Vulcanized Rubber (Part I).. 136
  Relaxation Phenomena of Polymers, II. Stress Relaxation of Vulcanized Rubber (Part II).. 139
  Relaxation Phenomena of Polymers, III. Motion of Junctions under Stress Relaxation.. 222
Tomono Y.: The Temperature Dependence of Initial Permeability of Iron Single Crystal under External Tension.. 196
  Several Experiments on the Permalloy Problem.......................... 298
Torikai Y.
  H. Kumagai, K. Shimoda, I. Ogawa, ——— & T. Kodama: Discharge Mechanism in Geiger-Müller Counters, Part I.. 39
  H. Kumagai, K. Shimoda, I. Ogawa, ——— & T. Kodama: Discharge Mechanism in Geiger-Müller Counters, Part II.. 44
  H. Kumagai, K. Shimoea, I. Ogawa, ——— & T. Kodama: Discharge Mechanism in Geiger-Müller Counters, Part III.. 48
Uchida Y.
  ——— & M. Ueta & Y. Nakai: A New Absorption Band in Colored Rock-Salt Crystal.. 57
Ueda R.: X-ray and Thermal Studies on the Phase Transitions of Cuprous Sulphide Cu_2S. 287
Ueta M.
  ———, Y. Uhida & Y. Nakai: A New Absorption Band in Colored Rock-Salt Crystal.. 57
Wada Y.: On the Relation between Compressibility and Molal Volume of Organic Liquid. 280
Watanabe I.
  T. Muto, K. Inoce & ———: On the Magnetic Scattering of Fast Electrons in the Ferromagnetic Crystal.. 251
Watanabe M.: Ionization of Negative Oxygen Ion by Electron Impact, (I)............ 203
  Ionization of Negative Oxygen Ion by Electron Impact, (II).................... 208
Wu, Ta-you: On Araki's Theory of Inverted Alkali Doublet.......................... 343
Yamashita J.: Theory of Thermoelectromotive Foree in Semiconductors............... 310
Yokota I.: Thomas-Fermi-Dirac Equation for Incompletely Degenerate Electron Gases. 82
Yoshioka H.: A Study of Corrosion of Iron by Electron Diffraction........................ 270